MULTIFRACTAL APPROACH TO THE STUDY OF GORKHA EARTHQUAKE OF 25 APRIL, 2015 NEPAL

A THESIS SUBMITTED TO THE

CENTRAL DEPARTMENT OF PHYSICS

INSTITUTE OF SCIENCE AND TECHNOLOGY

TRIBHUVAN UNIVERSITY

NEPAL

FOR THE AWARD OF

DOCTOR OF PHILOSOPHY

IN PHYSICS

By

RAM KRISHNA TIWARI

February 2023

MULTIFRACTAL APPROACH TO THE STUDY OF GORKHA EARTHQUAKE OF 25 APRIL, 2015 NEPAL

A THESIS SUBMITTED TO THE

CENTRAL DEPARTMENT OF PHYSICS

INSTITUTE OF SCIENCE AND TECHNOLOGY

TRIBHUVAN UNIVERSITY

NEPAL

FOR THE AWARD OF

DOCTOR OF PHILOSOPHY

IN PHYSICS

By

RAM KRISHNA TIWARI

February 2023

TRIBHUVAN UNIVERSITY

Institute of Science and Technology

DEAN'S OFFICE

Kirtipur, Kathmandu, Nepal

Reference No.:

Institute of Science & Technology
Dean's Office
Kirtipur 2045

EXTERNAL EXAMINERS

The Title of Ph.D. Thesis: " Multifractal approach to the study of Gorkha Earthquake of 25 April, 2015 Nepal "

Name of Candidate: Mr. Ram Krishna Tiwari

External Examiners:

(1) Dr. Subesh Ghimire
Central Department of Geology
Tribhuvan University, NEPAL

(2) Prof. Dr. Ambrish Kumar Mahajan
Central University of Himachal
Himachal Pradesh, INDIA

(3) Prof. Papadimitriou Eleftheria
Aristotle University of Thessaloniki
Thessaloniki, GREECE

November 9, 2023

(Dr. Surendra Kumar Gautam)
Asst. Dean

DECLARATION

I hereby declare that the Ph. D. dissertation entitled **"MULTIFRACTAL APPROACH TO THE STUDY OF GORKHA EARTHQUAKE OF 25 APRIL, 2015 NEPAL"** submitted to the Central Department of Physics, Institute of Science and Technology (IoST), Tribhuvan University, Nepal for the award of the degree of Doctor of Philosophy (Ph. D.), is my original work. It has been done after registration for the degree of Ph. D. at Tribhuvan University and carried under the supervision of Prof. Harihar Paudyal, Department of Physics, Birendra Multiple Campus (BMC), Tribhuvan University, Bharatpur, Chitwan, Nepal.

The results of this work or parts of this thesis have not been submitted to any other university or institution, for the award of any degree before. I shall be solely responsible if any evidences are found against my declaration.

Ram Krishna Tiwari

RECOMMENDATION

I have great pleasure in recommending that **Mr. Ram Krishna Tiwari** has carried out research entitled **"MULTIFRACTAL APPROACH TO THE STUDY OF GORKHA EARTHQUAKE OF 25 APRIL, 2015 NEPAL"** for the award of Doctor of Philosophy (Ph. D.) in **Physics** under my supervision. I hereby certify that he has completed the present work for the prescribed full period and fulfilled all the requirements approved by the Institute of Science and Technology (IoST), Tribhuvan University, Kirtipur for the submission of the thesis for the award of Ph. D. degree.

To my knowledge, this work embodies the results of his investigations conducted as a Ph. D. research scholar and has not submitted for any other degree.

.....

Dr. Harihar Paudyal
Supervisor
(Professor)
Department of Physics, Birendra Multiple Campus (BMC),
Tribhuvan University, Bharatpur
Chitwan, Nepal

February 2023

TRIBHUVAN UNIVERSITY
CENTRAL DEPARTMENT OF PHYSICS
Kirtipur, Kathmandu, Nepal

☎ 4331054
www.tucdp.edu.np

Tribhuvan University Central Department of Physics Kirtipur

Ref. No.: (F.No .....) CDP .....

Date: 2079-12-27

LETTER OF APPROVAL

Date: 04/10/2023

On the recommendation of **Prof. Harihar Paudyal**, this Ph. D. thesis submitted by **Ram Krishna Tiwari**, entitled **"MULTIFRACTAL APPROACH TO THE STUDY OF GORKHA EARTHQUAKE OF 25 APRIL, 2015 NEPAL"** is forwarded by Central Department of Research Committee (CDRC) to the Dean, Institute of Science and Technology (IoST), Tribhuvan University.

O.P. Niraula

Dr. Om Prakash Niraula
(Professor)
Head,
Central Department of Physics (CDP),
Tribhuvan University,
Kirtipur, Kathmandu, Nepal

ACKNOWLEDGMENTS

I would like to express my deep gratitude and appreciation to my supervisor Prof. Dr. Harihar Paudyal for his guidance, support, and encouragement throughout my Ph. D. journey. His expertise, patience, and dedication have been invaluable to me and have helped shape my research in countless ways. I am incredibly thankful for the countless hours of discussions and feedback that have greatly improved my thesis. I am grateful for the opportunities he has provided me to present my work at conferences and for his help in securing funding for my research. I am proud to have him as my supervisor and will always remember the positive impact he has had on my life and career. I feel privileged to have had the opportunity to work with such a knowledgeable and dedicated supervisor.

I would like to acknowledge Prof. Dr. Om Prakash Niraula, Head of Central Department of Physics and and the whole CDRC member for their valuable help to complete this work. Also, I am thankful to all members of the Central Department of Physics, Kirtipur and Birendra Multiple Campus, Chitwan. My sincere reverence goes to Prof. Dr. Binil Aryal, Dean, IoST, TU for his encouragement and motivation throughout the work. Also, I would like to express my deep thanks to Prof. Dr. Narayan Prasad Adhikari, Prof. Dr. Raju Khanal, Prof. Dr. Sitaram Bahadur Thapa, Prof. Arun Kumar Shrestha, Prof. Dayaram Paudel, and Dr. Keshav Raj Chalise for their valuable suggestion, cooperation and encouragement.

I am grateful to Dr. Sri Krishna Bhattarai, and Prakash Man Shrestha for sharing the knowledge of Python software, Dr. Hariram Thapa for sharing GMT software knowledge, and Dr. Suresh Basnet for sharing knowledge of Latex. Also, I would like to acknowledge Prof. Daya Shanker of IIT Roorke, and Prof. Paresh Nath Singh Roy of IIT Kharagpur, India for their fruitful suggestions while preparing manuscript for different international journals. Additionally, I am grateful to my friends, Hari Krishna Neupane, Jhulan Paurel, Arjun Dhungana, Sangeeta Maharjan, Anil Khadka, Sajan Shrestha, Narayan Panthi, Umakanta lal Karna, Arun Kumar Shaha, Shyam Khanal, and other colleagues with whom I spent significant hours during the period of my Ph. D. work.

In addition, I would like to thank Tribhuvan University in Nepal for the sabbatical leave and the University Grants Commission (UGC) of Nepal for the Ph.D. fellowship. I am equally thankful to Birendra Multiple Campus family. Last but not the least, I would like to thank my family: my parents and to my wife (Shanti Duwadi), my daughter (Aarohi

Tiwari), son (Aarav Tiwari), brother (Shyam Krishna Tiwari) and sister (Shanta Dawadi) for their continuous pray for the fruitful outcome of my hard work. I would also like to express my thanks to Mr. Nishkarsha Dawadi (my older nephew) for providing research articles and Nikesh Dawadi (younger nephew), and Mr. Damodar Dawadi (brother in law) for immense love and support. At last, I want to acknowledge to all my relatives, friends (Suvash Chandra Shah, Roshan Thapa, Sarun Shrestha, Bimal Kumar Chhetri, and Udaya Bahadur Thapa Kshetri) and well wishers for their inspiration.

Ram Krishna Tiwari
February 2023

ABSTRACT

The devastating earthquake that occurred in the Barpak area of the Gorkha district of Nepal on April 25, 2015, known as the Gorkha earthquake, caused widespread damage and the loss of lives. This study focuses on the central Himalaya region, particularly the area directly impacted by the Gorkha earthquake in 2015, as well as the surrounding regions. This study estimates the fractal dimension of the distribution pattern of the Gorkha earthquake aftershock sequence and the *b*-value of Gutenberg-Richter law for the earthquakes that occurred between 1964 and 2020 in central Himalaya and vicinity. The data set containing 1126 earthquakes with a completeness magnitude of ≥3.8 is created from the revised International Seismological Centre (ISC) catalogue for the rectangular boundary 26.45°N-30.5°N and 80°E-88.2°E for the study of *b*-value change. The b-value is estimated by the maximum likelihood estimation (MLE) method.

The temporal variation of *b*-value for the fixed event window (100) shows the increment from 0.44 ± 0.02 to 1.02 ± 0.09 for the period of 21 years (1980 to 2001). The U-shaped variation in b-value was noticed from 2005 to 2015, during which earthquakes from Gorkha to Kodari happened in the region. When the variation in *b*-value is studied on a long-term basis, the lowest *b*-value of 0.44 ± 0.06 was noticed for the period between 1984 and 1994, and after 1994, the *b*-value shows a gradual increase and settles around 1.0 after 2020.

The spatial variation of the *b*-value for the fixed width window shows the variation in the range between 0.59 and 1.0, suggesting the region under study is tectonically active. The *b*-value around 1.0 for 0 to 11 km of depth suggests the heterogeneity and low strength of the rock. The depth-dependent *b*-value reveals a significant boundary around the depth 32 km. The contour map shows the low *b*-value patches (areas) ≤ 0.7, one west and the other east of the 2015 earthquakes,and the areas are overlapped with the zones of the major faults.

More importantly, a multifractal analysis of the 2015 Gorkha earthquake's aftershock sequence is presented, focusing on the spatio-temporal distribution of earthquakes from April 25, 2015, to May 14, 2016 for the regions 81.77°–90.41°E and 25.22°–30.15°N. The analysis uses 10,500 earthquakes (Mc = 2.0 ML), divided into 101 windows of 500 events with 100 event shifts. During this period, the box counting dimension (D_0) ranged from 0.84 ± 0.07 to 2.39 ± 0.03, and the correlation dimension (D_2) ranged from 1.11 ± 0.04 to 1.38 ± 0.03. The generalized dimension spectrum (D_q) showed oscillations in positive q values with consistent peaks from q = 0 to q = 22.

From the study, the highest values of the capacity dimension, D_0, were found to be 2.28 ± 0.02, 2.39 ± 0.03, and 2.15 ± 0.03 for the temporal windows spanning from 2015-08-15 to 2015-08-26, 2015-11-01 to 2015-11-20, and 2015-11-30 to 2016-01-11, respectively. The study found that the fractal spectrum deviated between D_2 and D_{22}, with values ranging from 2.0 to 0.7. This deviation suggests a buildup of strain around an asperity and its subsequent release in the tectonic stress field. The knee-shaped structure of the fractal spectrum suggests that the aftershocks of the Gorkha earthquake show a multifractal structure described by a spectrum of generalized dimensions. Additionally, we found that the distribution of epicenters is not random but rather clusters in certain regions.

The temporal correlation dimension (D_t) varies between 0.27 and 0.30 across different time windows, and when calculated for the entire study duration spanning from 1964 to 2020, it yields a value of 0.31 ± 0.004. The low temporal correlation dimension value indicates a high temporal clustering of aftershocks. This high temporal clustering of aftershocks may be due to the interplay of different physical processes, such as stress transfer, and the temporal evolution of the fault system, which can lead to a temporal clustering of aftershocks. The seismic moment release curves for the Gorkha and Kodari (Dolakha) earthquakes in 2015 showed that the majority of the seismic moment was released during the Kodari earthquake. This suggests that the strongest aftershocks tend to carry the most seismic moment in an earthquake sequence. Additionally, it is possible that the high seismic moment release during the Dolakha earthquake was caused by an increase in the rate of plate subduction. A very weak negative correlation between *b*-value and fractal dimensions of aftershocks distribution means that as the *b*-value increases (indicating a greater number of small earthquakes relative to larger ones), the fractal dimension decreases (indicating a less complex distribution of aftershocks). This may indicate that as the number of small earthquakes increases, the distribution of aftershocks becomes more homogeneous and less complex.

The decline in the number of aftershocks is observed following the Gorkha earthquake within the first 45 days. It is observed that the rate of decline is steep in the first 10 days after the main shock and then gradually slows down. The modified Omori parameter *(p)* is calculated to be 0.86 ± 0.04, indicating a relatively low temporal decay rate. Additionally, the parameters c and K are calculated to be 0.051 ± 0.019, and 57.9 ± 3.7, respectively. The low value of p compared to the typical value of 1.0 for this study period suggests that the rate of decline in aftershocks has not yet reached equilibrium, and the possibility of additional aftershocks cannot be ruled out. This study provides valuable understandings regarding the spatial distribution of seismic activity in the central Himalayan region and thereby contributing to potential applications in risk evaluation endeavors in the times to come.

शोधसार

वि.सं. २०७२ साल बैशाख १२ गते (२५ अप्रिल २०१५) मा मध्य नेपालको गोरखा जिल्लास्थित बारपाक केन्द्रविन्दु बनाएर गएको गोरखा भूकम्पले धेरै जनधनको क्षति गरेको थियो । यस शोधमा सो भूकम्पको प्रभावमा परेको आयाताकार क्षेत्र (२६.४५° उत्तर - ३०.५०° उत्तर र ८०.००° पूर्व - ८८.२° पूर्व) मा पर्ने विगतका भूकम्पहरूको अध्ययन गरी बी–मान (बी–भ्यालु) को मापन र गोरखा भूकम्पको पराकम्पनहरूको अध्ययन गरी भग्न आयाम (फ्रेक्टल डाइमेन्सन) को मापन गरिएको छ। यस अध्ययनमा बी–मानको मापन अधिकतम सम्भावनाको अनुमान (म्याक्सिमम लाइक्लिहुड मेथड) बाट गरिएको छ।

प्रत्येकमा १०० वटा भूकम्पहरू समेटेर बनाइएको निश्चित विन्डोको आधारमा बी–मानको समयअनुसार (टेम्पोरल) परिवर्तन हेर्दा सन १९८० देखि २००१ सम्मको २१ वर्षको समयमा बी–मान ०.४४$\pm$०.०२ देखि १.०२$\pm$०.०९ सम्म बढेको पाइएको छ भने अङ्ग्रेजीको यु आकारको परिवर्तन २००५ देखि २०१५ सम्ममा देखिएको छ। दशक अवधिको आधारमा बी–मानको परिवर्तन हेर्दा सबैभन्दा कम (०.४४$\pm$०.०६) १९८४ देखि १९९४ को दशकमा देखिन्छ भने १९९४ पछि क्रमिक वृद्धि भई वैशिक औसत (ग्लोबल एभरेज) मान १.० को वरिपरि स्थिर भएको देखिन्छ। निश्चित चौडाइ (फिक्स्ड बीइड्थ) विन्डो बनाएर स्थान अनुसार भिन्नता (स्पेटियल भ्यारिएसन) को आधारमा बी–मानमा गरिएको अध्ययनले ०.५९ देखि १.० सम्म परिवर्तन भएको देखाउँछ। यस परिणामले अध्ययनमा समेटिएको क्षेत्र विवर्तनिक (टेक्टोनिक) रुपले सक्रिय रहेको सङ्केत गर्दछ।

हिमालयको सतहभन्दा मुनि गरिएको बी–मानको अध्ययनमा ०–११ कि.मी. गहिराइमा बी–मान १.० को वरिपरि पाइएको छ भने ३२ कि.मि. गहिराइमा बी–मानमा सार्थक परिवर्तन देखिएको छ। बी–मान १.० को वरिपरि रहनुले सक्रिय विवर्तनिक, भूपर्पटी (क्रस्ट) मा रहेको विजायीयता (हेटेरोजिनीटी) र भूपर्पटीमा रहेको चट्टानको तनाब (स्ट्रेस) धान्न सक्ने क्षमताको न्युनतालाई दर्साउँछ। बी–मानका रूपरेखा नक्शा (कन्टुर म्याप) को अध्ययन गर्दा गोरखा भूकम्पको पूर्वतिर र पश्चिमतिर न्यून बी–मान सूचित गर्ने क्षेत्रहरू पाइएको छ र यी क्षेत्रहरू हिमालयमा बिध्यमान मुख्य भ्रंश (थ्रष्ट) सँग अतिव्याप्ति (ओभरलेप) भएको पाइएको छ।

यस शोधमा ८१.७७° पूर्व - ९०.४१° पूर्व र २५.२२° उत्तर - ३०.१५° उत्तरमा २५ अप्रिल २०१५ देखि १४ मे २०१६ सम्मका गोरखा भूकम्पको पराकम्पनहरूको भग्न आयाम अध्ययनलाई विशेष जोड दिइएको छ। तीव्रता (म्याग्निचुड) २.० वा सो भन्दा बढी (रिक्टर स्केल) का १०,५०० पराकम्पनहरूलाई प्रत्येकमा ५०० वटा पराकम्पनहरू समाबेश गरी १०१ वटा विन्डो बनाईएको छ। प्रत्येक विन्डोमा पराकम्पनहरू १०० को सङ्ख्यामा सर्दै गएका छन् वा ४०० वटा पराकम्पनहरू अतिव्याप्ति भएका छन्। बाक्शा गणना आयाम (बक्स काउन्टीङ्ग डाइमेन्सन) वा क्षमता आयाम (क्यापासिटी डाइमेन्सन)

को मान ०.८४±०.०७ देखि २.३९±०.०३ सम्म र सहसम्बन्ध आयम (कोरिलेसन डाइमेन्सन) को मान १.११±०.००४ देखि १.३८ ±०.०३ सम्म परिवर्तन भएको देखिन्छ। सामान्यीकृत आयाम (जेनेरलाईज्ड डाइमेन्सन) वर्णक्रम (स्पेक्ट्रम) मानहरू दोलन (ओस्किलेसन) भएको देखिन्छ।

सामान्यीकृत आयाम वर्णक्रमको विस्तृत अध्ययन गर्दा बाक्शा गणना आयामको उच्चतम मानहरू २.२८±०.०२, २.३९± ०.०३ र २.१५±०.०३ क्रमशः २०१५–०८–१५ देखि २०१५–०८–२६, २०१५–११–०१ देखि २०१५–११–२० र २०१५–११–३० देखि २०१६–१–११ को समयकालिक विन्डोको लागि पाइएको छ। आयाम वर्णक्रम (डाइमेन्सन स्पेक्ट्रम) मा क्यु (अङ्ग्रेजी अक्षर) को मान २ देखि २२ सम्म परिवर्तन गरी हेर्दा भग्न आयाम २.०–०.७ सम्म घटेको पाइयो। यो विचलनले रूक्षता (एस्पेरिटि) को वरिपरि तनाव (स्ट्रेस) निर्माण र तनावबाट छुटकारा को सङ्केत गर्दछ। भग्न वर्णक्रम (फ्रेक्टल स्पेक्ट्रम) को घुँडा जस्तो वा अवग्रह (सिगमोईड) आकारले गोरखा भूकम्पको पराकम्पनको बाँडफाँड बहुभग्न संरचनामा भएको देखिन्छ। यसको साथै भूकम्पको केन्द्रविन्दु (एपिसेन्टर) हरू निश्चित क्षेत्रहरूमा झुण्ड (क्लष्टर) को रुपमा पाइएको छ। समयकालिक सहसम्बन्ध आयाम (टेम्पोरल कोरिलेसन डाइमेन्स) को मान फरक फरक समय विन्डो को लागि ०.२७ देखि ०.३० बिच रहेको पाइएको छ भने १९६४ देखि २०२० सम्म यसको मान ०.३१±०.००४ रहेको पाइएको छ। यी न्यून मानहरूले पराकम्पनहरूको उच्च अस्थायी झुण्डको सङ्केत गर्दछ। यो उच्च झुण्डको कारण तनावको अन्तरक्रिया, नयाँ भ्रंशहरूको निर्माण हुन सक्छ।

भूकम्पजनिक मोमेन्ट प्रसारण वक्र (साइजमिक मोमेन्ट रिलिज कर्व) हेर्दा कोदारी (दोलखा) भूकम्प पछि भूकम्पजनिक शक्तिको रिलिज बढी भएको पाइएको छ। जसले शक्तिशाली पराकम्पनले बढी असर गर्छ भन्ने कुरालाई प्रष्टयाउँछ। भूकम्पजनिक शक्ति बढी रिलिज हुनुको कारण भू-पाता सबडक्सन दर बढेको पनि हुन सक्छ। यस अध्ययनमा बी–मान र भग्न आयामको बिचमा कमजोर नकरात्मक सहसम्बन्ध देखिएको छ जसले बी–मान बढ्दै जाँदा भग्न आयमको मान घट्दै जाने सकेत गर्दछ। यसको साथसाथै स–साना पराकम्पनहरूले भूकम्पीय क्षेत्रमा कम जटिल स्थिति बन्दै गएको पनि सङ्केत गर्दछ।

गोरखा भूकम्पको पहिलो ४५ दिन सम्मको पराकम्पनहरूको ओमरी नियम अनुसार अध्ययन गर्दा पराकम्पनहरूको सङ्ख्या पहिलो १० दिनमा तीब्र रुपमा घटेको देखिन्छ र त्यसपछि क्रमिक रुपमा घटेको पाईएको छ। परिमार्जित ओमरी मापदण्ड (प्यारामिटर) पि (अङ्ग्रेजी अक्षर) को मान ०.८६±०.०४ मापन गरिएको छ जसले अपेक्षाकृत कम अस्थायी क्षयदर सङ्केत गर्दछ। अन्य मापदण्डहरू सी (अङ्ग्रेजी अक्षर) र के (अङ्ग्रेजी अक्षर) को मान क्रमशः ०.०५१±०.०१९ र ५७.९±३.७ मापन गरिएको छ। यस अध्ययनबाट प्राप्त पी को मान सामान्य मानिने पी को मान (१.०) भन्दा कम छ जसले पराकम्पनमा आएको

गिरावट दर अझै सन्तुलनमा पुग्न नसकेको सङ्केत गर्दछ र अतिरिक्त पराकम्पनहरूको सम्भावनालाई नर्कान नसकिने बताउँछ।

अन्तमा यस अध्ययनले मध्य हिमाली क्षेत्रमा भूकम्पीय गतिविधिको जानकारी गराई समयमा जोखिम मुल्याङ्कनका प्रयासहरूमा लाग्न जोड दिन्छ। यसले गर्दा भविष्यमा हुने धनजनको क्षतिमा कमी ल्याउन सकिने छ।

LIST OF ACRONYMS AND ABBREVIATIONS

GR	Gutenberg Richter
MLE	Maximum Likelihood Estimation
ISC	International Seismological Centre
NEMRC	National Earthquake and Research Centre
MCT	Main Central Thrust
MBT	Main Boundary Thrust
MFT	Main Frontal Thrust
HFT	Himalayan Frontal Thrust
MHT	Main Himalayan Thrust
ITSZ	Indus-Tsangpo Suture Zone
TH	Tethyan Himalaya
STDS	South Tibetan Detachment System
HH	Higher Himalaya
LH	Lesser Himalaya
SH	Sub Himalaya
KL	Karnali Lineament
JL or JF	Judi Lineament or Fault
TL or TF	Thaple Lineament or Fault
KTML or KTMF	Kathmandu Lineament or Fault
MGL or MGF	Motihari-Gaurishanker Lineament or Fault
MEL or MEF	Motihari-Everest Lineament or Fault
DKL	Dudhkoshi Lineament
AL	Arun Lineament
KAL	Kanchenjunga Lineament
HHC	Higher Himalayan Crystalline
LHSZ	Lesser Himalayan Sedimentary Zone
IGP	Indo-Gangetic Plain
SAR	Synthetic Aperture Radar
InSAR	Interferometric Synthetic Aperture Radar
NAMASTE	Nepal Array Measuring Aftershock Seismicity Trailing Earthquake
GPS	Global Positioning System
WTMM	Wavelet Transform Modulus Maxima
GCMT	Global Centroid Moment Tensor
WR	Walker's Ruler
PDF	Probability Density Function

CSC	Coulomb Stress Changes
SOC	Self Organised Critical
GMT	Generic Mapping Tools
CMT	Centroid Moment Tensor

LIST OF SYMBOLS

Mw	Moment magnitude
mb	Body wave magnitude
ML	Local magnitude or Richter magnitude
Mc	Magnitude of completeness
Mrr	Element of moment tensor where r stands for vertical direction
Mtt	Element of moment tensor where t stands for south direction
Mpp	Element of moment tensor where p stands for east direction
Mrt	Element of moment tensor in vertical and south direction
Mrp	Element of moment tensor in vertical and east direction
Mtp	Element of moment tensor in south and east direction
a	a-value of earthquake distribution (Seismicity)
b	b-value of earthquake distribution
p	p-value of aftershocks decay rate
D_0	Box Counting dimension
D_2	Correlation fractal dimension
D_q	Generalised fractal dimension
$C(r)$	Correlation integral function
$C_q(r)$	Generalised correlation integral function

LIST OF TABLES

Page No.

LIST OF FIGURES

Page No.

TABLE OF CONTENTS

CHAPTER 1

INTRODUCTION

1.1 General

Earthquakes are among the deadliest natural hazards as they strike without any warnings. They continuously pose unremitting threats to human civilization because many earthquake zones coincide with areas of high population density. A strong earthquake can damage and obliterate lives and property up to several hundred kilometers from its origin. The damage due to an earthquake depends upon the magnitude of the earthquake and geotectonic setup of a region. Thus, there is a desperate need to understand the basics of science related to the earthquake and to discover different methods of mitigation and if possible, to develop the theory that can predict the future earthquake.

As earthquakes result in devastating consequences, earthquake prediction is a matter of great challenge among the research communities, public and emergency service sectors. In recent years, the short-term forecasting of earthquakes from a machine learning (ML), and artificial Intelligence (AI) approach are popular among the researchers (Chelidze et al., 2020, 2022; Matcharashvili et al., 2018; Kaiser & Al Banna, 2020), and numerous works on prediction of earthquake has been attempted by various scientists from all over the world in past (Rikitake, 1968; Crampin et al., 1984). But, because of the complex and unpredictable nature of earthquake occurrence phenomenon, the success over it has not been achieved yet (K. Wang et al., 2006; Geller, 1997; Wyss, 1997). Nevertheless, each attempt and approach of study has unlocked some interesting facts, behavior, and mechanics of earthquake occurrences. Each of the different approaches towards studying the processes leading to different seismicity patterns can help in finding new ways of understanding the earthquake mechanisms. A new applicable model can identify the most vulnerable zone or highly seismic hazardous zone and helps society to prepare for challenges and implementation of hazard mitigation process. This study is an endeavor for identifying the earthquake patterns to declare the hazardous zone in central Himalaya

region after 2015 Gorkha earthquake.

The Himalayan belt stretching west to east from Nanga Parbat with an elevation of 8138 m to Namche Barwa reaching a height of 7755 m (Le Fort, 1975) trends mostly in northwest to southeast with a length ~2500 km and variation in width between 200 to 250 km from south to north. India, Nepal, and Bhutan occupy most of the Himalayas while some parts of them are also occupied by China, and Pakistan (Malik & Nakata, 2003; Molnar & Pandey, 1989). Geographical bordered of the Himalayas are Karakoram and Hindu Kush ranges to the northwest, plateau of Tibet to the north, and Indo-Gangetic plain to the south reflecting the extensive geological and tectonic processes happening in the region (Khattri & Tyagi, 1983; Ni et al., 1989).

Himalaya is the most geologically and tectonically complex, and one of the world's most seismically active areas where one continental crust is attempting to under-thrust another continental crust (Bilham et al., 2017; Dal Zilio et al., 2021; Duputel & Rivera, 2017). As the Indian plate collides with the Eurasian plate, Himalaya deforms downhill in response to an increased orogenic load, maintaining the entire Himalayan mountain arc seismically active (Dal Zilio et al., 2021; Mandal et al., 2000; Verma & Kumar, 1987). The Himalayan topography is created by a variety of discontinuous process (displacements on faults) and continuous processes (folding). Even today the Himalayas are developing continuously and changing their structures by the interplay between Indian and the Eurasian plates (Jouanne et al., 2004; D. Singh, 2000; Tandon & Gupta, 2020).

The convergence boundary of India with Eurasia is a continuous arc spanning from longitude 77°E and 89°E, referred to as Main Himalayan Thrust (MHT), a wedge-shape structure when seen in cross-section (Kayal, 2010; Mitra et al., 2015). The present-day convergence of the Himalaya captivates nearly half of the total convergence between India and Eurasia (about 2cm/yr.) (Bilham, 2004; Wobus et al., 2005). Three segments, namely-western segment (the region west of 75°E), central segment (the region between 75°E to 90°E), and eastern segment (the region east of 90°E) are geographical division of the Himalayan mountain system (Hodges, 2000).

The ramp structures within the MHT significantly contribute to the generation of seismic activity in the Himalayas and neighboring regions (Bai et al., 2019; Parameswaran & Rajendran, 2017; Whipple et al., 2016). Earthquakes in the Himalaya are mainly due to release of elastic strain energy created and restored by persistent collision of India and Eurasia (Ader et al., 2012; Mandal et al., 2000; Verma, 1991; Webb et al., 2011; Paudyal et al., 2008). Earthquakes of different (low to very high) magnitudes have clustered in the NW-SE trending Himalayan terrain (Bai et al., 2019; Jena et al., 2020). Generally, earthquakes do not occur uniformly throughout the world but occur repeatedly in certain

limited areas, particularly in active seismic belt like Himalaya. Although, the earthquake activity in the Himalaya compression zone is influenced by numerous factors such as highly distorted structures and large crustal thickness, strong geothermal movement, high vertical thermal gradients, tectonics features of the area of influence etc., it is mainly due to under-thrusting of aforementioned plates (DeCelles et al., 2002; Jouanne et al., 2004; D. Singh, 2000; Verma & Kumar, 1987; Whipple et al., 2016). Nearly all of the tectonic stresses in Himalaya have alignment along the north-south to the north northeast-south direction whereas in the adjoining Tibet region, north-south striking normal faults are prevalent (Bollinger et al., 2004, 2014). An area bounded by 26°-32°N and 80°- 89°E is considered in the present study which covers the central Himalaya and special focus is given to the epicenter area of 2015 Gorkha earthquake (Figure 1).

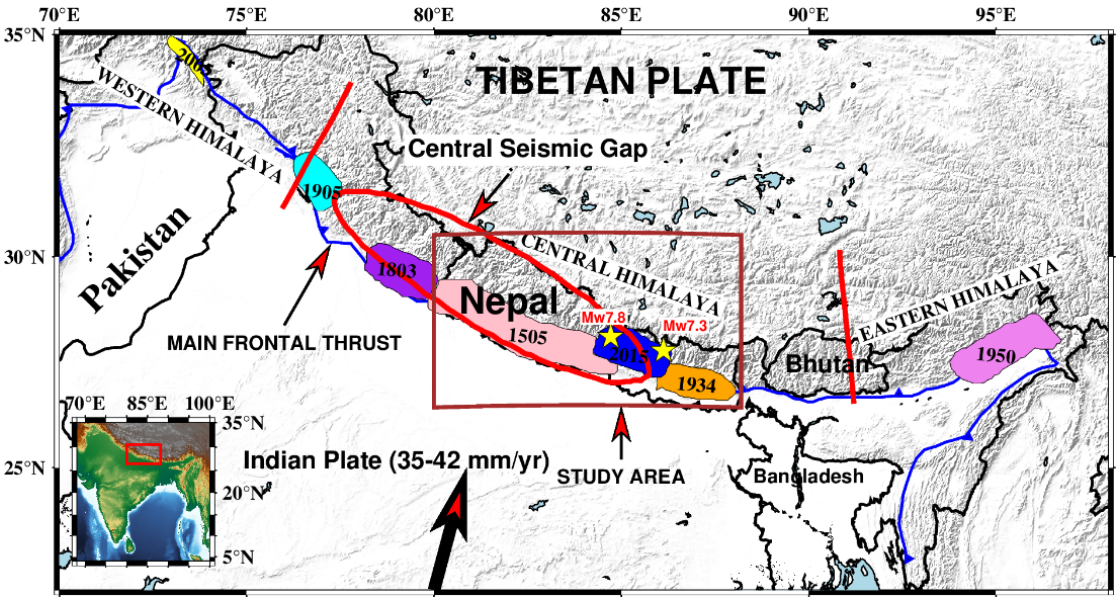

Figure 1: Map showing Himalayan arc and rupture zones of strong earthquakes (Gahalaut, 2008; Hodges, 2000; S. Gupta et al., 2021; Qureshi & Khan, 2020; C. Rajendran et al., 2015; Thakur et al., 2019; J. Yin et al., 2017). Yellow shaded zone represents the rupture area of 2005 Muzaffarabad–Kashmir earthquake, cyan shaded zone represents the rupture area of 1905 Uttarkashi earthquake or Kangra earthquake, purple shaded zone represents the rupture area of 1803 Garhwal earthquake, pink shaded zone represents the rupture area of 1505 Lo Mustang earthquake, blue shaded zone represents the rupture area of 2015 Gorkha earthquake, orange shaded zone represents the rupture area of 1934 Nepal–Bihar earthquake, violet shaded zone represents the rupture area of 1950 Assam earthquake. Red oval structure represents the central seismic gap. The red rectangular box in the inset map represents the study area at the global level, and the brown rectangular box denotes the study area at the regional level. The geodetic convergence velocity 35-42 mm/year between the India and Eurasia plates is adapted from past literature (Qureshi & Khan, 2020)

.

Because of the highly complex geological and tectonic structure (Ni et al., 1989; C. Rajendran & Rajendran, 2005), several significant earthquakes have previously occurred in the central Himalaya region. Few of them are worth mentioning here. The 1505 Lo Mustang earthquake is a plate boundary event that was strongly felt in the southern Tibet and northern Nepal with rupture length of 400-700 km (Ambraseys & Bilham,

2003; Ambraseys & Jackson, 2003). The 1803 Garhwal earthquake (Mw 7.4) possibly occurred on a subordinate thrust of the Main Central Thrust (MCT) damaging the hills of Garhwal Himalaya and ruptured ~200 km long sector of the MHT farther to east (Ambraseys & Douglas, 2004; C. Rajendran et al., 2018; C. Rajendran & Rajendran, 2005). The first major instrumentally documented event in the central Himalaya, the Uttarkashi or Kangra earthquake of April 4, 1905 (Mw 7.4), occurred south of the Main Boundary Thrust (MBT) (Ambraseys & Douglas, 2004; C. Rajendran et al., 2018; Kayal, 2010). The event was identified as pure thrust that extended over the width of the tectonic plate boundary for ~300 km, indicating its source on the MHT (Ni & Barazangi, 1984; T. Singh et al., 2012). The other remarkable earthquakes hosted by the Himalayan arc are Nepal-Bihar earthquake with a magnitude of Mw 8.1 on January 15, 1934, Assam earthquake of magnitude Mw 8.4 on August 15, 1950, Muzaffarabad–Kashmir earthquake registering Mw 7.6 on October 8, 2005, and the most recently Gorkha earthquake reaching a magnitude of Mw 7.8 on April 25, 2015 (Ambraseys & Douglas, 2004; Avouac et al., 2015). During the 1934 Nepal-Bihar earthquake nearly 100-300 km length of the Himalayan arc had ruptured (Molnar & Pandey, 1989) and after sixteen years of this event, the 15 August 1950 great Assam earthquake occurred in the eastern syntaxis zone of the Himalaya which did not reveal any surface rupture (Priyanka et al., 2017). Since the Assam quake, the Himalayan arc was silent until the occurrences of Muzaffarabad–Kashmir earthquake of magnitude (Mw 7.6) in 2005 and Gorkha earthquakes (Mw 7.8) in 2015, (C. Rajendran et al., 2019). Muzaffarabad–Kashmir earthquake was the lethal in the history of the Indian subcontinent that destroyed more than 80,000 lives (Teotia & Kumar, 2011; Wyss, 2005).

The section of an active fault where no great earthquake has happened for an extended period can be considered as a seismic gap. Several researchers (Arora et al., 2012; Khattri & Tyagi, 1983; Molnar & Pandey, 1989; Qureshi & Khan, 2020; Bilham, 2019) have classified the Himalayas as three seismic gap zones where future large earthquakes are possible. The segment of the Himalaya located to the westward of the 1905 Kangra earthquake is stated as the Kashmir gap (Schiffman et al., 2013; Khattri & Tyagi, 1983; Gahalaut, 2008), ~700 km long segment sandwiched between the 1905 Kangra earthquake and the 1934 Nepal-Bihar earthquake is stated as the central gap (Morell et al., 2015; C. Rajendran & Rajendran, 2005), the segment sandwiched between the 1934 and 1950 Assam earthquakes is stated as the Assam gap (Khattri et al., 1983; I. Singh et al., 2021).

It is believed that the central seismic gap is conducive to generate an Mw > 8 earthquake in near future (Khattri & Tyagi, 1983; Ghazoui et al., 2019; D. Gupta et al., 2015; Mugnier et al., 2013; K. Rajendran et al., 2017; Shrivastava, 2021). The absence of major historical earthquakes in western Nepal could be either by aseismic slip on the

MHT or enduring elastic strain growth (Bollinger et al., 2016; Ghazoui et al., 2019). The sealed zone between the MFT and the creeping zone is more extensive in western Nepal as compared to central Nepal. Therefore, the probability of the occurrence of M > 8 earthquakes in western Nepal could not be avoided (Jouanne et al., 2004). The investigations conducted by numerous researchers (Arora et al., 2012; Bilham, 2019; Morell et al., 2015; A. Tiwari et al., 2021; Mencin et al., 2016; Qiu et al., 2016) suggest that the central seismic gap is more vulnerable for future large earthquakes. Seeing convergence rates 35-42 mm per year (Qureshi & Khan, 2020), it is astonishing that the Himalayan plate boundary has produced only two great earthquakes in the last century thus scarcity of great earthquakes could only be justified as a kinematic mismatch in the region (C. Rajendran et al., 2019).

The release of the cumulative geodetic strain requires the occurrences of Mw 9.0 events in every thousand years for the Himalayan mountain system. The nonexistence of great earthquakes having capability to steadiness the accumulated strain in the middle portion keeps on mystifying the researchers who believe that the central Himalaya is geared up for a great earthquake (Arora et al., 2017; Jing et al., 2015; Molnar & Lyon-Caent, 1989; Sreejith et al., 2018). These conjectures have raised issues about the high seismic hazard for the central Himalaya and adjoining regions and demands the proper study of the nature of earthquake's occurrence and estimation of the hazardous zone.

1.2 An overview of Gorkha earthquake

The earthquake that occurred in the Barpak area of the Gorkha district in Nepal on April 25, 2015, also known as the Gorkha earthquake, was a devastating natural disaster. The earthquake had a magnitude of Mw 7.8 and its epicenter was positioned at around latitude 28.23°N and longitude 84.73°E, approximately 77 kilometers in the northwestern direction of Nepal's capital, Kathmandu (Bollinger et al., 2016; Bilham et al., 2017). The Gorkha earthquake occurred in a central seismic gap in close proximity to the MHT fault line. The earthquake resulted in extensive destruction and loss of lives in Nepal, with an estimated 9,000 people killed and 22,000 injured (Wyss & Chamlagain, 2019). It is the major earthquake after the Mw 8.7 Assam earthquake in the entire orogenic area of Himalaya (Coudurier-Curveur et al., 2020) and the last biggest earthquake after the 1934 Nepal-Bihar Mw 8.1 earthquake in central Nepal (S. Gupta et al., 2021). The main shock spread eastward along ~117° azimuth (A. Kumar et al., 2017) and partially ruptured a previously identified seismic gap (Diao et al., 2015) resulting in over 8,800 fatalities (Adhikari et al., 2015; Baillard et al., 2017). The faulting geometry of the main shock is a low-angle thrust fault dipping at ~11° north and broke a small eastern piece of the MHT, at the 800 km wide seismic gap between the 1905 M 7.4 Kangra earthquake in the west and the Mw 8.1 1934 Nepal-Bihar earthquake in the east (Kumahara et al.,

2016; Jing et al., 2015; McNamara et al., 2017). Within an hour of the main shock, two aftershocks took place at either end of the rupture, with magnitudes ranging from 6.6 Mw to 6.7 Mw. Two and a half weeks later, the largest aftershock, referred to as the Kodari (Dolakha) earthquake, took place at the north-eastern end of the key rupture with a magnitude of 7.3 Mw, leading to additional fatalities. (A. Kumar et al., 2017; Ogata & Tsuruoka, 2016; G. Zhang et al., 2015). There are 3 large aftershocks (Mw 6.7, 6.8 and 7.3) until May 12, 2015. A novel waveform inversion formula shows that the rupture was grown from the hypocenter at 30.0 km/s which goes on triggerring a large slip-event centered about 50 km to the east (Yagi & Okuwaki, 2015). The rupture was believed to nucleate at the downdip border of the MHT close to the transition from inter-seismic locking to aseismic creep beneath the Tibetan plateau, and propagated partially towards the MFT (Bilham et al., 2017). The mechanism behind the occurrence of major aftershock (Mw 7.3) was explained to be the reduction in shear strength along the hidden thrust fault that may be caused by the diffusion of high pore pressure fluids (Arora et al., 2017).

Distinguished features of the Gorkha event include time duration of 6s within which slip pulse unlocked the lower edge of the MHT (Y. Wang et al., 2019). The rupture extended in an eastward direction beneath Kathmandu, covering a distance of roughly 140 kilometers (K. Wang & Fialko, 2015) while the overall rupture area of the main-shock is $\sim$140$\times$ 70 km^2 on the fault interface (J. Yin et al., 2017). Early observations suggest that rupture did not stretch to the surface, conflicting with past events, such as the 1934 Nepal-Bihar earthquake and the 2005 Muzaffarabad–Kashmir earthquake. (Elliott et al., 2016; Kurashimo et al., 2019; Qiu et al., 2016; S. Li et al., 2019; Roback et al., 2018). A day plot of seismograph and three components of waveform of Gorkha earthquake are depicted in figure 2 and figure 3.

1.2.1 *b*-value of earthquake distribution

An ensemble of earthquakes can be described by the basic and important seismological parameter known as *b*-value (Gutenberg & Richter, 1944). This parameter follows the power law and signifies the distribution of earthquakes for the given range of magnitudes and estimated by the relation (Aki, 1965)

$$b = \frac{\log e}{\overline{M} - Mc} \tag{1.1}$$

where $\overline{M}$ is the average of magnitude of the earthquakes, and Mc is the completeness magnitude. The *b*-value is normally 1.0, but it differs from 0.5 to 1.5 based on the occurrence of earthquakes and tectonic setting of a region (Chiba & Shimizu, 2018; Prasath et al., 2019).

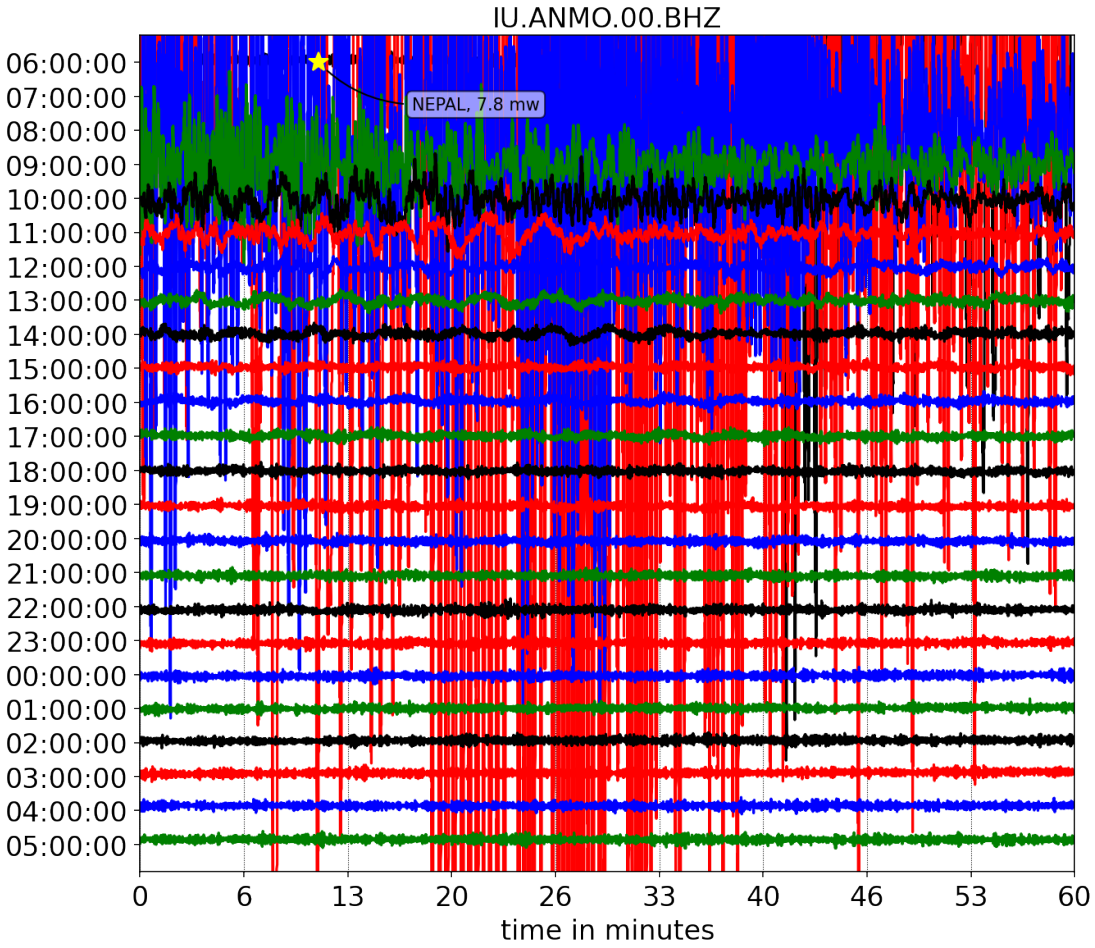

Figure 2: A Day plot of seismogram of Gorkha earthquake from network IRIS-USGS (IU), station Albuquerque New Mexico (ANMO), location =00, channel BHZ. The channel BHZ indicates a broadband (B) signal of high gain seismometer (H) recording the vertical (Z) component of the ground motion while 00 for the STS-1 (primary stream).

It is probable that there is a gradual decline in the b value before a significant earthquake which is thought to be precursor of the impending major fracture (Mizrahi et al., 2021; R. Wang et al., 2021; Wyss et al., 2008). Regardless of the mechanism, it is admitted that *b*-value tends to decline before a large earthquake, so arguably it gives a hint in predicting earthquakes (E. Bayrak et al., 2017; Han et al., 2015). Moreover, temporal variation of *b*-values and its relation to future destructive earthquakes have been studied and discussed by numerous researchers. For the central Himalayan region after the Gorkha earthquake, *b*-value of 1.11 ± 0.08 is obtained for the distribution of the aftershocks (Nampally et al., 2018). The low b values (0.75 ± 0.02) observed in the vicinity of the source zone of Gorkha earthquake, reflects the immense stress and the region could be the source zone for earthquakes in a time to come (Ghosh, 2020). Also, the outcome of the study based on the data over the period 1973 to 2015, shows the increment in *b*-value while moving from the northwest to northeast Himalayas which could be the reflection of the stress level and material heterogeneity (Jena et al., 2021).

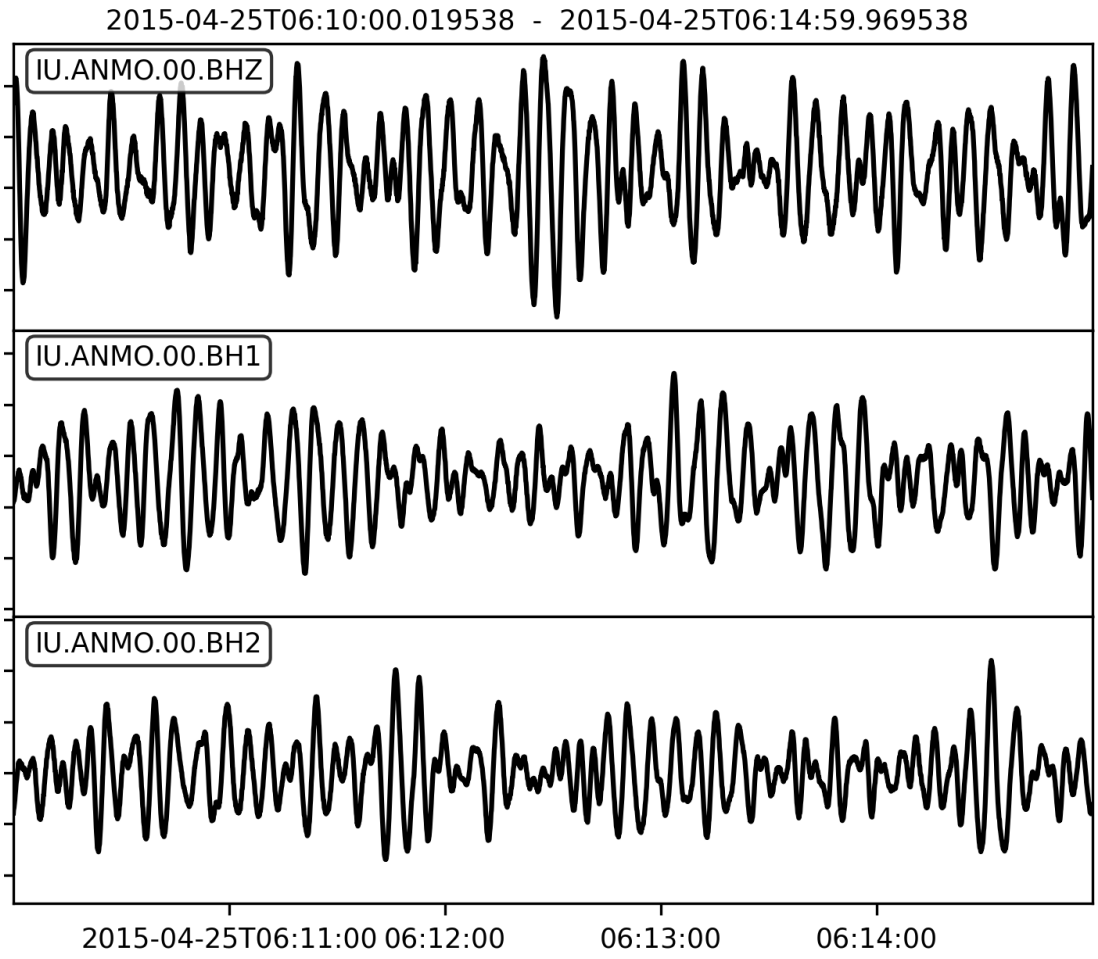

Figure 3: Three components of waveform of Gorkha earthquake BHZ, BH1, BH2. Channel BHZ indicates the broadband (B) signal of high gain seismometer (H) giving vertical (Z) component of ground motion. BH1 and BH2 indicate the same signal in the east-west and north-south direction, respectively. The start time is 2015-04-25T06:10:00.000 and the end time is 2015-04-25T06:14:59.969

1.2.2 Fractals and Faults

Fractals are infinitely complex, self-similar objects in which the laws of nature repeat at different scales and sizes. Many natural objects are fractal to some degree. Trees are natural fractals. The patterns formed by the repetition of smaller and smaller copies of themselves are responsible for the creation of the whole forest. Furthermore, a small branch taken out of the leaf of a fern look like the whole leaf itself (Figure 4a and 4b). The fractals belong to the family of mathematical functions whose dimension strictly exceeds the topological dimension. These functions are continuous but nowhere differentiable. In a perfect mathematical fractal like Mandelbrot set (Figure 5a) and Koch-curve (Figure 5b), self-similarity goes noticeably deep in which every pattern is made up of its smaller copies and shows the same statistical character as whole. A simple example of the geological fractal is the aerial view of a coastline initially from a great height and then from points nearer the earth (Brown & Scholz, 1985). Furthermore, joints and faults

in the rocks are fractals (Hirata et al., 1987; Lei & Kusunose, 1999) that reflects the mechanical and hydraulic behavior of discontinuities in rock. Joints are usually caused by tensional force and do not go through the movement while a fault is a break in the rock where movement has taken place. The seismicity of a region is associated to the definite fault system which can be described by the physical process of stress buildup and strain discharge and one can expect more earthquake to occur nearby faults (Jiang et al., 2018; Okubo & Aki, 1987). Fractal dimension of active fault system can be known by fractal dimension of earthquakes. Earthquakes are physically triggered by the slip movements of adjoining fault planes along the contact of droopy wall (hanging wall) and foot wall (head wall) asperities and by the discharge of the strain gathered during the era of sticking (Amitrano, 2012; Kame et al., 2013). The fractal distributions of earthquakes can be described by two models. The first model talks about the fractal distribution of the faults with every fault having own particular earthquake and the second model says that every fault has a fractal distribution of earthquakes (Huang & Turcotte, 1988; Meng et al., 2019). Here, we accept the hypothesis that every fault has a particular earthquake and a fractal distribution of earthquakes infers a fractal distribution of faults.

1.2.3 Self-organized criticality

Self-organized criticality (SOC) is a concept that has been proposed to explain the behavior of natural systems and equally acceptable for the study of earthquakes. The basic idea is that the natural systems are driven by internal processes that eventually lead them to a critical state, where small disturbances is enough to trigger large-scale events (Bak et al., 2002). In the earthquake generation mechanism, self-organized criticality suggests that small tectonic movements in the earth's crust leads to the gradual accumulation of stress on a fault line. When the accumulated stress exceeds the threshold value of stress, a small tremor or a slight movement of the earth's crust, can trigger a destructive earthquake (Teotia & Kumar, 2011; Mandal et al., 2005). The critical state is characterized by a delicate balance between the forces that cause the crust to deform and the forces that resist deformation. One key aspect of self-organized criticality as it applies to earthquakes is the idea of power-law distributions which is very useful to study occurrence of aftershocks following a large earthquake and the frequency magnitude distribution of earthquakes (Mandal et al., 2005; Pastén & Comte, 2014).

1.2.4 Fractal dimension

Tectonic processes like fault displacement and folding are complex and follow fractal statistics, as demonstrated by research (Turcotte, 1989). Seismicity is another complex phenomenon that can be quantified using the concept of fractals, as it too conforms to fractal statistics (Radziminovich et al., 2019; Rundle et al., 2016; Sianturi et al., 2019).

Tectonic models to clarify the fractal distribution of faults have been recommended by investigators in the decade 1980 to 1990 (Hirata, 1989; King, 1983). In the Euclidean geometry, the dimension of the object is the number of distinct coordinates required to specify the position. Accordingly, the dimension of a point is zero. It is one for a line segment, two for a square, and three for a cube. But to describe the natural objects with irregularities and fragmentation like jagged surfaces of mountains, the shape of cumulus clouds, the turbulence of flowing water etc., one needs different sets of coordinates. The dimension then takes the non-integer or a fractional value called fractal dimension. It is equivalent to a Euclidean dimension only when its value is integer. The fractal dimension (D) lies between the topological dimension (D_T) and Euclidean dimension (D_E) i.e., D_T < D < D_E and describes the roughness or degree to which the fractal structure fills up the Euclidean space (Brown & Scholz, 1985).

The concept of fractal geometry (Mandelbrot, 1967) allows us to look at nature with a distinct perspective and to consider irregularities as intrinsic entities. An object has a fractal structure if one obtains a structure of the same complexity by magnifying a portion of it (De Rubeis et al., 2010; Meng et al., 2019; Pietronero, 1989). The application of fractal in earthquakes reveals so many valuable informations regarding the nature of earthquake occurrences. The spatio-temporal distribution of the seismicity of a region may be measured by its fractal dimensions (Y. Tang et al., 2020). Further, a variation in the fractal dimension may resemble the energetic progression of the states of the system (Sri Lakshmi & Banerjee, 2019). The degree of heterogeneity of seismic activity in fault systems can be quantify by the estimation fractal dimension (Öncel et al., 1996). The results of numerous studies show that the seismicity of spatial and temporal distribution reveals statistically self-similar fractal properties in wide range of scales (Telesca et al., 2002; Tosi et al., 2004; F. Wang & Zai, 2021).

(a)

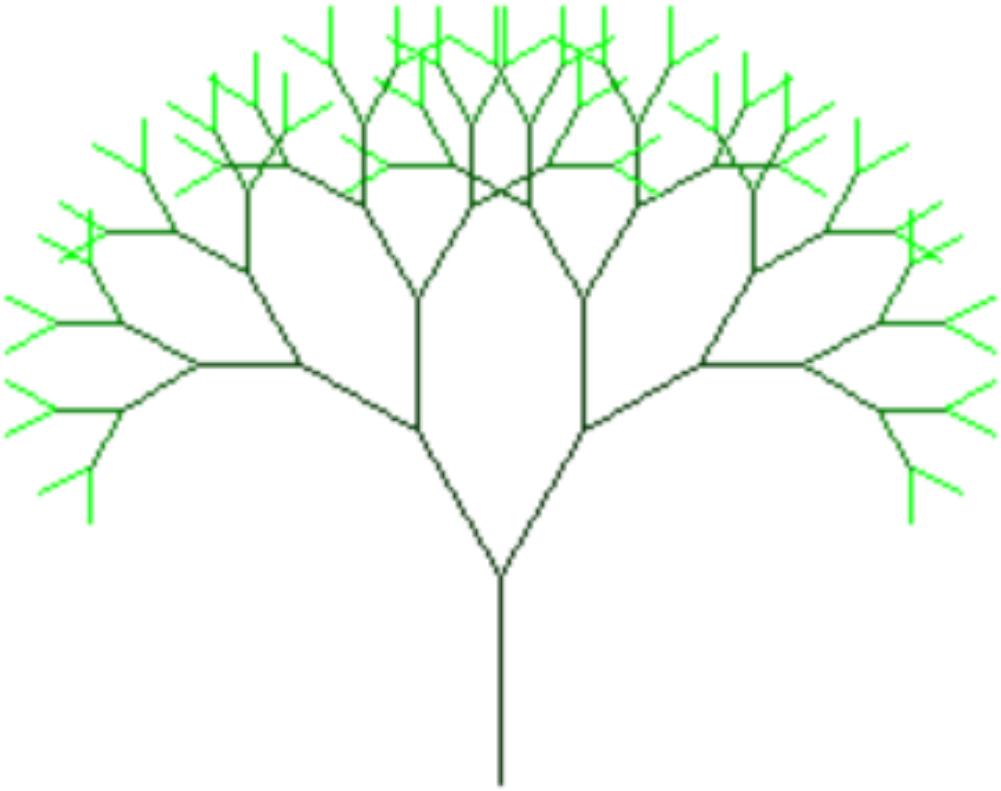

(b)

Figure 4: Examples of the fractal object (a) A leaf of a fern (b) A fractal tree

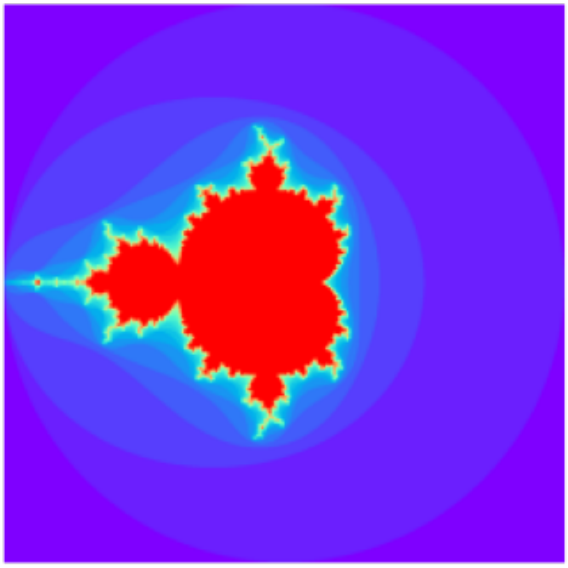

(a)

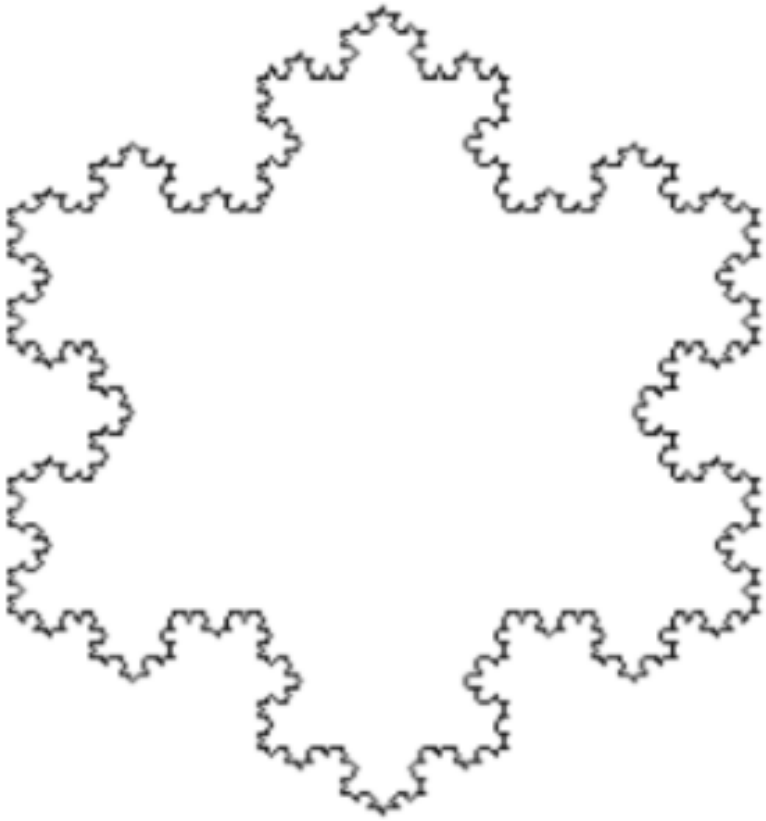

(b)

Figure 5: Examples of the fractal object (a) The Mandelbrot set (b) A Koch-curve

The box-counting method, a specific form of generalized fractal dimension, has been utilized by various researchers to determine the fractal dimension of earthquake epicenter distributions across the world. These studies have focused on earthquake sequences in the Kachchh, Bhuj area during 2001 to 2012 (Aggarwal et al., 2017), Mount St. Helens, Washington from 1980-2002 (Caruso et al., 2006), the 20th September 1999 Chi-Chi earthquake in Taiwan (D'Amico et al., 2010), three large earthquakes in Chile (Antofagasta 1995, Valparaiso 1985, and Maule 2010) (Pastén & Comte, 2014), and north-western Himalaya region earthquake (Teotia & Kumar, 2011). Using the same technique, the box counting dimension of epicenter distribution in central Himalayan region has been successfully estimated in this study. Spatial correlation dimension (D_2) is estimated to measure the spatial and temporal clustering of earthquakes (Grassberger & Procaccia, 1983; Jena et al., 2021; Telesca et al., 2001; J.-H. Wang et al., 2014). The highest clustering of earthquakes is observed with lowest fractal dimension value D_2 (Mondal et al., 2019). Furthermore, these clustering regions have been suggested as highly stressed zone and are the expected areas where nucleation for large earthquake may appear in future (N. Kumar et al., 2013; Roy & Mondal, 2012). Low fractal dimensions have been observed prior to large earthquakes in several places of the world, as reported in literary works. For example, the New Zealand earthquake that occurred on July 15th, 2009 (Mw 7.8) had low fractal dimensions before it struck (Mondal et al., 2019), as did the 2012-2013 seismic swarm in Torreperogil-Sabiote (southern Spain) (Hamdache et al., 2016), the 2001 Bhuj earthquake in Gujarat, India (Ram & Roy, 2005), and the series of aftershocks that followed the 1999 Chi-Chi, Taiwan, earthquake (Chen et al., 2006). Several subsets (100, 200, and 500 events windows) of earthquakes are considered for the estimation of D_0, D_2 and D_q in this work. Furthermore, the correlation between parameters b-value and D_2 is also studied.

1.2.5 Multifractality

Fractures and faults have multifractal structure and the occurrence of earthquakes could be related to those structures (Teotia & Kumar, 2011; Roy & Padhi, 2007). Multifractal analysis helps to understand the heterogeneity of fractures, the preparation mechanism of generous size earthquake, and complex dynamics of seismotectonic processes. Multifractal characterization is achieved by measuring the so-called generalized dimensions (D_q). The spatial variation of D_q gives a quantitative measure of the spatial clustering of events (Davidsen & Goltz, 2004; Radziminovich et al., 2019) and the temporal variation of D_q reflects the temporal clustering of events (Mondal & Roy, 2016; Nakaya & Hashimoto, 2002). Several studies have utilized the multifractal approach to examine the temporal patterns of earthquakes in different seismic regions. For instance, the multifractal pattern was applied to the aftershocks of the 1994 Northridge earthquake (MW 6.7) (Telesca et al., 2002), the seismicity in Kachchh, India (Telesca et al., 2015),

and the Alborz and Zagros regions of Iran (Zamani & Agh-Atabai, 2009).

1.2.6 Omori-Utsu law

The Omori-Utsu law (Hirose & Maeda, 2011; Utsu & Ogata, 1995) is a statistical law that describes the temporal decay of the frequency of aftershocks following a main shock. It is often used to study the aftershock activity of earthquakes. After the large earthquakes, the rate of the seismic activity increases and continues to be high for up to month or even years and decreases hyperbolically with time. This law is thought to be related to the redistribution of stress in the earth's crust following a main shock. The main shock causes a redistribution of stress in the surrounding area, and this stress can trigger aftershocks. As time goes on, the stress in the surrounding area decreases, leading to a decrease in the frequency of aftershocks. The p-value of Omori-Utsu law is important because it can be used to infer the physical processes that control the aftershock activity. The values of p that are observed for different earthquakes can vary between 0.5 and 1.5, with some studies indicating that it is around 1.0 (Omori, 1895; Hainzl & Marsan, 2008). This study estimates the p-value of the Omori-Utsu formula for the 2015 Gorkha earthquake aftershock sequence.

1.3 Rationale of the Study

Himalayan Subduction zone is capable enough to produce an Mw ~9 earthquake as other subduction zone of the earth (H. Gupta & Gahalaut, 2015). From the hazard perspective a great earthquake of Mw > 8 could happen anywhere along the Himalayan belt that may ended up taking lives of about one million people in the Himalaya and adjoining Indo-Gangetic plain (Mencin et al., 2016; Wyss, 2005). Since the shallow segment of the MHT that did not rupture in 2015 was loaded by the after slip, up dip of the rupture area of the Gorkha earthquake and the area west of Kathmandu are the risk zone for future large earthquakes (Gualandi et al., 2017). Although the 1934 Nepal-Bihar earthquake and the 2015 Gorkha earthquake abolished the stored strain energy, the possibility of a major event is still high in the west of epicenter of 2015, Gorkha earthquake (Wyss & Chamlagain, 2019; Sreejith et al., 2018). The MHT is likely to get ruptured in earthquakes (Mw 8.7) for every period greater than 200 years (Michel et al., 2021). The aforementioned statements strongly demand the understanding of the tectonic of the source zone and undergoing mechanism in the region to mitigate the eathquake hazard in future. The aim of the study is to utilize fractal analysis in seismicity and determine the most hazardous zone for potential future large earthquakes in the central seismic gap.

1.4 Objectives of the Study

This thesis aims to assess the possibility of significant earthquakes in the central Himalaya and surrounding regions by utilizing data from the International Seismic Centre (ISC), National Earthquake Monitoring and Research Centre (NEMRC), Nepal, and published research. The general and specific objectives are:

General Objective

Identification of the random fault's distribution of Gorkha region (central Himalayan region) and its surrounding and to understand the variation in stress level before and after the earthquake.

Specific Objectives

1) To use box counting technique to calculate capacity dimension (Hausdorff dimension).

2) To characterise and quantify the spatial and temporal clustering of the earthquake and its variation with time using correlation integral approach.

3) To study the correlation between the fractal dimension and b-value of G-R formula

$$\log_{10} N = a - bMc \tag{1.2}$$

The earthquake potential is evaluated based on b-value and multifractality for the region and hence the high-risk zone for future large events has been demarcated. This research output will be beneficial in accurately assessing potential hazards and in taking measures to safeguard both property and human lives through proper emergency planning and construction regulations.

1.5 Organization of the Thesis

More explicitly chapters of the thesis are organized as follows: -

(i) Chapter 1 is introductory, in which importance of earthquake study and more interestingly in the study region of the Himalayan is explained. A brief overview of the different parameters used in this thesis is presented.

(ii) Chapter 2 reviews the relevant literature and sets a departure on how proposed work is important. Also the tectonic setting of Himalaya and more specifically the central Himalayan region is reported. The tectonic plates that are responsible for

majority of the seismicity in the region are discussed. Major thrust faults and other structural elements, such as lineaments and surface faults, and their relationship to seismicity are analysed.

(iii) Chapter 3 explains the data and methods used in this work. The method to calculate the earthquake distribution's b-value, the box counting technique to determine capacity dimension (D_0), correlation integral function to calculate the correlation dimension (D_2), multifractal spectrum (D_q) of generalized fractal dimension, and the method to estimate the p-value of aftershocks decay are explained in details.

(iv) Chapter 4 focuses on the calculation of the b-value. The b-value's variation over time and depth is analyzed using various temporal and spatial window sizes. More importantly, the chapter employs fractal and multifractal analysis techniques to examine the sequence of aftershocks that occurred following the Gorkha earthquake. Determination of spatial correlation dimension (D_2) and generalized multifractal dimension (D_q) have been done using the correlation integral approach. It deals with all the aspects of D_2 value variation that are important to understand the earthquakes clustering for future large events in the region.

(v) The conclusion of the thesis work is presented in chapter 5, where the results obtained from the multi-fractal approaches are discussed. Future research directions and recommendations are also provided. The summary of the entire work is provided in the final chapter, Chapter 6, followed by the bibliography and appendix.

CHAPTER 2

LITERATURE REVIEW

The past relevant literature gives a way to focus on the identified problem and this chapter explains the literature relevant to geology and tectonics of the Himalaya, fault plane solutions or rupture plane characteristics of notable past earthquakes as well as the fault plane solution pertaining to the 2015 Gorkha earthquake in central Himalaya.

2.1 Himalayan geology and tectonics

Himalaya or the Himalayas, the continent-continent collisional belt (~2500 km) is the most noticeable innovation of plate tectonic forces and extended to the Arabian Sea and the Bay of Bengal and provide a natural laboratory for studying subduction processes (A. Yin, 2006; A. Yin et al., 2010). It separates the plains of the Indian subcontinent from those of the Tibetan plateau and encompasses the territories of six countries: Afghanistan, Pakistan, India, Nepal, China, and Bhutan. (K. Rajendran et al., 2017; Tandon & Gupta, 2020; Webb et al., 2017). Structurally, it is bordered by the Indus-Tsangpo Suture Zone (ITSZ) in the north, the Main Frontal Thrust (MFT) or Himalayan Frontal Thrust (HFT) in the south and by the left slip or sinistral Chaman Fault and the right slip or dextral Sagaing Fault in its western and eastern boundaries (Jouanne et al., 2004; Le Fort, 1975). The formation of the Himalaya is accredited to (a) a collision between the Indian plate and the Eurasian plate starting in early Tertiary time (about 50 Ma) on the Indus suture zone and (b) the steady convergence that give rise a shortening around 2000 – 3000 km afterwards (Arita, 1983; Valdiya & Goel, 1983; Valdiya, 1980; Guillot et al., 2008). Later, the thrusting mechanism shifted in the south direction, which pulled back the northerly edge of the Indian continent onto itself along the Main Central thrust (MCT) and Main Boundary thrust (MBT) that ultimately uplifted the Himalaya (Sinha, 1989; Upreti & Le Fort, 1999; Gansser, 1981).

The convergence in Himalaya is not only due to the frontal thrusting of the Himalaya, but

also by the east-west extension on the South Tibet creating normal faults (Armijo et al., 1989). The convergence rate at the Himalaya is about 9-14 mm/year at the Himalayan frontal zone (Baker et al., 1988), ~35 mm/year at the northerly border of the India plate, and 50 mm/year near the eastern Himalayan Syntaxis (DeMets et al., 2010; Molnar & Lyon-Caent, 1989). The current tectonic convergence is absorbed along the HFT which marks the tectonic and topographic front of the Himalayan orogeny (Ader et al., 2012; Lavé & Avouac, 2000). Additionally, the Himalayan convergence caused earthquakes to occur in the area (K. Rajendran et al., 2017). The concept of underthrusting of Indian lithosphere beneath Eurasian lithosphere that leads to the building of mountain and upliftment of the plateau was explained by different models (Matte et al., 1997; J. Zhang et al., 2012).

One model assumed that the Himalaya was carved exclusively by the collision between Atlantic type (having longer period stability) continental margin and the Asian continent when the buoyancy of the continental lithosphere prevents further subduction (Dewey & Bird, 1970). But the model overlooked the possible significance of intra-continental thrusts. According to plate tectonic theory, the present-day tectonics of the Himalayan belt and Tibetan plateau results from the north-south shortening and crustal thickening during convergence between the Indian and Eurasian plates after their collision (Powell & Conaghan, 1973). They believe collision itself could not produce the present-day Himalaya and disagree with the straightforward model of continent-continent collision proposed by Dewey and Bird in 1970. Alternatively, they proposed two phases of orogeny for the formation of the Himalayas (Powell & Conaghan, 1973, 1975). The early connection of the Indian and Asian continental junctions occurred at the Paleocene/Eocene boundary at some point between 55 ± 2 Ma, which slowed down the rate of northward drift of the Indian continental plate (Gansser, 1981; Guillot et al., 2008; Le Fort, 1975).

This slowdown marks the beginning of the Indian land mass collision with the Eurasian land mass, the closing of the former Tethys Ocean, and creation of the Indus. In the second phase, the Indian plate under thrusted further beneath the Eurasian plate and leads to the formation of intra continental fractures within the northern Indian margin. At about 20 Ma, the thrusting process occurs along a gentle northwardly dipping main basal detachment known as Main Himalaya Thrust (MHT) (Hodges, 2000; Jouanne et al., 2004; Searle & Treloar, 2019). The subdivision of the Himalaya into different lithotectonics units demarcated by five major structural elements are Indus-Tsangpo Suture Zone (ITSZ) (Guillot et al., 2008; Sharma, 1998; A. Yin, 2006), the South Tibetan Detachment System (STDS) or North Himalayan Normal Fault (Pêcher, 1989; J. Zhang et al., 2012), MCT (Nakata, 1989; Verma, 1991), MBT (Gansser, 1981; Le Fort, 1975) , and MFT or HFT (Lavé & Avouac, 2000; Valdiya, 1980). The northern boundary

is nearly east-west trending and more than 2000 km long ITSZ and the southern limit is bounded by HFT.

2.1.1 Tibetan plateau

The Tibetan plateau lying north of the ITSZ has an average elevation of 3 km and surrounded by super tall mountain including Mount Everest and Mount K2 (Powell & Conaghan, 1975). It is the highest plateau with the largest area 2.5×10^6 km^2, known as the roof of the world. The crustal thickness is about 70 km in the central part of the plateau and its present position was uplifted 10 Ma ago (Hodges, 2000; J. Zhang et al., 2012). Rocks exposed on the Tibetan plateau reflect a long Paleozoic and Mesozoic history and it is believed that in the latter part of Tertiary time the plateau shape was superimposed on these earlier trends (Hauck et al., 1998; Ni et al., 1989). The genesis and the growth of the plateau are linked to the collision of India and Asia along the Himalayan arc (Molnar & Tapponnier, 1975).

2.1.2 Indus Tsangpo suture zone (ITSZ) or Yarlung- Tsangpo Suture Zone (YTSZ) or Indus-Yarlung Zangbo (IYZ) or Indus-Yarlung Suture (IYS)

The Indus-Tsangpo suture zone (ITSZ) is a tectonic line located in the southern Tibet region, with a length of over 2000 kilometers. It coincides with the subduction zone that was accountable for terminating the gape of the Tethys Ocean (Thakur, 1990). Its traces start from Kohistan region of Pakistan in the west and end at Lhasa regions of south Tibet in the east. The Ladakh region of India also shows a well-exposed trace of the ITSZ (Chingtham et al., 2014; Guillot et al., 2008). ITSZ also differentiates the Tethyan Himalaya from the Lhasa terrane (Eurasia) (Xu et al., 2015). It is the deepest structural boundary where the Indian plate collides with the Eurasian plate, resulting in their junction. The convergence between these plates takes place in a north-south direction along this line. Structurally, the ITSZ is circumscribed by a Triassic-Cretaceous flysch unit and southerly dipping Great Counter Thrust (GCT) from south and north respectively (Xu et al., 2015; A. Yin, 2006). It contains remnants of Neotethyan oceanic lithotectonic belts and shows a complex structural anatomy. The complex structure is resulted from multiple phases of collision related tectonic displacement and responsible for producing the Himalaya–Southern Tibet orogenic system. Ductile and brittle deformation fabrics found in this zone are the consequences of these multiple collisional events. This zone is also characterized by both south and north directed thrust faults (DeCelles et al., 2002, 2014).

2.1.3 The Alpine Himalaya or Tethyan Himalaya (TH)

The Tethyan mountain, a rugged terrain having beautifully sculptured landscape is developed after the consumption of Tethys Ocean by subduction process. It stretches from northwestern Africa and western Europe to the southwest Pacific Ocean to the Himalayan arc, and continues towards Tibet and Myanmar (Moritz & Baker, 2019). The TH are rocks situated south of ITSZ, north of the South Tibetan Detachment and bordered by the Great Counter Thrust (Guillot et al., 2008; A. Yin et al., 2010). The Tethyan Himalayan sequence mostly settled at the south edge of the windswept Tibetan Plateau and separated from HHC by north dipping normal faults to the south. TH, the northern edge of the India and Lhasa terrane is considered as the southernmost terrane of the Asia before the Cenozoic India-Asia collision (A. Yin & Harrison, 2000). Within the territory of Nepal, Tethyan rocks extends from the Mahakali River and Tinkar Lipu on the western border to Langtang Himal on the eastern border (Dhital, 2015). In central and western Nepal, TH is considered stratigraphic cover of Higher Himalayan Crystalline (HHC) (Thiede et al., 2006; Wiesmayr & Grasemann, 2002).

2.1.4 South Tibetan Detachment System (STDS)

The South Tibetan Detachment System (STDS) is the upper boundary of the Himalayan mid-crust which is traceable along the length of the Himalaya (Burchfiel et al., 1992; DiPietro & Pogue, 2004; Pye et al., 2022). The STDS is actually a system of north dipping syn-convergent low angle normal faults, ductile shear zone of thickness up to kilometers and brittle low-angle extensional faults that separates metamorphic rocks from Tibetan sedimentary sequence (Carosi et al., 1999; Kellett et al., 2019). It is the border of the Higher Himalayan zone and the Tibetan Himalayan zone (Burchfiel et al., 1992; Dhital, 2015). In Nepal, the STDS occupies a few kilometers wide zone. In western Nepal, the expression of the STDS is characterized by a lower shear zone (Carosi et al., 2013), east-west striking, low-angle, north-dipping normal faults in central Nepal Himalaya Pye et al. (2022), and in eastern Nepal, it is most evident and accessible in the Rongbuk valley in the Everest region (Carosi et al., 1999). The initial activity of STDS (28–17 Ma) was ahead of the MCT (19.8–8.5 Ma) and it was ended between 18.4 and 17.4 Ma (L.-K. Zhang et al., 2020).

2.1.5 Greater or Higher Himalaya (HH)

The Greater or Higher Himalaya (HH) is the pillar of the Himalaya and made up of 10-20 km thick metamorphic rocks also known as Tibetan slab in Nepal or Higher Himalayan Crystalline (HHC) zone (McNamara et al., 2017; Upreti & Le Fort, 1999). It is basement of the Tethyan belt and bounded by STDS and the MCT (Bilham et al., 1997; Sakai et al., 2017). The Higher Himalaya (HH) is bounded on the north by the STDS and on the

south by the Lesser Himalaya, which serves as the foundation for the Higher Himalaya sequence (HSS) (Gansser, 1981; Valdiya, 1980). The Greater Himalaya has an average elevation of more than 6.1 km and straddle the Tibet throughout their length of around 2400 km. Structurally, they extend southeastward across the northern Pakistan, northern India, and Nepal and then stretches eastward across Sikkim, and Bhutan. From there they turn northeastward across northern Arunachal Pradesh (Dasgupta et al., 2021; Feldl & Bilham, 2006; R. Singh & Singh, 2014).

2.1.6 Main Central Thrust (MCT)

The MCT is north dipping low angle major intracontinental thrust fault which divides high-grade metamorphic rock of the Higher Himalaya Crystalline from low-grade unmetamorphosed rock of the Lesser Himalaya (DiPietro & Pogue, 2004; Searle et al., 2008). The formation of the MCT took place during an intermediate stage of the collision between India and Eurasia in the north at the ITSZ, along with the more recent underthrusting at the MBT in the south (Sinha-Roy, 1982). In Nepal, the MCT is expressed as a shear zone having thickness between 2 to 10 km (Searle et al., 2008; Searle & Treloar, 2019) and exhibits a flat-ramp geometry (DeCelles et al., 2001). The location of MCT is still the topic of debate (Pêcher, 1989). Below the MCT fault defined by Le Fort and Pecher, a sudden change in lithology and metamorphic grade are noticed (Arita, 1983) and termed as the MCT-I or lower MCT (Paudel & Arita, 2000) while the upper limiting boundary of the MCT zone was termed as the MCT-II or upper MCT (Le Fort, 1975). The shearing zone between MCT I and MCT II is termed as the MCT zone which undertook a significant role of sliding planes during thrust movement of the Himalayan gneisses towards south. The MCT is folded by the younger structure of Lesser Himalayan Duplex (DeCelles et al., 2001; S. Li et al., 2019). In the hanging wall of the MCT, there exists regionally persistent northward dipping stratigraphically coherent block known as Tibetan slab in Nepal (Le Fort, 1975). In the footwall block below the MCT there exists strongly imbricated and folded Lesser Himalayan Sedimentary Zone (LHSZ) (Guillot et al., 2008; Pêcher, 1989).

2.1.7 Lesser Himalaya or Lower Himalaya (LH)

The Lesser Himalaya (LH), also known as the Inner Himalaya, is the central component of the Himalayan chain. It is a 60-80 km wide zone that trends northwest-southeast to east-west and west-southwest to east-northeast for nearly 2500 km, and is situated between the MBT in the south and the MCT in the north (Kumahara et al., 2016; Matin & Mukul, 2020). It is the fold and thrust belt with elevation between 3,500 and 4,500 meters above sea level (Herman et al., 2010) and divided into diverse tectonic blocks by a succession of northerly dipping thrusts and faults. The tectonic of the Lesser

Himalaya shows a wide variety from eastern to the western Nepal. In western Nepal, it is located between the Marsyangdi and Bheri Rivers and shows a comparatively broad tectonic zone. The central part of Lesser Himalaya geographically corresponds to the Mahabharat Range in Nepal (Upreti & Le Fort, 1999). In Central Nepal, LH is divided into two groups as lower LH and upper LH (Le Fort, 1975; Pêcher, 1989) and it is occupied by the Kathmandu nappe, a massive folded thrust sheet of the HHC with no visible roots and, thus represent unusual slices in LH (Arita et al., 1997; Schelling, 1992). In eastern Nepal, tectonic of LH can be described as pinched type due to the thrusting of the HHC over LH. LH shear zone thins towards the south and attains the thickness of 50-60 km (Paudel & Arita, 2000).

2.1.8 Main Boundary Thrust (MBT)

The Main Boundary Thrust (MBT) is a wide-angle reverse fault whose surface trace separates the hanging wall block of the LH from the footwall block of the Sub-Himalaya (Siwalik range). From the changes in subsidence rates its age is believed to be 11Ma (Meigs et al., 1995) and it is inferred to be 55 Ma old as suggested by the influx of coarse clastic sediments from the MBT hanging wall (DeCelles et al., 2002). The nature of the slope across the MBT is gentle and along the MBT is steep reflected by the young rejuvenated topography of MBT. An intermediate thrust between the MCT and MBT is the Mahabharat Thrust (MT) that carries the Kathmandu nappe and separates the upper Nawakot Groups (foot wall) in the south from the Kathmandu complex (hanging wall) in the north (Mugnier et al., 2017; Subedi & Acharya, 2016). The rocks present in hanging wall and foot wall of the MT are characterized by the simple shear and prominent pure shear component. This characterizes MT as stretching thrust system (Subedi & Acharya, 2016). The MCT and the MBT are unexpected to be dynamic seismogenic faults as they get folded by younger footwall faults in the fold-thrust belt (Boyer & Elliott, 1982).

2.1.9 Sub-Himalaya (SH) or Outer Himalaya or the Siwalik range

The sub- Himalaya (SH), also known as the Siwalik or Churia zone in Nepal, forms low altitude hills limited between the MFT and the MBT in the southern and northern boundary, respectively. It extends from east to west throughout Nepal and consists of Neogene to Quaternary molasses like fluvial sediments forming the Churia hills. The Siwalik belt is about 10 to 20 km wide and average elevation varies between 250 and 800 meters forms topographic front of the Himalaya. The age of the visible Siwalik group spans from 14 Ma to less than 2 Ma and approximately one million years ago, the Siwalik foothills were elevated along high-angle active reverse faults known as the Himalayan Frontal Thrust (HFT) (Nakata, 1982). In Nepal, Siwalik range is known as Churia range. The most magnificent topographic trademark of the sub- Himalayan belt

is the structurally controlled tectonic basins commonly known as duns like Dehra Dun in India and Chitwan in Nepal (Powers et al., 1998; Yeats & Lillie, 1991). At 3–2.5 Ma, the plate boundary fault shifted to the Main Frontal Thrust (MFT) which caused rapid elevation of the marginal range of the LH and the Siwalik Hills. The half of the present convergence of the Indian and the Asian plate is consumed by uplift of the Siwalik Hills along the MFT (Sakai et al., 2017).

2.1.10 Himalayan Frontal Thrust (HFT) or Main Frontal Thrust (MFT)

The Main Frontal Thrust (MFT) is a wide-angle thrust line where the last compressional force in the Himalayas orogeny has taken place. It defines the present time tectonic border between the Indian plate and the Himalayan orogenic prism (Thakur et al., 2019) and it is the youngest and southernmost structure in the Himalayan (Gahalaut, 2008). The MFT roots into underlying bed parallel fault known as MHT which is also the junction between the India and Asia (Seeber & Armbruster, 1981; Zhao, 2012). At the surface, the MFT is well expressed and defines the boundary between the Himalayan foothills and Indo-Gangetic Plain (IGP) (Webb et al., 2017; A. Yin et al., 2010). IGP, the southernmost part of MFT is characterized by the major sedimentary sinking basin filled with alluvial deposits (loose clay, sand, gravel etc.,) of major rivers Ganga, Yamuna, and Indus. MFT comes into existence 50 Ma ago due to epeirogenic movement of Himalaya and stretches from the Indus valley in the west to Assam in the east with width variation between 400-800 km (Nakata, 1989; Tandon & Gupta, 2020).

2.1.11 Main Himalayan Thrust (MHT)

The major thrust present in the Himalaya namely MFT, MBT, and MCT sole into a low angle fault in the southern sector of Himalaya termed as Main Himalayan Thrust (MHT) (Ader et al., 2012; Ghoshal et al., 2020; Bai et al., 2016). The near-surface equivalent of MHT is postulated to be the Main Frontal Thrust (MFT) (Avouac et al., 2015; Hazarika et al., 2017; Srivastava et al., 2015). The shape of the MHT has been described in many ways. Some literature describes MHT as a ramp-flat-ramp structure (Elliott et al., 2016; Duan et al., 2020), some as a duplex system (Mendoza et al., 2019), and also as the structure having an additional ramp in the mid portion of the seismogenic zone (Sathiakumar & Barbot, 2021). MHT is the horizon between distorted SH strata and Precambrian basement and at the northern side, it brings Precambrian crystalline rocks of the HH southward over the deformed strata of the LH. The surface traces of MCT, MBT and HFT are found to lie much close together in the eastern Himalaya compared to central and western Himalaya. This could be because of the active shortening along the Himalayan strike (A. Yin, 2006). MHT accumulates strain during the interseismic period when it is locked and the accumulated strain is released through sudden slip during

infrequent and large mega thrust earthquakes (Bilham et al., 2017; Ni & Barazangi, 1984). Within Nepal, a mid-crustal ramp of the MHT was reported under the boundary between LL and HH and the small to moderate earthquakes occur on the down dip part of the mid-crustal ramp (Lavé & Avouac, 2000).

Nepal secures a nearly trapezoidal shape, and located between 26°–31°N and 80°–89°E (K. Ansari, 2018). It covers almost one-third (800 km) length and 200 km width of the Himalaya so it entirely resides in the collisional zone of the Himalayan arc (Bilham, 2004; Bollinger et al., 2004; Elliott et al., 2016). Several north-dipping thrust faults are found within the country, and more importantly three major faults MFT, MBT and the MCT trending 120°N in western Nepal to 90°N in the eastern Nepal (Mugnier et al., 2013). Some other regional transverse faults cut across the major thrust systems (Figure 6) and play important roles in Himalayan geodynamics. They include Karnali Lineament (KL), Judi Lineament (JL), Thaple Lineament (TL), Kathmandu Lineament (KTML), Motihari-GauriShankar Lineament (MGL), Motihari-Everest Lineament (MEL), Dudhkoshi Lineament (DKL), Arun Lineament (AL), and Kanchenjunga Lineament (KAL). In the central Himalaya, the most notable structures are the Judi or Trisuli transfer Lineament (Mugnier et al., 2011) and Gauri-Shankar or Chautara lineament (Mugnier et al., 2017). They run from SSW to NNE, traversing the entire Himalayan range, covering both the western and eastern areas around Kathmandu.

At the present- time surface motion along the MGL and JL is very little, nonetheless the JL offsets the trace of MCT and the Siwalik structures (Mugnier et al., 2017; R. Tiwari et al., 2022) and in the region located south of the Kathmandu, the MGL also offset the MCT and MBT. The JL is believed to be situated above the deformation of the Indian crust, as indicated by the Gandak depression's deepening and the accretionary wedge's wider size (Mugnier et al., 2011) and the location of the MGL found to coincide with the pierce point of the branch line, between the MBT and MCT in front of the Kathmandu Nappe (Jouanne et al., 2004; Mugnier et al., 2017). The MGL delineates the eastern side of the aftershock's sequence of 2015 central Himalayan earthquakes sequences. Particularly, 12 May earthquake and aftershocks associated with it are concentrated between MGL and MEL (Figure 6). The major rupture area of the 2015 event stretches from JL in the west to the MEL to the east (Mugnier et al., 2017). The cross sectional along AA' (Figure 7) shows the concentration of the aftershocks around the ramp structure of the MHT. The structure of MHT may have play a major role for limiting the magnitude and the propagation of the rupture in lateral direction (M. Hubbard et al., 2021).

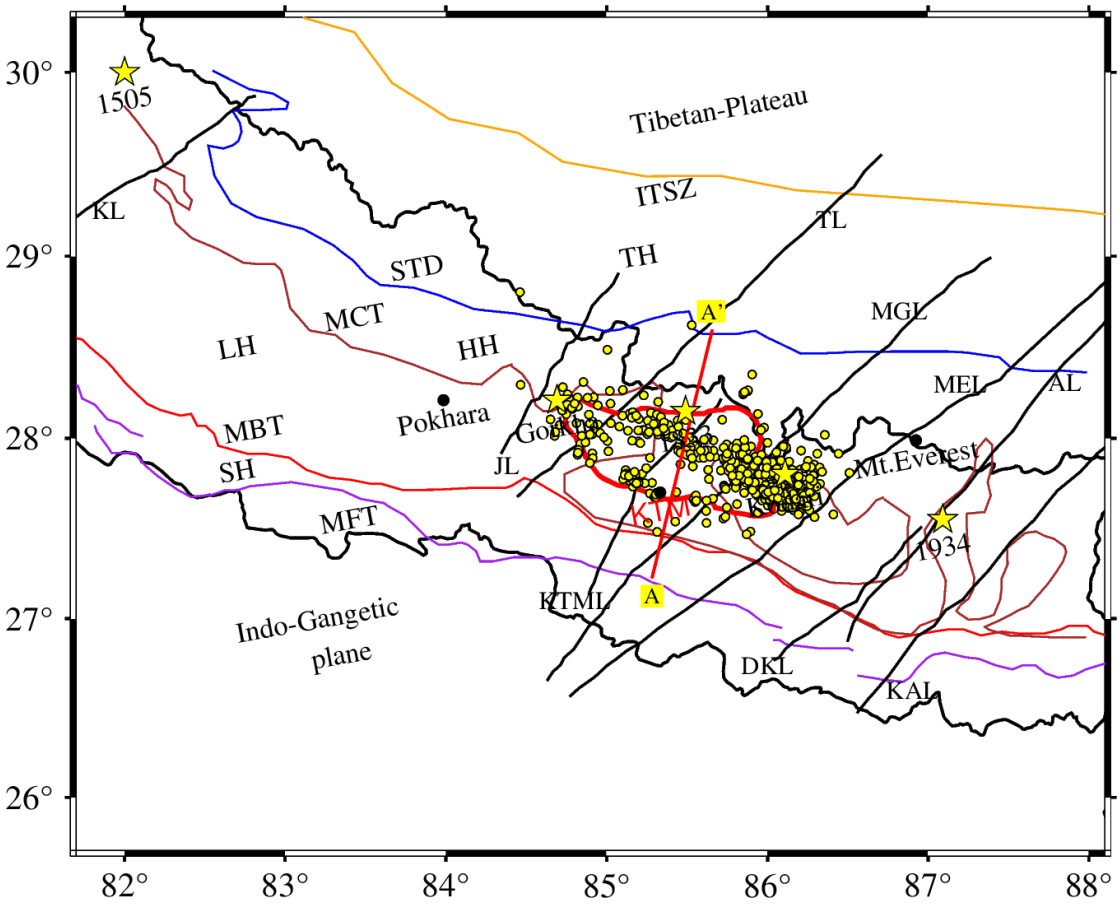

Figure 6: Tectonic map showing MFT (Sreejith et al., 2018), MBT (Mugnier et al., 2013), MCT, STD, ITSZ (Bai et al., 2016) from south to north. TH is the Tethyan Himalaya between ITSZ and STD, HH is the Higher Himalaya between STD and MCT, LH is the Lesser Himalaya between MCT and MBT, and SH is the Sub-Himalaya between MBT and MFT. KL is the Karnali Lineament, JL is Judi Lineament, TL is Thaple Lineament, KTML is Kathmandu Lineament, MGL is Motihari-Gaurishanker Lineament, MEL is Motihari-Everest Lineament, DKL is Dudhkoshi Lineament, AF is Arun Lineament, and KAL is Kanchenjunga Lineament (Dasgupta et al., 1987; Som et al., 2016). Yellow stars stand for 1505 Lo Mustang earthquake, 2015 Gorkha earthquake, 1833 earthquake, 2015 Kodari earthquake, and 1934 Nepal-Bihar earthquake. The 1833 earthquake occurred in a region between epicenter of Gorkha earthquake and Kodari earthquake while remaining earthquakes are along MCT. The profile point A is at the location 85.28°E and 27.23°N while the point A' is at 85.66°E and 28.59°N. The earthquakes cluster represented by yellow spheres are aftershocks of 2015 Gorkha earthquake and Kodari earthquke (Adhikari et al., 2015).

At the present time, the northward movement of Indian plate towards the Asian plate is putting enormous pressure on the Asian plate, and consequently Tibet presses on the landmass surrounding it to the north. This action is squeezing parts of Asia eastward toward the Pacific Ocean developing the tremendous stress within the earth's crust called domino effect (Sobolev, 2011). This continuing tectonic process assumed to be accommodated mainly along a MHT which reaches the surface in the Siwalik Hills of southern Nepal and had caused some of the world's most destructive earthquakes in the Himalayan arc (Ader et al., 2012; Cattin & Avouac, 2000; Elliott et al., 2016).

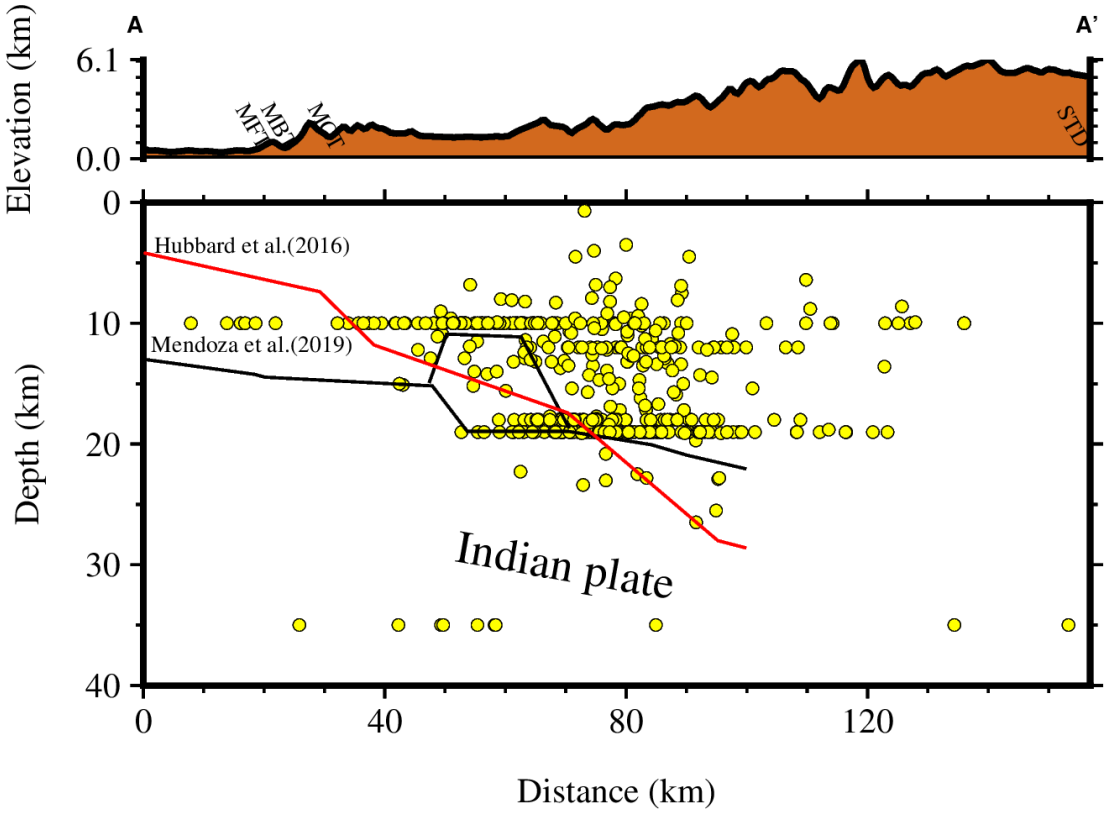

Figure 7: Cross sectional profile along AA'. The cross-section AA' covers 156.85 km from MFT to STD. The red lines (J. Hubbard et al., 2016) and black lines (Mendoza et al., 2019) indicating the MHT. The yellow circles indicate the aftershocks of the April/May 2015 Gorkha to Kodari earthquake (Adhikari et al., 2015)

.

2.2 Fault plane solutions of earthquakes in central Himalaya

Fault plane solutions, also known as focal mechanism solutions or beachball diagrams, are used in earthquake seismology to describe the dynamic process of seismic wave generation. They provide information on the slip and orientation of the fault on which an earthquake occurred, as well as the stress patterns that existed along tectonic regimes (Nakamura, 2002; Ousadou et al., 2014). These diagrams are typically generated using data from seismic waves recorded at various locations and can be used to infer the type of faulting that occurred during the earthquake, such as strike-slip or thrust faulting. They are an important tool for understanding the mechanics of earthquakes and can be used to help predict future seismic activity in a given area. They correspond to azimuthal projections of the nodal plane onto the lower hemisphere in hypocenter. The focal mechanisms are results of the positive direction or negative direction of the first P-wave impulse recorded at each station on a large area (Khalid et al., 2016; Wu et al., 2018; Xiaoshan et al., 2012; Paudyal et al., 2010). They are also a moment tensor (MT) solutions and depicted by beachball diagram in a map. A pattern, size, and orientation of beach ball is decided by the eigenvalues and eigenvectors of the MT. Eigenvalues

of moment tensor decide the size and eigenvectors decide the orientation of the beach balls (Tape & Tape, 2012). The MT is like stress tensor and describes the fault as a set of equivalent forces. The estimation of MT immediately after the earthquake gives the best idea about the nature of active faulting and interprets the dynamics of source and kinematics of a region. In this study, all the components of the moment tensor of earthquake dynamics are taken from the Global Centroid Moment Tensor (GCMT) webpage (Dziewonski et al., 1981; Ekström et al., 2012; Yagi & Okuwaki, 2015).

2.2.1 Faulting pattern between 80.00°E-82.50°E and 28.00°N-30.50°N in western Nepal and vicinity

Focal mechanism solutions for nine earthquakes located in the western Nepal and its vicinity from 2005 to 2019 were shown in the table 1 and figure 8. The focal depth of these events ranges from 15 to 47 km.

Table 1: Date, location, and depth of the earthquakes that occurred in and around western Nepal with six elements of seismic moment tensor viz. Mrr, Mtt, Mpp, Mrt, Mrp and Mtp where the alphabet r stands for up (vertical) direction, t stands for south direction, and p stand for east direction. The identification of beachballs is presented in the ID column.

ID	Date	Long	Lat	Depth	Mrr	Mtt	Mpp	Mrt	Mrp	Mtp
1	2005/10/31	81.28	29.39	47	0.23	0.13	− 0.37	0.84	−0.35	1.13
2	2008/12/08	82.01	29.65	20	−0.26	−0.68	0.94	0.39	−0.24	0.26
3	2010/07/06	80.33	29.55	14	2.02	−1.7	−0.32	2.98	0.84	1.01
4	2011/04/04	80.71	29.43	19	1.07	−0.97	−0.1	1.02	0.09	0.59
5	2013/06/28	82.18	28.49	18	2.78	−2.74	−0.04	2.3	−0.72	1.22
6	2015/04/21	82.35	28.65	26	3.81	−1.97	−1.84	0.58	1.19	1.9
7	2015/12/18	81.6	29.04	23	0.75	−0.66	−0.1	0.47	0.03	0.4
8	2016/12/01	80.38	29.57	34	1.22	−1.25	0.02	1.31	−0.49	1.1
9	2019/11/19	81.16	29.22	15	2.23	−2.22	−0.01	1.3	0.06	0.5

The fault-plane solutions related with earthquake show thrust mechanism with north west to north east dipping nodal planes which supports northward under-thrusting of Indian plate along the major thrusts of the Himalayas. Seven out of nine focal mechanism solutions clearly show a thrust faulting nature with nodal planes dipping north or north-east and the remaining two shows a strike-slip solution with major thrust component. Event 1 shows oblique reverse character. Event 2 has oblique normal mechanism with major component of normal fault. Events 3 and 4 show major thrust faulting nature with very small component of strike slip. Events 5, and 8 show pure thrusting nature dipping in northeast direction. Events 6 and 7 shows major thrust faulting with very small oblique component in it. Event 9 shows north dipping thrust character. Almost all of the fault plane solutions have shallow north dipping nodal planes reflecting the trend of the major thrusts.

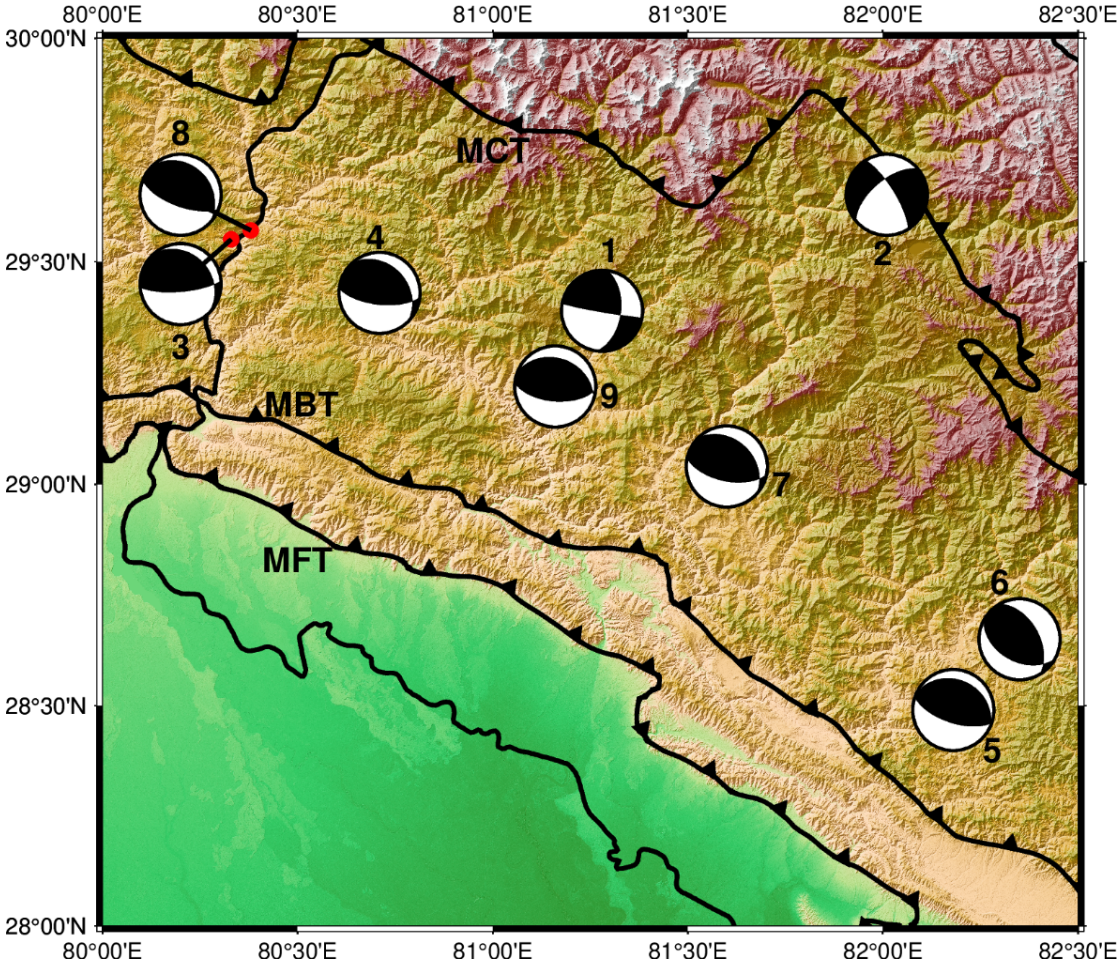

Figure 8: Faulting pattern in western Nepal and surrounding areas. The shaded quadrants signify compression as the primary motion, while the open quadrants indicate dilation as the primary motion. The numbers accompanying each beachball are serial numbers.

2.2.2 Faulting pattern between 82.50°E-85.50°E and 27.50°N-30.00°N in central Nepal and vicinity

The faulting pattern inferred from the MT solutions (Figure 9 and table 2) is consistent with the trend and the nature of the structural features present in the region and show similar characteristics as observed in the adjacent western Nepal region. The collective dips of the nodal planes indicate northward under-thrusting of the Indian plate at shallow angle, though the nodal plane of the specific event varies marginally in their alignment. All the earthquakes are confined within the upper crustal region from 12.0 to 29.0 km. Events 1 and 2 show thrust mechanism with nodal planes dipping towards NE direction. Events 3, 4, and 5 are associated with 2015 Gorkha earthquakes also shows the thrust mechanism and dip towards the north. Events 3 is the focal mechanism solution of the mainshock while 4 and 5 are the aftershocks on the same day. Event 5 exhibits oblique slip behavior with a significant component of normal slip and nodal planes oriented east-west, which might be regarded as an extension following the mainshock (R. Tiwari et al., 2022).

Table 2: Date, location, and depth of the earthquakes that occurred in and around central Nepal with six elements of seismic moment tensor viz. Mrr, Mtt, Mpp, Mrt, Mrp and Mtp where the alphabet r stands for up (vertical) direction, t stands for south direction, and p stand for east direction. The identification of beachballs is presented in the ID column.

ID	Date	Long	Lat	Depth	Mrr	Mtt	Mpp	Mrt	Mrp	Mtp
1	2005/10/31	84.88	28.38	22	1.59	−1.18	−0.41	−0.22	−0.06	0.47
2	2012/08/23	82.65	28.05	29	2.23	−1.83	−0.4	2.45	−1.01	1.2
3	2015/04/25	85.33	27.91	12	1.76	−1.82	0.06	8.04	−1.51	0.48
4	2015/04/25	84.93	27.86	21	0.68	−0.74	0.06	0.96	0.19	0.25
5	2015/04/25	84.96	27.61	15	−2.08	−2.46	4.54	5.53	−0.9	−1.2
6	2016/09/10	82.56	29.85	22	−1.76	−0.06	1.83	0.17	−0.17	0.3

Event 6 is normal fault having strike in north-south direction and dipping in east direction. The northward low-dipping planes (∼7° dip) of the focal mechanism solutions suggest that events had ruptured the MHT (Duputel et al., 2016; L. Zhang et al., 2016).

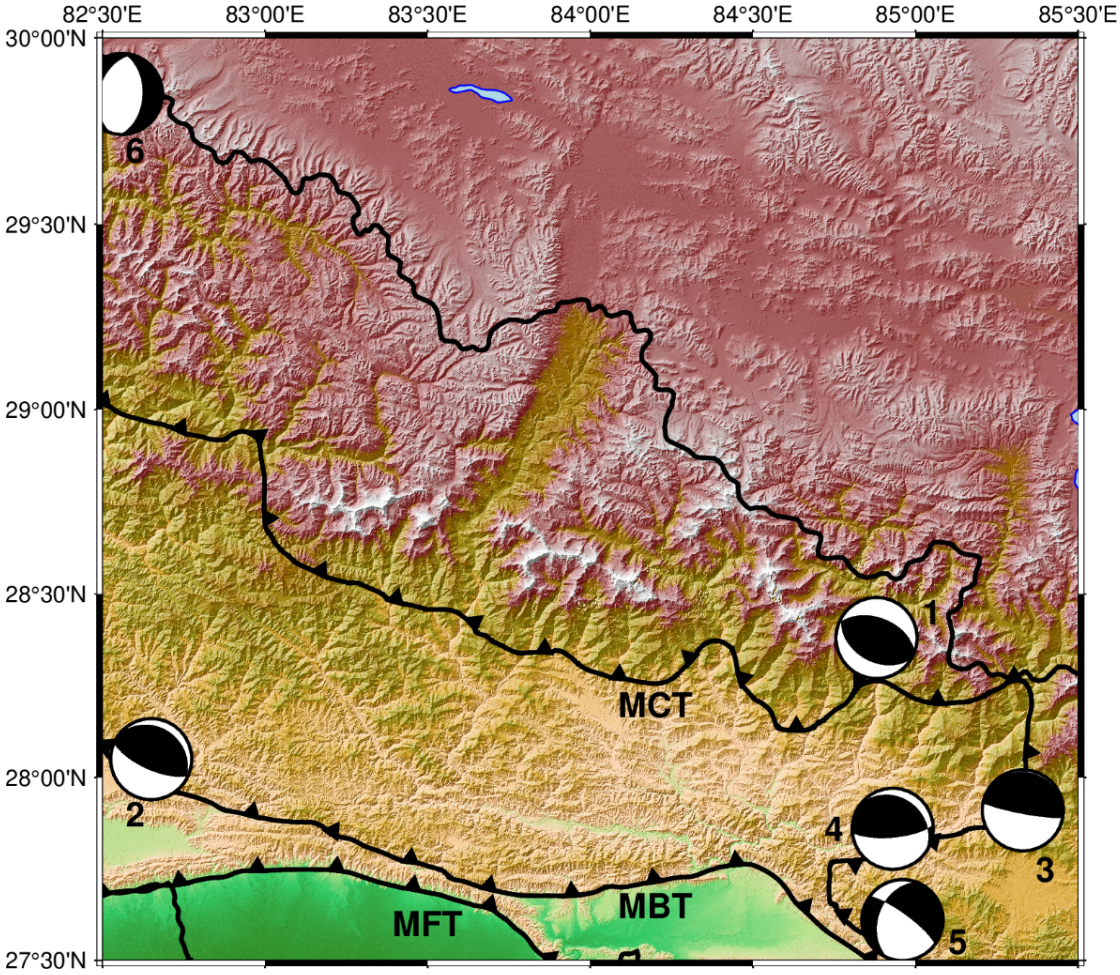

Figure 9: Faulting pattern in central Nepal and surrounding regions. The shaded quadrants indicate compression as the initial motion, while the open quadrants denote dilation as the initial motion. The numbers accompanying each beachball represent the respective serial numbers.

2.2.3 Faulting pattern between 85.50°E– 88.20°E and 26.45°N–28.35°N in eastern Nepal and vicinity

The seismicity in the eastern Nepal Himalaya is noticeably high and offset towards north. The depth of the events ranges from 12 to 35 km (Table 3). Most of the solutions show thrust nature with east-west striking nodal planes except event 3 which shows normal characteristics with nearly north-south trending nodal planes (Figure 10). Event 1 shows nearly north dipping and east west strike thrust fault. Event 2 shows thrust nature with small component of oblique slip character. Event 3 shows normal fault character with north-south strike and dipping in east direction. Event 4 shows pure thrust nature with small dip angle. Event 5 shows thrust fault character with very small component of oblique slip. Event 6 shows pure thrust nature with northeast dipping angle. Event 7 shows thrust character like event 5 with different strike direction from event 5. Event 9 and 10 show similar character as event 5.

Table 3: Date, location, and depth of the earthquakes that occurred in and around eastern Nepal with six elements of seismic moment tensor viz. Mrr, Mtt, Mpp, Mrt, Mrp and Mtp where the alphabet r stands for up (vertical) direction, t stands for south direction, and p stand for east direction. The identification of beachballs is presented in the ID column .

ID	Date	Long	Lat	Depth	Mrr	Mtt	Mpp	Mrt	Mrp	Mtp
1	2006/02/03	86.70	26.94	31	1.43	−1.32	−0.11	0.83	−0.1	0.17
2	2014/12/18	86.56	27.46	30	1.2	−3.08	1.88	2.48	−0.64	1.07
3	2015/04/25	85.89	28.06	21	−1.04	0.16	0.87	0.16	0.26	−0.17
4	2015/04/26	85.95	27.56	21	0.6	−0.67	0.07	1.2	−0.23	0.2
5	2015/04/26	85.90	27.56	20	5.38	−5.14	−0.24	5.14	−0.18	2.23
6	2015/05/12	86.08	27.67	12	2.7	−2.62	−0.08	8.25	−1.28	1.22
7	2015/05/12	86.35	27.37	20	1.37	−1.54	0.17	1.24	0.14	0.43
8	2015/05/16	86.26	27.37	12	0.75	−0.95	0.2	0.83	0.04	0.63
9	2016/11/27	86.53	27.35	35	0.56	−0.61	0.05	0.62	−0.08	0.29
10	2020/09/15	85.88	27.53	27	3.81	−3.61	−0.2	4.33	−1.07	2.01

Focal mechanism solutions discussed are relevant with past studies. The forward modelling technique indicates thrust faulting in the region with one gentle dipping nodal plane (< 30 ∼ north or northeast) and other steeply dipping nodal plane towards south (Bollinger et al., 2004; Letort et al., 2016). This shallow northward dipping zone has been taken as a part of the MHT (Ni & Barazangi, 1984). Furthermore, focal-mechanism solutions indicate that earthquakes in the southern foothills of the Himalaya are thrust nature with small components of strike slip. In Tibetan region there are mainly normal fault events which also contain the small subsets of strike-slip (Baranowski et al., 1984; Ni & Barazangi, 1984). Thus, the conclusion can be made that the Himalayan frontal arc within territory of Nepal is in compressed state and seismicity of the region is controlled by thrust faulting.

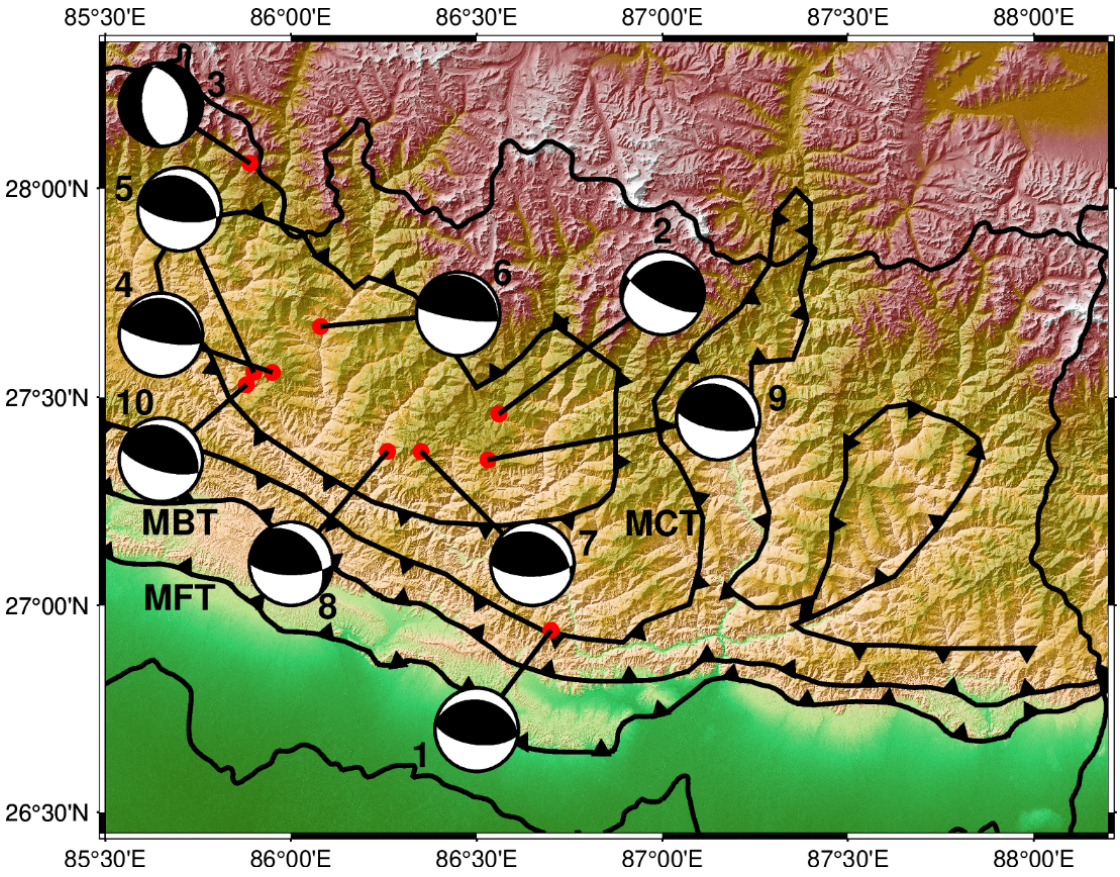

Figure 10: Faulting pattern in eastern Nepal and adjacent regions. The shaded quadrants demonstrate compression as the primary motion, while the open quadrants exhibit dilation as the primary motion. The numbers associated with each beachball are the serial numbers. The epicenters of earthquakes are represented by solid red circles.

2.3 Central Himalayan earthquakes of 2015

Because of the availability of large data and the global participation, 2015 Gorkha earthquake is one of the most studied earthquakes by various groups with different methods. It is the largest earthquake in the Himalaya having large tele seismic seismological records and studied by Synthetic Aperture Radar (SAR) imagery method (Avouac et al., 2015; Fan & Shearer, 2015), by Interferometric Synthetic Aperture Radar (InSAR) imagery method (Lindsey et al., 2015), from strong-motion, high-rate GPS (Global Positioning System), and static GPS (Grandin et al., 2015), and with the data recorded by local seismic networks (Adhikari et al., 2015) and by many more methods.

The following literature extensively examines the rupture mechanism of the Gorkha earthquake and the sequence of aftershocks. The ruptures during 25 April and 12 May earthquakes neither lead to the MFT nor induce any notable vertical slip (Parameswaran & Rajendran, 2017). The origin of the Gorkha earthquake was situated in the foreland of the elevated Himalayan region, positioned on the eastern side of the central gap, to the west of the rupture zone of the 1934 Nepal-Bihar earthquake (Avouac et al.,

2015). Based on 3-D model of the MHT, it was suggested that dissimilarities in fault alignment at depth were accountable for restricting the size of the Gorkha earthquake (J. Hubbard et al., 2016). The rupture zone is bordered by N-S oriented Judi lineament and Gaurishankar lineament in the western and the eastern limit respectively (Mugnier et al., 2017). The Gorkha earthquake is exemplified as structurally segmented seismicity controlled by the duplex above the MHT (Baillard et al., 2017) whose rupture length was controlled by the lateral variation on MHT (Bai et al., 2019). The surface deformation measurements specify that the 2015 Gorkha earthquake broke a deep down part of the seismogenic area conflicting to the 1934 Nepal-Bihar earthquake which broke a surface part of the nearby fault sector (Feng et al., 2017).

The concentration of the aftershocks is noticed to the south east of the main event suggesting the up-dip segments of the MHT favorable for impending earthquakes (McNamara et al., 2017). The spatial distribution and rupture patterns of aftershocks sequence explains the ramp and flat geometry of the MHT. The MHT comprises two north-dipping subhorizontal planes known as duplex that accomodates tectonic stress along the complex systems of the faults (Mendoza et al., 2019). In addition, a substantial portion of MHT located south of the Kathmandu remains unbroken that may present a continuous seismic hazard in the region (Elliott et al., 2016). The depth varying rupture properties suggests that the up dip portions are continuoulsy rupture while down dip portions are cascadedly rupture (Yue et al., 2017). In the investigation of rupture process, $\sim$ 15 km deep rupture noticed along the base of the coupled fragment of the MHT which fails to break the area ranging from Kathmandu to the front (Grandin et al., 2015). The source rupture process of the 2015 Gorkha earthquake shows unilateral rupture toward the east and a large-slip area toward the north of Kathmandu (Kubo et al., 2016). It is suggested that a heterogeneous duplex structure located above the MHT beneath the Lesser Himalayas may have played a role in regulating the rupture behavior during the Gorkha earthquake (Zhao, 2012). The abrupt northeast trending aftershocks distribution indicates the existence cross fault that could have limited the slip during the earthquakes and play a role in segmented deformation style and seismic activity along the entire Himalaya (J. Hubbard et al., 2016).

The study based on the fault slip model is also found many in numbers. The study carried out by the group (Mencin et al., 2016) suggests that after slip courses in southern Nepal have not distant the strain transmitted to the southern edge of the April 2015 rupture and the other study shows that the strain lasting near Kathmandu prerequisites major earthquake rupture for it to be free (J. Zhang et al., 2021). It is believed that earthquakes on the MHT have two modes of slip. One is the slip that travels all the way to MFT and the other that trapped at the mid–crustal ramp. As seen after the 1833 earthquake along the MHT, the slip deficit between Kathmandu and the Gangetic-plain would possibly be

shifted alongside MHT by an earthquake of generous size (Jouanne et al., 2019). The 1833 and 2015 earthquakes released only a small fraction of the accumulated slip deficit on a deep thrust segment north of the Siwaliks. It is suggested that the 1344 or 1408 AD earthquake may have ruptured the entire megathrust system in Nepal and that the current situation in the Himalayan seismic sequence may be similar to that of the 14th century (Bollinger et al., 2016).

The unified model based on GPS studies, InSAR data, tele seismic waveforms, and strong ground motion reveals that the slip zone of mainshock extends nearly 140 km along strike direction and nearly 80 km down dip while the slip of major aftershock is nearly 30 km along strike direction and nearly 20 km down dip (Liu et al., 2016). An investigation using earthquake reflection imaging has uncovered the geometry of the MHT located 75 km from the MFT and at a depth of approximately 10 km (Kurashimo et al., 2019). The InSAR based slip model implies that maximum slip of largest aftershocks is ~6 m at a depth of ~13 km located next to the eastern lower end of the mainshock rupture (Feng et al., 2017). A Bayesian study suggests that the spread of the Gorkha earthquake was about 140 km in a southeast direction and the slip was limited to 30-40 km in the direction of dip and near major aftershocks. The rupture then propagated to the north and southeast, creating a gap in the slip resembling the open mouth of a crocodile (Duan et al., 2020).

The following paragraph summarizes the studies based on the GPS, InSAR, and seismic waves along with their distinct phases. The post seismic deformation in the Gorkha region is dominated by afterslip as confirmed by the observations from InSAR and GPS and shallow updip part of the MFT has been identified as potential earthquake zone for future as the region is unruptured by coseismic slip (Hong & Liu, 2021). The analysis of the SAR interferograms suggests that the 2015 event was a blind thrust which was unable to produce surface ruptures related with the seismogenic fault (Kumahara et al., 2016). The different rupture features of the main shock and the aftershock as seen from 3D simulation were related with differences in fault zone structure. The extensive ground motion in Kathmandu valley is because of the trapping of the wave-field by the basin structure of the valley (Wei et al., 2018). The analysis of p wave spectra of the main shock (Mw 7.8) and of two large aftershocks (Mw 7.3, and Mw 6.8), reflects the fact that the start of the earthquake possibly gone through a dynamic weakening mechanism trailed by an sudden variation in the geometry of the fault (Denolle et al., 2015).

Coseismic radiation of the Gorkha earthquake shows the depth-varying frictional properties on the plate interface of the Nepal section in the MHT as in oceanic subduction zones (J. Yin et al., 2017). From time interruptions between tele seismic P phases and depth phases pP and sP of 61 aftershocks of 2015 earthquake, a lateral structural variation was identified as a likely barrier to the dynamic rupture transmission (Letort et

al., 2016). The Coulomb stress change after the Gorkha earthquake is also extensively studied. The study on Coulomb stress changes (CSC) showed that the aftershock of 12 May slightly enhanced CSC region in the India-Eurasia collision belt (Shrivastava, 2021). A significant increase Coulomb failure stress from 0.2 to 0.5 MPa at the shallow slope of the seismic gap suggests an added seismic threat around the locality of Kathmandu (Xiong et al., 2020). The areas that are laterally stretching the active fault zone have encountered the increase in stress value at the location of the largest aftershock on 12 May, 2015 (Diao et al., 2015). The static stress change calculated reflects that the loading of the fault around the main asperity (aftershock concentrated area) was due to the triggering caused by stress transfer (Galetzka et al., 2015). From the study of the historical catalogue and paleo-seismicity, the Lalitpur and Lamjung segments of the MHT were identified as high seismic potential where stress was enhanced by main shock and major aftershock (Chan et al., 2017).

The change observed in Coulomb failure stress indicates that despite the Gorkha earthquake and its aftershock sequence reducing the accumulated strain on the Main Himalayan Thrust, seismicity in the Himalayan front will persist in high stress areas to balance the slip deficit (Yang et al., 2019). By comparing the intensities of 1833 earthquake sequence with the intensities of Gorkha earthquake, the location of the both events are found to be on the same fault (Martin et al., 2015). The study based on four years of GPS data from Nepal and south Tibet, the sectors to the west and south of Kathmandu is identified as the potential region to host the future large earthquake (Tian et al., 2020). The multistage rupture and aftershock distribution observed in 2015 Gorkha earthquake agree with multiple-asperity model based on globally recorded tele seismic P waves (Fan & Shearer, 2015). Three fringes of the fault plane, namely the western, southern, and northern show a high value of positive Coulomb change after 2015 Gorkha earthquake so those areas must be considered for the probable future earthquakes (Mullick & Mukhopadhyay, 2017).

Previous literature has conducted statistical analysis of the aftershocks of the Gorkha earthquake. Based on 553 aftershocks recorded within a month and a half of the event, the study not only determined the ~140 km long rupture plane abutting on the 1934 Nepal-Bihar earthquake but also identified a second belt of seismicity in the northern part of the Mahabarat range located under the Kathmandu basin (Adhikari et al., 2015). An aftershock catalog prepared from events detected by the NAMASTE temporary seismic network shows the distribution of aftershocks on the slip surface of the entire hanging wall and the observed clustered distribution pattern reflects the complex geometry of the MHT (Yamada et al., 2020). From the record of mainshock and aftershocks provided by the seismographic array operated by Hokkaido University and Tribhuvan University, rapid aftershocks decay rate with Omori's p value = 1.35 was noticed and concentration

of aftershocks is found to be in the eastern margin of the major slip region of the main shock (Ichiyanagi et al., 2016). The scaling exponent (β)'s scale invariance behavior before and after the April 2015 Gorkha, Nepal earthquake has identified the south Himalayan region of India as a region of accumulated stress (S. Gupta et al., 2021). The Wavelet Transform Modulus Maxima (WTMM) method shows that the multifractal nature of strong ground motion is more pronounced near the epicenter site than at distant sites of Gorkha earthquake (B. Tiwari et al., 2020).

In a separate study of aftershock sequences, the magnitude of completeness (Mc), *a*-values, and *b*-values of the Gutenberg-Richter relationship, correlation dimension (Dc) values, and Omori's *p*-values were found to be 3.0, 4.74, 0.75 ± 0.03, 1.84 ± 0.05, and 1.01 ± 0.05, respectively, and 3.3, 5.46, 0.90 ± 0.04, 1.91 ± 0.05, and 0.95 ± 0.04, respectively. These values indicate the rapid temporal decay of aftershocks and clustering patterns of earthquakes in the 2D space of the ruptured fault systems of Nepal's Himalaya (Chingtham et al., 2016). In other similar works for the same earthquake sequence gives GR *b*-value of 1.11 ± 0.08 which could be the possible representation of the highly heterogeneous and low stress regime. In the same study the spectrum of generalised dimension shows the multifractal nature with D_q varying from 1.66 for q = 2 to 0.11 for q = 22 explaining the geo-dynamics of the region in which a small disturbances in stress is adequate to provoke aftershocks (Nampally et al., 2018). Furthermore, from monitoring of aftershocks sequence, the aftershock productivity of the major aftershock (12 May Kodari earthquake) is noticed to be approximately twice as large as that of the M 7.8 main shock (Ogata & Tsuruoka, 2016).

The past studies in central Himalaya reveal that a major earthquake, potentially exceeding Mw 8, is inevitable due to the partial rupture of the active fault caused by the 2015 earthquake between the 1934 and 1505 historical earthquakes (Bilham, 2015, 2019). Although, the 2015 earthquake ruptured an asperity with high strain, asperity with same nature holding high strain energy is recognized towards west of the epicenter. This could seed a subsequent large earthquake having magnitude similar to the 2015 Gorkha event towards west or south of Gorkha event (Sreejith et al., 2018). From the study of the dynamic mechanisms of post seismic deformation processes following the 2015 earthquake, afterslip deficiency is noticed in the shallow portion of the MHT shows the potential seismic risk on the south and west of Kathmandu in future (J. Zhang et al., 2021). Based on the previously mentioned literature, the distribution of earthquake epicenters in the central Himalayan region is analyzed using fractal statistics. Specifically, the *b*-value described in the G-R frequency magnitude distribution relation, box counting dimension (D_0), correlation dimension (D_2), and the multifractality (D_q) spectrum of the epicenter distribution are studied using a power law technique.

CHAPTER 3

MATERIALS AND METHODOLOGY

This chapter makes extensive discussion about the power laws that are useful to explain the complexity associated with dynamics of seismic process.

3.1 Power law distribution

When one physical parameter can be expressed in terms of another quantity raised to some power, then they obey a power law. The simple example is the relation between distance $s(t)$ covered by the object for time (t) during free fall

$$s(t) = \frac{1}{2}gt^2 \tag{3.1}$$

For the constant value of g, this equation tells that $s(t)$ is proportional to the square of t and the plot of the above equation is a parabola. Taking the logarithm of both sides of the equation, the power law relationship can be converted into straight line

$$\log s(t) = 2\log(t) + \log(\frac{g}{2}) \tag{3.2}$$

The plot of $\log s(t)$ and $\log(t)$ gives a straight-line having slope 2. The slope of the straight line is equal to the exponent of t (Figure 11).

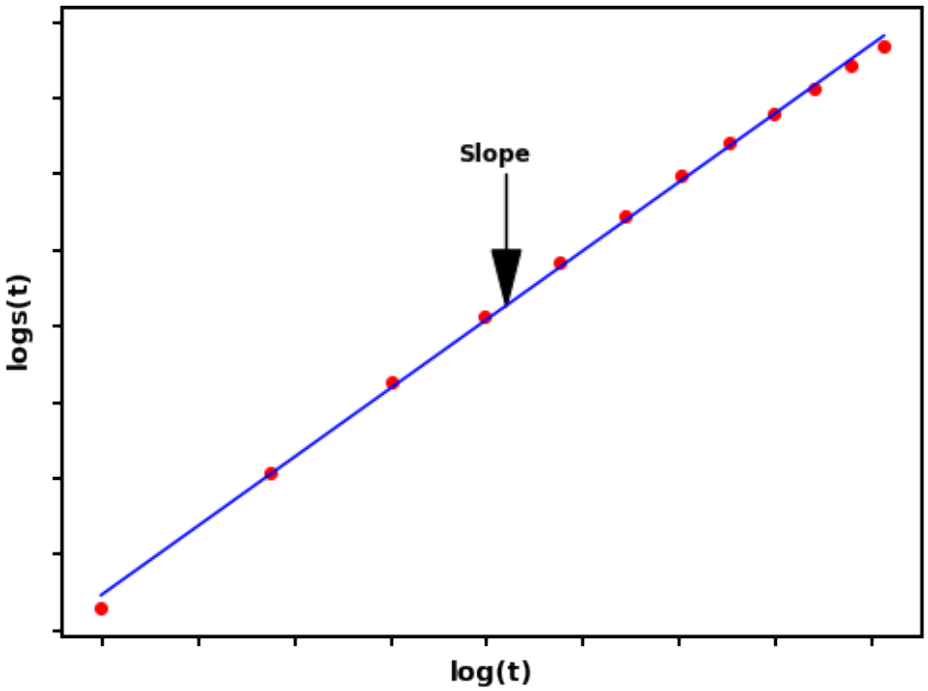

Figure 11: The slope of the graph gives the exponent of t.

This is a simple relation obeying the power law. In a broad sense, a power law or scaling law is the nonlinear scale free and self-similar distribution originated from the theory of complexity and tells that the probability of larger events decays more slowly than exponential. Power laws are often used in geophysics to describe phenomena such as earthquakes, volcanic eruptions, and landslides, as well as patterns in geological data such as rock formations and mineral deposits. The spatial parameters (latitude, longitude, depth), the temporal parameters (occurrence instant), and energy or magnitude parameters of earthquakes are governed by power law behaviour. Furthermore, the distribution of released energy follows a power law (Gutenberg & Richter, 1944), the distribution of earthquake epicenters also conforms to a power law (Kagan, 2007), and the number of aftershocks decreases as a power law (Utsu & Ogata, 1995). These statistics reflects the outcome of the earth's crust being in a self-organized critical state. (Bak et al., 2002). These laws are important in revealing an underlying regularity in the properties of the system. After the appealing work of Mandelbrot on fractals (Mandelbrot, 1982, 1989), geoscience researcher gave considerable attention in power law distributions to study the size of diverse geological structures like fault, coastlines (Turcotte & Brown, 1993), oil reservoirs (Kraaijpoel et al., 2022), the distribution of magnitude of 2015 Gorkha earthquake sequence (Nampally et al., 2018), space time distribution of Californian and global earthquakes (Corral & González, 2019),

aftershocks decay rate of Gorkha earthquake (R. Tiwari & Paudyal, 2022) etc. In earthquake science, the earliest known power law may be the law which describes the frequency distribution of amplitude of the seismograms (Ishimoto, 1939). It is expressed in the form $n(a) = Ka^{-m}$, where a is the amplitude, $n(a)$ is the number of events, while m and K are constants. Undermentioned power laws are used in this study.

3.1.1 Gutenberg-Richter (G-R) frequency magnitude distribution (FMD)

The most generally accepted log linear relation (Gutenberg & Richter, 1944) is power law between the frequency of occurrence earthquakes and the magnitude for defined region and time interval:

$$\log \dot{N} = -bm + \log \dot{a} \tag{3.3}$$

In above relation logarithm is to the base 10, b and $\dot{a}$ are constants, and $\dot{N}$ is the frequency of earthquakes per unit time with a magnitude > minimum magnitude (m) (Turcotte & Brown, 1993). The FMD relation is appropriate for a wide range of earthquake sizes in both global and local scale. The constant b or b-values vary for different sectors but are usually in the range between 0.8 and 1.2 (Bridges & Gao, 2006). It gives idea on the comparative scaling between large and small earthquakes (Spada et al., 2013), and it was often used to infer tectonic stress (El-Isa, 2013; Mandal et al., 2021), predict impending large earthquakes (Hirata et al., 1987; Kalafat & Görgün, 2019) and aid seismic hazard assessments (Ali, 2016; Pailoplee & Choowong, 2014). The constant $\dot{a}$ quantifies the regional value of seismicity. The b-value in this study is estimated by maximum likelihood estimation method (Aki, 1965).

3.1.2 Magnitude and energy relation

The magnitude of the earthquake (m) is an empirical measure of its size and can be related to the total energy released by the earthquakes E_s from the relation

$$\log E_s = 1.44m + 5.24 \tag{3.4}$$

Moment of earthquake or seismic moment *(M)* is proportional to the product of mean displacement *(D)* along the fault and the area of the fault surface *(A)* that slips during the earthquake. It is related with total energy release during the earthquakes as,

$$M = \mu AD \tag{3.5}$$

where μ is the shear modulus of the rock associated with the fault and unit of the seismic moment is Joule. Furthermore, the seismic moment *(M)* and magnitude *(m)* of the

magnitude of the earthquake can be defined as

$$\log M = cm + d \tag{3.6}$$

Where c and d are constants. For $c = 1.5$ and $d = 9.1$ equation (3.6) can be considered as a definition of magnitude, provided M in Joules (Hanks & Kanamori, 1979; Kanamori & Anderson, 1975). The approximate relationship between the seismic moment and the area of the ruptured fault *(A)* (Kanamori & Anderson, 1975) is

$$M = \alpha A^{3/2} \tag{3.7}$$

In above equation, α is a constant. On combining equation (3.3), (3.6), and (3.7) yields

$$\log \dot{N} = -3b/c + \log A + \log \dot{\beta} \tag{3.8}$$

With

$$\log \dot{\beta} = bd/c + \log \dot{a} - b/c \log \alpha \tag{3.9}$$

Now equation (3.8) can be written as

$$N = \dot{\beta} A^{-3b/2c} \tag{3.10}$$

The area of rupture $(A) \sim r^2$, where r is the linear dimension of the rupture. So, equation (3.10) takes the form

$$N = \dot{\beta} r^{-3b/c} \tag{3.11}$$

The number of objects *(N)* characterised by the linear dimension *(r)* can be defined as a power law

$$N = cr^{-D} \tag{3.12}$$

Where c is the proportionality constant and D is the fractal dimension. Comparing (3.11) with (3.12), we get

$$D = 3b/c \tag{3.13}$$

For the theoretical value of $c = 1.5$,

$$D = 2b \tag{3.14}$$

Thus, the fractal dimension of seismicity in both regional and global scale is two times the b-value (Aki, 1965; Turcotte, 1989).

3.1.3 Fractal dimension

A conventional knowledge of the dimension is a Euclidean dimension where a straight line has a dimension 1, a plane has a dimension of 2 and a volume has a dimension 3. To describe the roughness, complexity, or irregularity of an object, it is necessary to go beyond conventional knowledge, where the dimension is expressed by a non-integer or fractional value known as the fractal dimension, rather than the Euclidean dimension. Fractal objects/structures are rough, non-scaled objects that can only be scaled using non-traditional fractal dimensions. The idea of the fractal dimension was put forward while attempting to calculate the coastline's length (Mandelbrot, 1967, 1989). The length of the coastline (P_i) in terms of the length of the measuring rod (r_i) can be stated by the relation

$$P_i = \frac{C}{r_i^{D-1}} \tag{3.15}$$

Where C is the proportionality constant and D is the fractal dimension. Using the scale of map, the length of the coastline is plotted against the divider length on log-log paper, the slope of the linear component of the plot can then be used to determine the fractal dimension of the coast line. The smaller value of D signifies smooth coastlines and larger value signifies jagged coastlines (Smalley Jr et al., 1987). Thereafter, this technique of obtaining the fractal dimension is used for different topography (Gonzato et al., 1998; Klinkenberg & Goodchild, 1992). Although the Walker's Ruler (WR) or ruler divider method was the first method used for the calculation of the fractal dimension (Gonzato et al., 1998; Mandelbrot, 1982), it can only be employed for measuring the dimension of connected self-similar objects. The problem associated with WR method is that it has a finite remainder because for each ruler length L, part of the object left uncover creating considerable errors in the estimation of D (Aviles et al., 1987).

3.1.4 Hausdorff dimension and Box counting or capacity dimension

Hausdorff dimension and the capacity or box counting dimension are numerically equal for self-similar objects or for fractals generated by smooth dynamical systems, even though they are not equal in general (Mainieri, 1993). Hausdorff dimension is purely mathematical tools and is not suited for experimentation while box counting dimension

is well suited for numerical investigation. In both cases the efficiency of covering the object by the boxes or disks are measured, however Hausdorff dimension uses diverse box sizes for covering and box counting dimension uses the boxes of same size (El-Nabulsi & Anukool, 2022). The value of Hausdorff dimension is always less than equal to box counting dimension. The box counting method incorporates the best fitting procedure and much more applicable than the ruler method (De Santis, 1997). For N_i number of boxes of size r_i required to cover the fractal object, the plot is obtained on log-log scale as a function of r_i. For the straight-line correlation, the fractal dimension can be obtained by the formula

$$D = -\lim_{r_i \to 0} \frac{\log N_i(r_i)}{\log r_i} \tag{3.16}$$

The limitation of this method is that no provision is made for selecting the box according to whether there are no points or some points in the box. It is more of geometrical nature and provides very limited information about the degree of clumpiness of the distribution. Therefore, the correlation dimension is used to get more detailed information on clustering of the epicenter distribution.

3.1.5 Correlation fractal dimension

The correlation dimension (D) of epicenter distribution is calculated by defining correlation integral function $C(r)$ (Mondal et al., 2019; Roy & Mondal, 2012) as,

$$C(r) = \frac{2}{N(N-1)} \sum_{i,j=1, i \neq j}^{N} H(r - |x_i - x_j|) \tag{3.17}$$

In the above equation, $H(r - |x_i - x_j|) = \left\{ \begin{array}{ll} 1, & \text{if } |x_i - x_j| \leq r \\ 0, & \text{if } |x_i - x_j| > r \end{array} \right\}$ is the Heaviside step or also known as unit step function, r is the scaling factor, $|x_i - x_j|$, the angular distance between position vectors i and j of epicenters and can be obtained by the spherical triangle approach (Hirata, 1989), N is the sample volume (number of earthquakes within the sample taken). For small value of r, $C(r)$ has power law behavior which motivates to define the correlation dimension (Kagan, 2007)

$$C(r) \sim r^D \tag{3.18}$$

The slope of the linear part of plot for $\log r - \log C(r)$ give the correlation fractal dimension (D).

3.1.6 Generalized fractal dimension

A multifractal object exhibit different self-similarities and can only be described by a multifractal spectrum of dimensions. A full spectrum of fractal dimensions known as the Renyi dimension or the generalized dimension (D_q) (El-Nabulsi & Anukool, 2022) based on the value of generalized correlation integral (Grassberger & Procaccia, 1983).

$$C_q(r) = [\frac{1}{N}\sum_{i=1}^{N}[\frac{1}{(N-1)}\sum_{i,j=1,i\neq j}^{N} H(r-|x_i-x_j|)]^{q-1}]^{\frac{1}{q-1}} \tag{3.19}$$

The ratio of the logarithm of the generalized correlation integral to the logarithm of the scaling factor can be utilized to figure out the generalized dimension(D_q) as,

$$D_q = \lim_{r\to 0}\frac{1}{q-1}\frac{\log C_q(r)}{\log r} \tag{3.20}$$

Geometrically, D_q is obtained for each value of q by using the gradient of the linear section of the plot between $logr$ and $logC_q(r)$ for $r \to 0$. D_q provides a countable measure of the space-time clustering of earthquakes and hence information regarding the crustal deformation in space and time (Godano & Caruso, 1995; Mondal et al., 2019). For $q = 0$ the formula above provides the capacity dimension, for $q = 1$ it is equal to the information dimension and for $q = 2$ it is termed as correlation dimension (Grassberger & Procaccia, 1983). If the structure is monofractal then D_q is independent of q.
The temporal fractal dimension spectrum can be obtained by defining the correlation integral (Y.-J. Tang et al., 2012) $C_q(t)$ as

$$C_q(t) = [\frac{1}{N}\sum_{i=1}^{N}[\frac{1}{(N-1)}\sum_{i,j=1,i\neq j}^{N} H(t-|T_i-T_j|)]^{q-1}]^{\frac{1}{q-1}} \tag{3.21}$$

In the above equation, $H(t-|T_i-T_j|) = \left\{\begin{array}{ll} 0, & \text{if } |T_i-T_j| > t \\ 1, & \text{if } |T_i-T_j| \leq t \end{array}\right\}$ is the Heaviside step or unit step function, t is the period between the occurrences of two earthquakes, $|T_i-T_j|$ is the time interval of the ith and jth earthquake occurrences and N is the sample volume. The ratio of the logarithm of the generalized correlation integral to the logarithm of the scaling radius can be used to determine the temporal generalized dimension $D_q(t)$ as,

$$D_q(t) = \lim_{t\to 0}\frac{1}{q-1}\frac{\log C_q(t)}{\log t} \tag{3.22}$$

For each value of q between $-\infty$ and $+\infty$, the gradient of the linear section of the plot between $logt$ and $logC_q(t)$ for $t \to 0$ is used to calculate D_q.

3.2 Maximum likelihood estimation of *b*-value

Let us suppose seismic event catalog is divided into s sub catalogs having magnitude of completeness $m_c^1, m_c^2, \ldots\ldots\ldots, m_c^s$. Let each of sub catalogs contain a record of $n_i (i = 1, 2, \ldots., s)$ numbers of events having known magnitude. If the magnitude of each seismic event is assumed to be independent and identically distributed random variables following the G-R frequency magnitude distribution, then the earthquake magnitude probability density function (PDF) has the form

$$L(\beta) = \prod_{i=1}^{s} \prod_{i=1}^{n_i} f(m_j^i, \beta) \tag{3.23}$$

Where $L(\beta)$ is the likelihood function, β is the maximum likelihood estimate of the b-value and $f(m, \beta) = \left\{ \begin{array}{ll} 0, & \text{for } m \leq m_c \\ \beta \exp[-\beta(m - m_c)], & \text{for } m \geq m_c \end{array} \right\}$ is the PDF of the earthquake magnitude (Aki, 1965).

$$L(\beta) = \prod_{i=1}^{s} \prod_{i=1}^{n_i} \beta \exp[-\beta(m_j^i - m_c^i)] \tag{3.24}$$

For $s = 2$

$$L(\beta) = \prod_{i=1}^{2} \prod_{i=1}^{n_i} \beta \exp[-\beta(m_j^i - m_c^i)] \tag{3.25}$$

Taking log likelihood

$$\ln L(\beta) = \ln \prod_{i=1}^{2} \prod_{i=1}^{n_i} \beta + \ln \prod_{i=1}^{2} \prod_{i=1}^{n_i} \beta \exp[-\beta(m_j^i - m_c^i)] \tag{3.26}$$

Taking differentiation with respect to β, we get

$$\frac{d \ln L(\beta)}{d\beta} = \sum_{i=1}^{2} \sum_{j=1}^{n_i} \frac{1}{\beta} + \frac{d[\ln \prod_{i=1}^{2} \prod_{i=1}^{n_i} \beta \exp[-\beta(m_j^i - m_c^i)]]}{d\beta} \tag{3.27}$$

$$\frac{d \ln L(\beta)}{d\beta} = \sum_{i=1}^{2} \sum_{j=1}^{n_i} \frac{1}{\beta} - \sum_{i=1}^{2} \sum_{j=1}^{n_i} (m_j^i - m_c^i) \tag{3.28}$$

For $\frac{d \ln L(\beta)}{d\beta} = 0$

$$\sum_{i=1}^{2} \sum_{j=1}^{n_i} \frac{1}{\beta} = \sum_{i=1}^{2} \sum_{j=1}^{n_i} (m_j^i - m_c^i) \tag{3.29}$$

$$\sum_{j=1}^{n_1} \frac{1}{\beta} + \sum_{j=1}^{n_2} \frac{1}{\beta} = \sum_{j=1}^{n_1} (m_j^1 - m_c^1) + \sum_{j=1}^{n_2} (m_j^2 - m_c^2) \tag{3.30}$$

$$\frac{n_1}{\beta_1} + \frac{n_2}{\beta_2} = \sum_{j=1}^{n_1} (m_j^1 - n_1 m_c^1) + \sum_{j=1}^{n_2} (m_j^2 - n_2 m_c^2) \tag{3.31}$$

$$\frac{n_1 + n_2}{\beta} = \frac{n_1}{\beta_1} + \frac{n_2}{\beta_2} \tag{3.32}$$

where $\frac{1}{\beta_1} = \frac{\sum_{j=1}^{n_1} m_j^1}{n_1} - m_c^1$ and $\frac{1}{\beta_2} = \frac{\sum_{j=1}^{n_2} m_j^2}{n_2} - m_c^2$

Furthermore,

$$\frac{1}{\beta} = \frac{n_1}{n_1 + n_2} \frac{1}{\beta_1} + \frac{n_2}{n_1 + n_2} \frac{1}{\beta_2} \tag{3.33}$$

$$\frac{1}{\beta} = \frac{r_1}{\beta_1} + \frac{r_2}{\beta_2} \tag{3.34}$$

where $r_1 = \frac{n_1}{n_1 + n_2}$ and $r_2 = \frac{n_2}{n_1 + n_2}$

Equivalently,

$$\hat{\beta} = \left(\frac{r_1}{\beta_1} + \frac{r_2}{\beta_2} \right)^{-1} \tag{3.35}$$

In general,

$$\hat{\beta} = \left(\frac{r_1}{\hat{\beta}_1} + \frac{r_2}{\hat{\beta}_2} + \frac{r_3}{\hat{\beta}_3} + \ldots\ldots + \frac{r_s}{\hat{\beta}_s} \right)^{-1} \tag{3.36}$$

where $\hat{\beta}$ is the generalized Aki-Utsu b-value estimator (Kijko & Smit, 2012) used to calculate the b-value when the seismic event catalog can be divided into sub catalogs s each with a different level of completeness. The b-value estimator therefore can simply

be calculated by the formula

$$\frac{1}{\beta} = \frac{\sum_{j=1}^{n} m_j}{n} - m_c \tag{3.37}$$

Or,

$$\frac{1}{\beta} = \overline{m} - m_c \tag{3.38}$$

Where $\overline{m}$ is the mean magnitude and m_c is the completeness magnitude
Or,

$$b = \frac{\ln e}{\overline{m} - m_c} \tag{3.39}$$

Equivalently,

$$b = \frac{\log e}{\overline{m} - m_c} \tag{3.40}$$

The formula above is used in our study to estimate the b-value.

3.3 Spherical Triangle method

The arc distances r between two epicenters (θ_i, ϕ_i) and (θ_j, ϕ_j) is calculated by the spherical triangle method (Teotia et al., 1997; Öncel et al., 1996) given by the formula

$$r = \cos^{-1}(\cos\theta_i \cos\theta_j + \sin\theta_i \sin\theta_j \cos(\phi_i - \phi_j)) \tag{3.41}$$

The distance obtained by this formula is used to obtain correlation integral function $C(r)$ and generalised correlation integral function $C_q(r)$.

3.4 Correlation integral function

The Grassberger-Procaccia (GP) correlation integral is a mathematical technique to quantify the similarity or dissimilarity of time series data (Grassberger & Procaccia, 1983). It is used to quantify the degree of clustering or regularity in a point pattern. The basic idea behind the algorithm is to measure the degree of self-similarity in the data by comparing the similarity of pairs of points at different scales. Here is a general outline of the steps to develop the GP correlation function:

- A scaling radius (r) is defined
- A sphere of radius r is drawn for each point in the pattern

- The number of points that are enclosed inside each sphere are counted and noted as $n(r)$.
- Probability of falling two randomly selected points within the sphere is obtained by dividing $n(r)$ by total number of points (N) in a sample.
- The process is repeated for different value of r to plot the probability as a function of r.
- Heaviside step function is used to assign a value of 1 and 0 to pairs of points which are closer than r and farther than r.
- By summing the values over all pairs of points, the numerator of the correlation integral function is obtained.
- The numerator is divided by total number of pairs of points to get the correlation integral function $C(r)$ as

$$C(r) = \frac{2}{N(N-1)} \sum_{i}^{N} \sum_{j=i+1}^{N} H(r - ||x_i - x_j||) \tag{3.42}$$

  Where $H(r-||x_i-x_j||)$ is the Heaviside step function, x_i and x_j are the coordinates of two earthquake epicenters, and $||x_i - x_j||$ is the distance between the two epicenters.
- The correlation integral function as a function of scaling radius (r) is plotted on a log-log scale.
- For a power-law relationship, the slope of the linear region of the $log - log$ plot is the fractal dimension of the point pattern as

$$D = \frac{log(C(r)}{log(r)} \tag{3.43}$$

It is important to note that the choice of the radius r can have an impact on the final result, the common practice is to use multiple values of r and average the results to get a more accurate fractal dimension (Nerenberg & Essex, 1990; Aggarwal et al., 2017). The GP correlation function can be used to analyze a wide range of point patterns, including patterns in two-dimensional or three-dimensional space, and can be applied to both continuous and discrete data (Grassberger & Procaccia, 1983; Gonzato et al., 1998). The correlation integral is calculated for a range of distances, and the slope of the plot of the correlation integral versus distance is used to determine the degree of clustering.

3.5 Omori-Utsu law

The occurrence of aftershocks following the major shock is the indication that the complete strain energy is not released after the majorshock (Ouillon et al., 2009; Utsu, 1972). The aftershock sequence carries the information regarding earth's crust and help to understand the physics behind the occurrence of earthquakes. The Omori Law (Omori, 1895; Žalohar, 2018) stated as the frequency of aftershocks decays over time in hyperbolic manner. The displacement on the primary fault by the initial earthquake transforms stress in some adjacent faults from where sequences of aftershocks emerge. The temporal decay of aftershock following a main shock can be described by power law known as the Omori-Utsu law (Corral, 2003; Hainzl & Marsan, 2008).

$$R(t) = \frac{K}{(t+c)^p} \tag{3.44}$$

where $R(t)$ is the rate of decrease of aftershock and K and c are constants. p is the decay rate of aftershocks, known as p-value and varies from location to location and from case to case in wide limits and has a value close to 1.0 for longer period of time. For example, p values are usually found in the range 0.8 to 1.2 for tectonic seismicity (Utsu & Ogata, 1995), p variation from 0.5 to 1.5 is observed in California (Guglielmi, 2016; Reasenberg & Jones, 1989). The heterogeneity, stress, and temperature in the crust are connected to the fluctuation in p. (Mogi, 1967; Trivedi, 2015). Since, the accurate value of p represents the friction law and the stress relaxation mechanism in seismogenic zones, it is important to derive the reliable value of p (Hainzl et al., 1999; Helmstetter & Shaw, 2006). The constant K or K-value is controlled by the total number of the aftershocks in the sequence. K-value, also called as aftershock productivity, is a normalizing parameter that is dependent on the total number of aftershocks and the threshold magnitude (Kisslinger & Jones, 1991; S. Ansari, 2017). The other constant also known as c-value is generally considered as a delay between the mainshock rupture end and the start of the power law aftershock decay rate (Narteau et al., 2009). The value of c is typically positive, and $t + c$ is used to adjust the time of aftershock counting, so it starts at the time of main shock (Utsu, 1972).

3.6 Preparation of homogeneous database

An earthquake study demands the need of earthquake data recorded by a local and dense seismic network in the source area for the estimation of D_q with minimum bias (Nampally et al., 2018). To investigate variations in the b-value, a dataset of 1126 earthquakes with a magnitude of 3.8 or higher was compiled from the revised catalogue of the International Seismological Centre (ISC) (Storchak et al., 2020; Di Giacomo et al., 2018) for the region between 26.45°N to 30.50°N and 80.0°E to 88.20°E. The b-value was determined

using the maximum likelihood estimation (MLE) method. For the multifractal study of aftershocks, data was extracted from published literature. Following the mainshock of 2015 Gorkha earthquake, 4401 events were manually picked and located between May 25, 2015 to the June that includes 1802 events (> 3.0 ML) and 553 events (> 4.0 ML) (Adhikari et al., 2015). After the six weeks of the Gorkha earthquake a dense seismic network named as NAMASTE (Nepal Array Measuring Aftershock Seismicity Trailing Earthquake) installed in the source region of the earthquake. It has existed for approximately 11 months and recorded more than 8000 earthquakes (Yamada et al., 2020). From above sources we have prepared the dataset of 10500 events (Mc=2.0 ML) within the geographical range 25.22°N-30.15°N in latitude and 81.77°E-90.41°E in longitude from 2015-04-25 to 2015-06-14 for the study. To analyze the rate of decay in aftershocks (Omori, 1895; Utsu, 1971), a 2015 earthquake catalog (Adhikari et al., 2015) was utilized, covering the brief time period of April 25th to June 7th, within the latitude range of 26.50°N to 29.0°N and longitude range of 84.0°E to 87.0°E in the central Himalaya.

CHAPTER 4

RESULTS AND DISCUSSION

This chapter focuses on analyzing b-values and generalised fractal dimension D_q of earthquakes distribution in central Himalaya and adjoining region. we study the temporal variation of b-values for fixed event window and fixed time window, spatial distributions of b-values for fixed width, depth variation of b-values for fixed depth window, and spatial mapping of the region's b-value. More importantly, the multifractal spectrum ($D_q - q$) curve is also obtained for q = -10 to q = 22.

4.1 Spatio-temporal variation of *b*-value pre and post Gorkha earthquake

To examine the fluctuation in the b-value over both space and time, a homogeneous earthquake dataset is prepared from the ISC revised catalog. This catalog comprises of 2031 earthquake for the time frame of February 1, 1964 to June 16, 2020. The data was collected within the rectangular boundary marked by the red box in the inset map, with coordinates ranging from 26.45°N to 30.5°N and 80°E to 88.2°E (Figure 12). The declusterisation of the catalogue (Reasenberg, 1985) found 46 clusters of the earthquakes comprising 458 earthquakes. After omitting the cluster events, the subset of catalogue includes 1619 earthquakes. The magnitude of completeness (Mc) is computed from the software ZMAP-7.1 (Wiemer, 2001) and the final catalog contains 1126 events having magnitude of completeness $\geq$ 3.8. The b-value is calculated using the maximum likelihood estimation (MLE) method, which has the advantage of not being influenced by earthquakes of large magnitude, compared to other methods.

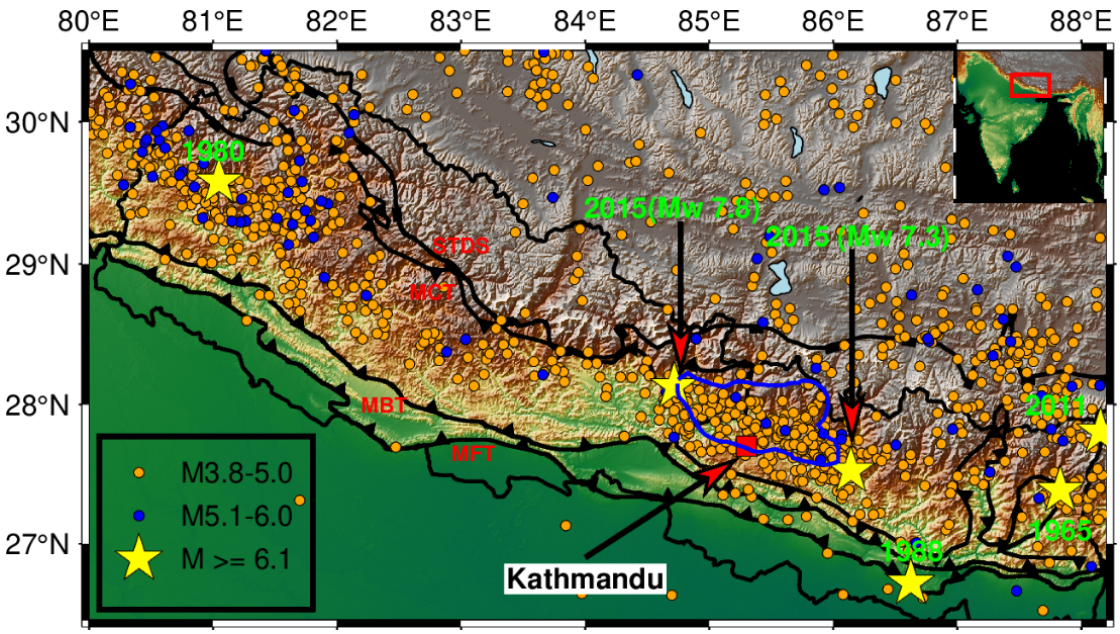

Figure 12: Seismicity of central Himalaya and adjoining region for the earthquakes under study (1126 events) (Di Giacomo et al., 2015, 2018). Earthquakes with magnitude greater than equal to 6.1 mb for the study period are depicted by yellow stars. Major faults within the study region viz., STDS, MCT, MBT, and MFT are also depicted along with blue contour, the rupture area of 2015 Gorkha earthquake.

For a single window of 1126 occurrences,the *b*-value is computed as 0.79 ± 0.02 and depicted in figure 13.

4.1.1 Temporal variation of *b*-value for fixed events window

The temporal variation of *b*-value was calculated from sliding as well as moving window technique containing a constant number of events to ensure the reliable value. The temporal variation of *b* provides the information regarding the stress condition with respect to time. It was found that *b*-values decrease before medium or large earthquake, and its value increases after the main shock (E. Bayrak et al., 2017; Kanamori & Anderson, 1975; R. Tiwari & Paudyal, 2021b). Table 4 displays estimated values of *a* and *b* for 100-event windows with their standard errors (Shi & Bolt, 1982) and figure 14 shows the temporal changes of *b*-values for same windows.

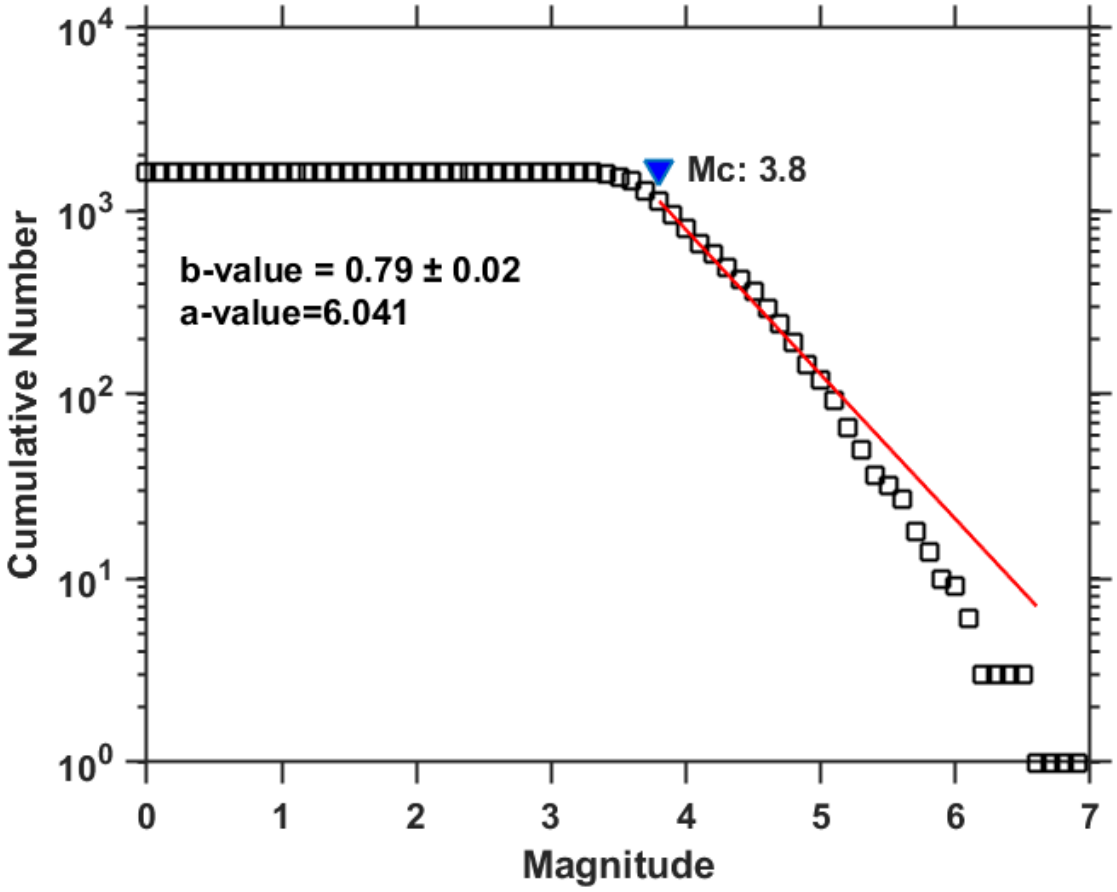

Figure 13: Magnitude of completeness (Mc) value, b-value of frequency size distribution, and a-value (number of earthquakes in a sample) for the earthquake data set of 58 years (1964 to 2020) in the central Himalaya and adjoining region.

Table 4: Fixed and movable temporal window presenting a-value and b-value of Gutenberg-Richter (GR) relation

Window	Number of earthquakes	Time period	a-value	b-value
1	0-100	1964-02-01-1984-05-19	4.274	0.54 ± 0.03
2	20-120	1967-12-18-1987-08-09	4.576	0.61 ± 0.03
3	40-140	1974-12-23-1988-12-27	4.020	0.50 ± 0.03
4	60-160	1978-08-13-1991-12-09	4.085	0.52 ± 0.03
5	80-180	1980-11-20-1993-08-19	3.674	0.44 ± 0.02
6	100-200	1984-05-30-1995-02-02	3.788	0.47 ± 0.02
7	120-220	1988-01-23-1996-01-25	4.003	0.53 ± 0.03
8	140-240	1989–5-22-1996-07-03	4.267	0.60 ± 0.03
9	160-260	1991-12-21-1996-09-07	3.960	0.69 ± 0.04
10	180-280	1993-09-05-1997-04-05	4.937	0.77 ± 0.05
11	200-300	1995-02-18-1998-01-16	5.230	0.85 ± 0.06
12	220-320	1996-02-07-1998-08-01	5.410	0.90 ± 0.07

13	240-340	1996-07-03-1998-10-04	5.572	0.94 ± 0.08
14	260-360	1996-10-03-1999-10-03	5.595	0.95 ± 0.09
15	280-380	1997-04-07-2001-04-15	5.883	1.02 ± 0.09
16	300-400	1998-01-16-2002-01-31	5.603	0.95 ± 0.09
17	320-420	1998-08-24-2002-06-04	5.619	0.95 ± 0.09
18	340-440	1998-10-14-2002-09-29	6.676	0.97 ± 0.09
19	360-460	1999-12-01-2003-02-26	5.776	0.99 ± 0.09
20	380-480	2001-04-28-2003-11-11	5.929	1.03 ± 0.09
21	400-500	2002-03-07-2004-05-29	6.509	1.19 ± 0.10
22	420-520	2002-06-06-2005-01-15	6.497	1.18 ± 0.09
23	440-540	2002-10-11-2005-06-14	6.116	1.08 ± 0.09
24	460-560	2003-03-21-2005-02-03	5.811	1.00 ± 0.09
25	480-580	2003-11-14-2007-02-06	5.603	0.95 ± 0.08
26	500-600	2004-06-24-2008-04-08	5.534	0.93 ± 0.08
27	520-620	2005-01-16-2008-12-26	5.410	0.90 ± 0.08
28	540-640	2005-06-17-2010-02-27	5.603	0.95 ± 0.09
29	560-660	2006-02-14-2011-05-04	5.474	0.91 ± 0.08
30	580-680	2007-02-12-2012-06-09	5.467	0.91 ± 0.09
31	600-700	2008-05-08-2012-12-29	5.348	0.88 ± 0.09
32	620-720	2009-01-23-2013-08-30	5.375	0.89 ± 0.09
33	640-740	2010-02-28-2014-08-12	5.611	0.95 ± 0.10
34	660-760	2011-05-24-2015-04-25	5.375	0.89 ± 0.10
35	680-780	2012-07-02-2015-04-27	5.467	0.91 ± 0.10
36	700-800	2013-01-02-2015-04-30	5.838	1.01 ± 0.13
37	720-820	2013-09-04-2015-05-04	6.210	1.11 ± 0.13
38	740-840	2014-08-22-2015-05-12	6.065	1.07 ± 0.13
39	760-860	2015-04-25-2015-05-21	6.770	1.26 ± 0.15
40	780-880	2015-04-27-2015-06-5	6.868	1.28 ± 0.14
41	800-900	2015-05-01-2015-07-02	6.413	1.16 ± 0.12
42	820-920	2015-05-04-2015-08-17	6.287	1.13 ± 0.11
43	840-940	2015-05-12-2015-11-19	5.967	1.04 ± 0.09
44	860-960	2015-05-22-2016-03-14	5.883	1.02 ± 0.08
45	880-980	2015-06-07-2016-05-23	5.929	1.03 ± 0.09
46	900-1000	2015-07-03-2016-11-06	6.116	1.08 ± 0.10
47	920-1020	2005-08-20-2017-08-24	5.759	0.99 ± 0.09
48	940-1040	2015-11-24-2018-04-29	6.025	1.06 ± 0.10
49	960-1060	2016-03-30-2018-10-24	6.147	1.09 ± 0.10

50	980-1080	2016-05-23-2019-03-07	5.742	0.98 ± 0.09
51	1000-1100	2016-11-12-2019-08-27	5.557	0.94 ± 0.08
52	1020-1126	2017-09-21-2020-05-30	5.610	0.94 ± 0.08

The *b*-value increased steadily from 0.44 ± 0.02 to 1.02 ± 0.09 over a 20-year period from 1980 to 2001. In 2002, it decreased to 0.95 ± 0.09, then rose to 1.19 ± 0.10 between 2002 and 2004. From 2005 to 2015, the *b*-value showed a U-shape variation with a peak at the end of May 2015 in the Gorkha to Kodari region where a cluster of earthquakes took place. This was followed by a sharp increase to 1.28 ± 0.14. Afterward, the *b*-value trended downward, settling around 0.94. A sudden rise in the *b*-value after April 25, 2015, may be linked to the release of energy in the earthquake region, returning the *b*-value to its average value of around 1.0 (Al-Heety & Mohammad, 2021; Y. Bayrak & Öztürk, 2004; Khalil et al., 2021). Therefore, a significant decrease in the *b*-value can be considered as a sign of a potential impending large rupture.

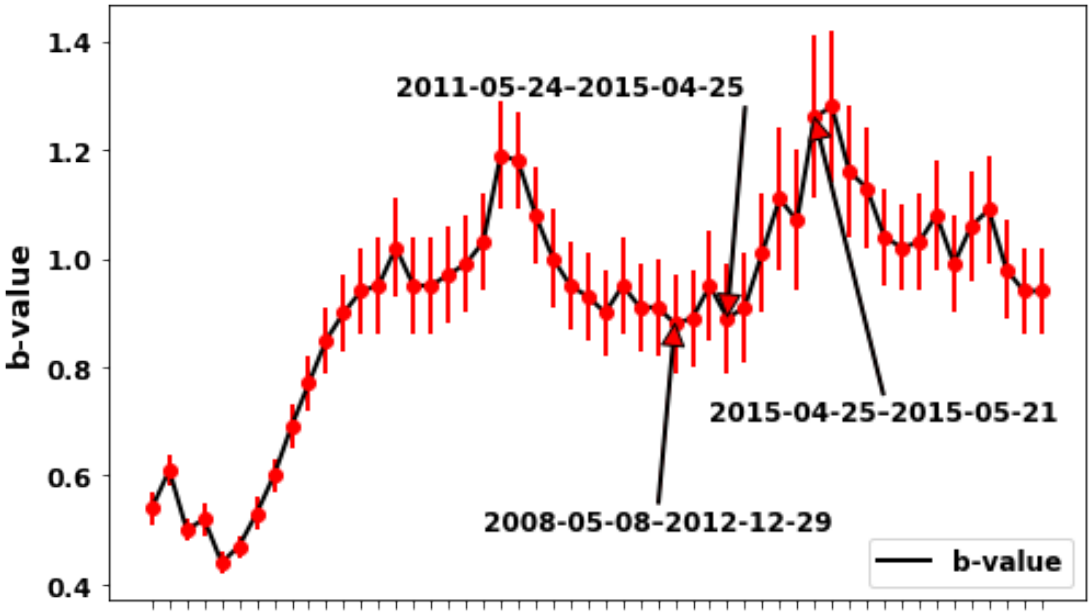

Figure 14: Temporal variation of *b*-value where vertical red bars represent the calculated standard errors in the estimation of *b*-value

4.1.2 Temporal variation of *b*-value for 10 year time window

Table 5 shows the long-term temporal changes in *b*-values estimated using constant 10-year windows with a 2-year moving step. However, the table does not display the *a*-values and *b*-values for windows 1, 2, 3, and 4 as only windows with 50 or more earthquakes were considered for a reliable *a*-value and *b*-value analysis.

Table 5: Movable temporal window of 10 year period

Window	Number of earthquakes	Time period	*a*-value	*b*-value
1	35	1964-1974	-	-
2	38	1966-1976	-	-
3	33	1968-1978	-	-
4	46	1970-1980	-	-
5	55	1972-1982	4.184	0.58 ± 0.04
6	59	1974-1984	4.361	0.62 ± 0.05
7	62	1976-1986	4.692	0.69 ± 0.05
8	66	1978-1988	4.639	0.67 ± 0.05
9	72	1980-1990	3.878	0.51 ± 0.03
10	76	1982-1992	4.056	0.54 ± 0.03
11	92	1984-1994	3.643	0.44 ± 0.02
12	107	1986-1996	3.933	0.50 ± 0.03
13	179	1988-1998	4.663	0.63 ± 0.03
14	220	1990-2000	5.219	0.77 ± 0.04
15	237	1992-2002	5.439	0.81 ± 0.04
16	302	1994-2004	6.102	0.95 ± 0.04
17	338	1996-2006	6.228	0.97 ± 0.05
18	296	1998-2008	6.294	1.01 ± 0.05
19	272	2000-2010	6.248	1.00 ± 0.05
20	274	2002-2012	6.181	0.99 ± 0.06
21	237	2004-2014	5.906	0.93 ± 0.06
22	388	2006-2016	6.403	1.00 ± 0.05
23	434	2008-2018	6.499	1.02 ± 0.05
24	478	2010-2020	6.472	1.00 ± 0.04
25	454	2012-2020	6.561	1.03 ± 0.05

The lowest *b*-value, 0.44 ± 0.06, was estimated for the period between 1984 and 1994, while the highest *b*-value, 1.03 ± 0.05, was estimated for the period between 2012 and 2020 (as shown in figure 15 and table 5). The *b*-value gradually increased after 1994 and settled around the global average of 1.0 by the end of 2020. High *a*-value over 6.0 and *b*-value around 1.0 after 1994 suggests a significant number of small earthquakes in the region. The slight drop in *b*-value from 1.01 ± 0.05 over the 1998-2008 decade to 0.93 ± 0.06 over the 2004-2014 decade, just before the Gorkha earthquake, supports the

idea that *b*-value increases long before an earthquake, followed by a drop just before the event (El-Isa, 2013; El-Isa & Eaton, 2014).

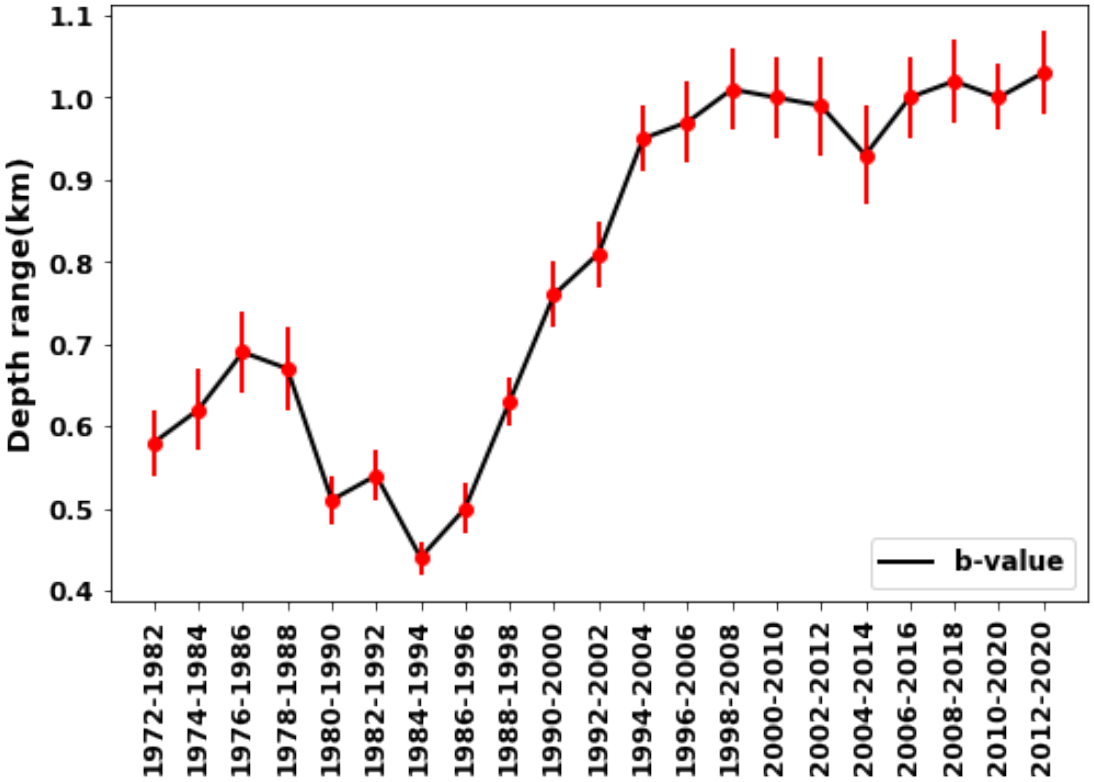

Figure 15: *b*-value variation for successive time windows of 10 years, with a 2-year shift.

4.1.3 Spatial variation of *b*-value for fixed width spatial window

To examine the spatial variation of the *b*-value, a window width of 1° with a shift of 0.2° along the longitude direction was used while maintaining a constant height (26.45°N-30.5°N) along the latitude direction (as shown in table 6).

Table 6: Movable spatial window of width 1° in the longitude direction and height of ~ 4° along latitude direction presenting *a*-value and *b*-value of Gutenberg-Richter (GR) relation.

Window	Number of earthquakes	Range	*a*-value	*b*-value
1	103	80.0°E-81.0°E and 26.45°N-30.5°N	4.349	0.61 ± 0.05
2	115	80.2°E-81.2°E and 26.45°N-30.5°N	4.300	0.59 ± 0.04
3	115	80.4°E-81.4°E and 26.45°N-30.5°N	4.343	0.60 ± 0.04
4	136	80.6°E-81.6°E and 26.45°N-30.5°N	4.603	0.65 ± 0.04
5	173	80.8°E-81.8°E and 26.45°N-30.5°N	4.823	0.68 ± 0.04
6	169	81.0°E-82.0°E and 26.45°N-30.5°N	4.906	0.70 ± 0.04
7	164	81.2°E-82.2°E and 26.45°N-30.5°N	5.099	0.76 ± 0.04

8	157	81.4°E-82.4°E and 26.45°N-30.5°N	4.983	0.73 ± 0.04
9	115	81.6°E-82.6°E and 26.45°N-30.5°N	4.774	0.71 ± 0.05
10	66	81.8°E-82.8°E and 26.45°N-30.5°N	4.556	0.72 ± 0.07
11	60	82.0°E-83.0°E and 26.45°N-30.5°N	4.536	0.73 ± 0.07
12	46	82.2°E-83.2°E and 26.45°N-30.5°N	4.345	0.71 ± 0.07
13	38	82.4°E-83.4°E and 26.45°N-30.5°N	4.566	0.79 ± 0.10
14	46	82.6°E-83.6°E and 26.45°N-30.5°N	5.007	0.88 ± 0.11
15	58	82.8°E-83.8°E and 26.45°N-30.5°N	4.767	0.79 ± 0.10
16	60	83.0°E-84.0°E and 26.45°N-30.5°N	5.068	0.87 ± 0.11
17	65	83.2°E-84.2°E and 26.45°N-30.5°N	5.029	0.85 ± 0.10
18	60	83.4°E-84.4°E and 26.45°N-30.5°N	5.101	0.87 ± 0.11
19	60	83.6°E-84.6°E and 26.45°N-30.5°N	5.204	0.90 ± 0.12
20	68	83.8°E-84.8°E and 26.45°N-30.5°N	5.030	0.84 ± 0.10
21	81	84.0°E-85.0°E and 26.45°N-30.5°N	4.923	0.79 ± 0.08
22	98	84.2°E-85.2°E and 26.45°N-30.5°N	5.162	0.83 ± .08
23	127	84.4°E-85.4°E and 26.45°N-30.5°N	5.531	0.90 ± 0.08
24	162	84.6°E-85.6°E and 26.45°N-30.5°N	5.811	1.00 ± 0.09
25	183	84.8°E-85.8°E and 26.45°N-30.5°N	5.925	0.96 ± 0.06
26	207	85.0°E-86.0°E and 26.45°N-30.5°N	6.023	0.98 ± 0.06
27	227	85.2°E-86.2°E and 26.45°N-30.5°N	5.820	0.91 ± 0.06
28	216	85.4°E-86.4°E and 26.45°N-30.5°N	5.934	0.94 ± 0.07
29	191	85.6°E-86.6°E and 26.45°N-30.5°N	5.563	0.86 ± 0.06
30	163	85.8°E-86.8°E and 26.45°N-30.5°N	5.196	0.79 ± 0.06
31	135	86.0°E-87.0°E and 26.45°N-30.5°N	4.978	0.75 ± 0.06
32	111	86.2°E-87.2°E and 26.45°N-30.5°N	5.017	0.78 ± 0.07
33	108	86.4°E-87.4°E and 26.45°N-30.5°N	4.792	0.73 ± 0.06
34	130	86.6°E-87.6°E and 26.45°N-30.5°N	4.714	0.68 ± 0.05
35	148	86.8°E-87.8°E and 26.45°N-30.5°N	5.467	0.68 ± 0.05
36	197	87.0°E-88.0°E and 26.45°N-30.5°N	5.688	0.88 ± 0.06
37	288	87.2°E-88.2°E and 26.45°N-30.5°N	5.584	0.82 ± 0.04

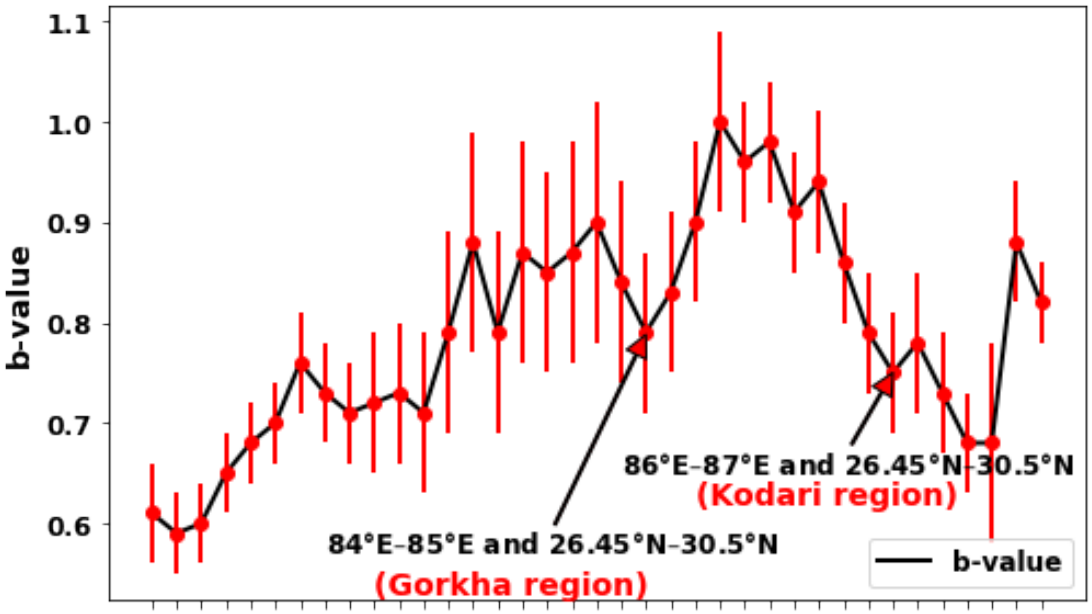

Figure 16: The inverted U-shaped variation of *b*-value for different spatial window.

Table 6 displays varying *b*-values between 0.59 ± 0.04 (80.2° - 81.2° and 26.45° - 30.5°) and 1.00 ± 0.09 (84.6° - 85.6° and 26.45° - 30.5°) with a mean of 0.79. Spatially, the *b*-value is below 0.70 from window 1 to window 5, below 0.80 from window 6 to window 15 except for window 14 (0.88 ± 0.11), less than or equal to 0.90 from window 16 to window 23 except window 21 (0.88 ± 0.11), and within the range of 0.90-1.00 from window 24 to window 28. From window 29 to window 35, it decreases below 0.70 and then rises above 0.80 (Figure 16). The *b*-value is related to the distribution of stress (Mogi, 1967; Scholz, 1968) and often falls between 0.5 and 1.5 in tectonically active regions (Pacheco et al., 1992; Wiemer and Wyss, 1997). The *b*-values in the region under study indicate seismic activity. The entire range of *b*-values from 0.59 to 1.0 agrees with values for aftershocks of the Gorkha earthquake (0.61 ± 0.01 (R. Tiwari et al., 2022), 0.93 ± 0.03 (Thapa et al., 2018), 1.11 ± 0.08 (Nampally et al., 2018).

4.1.4 Depth variation of *b*-value

To study the variability of *b*-value with depth, sliding windows were generated with a minimum of 114 earthquakes and a maximum of 499 earthquakes, and the study was focused on depths ranging from 0 to 47 km, as there are very few earthquakes recorded at deeper depths. The data was divided into depth range of 0-10 km and window was shifted by the advances of 0.5 km. A systematic decrease of *b*- value from 0 to 32 km is noticed followed by the reverse trend below the depth of 32 km.

Table 7: Movable depth window containing number of earthquakes, depth range (Z), a-value, and b-value of earthquake frequency magnitude distribution.

Window	Number of earthquakes	Depth range	a-value	b-value
1	208	$0.0 \leq Z \leq 10.0$	6.162	1.01 ± 0.07
2	217	$0.5 \leq Z \leq 10.5$	6.081	0.99 ± 0.06
3	230	$1.0 \leq Z \leq 11.0$	6.120	0.99 ± 0.06
4	237	$1.5 \leq Z \leq 11.5$	6.116	0.98 ± 0.06
5	266	$2.0 \leq Z \leq 12.0$	6.077	0.96 ± 0.06
6	275	$2.5 \leq Z \leq 12.5$	6.028	0.94 ± 0.05
7	285	$3.0 \leq Z \leq 13.0$	5.971	0.93 ± 0.05
8	292	$3.5 \leq Z \leq 13.5$	5.876	0.90 ± 0.05
9	307	$4.0 \leq Z \leq 14.0$	5.734	0.85 ± 0.05
10	312	$4.5 \leq Z \leq 14.5$	5.669	0.84 ± 0.04
11	317	$5.0 \leq Z \leq 15.0$	5.654	0.83 ± 0.04
12	327	$5.5 \leq Z \leq 15.5$	5.571	0.80 ± 0.04
13	338	$6.0 \leq Z \leq 16.0$	5.569	0.80 ± 0.04
14	342	$6.5 \leq Z \leq 16.5$	5.508	0.78 ± 0.04
15	383	$7.0 \leq Z \leq 17.0$	5.521	0.77 ± 0.04
16	389	$7.5 \leq Z \leq 17.5$	5.477	0.76 ± 0.03
17	429	$8.0 \leq Z \leq 18.0$	5.605	0.78 ± 0.03
18	431	$8.5 \leq Z \leq 18.5$	5.574	0.77 ± 0.03
19	477	$9.0 \leq Z \leq 19$	5.727	0.80 ± 0.03
20	484	$9.5 \leq Z \leq 19.5$	5.713	0.80 ± 0.03
21	499	$10.0 \leq Z \leq 20.0$	5.677	0.78 ± 0.03
22	338	$10.5 \leq Z \leq 20.5$	5.104	0.83 ± 0.08
23	342	$11.0 \leq Z \leq 21$	5.108	0.68 ± 0.03
24	332	$11.5 \leq Z \leq 21.5$	5.061	0.67 ± 0.03
25	320	$12.0 \leq Z \leq 22$	5.061	0.67 ± 0.03
26	299	$12.5 \leq Z \leq 22.5$	4.929	0.65 ± 0.03
27	315	$13.0 \leq Z \leq 23.0$	5.978	0.65 ± 0.03
28	310	$13.5 \leq Z \leq 23.5$	4.987	0.66 ± 0.03
29	299	$14.0 \leq Z \leq 24.0$	4.967	0.66 ± 0.03
30	299	$14.5 \leq Z \leq 24.5$	4.981	0.66 ± 0.03
31	296	$15.0 \leq Z \leq 25.0$	4.987	0.65 ± 0.03
32	290	$15.5 \leq Z \leq 25.5$	4.971	0.66 ± 0.03
33	286	$16.0 \leq Z \leq 26$	4.986	0.67 ± 0.03
34	276	$16.5 \leq Z \leq 26.5$	4.986	0.67 ± 0.03

35	310	$17.0 \leq Z \leq 27$	5.152	0.70 ± 0.03
36	197	$17.5 \leq Z \leq 27.5$	5.083	0.70 ± 0.03
37	260	$18 \leq Z \leq 28.0$	5.120	0.71 ± 0.04
38	220	$18.5 \leq Z \leq 28.5$	4.844	0.66 ± 0.03
39	218	$19.0 \leq Z \leq 29.0$	4.844	0.66 ± 0.03
40	159	$19.5 \leq Z \leq 29.5$	4.846	0.60 ± 0.04
41	153	$20.0 \leq Z \leq 30.0$	4.450	0.60 ± 0.04
42	144	$20.5 \leq Z \leq 30.5$	4.441	0.60 ± 0.04
43	159	$21.0 \leq Z \leq 31.0$	4.535	0.61 ± 0.04
44	148	$21.5 \leq Z \leq 31.5$	4.449	0.60 ± 0.04
45	151	$22 \leq Z \leq 32$	4.441	0.60 ± 0.04
46	151	$22.5 \leq Z \leq 32.5$	4.496	0.61 ± 0.04
47	165	$23.0 \leq Z \leq 33.0$	4.788	0.68 ± 0.04
48	140	$23.5 \leq Z \leq 33.5$	4.633	0.65 ± 0.04
49	141	$24.0 \leq Z \leq 34.0$	4.783	0.69 ± 0.05
50	133	$24.5 \leq Z \leq 34.5$	4.832	0.71 ± 0.05
51	292	$25.0 \leq Z \leq 35.0$	5.627	0.83 ± 0.04
52	285	$25.5 \leq Z \leq 35.5$	5.675	0.85 ± 0.04
53	293	$26.0 \leq Z \leq 36.0$	5.740	0.86 ± 0.04
54	289	$26.5 \leq Z \leq 36.5$	5.722	0.86 ± 0.04
55	372	$27.0 \leq Z \leq 37.0$	6.051	0.92 ± 0.04
56	330	$27.5 \leq Z \leq 29.5$	6.016	0.92 ± 0.04
57	331	$28.0 \leq Z \leq 38.0$	6.025	0.92 ± 0.04
58	329	$28.5 \leq Z \leq 38.5$	6.067	0.93 ± 0.04
59	328	$29.0 \leq Z \leq 39.0$	6.056	0.93 ± 0.04
60	326	$29.5 \leq Z \leq 39.5$	6.088	0.94 ± 0.04
61	327	$30.0 \leq Z \leq 40.0$	6.194	0.97 ± 0.04
62	326	$30.5 \leq Z \leq 40.5$	6.216	0.97 ± 0.04
63	330	$31.0 \leq Z \leq 41.0$	6.244	0.98 ± 0.04
64	316	$31.5 \leq Z \leq 41.5$	6.279	0.99 ± 0.05
65	31	5 $32.0 \leq Z \leq 42.0$	6.300	1.00 ± 0.05
66	312	$32.5 \leq Z \leq 42.5$	6.297	1.00 ± 0.05
67	311	$33.0 \leq Z \leq 43.0$	6.302	1.00 ± 0.05
68	290	$33.5 \leq Z \leq 43.5$	6.288	1.01 ± 0.05
69	291	$34.0 \leq Z \leq 44.0$	6.280	1.00 ± 0.05
70	283	$34.5 \leq Z \leq 44.5$	6.260	1.00 ± 0.05
71	282	$35.0 \leq Z \leq 45.0$	6.262	1.00 ± 0.05

72	122	$35.5 \leq Z \leq 45.5$	6.204	1.08 ± 0.07
73	123	$36.0 \leq Z \leq 46.0$	6.203	1.08 ± 0.07
74	114	$36.5 \leq Z \leq 46.5$	6.034	1.05 ± 0.07
75	117	$37.0 \leq Z \leq 47.0$	5.981	1.03 ± 0.07

As a function of depth, the *b*-value varies from 0.60 ± 0.04 to 1.08 ± 0.07, with an average value close to 0.82. Within the depth range of 0-10 km, the *b*-value is 1.01 ± 0.07. However, its value decreases to 0.60 ± 0.04 in the depth range of 22-32 km. For depths beyond 32 km, the *b*-value increases with increasing depth. It rises to 1.08 ± 0.07 for the depth range of 36-46 km (Table 7 and figure 17). The *b*-value showed a significant boundary around 32 km. The *b*-value above this depth displays a diminishing trend, and the *b*-value below this depth displays an ascending trend. Two peaks in *b*-value are observed in the depth range of 35.5-46 km, which may indicate areas of high crack density and/or elevated pore pressure.

The uppermost crust shows a higher value of *b* (1.01 ± 0.07). Some low *b*-value areas (around 0.60) within a depth range of 20-32 km could be the potential zone of future earthquakes. Higher *b*-value obtained for the uppermost crust agrees with this description of earthquake stability. Physical mechanism responsible for decreasing the *b*-value with increasing depth could be related with material heterogeneity and lithostatic stress condition in upper crust. Increase in *b*-value at greater depth (beyond 32 km) may indicate existence of pore fluid responsible to reduce the effective stress (Wyss & Stefansson, 2006).

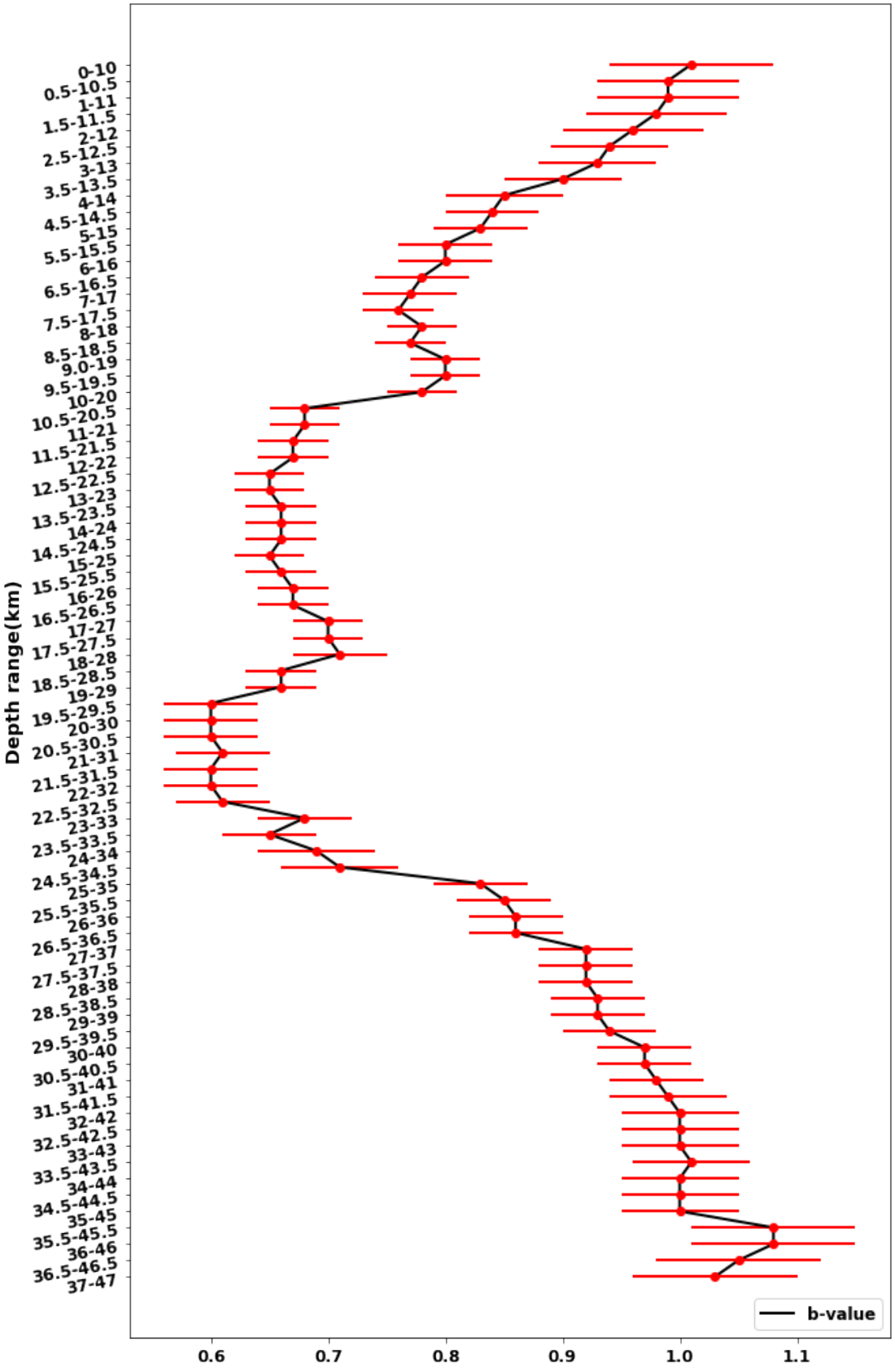

Figure 17: The b-value versus depth for the data. Horizontal bars represent the error-bars in b-value with 95% confidence limits using the maximum likelihood estimate.

4.1.5 *b*-value mapping in the region

The *b*-value contour map is prepared for the entire study area. The window size of 1°× 1° is set with moving step of 0.5° along the direction of latitude and results are presented in the table 8. Windows containing less than 50 events are excluded for the reliable estimation of *b*-value.

Table 8: Different window showing longitude range, latitude range, mean longitude, mean latitude and *b*-value

Window	Number of earthquakes	Lon.	Lat.	Mean long.	Mean lat.	*b*-value
1	56	80-81	28.80-29.80	80.5	29.30	0.61 ± 0.06
2	62	80-81	28.85-29.85	80.5	29.35	0.60 ± 0.06
3	68	80-81	28.90-29.90	80.5	29.40	0.58 ± 0.05
4	79	80-81	28.95-29.95	80.5	29.45	0.57 ± 0.05
5	80	80-81	29.00-30.00	80.5	29.50	0.57 ± 0.05
6	80	80-81	29.05-30.05	80.5	29.55	0.57 ± 0.05
7	81	80-81	29.10-30.10	80.5	29.60	0.57 ± 0.05
8	83	80-81	29.15-30.15	80.5	29.65	0.58 ± 0.05
9	85	80-81	29.20-30.20	80.5	29.70	0.59 ± 0.05
10	92	80-81	29.25-30.25	80.5	29.75	0.61 ± 0.05
11	94	80-81	29.30-30.30	80.5	29.80	0.60 ± 0.05
12	92	80-81	29.35-30.35	80.5	29.85	0.61 ± 0.05
13	89	80-81	29.40-30.40	80.5	29.90	0.60 ± 0.05
14	85	80-81	29.45-30.45	80.5	29.95	0.60 ± 0.05
15	82	80-81	29.50-30.50	80.5	30.0	0.60 ± 0.05
16	52	81-82	28.30-29.30	81.5	28.80	0.65 ± 0.06
17	67	81-82	28.35-29.35	81.5	28.85	0.64 ± 0.05
18	77	81-82	28.40-29.40	81.5	28.90	0.65 ± 0.05
19	87	81-82	28.45-29.45	81.5	28.95	0.63 ± 0.05
20	104	81-82	28.50-29.50	81.5	29.00	0.67 ± 0.05
21	116	81-82	28.55-29.55	81.5	29.05	0.64 ± 0.04
22	128	81-82	28.60-29.60	81.5	29.10	0.65 ± 0.04
23	130	81-82	28.65-29.65	81.5	29.15	0.65 ± 0.04
24	131	81-82	28.70-29.70	81.5	29.20	0.66 ± 0.04
25	132	81-82	28.75-29.75	81.5	29.25	0.64 ± 0.04
26	130	81-82	28.80-29.80	81.5	29.30	0.64 ± 0.04
27	128	81-82	28.85-29.85	81.5	29.35	0.64 ± 0.04
28	130	81-82	28.90-29.90	81.5	29.40	0.64 ± 0.04

29	127	81-82	28.95-29.95	81.5	29.45	0.64 ± 0.04
30	127	81-82	29.00-30.00	81.5	29.50	0.64 ± 0.04
31	126	81-82	29.05-30.05	81.5	29.55	0.64 ± 0.04
32	130	81-82	29.10-30.10	81.5	29.60	0.64 ± 0.04
33	125	81-82	29.15-30.15	81.5	29.65	0.65 ± 0.04
34	120	81-82	29.20-30.20	81.5	29.70	0.67 ± 0.05
35	118	81-82	29.25-30.25	81.5	29.75	0.71 ± 0.05
36	105	81-82	29.30-30.30	81.5	29.80	0.71 ± 0.06
37	91	81-82	29.35-30.35	81.5	29.85	0.74 ± 0.07
38	87	81-82	29.40-30.40	81.5	29.90	0.77 ± 0.07
39	80	81-82	29.45-30.45	81.5	29.95	0.84 ± 0.07
40	64	81-82	29.50-30.50	81.5	30.00	0.78 ± 0.09
41	56	84-85	27.20-28.20	84.5	27.70	0.73 ± 0.09
42	59	84-85	27.25-28.25	84.5	27.75	0.73 ± 0.08
43	61	84-85	27.30-28.30	84.5	27.80	0.71 ± 0.08
44	62	84-85	27.35-28.35	84.5	27.85	0.72 ± 0.08
45	63	84-85	27.40-28.40	84.5	27.90	0.72 ± 0.08
46	63	84-85	27.45-28.45	84.5	27.95	0.72 ± 0.08
47	64	84-85	27.50-28.50	84.5	28.00	0.71 ± 0.08
48	63	84-85	27.55-28.55	84.5	28.05	0.70 ± 0.07
49	63	84-85	27.60-28.60	84.5	28.10	0.70 ± 0.07
50	63	84-85	27.65-28.65	84.5	28.15	0.70 ± 0.07
51	62	84-85	27.70-28.70	84.5	28.20	0.70 ± 0.08
52	61	84-85	27.75-28.75	84.5	28.25	0.69 ± 0.07
53	56	84-85	27.80-28.80	84.5	28.30	0.69 ± 0.08
54	51	84-85	27.85-28.85	84.5	28.35	0.70 ± 0.08
55	59	85-86	26.70-27.70	85.5	27.20	1.01 ± 0.11
56	73	85-86	26.75-27.75	85.5	27.25	0.99 ± 0.09
57	91	85-86	26.80-27.80	85.5	27.30	0.97 ± 0.08
58	112	85-86	26.85-27.85	85.5	27.35	0.95 ± 0.07
59	129	85-86	26.90-27.90	85.5	27.40	0.98 ± 0.07
60	138	85-86	26.95-27.95	85.5	27.45	1.00 ± 0.07
61	145	85-86	27.00-28.00	85.5	27.50	1.01 ± 0.07
62	155	85-86	27.05-28.05	85.5	27.55	1.02 ± 0.07
63	158	85-86	27.10-28.10	85.5	27.60	1.01 ± 0.07
64	160	85-86	27.15-28.15	85.5	27.65	1.01 ± 0.07
65	159	85-86	27.20-28.20	85.5	27.70	1.04 ± 0.07

66	161	85-86	27.25-28.25	85.5	27.75	1.03 ± 0.07
67	164	85-86	27.30-28.30	85.5	27.80	1.02 ± 0.07
68	165	85-86	27.35-28.35	85.5	27.85	1.04 ± 0.07
69	162	85-86	27.40-28.40	85.5	27.90	1.03 ± 0.07
70	160	85-86	27.45-28.45	85.5	27.95	1.02 ± 0.07
71	155	85-86	27.50-28.50	85.5	28.00	1.03 ± 0.07
72	146	85-86	27.55-28.55	85.5	28.05	1.03 ± 0.08
73	143	85-86	27.60-28.60	85.5	28.10	1.00 ± 0.08
74	133	85-86	27.65-28.65	85.5	28.15	0.99 ± 0.08
75	118	85-86	27.70-28.70	85.5	28.20	0.97 ± 0.08
76	105	85-86	27.75-28.75	85.5	28.25	0.97 ± 0.09
77	88	85-86	27.80-28.80	85.5	28.30	1.00 ± 0.11
78	68	85-86	27.85-28.85	85.5	28.35	1.05 ± 0.13
79	51	85-86	27.90-28.90	85.5	28.40	1.00 ± 0.14
80	53	86-87	26.70-27.70	86.5	27.20	0.66 ± 0.08
81	60	86-87	26.75-27.75	86.5	27.25	0.71 ± 0.07
82	62	86-87	26.80-27.80	86.5	27.30	0.67 ± 0.07
83	64	86-87	26.85-27.85	86.5	27.35	0.65 ± 0.07
84	65	86-87	26.90-27.90	86.5	27.40	0.65 ± 0.07
85	66	86-87	26.95-27.95	86.5	27.45	0.67 ± 0.07
86	66	86-87	27.00-28.00	86.5	27.50	0.67 ± 0.07
87	64	86-87	27.05-28.05	86.5	27.55	0.70 ± 0.07
88	64	86-87	27.10-28.10	86.5	27.60	0.71 ± 0.08
89	63	86-87	27.15-28.15	86.5	27.65	0.71 ± 0.08
90	63	86-87	27.20-28.20	86.5	27.70	0.72 ± 0.08
91	60	86-87	27.25-28.25	86.5	27.75	0.73 ± 0.08
92	62	86-87	27.30-28.30	86.5	27.80	0.73 ± 0.08
93	61	86-87	27.35-28.35	86.5	27.85	0.74 ± 0.09
94	59	86-87	27.40-28.40	86.5	27.90	0.72 ± 0.08
95	62	86-87	27.45-28.45	86.5	27.95	0.73 ± 0.08
96	65	86-87	27.50-28.50	86.5	28.00	0.75 ± 0.09
97	66	86-87	27.55-28.55	86.5	28.05	0.82 ± 0.10
98	61	86-87	27.60-28.60	86.5	28.10	0.84 ± 0.11
99	52	86-87	27.65-28.65	86.5	28.15	0.86 ± 0.12
100	55	87-88.2	26.80-27.80	87.6	27.30	0.65 ± 0.07
101	59	87-88.2	26.85-27.85	87.6	27.35	0.62 ± 0.07
102	61	87-88.2	26.90-27.90	87.6	27.40	0.63 ± 0.07

103	65	87-88.2	26.95-27.95	87.6	27.45	0.64 ± 0.07
104	71	87-88.2	27.00-28.00	87.6	27.50	0.67 ± 0.07
105	77	87-88.2	27.05-28.05	87.6	27.55	0.70 ± 0.07
106	79	87-88.2	27.10-28.10	87.6	27.60	0.69 ± 0.07
107	88	87-88.2	27.15-28.15	87.6	27.65	0.70 ± 0.07
108	89	87-88.2	27.20-28.20	87.6	27.70	0.69 ± 0.06
109	90	87-88.2	27.25-28.25	87.6	27.75	0.69 ± 0.06
110	88	87-88.2	27.30-28.30	87.6	27.80	0.68 ± 0.06
111	90	87-88.2	27.35-28.35	87.6	27.85	0.72 ± 0.07
112	97	87-88.2	27.40-28.40	87.6	27.90	0.78 ± 0.07
113	100	87-88.2	27.45-28.45	87.6	27.95	0.81 ± 0.08
114	95	87-88.2	27.50-28.50	87.6	28.00	0.82 ± 0.08
115	95	87-88.2	27.55-28.55	87.6	28.05	0.83 ± 0.08
116	97	87-88.2	27.60-28.60	87.6	28.10	0.84 ± 0.08
117	98	87-88.2	27.65-28.65	87.6	28.15	0.82 ± 0.08
118	100	87-88.2	27.70-28.70	87.6	28.20	0.81 ± 0.08
119	100	87-88.2	27.75-28.75	87.6	28.25	0.83 ± 0.08
120	95	87-88.2	27.80-28.80	87.6	28.30	0.84 ± 0.08
121	92	87-88.2	27.85-28.85	87.6	28.35	0.87 ± 0.08
122	89	87-88.2	27.90-28.90	87.6	28.40	0.89 ± 0.09
123	84	87-88.2	27.95-28.95	87.6	28.45	0.88 ± 0.09
124	79	87-88.2	28.00-29.00	87.6	28.50	0.83 ± 0.09
125	72	87-88.2	28.05-29.05	87.6	28.55	0.81 ± 0.09
126	71	87-88.2	28.10-29.10	87.6	28.60	0.81 ± 0.09
127	62	87-88.2	28.15-29.15	87.6	28.65	0.81 ± 0.09
128	59	87-88.2	28.20-29.20	87.6	28.70	0.79 ± 0.09
129	57	87-88.2	28.25-29.25	87.6	28.75	0.81 ± 0.10
130	54	87-88.2	28.30-29.30	87.6	28.80	0.82 ± 0.10
131	50	87-88.2	28.95-29.95	87.6	29.45	0.93 ± 0.11
132	64	87-88.2	29.00-30.00	87.6	29.50	0.99 ± 0.09
133	79	87-88.2	29.05-30.05	87.6	29.55	1.03 ± 0.09
134	101	87-88.2	29.10-30.10	87.6	29.60	1.00 ± 0.08
135	110	87-88.2	29.15-30.15	87.6	29.65	1.01 ± 0.07
136	120	87-88.2	29.20-30.20	87.6	29.70	1.03 ± 0.07
137	128	87-88.2	29.25-30.25	87.6	29.75	1.01 ± 0.07
138	138	87-88.2	29.30-30.30	87.6	29.80	0.99 ± 0.06
139	147	87-88.2	29.35-30.35	87.6	29.85	0.95 ± 0.06

140	150	87-88.2	29.40-30.40	87.6	29.90	0.96 ± 0.06
141	152	87-88.2	29.45-30.45	87.6	29.95	0.96 ± 0.06
142	150	87-88.2	29.50-30.50	87.6	30.00	0.96 ± 0.06

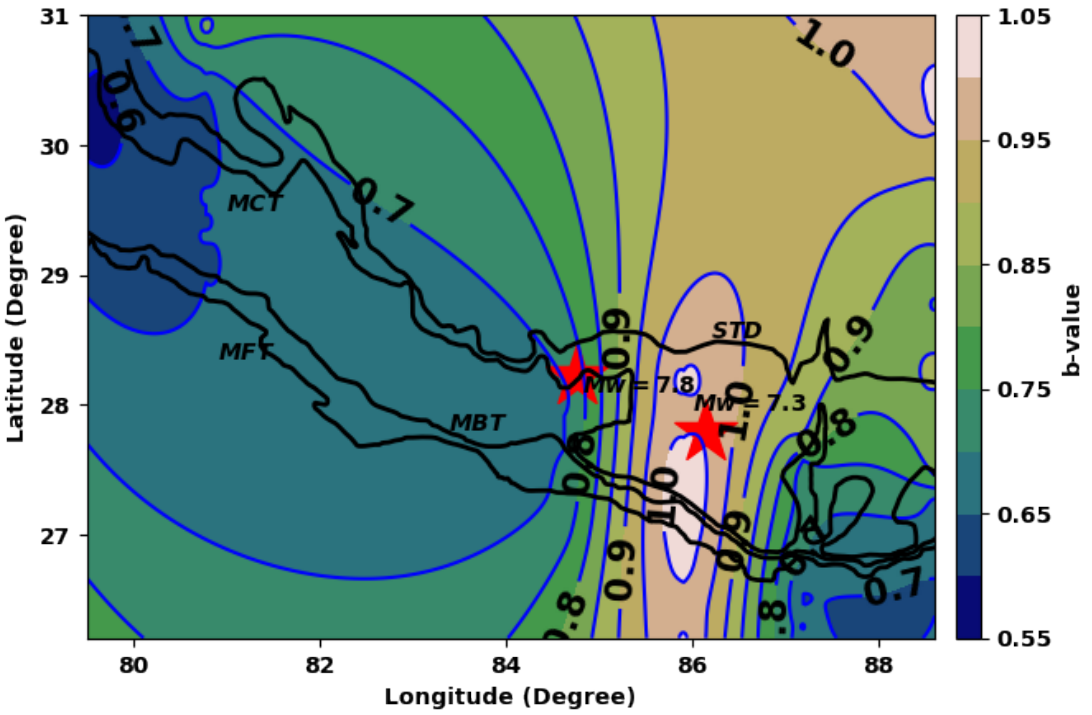

Figure 18: *b*-value contour map of the region of study. Two red stars stands for the epicenter location of 25th April 2015 Gorkha earthquake and 12th May Kodari earthquake

Upon initial examination of the *b*-value map, two regions of low *b*-values ($b \leq 0.7$ in blue) are observed, located to the west and east of the area affected by the 2015 earthquakes. These areas overlap with the zone of the major faults MBT, MCT, MFT in western Nepal. The eastern low *b*-value area is smaller than the western low *b*-value area which indicates that differential stress on asperities in the western part is higher than that in the eastern part. The western and the eastern low *b*-value areas sandwiched the zones of Gorkha-Kodari earthquake zone where *b*-values are relatively high ($\sim 0.9 - 1.0$). The existence of the high *b*-value area between two low *b*-value patches is unique, reflecting the segmented nature of the plate interface and could be the warning of impending two separate megathrust earthquakes. Low *b*-values have been correlated with locked part of a fault or areas of asperity as mentioned in past literature (Fan & Shearer, 2015; Sreejith et al., 2018; J. Yin et al., 2017), from where the nucleation of earthquakes is likely to happen.

4.1.6 *b*-value variation along transverse faults

The primary cluster of aftershocks is observed along the faults that originate in the footwall (lower side) of MHT and extend up to the hanging wall. These faults include Judi Fault or Lineament (JF or JL), Thaple Fault or Lineament (TF or TL), Kathmandu Fault or Lineament (KTMF or KTML), Motihari-GauriShanker Fault or Lineament (MGF or MGL), and Motihari-Everest Fault or Lineament (MEF or MEL) (Figure 19). The Gaurishankar transverse fault separates the ruptures of April 25 and May 12 at the eastern limit and at the western boundary the Judi transverse fault demarcates the main rupture from the nucleation area. Consequently, it may be claimed that transversal faults in the Himalaya governed the rupture progression during the 2015 earthquake (Mugnier et al., 2017; R. Tiwari et al., 2022).

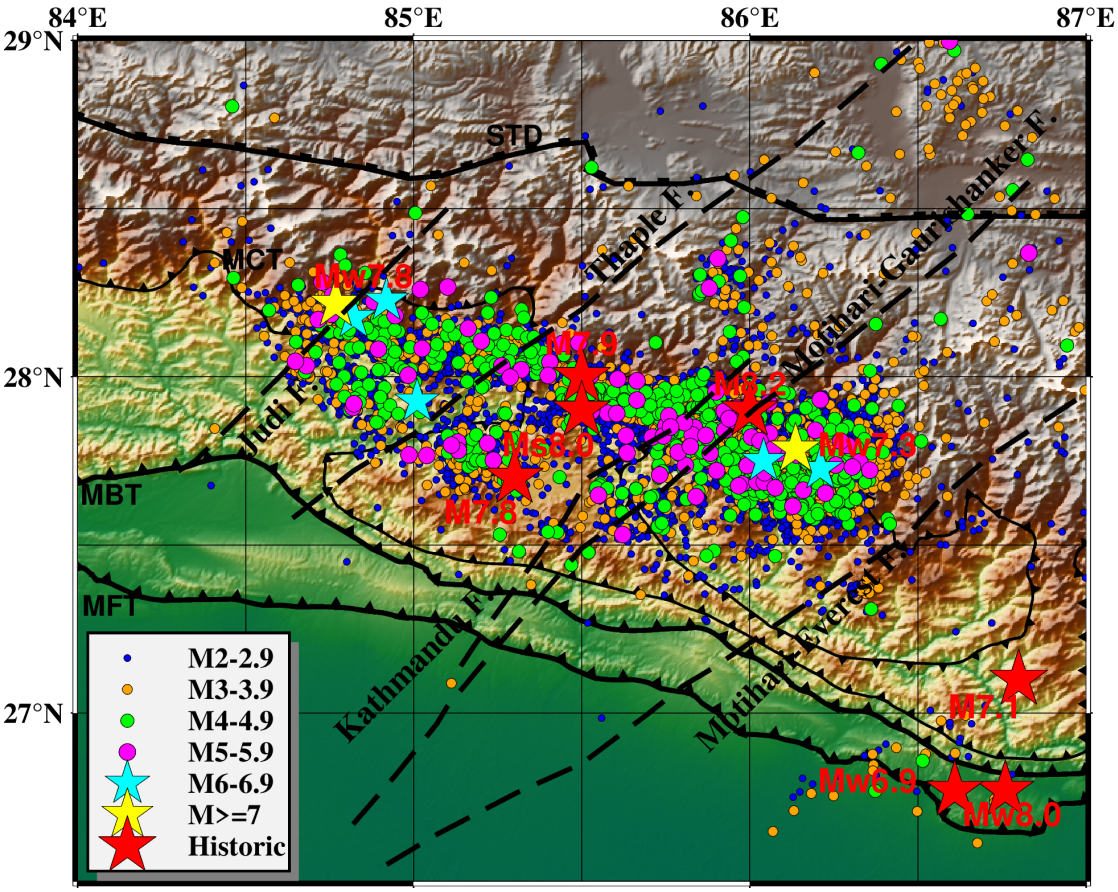

Figure 19: A map showing the 10500 earthquake events (ML ≥2.0). MCT, MBT, MFT, and STD are major thrust of the Himalaya. Historical major earthquakes in the region are shown by red stars. The Gorkha earthquake (ML 7.7) and the Kodari earthquake (ML 7.0) are represented by yellow stars. The dashed black lines represent aforementioned transverse faults (Dasgupta et al., 1987; R. Tiwari et al., 2022)

To understand the fall and rise in the *b*-value of aftershocks sequences of the 25 April 2015 Gorkha earthquake, an area of fixed-width 20 km and different length is considered along the aforementioned faults. A sharp rise and fall in the *b*-value was observed over

a span of a week along the JF, with a value of 0.76 on 12 August 2015 and a value of 0.67 on 18 August 2015. After September 2015, it settles between 0.75 and 0.8. The fluctuation of b with depth shows the lowest value ($\sim 0.26 - 0.27$) below 10 km, possibly reflecting the accumulation of stress around that depth. A seemingly cyclical variation in b-value was observed for the area along the TF, with a peaked on September 1 at 0.97. The b-value (~ 0.39) was estimated at a depth of around 13 km while the smallest value of b (~ 0.23) was estimated around a depth of 10 km, which may be an indication of the stress concentration at this depth. A similar, nearly cyclic variation in the b-value was observed for the region around the KTMF, but with a declining pattern. The minimum value of b (0.55) was observed on January 29 and the maximal value of b (1.10) was noticed on June 7. The b-value (~ 0.38) was estimated at a depth of 15 km and the smallest b-value (< 0.2) was adjudged at a depth of 10 km, indicating that stress had accumulated close to this depth.

A month-long period (from June 22 to July 22) saw a substantial change in the b-value along the MGF between 0.42 and 1.22. After that, there was a little decline in the value of b. The b-value varied from 0.3 to 0.55 between depths of 10 km and 17 km. The smallest b-value, around 0.2, was observed at a depth of around 10 km, indicating the area of greatest stress within this depth range. There was a sharp rise and fall in the value of b along the MEF zone. Between September 7 and September 14, 2015, there was volatility between 0.74 and 0.67; after that, it appeared to be constant at around 0.7. The b-value was at its lowest limit (~ 0.30) at a depth of ~7 km. The release of strain from this region is in step-wise pattern as indicated by the cumulative moment release curve (R. Tiwari et al., 2022) (Figure 20)

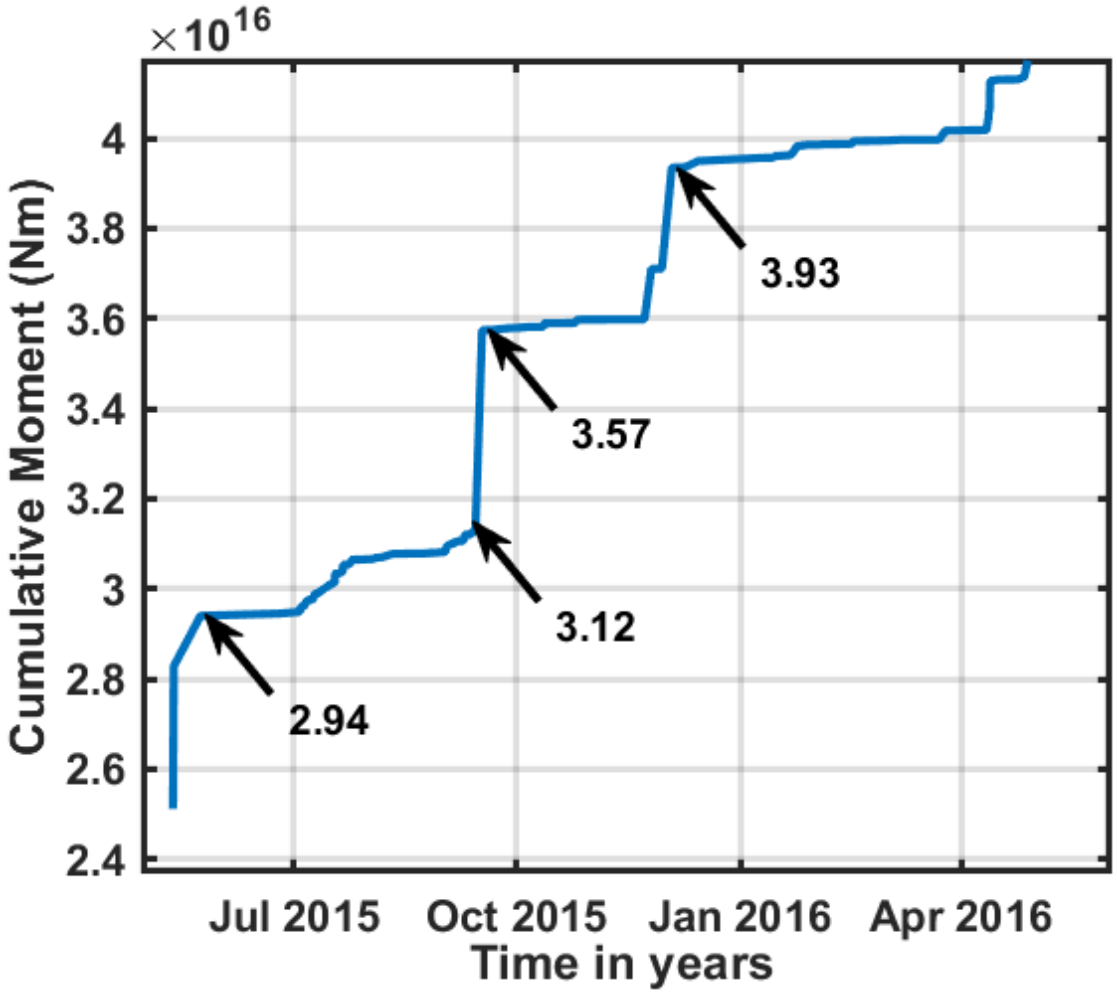

Figure 20: Variation of cumulative seismic moment release as a function of time for the area along MEF (R. Tiwari et al., 2022)

.

Although, the *b*-values range between 0.45 and 0.69 do not match up to the global mean value of 1.0, they can be justified for the aftershocks. These values correlate with the thrust type of faulting and signify the asperities (fault locked area) found in the region (Schorlemmer et al., 2005; Wyss et al., 2004). The small *b*-values, specifically 0.45 ± 0.02 and 0.55 ± 0.4 for area along JF and MEF, respectively suggest the high stress level in those area, capable of hosting two separate major earthquakes as mentioned in the past literature (Yagi & Okuwaki, 2015; Sreejith et al., 2018). The cumulative moment curve also shows the lowest value of the strain energy (of the order 10^{16}) is released from the MEF fault area compared to other four areas. The outcomes of this study is comparable with preceding works. The preceding studies reported *b*-value 0.75 ± 0.03 (Chingtham et al., 2016), 0.93 (Thapa et al., 2018), and 0.78 ± 0.08 (R. Tiwari & Paudyal, 2021b) for the 2015 earthquakes in Gorkha region and Kodari region.

4.2 Multifractality in Aftershocks Sequence of the 2015 Gorkha Earthquake

4.2.1 Multifractal analysis

The earth is a heterogeneous medium due to its complex distribution of physical properties, leading to chaotic behavior in many natural phenomena, such as earthquakes. Predictive analysis of these chaotic movements can only be done over limited time periods. The reason is that they lose their information exponentially (Aggarwal et al., 2017; Posadas et al., 2005). When a strong earthquake occurs, the background seismicity gets perturbed from the equilibrium state that results in the remarkably diverse distribution of aftershocks in both space and time. The perturbation in stress is responsible for the increased seismicity after the mainshock (Bak et al., 2002). The distribution of the earthquakes is not uniform or random rather cluster in magnitude, space, and time (Gutenberg & Richter, 1950; Tosi, 1998; Telesca et al., 2001). The fractal/multifractal distribution of earthquakes in space and time can be scaled by the power law behavior both regionally and globally (Dimri et al., 2005; Dimri & Srivastava, 2015). Multifractal theory that proceeds with the description of the spectrum of the generalized fractal dimensions (D_q) can characterize the temporal and spatial variations of earthquake phenomena in a fully quantitative fashion over a wide range of scales (Pastén & Comte, 2014; Posadas et al., 2005). The complexity of the system is determined by the shape and the variability of the fractal dimension spectrum.

$D_{+\infty}$ is the lower bound and $D_{-\infty}$ is the upper bound of multifractal spectrum and they carry the information about the most strong and the least strong bunching of the seismicity, respectively. Capacity dimension or box counting dimension, correlation dimension etc., can be easily retrieved from the spectrum ($D_q - q$ curve) and the variations of their characteristics contain information about evolution of the system towards main rupture. The slope of $D_q - q$ spectrum has a gentle type and a steep type of variation. For the extended distribution of the earthquake, the curve becomes gentle and for clustered type of the distribution it shows steepness. The steep part of the curve corresponds to an intensely heterogeneous multifractal, which appears during seismic swarm. The negative value of D_q has higher sensitivity to the variation in fractal structure of earthquakes compared to D_q for $q \geq 2$ and can possess a value even larger than the spatial dimension d, so $D_q > d$ does not have geometric sense (Hirabayashi et al., 1992; Mandelbrot, 1989). The 10,500 earthquakes used in the multifractal analysis within the latitude range of 25.22°N to 30.15°N and longitude range of 81.77°E to 90.41°E, from April 25th, 2015 to June 14th, 2015, are shown as a distribution graph in Figure 21. The 3D distribution of these earthquakes is presented in figure 22.

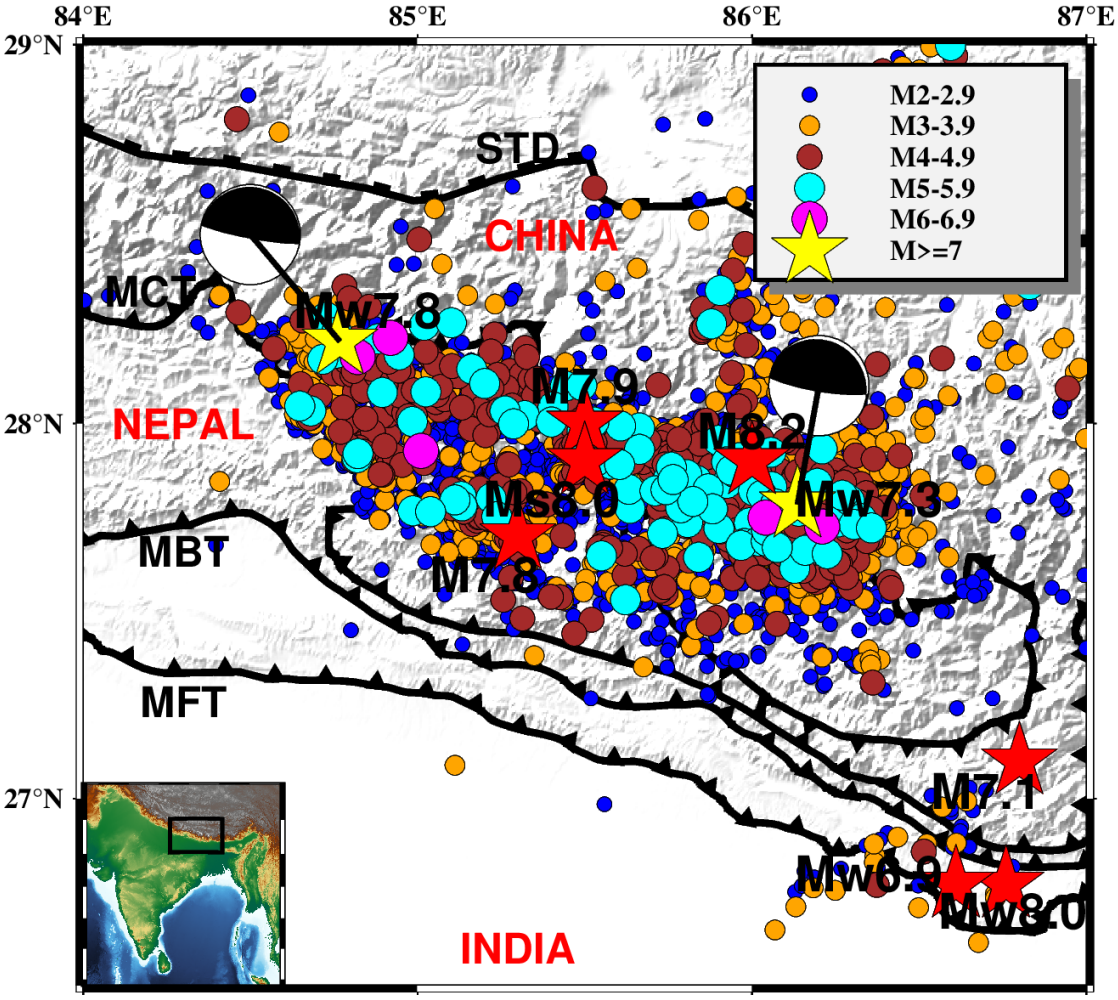

Figure 21: Distribution of the earthquakes in the study region. For clear visualization of the image the study region between 84°–87°E and 26.5°–29°N is only depicted. The black box in the inset map indicates the study area in details. The two yellow stars stand for Gorkha earthquake and Dolakha or Kodari earthquake. The focal mechanism solutions of these earthquakes indicate the low angle thrust faulting nature. The red stars are for the historic earthquakes in the study region. The major faults of the region are depicted by solid black lines as MCT, MBT, MFT. The map is plotted by the software GMT (Generic Mapping Tools) (Wessel et al., 2013)

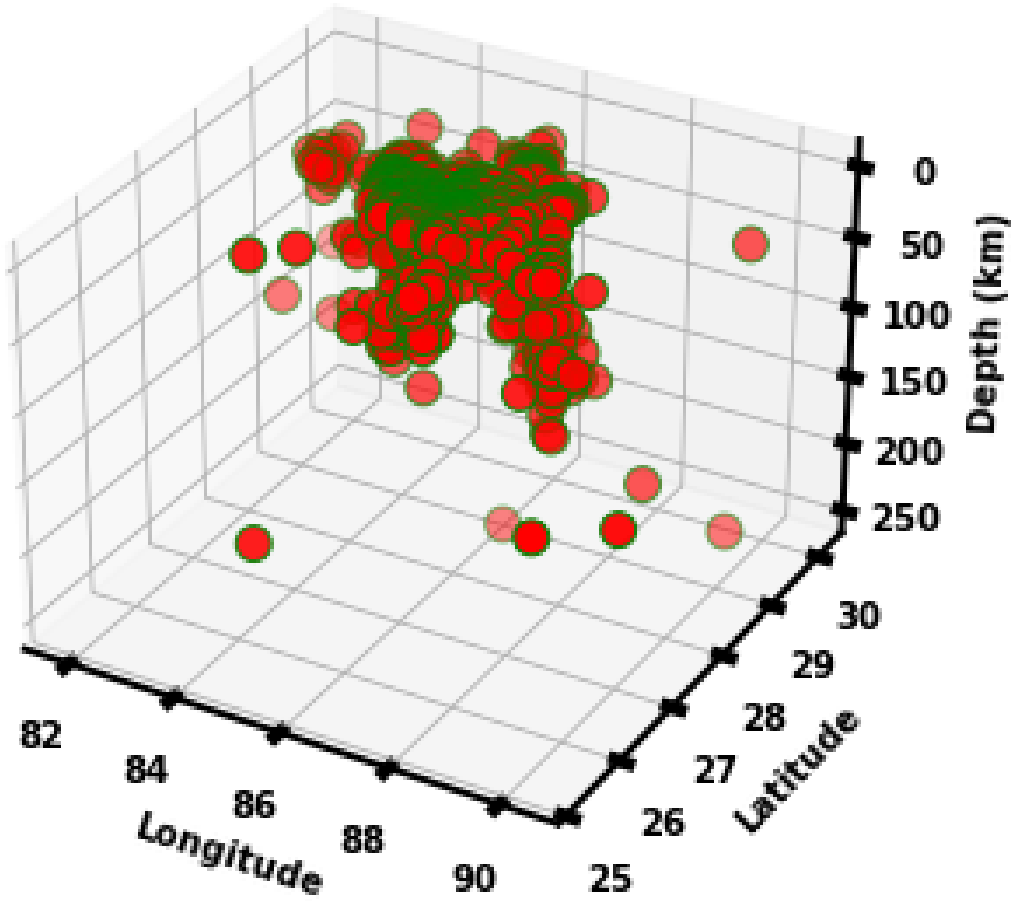

Figure 22: Distribution of the earthquakes based on the longitude, latitude and depth showing the clustering of earthquakes in the study area.

The completeness of database is checked by the maximum curvature technique in the software ZMAP (Wiemer, 2001) and found to be 2.0. The *b*-value estimation is done through the maximum likelihood method (Aki, 1965) and found to be 0.61 ± 0.01 (Figure 23).

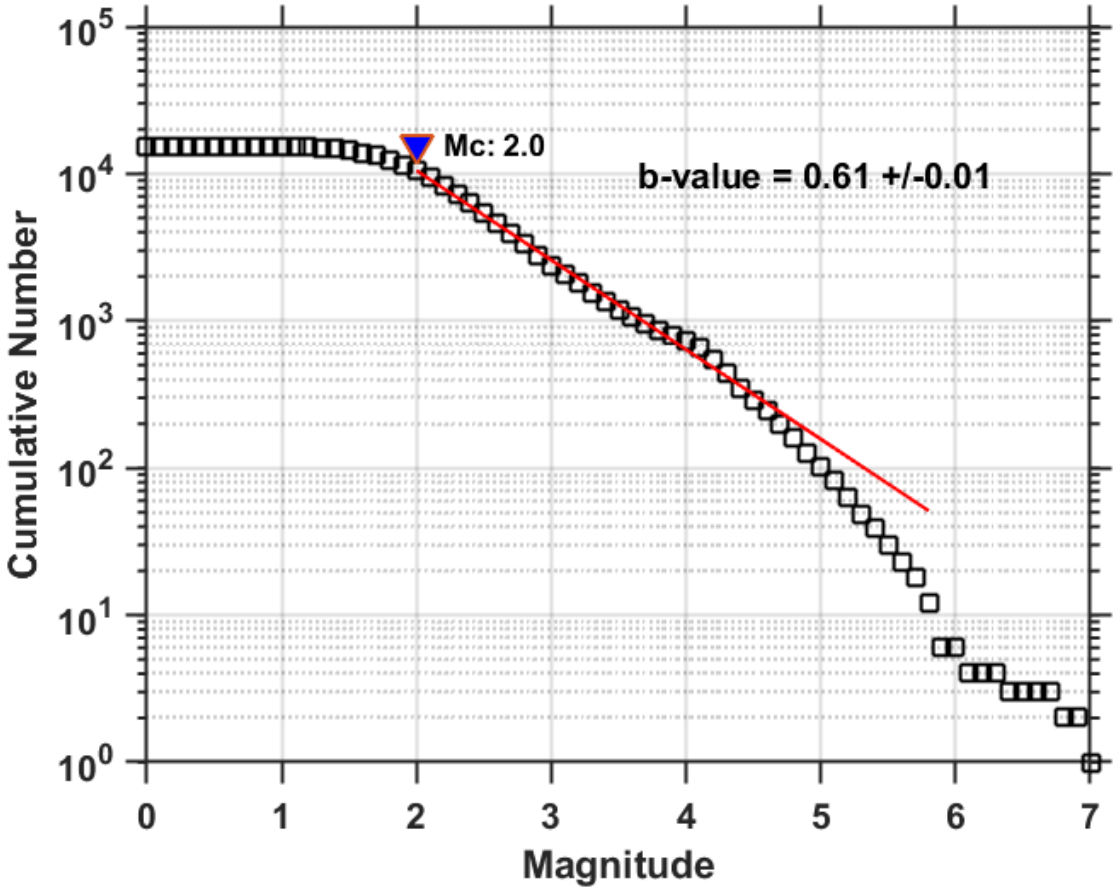

Figure 23: Magnitude of completeness and b-value of the dataset prepared for the study.

4.2.2 Multifractal spectrum

For the study of the aftershocks occurring in a short period, a longer time span (time window) is crucial condition for dependable assessment of D_q and it is mentioned that the larger number of events helps to get the smoother variation of the measured parameter (Lei, 2019). In a multifractal analysis, the number of points in a sample window should be as large as possible and should not less than 200 (Hui et al., 2020; L. Yin et al., 2019). With the small sample size, computed value of the fractal dimension may give pseudo-multifractal characteristics. After several tests, the moving windows with a constant number of epicenters (500) are taken to guarantee the precise estimation of the fractal dimensions. Multifractal spectrum ($D_q - q$) analysis was thus carried out for a running window of 500 earthquakes (D. Li et al., 1994; Monterrubio et al., 2020) which shifts forward by one fifth of the window length i.e., with a sliding window of 100 events overlaid by 400 events on 10500 earthquakes of magnitude of completeness ($Mc = 2.0$) in local scale.

The scaling range is chosen between depopulation and saturation and it is adjusted by searching the linear portion in the plot of $\log C_q(r)$ versus $\log r$ by means of the linear regression technique in Python language. For the large values of $|q|$, the multifractal

spectrum shows asymptotic behavior and this restricts the selection of the values of q. The previous works are found for both positive and negative values of q. For example, q = -6 to +6 (Teotia & Kumar, 2011), $|q|$ = 15 (Oncel & Wilson, 2006) and taking only positive values of q from 0 to 20 for 2001 Bhuj earthquake (Aggarwal et al., 2017) etc. The upper and lower value of the weighting factor q in this work is adjusted based on the saturation of D_q value, the final range of q is set from -10 to 22 with a step size of 2 (Lin & Wu, 2012; Y.-J. Tang et al., 2012).

4.2.3 Variation of fractal dimension

An infinite number of singularities are normally found in any fractal measure so the multifractal structure can be exemplified by the chain of cross-connected subsets in which particular fractal dimension depends on the singularities that describe them. So, one needs to rely on generalized dimensions (D_q). In the spectrum of D_q, q shows an asymptotic behavior for both positive and negative values of the infinity and the fractal dimensions $D_{-\infty}$ and $D_{+\infty}$ are correspondingly linked to the utmost and lowest values of the measure (Monterrubio et al., 2020). The difference of two extreme generalized dimensions $D_{-\infty}$ - $D_{+\infty}$ indicates the heterogeneity of the investigated structure (D. Li et al., 1994) while the values of the D_q express the grade of heterogeneity at diverse scales in the system of faults (Nampally et al., 2018; Öncel et al., 1996).

If D_q is a constant for all q, then the system of faults is monofractal. When D_q changes with q reflecting a different epicenter density within the fault system then the fault system is multifractal nature. Therefore, the D_q curves are representative of the strength of the multifractality of the structure. The more constant the plot is, the weaker the multifractality is known to be. Although we have calculated the dimension from q = -10 to q = 22, the fractal dimension values D_2, D_0 and D_{-2} are only presented for all 101 windows in table 9. The variation of generalized fractal dimension with temporal windows for negative value of q (from q = -10 to -2) is shown in figure 25 and for positive values of q (from q = 0 to q = 22) is depicted in figure 26.

The spectrum of the generalized fractal dimension or ($D_q - q$) curve reveals the multifractal structure (Figure 27). For the purpose of simplicity, we have only presented the fractal dimension curve for temporal windows 1, 2, 3, 4, and 5, which cover the period from April 25, 2015 to June 30, 2015. The values of D_0, D_2, and D_{-2} have different ranges from 2015-04-25 to 2016-05-15. The range of D_0 is from 0.84 ± 0.07 to 2.39 ± 0.03, the range of D_2 is from 1.11 ± 0.04 to 1.38 ± 0.03, and the range of D_{-2} is from 0.35 ± 0.02 to 11.28 ± 0.02. The lower value of D_2 obtained for the region shows that the fracture distribution is tending to fill a two-dimensional space through primary and secondary faulting (Teotia et al., 1997). The temporal variation of dimension from $D_2 - D_{22}$ shows periodic nature. The existence of this type of variation may be due to

the predominance of asperity/barrier in the central Himalaya region and the associated growth and release of stress or may be because of the clustering and declustering of earthquake. The amount of seismic energy release after Gorkha earthquake and Kodari earthquake as presented in figure 28 also supports this facts. It should be noticed that 3.30×10^{20} Nm and 3.74×10^{20} Nm energy gets released through the respective events. The existence of asperities/barriers as stress-controlling mechanisms has been supported by past studies to explain the fractal structure of earthquake distribution and high energy release in intra-plate earthquakes like the Gorkha event. Examples of such studies include those conducted in the northwest to northeast Himalayas (Jena et al., 2021), the Kachchh region of Gujarat (Roy & Ram, 2006), and the Garhwal–Kumaun region of Himalaya (A. Tiwari et al., 2021).

Table 9: The temporal windows describing number of events, their occurrence period along with fractal dimension for q = -2, q = 0, q = 2 and their standard deviations.

Window	Number of earthquakes	Period	D_{-2}	D_0	D_2
1	0-500	2015-04-25-2015-05-22	6.10 ± 0.05	1.42 ± 0.07	1.38 ± 0.03
2	100-600	2015-04-25-2015-06-25	8.56 ± 0.11	1.57 ± 0.07	1.33 ± 0.04
3	200-700	2015-04-26-2015-06-27	7.90 ± 0.06	1.56 ± 0.08	1.31 ± 0.04
4	300-800	2015-04-30-2015-06-29	6.13 ± 0.02	1.43 ± 0.07	1.26 ± 0.05
5	400-900	2015-05-12-2015-06-30	6.12 ± 0.08	1.48 ± 0.06	1.27 ± 0.05
6	500-1000	2015-05-22-2015-07-01	3.63 ± 0.00	1.52 ± 0.02	1.32 ± 0.04
7	600-1100	2015-06-25-2015-07-02	6.27 ± 0.02	1.55 ± 0.05	1.30 ± 0.04
8	700-1200	2015-06-27-2015-07-03	5.11 ± 0.01	1.41 ± 0.02	1.28 ± 0.04
9	800-1300	2015-06-29-2015-07-04	3.44 ± 0.11	1.64 ± 0.04	1.26 ± 0.04
10	900-1400	2015-06-30-2015-07-06	3.64 ± 0.09	1.66 ± 0.05	1.24 ± 0.04
11	1000-1500	2015-07-01-2015-07-06	7.39 ± 0.16	1.61 ± 0.07	1.20 ± 0.04
12	1100-1600	2015-07-02-2015-07-07	4.05 ± 0.07	1.34 ± 0.04	1.17 ± 0.04
13	1200-1700	2015-07-03-2015-07-09	3.42 ± 0.05	1.38 ± 0.04	1.20 ± 0.04
14	1300-1800	2015-07-04-2015-07-10	3.04 ± 0.05	1.30 ± 0.02	1.22 ± 0.04
15	1400-1900	2015-07-06-2015-07-11	3.04 ± 0.05	1.32 ± 0.04	1.23 ± 0.04
16	1500-2000	2015-07-06-2015-07-12	4.14 ± 0.12	1.46 ± 0.04	1.26 ± 0.03
17	1600-2100	2015-07-07-2015-07-13	4.63 ± 0.07	1.72 ± 0.03	1.31 ± 0.03
18	1700-2200	2015-07-09-2015-07-14	5.29 ± 0.11	1.68 ± 0.03	1.33 ± 0.03
19	1800-2300	2015-07-10-2015-07-16	10.75 ± 0.06	1.45 ± 0.10	1.33 ± 0.03
20	1900-2400	2015-07-11-2015-07-17	8.58 ± 0.04	1.34 ± 0.09	1.32 ± 0.03
21	2000-2500	2015-07-12-2015-07-18	3.47 ± 0.06	1.95 ± 0.06	1.34 ± 0.03
22	2100-2600	2015-07-13-2015-07-20	8.65 ± 0.06	1.21 ± 0.01	1.32 ± 0.03

23	2200-2700	2015-07-14-2015-07-21	9.24 ± 0.05	1.21 ± 0.02	1.31 ± 0.04
24	2300-2800	2015-07-16-2015-07-23	3.20 ± 0.04	1.43 ± 0.06	1.30 ± 0.04
25	2400-2900	2015-07-14-2015-07-24	3.50 ± 0.07	1.20 ± 0.04	1.17 ± 0.05
26	2500-3000	2015-07-18-2015-07-25	4.25 ± 0.05	1.13 ± 0.05	1.27 ± 0.04
27	2600-3100	2015-07-20-2015-07-27	7.77 ± 0.04	1.10 ± 0.05	1.23 ± 0.04
28	2700-3200	2015-07-21-2015-07-29	3.70 ± 0.05	1.19 ± 0.05	1.23 ± 0.04
29	2800-3300	2015-07-23-2015-07-30	3.87 ± 0.06	1.04 ± 0.05	1.23 ± 0.04
30	2900-3400	2015-07-24-2015-08-01	0.49 ± 0.05	1.00 ± 0.05	1.21 ± 0.04
31	3000-3500	2015-07-25-2015-08-02	5.80 ± 0.11	1.75 ± 0.09	1.20 ± 0.04
32	3100-3600	2015-07-27-2015-08-03	6.09 ± 0.10	0.91 ± 0.07	1.23 ± 0.04
33	3200-3700	2015-07-29-2015-08-05	0.68 ± 0.01	0.84 ± 0.07	1.21 ± 0.05
34	3300-3800	2015-07-30-2015-08-07	0.60 ± 0.02	0.85 ± 0.06	1.24 ± 0.04
35	3400-3900	2015-08-01-2015-08-09	2.42 ± 0.05	0.99 ± 0.06	1.26 ± 0.04
36	3500-4000	2015-08-02-2015-08-10	0.94 ± 0.08	1.39 ± 0.04	1.27 ± 0.04
37	3600-4100	2015-08-03-2015-08-13	0.35 ± 0.02	1.10 ± 0.03	1.25 ± 0.04
38	3700-4200	2015-08-05-2015-08-15	3.26 ± 0.08	0.95 ± 0.04	1.27 ± 0.03
39	3800-4300	2015-08-07-2015-08-17	2.26 ± 0.05	1.11 ± 0.06	1.24 ± 0.04
40	3900-4400	2015-08-09-2015-08-19	2.20 ± 0.05	1.21 ± 0.07	1.26 ± 0.04
41	4000-4500	2015-08-10-2015-08-21	4.58 ± 0.05	1.03 ± 0.12	1.26 ± 0.05
42	4100-4600	2015-08-13-2015-08-24	3.91 ± 0.06	2.19 ± 0.02	1.26 ± 0.05
43	4200-4700	2015-08-15-2015-08-26	4.02 ± 0.05	2.28 ± 0.02	1.24 ± 0.05
44	4300-4800	2015-08-17-2015-08-29	1.50 ± 0.04	1.25 ± 0.08	1.24 ± 0.05
45	4400-4900	2015-08-19-2015-09-01	4.34 ± 0.03	1.43 ± 0.08	1.22 ± 0.05
46	4500-5000	2015-08-21-2015-09-03	4.27 ± 0.06	1.22 ± 0.02	1.21 ± 0.05
47	4600-5100	2015-08-24-2015-09-06	2.64 ± 0.12	1.17 ± 0.06	1.24 ± 0.05
48	4700-5200	2015-08-26-2015-09-08	2.34 ± 0.08	1.41 ± 0.06	1.27 ± 0.04
49	4800-5300	2015-08-29-2015-09-11	0.65 ± 0.03	0.95 ± 0.09	1.30 ± 0.04
50	4900-5400	2015-09-01-2015-09-14	2.25 ± 0.04	1.22 ± 0.09	1.30 ± 0.03
51	5000-5500	2015-09-03-2015-09-16	3.54 ± 0.05	1.27 ± 0.08	1.31 ± 0.03
52	5100-5600	2015-09-06-2015-09-19	4.83 ± 0.06	1.29 ± 0.09	1.28 ± 0.04
53	5200-5700	2015-09-08-2015-09-22	4.99 ± 0.05	1.21 ± 0.08	1.27 ± 0.04
54	5300-5800	2015-09-11-2015-09-25	5.83 ± 0.04	1.25 ± 0.07	1.26 ± 0.04
55	5400-5900	2015-09-14-2015-09-28	2.20 ± 0.06	1.21 ± 0.06	1.26 ± 0.06
56	5500-6000	2015-09-16-2015-10-01	5.17 ± 0.35	1.29 ± 0.09	1.27 ± 0.04
57	5600-6100	2015-09-19-2015-10-03	3.13 ± 0.04	1.18 ± 0.07	1.29 ± 0.04
58	5700-6200	2015-09-22-2015-10-06	6.81 ± 0.09	1.18 ± 0.05	1.31 ± 0.04
59	5800-6300	2015-09-25-2015-10-09	6.51 ± 0.03	1.95 ± 0.07	1.32 ± 0.04

60	5900-6400	2015-09-28-2015-10-12	3.30 ± 0.04	1.26 ± 0.05	1.35 ± 0.04
61	6000-6500	2015-10-01-2015-10-15	3.05 ± 0.02	1.25 ± 0.06	1.32 ± 0.04
62	6100-6600	2015-10-03-2015-10-19	1.97 ± 0.02	1.30 ± 0.05	1.32 ± 0.04
63	6200-6700	2015-10-06-2015-10-22	2.13 ± 0.03	1.30 ± 0.05	1.32 ± 0.03
64	6300-6800	2015-10-09-2015-10-25	5.40 ± 0.07	1.18 ± 0.06	1.30 ± 0.03
65	6400-6900	2015-10-12-2015-10-28	10.45 ± 0.10	1.14 ± 0.09	1.30 ± 0.03
66	6500-7000	2015-10-16-2015-11-01	11.28 ± 0.12	1.14 ± 0.08	1.32 ± 0.03
67	6600-7100	2015-10-19-2015-11-05	11.02 ± 0.13	1.16 ± 0.10	1.33 ± 0.03
68	6700-7200	2015-10-22-2015-11-09	11.02 ± 0.02	1.21 ± 0.09	1.35 ± 0.03
69	6800-7300	2015-10-25-2015-11-13	7.29 ± 0.04	1.29 ± 0.09	1.38 ± 0.03
70	6900-7400	2015-10-28-2015-11-16	7.56 ± 0.07	1.77 ± 0.06	1.35 ± 0.03
71	7000-7500	2015-11-01-2015-11-20	7.51 ± 0.06	2.39 ± 0.03	1.33 ± 0.03
72	7100-7600	2015-11-05-2015-11-26	1.55 ± 0.04	0.97 ± 0.05	1.32 ± 0.04
73	7200-7700	2015-11-09-2015-11-30	1.57 ± 0.02	1.09 ± 0.07	1.27 ± 0.03
74	7300-7800	2015-11-13-2015-12-05	4.92 ± 0.05	1.48 ± 0.06	1.23 ± 0.04
75	7400-7900	2015-11-16-2015-12-20	5.16 ± 0.06	1.63 ± 0.06	1.28 ± 0.04
76	7500-8000	2015-11-20-2015-12-27	6.19 ± 0.07	1.63 ± 0.06	1.28 ± 0.00
77	7600-8100	2015-11-26-2015-12-27	3.29 ± 0.04	1.95 ± 0.02	1.27 ± 0.04
78	7700-8200	2015-11-30-2016-01-11	2.95 ± 0.07	2.15 ± 0.03	1.31 ± 0.04
79	7800-8300	2015-12-05-2016-01-16	3.48 ± 0.04	1.76 ± 0.05	1.32 ± 0.04
80	7900-8400	2015-12-10-2016-01-21	4.40 ± 0.06	1.93 ± 0.03	1.28 ± 0.04
81	8000-8500	2015-12-17-2016-01-25	3.68 ± 0.05	1.67 ± 0.05	1.28 ± 0.04
82	8100-8600	2015-12-27-2016-01-31	2.85 ± 0.06	1.75 ± 0.05	1.28 ± 0.04
83	8200-8700	2016-01-11-2016-02-04	2.45 ± 0.06	1.58 ± 0.05	1.27 ± 0.04
84	8300-8800	2016-01-16-2016-02-10	9.46 ± 0.08	1.44 ± 0.07	1.28 ± 0.04
85	8400-8900	2016-01-21-2016-02-13	6.82 ± 0.03	1.42 ± 0.08	1.26 ± 0.03
86	8500-9000	2016-01-25-2016-02-17	6.33 ± 0.06	1.48 ± 0.07	1.25 ± 0.03
87	8600-9100	2016-01-31-2016-02-22	3.98 ± 0.04	1.90 ± 0.06	1.25 ± 0.03
88	8700-9200	2016-02-04-2016-02-26	3.82 ± 0.03	1.64 ± 0.06	1.21 ± 0.03
89	8800-9300	2016-02-10-2016-03-04	3.96 ± 0.04	1.77 ± 0.04	1.11 ± 0.04
90	8900-9400	2016-02-13-2016-03-10	3.64 ± 0.06	1.86 ± 0.04	1.22 ± 0.03
91	9000-9500	2016-02-17-2016-03-15	3.31 ± 0.05	1.62 ± 0.06	1.23 ± 0.03
92	9100-9600	2016-02-22-2016-03-20	4.28 ± 0.03	1.71 ± 0.04	1.21 ± 0.03
93	9200-9700	2016-02-22-2016-03-20	4.46 ± 0.03	1.88 ± 0.02	1.27 ± 0.03
94	9300-9800	2016-03-04-2016-03-31	4.31 ± 0.03	1.79 ± 0.05	1.28 ± 0.03
95	9400-9900	2016-03-11-2016-04-07	3.13 ± 0.03	1.77 ± 0.04	1.29 ± 0.04
96	9500-10000	2016-03-15-2016-04-12	3.37 ± 0.07	1.82 ± 0.05	1.26 ± 0.04

97	9600-10100	2016-03-20-2016-04-18	3.16 ± 0.03	1.50 ± 0.04	1.24 ± 0.04
98	9700-10200	2016-03-26-2016-04-24	2.91 ± 0.03	1.33 ± 0.03	1.22 ± 0.04
99	9800-10300	2016-03-31-2016-04-29	4.39 ± 0.06	1.37 ± 0.06	1.21 ± 0.04
100	9900-10400	2016-04-07-2016-05-06	4.83 ± 0.05	1.34 ± 0.07	1.20 ± 0.04
101	10000-10500	2016-04-13-2016-05-14	4.24 ± 0.03	1.58 ± 0.07	1.21 ± 0.04

The relationship between $\log C_q(r)$ and $\log r$ for the time window 1 including both Gorkha earthquake and Kodari earthquake with different embedding dimension $D = 0$ to 22 with step size of 2 is depicted in the figure 24. It shows the gradual saturation value of the scaling exponents showing the existence of the power law relation in the earthquake epicenter distribution for different q values. The D_q curve are not straight lines indicating the existence of multifractality in the earthquake distribution.

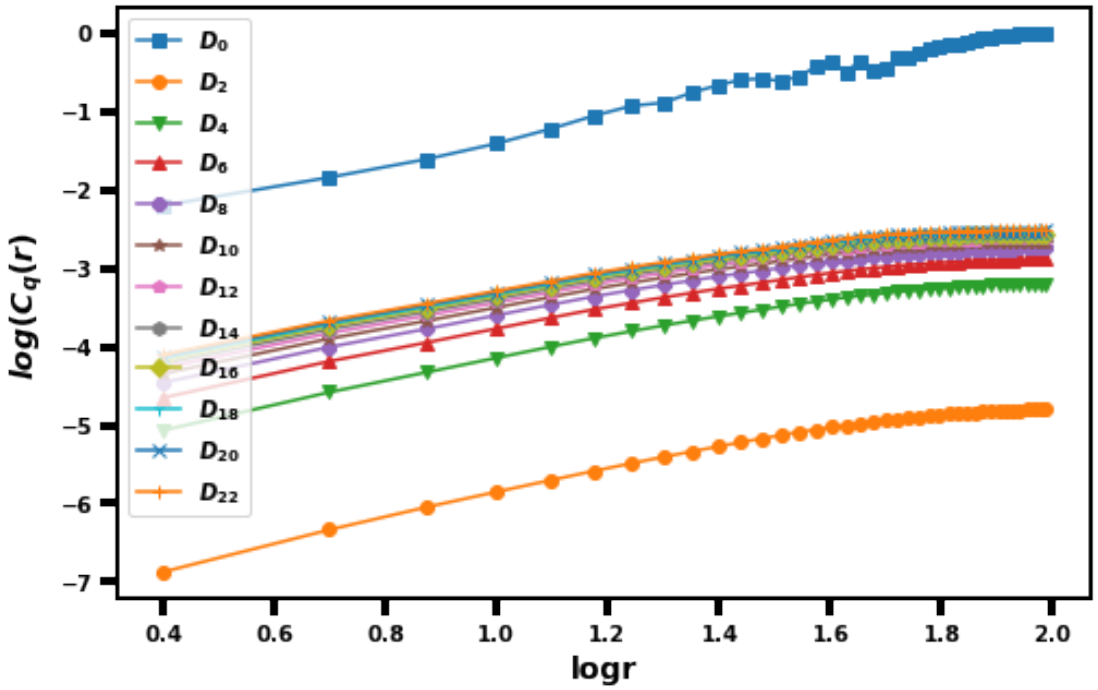

Figure 24: The log – log relations for generalized correlation function $C_q(r)$ and correlation distance (r) of spatial distribution of earthquakes for window1 (2015-04-25 to 2015-05-22). The slope of the linear portion ($r_{min.} = 10^{0.9}$ km = 7.94 km to $r_{max.} = 10^{1.6}$ km = 39.81 km) of these plots give the value of fractal dimension for $q = 0$ to 22. The lower limit and upper limit for scaling distance is chosen by searching the linear part in the plot from linear regression technique in python language.

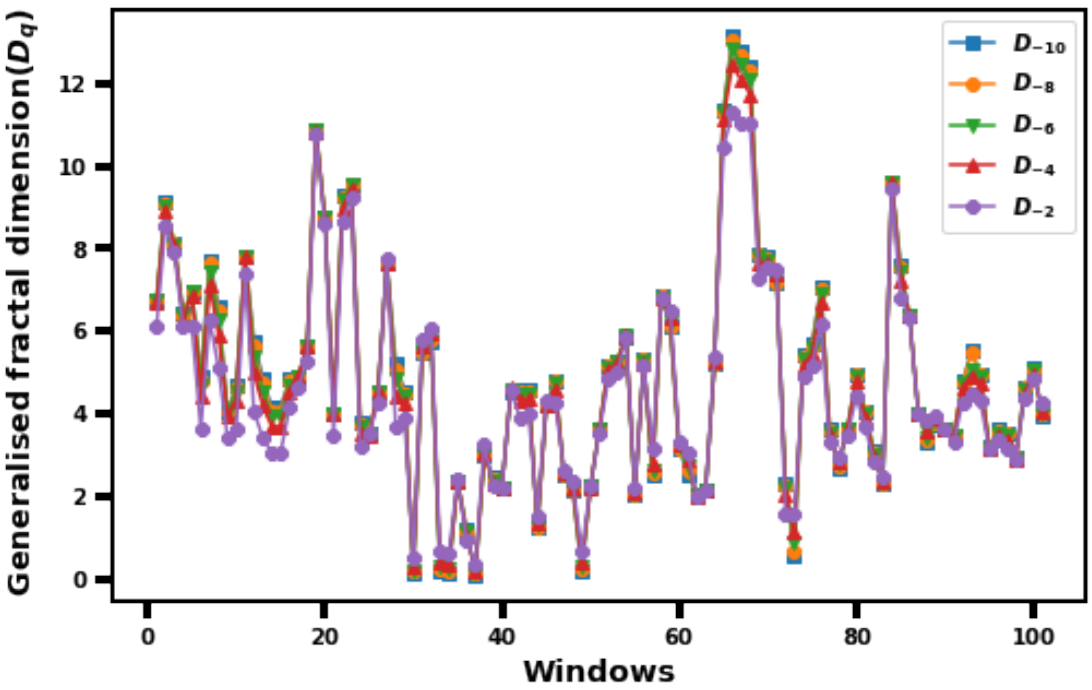

Figure 25: Continuum of dimension for negative q i.e., from q = -10 to -2 for different temporal windows. The time window numbers correspond to the data of table 9. The Gorkha earthquake Mw 7.8 is included by window 1 (2015-04-25 to 2015-05-22) and window 2 (2015-04-25 to 2015-06-25) and Dolakha earthquake Mw 7.3 is included by the windows (1 to 5) for period 2015-04-25 to 2015-06-30.

The values of D_q display a jagged pattern for negative values of q, ranging from -10 to -2, with some values even exceeding 13 (13.16 ± 0.13 for window 66 of the period 2015-10-16-2015-11-01) (Figure 25). Despite the high fluctuations for small negative values of q, the D_q values for negative q are useful in characterizing the scaling properties of areas with seismic gap (low seismic activity area). The high values of D_q for negative q in multifractal time series indicate the dimension of the sparsest part of the earthquake distribution (Aggarwal et al., 2015; Zamani & Agh-Atabai, 2011). However, these high fluctuations make it difficult to accurately approximate the values of D_q (Nie et al., 2020). The results indicate that the distribution of epicenters is not uniform in the study area. The D_q values for negative values of q can exceed the dimension (d) of the topology, which goes against the geometric aspect of fractal dimension (Mandelbrot, 1989). To preserve the physical meaning of D_q, it is recommended to restrict the range of q such that $D_q \leq d$. The study also observes an increase in the fractal dimension preceding the Gorkha earthquake (window 1, 2015-04-25-2015-05-22) and the Dolakha or Kodari earthquake (window 5, 2015-05-12-2015-06-30).

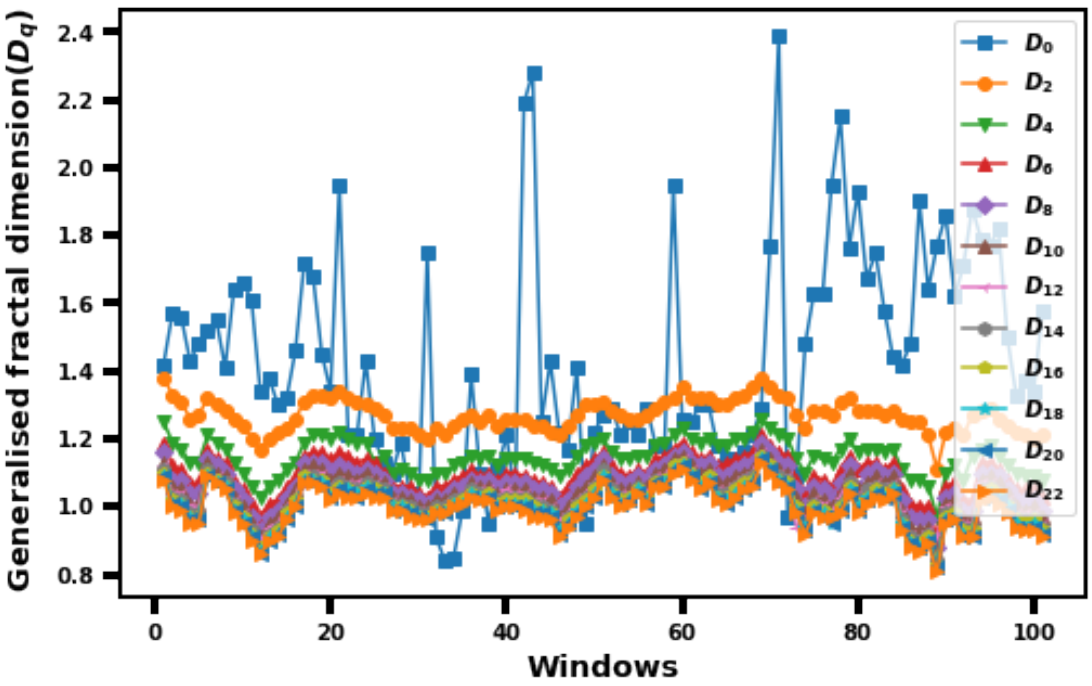

Figure 26: Continuum of dimension for positive q i.e., from q = 0 to 22 for temporal window 1 to the temporal window 101. The time window numbers correspond to the data of table 9

The variation of D_q for $q \geq 0$ can be seen in figure 26 for the temporal window 1 to 101. It shows the gentle oscillating nature (between ~0.4 to ~1.5) for q = 2 to q = 22. D_q values show number of consistent peaks from $q = 0$ to $q = 22$. This is the global behavior of the multifractal pattern. Following the main shock, D_q marks a local minimum value for a brief period due to the clustered sequence. Thereafter D_q increases to get the local high value. The D_q now tends to decrease until a new event occurs and the cycle repeats itself. when the D_q spectra of different temporal window is compared, capacity dimension, D_0 (D_q values for $q = 0$) is found greater than 2 for window 43 (2.28 ± 0.02), for window 71 (2.39 ± 0.03) and for window 78 (2.15 ± 0.03) and are the highest spectra of all the windows (Table 9 and figure 26). They exhibit the two-dimensional tendency of the fault system.

The temporal correlation dimension (D_t) is a measure of the complexity of the temporal distribution of aftershocks. The value of (D_t) ranged from 0.27 to 0.30 for different time windows, and it was calculated to be 0.31 ± 0.004 for the study period of 1964 to 2020 (R. Tiwari & Paudyal, 2021a). A low value of the temporal fractal dimension indicates that the earthquakes tend to occur in groups or clusters rather than being spaced out over time. Furthermore, this suggests that the temporal and spatial distribution of aftershocks was relatively complex and self-similar over the entire study period. The temporal spatial correlation dimension can provide insights into the dynamics of the aftershock sequences and can be used to identify the possible triggering mechanisms

and source properties of the earthquakes. The 1905 Kangra earthquake study revealed a low value of D_0 (0.84 ± 0.07), which represents a high stress region with potential barriers and asperities (N. Kumar et al., 2013). The deviation of the fractal spectrum D_2 and D_{22} between 2.0 and 0.7 indicated strain buildup and discharge around an asperity in the tectonic stress field (Nakaya & Hashimoto, 2002). This study thus supports and builds upon similar previous research.

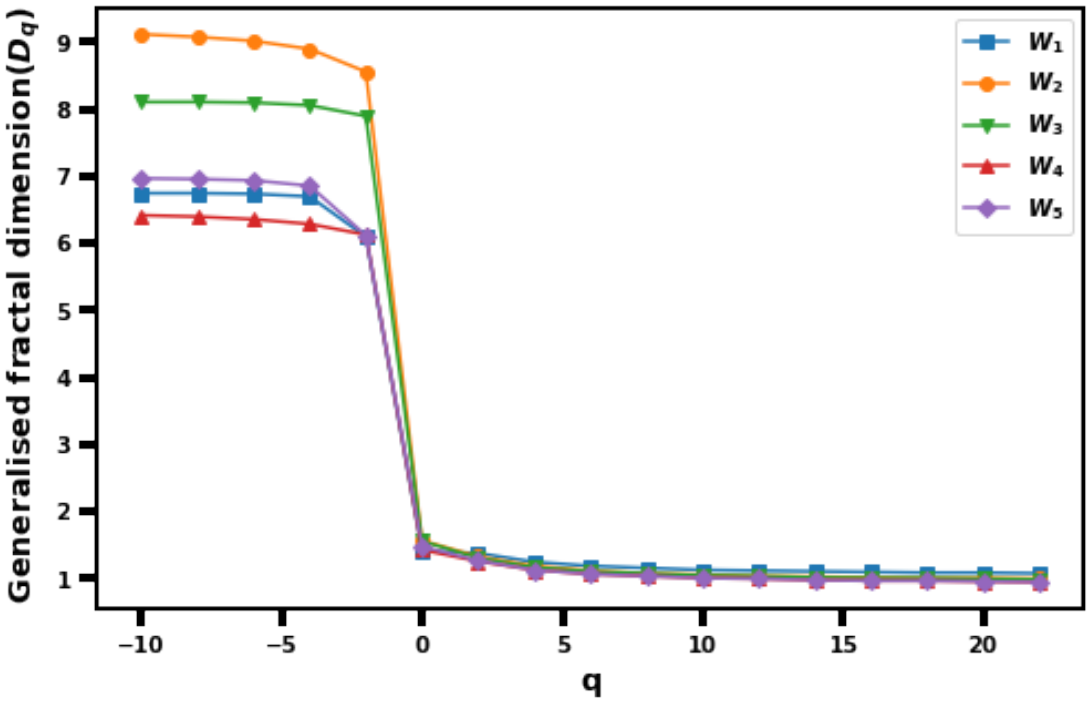

Figure 27: Graph for realization of multifractal distribution. Fractal dimension for window1 (2015-04-25 to 2015-05-22), window 2 (2015-04-25 to 2015-06-25), window 3 (2015-04-26 to 2015-06-27) window 4 (2015-04-30 to 2015-06-29) and window 5 (2015-05-12 to 2015-06-30). For the clear and distinct presentation, we have only depicted the $D_q - q$ curve for the period covering Gorkha earthquake and Dolakha or Kodari earthquake (the major aftershock).

From the representative multifractal spectrum depicted in figure 27, a non-linear dependence between D_q and q can be observed for each considered temporal window. A hallmark of multifractal processes is a sigmoidal shape in the plot of D_q versus q. In this work, the D_q spectrum shows a change in slope around $q = 0$, with a sharp decrease and then a horizontal trend approaching a finite value around 1.0. This knee shape of the spectrum indicates the multifractal nature of the epicenter distribution (Mach et al., 1995). The width of the multifractal spectrum ($W = D_{max}$-$D_{min} = D_{-\infty}$- $D_{+\infty}$) is proportional to the heterogeneity of the complexities or densities in the distribution, with a high degree of heterogeneity being indicated by a large value of W (Macek, 2012; Tarquis et al., 2006). Thus, the presence of a wide range in the values of $D_{-\infty}$ above 6.0 and $D_{+\infty}$ around 1.5 supports the existence of a high degree of multifractality in the distribution of earthquakes.

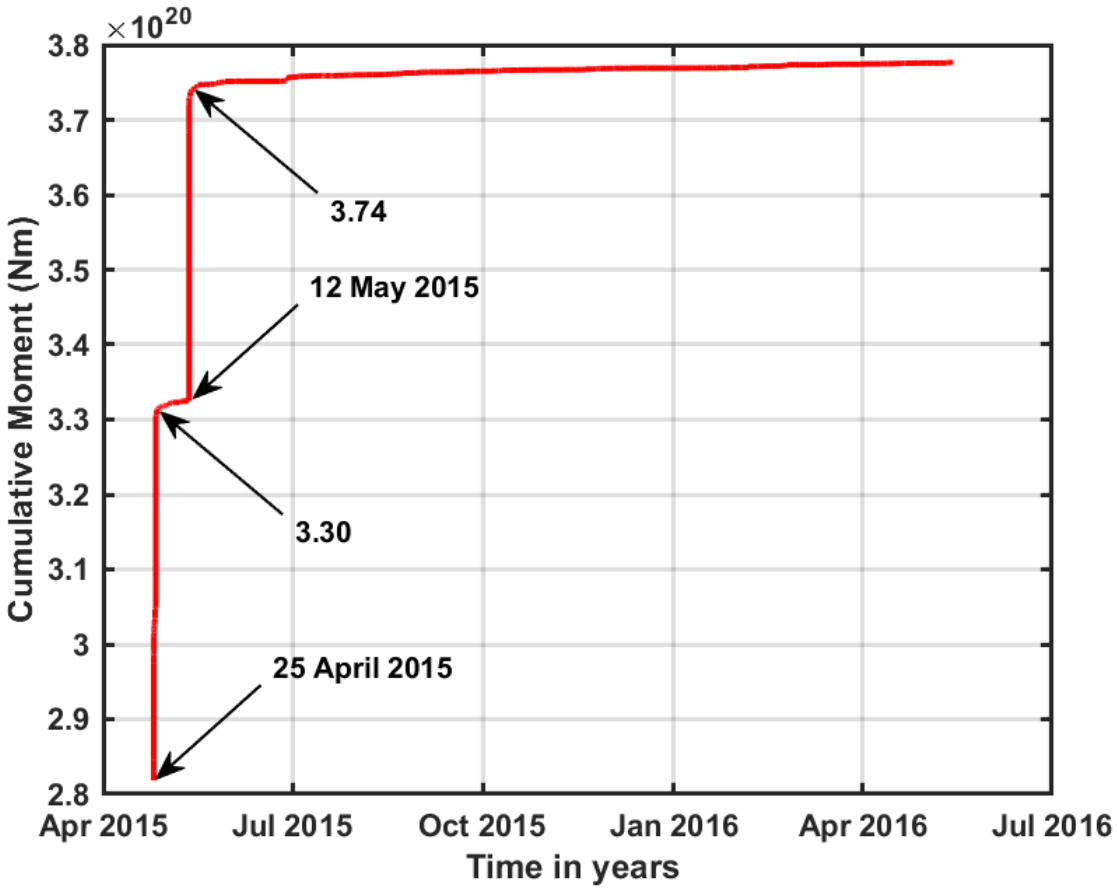

Figure 28: Temporal energy released pattern for the period of the study.

The seismic moment release curves after the Gorkha earthquake (25 April 2015) and the Kodari earthquake (12 May 2015) is depicted in figure 28. The higher value of the moment release after the Kodari earthquake (Major aftershock) justified the fact that most of the moment in a sequence is carried by the strongest aftershocks. It is realistic to accept that a growth in plate subduction rate may have led to the release of high seismic moment release.

4.2.4 Correlation between Box counting dimension and *b*-value

The *b*-value and box counting fractal dimension are estimated for the 101 windows (Table 9) and correlation plot is presented in the figure 29.

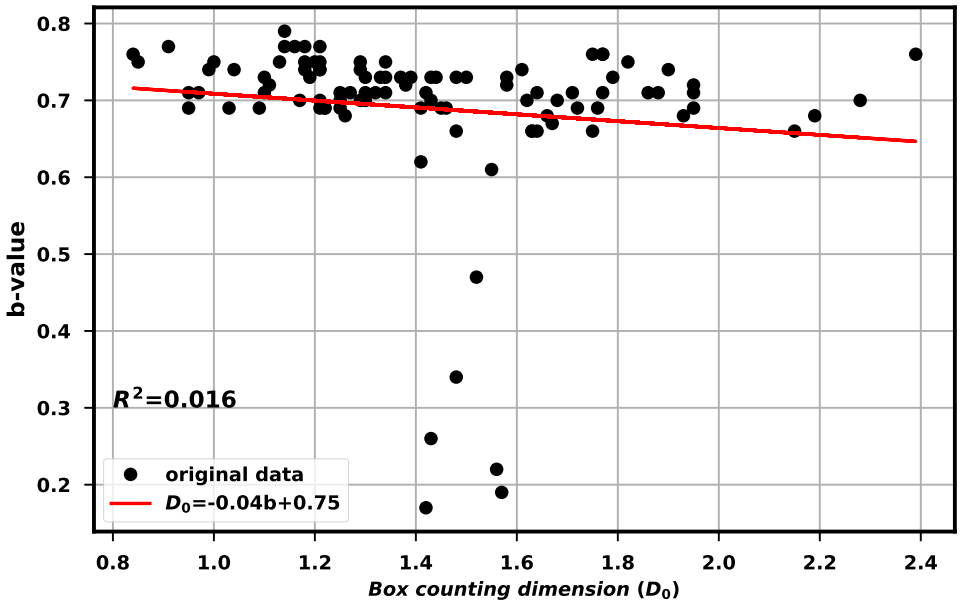

Figure 29: Negative correlation between b-value and box counting dimension

We can see the very weak negative correlation between b-value and box counting fractal dimension of aftershocks distribution defined by the equation $D_0 = -0.04b + 0.75$ with coefficient of determination $(R^2) = 0.016$.

4.2.5 Correlation between correlation dimension and b-value

Figure 30 displays the correlation plot for 101 windows (table 9) between the b-value and correlation fractal dimension. The very faint negative association between the correlation fractal dimension and the b-value is visible for aftershocks distribution defined by the equation $D_2 = -0.56b + 1.39$ with coefficient of determination $(R^2) = 0.056$. Both D_0 and D_2 are negatively correlated supporting the past work related with spatial distribution of earthquake in Tohuku region of Japan (Hirata, 1989) and recent work related with earthquake distribution in central Himalaya (R. Tiwari & Paudyal, 2022, 2021a). It is worth noting that the correlation between b-value and fractal dimension can be affected by other factors such as the earthquake magnitude, stress drop, and the tectonic setting.

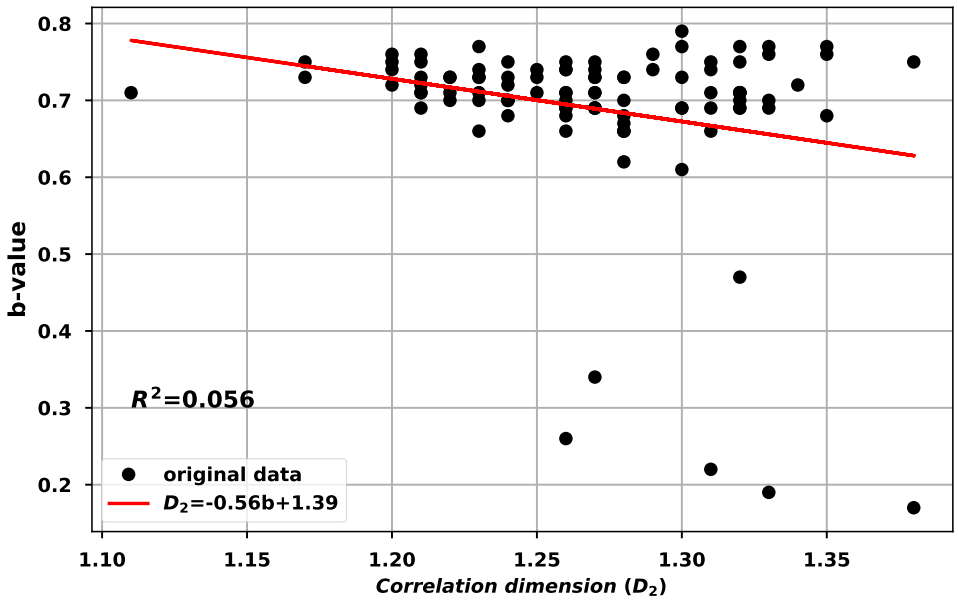

Figure 30: Negative correlation between b-value and correlation dimension

4.3 Omori- Utsu law

An earthquake catalog from the recent period 2015 – 4 – 25 to 2015 – 06 – 07 (Adhikari et al., 2015) was used for the 26.5°N-29°N latitude and 84°E- 87°E longitude in the central Himalaya region to examine the decay rate of aftershocks (Omori, 1895; Utsu, 1971). Figure 31 shows the aftershock decay rate for the first 45 days following the Gorkha earthquake. It is noticed that the decay rate is high for the first 10 days of main shock and increases steadily thereafter. The p-value of modified Omori parameter (p = 0.86 ± 0.04) is estimated for the aftershocks decay and the other two parameters estimated are c = 0.0051 ± 0.019,and K= 57.9 ± 3.76. The value of p is low in comparison with the universal value (1.0) for the study period, suggesting the temporal disintegration rate has not attained the equilibrium and possibility of occurrence of aftershocks could not be denied.

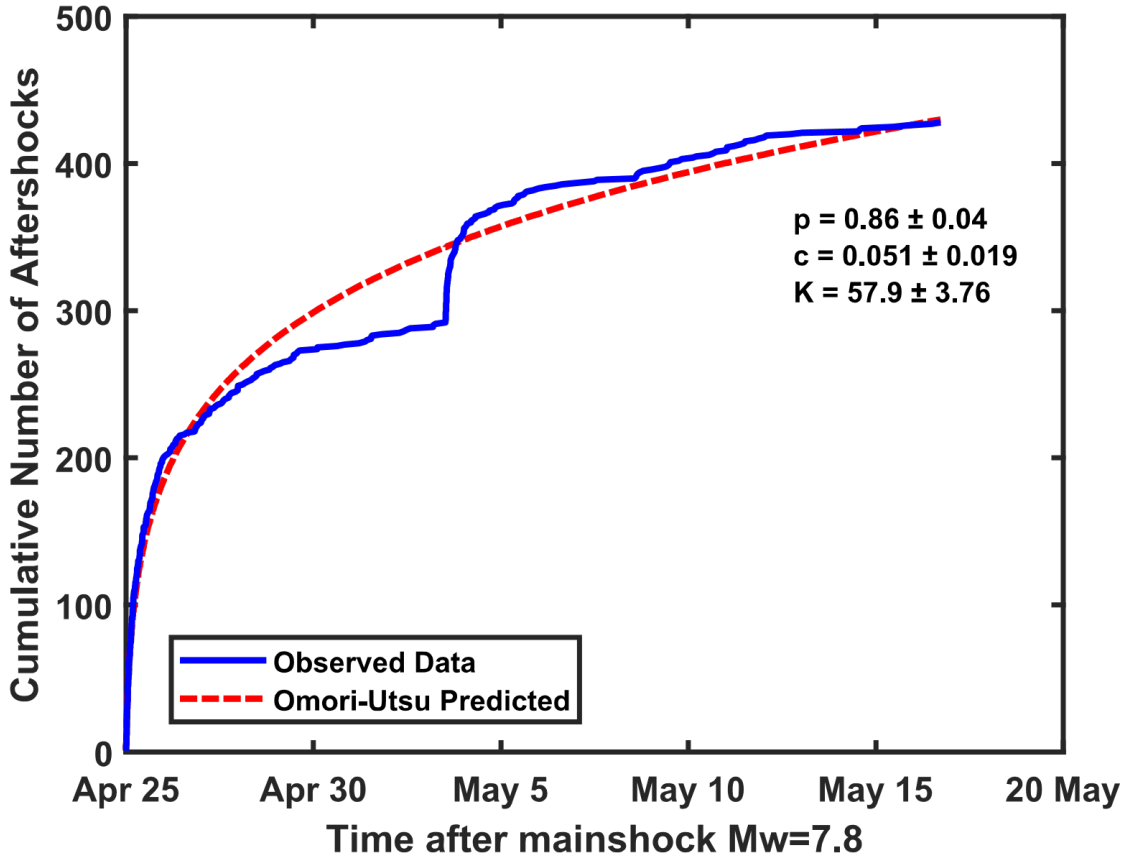

Figure 31: Aftershocks decay rate plot for 429 aftershocks of Gorkha earthquake along with Omori-Utsu parameters (R. Tiwari & Paudyal, 2022).

Based on the estimated parameters, Omori-Utsu law appears to be a useful model for analyzing the aftershock decay patterns of the 2015 Gorkha earthquake (Utsu & Ogata, 1995; Utsu, 1971). The lower p-value also signifies the fact that the region did not experience significant rupture during the period of earthquake. The Omori's law parameters can be associated with the style of faulting. The low p value and larger K-value estimated from the study correlate with thrust type of faulting found in the Himalaya region (Tahir & Grasso, 2015). The p-value (0.86) estimated in this study is slightly higher than 0.80 ± 0.4 estimate for the primary cluster of 2015 earthquakes (Adhikari et al., 2015), 0.82 ± 0.02 estimated as a function of earthquake-faulting styles (Tahir & Grasso, 2015), and 0.79 ± 0.24 for 298 aftershocks of Gorkha earthquake (Thapa et al., 2018). A small value of c (0.051 ± 0.019) obtained for aftershocks could be the result of a diverse stress adjustment process (Dieterich, 1994; Helmstetter & Shaw, 2006). By characterising the aftershocks decay parameter, this study provides the significant contribution in aftershock risk assessments.

CHAPTER 5

CONCLUSIONS AND RECOMMENDATIONS

5.1 Conclusion

This study examines the stress level in the central Himalaya region before and after the Gorkha earthquake using earthquake precursor parameters such as *b*-value, and assesses the heterogeneity of the seismogenic sources through the generalized fractal dimension spectrum. It also analyzes the *p*-value of the aftershocks decay rate of the Gorkha earthquake sequence. Additionally, the study investigates the correlation between the *b*-value and fractal dimensions for the 2015 Gorkha earthquake aftershocks.

The temporal and spatial variations in *b*-values during 1964 to 2020 is analyzed for central Himalaya and adjoining thrusts region. The temporal variation of *b*-value for the fixed event (100) shows the increment from 0.44 ± 0.02 to 1.02 ± 0.09 for the period of 21 years (1980 to 2001). The U-shaped variation in *b*-value is noticed from 2005 to 2015 during which earthquakes from Gorkha to Kodari happened in the region. A quick rise in *b*-value is noticed after 25 April 2015 which could be related with the release of the accumulated energy from the respective earthquake regions. When the variation in *b*-value is studied in long term basis, the lowest *b*-value 0.44 ± 0.06 was noticed for the period between 1984 and 1994 and after 1994, the *b*-value shows gradual increase and settles around 1.0 after 2020. The temporal variation of *b*-value can also be related to the density of the station operating in the region.

The spatial variation of *b*-value for fixed width window shows the variation in the range between 0.59 and 1.0 suggesting the region under study is tectonically active. The *b*-value around 1.0 for 0 to 11 km depth suggests the heterogeneity present in the crust. It may also indicate the low strength of the crust.The *b*-value shows a significant boundary around the depth of 32 km. Increase in *b*-value beyond 32 km depth may indicate the

existence of pore fluid which may be the cause of reduced stress. The contour map of b-value shows the low b-value patches (≤ 0.7), one west and the other east of the 2015 earthquakes and the area governs by the low b-values found to overlap with the zone of the major faults. This result reflects the segmented structure of mega-thrust capable of hosting two major earthquakes separately. This study has found that the stress has not completely released from the focal region of the 2015 earthquakes. On the basis that a transient change in a b-value provides significant information about the evolution of stress and a decrease in the b-value is a prospective precursor to the next inter-plate earthquake, we suggest the monitoring of the b-value is crucial for the evaluation of impending series of earthquakes in the central Himalaya earthquakes.

The examination of spatio-temporal distribution of b-value for areas along the JF ,TF, KTMF, MGF, and MEF could potentially yield valuable insight into how the b-value changes following the significant earthquake. The variation in b-values between 0.45 and 0.69 for aforementioned areas could be justified for the aftershock sequences. Low levels of material heterogeneity and high levels of stress are the characteristics of these regions as suggested by low b-values. The focal mechanism solutions of both the mainshock (25 April earthquake) and its aftershocks further corroborate the existence of the thrust faulting in the region, inline with the observed low b-values linked with the faults. The findings back with the claim that the Gorkha earthquake took place on a low-angle fault plane. From the study of temporal variation of the cumulative moment release, a rapid discharge of strain energy is noticed for the area along Judi fault and the step-wise pattern of strain energy release is noticed for the area along the MEF.

The spatial distribution of aftershocks in the central Himalaya region shows the heterogeneous multifractal character. The D_q spectrum obtained for the region shows a gentle nature for $q > 0$ having gradual saturation towards $D_{+\infty}$ and the steep convergence towards the $D_{-\infty}$. A decrease in D_q observed for $q > 2$ in the fractal spectrum indicates spatial clustering, while an increase in D_q observed for $q < 0$ indicates spatial spreading. The rapid convergence for negative q values indicates greater heterogeneity in sparsely populated regions. The shape of the multifractal curve may reflect the diverse dynamics of the regions. Furthermore, the non-integer fractal dimension characterizes the reality of voids in the region. The presence of voids specifies the reality of small areas deprived of earthquakes. The large number of voids resulted in a high degree of heterogeneity of the seismogenic sources and a smaller value of the fractal dimension. The gradual oscillating behavior of the fractal dimension (ranging from approximately 0.4 to 1.5) from $q = 2$ to $q = 22$ supports this observation.

The self-similar characters of the seismogenic sources, i.e., whether earthquake give the same fractal dimension upon clustering is investigated by considering the earthquake events in different temporal windows. The computed values of dimensions for

the temporal window show a slight difference from D_2 to D_{22} which confirms the scale invariant multi-dimensionality nature of earthquake distribution. The sigmoidal nature of the multifractal spectrum, confirming that earthquake distributions are not monofractal. Also, the higher value of box counting dimension close to or above 2 depicts the complexity of the system. The decrease in the value of D_q with increasing value of q implies a clustered behavior in the spatial distribution of seismic events. This variation can also be related as a decrease in the inhomogeneity of the structure before getting a self organized critical state. The temporal correlation dimension (D_t) computed for the study period between 1964 to 2020 varies between 0.27 to 0.30 for different windows of time whereas for the duration of investigation, the D_t was calculated to be 0.31 ± 0.004. This suggests that the temporal distribution of aftershocks is not a random process, but it has a certain degree of complexity. These results highlight the significance of multifractal approach in the study of the spatial distribution of aftershock sequence.

A subtle and negative association between b-value and fractal dimension can be attributed to the complex tectonic setting of the region which has multiple active faults and different seismic behaviors. The negative correlation also indicates that as the b-value decreases (indicating a higher occurrence of small events), the fractal dimension of the aftershock distribution increases (indicating a more complex and self-similar distribution of events). The aftershocks of Gorkha earthquake found to obey Omori-Utsu law. A p-value of 0.86 ± 0.04 for the decay rate of aftershocks means that the number of aftershocks decreases at a moderate rate. The aftershocks will continue to happen for a longer period of time. The estimated p-value for a study area can be used to mitigate the potential hazards of aftershocks. For example, if a high p-value is observed for a specific area, this would suggest that the risk of aftershocks is relatively high. Additionally, the Omori-Utsu law can be used to predict the number and timing of aftershocks following a main shock. This information can be used to help emergency responders to plan for and respond to aftershocks. This type of study is particularly useful for the understanding of the preparation zone of large and generous size earthquake in the Himalayan region that could be helpful for future earthquake hazard assessment. Nevertheless, it is very crucial to have a complete and homogeneous catalogue of seismicity for this type of study.

5.2 Recommendations

A sound knowledge of geology, tectonics and seismicity of the region are prerequisites to understand the mechanism behind the occurrence of strong earthquakes. This study has made every possible effort to explain the seismotectonic parameters to carry meaningful conclusion about seismic hazard assessment in the central Himalayan region. Although prediction and prevention of earthquakes occurrence is not possible so far, but its effect on

human lives and properties can be reduced significantly through scientific understanding of their nature of occurrence. This thesis would be very useful and fruitful in the field of earthquake hazard assessments not only in the central Himalayan region but also in other regions having similar tectonic set up.

The seismotectonic parameters viz., b-value of earthquake frequency magnitude distribution, box counting dimension or capacity dimension (D_0) value, spatial fractal dimension (D_2) value, temporal fractal dimension (D_t) value, correlation of b-value with (D_0) value, correlation of b-value with (D_2) value, multifractal dimension (D_q), and spatial mapping of b-value of the region are important for understanding the earthquakes preparation process statistically. This knowledge will lead future researchers towards the study of crust dynamics for future large earthquakes. Furthermore, the high risk zone for future large earthquakes has been demarcated on the basis of earthquake's potential. It also suggests to install the more seismic network in study region to record more number of earthquakes from which meaningful conclusion can be drawn about the strain accumulation and distribution to understand the nature of crust deformation leading to earthquakes. Some future recommendations for studying earthquake distribution in the central Himalaya using multifractal analysis are

1) To conduct a multifractal study of earthquakes distribution in the central Himalaya region where risk of future earthquakes is very high.

2) To compare the results of multifractal study of earthquake epicenter distribution with multifractal detrended fluctuation analysis of magnitude time series.

3) To collaborate with other researchers and institutions to gather more data on the distribution of earthquakes in the central Himalaya to improve the accuracy of analysis.

4) To conduct the multifractal variability of geoelectrical signal and to study the correlation with seismicity.

5) To apply the multifractal approach to study other natural processes like rain fall and river flows, relative air humidity time series etc.

CHAPTER 6

SUMMARY

6.1 Summary

The present chapter is the output of the overall study of the thesis. The chapter elaborately summarizes the importance of earthquakes study from the theory of power law in one of the most well known and geologically complex central Himalayan region. The region is one of the most tectonically and seismically active part of the Himalaya since it accommodates the most of the India and Eurasia collision. The dynamics and complexities of earthquakes occurrence in the region have been studied with the help of b-value of GR frequency magnitude distribution of past seismicity, and box counting dimension or Capacity dimensions (D_0), correlation dimension (D_2) and multifractal spectrum (D_q) of aftershocks sequence of 2015 Gorkha earthquake.

The correlation dimension values of aftershocks distribution suggests that epicenters are more clustered and reflects the distribution of seismogenic sources in more than linear space. Correlation study of D_0, D_2 and b-value indicates that they have very weak negative correlation. For the entire central Himalaya region, there is neither positive nor negative correlation between these exponents. The low b-value suggests the likelihood of a significant earthquake, and the low D_2 value reveals that the events are concentrated in highly stressed zones. Spatial multifractal spectrum gives D_q versus q variation plot or D_q spectrum for five hundred events windows. The plot shows the multifractal nature indicating the events are distributed in clusters. The notable difference between D_2 and D_{22} suggests the existence of revealing heterogeneity within the epicentre area attributed to the fault complexity at local scales. The change of D_q from $q = 2$ to $q = 22$ suggests the presence of the cluster within cluster indicating heterogeneity of the crust. The curve of the multifractal spectrum provides important information about the underlying physical processes that control the distribution of earthquakes. A multifractal spectrum suggest that the distribution of earthquakes in central Himalaya is controlled by multiple

physical processes happening inside the crust. The negative correlation between the *b*-value and the fractal dimension suggest that regions with a more complex and fragmented distribution of epicenters also have a higher frequency of smaller earthquakes and a lower frequency of larger earthquakes. This may indicate that the complexity of the tectonic environment affects the distribution of earthquake magnitudes. The observed decrease in the number of aftershocks is consistent with the mathematical relationship described by the Omori-Utsu law. This would provide evidence supporting the use of the Omori-Utsu law to model aftershock decay for the 2015 Gorkha earthquake.

The outcomes of the work can be considered as hazard indicators. There is a possibility of strong earthquake equal to or even greater than Gorkha earthquake which may dissipate a huge amount of the accumulated regional strain and brings the region out of a self-organized critical (SOC) state. Thus, this study helps in better hazard mitigation and disaster management for the central Himalaya and its surrounding region.

REFERENCES

Ader, T., Avouac, J.-P., Liu-Zeng, J., Lyon-Caen, H., Bollinger, L., Galetzka, J., ... Flouzat, M. (2012). Convergence rate across the Nepal Himalaya and interseismic coupling on the Main Himalayan Thrust: Implications for seismic hazard. *Journal of Geophysical Research: Solid Earth*, *117*(B4). https://doi.org/10.1029/2011JB009071

Adhikari, L., Gautam, U., Koirala, B., Bhattarai, M., Kandel, T., Gupta, R., ... Bollinger, L. (2015). The aftershock sequence of the 2015 April 25 Gorkha–Nepal earthquake. *Geophysical Journal International*, *203*(3), 2119–2124. https://doi.org/10.1093/gji/ggv412

Aggarwal, S., Lovallo, M., Khan, P., Rastogi, B., & Telesca, L. (2015). Multifractal detrended fluctuation analysis of magnitude series of seismicity of Kachchh region, Western India. *Physica A: Statistical Mechanics and its Applications*, *426*, 56–62. https://doi.org/10.1016/j.physa.2015.01.049

Aggarwal, S., Pastén, D., & Khan, P. K. (2017). Multifractal analysis of 2001 Mw 7.7 Bhuj earthquake sequence in Gujarat, Western India. *Physica A: Statistical Mechanics and its Applications*, *488*, 177–186. https://doi.org/10.1016/j.physa.2017.06.022

Aki, K. (1965). Maximum likelihood estimate of b in the formula logn= a-bm and its confidence limits. *Bulletin of the Earthquake Research Institute University of Tokyo*, *43*, 237–239.

Al-Heety, E. A., & Mohammad, O. J. (2021). The reliance of the earthquake b-value on depth and focal mechanism. *The Iraqi Geological Journal*, 1–10.

Ali, S. M. (2016). Statistical analysis of seismicity in Egypt and its surroundings. *Arabian Journal of Geosciences*, *9*(1), 1–16. https://doi.org/10.1007/s12517-015-2079-x

Ambraseys, N., & Bilham, R. (2003). Reevaluated intensities for the great Assam earthquake of 12 June 1897, Shillong, India. *Bulletin of the Seismological Society of America*, *93*(2), 655–673. https://doi.org/10.1785/0120020093

Ambraseys, N., & Douglas, J. (2004). Magnitude calibration of north Indian earthquakes. *Geophysical Journal International*, *159*(1), 165–206. https://doi.org/10.1111/j.1365-246X.2004.02323.x

Ambraseys, N., & Jackson, D. (2003). A note on early earthquakes in northern India and southern Tibet. *Current Science*, 570–582.

Amitrano, D. (2012). Variability in the power-law distributions of rupture events. *The European Physical Journal Special Topics*, *205*(1), 199–215. https://doi.org/10.1140/epjst/e2012-01571-9

Ansari, K. (2018). Crustal deformation and strain analysis in Nepal from GPS time-series measurement and modeling by ARMA method. *International Journal of Earth Sciences*, *107*(8), 2895–2905. https://doi.org/10.1007/s00531-018-1633-7

Ansari, S. (2017). Aftershocks properties of the 2013 Shonbe Mw 6.3 earthquake, central Zagros, Iran. *Journal of Asian Earth Sciences*, *147*, 17–27. https://doi.org/10.1016/j.jseaes.2017.07.042

Arita, K. (1983). Origin of the inverted metamorphism of the lower Himalayas, central Nepal. *Tectonophysics*, *95*(1-2), 43–60. https://doi.org/10.1016/0040-1951(83)90258-5

Arita, K., Dallmeyer, R. D., & Takasu, A. (1997). Tectonothermal evolution of the Lesser Himalaya, Nepal: Constraints from 40Ar/39Ar ages from the Kathmandu Nappe. *Island Arc*, *6*(4), 372–385. https://doi.org/10.1111/j.1440-1738.1997.tb00047.x

Armijo, R., Tapponnier, P., & Han, T. (1989). Late Cenozoic right-lateral strike-slip faulting in southern Tibet. *Journal of Geophysical Research: Solid Earth*, *94*(B3), 2787–2838. https://doi.org/10.1029/JB094iB03p02787

Arora, B., Bansal, B., Prajapati, S. K., Sutar, A. K., & Nayak, S. (2017). Seismotectonics and seismogenesis of Mw 7.8 Gorkha earthquake and its aftershocks. *Journal of Asian Earth Sciences*, *133*, 2–11. https://doi.org/10.1016/j.jseaes.2016.07.018

Arora, B., Gahalaut, V., & Kumar, N. (2012). Structural control on along-strike variation in the seismicity of the northwest Himalaya. *Journal of Asian Earth Sciences*, *57*, 15–24. https://doi.org/10.1016/j.jseaes.2012.06.001

Aviles, C., Scholz, C. H., & Boatwright, J. (1987). Fractal analysis applied to characteristic segments of the San Andreas fault. *Journal of Geophysical Research: Solid Earth*, *92*(B1), 331–344. https://doi.org/10.1029/JB092iB01p00331

Avouac, J.-P., Meng, L., Wei, S., Wang, T., & Ampuero, J.-P. (2015). Lower edge of locked Main Himalayan Thrust unzipped by the 2015 Gorkha earthquake. *Nature Geoscience*, *8*(9), 708–711. https://doi.org/10.1038/ngeo2518

Bai, L., Klemperer, S. L., Mori, J., Karplus, M. S., Ding, L., Liu, H., ... Dhakal, S. (2019). Lateral variation of the Main Himalayan Thrust controls the rupture length of the 2015 Gorkha earthquake in Nepal. *Science Advances*, *5*(6), 1–8. https://doi.org/10.1126/sciadv.aav0723

Bai, L., Liu, H., Ritsema, J., Mori, J., Zhang, T., Ishikawa, Y., & Li, G. (2016). Faulting structure above the Main Himalayan Thrust as shown by relocated aftershocks of the 2015 Mw 7.8 Gorkha, Nepal, earthquake. *Geophysical Research Letters*, *43*(2), 637–642. https://doi.org/10.1002/2015GL066473

Baillard, C., Lyon-Caen, H., Bollinger, L., Rietbrock, A., Letort, J., & Adhikari, L. B. (2017). Automatic analysis of the Gorkha earthquake aftershock sequence: Evidences of structurally segmented seismicity. *Geophysical Journal International*, *209*(2), 1111–1125. https://doi.org/10.1093/gji/ggx081

Bak, P., Christensen, K., Danon, L., & Scanlon, T. (2002). Unified scaling law for earthquakes. *Physical Review Letters*, *88*(17), 178501. https://doi.org/10.1103/PhysRevLett.88.178501

Baker, D. M., Lillie, R. J., Yeats, R. S., Johnson, G. D., Yousuf, M., & Zamin, A. S. H. (1988). Development of the Himalayan frontal thrust zone: Salt Range, Pakistan. *Geology*, *16*(1), 3–7. https://doi.org/10.1130/0091-7613(1988)016<3C0003:DOTHFT>3E2.3.CO;2

Baranowski, J., Armbruster, J., Seeber, L., & Molnar, P. (1984). Focal depths and fault plane solutions of earthquakes and active tectonics of the Himalaya. *Journal of Geophysical Research: Solid Earth*, *89*(B8), 6918–6928. https://doi.org/10.1029/JB089iB08p06918

Bayrak, E., Yılmaz, Ş., & Bayrak, Y. (2017). Temporal and spatial variations of Gutenberg-Richter parameter and fractal dimension in Western Anatolia, Turkey. *Journal of Asian Earth Sciences*, *138*, 1–11. https://doi.org/10.1016/j.jseaes.2017.01.031

Bayrak, Y., & Öztürk, S. (2004). Spatial and temporal variations of the aftershock sequences of the 1999 İzmit and Düzce earthquakes. *Earth, planets and space*, *56*(10), 933–944. https://doi.org/10.46717/igj.54.1D.1Ms-2021-04-21

Bilham, R. (2004). Earthquakes in India and the Himalaya: tectonics, geodesy and history. *Annals of Geophysics*(2–3), 839–858. https://doi.org/10.4401/ag-3338

Bilham, R. (2015). Raising Kathmandu. *Nature Geoscience*, *8*(8), 582–584. https://doi.org/10.1038/ngeo2498

Bilham, R. (2019). Himalayan earthquakes: a review of historical seismicity and early 21st century slip potential. *Geological Society, London, Special Publications*, *483*(1), 423–482. https://doi.org/10.1144/SP483.16

Bilham, R., Larson, K., & Freymueller, J. (1997). GPS measurements of present-day convergence across the Nepal Himalaya. *Nature*, *386*(6620), 61–64. https://doi.org/10.1038/386061a0

Bilham, R., Mencin, D., Bendick, R., & Bürgmann, R. (2017). Implications for elastic energy storage in the Himalaya from the Gorkha 2015 earthquake and other incomplete ruptures of the Main Himalayan Thrust. *Quaternary International*, *462*, 3–21. https://doi.org/10.1016/j.quaint.2016.09.055

Bollinger, L., Avouac, J., Cattin, R., & Pandey, M. (2004). Stress buildup in the Himalaya. *Journal of Geophysical Research: Solid Earth*, *109*(B11). https://doi.org/10.1029/2003JB002911

Bollinger, L., Sapkota, S. N., Tapponnier, P., Klinger, Y., Rizza, M., Van der Woerd, J., . . . Bes de Berc, S. (2014). Estimating the return times of great Himalayan earthquakes in eastern Nepal: Evidence from the Patu and Bardibas strands of the Main Frontal Thrust. *Journal of Geophysical Research: Solid Earth*, *119*(9), 7123–7163. https://doi.org/10.1002/2014JB010970

Bollinger, L., Tapponnier, P., Sapkota, S., & Klinger, Y. (2016). Slip deficit in central Nepal: Omen for a repeat of the 1344 AD earthquake? *Earth, Planets and Space*, *68*(1), 1–12. https://doi.org/10.1186/s40623-016-0389-1

Boyer, S. E., & Elliott, D. (1982). Thrust systems. *American Association of Petroleum Geologists Bulletin*, *66*(9), 1196–1230. https://doi.org/10.1306/03B5A77D-16D1-11D7-8645000102C1865D

Bridges, D. L., & Gao, S. S. (2006). Spatial variation of seismic b-values beneath Makushin Volcano, Unalaska Island, Alaska. *Earth and Planetary Science Letters*, *245*(1-2), 408–415. https://doi.org/10.1016/j.epsl.2006.03.010

Brown, S. R., & Scholz, C. H. (1985). Broad bandwidth study of the topography of natural rock surfaces. *Journal of Geophysical Research: Solid Earth*, *90*(B14), 12575–12582. https://doi.org/10.1029/JB090iB14p12575

Burchfiel, B. C., Zhiliang, C., Hodges, K. V., Yuping, L., Royden, L. H., Changrong, D., & Jiene, X. (1992). *The South Tibetan detachment system, Himalayan orogen: Extension contemporaneous with and parallel to shortening in a collisional*

mountain belt. Geological Society of America. https://doi.org/10.1130/SPE269-p1

Carosi, R., Montomoli, C., Rubatto, D., & Visonà, D. (2013). Leucogranite intruding the South Tibetan Detachment in western Nepal: implications for exhumation models in the Himalayas. *Terra Nova*, *25*(6), 478–489. https://doi.org/10.1111/ter.12062

Carosi, R., Musumeci, G., & Pertusati, P. (1999). Extensional tectonics in the higher Himalayan crystallines of Khumbu Himal, eastern Nepal. *Geological Society Of America*, 211–224. https://doi.org/10.1130/0-8137-2328-0.211

Caruso, F., Vinciguerra, S., Latora, V., Rapisarda, A., & Malone, S. (2006). Multifractal analysis of Mount St. Helens seismicity as a tool for identifying eruptive activity. *Fractals*, *14*(03), 179–186. https://doi.org/10.1142/S0218348X06003180

Cattin, R., & Avouac, J. (2000). Modeling mountain building and the seismic cycle in the Himalaya of Nepal. *Journal of Geophysical Research: Solid Earth*, *105*(B6), 13389–13407. https://doi.org/10.1029/2000JB900032

Chan, C.-H., Wang, Y., Almeida, R., & Yadav, R. (2017). Enhanced stress and changes to regional seismicity due to the 2015 Mw 7.8 Gorkha, Nepal, earthquake on the neighbouring segments of the Main Himalayan Thrust. *Journal of Asian Earth Sciences*, *133*, 46–55. https://doi.org/10.1016/j.jseaes.2016.03.004

Chelidze, T., Kiria, T., Melikadze, G., Jimsheladze, T., & Kobzev, G. (2022). Earthquake Forecast as a Machine Learning Problem for Imbalanced Datasets: Example of Georgia, Caucasus. *Frontiers in Earth Science*, *10*, 1-11. https://doi.org/10.3389/feart.2022.847808

Chelidze, T., Melikadze, G., Kiria, T., Jimsheladze, T., & Kobzev, G. (2020). Statistical and non-linear dynamics methods of earthquake forecast: Application in the Caucasus. *Frontiers in Earth Science*, *8*, 194. https://doi.org/10.3389/feart.2020.00194

Chen, C.-C., Wang, W.-C., Chang, Y.-F., Wu, Y.-M., & Lee, Y.-H. (2006). A correlation between the b-value and the fractal dimension from the aftershock sequence of the 1999 Chi-Chi, Taiwan, earthquake. *Geophysical Journal International*, *167*(3), 1215–1219. https://doi.org/10.1111/j.1365-246X.2006.03230.x

Chiba, K., & Shimizu, H. (2018). Spatial and temporal distributions of b-value in and around Shinmoe-dake, Kirishima volcano, Japan. *Earth, Planets and Space*, *70*(1), 1–9. https://doi.org/10.1186/s40623-018-0892-7

Chingtham, P., Chopra, S., Baskoutas, I., & Bansal, B. (2014). An assessment of seismicity parameters in northwest Himalaya and adjoining regions. *Natural hazards*, *71*(3), 1599–1616. https://doi.org/10.1007/s11069-013-0967-5

Chingtham, P., Sharma, B., Chopra, S., & SinghaRoy, P. (2016). Statistical analysis of aftershock sequences related with two major nepal earthquakes: April 25, 2015, Mw 7.8, and May 12, 2015, Mw 7.2. *Annals of Geophysics*, *59*(5). https://doi.org/10.4401/ag-7025

Corral, Á. (2003). Local distributions and rate fluctuations in a unified scaling law for earthquakes. *Physical Review E*, *68*(3), 035102. https://doi.org/10.1103/PhysRevE.68.035102

Corral, Á., & González, Á. (2019). Power law size distributions in geoscience revisited. *Earth and Space Science*, *6*(5), 673–697. https://doi.org/10.1029/2018EA000479

Coudurier-Curveur, A., Tapponnier, P., Okal, E., Van der Woerd, J., Kali, E., Choudhury, S., . . . Karakaş, Ç. (2020). A composite rupture model for the great 1950 Assam earthquake across the cusp of the East Himalayan Syntaxis. *Earth and Planetary Science Letters*, *531*, 115928. https://doi.org/10.1016/j.epsl.2019.115928

Crampin, S., Evans, R., & Atkinson, B. K. (1984). Earthquake prediction: a new physical basis. *Geophysical Journal International*, *76*(1), 147–156. https://doi.org/10.1111/j.1365-246X.1984.tb05030.x

Dal Zilio, L., Hetényi, G., Hubbard, J., & Bollinger, L. (2021). Building the Himalaya from tectonic to earthquake scales. *Nature Reviews Earth & Environment*, *2*(4), 251–268. https://doi.org/10.1038/s43017-021-00143-1

Dasgupta, S., Mukhopadhyay, B., Mukhopadhyay, M., & Pande, P. (2021). Geo-and seismo-tectonics of Eastern Himalaya: Exploring earthquake source zones from foredeep to Tibetan hinterland. *Physics and Chemistry of the Earth, Parts A/B/C*, *123*, 103013. https://doi.org/10.1016/j.pce.2021.103013

Dasgupta, S., Mukhopadhyay, M., & Nandy, D. (1987). Active transverse features in the central portion of the Himalaya. *Tectonophysics*, *136*(3-4), 255–264. https://doi.org/10.1016/0040-1951(87)90028-X

Davidsen, J., & Goltz, C. (2004). Are seismic waiting time distributions universal? *Geophysical research letters*, *31*(21). https://doi.org/10.1029/2004GL020892

DeCelles, P., Kapp, P., Gehrels, G., & Ding, L. (2014). Paleocene-Eocene foreland basin evolution in the Himalaya of southern Tibet and Nepal: Implica-

tions for the age of initial India-Asia collision. *Tectonics*, *33*(5), 824–849. https://doi.org/10.1002/2014TC003522

DeCelles, P., Robinson, D. M., Quade, J., Ojha, T., Garzione, C. N., Copeland, P., & Upreti, B. N. (2001). Stratigraphy, structure, and tectonic evolution of the Himalayan fold-thrust belt in western Nepal. *Tectonics*, *20*(4), 487–509. https://doi.org/10.1029/2000TC001226

DeCelles, P., Robinson, D. M., & Zandt, G. (2002). Implications of shortening in the Himalayan fold-thrust belt for uplift of the Tibetan Plateau. *Tectonics*, *21*(6), 12–1. https://doi.org/10.1029/2001TC001322

DeMets, C., Gordon, R. G., & Argus, D. F. (2010). Geologically current plate motions. *Geophysical journal international*, *181*(1), 1–80. https://doi.org/10.1111/j.1365-246X.2009.04491.x

Denolle, M. A., Fan, W., & Shearer, P. M. (2015). Dynamics of the 2015 M 7. 8 Nepal earthquake. *Geophysical Research Letters*, *42*(18), 7467–7475. https://doi.org/10.1002/2015GL065336

De Rubeis, V., Czechowski, Z., & Teisseyre, R. (2010). *Synchronization and triggering: from fracture to earthquake processes*. Springer. https://doi.org/10.1007/978-3-642-12300-9

De Santis, A. (1997). A direct divider method for self-affine fractal profiles and surfaces. *Geophysical research letters*, *24*(16), 2099–2102. https://doi.org/10.1029/97GL02002

Dewey, J. F., & Bird, J. M. (1970). Mountain belts and the new global tectonics. *Journal of geophysical Research*, *75*(14), 2625–2647. https://doi.org/10.1029/JB075i014p02625

Dhital, M. R. (2015). *Geology of the Nepal Himalaya: regional perspective of the classic collided orogen*. Springer. https://doi.org/10.1007/978-3-319-02496-7

Diao, F., Walter, T. R., Motagh, M., Prats-Iraola, P., Wang, R., & Samsonov, S. V. (2015). The 2015 Gorkha earthquake investigated from radar satellites: Slip and stress modeling along the MHT. *Frontiers in Earth Science*, *3*, 65. https://doi.org/10.3389/feart.2015.00065

Dieterich, J. (1994). A constitutive law for rate of earthquake production and its application to earthquake clustering. *Journal of Geophysical Research: Solid Earth*, *99*(B2), 2601–2618. https://doi.org/10.1029/93JB02581

Di Giacomo, D., Bondár, I., Storchak, D. A., Engdahl, E. R., Bormann, P., & Harris, J. (2015). Isc-gem: Global instrumental earthquake catalogue (1900–2009), III. Re-computed MS and mb, proxy MW, final magnitude composition and completeness assessment. *Physics of the Earth and Planetary Interiors*, *239*, 33–47. https://doi.org/10.1016/j.pepi.2014.06.003

Di Giacomo, D., Engdahl, E. R., & Storchak, D. A. (2018). The ISC-GEM earthquake catalogue (1904–2014): status after the extension project. *Earth System Science Data*, *10*(4), 1877–1899. https://doi.org/10.5194/essd-10-1877-2018

Dimri, V., & Srivastava, K. (2015). *Introduction for the special issue: the role of fractals in seismology* (Vol. 77) (No. 1). Springer.

Dimri, V., Vedanti, N., & Chattopadhyay, S. (2005). Fractal analysis of aftershock sequence of the Bhuj earthquake: A wavelet-based approach. *Current Science*, *88*(10), 1617–1620.

DiPietro, J. A., & Pogue, K. R. (2004). Tectonostratigraphic subdivisions of the Himalaya: A view from the west. *Tectonics*, *23*(5). https://doi.org/10.1029/2003TC001554

Duan, H., Wu, S., Kang, M., Xie, L., & Chen, L. (2020). Fault slip distribution of the 2015 Mw 7. 8 Gorkha (Nepal) earthquake estimated from InSAR and GPS measurements. *Journal of Geodynamics*, *139*, 101767. https://doi.org/10.1016/j.jog.2020.101767

Duputel, Z., & Rivera, L. (2017). Long-period analysis of the 2016 Kaikoura earthquake. *Physics of the Earth and Planetary Interiors*, *265*, 62–66. https://doi.org/10.1016/j.pepi.2017.02.004

Duputel, Z., Vergne, J., Rivera, L., Wittlinger, G., Farra, V., & Hetényi, G. (2016). The 2015 Gorkha earthquake: a large event illuminating the Main Himalayan Thrust fault. *Geophysical Research Letters*, *43*(6), 2517–2525. https://doi.org/10.1002/2016GL068083

Dziewonski, A. M., Chou, T.-A., & Woodhouse, J. H. (1981). Determination of earthquake source parameters from waveform data for studies of global and regional seismicity. *Journal of Geophysical Research: Solid Earth*, *86*(B4), 2825–2852. https://doi.org/10.1029/JB086iB04p02825

D'Amico, S., Caccamo, D., Parrillo, F., Lagana, C., & Barbieri, F. (2010). The 20th September 1999 Chi-Chi earthquake (Taiwan): a case of study for its aftershock seismic sequence. *Izvestiya, Physics of the Solid Earth*, *46*(4), 317–326. https://doi.org/10.1134/S106935131004004X

Ekström, G., Nettles, M., & Dziewoński, A. (2012). The global CMT project 2004–2010: Centroid-moment tensors for 13,017 earthquakes. *Physics of the Earth and Planetary Interiors*, *200*, 1–9. https://doi.org/10.1016/j.pepi.2012.04.002

El-Isa, Z. (2013). Continuous-cyclic variations in the b-value of the earthquake frequency-magnitude distribution. *Earthquake Science*, *26*(5), 301–320. https://doi.org/10.1007/s11589-013-0037-9

El-Isa, Z., & Eaton, D. W. (2014). Spatiotemporal variations in the b-value of earthquake magnitude–frequency distributions: Classification and causes. *Tectonophysics*, *615*, 1–11. https://doi.org/10.1016/j.tecto.2013.12.001

Elliott, J., Jolivet, R., González, P. J., Avouac, J.-P., Hollingsworth, J., Searle, M., & Stevens, V. (2016). Himalayan megathrust geometry and relation to topography revealed by the Gorkha earthquake. *Nature Geoscience*, *9*(2), 174–180. https://doi.org/10.1038/ngeo2623

El-Nabulsi, R. A., & Anukool, W. (2022). Fractal dimension modeling of seismology and earthquakes dynamics. *Acta Mechanica*, 1–16. https://doi.org/10.1007/s00707-022-03213-7

Fan, W., & Shearer, P. M. (2015). Detailed rupture imaging of the 25 April 2015 Nepal earthquake using teleseismic P waves. *Geophysical Research Letters*, *42*(14), 5744–5752. https://doi.org/10.1002/2015GL064587

Feldl, N., & Bilham, R. (2006). Great Himalayan earthquakes and the Tibetan plateau. *Nature*, *444*(7116), 165–170. https://doi.org/10.1038/nature05199

Feng, W., Lindsey, E., Barbot, S., Samsonov, S., Dai, K., Li, P., ... Xu, X. (2017). Source characteristics of the 2015 MW 7.8 Gorkha (Nepal) earthquake and its MW 7.2 aftershock from space geodesy. *Tectonophysics*, *712*, 747–758. https://doi.org/10.1016/j.tecto.2016.02.029

Gahalaut, V. (2008). Major and great earthquakes and seismic gaps in the Himalayan arc. *Golden Jubilee Memoir of Geological Society of India*, *66*, 373–393.

Galetzka, J., Melgar, D., Genrich, J. F., Geng, J., Owen, S., Lindsey, E. O., ... Maharjan, N. (2015). Slip pulse and resonance of the Kathmandu basin during the 2015 Gorkha earthquake, Nepal. *Science*, *349*(6252), 1091–1095. https://doi.org/10.1126/science.aac6383

Gansser, A. (1981). The geodynamic history of the Himalaya. *Zagros Hindu Kush Himalaya Geodynamic Evolution*, *3*, 111–121. https://doi.org/10.1029/GD003p0111

Geller, R. J. (1997). Earthquake prediction: a critical review. *Geophysical Journal International*, *131*(3), 425–450. https://doi.org/10.1111/j.1365-246X.1997.tb06588.x

Ghazoui, Z., Bertrand, S., Vanneste, K., Yokoyama, Y., Nomade, J., Gajurel, A., & van der Beek, P. (2019). Potentially large post-1505 AD earthquakes in western Nepal revealed by a lake sediment record. *Nature communications*, *10*(1), 1–9. https://doi.org/10.1038/s41467-019-10093-4

Ghosh, U. (2020). Seismic characteristics and seismic hazard assessment: Source region of the 2015 Nepal earthquake Mw 7.8 in central Himalaya. *Pure and Applied Geophysics*, *177*(1), 181–194. https://doi.org/10.1007/s00024-019-02318-w

Ghoshal, S., McQuarrie, N., Robinson, D. M., Adhikari, D., Morgan, L. E., & Ehlers, T. A. (2020). Constraining central Himalayan (Nepal) fault geometry through integrated thermochronology and thermokinematic modeling. *Tectonics*, *39*(9), e2020TC006399. https://doi.org/10.1029/2020TC006399

Godano, C., & Caruso, V. (1995). Multifractal analysis of earthquake catalogues. *Geophysical Journal International*, *121*(2), 385–392. https://doi.org/10.1111/j.1365-246X.1995.tb05719.x

Gonzato, G., Mulargia, F., & Marzocchi, W. (1998). Practical application of fractal analysis: problems and solutions. *Geophysical Journal International*, *132*(2), 275–282. https://doi.org/10.1046/j.1365-246x.1998.00461.x

Grandin, R., Vallée, M., Satriano, C., Lacassin, R., Klinger, Y., Simoes, M., & Bollinger, L. (2015). Rupture process of the Mw = 7.9 2015 Gorkha earthquake (Nepal): Insights into Himalayan megathrust segmentation. *Geophysical Research Letters*, *42*(20), 8373–8382. https://doi.org/10.1002/2015GL066044

Grassberger, P., & Procaccia, I. (1983). Measuring the strangeness of strange attractors. *Physica. D*, *9*(1-2), 189–208. https://doi.org/10.1016/0167-2789(83)90298-1

Gualandi, A., Avouac, J.-P., Galetzka, J., Genrich, J. F., Blewitt, G., Adhikari, L. B., ... Liu-Zeng, J. (2017). Pre-and post-seismic deformation related to the 2015, Mw 7. 8 Gorkha earthquake, Nepal. *Tectonophysics*, *714*, 90–106. https://doi.org/10.1016/j.tecto.2016.06.014

Guglielmi, A. V. (2016). Interpretation of the Omori law. *Izvestiya, Physics of the Solid Earth*, *52*(5), 785–786. https://doi.org/10.1134/S1069351316050165

Guillot, S., Mahéo, G., De Sigoyer, J., Hattori, K., & Pecher, A. (2008). Tethyan and Indian subduction viewed from the Himalayan high-to

ultrahigh-pressure metamorphic rocks. *Tectonophysics*, *451*(1-4), 225–241. https://doi.org/10.1016/j.tecto.2007.11.059

Gupta, D., Bhowmick, D., & Roy, P. (2015). Himalayan hazard study on the basis of stress and strain state of 1991 Uttarkashi earthquake using coulomb stress transfer model. *Geomatics, Natural Hazards and Risk*, *6*(2), 131–148. https://doi.org/10.1080/19475705.2013.820797

Gupta, H., & Gahalaut, V. (2015). Can an earthquake of Mw∼ 9 occur in the Himalayan region? *Geological Society, London, Special Publications*, *412*(1), 43–53. https://doi.org/10.1144/SP412.10

Gupta, S., Roy, P., & Pal, S. (2021). Scale invariance behavior for pre and post-2015 Nepal Gorkha earthquake GPS time series based on fractal analysis. *Chaos, Solitons & Fractals*, *152*, 111341. https://doi.org/10.1016/j.chaos.2021.111341

Gutenberg, B., & Richter, C. F. (1944). Frequency of earthquakes in California. *Bulletin of the Seismological society of America*, *34*(4), 185–188. https://doi.org/10.1785/BSSA0340040185

Gutenberg, B., & Richter, C. F. (1950). Seismicity of the earth and associated phenomena. *Mausam*, *1*(2), 174–176. https://doi.org/10.54302/mausam.v1i2.4568

Hainzl, S., & Marsan, D. (2008). Dependence of the Omori-Utsu law parameters on main shock magnitude: Observations and modeling. *Journal of Geophysical Research: Solid Earth*, *113*(B10). https://doi.org/10.1029/2007JB005492

Hainzl, S., Zöller, G., & Kurths, J. (1999). Similar power laws for foreshock and aftershock sequences in a spring-block model for earthquakes. *Journal of Geophysical Research: Solid Earth*, *104*(B4), 7243–7253. https://doi.org/10.1029/1998JB900122

Hamdache, M., Peláez, J., Henares, J., Damerdji, Y., & Sawires, R. (2016). Analysis of the 2012–2013 Torreperogil-Sabiote seismic swarm. *Physics and Chemistry of the Earth, Parts A/B/C*, *95*, 101–112. https://doi.org/10.1016/j.pce.2016.01.003

Han, Q., Wang, L., Xu, J., Carpinteri, A., & Lacidogna, G. (2015). A robust method to estimate the b-value of the magnitude–frequency distribution of earthquakes. *Chaos, Solitons & Fractals*, *81*, 103–110. https://doi.org/10.1016/j.chaos.2015.09.004

Hanks, T. C., & Kanamori, H. (1979). A moment magnitude scale. *Journal of Geophysical Research: Solid Earth*, *84*(B5), 2348–2350. https://doi.org/10.1029/JB084iB05p02348

Hauck, M., Nelson, K., Brown, L., Zhao, W., & Ross, A. (1998). Crustal structure of the Himalayan orogen at 90 east longitude from Project INDEPTH deep reflection profiles. *Tectonics*, *17*(4), 481–500. https://doi.org/10.1029/98TC01314

Hazarika, D., Wadhawan, M., Paul, A., Kumar, N., & Borah, K. (2017). Geometry of the Main Himalayan Thrust and Moho beneath Satluj valley, northwest Himalaya: Constraints from receiver function analysis. *Journal of Geophysical Research: Solid Earth*, *122*(4), 2929–2945. https://doi.org/10.1002/2016JB013783

Helmstetter, A., & Shaw, B. E. (2006). Relation between stress heterogeneity and aftershock rate in the rate-and-state model. *Journal of Geophysical Research: Solid Earth*, *111*(B7). https://doi.org/10.1029/2005JB004077

Herman, F., Copeland, P., Avouac, J.-P., Bollinger, L., Mahéo, G., Le Fort, P., ... Henry, P. (2010). Exhumation, crustal deformation, and thermal structure of the Nepal Himalaya derived from the inversion of thermochronological and thermobarometric data and modeling of the topography. *Journal of Geophysical Research: Solid Earth*, *115*(B6). https://doi.org/10.1029/2008JB006126

Hirabayashi, T., Ito, K., & Yoshii, T. (1992). Multifractal analysis of earthquakes. In *Fractals and chaos in the earth sciences* (pp. 591–610). Springer. https://doi.org/10.1007/978-3-0348-6191-5$_5$

Hirata, T. (1989). Fractal dimension of fault systems in Japan: fractal structure in rock fracture geometry at various scales. In *Fractals in geophysics* (pp. 157–170). Springer. https://doi.org/10.1007/BF00874485

Hirata, T., Satoh, T., & Ito, K. (1987). Fractal structure of spatial distribution of microfracturing in rock. *Geophysical Journal International*, *90*(2), 369–374. https://doi.org/10.1111/j.1365-246X.1987.tb00732.x

Hirose, F., & Maeda, K. (2011). Earthquake forecast models for inland Japan based on the GR law and the modified GR law. *Earth, planets and space*, *63*(3), 239–260. https://doi.org/10.5047/eps.2010.10.002

Hodges, K. V. (2000). Tectonics of the Himalaya and southern Tibet from two perspectives. *Geological Society of America Bulletin*, *112*(3), 324–350. https://doi.org/10.1130/0016-7606(2000)112<3C324:TOTHAS>3E2.0.CO;2

Hong, S., & Liu, M. (2021). Postseismic deformation and afterslip evolution of the 2015 Gorkha earthquake constrained by InSAR and GPS observations. *Journal of Geophysical Research: Solid Earth*, *126*(7), e2020JB020230. https://doi.org/10.1029/2020JB020230

Huang, J., & Turcotte, D. L. (1988). Fractal distributions of stress and strength and variations of b-value. *Earth and Planetary Science Letters*, *91*(1-2), 223–230. https://doi.org/10.1016/0012-821X(88)90164-1

Hubbard, J., Almeida, R., Foster, A., Sapkota, S. N., Bürgi, P., & Tapponnier, P. (2016). Structural segmentation controlled the 2015 Mw 7.8 Gorkha earthquake rupture in Nepal. *Geology*, *44*(8), 639–642. https://doi.org/10.1130/G38077.1

Hubbard, M., Mukul, M., Gajurel, A. P., Ghosh, A., Srivastava, V., Giri, B., ... Mendoza, M. M. (2021). Orogenic segmentation and its role in Himalayan mountain building. *Frontiers in Earth Science*, *9*, 641666. https://doi.org/10.3389/feart.2021.641666

Hui, C., Cheng, C., Ning, L., & Yang, J. (2020). Multifractal characteristics of seismogenic systems and b values in the Taiwan seismic region. *ISPRS International Journal of Geo-Information*, *9*(6), 384. https://doi.org/10.3390/ijgi9060384

Ichiyanagi, M., Takai, N., Shigefuji, M., Bijukchhen, S., Sasatani, T., Rajaure, S., ... Takahashi, H. (2016). Aftershock activity of the 2015 Gorkha, Nepal, earthquake determined using the Kathmandu strong motion seismographic array. *Earth, Planets and space*, *68*(1), 1–6. https://doi.org/10.1186/s40623-016-0402-8

Ishimoto, M. (1939). Observations of earthquakes registered with the microseismograph constructed recently. *Bulletin of Earthquake Research Institute*, *17*, 443–478.

Jena, R., Ghansar, T. A. A., Pradhan, B., & Rai, A. K. (2021). Estimation of fractal dimension and b-value of earthquakes in the Himalayan region. *Arabian Journal of Geosciences*, *14*(10), 1–15. https://doi.org/10.1007/s12517-021-07271-4

Jena, R., Pradhan, B., Al-Amri, A., Lee, C. W., & Park, H.-j. (2020). Earthquake probability assessment for the Indian subcontinent using deep learning. *Sensors*, *20*(16), 4369. https://doi.org/10.3390/s20164369

Jiang, Z., Yuan, L., Huang, D., Yang, Z., & Hassan, A. (2018). Postseismic deformation associated with the 2015 Mw 7.8 Gorkha earthquake, Nepal: Investigating ongoing afterslip and constraining crustal rheology. *Journal of Asian Earth Sciences*, *156*, 1–10. https://doi.org/10.1016/j.jseaes.2017.12.039

Jing, L., Chen, J., Zhang, J., Zhang, P., LingSen, Z., ZhanFei, L., & Wei, W. (2015). Tectonic setting and general features of coseismic rupture of the 25 April, 2015 MW 7.8 Gorkha, Nepal earthquake. *Chinese Science Bulletin*, *60*(27), 2640–2655. https://doi.org/10.1360/N972015-00559

Jouanne, F., Gajurel, A., Mugnier, J.-L., Bollinger, L., Adhikari, L. B., Koirala, B., ... Huyghe, P. (2019). Postseismic deformation following the April 25, 2015 Gorkha

earthquake (Nepal): Afterslip versus viscous relaxation. *Journal of Asian Earth Sciences*, *176*, 105–119. https://doi.org/10.1016/j.jseaes.2019.02.009

Jouanne, F., Mugnier, J.-L., Gamond, J., Le Fort, P., Pandey, M., Bollinger, L., ... Avouac, J.-P. (2004). Current shortening across the Himalayas of Nepal. *Geophysical Journal International*, *157*(1), 1–14. https://doi.org/10.1111/j.1365-246X.2004.02180.x

Kagan, Y. Y. (2007). Earthquake spatial distribution: the correlation dimension. *Geophysical Journal International*, *168*(3), 1175–1194. https://doi.org/10.1111/j.1365-246X.2006.03251.x

Kaiser, M. S., & Al Banna, M. (2020). Application of artificial intelligence in predicting earthquakes: state-of-the-art and future challenges. *IEEE Access*, *8*, 192880–192923. https://doi.org/10.1109/ACCESS.2020.3029859

Kalafat, D., & Görgün, E. (2019). Source characteristics and b-values of the Tuz Gölü fault zone in central Anatolia, Turkey. *Journal of Asian Earth Sciences*, *179*, 337–349. https://doi.org/10.1016/j.jseaes.2019.05.005

Kame, N., Fujita, S., Nakatani, M., & Kusakabe, T. (2013). Effects of a revised rate-and state-dependent friction law on aftershock triggering model. *Tectonophysics*, *600*, 187–195. https://doi.org/10.1016/j.tecto.2012.11.028

Kanamori, H., & Anderson, D. L. (1975). Theoretical basis of some empirical relations in seismology. *Bulletin of the seismological society of America*, *65*(5), 1073–1095. https://doi.org/10.1785/BSSA0650051073

Kayal, J. (2010). Himalayan tectonic model and the great earthquakes: an appraisal. *Geomatics, Natural Hazards and Risk*, *1*(1), 51–67. https://doi.org/10.1080/19475701003625752

Kellett, D. A., Cottle, J. M., & Larson, K. P. (2019). The South Tibetan Detachment System: history, advances, definition and future directions. *Geological Society, London, Special Publications*, *483*(1), 377–400. https://doi.org/10.1144/SP483.2

Khalid, P., Bajwa, A. A., Naeem, M., & Din, Z. U. (2016). Seismicity distribution and focal mechanism solution of major earthquakes of northern Pakistan. *Acta Geodaetica et Geophysica*, *51*(3), 347–357. https://doi.org/10.1007/s40328-015-0130-8

Khalil, U., Aslam, B., & Maqsoom, A. (2021). Afghanistan earthquake 2015 aftershocks analysis for a better understanding of the seismicity behavior for future assessment. *Acta Geophysica*, *69*(4), 1189–1197. https://doi.org/10.1007/s11600-021-00624-3

Khattri, K., & Tyagi, A. (1983). Seismicity patterns in the Himalayan plate boundary and identification of the areas of high seismic potential. *Tectonophysics*, *96*(3-4), 281–297. https://doi.org/10.1016/0040-1951(83)90222-6

Khattri, K., Wyss, M., Gaur, V., Saha, S., & Bansal, V. (1983). Local seismic activity in the region of the Assam gap, northeast India. *Bulletin of the Seismological Society of America*, *73*(2), 459–469. https://doi.org/10.1785/BSSA0730020459

Kijko, A., & Smit, A. (2012). Extension of the Aki-Utsu b-value estimator for incomplete catalogs. *Bulletin of the Seismological Society of America*, *102*(3), 1283–1287. https://doi.org/10.1785/0120110226

King, G. (1983). The accommodation of large strains in the upper lithosphere of the earth and other solids by self-similar fault systems: the geometrical origin of b-value. *Pure and Applied Geophysics*, *121*(5), 761–815. https://doi.org/10.1007/BF02590182

Kisslinger, C., & Jones, L. M. (1991). Properties of aftershock sequences in southern California. *Journal of Geophysical Research: Solid Earth*, *96*(B7), 11947–11958. https://doi.org/10.1029/91JB01200

Klinkenberg, B., & Goodchild, M. (1992). The fractal properties of topography: a comparison of methods. *Earth surface processes and landforms*, *17*(3), 217–234. https://doi.org/10.1002/esp.3290170303

Kraaijpoel, D., Martins, J. E., Osinga, S., Vogelaar, B., & Breunese, J. (2022). Statistical analysis of static and dynamic predictors for seismic b-value variations in the Groningen gas field. *Netherlands Journal of Geosciences*, *101*, e18. https://doi.org/10.1017/njg.2022.15

Kubo, H., Dhakal, Y. P., Suzuki, W., Kunugi, T., Aoi, S., & Fujiwara, H. (2016). Estimation of the source process of the 2015 Gorkha, Nepal, earthquake and simulation of long-period ground motions in the Kathmandu basin using a one-dimensional basin structure model. *Earth, Planets and Space*, *68*(1), 1–10. https://doi.org/10.1186/s40623-016-0393-5

Kumahara, Y., Chamlagain, D., & Upreti, B. N. (2016). Geomorphic features of active faults around the Kathmandu Valley, Nepal, and no evidence of surface rupture associated with the 2015 Gorkha earthquake along the faults. *Earth, Planets and Space*, *68*(1), 1–8. https://doi.org/10.1186/s40623-016-0429-x

Kumar, A., Singh, S. K., Mitra, S., Priestley, K., & Dayal, S. (2017). The 2015 April 25 Gorkha (Nepal) earthquake and its aftershocks: implications for lateral

heterogeneity on the Main Himalayan Thrust. *Geophysical Journal International*, *208*(2), 992–1008. https://doi.org//10.1093/gji/ggw438

Kumar, N., Yadav, D. K., Mondal, S., & Roy, P. (2013). Stress drop and its relation to tectonic and structural elements for the meizoseismal region of great 1905 Kangra earthquake of the NW Himalaya. *Natural hazards*, *69*(3), 2021–2038. https://doi.org/10.1007/s11069-013-0793-9

Kurashimo, E., Sato, H., Sakai, S., Hirata, N., Gajurel, A. P., Adhikari, D. P., ... Upreti, B. N. (2019). The 2015 Gorkha earthquake: Earthquake reflection imaging of the source fault and connecting seismic structure with fault slip behavior. *Geophysical Research Letters*, *46*(6), 3206–3215. https://doi.org/10.1029/2018GL081197

Lavé, J., & Avouac, J.-P. (2000). Active folding of fluvial terraces across the Siwaliks Hills, Himalayas of central Nepal. *Journal of Geophysical Research: Solid Earth*, *105*(B3), 5735–5770. https://doi.org/10.1029/1999JB900292

Le Fort, P. (1975). Himalayas: the collided range. Present knowledge of the continental arc. *American Journal of Science*, *275*(1), 1-44.

Lei, X. (2019). Evolution of b-value and fractal dimension of acoustic emission events during shear rupture of an immature fault in granite. *Applied Sciences*, *9*(12), 2498. https://doi.org/10.3390/app9122498

Lei, X., & Kusunose, K. (1999). Fractal structure and characteristic scale in the distributions of earthquake epicentres, active faults and rivers in Japan. *Geophysical Journal International*, *139*(3), 754–762. https://doi.org/10.1046/j.1365-246x.1999.00977.x

Letort, J., Bollinger, L., Lyon-Caen, H., Guilhem, A., Cano, Y., Baillard, C., & Adhikari, L. B. (2016). Teleseismic depth estimation of the 2015 Gorkha-Nepal aftershocks. *Geophysical Journal International*, *207*(3), 1584–1595. https://doi.org/10.1093/gji/ggw364

Li, D., Zheng, Z., & Wang, B. (1994). Research into the multifractal of earthquake spatial distribution. *Tectonophysics*, *233*(1-2), 91–97. https://doi.org/10.1016/0040-1951(94)90222-4

Li, S., Wang, Q., Chen, G., He, P., Ding, K., Chen, Y., & Zou, R. (2019). Interseismic coupling in the central Nepalese Himalaya: Spatial Correlation with the 2015 Mw 7.9 Gorkha Earthquake. *Pure and Applied Geophysics*, *176*(9), 3893–3911. https://doi.org/10.1007/s00024-019-02121-7

Lin, J.-Y., & Wu, W.-N. (2012). Spatio-temporal distribution of seismic moment release near the source area of the 2011 Tohoku-Oki earthquake. *Earth, planets and space*, *64*(12), 1067–1075. https://doi.org/10.5047/eps.2012.04.006

Lindsey, E. O., Natsuaki, R., Xu, X., Shimada, M., Hashimoto, M., Melgar, D., & Sandwell, D. T. (2015). Line-of-sight displacement from ALOS-2 interferometry: Mw 7.8 Gorkha Earthquake and Mw 7.3 aftershock. *Geophysical Research Letters*, *42*(16), 6655–6661. https://doi.org/10.1002/2015GL065385

Liu, G., Wang, Q., & Qiao, X. (2016). A unified source model of the 2015 Gorkha earthquake. In *Agu fall meeting abstracts* (Vol. 2016, pp. G31A–1036). https://doi.org/10.6038/cjg20170714

Macek, W. M. (2012). Multifractal turbulence in the heliosphere. *Exploring the Solar Wind*, 143–168. https://doi.org/10.1007/s11214-022-00914-2

Mach, J., Mas, F., & Sagués, F. (1995). Two representations in multifractal analysis. *Journal of Physics A: Mathematical and General*, *28*(19), 5607. https://doi.org/10.1088/0305-4470/2F28/2F19/2F015

Mainieri, R. (1993). On the equality of Hausdorff and box counting dimensions. *Chaos: An Interdisciplinary Journal of Nonlinear Science*, *3*(2), 119–125. https://doi.org/10.1063/1.165970

Malik, J. N., & Nakata, T. (2003). Active faults and related Late Quaternary deformation along the northwestern Himalayan Frontal Zone, India. *Annals of Geophysics*. https://doi.org/10.4401/ag-3462

Mandal, P., Mabawonku, A. O., & Dimri, V. P. (2005). Self-organized fractal seismicity of reservoir triggered earthquakes in the Koyna-Warna seismic zone, western India. *Pure and applied Geophysics*, *162*(1), 73–90. https://doi.org/10.1111/j.1365-246X.2009.04079.x

Mandal, P., Rastogi, B., & Gupta, H. K. (2000). Recent Indian earthquakes. *Current Science*, 1334–1346.

Mandal, P., Srinagesh, D., Suresh, G., Naresh, B., Naidu, M., Singh, D. K., . . . Saha, S. (2021). Characterization of earthquake hazard at the Palghar and Pulichintala swarm activity regions (India) through three-dimensional modelling of b-value and fractal (correlation) dimensions. *Natural Hazards*, *108*(1), 1183–1196. https://doi.org/10.1007/s11069-021-04726-5

Mandelbrot, B. B. (1967). How long is the coast of Britain? statistical self-similarity and fractional dimension. *science*, *156*(3775), 636–638. https://doi.org/10.1126/science.156.3775.636

Mandelbrot, B. B. (1982). *The fractal geometry of nature* (Vol. 1). WH freeman New York. https://doi.org/10.2307/2323761

Mandelbrot, B. B. (1989). Multifractal measures, especially for the geophysicist. In *Fractals in geophysics* (pp. 5–42). Springer. https://doi.org/10.1007/BF00874478

Martin, S. S., Hough, S. E., & Hung, C. (2015). Ground motions from the 2015 Mw 7.8 Gorkha, Nepal, earthquake constrained by a detailed assessment of macroseismic data. *Seismological Research Letters*, *86*(6), 1524–1532. https://doi.org/10.1785/0220150138

Matcharashvili, T., Chelidze, T., Javakhishvili, Z., Zhukova, N., Jorjiashvili, N., Shengelia, I., ... Sborshchikovi, A. (2018). Analysis of the complexity of seismic data sets: Case study for Caucasus. In *Complexity of seismic time series* (p. 3-24). Elsevier. https://doi.org/10.1016/B978-0-12-813138-1.00001-8

Matin, A., & Mukul, M. (2020). Himalayan cross faults affect thrust sheet geometry: An example from the Munsiari thrust sheet near the Gish Transverse fault zone, frontal Darjiling Himalaya, India. *Journal of Asian Earth Sciences*, *199*, 104400. https://doi.org/10.1016/j.jseaes.2020.104400

Matte, P., Mattauer, M., Olivet, J., & Griot, D. (1997). Continental subductions beneath Tibet and the Himalayan orogeny: a review. *Terra Nova*, *9*(5-6), 264–270. https://doi.org/10.1111/j.1365-3121.1997.tb00026.x

McNamara, D. E., Yeck, W. L., Barnhart, W. D., Schulte-Pelkum, V., Bergman, E., Adhikari, L., ... Earle, P. S. (2017). Source modeling of the 2015 Mw 7.8 Nepal (Gorkha) earthquake sequence: Implications for geodynamics and earthquake hazards. *Tectonophysics*, *714*, 21–30. https://doi.org/10.1016/j.tecto.2016.08.004

Meigs, A. J., Burbank, D. W., & Beck, R. A. (1995). Middle-late Miocene (> 10 Ma) formation of the Main Boundary thrust in the western Himalaya. *Geology*, *23*(5), 423–426. https://doi.org/10.1130/0091-7613(1995)023<3C0423:MLMMFO>3E2.3.CO;2

Mencin, D., Bendick, R., Upreti, B. N., Adhikari, D. P., Gajurel, A. P., Bhattarai, R. R., ... Bilham, R. (2016). Himalayan strain reservoir inferred from limited afterslip following the Gorkha earthquake. *Nature Geoscience*, *9*(7), 533–537. https://doi.org/10.1038/ngeo2734

Mendoza, M., Ghosh, A., Karplus, M., Klemperer, S., Sapkota, S., Adhikari, L., & Velasco, A. (2019). Duplex in the Main Himalayan Thrust illuminated by

aftershocks of the 2015 Mw 7.8 Gorkha earthquake. *Nature Geoscience*, *12*(12), 1018–1022. https://doi.org/10.1038/s41561-019-0474-8

Meng, F., Wong, L. N. Y., & Zhou, H. (2019). Power law relations in earthquakes from microscopic to macroscopic scales. *Scientific reports*, *9*(1), 1–11. https://doi.org/10.1038/s41598-019-46864-8

Michel, S., Jolivet, R., Rollins, C., Jara, J., & Dal Zilio, L. (2021). Seismogenic potential of the Main Himalayan Thrust constrained by coupling segmentation and earthquake scaling. *Geophysical Research Letters*, *48*(13), e2021GL093106. https://doi.org/10.1029/2021GL093106

Mitra, S., Paul, H., Kumar, A., Singh, S. K., Dey, S., & Powali, D. (2015). The 25 April 2015 Nepal earthquake and its aftershocks. *Current Science*, 1938–1943.

Mizrahi, L., Nandan, S., & Wiemer, S. (2021). The effect of declustering on the size distribution of mainshocks. *Seismological Society of America*, *92*(4), 2333–2342. https://doi.org/10.1785/0220200231

Mogi, K. (1967). Earthquakes and fractures. *Tectonophysics*, *5*(1), 35–55. https://doi.org/10.1016/0040-1951(67)90043-1

Molnar, P., & Lyon-Caent, H. (1989). Fault plane solutions of earthquakes and active tectonics of the Tibetan Plateau and its margins. *Geophysical Journal International*, *99*(1), 123–153. https://doi.org/10.1111/j.1365-246X.1989.tb02020.x

Molnar, P., & Pandey, M. (1989). Rupture zones of great earthquakes in the Himalayan region. *Proceedings of the Indian Academy of Sciences-Earth and Planetary Sciences*, *98*(1), 61-70. https://doi.org/10.1007/BF02880376

Molnar, P., & Tapponnier, P. (1975). Cenozoic tectonics of Asia: Effects of a Continental Collision: Features of recent continental tectonics in Asia can be interpreted as results of the India-Eurasia collision. *Science*, *189*(4201), 419–426. https://doi.org/10.1126/science.189.4201.419

Mondal, S., & Roy, P. (2016). Temporal multifractal pattern of seismicity in northwest Himalayan region. *Journal of the Geological Society of India*, *88*(5), 569–575. https://doi.org/10.1007/s12594-016-0522-6

Mondal, S., Roy, P. N. S., Catherine, J. K., & Pandey, A. K. (2019). Significance of fractal correlation dimension and seismic b-value variation due to 15th July 2009, New Zealand earthquake of Mw 7.8. *Annals of Geophysics*, *62*(5), SE568–SE568. https://doi.org/10.4401/ag-8020

Monterrubio, M., Lana, X., Martínez, M. D., Zúñiga, F. R., & Puente, J. d. l. (2020). Evolution of the multifractal parameters along different steps of a seismic activity. The example of Canterbury 2000–2018 (New Zealand). *AIP advances*, *10*(11), 115109. https://doi.org/10.1063/5.0010103

Morell, K. D., Sandiford, M., Rajendran, C., Rajendran, K., Alimanovic, A., Fink, D., & Sanwal, J. (2015). Geomorphology reveals active décollement geometry in the central Himalayan seismic gap. *Lithosphere*, *7*(3), 247–256. https://doi.org/10.1130/L407.1

Moritz, R., & Baker, T. (2019). Metallogeny of the Tethyan orogenic belt: From Mesozoic magmatic arcs to Cenozoic back-arc and postcollisional settings in southeast Europe, Anatolia, and the lesser Caucasus: An introduction. *Economic Geology*, *114*(7), 1227–1235. https://doi.org/10.5382/econgeo.4683

Mugnier, J.-L., Gajurel, A., Huyghe, P., Jayangondaperumal, R., Jouanne, F., & Upreti, B. (2013). Structural interpretation of the great earthquakes of the last millennium in the central Himalaya. *Earth-Science Reviews*, *127*, 30–47. https://doi.org/10.1016/j.earscirev.2013.09.003

Mugnier, J.-L., Huyghe, P., Gajurel, A. P., Upreti, B. N., & Jouanne, F. (2011). Seismites in the Kathmandu basin and seismic hazard in central Himalaya. *Tectonophysics*, *509*(1-2), 33–49. https://doi.org/10.1016/j.tecto.2011.05.012

Mugnier, J.-L., Jouanne, F., Bhattarai, R., Cortes-Aranda, J., Gajurel, A., Leturmy, P., ... Vassallo, R. (2017). Segmentation of the Himalayan megathrust around the Gorkha earthquake (25 April 2015) in Nepal. *Journal of Asian Earth Sciences*, *141*, 236–252. https://doi.org/10.1016/j.jseaes.2017.01.015

Mullick, M., & Mukhopadhyay, D. (2017). Quantitative analysis of the Nepal earthquake on 25 April, 2015 in the perspective of future earthquake hazard. *Geodesy and Geodynamics*, *8*(2), 77–83. https://doi.org/10.1016/j.geog.2017.02.003

Nakamura, M. (2002). Determination of focal mechanism solution using initial motion polarity of P and S waves. *Physics of the Earth and Planetary Interiors*, *130*(1-2), 17–29. https://doi.org/10.1016/S0031-9201(01)00306-5

Nakata, T. (1982). A photogrametric study on active faults in the Nepal Himalayas. *Journal of Nepal Geological Society*, *2*, 67–80. https://doi.org/10.1130/SPE232-p243

Nakata, T. (1989). Active faults of the Himalaya of India and Nepal. *Geological Society of America Special Paper*, *232*(1), 243–264. https://doi.org/10.1130/SPE232-p243

Nakaya, S., & Hashimoto, T. (2002). Temporal variation of multifractal properties of seismicity in the region affected by the mainshock of the october 6, 2000 western Tottori Prefecture, Japan, earthquake (M= 7.3). *Geophysical research letters*, *29*(10), 133–1. https://doi.org/10.1029/2001GL014216

Nampally, S., Padhy, S., & Dimri, V. P. (2018). Characterizing spatial heterogeneity based on the b-value and fractal analyses of the 2015 Nepal earthquake sequence. *Tectonophysics*, *722*, 154–162. https://doi.org/10.1016/j.tecto.2017.11.004

Narteau, C., Byrdina, S., Shebalin, P., & Schorlemmer, D. (2009). Common dependence on stress for the two fundamental laws of statistical seismology. *Nature*, *462*(7273), 642–645. https://doi.org/10.1038/nature08553

Nerenberg, M., & Essex, C. (1990). Correlation dimension and systematic geometric effects. *Physical Review A*, *42*(12), 7065. https://doi.org/10.1103/physreva.42.7065

Ni, J., & Barazangi, M. (1984). Seismotectonics of the Himalayan collision zone: Geometry of the underthrusting Indian plate beneath the Himalaya. *Journal of Geophysical Research: Solid Earth*, *89*(B2), 1147–1163. https://doi.org/10.1029/JB089iB02p01147

Ni, J., Guzman-Speziale, M., Bevis, M., Holt, W. E., Wallace, T. C., & Seager, W. R. (1989). Accretionary tectonics of Burma and the three-dimensional geometry of the Burma subduction zone. *Geology*, *17*(1), 68–71. https://doi.org/10.1130/0091-7613(1989)017<3C0068:ATOBAT>3E2.3.CO;2

Nie, Q., Shi, K., Gong, Y., Ran, F., Li, Z., Chen, R., & Hua, L. (2020). Spatial–temporal variability of land surface temperature spatial pattern: Multifractal detrended fluctuation analysis. *IEEE Journal of Selected Topics in Applied Earth Observations and remote Sensing*, *13*, 2010–2018. https://doi.org/10.1109/JSTARS.2020.2990479

Ogata, Y., & Tsuruoka, H. (2016). Statistical monitoring of aftershock sequences: a case study of the 2015 Mw 7. 8 Gorkha, Nepal, earthquake. *Earth, Planets and Space*, *68*(1), 1–13. https://doi.org/10.1186/s40623-016-0410-8

Okubo, P. G., & Aki, K. (1987). Fractal geometry in the San Andreas fault system. *Journal of Geophysical Research: Solid Earth*, *92*(B1), 345–355. https://doi.org/10.1029/JB092iB01p00345

Omori, F. (1895). *On the after-shocks of earthquakes* (Unpublished doctoral dissertation). The University of Tokyo.

Öncel, A. O., Main, I., Alptekin, Ö., & Cowie, P. (1996). Spatial variations of the fractal properties of seismicity in the Anatolian fault zones. *Tectonophysics*, *257*(2-4), 189–202. https://doi.org/10.1016/0040-1951(95)00132-8

Oncel, A. O., & Wilson, T. (2006). Evaluation of earthquake potential along the northern Anatolian Fault Zone in the Marmara Sea using comparisons of GPS strain and seismotectonic parameters. *Tectonophysics*, *418*(3-4), 205–218. https://doi.org/10.1016/j.tecto.2006.02.006

Ouillon, G., Sornette, D., & Ribeiro, E. (2009). Multifractal Omori law for earthquake triggering: new tests on the California, Japan and world-wide catalogues. *Geophysical Journal International*, *178*(1), 215–243. https://doi.org/10.1111/j.1365-246X.2009.04079.x

Ousadou, F., Dorbath, L., Ayadi, A., Dorbath, C., & Gharbi, S. (2014). Stress field variations along the Maghreb region derived from inversion of major seismic crisis fault plane solutions. *Tectonophysics*, *632*, 261–280. https://doi.org/10.1016/j.tecto.2014.06.017

Pailoplee, S., & Choowong, M. (2014). Earthquake frequency-magnitude distribution and fractal dimension in mainland Southeast Asia. *Earth, Planets and space*, *66*(1), 1–10. https://doi.org//10.1186/1880-5981-66-8

Parameswaran, R. M., & Rajendran, K. (2017). Structural context of the 2015 pair of Nepal earthquakes (Mw 7.8 and Mw 7.3): an analysis based on slip distribution, aftershock growth, and static stress changes. *International Journal of Earth Sciences*, *106*(3), 1133–1146. https://doi.org/10.1007/s00531-016-1358-4

Pastén, D., & Comte, D. (2014). Multifractal analysis of three large earthquakes in Chile: Antofagasta 1995, Valparaiso 1985, and Maule 2010. *Journal of seismology*, *18*(4), 707–713. https://doi.org/10.1007/s10950-014-9432-5

Paudel, L. P., & Arita, K. (2000). Tectonic and polymetamorphic history of the Lesser Himalaya in central Nepal. *Journal of Asian Earth Sciences*, *18*(5), 561–584. https://doi.org/10.1016/S1367-9120(99)00069-3

Paudyal, H., Shanker, D., Singh, H., Panthi, A., Kumar, A., & Singh, V. (2010). Current understanding of the seismotectonics of western Nepal Himalaya and vicinity. *Acta Geodaetica et Geophysica Hungarica*, *45*(2), 195–209. https://doi.org/10.1556/AGeod.45.2010.2.5

Paudyal, H., Singh, H., Shanker, D., & Singh, V. (2008). Stress pattern in two seismogenic sources in Nepal-Himalaya and its vicinity. *Acta Geophysica*, *56*, 313–323. https://doi.org/10.2478/s11600-008-00013-2

Pêcher, A. (1989). The metamorphism in the central Himalaya. *Journal of Metamorphic Geology*, *7*(1), 31–41. https://doi.org/10.1111/j.1525-1314.1989.tb00573.x

Pietronero, L. (1989). Theoretical concepts fpr fractal growth. *Physica D: Nonlinear Phenomena*, *38*(1-3), 279–286. https://doi.org/10.1016/0167-2789(89)90206-6

Posadas, A. N. D., Quiroz, R., Zorogastua, P., & León-Velarde, C. (2005). Multifractal characterization of the spatial distribution of ulexite in a Bolivian salt flat. *International Journal of Remote Sensing*, *26*(3), 615–627. https://doi.org/10.1080/01431160512331299261

Powell, C. M., & Conaghan, P. (1973). *Plate tectonics and the Himalayas: Earth and planetary science letters.* https://doi.org/10.1016/0012-821X(73)90134-9

Powell, C. M., & Conaghan, P. (1975). Tectonic models of the Tibetan plateau. *Geology*, *3*(12), 727–731. https://doi.org/10.1130/0091-7613(1975)3<3C727:TMOTTP>3E2.0.CO;2

Powers, P. M., Lillie, R. J., & Yeats, R. S. (1998). Structure and shortening of the Kangra and Dehra Dun reentrants, sub-Himalaya, India. *Geological Society of America Bulletin*, *110*(8), 1010–1027. https://doi.org/10.1130/0016-7606(1998)110<3C1010:SASOTK>3E2.3.CO;2

Prasath, R. A., Paul, A., & Singh, S. (2019). Earthquakes in the Garhwal Himalaya of the central seismic gap: a study of historical and present seismicity and their implications to the seismotectonics. *Pure and Applied Geophysics*, *176*(11), 4661–4685. https://doi.org/10.1007/s00024-019-02239-8

Priyanka, R. S., Jayangondaperumal, R., Pandey, A., Mishra, R. L., Singh, I., Bhushan, R., . . . Bhat, G. R. (2017). Primary surface rupture of the 1950 Tibet-Assam great earthquake along the eastern Himalayan front, India. *Scientific reports*, *7*(1), 1–12. https://doi.org/10.1038/s41598-017-05644-y

Pye, A. E., Hodges, K. V., Keller, C. B., Law, R. D., van Soest, M. C., Bhandari, B., & McDonald, C. S. (2022). Prolonged Slip on the South Tibetan Detachment Constrains Tectonic Models for Synorogenic Extension in the Central Himalaya. *Tectonics*, *41*(11), e2022TC007298. https://doi.org/10.1029/2022TC007298

Qiu, Q., Hill, E. M., Barbot, S., Hubbard, J., Feng, W., Lindsey, E. O., . . . Tapponnier, P. (2016). The mechanism of partial rupture of a locked megathrust: The role of fault morphology. *Geology*, *44*(10), 875–878. https://doi.org/10.1130/G38178.1

Qureshi, K. A., & Khan, S. D. (2020). Active Tectonics of the Frontal Himalayas: An Example from the Manzai Ranges in the Recess Setting, Western Pakistan. *Remote Sensing*, *12*(20), 3362. https://doi.org/10.3390/rs12203362

Radziminovich, N. A., Miroshnichenko, A. I., & Zuev, F. L. (2019). Magnitude of completeness, b-value, and spatial correlation dimension of earthquakes in the South Baikal Basin, Baikal Rift System. *Tectonophysics*, *759*, 44–57. https://doi.org/10.1016/j.tecto.2019.04.002

Rajendran, C., John, B., Anandasabari, K., Sanwal, J., Rajendran, K., Kumar, P., & Chopra, S. (2018). On the paleoseismic evidence of the 1803 earthquake rupture (or lack of it) along the frontal thrust of the kumaun himalaya. *Tectonophysics*, *722*, 227–234. https://doi.org/10.1016/j.tecto.2017.11.012

Rajendran, C., John, B., & Rajendran, K. (2015). Medieval pulse of great earthquakes in the central Himalaya: Viewing past activities on the frontal thrust. *Journal of Geophysical Research: Solid Earth*, *120*(3), 1623–1641. https://doi.org/10.1002/2014JB011015

Rajendran, C., & Rajendran, K. (2005). The status of central seismic gap: a perspective based on the spatial and temporal aspects of the large Himalayan earthquakes. *Tectonophysics*, *395*(1-2), 19–39. https://doi.org/10.1016/j.tecto.2004.09.009

Rajendran, C., Sanwal, J., John, B., Anandasabari, K., Rajendran, K., Kumar, P., ... Chopra, S. (2019). Footprints of an elusive mid-14th century earthquake in the central Himalaya: Consilience of evidence from Nepal and India. *Geological Journal*, *54*(5), 2829–2846. https://doi.org/10.1002/gj.3385

Rajendran, K., Parameswaran, R. M., & Rajendran, C. (2017). Seismotectonic perspectives on the Himalayan arc and contiguous areas: Inferences from past and recent earthquakes. *Earth-Science Reviews*, *173*, 1–30. https://doi.org/10.1016/j.earscirev.2017.08.003

Ram, A., & Roy, P. (2005). Fractal dimensions of blocks using a box-counting technique for the 2001 Bhuj earthquake, Gujarat, India. *Pure and applied geophysics*, *162*(3), 531–548. https://doi.org/10.1007/s00024-004-2620-4

Reasenberg, P. (1985). Second-order moment of central California seismicity, 1969–1982. *Journal of Geophysical Research: Solid Earth*, *90*(B7), 5479–5495. https://doi.org/10.1029/JB090iB07p05479

Reasenberg, P., & Jones, L. M. (1989). Earthquake hazard after a mainshock in California. *Science*, *243*(4895), 1173–1176. https://doi.org/10.1126/science.243.4895.1173

Rikitake, T. (1968). Earthquake prediction. *Earth-Science Reviews*, *4*, 245–282.

Roback, K., Clark, M. K., West, A. J., Zekkos, D., Li, G., Gallen, S. F., ... Godt, J. W. (2018). The size, distribution, and mobility of landslides caused by the 2015 Mw 7. 8 Gorkha earthquake, Nepal. *Geomorphology*, *301*, 121–138. https://doi.org/10.1016/j.geomorph.2017.01.030

Roy, P., & Mondal, S. (2012). Multifractal analysis of earthquakes in Kumaun Himalaya and its surrounding region. *Journal of earth system science*, *121*(4), 1033–1047. https://doi.org/10.1007/s12040-012-0208-4

Roy, P., & Padhi, A. (2007). Multifractal analysis of earthquakes in the southeastern Iran-Bam region. *Pure and Applied Geophysics*, *164*(11), 2271–2290. https://doi.org/10.1007/s00024-007-0272-x

Roy, P., & Ram, A. (2006). A correlation integral approach to the study of 26 January 2001 Bhuj earthquake, Gujarat, India. *Journal of Geodynamics*, *41*(4), 385–399. https://doi.org/10.1016/j.jog.2005.10.003

Rundle, J. B., Turcotte, D., Donnellan, A., Grant Ludwig, L., Luginbuhl, M., & Gong, G. (2016). Nowcasting earthquakes. *Earth and Space Science*, *3*(11), 480–486. https://doi.org/10.1002/2016EA000185

Sakai, H., Imayama, T., Yoshida, K., & Asahi, K. (2017). Tectonics of the Himalayas. *Journal of the Geological Society of Japan*, *123*, 403–421. https://doi.org/10.5575/geosoc.2017.0026

Sathiakumar, S., & Barbot, S. (2021). The stop-start control of seismicity by fault bends along the Main Himalayan Thrust. *Communications Earth & Environment*, *2*(1), 1–11. https://doi.org/10.1038/s43247-021-00153-3

Schelling, D. (1992). The tectonostratigraphy and structure of the eastern Nepal Himalaya. *Tectonics*, *11*(5), 925–943. https://doi.org/10.1029/92TC00213

Schiffman, C., Bali, B. S., Szeliga, W., & Bilham, R. (2013). Seismic slip deficit in the Kashmir Himalaya from GPS observations. *Geophysical Research Letters*, *40*(21), 5642–5645. https://doi.org/10.1002/2013GL057700

Scholz, C. (1968). The frequency-magnitude relation of microfracturing in rock and its relation to earthquakes. *Bulletin of the seismological society of America*, *58*(1), 399–415. https://doi.org/10.1785/BSSA0580010399

Schorlemmer, D., Wiemer, S., & Wyss, M. (2005). Variations in earthquake-size distribution across different stress regimes. *Nature*, *437*(7058), 539–542. https://doi.org/10.1038/nature04094

Searle, M. P., Law, R. D., Godin, L., Larson, K. P., Streule, M. J., Cottle, J. M., & Jessup, M. J. (2008). Defining the Himalayan main central thrust in Nepal. *Journal of the Geological Society*, *165*(2), 523–534. https://doi.org/10.1144/0016-76492007-081

Searle, M. P., & Treloar, P. J. (2019). *Introduction to Himalayan tectonics: a modern synthesis* (Vol. 483) (No. 1). Geological Society of London. https://doi.org/10.1144/SP483-2019-20

Seeber, L., & Armbruster, J. G. (1981). Great detachment earthquakes along the Himalayan arc and long-term forecasting. *Earthquake prediction: an international review*, *4*, 259–277. https://doi.org/10.1029/ME004p0259

Sharma, K. K. (1998). Geologic and tectonic evolution of the Himalaya before and after the India-Asia collision. *Proceedings of the Indian Academy of Sciences-Earth and Planetary Sciences*, *107*(4), 265–282. https://doi.org/10.1007/BF02841594

Shi, Y., & Bolt, B. A. (1982). The standard error of the magnitude-frequency b value. *Bulletin of the Seismological Society of America*, *72*(5), 1677–1687. https://doi.org/10.1785/BSSA0720051677

Shrivastava, M. N. (2021). The Gorkha earthquake 2015 and the largest aftershock in the Indian-Eurasian collision zone. *Arabian Journal of Geosciences*, *14*(13), 1–11. https://doi.org/10.1007/s12517-021-07557-7

Sianturi, H. L., Susilo, A., & Maryanto, S. (2019). Correlation Analysis of Spatial Distribution, Temporal Seismotectonics, and Return Period of Earthquake in East Nusa Tenggara, Indonesia. *International Journal of Geophysics*, *2019*. https://doi.org/10.1155/2019/5485783

Singh, D. (2000). Seismotectonics of the Himalaya and its vicinity from centroid-moment tensor (CMT) solution of earthquakes. *Journal of Geodynamics*, *30*(5), 507–537. https://doi.org/10.1016/S0264-3707(00)00007-7

Singh, I., Pandey, A., Mishra, R. L., Priyanka, R. S., Brice, A., Jayangondaperumal, R., & Srivastava, V. (2021). Evidence of the 1950 great Assam earthquake surface break along the Mishmi Thrust at Namche Barwa Himalayan Syntaxis. *Geophysical Research Letters*, *48*(11), e2020GL090893. https://doi.org/10.1029/2020GL090893

Singh, R., & Singh, A. (2014). Microstructural and geochemical studies of Higher Himalayan Leucogranite: implications for geodynamic evolution of Tertiary Leucogranite in the Eastern Himalaya. *Geological Journal*, *49*(1), 28–51. https://doi.org/10.1002/gj.2480

Singh, T., Awasthi, A., & Caputo, R. (2012). The sub-Himalayan fold-thrust belt in the 1905 Kangra earthquake zone: A critical taper model perspective for seismic hazard analysis. *Tectonics*, *31*(6). https://doi.org/10.1029/2012TC003120

Sinha, A. K. (1989). *Geology of the higher Central Himalaya*. John Wiley& Sons. https://doi.org/10.1017/S0016756800013911

Sinha-Roy, S. (1982). Himalayan Main Central Thrust and its implications for Himalayan inverted metamorphism. *Tectonophysics*, *84*(2-4), 197–224. https://doi.org/10.1016/0040-1951(82)90160-3

Smalley Jr, R. F., Chatelain, J.-L., Turcotte, D. L., & Prévot, R. (1987). A fractal approach to the clustering of earthquakes: applications to the seismicity of the New Hebrides. *Bulletin of the Seismological Society of America*, *77*(4), 1368–1381. https://doi.org/10.1785/BSSA0770041368

Sobolev, G. (2011). Seismicity dynamics and earthquake predictability. *Natural Hazards and Earth System Sciences*, *11*(2), 445–458. https://doi.org/10.5194/nhess-11-445-2011

Som, S., Dasarwar, P., Mohan, M., Hindayar, J., Kumar, N. T., Chowdhuri, S., . . . Singh, H. (2016). Comparing seismic susceptibility models of the Himalayan terrain. *Journal of Seismology*, *20*(3), 827–863. https://doi.org/10.1007/s10950-016-9562-z

Spada, M., Tormann, T., Wiemer, S., & Enescu, B. (2013). Generic dependence of the frequency-size distribution of earthquakes on depth and its relation to the strength profile of the crust. *Geophysical research letters*, *40*(4), 709–714. https://doi.org/10.1029/2012GL054198

Sreejith, K., Sunil, P., Agrawal, R., Saji, A. P., Rajawat, A., & Ramesh, D. (2018). Audit of stored strain energy and extent of future earthquake rupture in central Himalaya. *Scientific reports*, *8*(1), 1–9. https://doi.org/10.1038/s41598-018-35025-y

Sri Lakshmi, S., & Banerjee, P. (2019). Dynamic multifractality of seismic activity in Northeast India. *Pure and Applied Geophysics*, *176*(4), 1561–1577. https://doi.org/10.1007/s00024-018-02087-y

Srivastava, H., Verma, M., Bansal, B., & Sutar, A. K. (2015). Discriminatory characteristics of seismic gaps in Himalaya. *Geomatics, Natural Hazards and Risk*, *6*(3), 224–242. https://doi.org/10.1080/19475705.2013.839483

Storchak, D. A., Harris, J., Brown, L., Lieser, K., Shumba, B., & Di Giacomo, D. (2020). Rebuild of the bulletin of the international seismological centre (isc)—part 2: 1980–2010. *Geoscience Letters*, *7*(1).

Subedi, L., & Acharya, K. K. (2016). Tracing the Mahabharat Thrust (MT) on the basis of lithology and microstructures around Bhainse-Manahari area, central Nepal. *Journal of Nepal Geological Society*, *51*, 39–48. https://doi.org/10.3126/jngs.v51i0.24086

Tahir, M., & Grasso, J. R. (2015). Faulting style controls for the space–time aftershock patterns. *Bulletin of the Seismological Society of America*, *105*(5), 2480–2497. https://doi.org/10.1785/0120140336

Tandon, S. K., & Gupta, N. (2020). Introduction to geodynamics of the Indian plate: evolutionary perspectives. In *Geodynamics of the indian plate* (pp. 1–4). https://doi.org/10.1007/978-3-030-15989-4$_1$

Tang, Y., Liu, S., Li, X., Fan, Y., Deng, Y., Liu, Y., & Yin, L. (2020). Earthquakes spatio–temporal distribution and fractal analysis in the Eurasian seismic belt. *Rendiconti Lincei. Scienze Fisiche e Naturali*, *31*(1), 203–209. https://doi.org/10.1007/s12210-020-00871-4

Tang, Y.-J., Chang, Y.-F., Liou, T.-S., Chen, C.-C., & Wu, Y.-M. (2012). Evolution of the temporal multifractal scaling properties of the Chiayi earthquake (ML= 6.4), Taiwan. *Tectonophysics*, *546*, 1–9. https://doi.org/10.1016/j.tecto.2012.04.006

Tape, W., & Tape, C. (2012). A geometric comparison of source-type plots for moment tensors. *Geophysical Journal International*, *190*(1), 499–510. https://doi.org/10.1111/j.1365-246X.2012.05490.x

Tarquis, A. M., McInnes, K., Key, J., Saa, A., Garcia, M., & Diaz, M. (2006). Multiscaling analysis in a structured clay soil using 2D images. *Journal of Hydrology*, *322*(1-4), 236–246. https://doi.org/10.1016/j.jhydrol.2005.03.005

Telesca, L., Cuomo, V., Lapenna, V., & Macchiato, M. (2001). Identifying space–time clustering properties of the 1983–1997 Irpinia–Basilicata (southern Italy) seismicity. *Tectonophysics*, *330*(1-2), 93–102. https://doi.org/10.1016/S0040-1951(00)00221-3

Telesca, L., Cuomo, V., Lapenna, V., & Macchiato, M. (2002). Fractal characterization of the temporal distribution of aftershocks associated with the 1994 MW 6.7 Northridge earthquake. *Fractals*, *10*(01), 67–76. https://doi.org/10.1142/S0218348X02000756

Telesca, L., Lovallo, M., Aggarwal, S., & Khan, P. (2015). Precursory signatures in the visibility graph analysis of seismicity: An application to the Kachchh (Western India) seismicity. *Physics and Chemistry of the Earth, Parts A/B/C*, *85*, 195–200. https://doi.org/10.1016/j.pce.2015.02.008

Teotia, S., Khattri, K., & Roy, P. (1997). Multifractal analysis of seismicity of the Himalayan region. *Current Science*, 359–366.

Teotia, S., & Kumar, D. (2011). Role of multifractal analysis in understanding the preparation zone for large size earthquake in the North-Western Himalaya region. *Nonlinear Processes in Geophysics*, *18*(1), 111–118. https://doi.org/10.5194/npg-18-111-2011

Thakur, V. (1990). Indus Tsangpo suture zone in Ladakh—its tectonostratigraphy and tectonics. *Proceedings of the Indian Academy of Sciences-Earth and Planetary Sciences*, *99*(2), 169–185. https://doi.org/10.1007/BF02839388

Thakur, V., Jayangondaperumal, R., & Joevivek, V. (2019). Seismotectonics of central and NW Himalaya: plate boundary–wedge thrust earthquakes in thin-and thick-skinned tectonic framework. *Geological Society, London, Special Publications*, *481*(1), 41–63. https://doi.org/10.1144/SP481.8

Thapa, D. R., Tao, X., Fan, F., & Tao, Z. (2018). Aftershock analysis of the 2015 Gorkha-Dolakha (Central Nepal) earthquake doublet. *Heliyon*, *4*(7), e00678. https://doi.org/10.1016/j.heliyon.2018.e00678

Thiede, R. C., Arrowsmith, J. R., Bookhagen, B., McWilliams, M., Sobel, E. R., & Strecker, M. R. (2006). Dome formation and extension in the Tethyan Himalaya, Leo Pargil, northwest India. *Geological Society of America Bulletin*, *118*(5-6), 635–650. https://doi.org/10.1130/B25872.1

Tian, Z., Freymueller, J. T., & Yang, Z. (2020). Spatio-temporal variations of afterslip and viscoelastic relaxation following the Mw 7.8 Gorkha (Nepal) earthquake. *Earth and Planetary Science Letters*, *532*, 116031. https://doi.org/10.1016/j.epsl.2019.116031

Tiwari, A., Paul, A., Singh, R., & Upadhyay, R. (2021). Potential seismogenic asperities in the Garhwal–Kumaun region, NW Himalaya: Seismotectonic implications. *Natural Hazards*, *107*(1), 73–95. https://doi.org/10.1007/s11069-021-04574-3

Tiwari, B., Xu, J., Adhikari, B., & Chapagain, N. (2020). Multifractal analysis for seismic wave in Kathmandu valley after Gorkha Earthquake-2015, Nepal. *Journal of Nepal Physical Society*, *6*(2), 113–120. https://doi.org/10.3126/jnphyssoc.v6i2.34866

Tiwari, R., & Paudyal, H. (2021a). Statistics of the earthquakes in the central Himalaya and its vicinity in last 56 years, with an emphasis in the 25 April 2015 Gorkha, Nepal earthquake. *Contributions to Geophysics and Geodesy*, *51*(4), 321–343. https://doi.org/10.31577/congeo.2021.51.4.2

Tiwari, R., & Paudyal, H. (2021b). Variability of b-value before and after the Gorkha earthquake in the central Himalaya and vicinity. *Bibechana*, *18*(2), 32–42. https://doi.org/10.3126/bibechana.v18i2.31207

Tiwari, R., & Paudyal, H. (2022). Gorkha earthquake (MW 7.8) and after-shock sequence: A fractal approach. *Earthquake Science*, *35*(3), 193–204. https://doi.org/10.1016/j.eqs.2022.06.001

Tiwari, R., Paudyal, H., & Shanker, D. (2022). On the spatio-temporal variation in b-value after 25 April 2015 Gorkha, Nepal earthquake. *Geodesy and Geodynamics*. https://doi.org/10.1016/j.geog.2022.01.006

Tosi, P. (1998). Seismogenic structure behaviour revealed by spatial clustering of seismicity in the Umbria-Marche Region (Central Italy). *Annals of Geophysics*, *41*(2). https://doi.org/10.1007/s11069-015-1720-z

Tosi, P., De Rubeis, V., Loreto, V., & Pietronero, L. (2004). Space-time combined correlation integral and earthquake interactions. *Annals of Geophysics*, *47*(6), 1849–1854. https://doi.org/10.4401/ag-4404

Trivedi, P. C. (2015). Application of Omori's decay law to the 2001 Bhuj aftershock sequence for Kachchh region of Western India. *Open Journal of Earthquake Research*, *4*(03), 94. https://doi.org/10.4236/ojer.2015.43009

Turcotte, D. L. (1989). Fractals in geology and geophysics. *Pure and applied Geophysics*, *131*(1), 171–196. https://doi.org/10.1007/978-1-4419-7695-$6_3$1

Turcotte, D. L., & Brown, S. R. (1993). Fractals and chaos in geology and geophysics. *Physics Today*, *46*(5), 68. https://doi.org/10.1017/CBO9781139174695

Upreti, B. N., & Le Fort, P. (1999). Lesser Himalayan crystalline nappes of Nepal: Problems of their origin. *Geological Society of America*, 225–238. https://doi.org/10.1130/0-8137-2328-0.225

Utsu, T. (1971). Aftershocks and earthquake statistics (2): further investigation of aftershocks and other earthquake sequences based on a new classification of earthquake sequences. *Journal of the Faculty of Science, Hokkaido University. Series 7, Geophysics*, *3*(4), 197–266.

Utsu, T. (1972). Aftershocks and earthquake statistics (3): Analyses of the distribution of earthquakes in magnitude, time and space with special consideration to clustering characteristics of earthquake occurrence (1). *Journal of the Faculty of Science, Hokkaido University. Series 7, Geophysics*, *3*(5), 379–441.

Utsu, T., & Ogata, Y. (1995). The centenary of the Omori formula for a decay law of aftershock activity. *Journal of Physics of the Earth*, *43*(1), 1–33. https://doi.org/10.4294/jpe1952.43.1

Valdiya, K. (1980). The two intracrustal boundary thrusts of the Himalaya. *Tectonophysics*, *66*(4), 323–348. https://doi.org/10.1016/0040-1951(80)90248-6

Valdiya, K., & Goel, O. (1983). Lithological subdivision and petrology of the Great Himalayan Vaikrita group in Kumaun, India. *Proceedings of the Indian Academy of Sciences-Earth and Planetary Sciences*, *92*(2), 141–163. https://doi.org/10.1007/BF02866736

Verma, R. (1991). Seismicity of the Himalaya and the northeast India, and nature of continent-continent collision. *Physics and Chemistry of the Earth*, *18*, 345–370. https://doi.org/10.1016/0079-1946(91)90009-5

Verma, R., & Kumar, G. K. (1987). Seismicity and the nature of plate movement along the Himalayan arc, Northeast India and Arakan-Yoma: a review. *Tectonophysics*, *134*(1-3), 153–175. https://doi.org/10.1016/0040-1951(87)90255-1

Wang, F., & Zai, Y. (2021). Fractal and multifractal characteristics of shale nanopores. *Results in Physics*, *25*, 104277. https://doi.org/10.1016/j.rinp.2021.104277

Wang, J.-H., Chen, K.-C., Huang, W.-G., Chang, K.-H., Wang, J.-C., & Leu, P.-L. (2014). Multifractal Measures of M $\geq$ 3 Shallow Earthquakes in the Taipei Metropolitan Area. *Terrestrial, Atmospheric & Oceanic Sciences*, *25*(1). https://doi.org/10.3319/TAO.2013.09.09.01(T)

Wang, K., Chen, Q.-F., Sun, S., & Wang, A. (2006). Predicting the 1975 Haicheng Earthquake. *Bulletin of the Seismological Society of America*, *96*(3), 757-795. https://doi.org/10.1785/0120050191

Wang, K., & Fialko, Y. (2015). Slip model of the 2015 Mw 7.8 Gorkha (Nepal) earthquake from inversions of ALOS-2 and GPS data. *Geophysical Research Letters*, *42*(18), 7452–7458. https://doi.org/10.1002/2015GL065201

Wang, R., Chang, Y., Miao, M., Zeng, Z., Chen, H., Shi, H., ... Han, P. (2021). Assessing earthquake forecast performance based on b value in Yunnan Province, China. *Entropy*, *23*(6), 730. https://doi.org/10.3390/e23060730

Wang, Y., Day, S. M., & Denolle, M. A. (2019). Geometric controls on pulse-like rupture in a dynamic model of the 2015 Gorkha earthquake. *Journal of Geophysical Research: Solid Earth*, *124*(2), 1544–1568. https://doi.org/10.1029/2018JB016602

Webb, A. A. G., Guo, H., Clift, P. D., Husson, L., Müller, T., Costantino, D., ... Wang, Q. (2017). The Himalaya in 3D: Slab dynamics controlled mountain building and monsoon intensification. *Lithosphere*, *9*(4), 637–651. https://doi.org/10.1130/L636.1

Webb, A. A. G., Schmitt, A. K., He, D., & Weigand, E. L. (2011). Structural and geochronological evidence for the leading edge of the Greater Himalayan Crystalline complex in the central Nepal Himalaya. *Earth and Planetary Science Letters*, *304*(3-4), 483–495. https://doi.org/10.1016/j.epsl.2011.02.024

Wei, S., Chen, M., Wang, X., Graves, R., Lindsey, E., Wang, T., ... Helmberger, D. (2018). The 2015 Gorkha (Nepal) earthquake sequence: I. Source modeling and deterministic 3D ground shaking. *Tectonophysics*, *722*, 447–461. https://doi.org/10.1016/j.tecto.2017.11.024

Wessel, P., Smith, W. H., Scharroo, R., Luis, J., & Wobbe, F. (2013). Generic mapping tools: improved version released. *Eos, Transactions American Geophysical Union*, *94*(45), 409–410. https://doi.org/10.1002/2013EO450001

Whipple, K. X., Shirzaei, M., Hodges, K. V., & Ramon Arrowsmith, J. (2016). Active shortening within the Himalayan orogenic wedge implied by the 2015 Gorkha earthquake. *Nature Geoscience*, *9*(9), 711–716. https://doi.org/10.1038/ngeo2797

Wiemer, S. (2001). A software package to analyze seismicity: Zmap. *Seismological Research Letters*, *72*(3), 373–382. https://doi.org/10.1785/gssrl.72.3.373

Wiesmayr, G., & Grasemann, B. (2002). Eohimalayan fold and thrust belt: Implications for the geodynamic evolution of the NW-Himalaya (India). *Tectonics*, *21*(6), 8–1. https://doi.org/10.1029/2002TC001363

Wobus, C., Heimsath, A., Whipple, K., & Hodges, K. (2005). Active out-of-sequence thrust faulting in the central Nepalese Himalaya. *Nature*, *434*(7036), 1008–1011. https://doi.org/10.1038/nature03499

Wu, Y.-M., Chen, S. K., Huang, T.-C., Huang, H.-H., Chao, W.-A., & Koulakov, I. (2018). Relationship between earthquake b-values and crustal stresses in a young orogenic belt. *Geophysical Research Letters*, *45*(4), 1832–1837. https://doi.org/10.1002/2017GL076694

Wyss, M. (1997). Can not earthquakes be predicted? *Science*, *278*(5337), 487–490. https://doi.org/10.1126/science.278.5337.487

Wyss, M. (2005). Human losses expected in Himalayan earthquakes. *Natural hazards*, *34*, 305–314. https://doi.org/10.1007/s11069-004-2073-1

Wyss, M., & Chamlagain, D. (2019). Estimated casualties in possible future earthquakes south and west of the M 7.8 Gorkha earthquake of 2015. *Acta Geophysica*, *67*(2), 423–429. https://doi.org/10.1007/s11600-019-00265-7

Wyss, M., Pacchiani, F., Deschamps, A., & Patau, G. (2008). Mean magnitude variations of earthquakes as a function of depth: Different crustal stress distribution depending on tectonic setting. *Geophysical research letters*, *35*(1). https://doi.org/10.1029/2007GL031057

Wyss, M., Sammis, C. G., Nadeau, R. M., & Wiemer, S. (2004). Fractal dimension and b-value on creeping and locked patches of the San Andreas fault near Parkfield, California. *Bulletin of the Seismological Society of America*, *94*(2), 410–421. https://doi.org/10.1785/0120030054

Wyss, M., & Stefansson, R. (2006). Nucleation points of recent mainshocks in southern Iceland, mapped by b-values. *Bulletin of the Seismological Society of America*, *96*(2), 599–608. https://doi.org/10.1785/0120040056

Xiaoshan, W., Guiling, D., Xiangdong, F., & Yaqiong, Y. (2012). Characteristics of focal mechanisms in Chile subduction. *Geodesy and Geodynamics*, *3*(3), 23–28. https://doi.org/10.3724/SP.J.1246.2012.00023

Xiong, N., Niu, F., & Wang, R. (2020). Significance of Nonplanar Rupture of the Mainshock and Optimal Faulting in Forecasting Aftershocks of the 2015 Mw 7.8 Gorkha Earthquake. *Seismological Research Letters*, *91*(3), 1606–1616. https://doi.org/10.1785/0220190254

Xu, Z.-Q., Dilek, Y., Yang, J.-S., Liang, F.-H., Liu, F., Ba, D.-Z., ... Ji, S.-C. (2015). Crustal structure of the Indus–Tsangpo suture zone and its ophiolites in southern Tibet. *Gondwana Research*, *27*(2), 507–524. https://doi.org/10.1016/j.gr.2014.08.001

Yagi, Y., & Okuwaki, R. (2015). Integrated seismic source model of the 2015 Gorkha, Nepal, earthquake. *Geophysical Research Letters*, *42*(15), 6229–6235. https://doi.org/10.1186/s40623-016-0393-5

Yamada, M., Kandel, T., Tamaribuchi, K., & Ghosh, A. (2020). 3D Fault Structure Inferred from a Refined Aftershock Catalog for the 2015 Gorkha Earthquake

in Nepal. *Bulletin of the Seismological Society of America*, *110*(1), 26–37. https://doi.org/10.1785/0120190075

Yang, Y., Chen, Q., Xu, Q., Liu, G., & Hu, J.-C. (2019). Source model and Coulomb stress change of the 2015 Mw 7.8 Gorkha earthquake determined from improved inversion of geodetic surface deformation observations. *Journal of Geodesy*, *93*(3), 333–351. https://doi.org/10.1007/s00190-018-1164-9

Yeats, R. S., & Lillie, R. J. (1991). Contemporary tectonics of the Himalayan frontal fault system: folds, blind thrusts and the 1905 Kangra earthquake. *Journal of Structural Geology*, *13*(2), 215–225. https://doi.org/10.1016/0191-8141(91)90068-T

Yin, A. (2006). Cenozoic tectonic evolution of the Himalayan orogen as constrained by along-strike variation of structural geometry, exhumation history, and foreland sedimentation. *Earth-Science Reviews*, *76*(1-2), 1–131. https://doi.org/10.1016/j.earscirev.2005.05.004

Yin, A., Dubey, C., Webb, A., Kelty, T., Grove, M., Gehrels, G., & Burgess, W. (2010). Geologic correlation of the Himalayan orogen and Indian craton: Part 1. Structural geology, U-Pb zircon geochronology, and tectonic evolution of the Shillong Plateau and its neighboring regions in NE India. *Bulletin*, *122*(3-4), 336–359. https://doi.org/10.1130/B26460.1

Yin, A., & Harrison, T. M. (2000). Geologic evolution of the Himalayan-Tibetan orogen. *Annual review of earth and planetary sciences*, *28*(1), 211–280. https://doi.org/10.1146/annurev.earth.28.1.211

Yin, J., Yao, H., Yang, H., Liu, J., Qin, W., & Zhang, H. (2017). Frequency-dependent rupture process, stress change, and seismogenic mechanism of the 25 April 2015 Nepal Gorkha M W 7.8 earthquake. *Science China Earth Sciences*, *60*(4), 796–808. https://doi.org/10.1007/s11430-016-9006-0

Yin, L., Li, X., Zheng, W., Yin, Z., Song, L., Ge, L., & Zeng, Q. (2019). Fractal dimension analysis for seismicity spatial and temporal distribution in the circum-Pacific seismic belt. *Journal of Earth System Science*, *128*(1), 1–7. https://doi.org/10.1007/s12040-018-1040-2

Yue, H., Simons, M., Duputel, Z., Jiang, J., Fielding, E., Liang, C., ... Samsonov, S. V. (2017). Depth varying rupture properties during the 2015 Mw 7.8 Gorkha (Nepal) earthquake. *Tectonophysics*, *714*, 44–54. https://doi.org/10.1016/j.tecto.2016.07.005

Žalohar, J. (2018). Omori's law. In *Developments in Structural Geology and Tectonics* (Vol. 2, pp. 123–134). Elsevier. https://doi.org/10.1016/B978-0-12-814580-

7.00010-1

Zamani, A., & Agh-Atabai, M. (2009). Temporal characteristics of seismicity in the Alborz and Zagros regions of Iran, using a multifractal approach. *Journal of Geodynamics*, *47*(5), 271–279. https://doi.org/10.1016/j.jog.2009.01.003

Zamani, A., & Agh-Atabai, M. (2011). Multifractal analysis of the spatial distribution of earthquake epicenters in the Zagros and Alborz-Kopeh Dagh regions of Iran. *Iranian Journal of Science and Technology (Sciences)*, *35*(1), 39–51. https://doi.org/10.22099/IJSTS.2011.2127

Zhang, G., Hetland, E., & Shan, X. (2015). Slip in the 2015 MW 7.9 Gorkha and MW 7.3 Kodari, Nepal, earthquakes revealed by seismic and geodetic data: delayed slip in the Gorkha and slip deficit between the two earthquakes. *Seismological Research Letters*, *86*(6), 1578–1586. https://doi.org/10.1785/0220150139

Zhang, J., Santosh, M., Wang, X., Guo, L., Yang, X., & Zhang, B. (2012). Tectonics of the northern Himalaya since the India–Asia collision. *Gondwana Research*, *21*(4), 939–960. https://doi.org/10.1016/j.gr.2011.11.004

Zhang, J., Zhao, B., Wang, D., Yu, J., & Tan, K. (2021). Dynamic modeling of postseismic deformation following the 2015 Mw 7.8 Gorkha earthquake, Nepal. *Journal of Asian Earth Sciences*, *215*, 104781. https://doi.org//10.1016/j.jseaes.2021.104781

Zhang, L., Li, J., Liao, W., & Wang, Q. (2016). Source rupture process of the 2015 Gorkha, Nepal Mw 7.9 earthquake and its tectonic implications. *Geodesy and geodynamics*, *7*(2), 124–131. https://doi.org/10.1016/j.tecto.2016.05.034

Zhang, L.-K., Li, G.-M., Cao, H.-W., Zhang, Z., Dong, S.-L., Liang, W., ... Zhang, S. T. (2020). Activity of the south Tibetan detachment system: Constraints from leucogranite ages in the eastern Himalayas. *Geological Journal*, *55*(7), 5540–5573. https://doi.org/10.1002/gj.3756

Zhao, J. (2012). Lithospheric structure and geodynamic properties of the Tibetan plateau and its adjacent regions. *Earthquake Science*, *25*(5), 353–362. https://doi.org/10.1007/s11589-012-0861-3

APPENDIX

Academic Activities

A. Attended courses offered by IoST

In first semester:

PHS 911, Philosophy of Science (Cr. Hrs. 3)

PHS 912, Research Methodology (Cr. Hrs. 3)

PHS 913, Seminar (Cr. Hrs. 3)

In second semester:

PHS 951, Advanced Research Methodology (Cr. Hrs. 3)

PHS 957, Himalayan Seismology (Cr. Hrs. 3)

PHS 952, Seminar (Cr. Hrs. 3)

B. Paper publications

International

1) Tiwari, R. K., & Paudyal, H. (2021). Statistics of the earthquakes in the central Himalaya and its vicinity in last 56 years, with an emphasis in the 25 April 2015 Gorkha, Nepal earthquake. *Contributions to Geophysics and Geodesy*, *51*(4), 321-343.
https://doi.org/10.31577/congeo.2021.51.4.2

2) Tiwari, R. K., Paudyal, H., & Shanker, D. (2022). On the spatio-temporal variation in b-value after 25 April 2015 Gorkha, Nepal earthquake. *Geodesy and Geodynamics*, *13*(5), 525-533.
https://doi.org/10.1016/j.geog.2022.01.006

3) Tiwari, R. K., & Paudyal, H. (2022). Gorkha earthquake (MW7. 8) and aftershock sequence: A fractal approach. *Earthquake Science*, *35*(3), 193-204.
https://doi.org/10.1016/j.eqs.2022.06.001

4) Tiwari, R. K., & Paudyal, H. (2022). Frequency magnitude distribution and spatial correlation dimension of earthquakes in north-east Himalaya and adjacent regions. *Geologos*, *28*(2), 115-128.
https://doi.org/10.2478/logos-2022-0009

5) Tiwari, R. K., & Paudyal, H. (2023). Fractal Characteristics of the Seismic Swarm Succeeding the 2015 Gorkha Earthquake, Nepal. *Indian Geotechnical Journal*,

53, 789–804.
https://doi.org/10.1007/s40098-022-00704-1

6) Tiwari, R. K., Paudyal, H., & Shanker, D. (2022). Spatio-temporal distribution of earthquake occurrence in Eastern Himalaya and vicinity estimated based on b-value and fractal dimension. *Applied Geophysics*,*19*, 458–469.
https://doi.org/10.1007/s11770-022-0916-8

7) Tiwari, R. K., & Paudyal, H. (2022). Spatial mapping of b-value and Fractal Dimension Prior to November 8, 2022 Doti Earthquake, Nepal. *PLOS ONE*,*18*(8), 1–13.
https://doi.org/10.1371/journal.pone.0289673

National

1) Tiwari, R. K., & Paudyal, H. P. (2020). Geodynamics of Gorkha earthquake (Mw 7.9) and its aftershocks. *Himalayan Physics*, *9*, 103-109.
https://doi.org/10.3126/hp.v9i01.40208

2) Tiwari, R. K., & Paudyal, H. (2021). Variability of b-value before and after the Gorkha earthquake in the central Himalaya and vicinity. *Bibechana*, *18*(2), 32-42.
https://doi.org/10.3126/bibechana.v18i2.31207

3) Tiwari, R. K., & Paudyal, H. (2021). Seismic phases of 25 April 2015 (Mw 7.8) Earthquake and 12 May 2015 (Mw 7.3) Earthquake Predicted by AK135 Model-A comparison. *Journal of Nepal Physical Society*, *7*(2), 58-64.
https://doi.org/10.3126/jnphyssoc.v7i2.38623

4) Tiwari, R. K., & Paudyal, H. (2021). Box Counting Fractal Dimension and Frequency Size Distributon of Earthquakes in the Central Himalaya Region. *Journal of Institute of Science and Technology*, *26*(2), 127-136.
https://doi.org/10.3126/jist.v26i2.41664

5) Tiwari, R. K., & Paudyal, H. (2022). Fractal Structure of Seismic Signals of 2015 Gorkha-Kodari Earthquakes: A Box Counting Method. *BMC Journal of Scientific Research*, *5*(1), 18-26.
https://doi.org/10.3126/bmcjsr.v5i1.50667

Manuscript communicated

1) Tiwari, R. K., & Paudyal, H. (2022). Analysis of the b, p values, and the fractal dimension of aftershocks sequences following two major earthquakes in central Himalaya, *Heliyon*.

2) Tiwari, R. K., & Paudyal, H. (2023). Temporal clustering in aftershock sequences

of 2015 Gorkha earthquake, *Lithosphere*.

C. Participation

1) Oral presentation entitled "Ray path distribution of seismic wave of 25 April 2015, Gorkha earthquake (Mw 7.8) and its largest aftershock of 12 May 2015 (Mw7.3)" in the ANPA Conference organized by Association of Nepali Physicists in America (ANPA) during 17-19 July, 2020

2) Participated in an international virtual workshop on Global Seismology & tectonics (IVWGST-2020) organized by the Geo science and Technology Division of Council of Scientific and Industrial Research-North East Institute of Science and Technology, Jorhat, India from 14 to 25 September 2020

3) Participated and completed online workshop on Citizen Science with Application to Nuclear, Seismic and Air Quality Monitoring: Introduction organised by The Abdus Salam International Centre for Theoretical Physics (ICTP) Italy from 08-12 March 2021.

4) Participated and completed online workshop on Citizen Science with Application to Nuclear, Seismic and Air Quality Monitoring: Applications in Seismic Monitoring organised by The Abdus Salam International Centre for Theoretical Physics (ICTP) Italy from 15-19 March 2021.

5) Oral presentation entitled "Cumulative Frequency Magnitude Distribution and Fractal Dimension of Earthquakes Epicenter in Central Himalaya Region" in the ANPA Conference organized by Association of Nepali Physicists in America (ANPA) during 16-18 July, 2021

6) Poster presentation entitled "On the spatio-temporal variation in b-value After 25 April 2015 Gorkha, Nepal earthquake" in the virtual conference organized by International Association of Geomagnetism and Aeronomy and International Association of Seismology and Physics of the Earth's Interior (IAGA-IASPEI 2021), held in Hyderabad, India during August 21-27, 2021

7) Participated in an international virtual workshop on Global Seismology & tectonics (IVWGST-2021) organized by the Geo science and Technology Division of Council of Scientific and Industrial Research-North East Institute of Science and Technology, Jorhat, India from 20 to 30 September 2021

8) Participated and completed online/onsite workshop on Scientific Research Writing organised by Research Management Cell, Birendra Multiple Campus, Bharatpur and supported by UGC, Nepal from 15-19 September 2021.

9) Participated and completed online/onsite training program on Capacity Devel-

opment in Linux Operating System organised by Research Management Cell, Birendra Multiple Campus, Bharatpur and supported by UGC, Nepal from 19-25 September 2021

10) Oral presentation entitled "Study of 25 April 2015 Gorkha Earthquake (Mw 7.8) and aftershock Sequence: A Fractal Approach" in the 27th International Conference of International Academy of Physical Sciences (CONIAPS XXVII),organised by Institute of earth and environmental sciences DR. Rammanohar Lohia Avadh University,Ayodha, India during October 26 - 28, 2021 (Online)

11) Oral presentation entitled "Multifractal Nature of Aftershocks Sequence of the 2015 Gorkha earthquake" in the International Conference on Frontiers of Physics (ICFP)- 2022,(e - Conference) organised by Nepal Physical Society held in Kathmandu, Nepal from January 22 - 24.

12) Oral presentation entitled "The p and b values succeeding the 25 April and 12 May, 2015 Central Himalayan earthquakes" in the 58th Annual Convention of IGU "Recent Advances in Earth Sciences with Special Emphasis - Natural Hazards" jointly organised by Indian Geophysical Union and North-Eastern Hill University,Shillong between 2nd and 4th February 2022.

13) Oral presentation entitled " Fractal Characteristics Of the Seismic swarm Succeeding the 2015 Gorkha earthquake in Nepal" in the 9th National Conference on Science and Technology "Science for Society and Innovation for Prosperity" organized by Nepal Academy of Science and Technology (NAST) between June 26 - 28, 2022,Khumaltar, Lalitpur, Nepal.

14) Participated and completed the short course training program requirement for THE Generic Mapping TOOL (GMT) for Geodesy between July 5-7, 2022.

15) Participated on International Virtual Workshop on Global Seismology and Tectonics (IVWGST) between September 20-30, 2022 organized by Geoscience and Technology Division North East Institute of Science and Technology, Jorhat, Assam, India.

16) Participated on 2-day Hands-on Workshop on OpendTect Software through online platform on 25th and 26th March, 2023, organised by a collaboration of SEG Student Chapters of IIT Kharagpur, Dibrugarh University and Delhi University, India.

The published articles in PDF form can be accessed afterward.

Contributions to Geophysics and Geodesy Vol. 51/4, 2021 (321–343)

Statistics of the earthquakes in the central Himalaya and its vicinity in last 56 years, with an emphasis in the 25 April 2015 Gorkha, Nepal earthquake

Ram Krishna TIWARI[1,2,*], Harihar PAUDYAL[2]

[1] Central Department of Physics, Tribhuvan University, Kirtipur, Kathmandu, Nepal

[2] Birendra Multiple Campus, Tribhuvan University, Bharatpur, Chitwan, Nepal

Abstract: To understand the variation of stress levels in the region 80°E – 89°E and 26°N – 31°N, the statistical analysis of earthquake frequency-magnitude distribution and spatio-temporal variation of fractal correlation dimension of earthquake epicenter distribution are estimated. The analysis is carried out on declusterised catalogue containing 1185 events of 56 years from February 1964 to November 2020. The study area is divided into three regions the western Nepal and vicinity (Region A), central Nepal and vicinity (Region B) and eastern Nepal and vicinity (Region C), respectively. The magnitude of completeness (M_c) varies from 3.6 to 4.0 for the study period. The spatial fractal dimension (D_c) and b-value are calculated as 1.89 ± 0.02 and 0.68 ± 0.03 for the western Nepal, 1.76 ± 0.01 and 0.60 ± 0.05 for the central Nepal, whereas they are estimated as 1.85 ± 0.02 and 0.63 ± 0.03 for the eastern part of the Nepal. The b-values obtained for all three regions are very low comparing to global average value of 1. The time clustering of the events in the respective regions are 0.26 ± 0.003, 0.31 ± 0.004 and 0.26 ± 0.02 as indicated by temporal fractal dimension (D_t). The higher D_c, lower b and D_t values associated with the regions indicate high stress concentration and stronger epicenter clustering in these regions. The strongly increasing trend of fractal dimension and strongly decreasing trend of b-value show the high probabilities of occurring the large earthquake in both central Nepal (82.5°E – 85.5°E and 27.5°N – 30°N) and eastern Nepal (85.5°E – 88.2°E and 26.45°N – 28.6°N) as compared to western Nepal (80°E – 82.5°E and 28°N – 30.5°N). This statistical analysis of spatial and temporal characteristics of the earthquake activity may give significant signs of the future seismic hazard along central Himalaya region.

Key words: magnitude of completeness, b-value, fractal dimension, clustering of earthquakes

*corresponding author, e-mail: ram.tiwari@bimc.tu.edu.np

doi: 10.31577/congeo.2021.51.4.2

1. Tectonics of the Himalaya

The Himalaya, the youngest and the highest mountain range in the world is resulted from the collision of the Indian and Eurasian plates (*Bilham, 2019; Wang and Fialko, 2015*). After the collision, subsequent thrusting of Indian plate into the Eurasian plate led to the formation of the Himalaya range and the largest and highest plateau – Tibetan plateau (*Butler et al., 2007; DeCelles et al., 2014; Ni, 1989; Pandey et al., 1995*). The mechanism of the formation of the Himalaya is that at some point between 65 Ma (million years ago) and 45Ma, India collided with Eurasia creating the Indus Yarlung Suture (IYS) – a zone that delineates the approximate boundary between the Indian and Eurasian plate. Thereafter the elevation of the Himalayan Mountain range began to take place in which the Eurasian plate was partly crumpled and buckled up above the Indian plate. Finally, the Himalayas gain their present height between 2.5 Ma and 1.8 Ma (*Cattin et al., 2001; DeCelles et al., 2002; Molnar and Pandey, 1989; Webb et al., 2011*). The dominant push of the Indian continental crust breaks itself into a lower and upper block at a depth. The breaking plane separating these two blocks of the Indian crust is called the Main Himalayan Thrust (MHT). It is gentle north dipping fault with 75 km width and three splays (*DiPietro and Pogue, 2004*). The Main Central Thrust (MCT) is the oldest, the Main Boundary Thrust (MBT) is the younger and the Main Frontal Thrust (MFT) or Himalaya Frontal Thrust (HFT) is southernmost and the youngest splay which is also the surface exposure of MHT. These structures strike the entire length of the Himalayan Arc (*Shanker et al., 2011; Yin et al., 2010*). The Main Central Thrust is a major intra-continental fault along 2200 km of the Himalaya Mountain belt where the Indian plate has pushed under the Eurasian plate along the Himalaya (*DiPietro and Pogue, 2004*). The MCT and South Tibetan Detachment (STD) run in sub-parallel way and bound a thick bundle of mid-crustal rocks that extend from the Himalayan front to the north beneath southern Tibet (*Kellett et al., 2019*). The MBT is another major thrust fault that runs parallel to the MFT with a spacing distance of about 20 km. In addition, several lineaments like the Motihari Gaurishanker, Motihari Everest, Arun, Kanchenjunga etc. in eastern Nepal produce noticeable offsets on the MCT and MBT. Many others lineaments like Karnali, Judi, Thaple are establish faults as known from ground map-

ping in the west of the Kathmandu fault (*Dasgupta et al., 1987; Prakash et al., 2016; Upreti et al., 2007*) (Fig. 1).

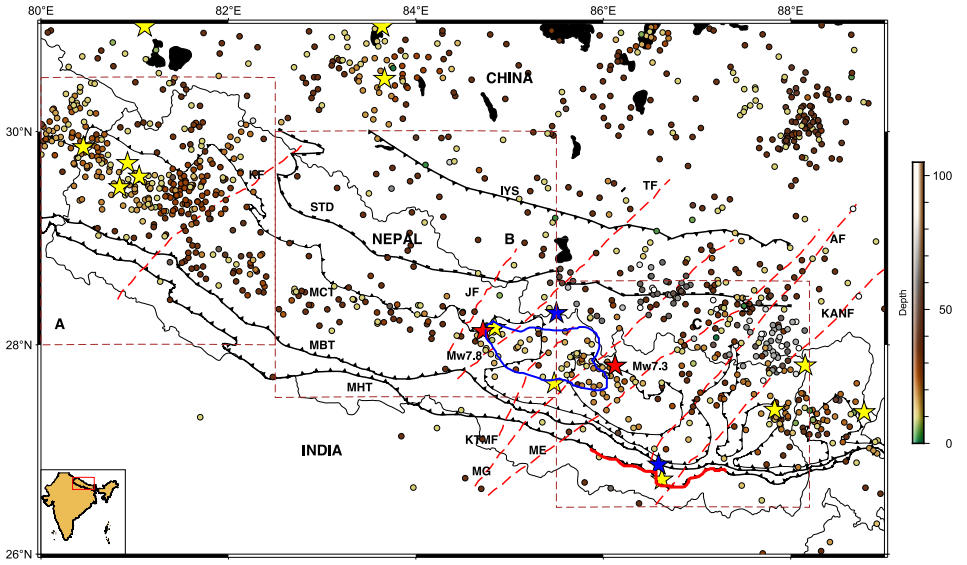

Fig. 1. Spatial distribution of 1185 earthquake events in the study region. 1170 earthquakes having magnitude ≤ 5.9 mb are shown by solid circle. Color of the circle indicates the depth of the earthquake events. 13 yellow stars stand for the earthquake events ≥ 6 mb and 2 red stars for Gorkha earthquake (Mw 7.8) and Dolakha earthquake (Mw 7.3). Blue stars for 1833 Kathmandu earthquake (M 7.7) and 1934 Nepal-Bihar earthquake (M 8.3). Regions of interest are demarcated by orange box into regions A, B and C. Inset map at bottom left corner of the map shows study region bounded by red box. Major thrusts of the region MHT, MBT, MCT and STD are shown along with IYS. Regional faults are depicted by dashed lines where KF is Karnali fault, JF is Judi fault, TF is Thaple fault, KTMF is Kathmandu fault, MG is Motihari Gaurishanker fault, ME is Motihari Everest fault, AF is Arun fault and KANF is Kanchenjunga fault. The blue contour indicates the approximate position of rupture rim of mainshock of Gorkha earthquake (*Grandin et al., 2015; Letort et al., 2016*) and red wavy line over MHT indicates the rupture length (∼150 km in Nepal) of the 1934 Bihar-Nepal earthquake (*Sapkota et al., 2013; Wei et al., 2018*).

2. History of earthquakes in Nepal

The cause of a major geo-hazard in the Himalayas is/are earthquakes. The Main Himalayan Thrust (MHT) constantly gathers the massive amounts

of strain and rupture process along it is the source of great earthquakes that have been documented along the range. (*Bilham, 2019; Hubbard et al., 2016*). Nepal measures about 880 km along its Himalayan axis by 150 to 250 km across so it is highly vulnerable to a disaster like earthquakes. In the earthquake history of Nepal two big earthquakes registered were 7.7 magnitude earthquake of 1833 that killed 414 people and 8.3 magnitude earthquake of 1934 that killed 8519 people (*Joshi and Kaushik, 2017*). The comparatively much smaller earthquakes that visited the nation were 1980 earthquake of 6.5 magnitude in western part of Nepal that killed 103 people, and 1988 earthquake of magnitude 6.5 in eastern part of Nepal that killed 721 people (*Chhetri, 2018; Miyake et al., 2017*). The most destructive earthquakes of 1934, 1980, 1988, and 2015 AD (Gorkha earthquake, 25 April) caused heavy fatalities and destruction of physical properties. The Gorkha event that ruptured a 50 km segment of the MHT has ended eastward in the area that was already broken during the 1934 Bihar-Nepal earthquake (*Adhikari et al., 2015; Elliott et al., 2016; Ramesh et al., 2018*). The earthquake is located at 15 km depth with epicenter at 28.147°N – 84.708°E. Among the intense aftershock sequences, two larger aftershocks of Mw 6.6 and Mw 6.7 were followed by the largest aftershock of magnitude Mw 7.3 on the southeastern end of the main rupture (*Avouac et al., 2015; Mitra et al., 2015*).

It is believed that the Gorkha earthquake did not release all the stress as it was expected to release. It would take the really big earthquake of Mw 8 and above for the strain to be relieved (*Bilham, 2019; Sreejith et al., 2018*). The partial rupture caused by the 1833 earthquake and the 2015 earthquake may initiate great earthquake in future by uncovering the shallow sealed slice of the MHT (*Sreejith et al., 2018*). They further recommended that some of this stress has shifted west to an area enlarging from Pokhara, Nepal to the Delhi, India (*Bilham, 2019; Grandin et al., 2015*). The central gap stretching from east Uttarakhand to central Nepal has been recognized that might fail, or collapse, either individually or in tandem with neighboring segments, in future earthquakes (Mw 8.5–8.7) (*Bilham, 2019*). Even though, there is a long history of Himalayan research, the seismic activity and seismogenic structures of the Himalayan range is not fully understood yet. The study therefore attempts to understand the seismic activity as well as stress level in central Himalaya region in terms of *b*-value of frequency

magnitude distribution and the spatio-temporal clustering of the earthquake events for the period of last 56 years.

3. Frequency magnitude distribution and fractal geometry

Earthquake epicenters/hypocenters can be considered as to be point events in space and time. If the occurrence of one earthquake is uncorrelated with other earthquakes events, then the distribution of events can be explained by Poisson (random) distribution having well-understood mathematics (*Greenhough and Main, 2008; Wu et al., 2019*). In regional seismicity studies, the distributions are not Poisson (*Smalley et al., 1987; Knopoff, 2000*) so cannot be explained by purely Poisson process. Then the distribution of events is explained by fractal geometry which applies scale invariant properties to study earthquakes. It is well known that earthquake phenomenon exhibit a scale-invariant character in several statistical features like Gutenberg-Richter (GR) earthquake sizes power law distribution (*Gutenberg and Richter, 1944*), fractal dimension of epicenters/hypocenters etc. The GR relationship is:

$$\log N = a - bM\,. \tag{1}$$

In the relation above, N is the cumulative number of events having magnitude $\geq M$, the constant 'a' is the seismicity of the region, and 'b' is the b-value of the earthquake frequency magnitude distribution. The b-value for earthquakes distribution that covers large area and extended time is typically equal to 1. The global study on b-value reveals that b-value varies significantly between individual fault zones, time, and space (*Nuannin, 2006; Schorlemmer et al., 2005*). Its variation is systematic in the period preceding a major earthquake (*Smith, 1981*). A high b-value means plenty of smaller events compared to larger ones and vice versa (*Yeken, 2016*). For the fractal behavior of earthquakes, fractal dimension is usually favored to investigate the clustering properties and size-scaling characteristics of earthquake parameters. Fractal distributions are the only distributions which do not include a typical length scale, and so, can be practicable to scale invariant phenomena (*Shcherbakov et al., 2015, 2004*). The temporal correlation dimension shows that earthquake occurrence is characterized by clustering properties with both short and long-time scales (*Mondal and Roy, 2016;*

Nakaya and Hashimoto, 2002).

4. Data and methodology

Our study is limited to the region 80°E – 89°E and 26°N – 31°N which covers the total area of Nepal and its vicinity. Analysis is done on the database prepared from the catalogue of ISC (International Seismological Centre) and USGS (United State Geological Survey). The time window of study is from 1964-01-01 to 2020-11-23. We retrieved the 2457 earthquakes data from the above-mentioned sources. After declusterisation (*Gardner and Knopoff, 1974*), 1185 events are retained for the region where 15 events are with magnitude ≥ 6 mb and 1170 events are less than 6 mb. The study region is further segmented into three regions containing 777 earthquake events altogether. The segmentation of the region is based on the nature of the faulting. The thrust dominated part appears in the western and central Nepal region, whereas, in the eastern Nepal, it is combination of thrust and strike-slip (*Shanker et al., 2011*). The regions segmented are:

(I) Western Nepal and its vicinity (Region A) 80°E – 82.5°E and 28°N – 30.5°N comprising 351 events.

(II) Central Nepal and its vicinity (Region B) 82.5°E – 85.5°E and 27.5°N – 30°N comprising 141 events.

(III) Eastern Nepal and its vicinity (Region C) 85.5°E – 88.2°E and 26.45°N – 28.6°N comprising 285 events.

The magnitude of completeness is computed by the first derivative of the frequency magnitude curve (*Wiemer and Wyss, 2000*). The maximum likelihood estimation (MLE) method (*Aki, 1965*) was used for the calculation of b-value. The error estimation of the b-value and M_c is based on the bootstrapping method (*Amorèse et al., 2010*):

$$b = \frac{\log_{10} \mathrm{e}}{M_a - (M - \Delta M/2)}\,, \tag{2}$$

where e is a constant, M_a is the average magnitude, M is the minimum magnitude in the catalogue and ΔM is the binning width of the catalogue (*Aki, 1965*). An estimate of the standard deviation (δb) of the b-value is given as suggested by (*Shi and Bolt, 1982*):

$$\delta b = 2.3\, b^2 \sqrt{\frac{\sum_{i}^{N} (M_i - M_a)^2}{n_s(n_s - 1)}}\,, \tag{3}$$

where n_s is the sample size (total number of events of the sample).

The *Grassberger and Procaccia (1983)* correlation dimension calculation method or sphere counting method is among the extensively used method to study space time characteristics of earthquake activity. It is based on power law and is used for spatio-temporal studies on the space-time characteristics of earthquake activity for various parts of the world (*Oncel and Wilson, 2007; Ormeni et al., 2017; Pailoplee and Choowong, 2014; Roy et al., 2011*). In this method the correlation integral function is defined as:

$$C(r) = \frac{2}{N(N-1)} \sum_{\substack{i,j=1 \\ i \neq j}}^{N} H(r - |X_i - X_j|)\,, \tag{4}$$

where N is the total number of earthquakes in the given window, $X_i - X_j$ is the angular distance between two events, calculated by using spherical triangle method (*Hirata, 1989*), and $H(r - |X_i - X_j|)$ is the Heaviside step function where r is the scaling radius.

The clue of possible approaching phase for large earthquakes can be better understood by investigating the temporal fluctuations of seismic sequences. It can be done by calculating the temporal correlation dimension based on the correlation integral function (*Mondal and Roy, 2016; Nakaya and Hashimoto, 2002*):

$$C(\tau) = \frac{2}{N(N-1)} \sum_{\substack{i,j=1 \\ i \neq j}}^{N} H(\tau - |t_i - t_j|)\,, \tag{5}$$

where N is the number of total earthquakes in the given window, τ is scaling time, $t_i - t_j$ is the inter occurrence time and $H(\tau - |t_i - t|)$ is the Heaviside step function. Now the correlation dimension can be defined from the power law relations:

$C(r) \sim r^D$, for spatial correlation dimension and

$C(\tau) \sim \tau^D$, for temporal correlation dimension.

The graphs are plotted for $\log r - \log C(r)$ and $\log \tau - \log C(\tau)$ then after respective fractal dimensions (D) can be obtained as the slope of the linear segment of the graph. The time variation of M_c and b-value are calculated by taking window size = 100, minimum number of events = 50, window overlap = 4%, bootstraps = 200, magnitude binning = 0.1 from Zmap software.

5. Results and discussion

The magnitude of earthquakes versus time in the western Nepal and vicinity is shown in Fig. 2a which shows the largest earthquake of the region was 6.1 mb on 1980. The b-value for the region was computed to be very low (0.68 ± 0.03) comparing to the global average value of 1 for the period of the study (Table 1 and Fig. 2c). The b-value before Gorkha earthquake (from window 1 to window 8) ranges from 0.84 ± 0.08 to 0.79 ± 0.08 and it is slightly high after Gorkha earthquake (0.90 ± 0.09) and thereafter it is around 0.86 to 0.87. The spatial correlation dimension (D_c) varied from 1.52 to 1.94 for different windows while it was noticed 1.89 ± 0.02 for entire region (Table 1 and Fig. 2e). It was suggested the D_c value of seismically active region ranges between 0 and 2 (*Singh et al., 2009; Tosi, 1998*). Thus, the western Nepal could be interpreted as being seismically active. Moreover, the spatial fractal dimension greater than 1.5 indicates the faults in the region are approaching to the near planar structure. The temporal correlation dimension (D_t) varied between 0.22 to 0.31 for different windows and it was computed as 0.26 ± 0.003 for entire study period (Table 1 and Fig. 2f). The results indicate that the time clustering of earthquakes could be homogeneous (or monofractal).

The maximum M_c above 5 is found at the beginning of the computations before 1980. Thereafter it is found decreasing and minimum M_c value is computed for the catalogue after 2010 between 3.6 and 3.8. After 2015 it is around 3.8 (see Fig. 2b). The M_c value for entire period of study is noticed to be 3.9 (Table 1). The temporal variation of b-value is constant around the global average value of 1. The lowest value of 0.81 was observed for 11 May 2010. It was noticed 0.88 for 14 January 2014 and just around 1 after 2015 Gorkha earthquake (Fig. 2d). There are no distinct earthquake precursors before the 2015 Gorkha earthquake according to the temporal

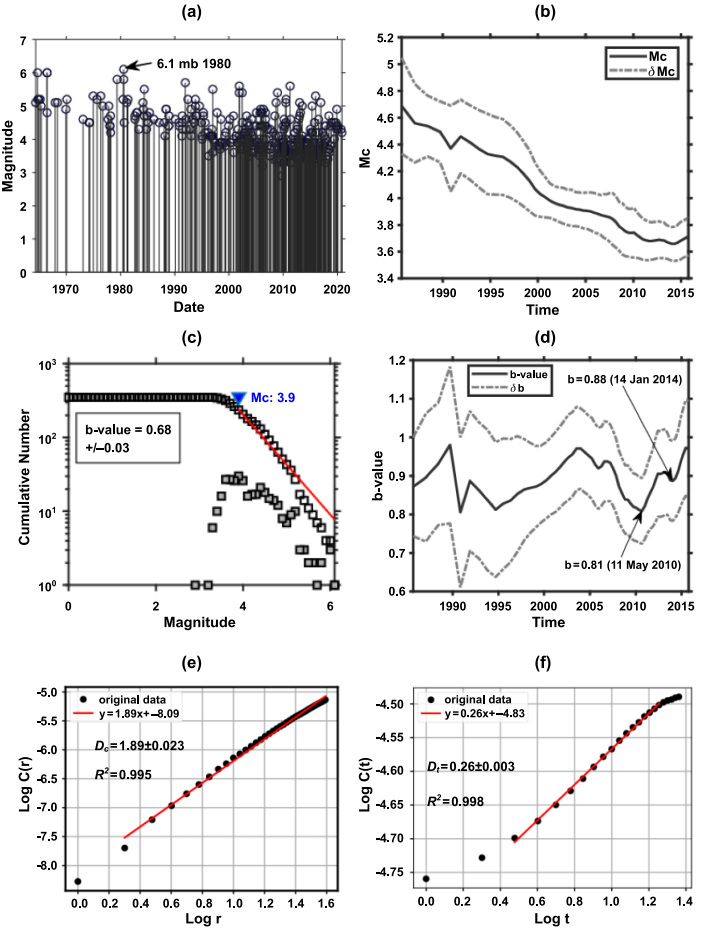

Fig. 2. Graphs showing (a) temporal variations of magnitude of the earthquake, (b) time variations of magnitude of completeness M_c with standard deviation (δM_c) shown by the dashed lines, (c) frequency magnitude distribution b-value (d) temporal variation of b-value with standard deviation (δb_c), (e) spatial correlation dimension (f) temporal correlation dimension for earthquake events from 1964 to 2020 in the demarcated region A.

variations of b-value in western part of the Nepal.

The magnitude of earthquakes versus time in the central Nepal and vicinity is shown in Fig. 3a showing 6.9 mb 2015 Gorkha earthquake as the biggest event in the region so far. The b-value in this region was computed to be very low (0.60 ± 0.05) than the global average value of 1 during pe-

Table 1. Time window, b-value with completeness magnitude M_c, temporal correlation dimension (D_t) and spatial correlation dimension (D_c) with their coefficient of determination (R^2) for 11 windows (10 windows each of 100 events and 11th window of 101 events) of region A.

Window	Time	b-value	M_c	D_t	R^2	D_c	R^2
1	1964-05-24 – 1998-05-20	0.84 ± 0.08	4.5	0.22 ± 0.004	0.995	1.68 ± 0.009	0.999
2	1978-03-07 – 2002-06-04	0.69 ± 0.06	4.1	0.24 ± 0.003	0.998	1.78 ± 0.02	0.994
3	1988-05-15 – 2004-04-03	0.87 ± 0.09	4.1	0.26 ± 0.003	0.998	1.72 ± 0.02	0.995
4	1994-07-17 – 2006-04-15	0.93 ± 0.10	3.9	0.31 ± 0.004	0.997	1.62 ± 0.01	0.999
5	1998-07-15 – 2008-12-26	0.86 ± 0.08	3.8	0.29 ± 0.003	0.998	1.58 ± 0.01	0.996
6	2002-06-04 – 2010-06-13	0.94 ± 0.09	3.8	0.23 ± 0.003	0.998	1.52 ± 0.02	0.991
7	2004-04-17 – 2012-07-11	0.80 ± 0.08	3.6	0.22 ± 0.002	0.999	1.70 ± 0.02	0.992
8	2006-05-05 – 2014-02-11	0.79 ± 0.08	3.6	0.26 ± 0.004	0.997	1.64 ± 0.02	0.991
9	2009-01-23 – 2015-10-19	0.90 ± 0.09	3.6	0.27 ± 0.003	0.998	1.94 ± 0.03	0.991
10	2010-06-13 – 2017-07-15	0.87 ± 0.09	3.6	0.26 ± 0.004	0.996	1.93 ± 0.03	0.991
11	2012-07-28 – 2020-10-28	0.86 ± 0.08	3.6	0.28 ± 0.003	0.994	1.70 ± 0.02	0.995
Entire region A	1964-05-24 – 2020-10-28	0.68 ± 0.03	3.9	0.26 ± 0.003	0.997	1.89 ± 0.02	0.995

riod of the study (Table 2 and Fig. 3c). The b-value decreases from 0.71 to the lowest value of 0.68 and then increases up to 0.82 for the period of study. The low b-values 0.71 ± 0.08 and 0.68 ± 0.07 are observed for the window 2 (1979-01-01 to 2015-4-25) and window 3 (1985-10-21 to 2015-07-01). The slight decrease in b-value before Gorkha earthquake may be because of occurrence of foreshocks and variations in b-value after the earthquake is attributed to the aftershock activity [46]. The calculated spatial correlation dimension (D_c) varied from 1.62 to 1.84 for different windows while it was

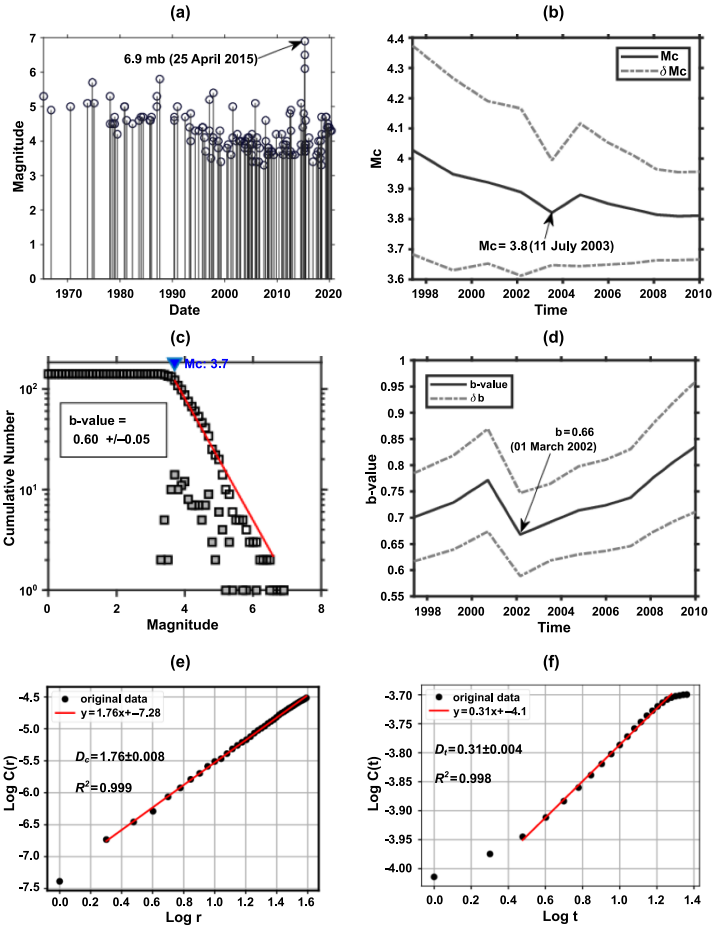

Fig. 3. Graphs showing (a) temporal variations of magnitude, (b) time variations of magnitude of completeness M_c with standard deviation (δM_c) shown by the dashed lines, (c) frequency magnitude distribution b-value, (d) temporal variation of b-value with standard deviation (δb_c), (e) spatial correlation dimension, (f) temporal correlation dimension for earthquake events from 1965 to 2020 in the demarcated region B.

noticed 1.76 ± 0.01 for entire study period (Table 2 and Fig. 3e). These results indicate that the central Nepal is seismically active with seismogenic structure of planar geometry. The temporal spatial correlation dimension (D_t) varied between 0.27 to 0.30 for different windows and it was computed as 0.31 ± 0.004 for entire study period (Table 2 and Fig. 3f). The results

Table 2. Time window, b-value with completeness magnitude M_c, temporal correlation dimension (D_t) and spatial correlation dimension (D_c) with their coefficient of determination (R^2) for 5 windows (4 windows each of 100 events and 5th window of 101 events) of region B.

Window	Time	b-value	M_c	D_t	R^2	D_c	R^2
1	1965-06-01 – 2012-08-23	0.71 ± 0.07	4.0	0.27 ± 0.002	0.999	1.78 ± 0.01	0.996
2	1979-01-01 – 2015-04-25	0.71 ± 0.08	4.0	0.29 ± 0.004	0.998	1.84 ± 0.02	0.996
3	1985-10-21 – 2015-07-01	0.68 ± 0.07	3.7	0.29 ± 0.003	0.998	1.75 ± 0.01	0.997
4	1993-07-05 – 2018-06-14	0.82 ± 0.10	3.7	0.30 ± 0.005	0.996	1.71 ± 0.01	0.998
5	1997-05-28 – 2020-05-30	0.79 ± 0.10	3.7	0.29 ± 0.004	0.997	1.62 ± 0.01	0.999
Entire region B	1965-06-01 – 2020-05-30	0.60 ± 0.05	3.7	0.31 ± 0.004	0.998	1.76 ± 0.01	0.996

indicate that the time clustering of earthquakes can be considered to be homogeneous (or monofractal) for this region as well.

The maximum M_c above 4.6, is found at the beginning of the computations before 1990. Thereafter it is found decreasing in linear trend. The minimum M_c value below 3.8 is computed for the catalogue around 2015 (Fig. 3b). The M_c value for entire period of study noticed to be 3.7 (Table 2). The temporal variations show b-value very lower than 1. The lowest value 0.66 is noted for 1 March 2002. Thereafter it seems rising gradually and it is just above 0.8 after 2010 (Fig. 3d).

The magnitude of earthquakes versus time in the eastern Nepal and vicinity is shown in Fig. 4a showing 6.7 mb earthquake on 12 May 2015 as the biggest one. The b-value in this region was computed to be very low (0.63 ± 0.03) than the global average value of 1 for the period of the study (Table 3 and Fig. 4c). The b-values before Gorkha earthquake (from window 1 to window 5) range from 1.12 ± 0.16 to 0.86 ± 0.10 and after Gorkha earthquake it ranges from 0.82 ± 0.11 to 0.70 ± 0.09 (from window 6 to window 9). The results show increase in b-value for several years before earthquake and followed by a decrease after the occurrence of the Gorkha earthquake. This may be the indication of smaller events before the major events. The

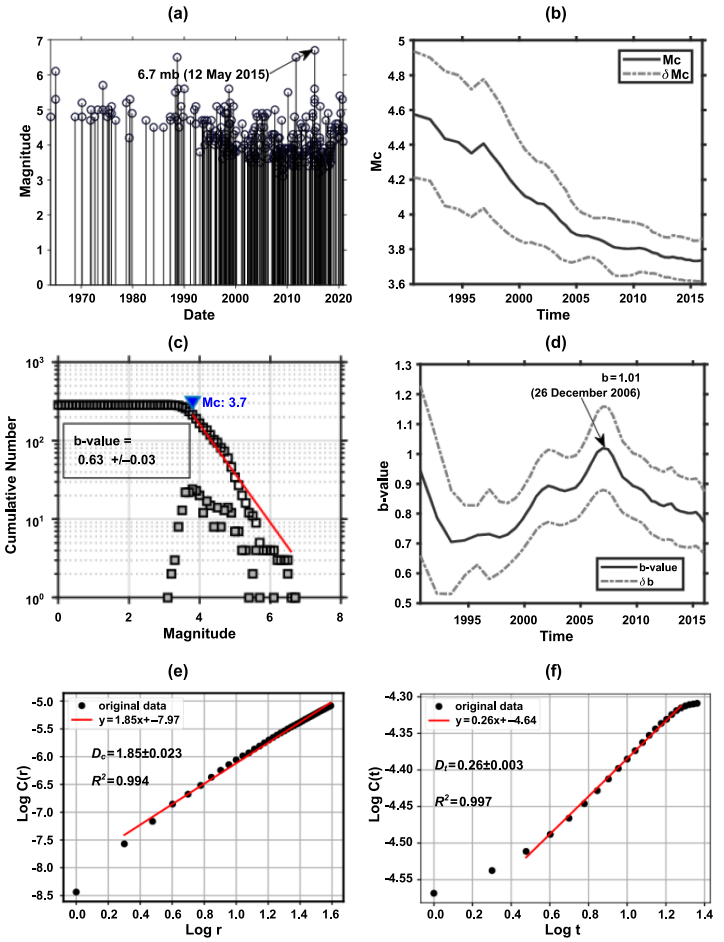

Fig. 4. Graphs showing (a) temporal variations of magnitude, (b) time variations of magnitude of completeness M_c with standard deviation (δM_c) shown by the dashed lines, (c) frequency magnitude distribution b-value, (d) temporal variation of b-value with standard deviation (δb_c), (e) spatial correlation dimension, (f) temporal correlation dimension for earthquake events from 1964 to 2020 in the demarcated region C.

calculated spatial correlation dimension (D_c) varied from 1.65 to 1.87 for different windows while it was noticed 1.82 ± 0.002 for entire study period (Table 3 and Fig. 4e). The D_c value of seismically active region ranges between 0 and 2 (*Tosi, 1998; Xu, 2011*), thus, the eastern Nepal could be interpreted as being seismically active. The temporal spatial correlation

Table 3. Time window, b-value with completeness magnitude M_c, temporal correlation dimension (D_t) and spatial correlation dimension (D_c) with their coefficient of determination (R^2) for 9 windows (8 window each of 100 events and 9th window of 85 events) of region C.

Window	Time	b-value	M_c	D_t	R^2	D_c	R^2
1	1964-02-01 – 2002-05-02	1.12 ± 0.16	4.7	0.26 ± 0.004	0.996	1.80 ± 0.02	0.996
2	1987-04-23 – 2005-02-08	0.71 ± 0.16	4.0	0.22 ± 0.003	0.998	1.80 ± 0.02	0.995
3	1995-02-18 – 2008-04-01	1.02 ± 0.12	4.2	0.29 ± 0.003	0.998	1.83 ± 0.02	0.995
4	1998-06-27 – 2010-09-28	0.93 ± 0.11	3.9	0.28 ± 0.004	0.997	1.66 ± 0.01	0.999
5	2002-05-03 – 2013-02-04	0.86 ± 0.10	3.7	0.25 ± 0.003	0.998	1.65 ± 0.01	0.998
6	2005-02-08 – 2015-04-27	0.82 ± 0.11	3.9	0.25 ± 0.004	0.996	1.82 ± 0.03	0.996
7	2008-04-12 – 2017-01-12	0.80 ± 0.11	3.7	0.28 ± 0.005	0.995	1.84 ± 0.02	0.997
8	2010-10-05 – 2019-06-17	0.76 ± 0.11	3.8	0.28 ± 0.004	0.996	1.87 ± 0.02	0.997
9	2013-02-05 – 2020-11-23	0.70 ± 0.09	3.8	0.26 ± 0.003	0.998	1.87 ± 0.02	0.997
Entire region C	1964-02-01 – 2020-11-23	0.63 ± 0.03	3.8	0.26 ± 0.003	0.997	1.85 ± 0.02	0.994

dimension (D_t) varied between 0.22 to 0.29 for different windows and it was computed as 0.26 ± 0.003 for entire study period (Table 3 and Fig. 4f). The results indicate that the time clustering of earthquakes can be considered to be near homogeneous monofractal) for eastern Nepal also.

The maximum M_c between 4.5 and 5, is found at the beginning of the computations before 1985. Thereafter it is found decreasing in linear trend. The minimum M_c value around 3.8 is computed for the catalogue after 2015 (Fig. 4b). The M_c value for entire period of study noticed to be 3.8 (Table 3). The temporal variation of b-value shows the highest b-value 1.01 for 26 December 2006 and ~ 0.8 before Gorkha earthquake (Fig. 4d).

The negative and weak correlation between b-value and spatial fractal dimension has been observed for all three regions (Fig. 5). The negative

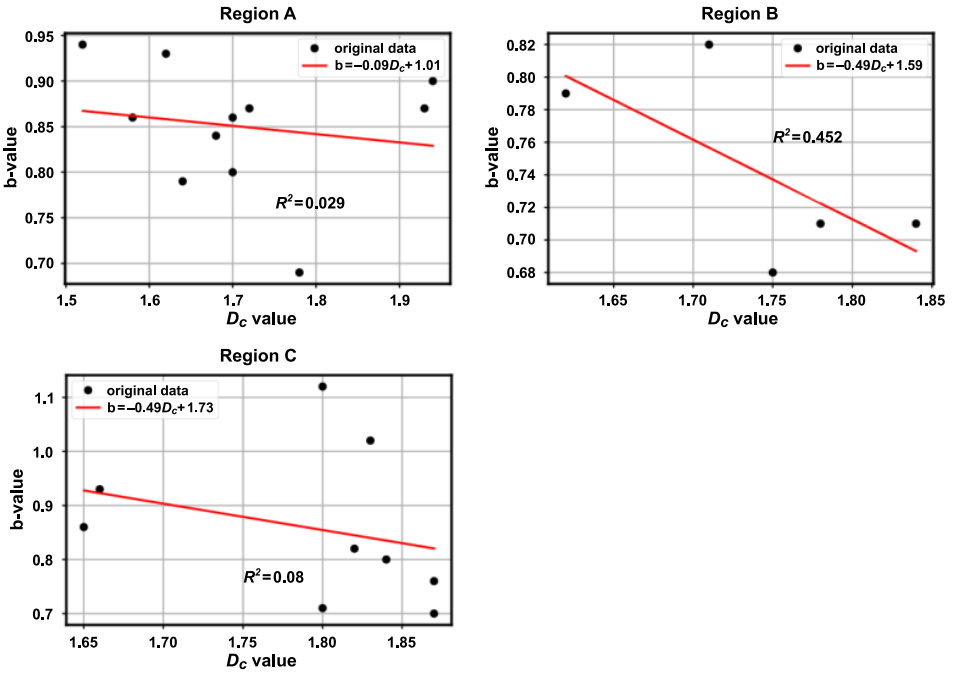

Fig. 5. Correlation between b-value and spatial correlation fractal dimension (D_c) for regions A, B and C, respectively.

correlation indicates the release of the stress along the faults of a larger surface so there is a substantial likelihood of occurrence of huge magnitude earthquakes in the regions. The distribution of epicenters on larger surface area could also be understood by high spatial correlation dimension value computed for the regions (Table 1, Table 2, and Table 3). The negative correlation is also obtained from the findings of previous articles (*Ghosh, 2020; Minocha and Parvez, 2020*) for central Himalaya region. The findings (*Minocha and Parvez, 2020*) show no significant relation between b-value and the correlation dimension as indicated by correlation coefficient 0.26.

The b-values obtained for all three regions acceptable for the region where dominant nature of the fault is thrust type. *Schorlemmer et al. (2005)* also indicated that the b-values of thrust mechanisms are low which also supports our study. Our results can also be compared numerically with the results of earlier researchers for the Himalayan region. For example, the

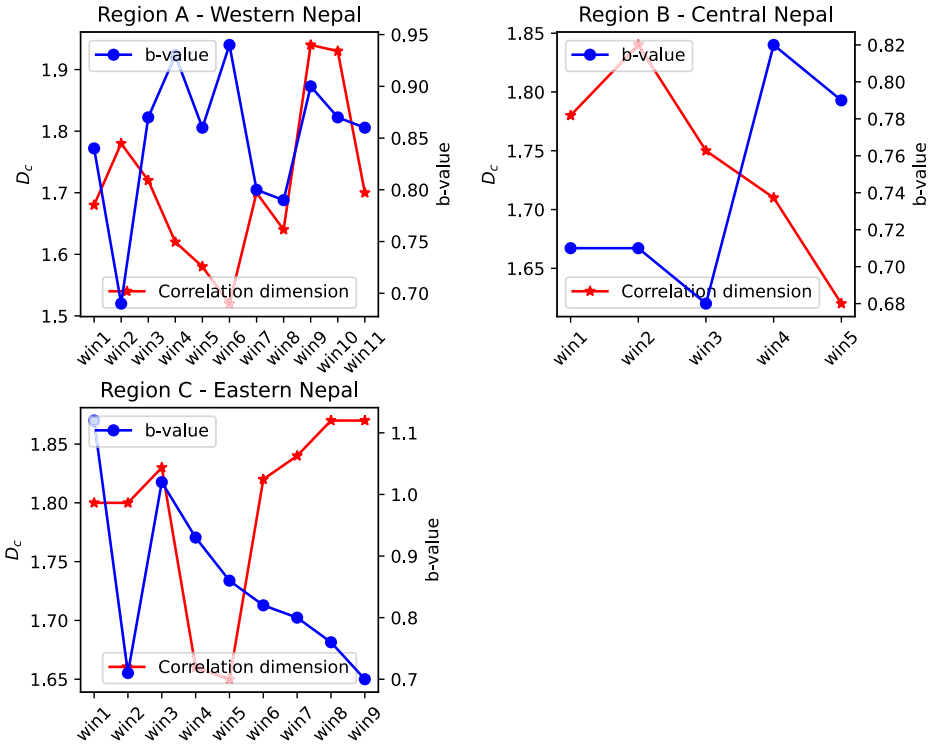

Fig. 6. Variations of the exponent b-value and D_c for different time window for Western Nepal (Region A), Central Nepal (Region B), and Eastern Nepal (Region C) during the study period.

b-values were computed between 0.85 to 0.86 for central Himalaya region before the Gorkha earthquake (*Ramesh et al., 2018*). The two low b-value patches ($b < 0.75$), towards east and west of the 2015 Gorkha earthquake epicenter had revealed in the preceding works (*Sreejith et al., 2018*). In the study carried out by *Tiwari and Paudyal (2021)* the b-value was noted as 0.78 ± 0.08 for aftershocks sequences after Dolakha earthquake. The fractal dimension computed from this study can also be compared with the preceding works (*Ghosh, 2020; Valerio et al., 2017*). *Valerio et al. (2017)* computed fractal dimension ranging from 1.5 to 1.57 with average value of $R^2 = 0.96$ for the Gorkha earthquake sequences that lasted for about 130 day (about 4 and a half months). The work (*Ghosh, 2020*) computed the fractal dimension ~ 2 near the source region of Gorkha earthquake. Higher

D_c value and low b-value computed for all three regions indicate the release of stress is on the smaller fault plane that will increase the complexity in the nearby fault system (*Nampally et al., 2018; Roy and Mondal, 2009*).

Temporal changes in b-value and D_c for different fixed events time window (Table 1, Table 2, and Table 3) are plotted in Fig. 6. These variations depict the possible temporal changes during the time 1964 and 2020. For Central Nepal (see Fig. 6) D_c values show a strong increasing tendency and b-values show a strong decreasing tendency from 1979-01-01 to 2015-04-25 (Table 2, Window 2) before the devastating Gorkha earthquake. Similar trend i.e., increasing value of D_c from 1.66 to 1.87 and decreasing b-value from 0.93 to 0.70 (Table 3 and Fig. 6) is noticed for eastern Nepal from 1998 onwards. This may suggest the adjacent large earthquake in the region. Since the higher value of the fractal dimension is more sensitive to heterogeneity in the magnitude distribution, it can be concluded that seismicity is more clustered at larger scales within smaller areas in the eastern Nepal. For western Nepal, no clear increasing or decreasing trend of both b-value and D_c value is observed.

In the bulk of the study area, M_c ranges from 3.6 to 4.0 and decrease of M_c with time is noted which might be related to the improvement of seismic networks in the region. *Chingtham et al. (2016)* estimated the three-dimensional distribution of M_c and showed that Himalayan regions have higher M_c as compared to Gangetic plain. The previous work (*Yadav et al., 2012*) have estimated the M_c for northwest Himalaya and adjacent region considering Mw$\geq$ 4.0 and the results showed that M_c varies from 4.3 to 4.7 which agrees the present study.

6. Conclusion

In this study, the completeness magnitude M_c, b-value of frequency magnitude distribution and fractal correlation dimension of earthquake's epicenter in Nepal and its vicinity were estimated by analyzing the homogeneous catalogue of 1185 events (1964-01-01 to 2020-11-23). The analysis is based on fixed event sliding window technique. M_c value for the different time windows varies between 3.6 and 4.7 with dominating value $\leq$ 4.0. For the most part of the study area, the value of b is observed $\leq$ 0.94, it suggests high stress in the crust that could increase as the result of the constant move-

ment of Indian plate towards Eurasian plate. Consequently, the probability of occurrence of future large earthquakes in this area of Himalaya increases. D_c value shows strong increasing trend and b-value shows strong decreasing trend before Gorkha earthquake in central Nepal region and similar trend is also noticed for eastern Nepal region. This could be the indication of impending large earthquake in the Eastern Nepal. For western Nepal, this study does not notice any pattern in the variation of these parameters. From temporal correlation dimension obtained for these three regions, it can be concluded that the time clustering of earthquake events is homogenous. This study enhances the knowledge of understanding the level of tectonic stress and the degree of heterogeneity of the earthquake sources in the central Himalayan region.

Acknowledgements. Author (RKT) would like to express acknowledgement to Tribhuvan University, Nepal for providing study leave and University Grants Commission (UGC), Nepal for providing monetary support for the PhD study. The authors would also like to thank the reviewers and editors for their suggestions and comments to improve the quality of this manuscript.

Software resources. The plotting software are Python, Generic Mapping Tools (*Wessel et al., 2013*) and ZMAP (*Wiemer, 2001*).

References

Adhikari L. B., Gautam U. P., Koirala B. P., Bhattarai M., Kandel T., Gupta R. M., Timsina C., Maharjan N., Maharjan K., Dahal T., Hoste-Colomer R., Cano Y., Dandine M., Guilhem A., Merrer S., Roudil P., Bollinger L., 2015: The aftershock sequence of the 2015 april 25 Gorkha–Nepal earthquake. Geophys. J. Int., **203**, 3, 2119–2124, doi: 10.1093/gji/ggv412.

Aki K., 1965: Maximum likelihood estimate of b in the formula $\log N = a - bM$ and its confidence limits. Bull. Earthq. Res. Inst. Univ. Tokyo, **43**, 2, 237–239, doi: 10.15083/0000033631.

Amorèse D., Grasso J.-R., Rydelek P. A., 2010: On varying b-values with depth: Results from computer-intensive tests for Southern California. Geophys. J. Int., **180**, 1, 347–360, doi: 10.1111/j.1365-246X.2009.04414.x.

Avouac J.-P., Meng L., Wei S., Wang T., Ampuero J.-P., 2015: Lower edge of locked Main Himalayan Thrust unzipped by the 2015 Gorkha earthquake. Nat. Geosci., **8**, 708–711, doi: 10.1038/ngeo2518.

Bilham R., 2019: Himalayan earthquakes: A review of historical seismicity and early 21st century slip potential. In: Treloar P. J., Searle M. P. (Eds.): Himalayan Tectonics: A Modern Synthesis. Geol. Soc. Spec. Publ., **483**, 423–482, doi: 10.1144/SP483.16.

Butler R. W. H., Graham R. H., Ries A. C., 2007: Introduction: The deformation of continental crust and Mike Coward's impact on its understanding. In: Ries A. C., Butler R. W. H., Graham R. H. (Eds.): Deformation of the Continental Crust: The Legacy of Mike Coward. Geol. Soc. Spec. Publ., **272**, 1–8, doi: 10.1144/GSL.SP.2007.272.01.01.

Cattin R., Martelet G., Henry P., Avouac J.-P., Diament M., Shakya T. R., 2001: Gravity anomalies, crustal structure and thermo-mechanical support of the Himalaya of Central Nepal. Geophys. J. Int., **147**, 2, 381–392, doi: 10.1046/j.0956-540X.2001.01541.x.

Chhetri M. B. P., 2018: Aftermath of Gorkha–Nepal Earthquake 2015: Lessons Learnt. Oceanogr. Fish. Open Access J., **8**, 2, 555735, doi: 10.19080/ofoaj.2018.08.555735.

Chingtham P., Sharma B., Chopra S., SinghaRoy P., 2016: Statistical analysis of aftershock sequences related with two major Nepal earthquakes: April 25, 2015, MW 7.8, and May 12, 2015, MW 7.2. Ann. Geophys., **59**,5, S0540, doi: 10.4401/ag-7025.

Dasgupta S., Mukhopadhyay M., Nandy D. R., 1987: Active transverse features in the central portion of the Himalaya. Tectonophysics, **136**, 3-4, 255–264, doi: 10.1016/0040-1951(87)90028-X.

DeCelles P. G., Kapp P., Gehrels G. E., Ding L., 2014: Paleocene-Eocene foreland basin evolution in the Himalaya of southern Tibet and Nepal: Implications for the age of initial India-Asia collision. Tectonics, **33**, 5 ,824–849, doi: 10.1002/2014TC003522.

DeCelles P. G., Robinson D. M., Zandt G., 2002: Implications of shortening in the Himalayan fold-thrust belt for uplift of the Tibetan Plateau. Tectonics, **21**, 6, 12-1–12–25, doi: 10.1029/2001TC001322.

DiPietro J. A., Pogue K. R., 2004: Tectonostratigraphic subdivisions of the Himalaya: A view from the west. Tectonics, **23**, 5, doi: 10.1029/2003TC001554.

Elliott J. R., Jolivet R., González P. J., Avouac J.-P., Hollingsworth J., Searle M. P., Stevens V. L., 2016: Himalayan megathrust geometry and relation to topography revealed by the Gorkha earthquake. Nat. Geosci., **9**, 174–180, doi: 10.1038/ngeo2623.

Gardner J. K., Knopoff L., 1974: Is the sequence of earthquakes in Southern California, with aftershocks removed, Poissonian? Bull. Seismol. Soc. Am., **64**, 5, 1363–1367, doi: 10.1785/BSSA0640051363.

Ghosh U., 2020: Seismic Characteristics and Seismic Hazard Assessment: Source Region of the 2015 Nepal Earthquake Mw 7.8 in Central Himalaya. Pure Appl. Geophys., **177**, 1, 181–194, doi: 10.1007/s00024-019-02318-w.

Grandin R., Vallée M., Satriano C., Lacassin R., Klinger Y., Simoes M., Bollinger L., 2015: Rupture process of the $Mw = 7.9$ 2015 Gorkha earthquake (Nepal): Insights into Himalayan megathrust segmentation. Geophys. Res. Lett., **42**, 20, 8373–8382, doi: 10.1002/2015GL066044.

Grassberger P., Procaccia I., 1983: Characterization of strange attractors. Phys. Rev. Lett., **50**, 5, 346–349, doi: 10.1103/PhysRevLett.50.346.

Greenhough J., Main I. G., 2008: A poisson model for earthquake frequency uncertainties in seismic hazard analysis. Geophys. Res. Lett., **35**, 19, L19313, 8–11, doi: 10.1029/2008GL035353.

Gutenberg B., Richter C. F., 1944: Frequency of earthquakes in California. Bull. Seismol. Soc. Am., **34**, 4, 185–188, doi: 10.1785/BSSA0340040185.

Hirata T., 1989: A correlation between the b value and the fractal dimension of earthquakes. J. Geophys. Res., **94**, B6,7507–7514, doi: 10.1029/JB094iB06p07507.

Hubbard J., Almeida R., Foster A., Sapkota S. N., Bürgi P., Tapponnier P., 2016: Structural segmentation controlled the 2015 MW 7.8 Gorkha earthquake rupture in Nepal. Geology, **44**, 8, 639–642, doi: 10.1130/G38077.1.

Joshi V. M., Kaushik H. B., 2017: Historic earthquake-resilient structures in Nepal and other Himalayan regions and their seismic restoration. Earthq. Spectra, **33**, 1_suppl, 299–319, doi: 10.1193/121616eqs240m.

Kellett D. A., Cottle J. M., Larson K. P., 2019: The South Tibetan Detachment System: History, advances, definition and future directions. Geol. Soc. Spec. Publ., **483**, 1, 377–400, doi: 10.1144/SP483.2.

Knopoff L., 2000: The magnitude distribution of declustered earthquakes in Southern California. Proc. Natl. Acad. Sci. U.S.A., **97**, 22, 11880–11884, doi: 10.1073/pnas.190241297.

Letort J., Bollinger L., Lyon-Caen H., Guilhem A., Cano Y., Baillard C., Adhikari L. B., 2016: Teleseismic depth estimation of the 2015 Gorkha−Nepal aftershocks. Geophys. J. Int., **207**, 3, 1584–1595, doi: 10.1093/gji/ggw364.

Minocha S., Parvez I. A., 2020: Self-organized fractal seismicity and b-value of aftershocks of the 2015 Gorkha earthquake, Nepal. Int. J. Geosci., **11**, 8, 562–579, doi: 10.4236/ijg.2020.118030.

Mitra S., Paul H., Kumar A., Singh S. K., Dey S., Powali D., 2015: The 25 April 2015 Nepal earthquake and its aftershocks. Curr. Sci., **108**, 10, 1938–1943, doi: 10.18520/cs/v108/i10/1938-1943.

Miyake H., Sapkota S. N., Upreti B. N., Bollinger L., Kobayashi T., Takenaka H., 2017: Special issue "the 2015 Gorkha, Nepal, earthquake and Himalayan studies: First results". Earth Planets Space, **69**, 12, 2015–2016, doi: 10.1186/s40623-016-0597-8.

Molnar P., Pandey M. R., 1989: Rupture zones of great earthquakes in the Himalayan region. Proc. Indian Acad. Sci. – Earth Planet. Sci., **98**, 1, 61–70, doi: 10.1007/BF02880376.

Mondal S. K., Roy P. N. S., 2016: Temporal multifractal pattern of seismicity in northwest Himalayan region. J. Geol. Soc. India, **88**, 5, 569–575, doi: 10.1007/s12594-016-0522-6.

Nakaya S., Hashimoto T., 2002: Temporal variation of multifractal properties of seismicity in the region affected by the mainshock of the October 6, 2000 Western Tottori Prefecture, Japan, earthquake ($M = 7.3$). Geophys. Res. Lett., **29**, 10, 133-1–133-4, doi: 10.1029/2001gl014216.

Nampally S., Padhy S., Dimri V. P., 2018: Characterizing spatial heterogeneity based on the b-value and fractal analyses of the 2015 Nepal earthquake sequence. Tectonophysics, **722**, 154–162, doi: 10.1016/j.tecto.2017.11.004.

Ni J. F., 1989: Active tectonics of the Himalaya. Proc. Indian Acad. Sci. – Earth Planet. Sci., **98**, 71–89, doi: 10.1007/BF02880377.

Nuannin P., 2006: The Potential of b-value Variations as Earthquake Precursors for Small and Large Events. PhD thesis, Uppsala University, SE-75236, Uppsala, Sweden.

Oncel A. O., Wilson T., 2007: Anomalous seismicity preceding the 1999 Izmit event, NW Turkey. Geophys. J. Int., **169**, 1, 259–270, doi: 10.1111/j.1365-246X.2006.03298.x.

Ormeni R., Öztürk S., Fundo A., Çelik K., 2017: Spatial and temporal analysis of recent seismicity in different parts of the Vlora-Lushnja-Elbasani-Dibra transversal fault zone, Albania. Austrian J. Earth Sci., **110**, 2, doi: 10.17738/ajes.2017.0015.

Pailoplee S., Choowong M., 2014: Earthquake frequency-magnitude distribution and fractal dimension in mainland Southeast Asia. Earth Planets Space, **66**, 8, 1–10, doi: 10.1186/1880-5981-66-8.

Pandey M. R., Tandukar, R. P., Avouac J.-P., Lavé J., Massot J. P., 1995: Interseismic strain accumulation on the Himalayan crustal ramp (Nepal). Geophys. Res. Lett., **22**, 7, 751–754, doi: 10.1029/94GL02971.

Prakash R., Singh R. K., Srivastava H. N., 2016: Nepal earthquake 25 April 2015: source parameters, precursory pattern and hazard assessment. Geomatics, Nat. Hazards Risk, **7**, 6, 1769–1784, doi: 10.1080/19475705.2016.1155504.

Ramesh P., Martha T. R., Kumar K. V., 2018: Regional variation of stress level in the Himalayas after the 25 April 2015 Gorkha earthquake (Nepal) estimated using *b*-values. J. Geophys. Eng., **15**, 3, 921–927, doi: 10.1088/1742-2140/aaa26c.

Roy P. N. S., Mondal S. K., 2009: Fractal nature of earthquake occurrence in northwest Himalayan region. J. Indian Geophys. Union, **13**, 2, 63–68.

Roy S., Ghosh U., Hazra S., Kayal J. R., 2011: Fractal dimension and *b*-value mapping in the Andaman-Sumatra subduction zone. Nat. Hazards, **57**, 1, 27–37, doi: 10.1007/s11069-010-9667-6.

Sapkota S. N., Bollinger L., Klinger Y., Tapponnier P., Gaudemer Y., Tiwari D., 2013: Primary surface ruptures of the great Himalayan earthquakes in 1934 and 1255. Nat. Geosci., **6**, 71–76, doi: 10.1038/ngeo1669.

Schorlemmer D., Wiemer S., Wyss M., 2005: Variations in earthquake-size distribution across different stress regimes. Nature, **437**, 539–542, doi: 10.1038/nature04094.

Shanker D., Paudyal H., Singh H. N., 2011: Discourse on seismotectonics of Nepal Himalaya and vicinity: Appraisal to earthquake hazard. Geosciences, **1**, 1, 1–15, doi: 10.5923/j.geo.20110101.01.

Shcherbakov R., Turcotte D. L., Rundle J. B., 2015: Complexity and Earthquakes. In: Schubert G. (Ed.): Treatise on Geophysics: Second Edition. Elsevier B.V., 627–653, doi: 10.1016/B978-0-444-53802-4.00094-4.

Shcherbakov R., Turcotte D. L., Rundle J. B., 2004: A generalized Omori's law for earthquake aftershock decay. Geophys. Res. Lett., **31**, 11, L11613, doi: 10.1029/2004GL019808.

Shi Y., Bolt B. A., 1982: The standard error of the magnitude-frequency *b* value. Bull. Seismol. Soc. Am., **72**, 5, 1677–1687, doi: 10.1785/BSSA0720051677.

Singh C., Singh A., Chadha R. K., 2009: Fractal and b-value mapping in eastern Himalaya and southern Tibet. Bull. Seismol. Soc. Am., **99**, 6, 3529–3533, doi: 10.1785/0120090041.

Smalley R. F., Chatelain J.-L., Turcotte D. L., Prévot R., 1987: A fractal approach to the clustering of earthquakes: Applications to the seismicity of the New Hebrides. Bull. Seismol. Soc. Am., **77**, 4, 1368–1381, doi: 10.1785/BSSA0770041368.

Smith W. D., 1981: The *b*-value as an earthquake precursor. Nature, **289**, 136–139, doi: 10.1038/289136a0.

Sreejith K. M., Sunil P. S., Agrawal R., Saji A. P., Rajawat A. S., Ramesh D. S., 2018: Audit of stored strain energy and extent of future earthquake rupture in central Himalaya. Sci. Rep., **8**, 16697, 1–9, doi: 10.1038/s41598-018-35025-y.

Tiwari R. K., Paudyal H., 2021: Variability of b-value before and after the Gorkha earthquake in the central Himalaya and vicinity. BIBECHANA, **18**, 2, 32–42, doi: 10.3126/bibechana.v18i2.31207.

Tosi P., 1998: Seismogenic structure behaviour revealed by spatial clustering of seismicity in the Umbria-Marche Region (Central Italy). Ann. Geophys., **41**, 2, 215–224, doi: 10.4401/ag-4331.

Upreti B. N., Kumahara Y., Nakata T., 2007: Paleoseismological study in the Nepal Himalaya – present status. Proceedings of the Korea-Nepal Joint symposium on slope stability and landslides, April 1, 2007, 1–9.

Valerio E., Tizzani P., Carminati E., Doglioni C., 2017: Longer aftershocks duration in extensional tectonic settings. Sci. Rep., **7**, 16403, 1–12, doi: 10.1038/s41598-017-14550-2.

Wang K., Fialko Y., 2015: Slip model of the 2015 *Mw* 7.8 Gorkha (Nepal) earthquake from inversions of ALOS-2 and GPS data. Geophys. Res. Lett., **42**, 18, 7452–7458, doi: 10.1002/2015GL065201.

Webb A. A. G., Schmitt A. K., He D., Weigand E. L., 2011: Structural and geochronological evidence for the leading edge of the Greater Himalayan Crystalline complex in the central Nepal Himalaya. Earth Planet. Sci. Lett., **304**, 3-4, 483–495, doi: 10.1016/j.epsl.2011.02.024.

Wei S., Chen M., Wang X., Graves R., Lindsey E., Wang T., Karakaş Ç., Helmberger D., 2018: The 2015 Gorkha (Nepal) earthquake sequence: I. Source modeling and deterministic 3D ground shaking. Tectonophysics, **722**, 447–461, doi: 10.1016/j.tecto.2017.11.024.

Wessel P., Smith W. H. F., Scharroo R., Luis J., Wobbe F., 2013: Generic mapping tools: Improved version released. Eos (Washington DC), **94**, 45, 409–410, doi: 10.1002/2013EO450001.

Wiemer S., 2001: A software package to analyze seismicity: ZMAP. Seismol. Res. Lett., **72**, 3, 373–382, doi: 10.1785/gssrl.72.3.373.

Wiemer S., Wyss M., 2000: Minimum magnitude of completeness in earthquake catalogs: Examples from Alaska, the Western United States, and Japan. Bull. Seismol. Soc. Am., **90**, 4, 859–869, doi: 10.1785/0119990114.

Wu M.-H., Wang J. P., Ku K.-W., 2019: Earthquake, Poisson and Weibull distributions. Physica A, **526**, 121001, doi: 10.1016/j.physa.2019.04.237.

Xu J., 2011: Fractal analysis to study the structural distribution of Wenchuan earthquake in China. Adv. Mat. Res., **243–249**, 4097–4100, doi: 10.4028/www.scientific.net/AMR.243-249.4097.

Yadav R. B. S., Bayrak Y., Tripathi J. N., Chopra S., Bayrak E., 2012: Regional variation of the ω-upper bound magnitude of GIII distribution in Hindukush-Pamir Himalaya and the adjacent regions: A perspective on earthquake hazard. Tectonophysics, **544–545**, 1–12, doi: 10.1016/j.tecto.2012.03.015.

Yeken T., 2016: Spatial Analysis of b-value Variability in Armutlu Peninsula (NW Turkey). Open Geosci., **8**, 548–555, doi: 10.1515/geo-2016-0048.

Yin A., Dubey C. S., Webb A. A. G., Kelty T. K., Grove M., Gehrels G. E., Burgess W. P., 2010: Geologic correlation of the Himalayan orogen and Indian craton: Part 1. Structural geology, U-Pb zircon geochronology, and tectonic evolution of the Shillong Plateau and its neighboring regions in NE India. Geol. Soc. Am. Bull., **122**, 3-4, 336–359, doi: 10.1130/B26460.1.

Geodesy and Geodynamics 13 (2022) 525–533

Contents lists available at ScienceDirect

Geodesy and Geodynamics

journal homepage: http://www.keaipublishing.com/geog

On the spatio-temporal variation in *b*-value after 25 April 2015 Gorkha, Nepal earthquake

Ram Krishna Tiwari [a, b, *], Harihar Paudyal [b], Daya Shanker [c]

[a] Central Department of Physics, Tribhuvan University, Kirtipur, Kathmandu, Nepal
[b] Birendra Multiple Campus, Tribhuvan University, Bharatpur, Chitwan, Nepal
[c] Department of Earthquake Engineering, Indian Institute of Technology Roorkee, Roorkee, Uttarakhand, India

ARTICLE INFO

Article history:
Received 11 November 2021
Accepted 12 January 2022
Available online 20 May 2022

Keywords:
Frequency-magnitude distribution
Time series analysis
Thrust fault
Stress
Central Himalaya

ABSTRACT

In the present study, the spatial-temporal distribution of *b*-value along the five faults area (the Judi fault, Thaple fault, Kathmandu fault, Motihari-GauriShanker fault, and Motihari-Everest fault) was investigated after the Gorkha earthquake (M_W7.8). The earthquake catalog of 10,500 events was prepared by compiling the published catalogs. The study area is bounded in the central Himalaya from 26.5° to 29° in latitude direction and 84° to 87° in longitude direction. The frequency magnitude distribution shows the variation of the *b*-value along with fault areas from 0.45 to 0.69, indicating a common characteristic of aftershock sequences. In particular, the Judi fault area, Thaple fault area, and Motihari-Everest fault area are characterized by the low *b*-values of 0.45 ± 0.02, 0.48 ± 0.02, and 0.55 ± 0.04, respectively. These regions could be the source region for future earthquakes. The low *b*-value observed for fault areas are also consistent with the thrust faulting pattern in the region as indicated by the focal mechanism of mainshock and major aftershocks. The temporal variation of *b*-value shows inevitable fluctuations during 25 April to 12 May 2015. Among the area selected, the Motihari-Everest fault area is in critical strain (mechanically locked) conditions, as indicated by the stepwise energy release pattern.

1. Introduction

Nepal has a long history of devastating earthquakes because of its location in an earthquake-prone plate tectonic zone. Two major earthquakes that occurred in the last 200 years are the 26 August 1833 earthquake (VII-IX in Modified Mercalli Intensities scale) [1] and the tremendous Nepal-Bihar earthquake (M_W8.1) on 15 January 1934. The epicenter of the 1934 earthquake was 9.5 km south of Mount Everest [2]. Recently the nation was struck by an earthquake of moment magnitude M_W7.8 or local magnitude 7.6 on 25 April 2015 at 06:11:26 UTC [3]. The epicenter of this event was in the Nepal-Bihar seismic gap, located 36 km east of Khudi, Nepal, about 80 km northwest of Kathmandu [4]. The Gorkha earthquake was the largest in Nepal after the 1934 Bihar-Nepal Earthquake [5]. The main event broke the Main Himalayan Thrust (MHT) locked lower section from west to east and left the locked upper section unbroken [6–8]. The event killed nearly 9000 people, and many thousands more were injured. It destroyed or damaged more than 600,000 structures in Kathmandu and nearby towns [9].

Following the main shock, the series of moderate to strong aftershocks are recorded, including the two largest aftershocks M_L6.0 and M_L6.7 on the same day within 35 min of the mainshock. On 26 April the second-largest aftershock of M_L6.9 was registered while the strongest and severely damaging one (M_L7.0) was noticed on 12 May 2015 which further ruptured the eastern end of the rupture zone. The rupturing process left a small gap unbroken between the mainshock and aftershock slip zones [10]. After 30 min of this event, another large aftershock M_W6.3 was registered [11–13]. The aftershock sequences are concentrated in a narrow band of width 40 km at mid-crustal to shallow depths (i.e., within the range of 2–25 km) along the strike of

* Corresponding author. Central Department of Physics, Tribhuvan University, Kirtipur, Kathmandu, Nepal.
E-mail addresses: ram.tiwari@bimc.tu.edu.np (R.K. Tiwari), harihar.paudyal@bimc.tu.edu.np (H. Paudyal).

Peer review under responsibility of Institute of Seismology, China Earthquake Administration.

Production and Hosting by Elsevier on behalf of KeAi

https://doi.org/10.1016/j.geog.2022.01.006

the southern slope of the high Himalayan range [3]. From the prepared dataset, it can be noticed that the most of the aftershocks were spread over an area of about 222 km × 111 km, with an increasing concentration towards the east of the mainshock (Fig. 1). These aftershocks caused further loss of life and infrastructures in the northern part of central Nepal.

2. Tectonic process and earthquake

The mechanism behind these Himalayan earthquakes is governed by the northward thrusting of the Indian plate below the overriding Eurasian plate. This long tectonic process dating back to 61 Ma [14] maintains the height of the Himalayas mountains and causes large earthquakes that can exceed magnitude 8 [15]. From the south to the north, the major faults of the Himalayas are the Main Frontal Thrust (MFT), Main Boundary Thrust (MBT), Main Central thrust (MCT), South Tibetan detachment system (STD), and the Indus-Tsangpo suture zone (ITSZ) [16,17]. The source region of the Gorkha event is the Main Himalayan Thrust (MHT) fault which is the most active structure running along the Himalayan arc. The MHT reaches the surface as MFT and absorbs about 20 mm per year of the India-Eurasia convergence in Nepal [8,18]. The coseismic rupture of the Gorkha earthquake has been controlled by the local heterogeneity in the stress/strain regime [19]. Transversal structures have controlled the rupture propagation during the earthquake. The Judi fault is the western boundary of the central rupture zone, while the eastern boundary is the Gaurishankar fault separating the 25 April 2015 rupture from the 12 May 2015 rupture [20]. The well-marked concentration of these aftershocks (Fig. 1) near MHT could activate the Judi fault, Thaple fault, Kathmandu fault, Motihari-GauriShanker fault, and Motihari-Everest fault [21]. This study selected the fault that started in the footwall of the MHT and extending up to the hanging wall (i.e., from the Judi fault on the western boundary to the Motihari-Everest fault on the eastern boundary), to investigate the spatio-temporal variation of aftershocks sequences of the Gorkha earthquake in the central Himalaya.

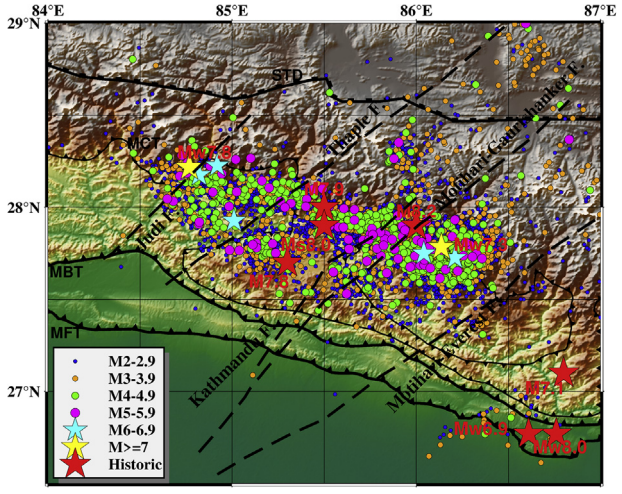

Fig. 1. Seismotectonic map showing the 10,500 earthquake events ($M_L \geq 2.0$) along with the major faults MCT, MBT, MFT, and STD. From the historical period to date, the red stars represent seven major earthquakes in the region. The yellow stars are the mainshock (M_L7.6) and major aftershock (M_L7.0) of the Gorkha earthquake sequences. The dashed black lines represent the Judi fault, Thaple fault, Kathmandu fault, Motihari-GauriShanker fault, and Motihari-Everest fault [22,23].

3. Frequency magnitude distribution

Numerous workers have suggested the *b*-value of the frequency magnitude distribution as an earthquake precursor [24–26]. The frequency magnitude distribution equation [27] describes the number of earthquakes that occurred in the region as a function of their magnitude *M* as:

$$\log N(M) = a - bM \quad (1)$$

In the relation, *N* is the cumulative number of earthquakes with a magnitude greater than equal to *M*, while the parameter *a* and *b* are real constants with a spatial-temporal variation. The constant *a* characterizes the seismicity of the region. The high value of *a* corresponds to high seismicity and vice versa. The other constant *b*-value has the potential to describe the relative number of minor to major earthquakes in the given area. The stable *b*-value is reported to be 1, but values ranging from 0.3 to 2.5 have also been mentioned in the kinds of literature [28–31]. The variation in the *b*-value is suggested to depend on tectonic characteristics and focal mechanisms. It takes a small value for a thrust faulting earthquake than a normal faulting earthquake and an intermediary value for strike-slip earthquakes [32–34]. In addition, parameter *b* is thought to depend on the stress regime as well as the tectonic character of the region [35,36]. Moreover, the creeping nature of faults is associated with high *b*-values, while asperities type faults are reported to be described by peculiarly low *b*-values [34,37]. The *b*-value increases when the asperities present in the region get isolated, and when the asperities become more organized, its value decreases [38]. The *b*-value as a function of depth has also been studied [39] and found that the *b*-value decreases down to depth. Following the Gorkha earthquake, many investigators have studied the change in frequency magnitude distribution of earthquakes (*b*-value) in the central Himalayan region. The investigators [3] noticed that the *b*-value (0.80 ± 0.05) lesser than the normal *b*-value of 1.0 observed worldwide after the major earthquake. The *b*-value (0.92) was noticed for around 3 months of data from April 25, 2015, to July 31 2015, documented at the National Seismological Centre (NSC) network [11]. The findings [40] conclude that the triggering of aftershocks around the mainshock was delayed, and expansion occurred towards the eastern end near the Kodari earthquake (major aftershock). The previous finding [41] showed that *b*-values in the eastern zone are lower than that in the source region of the 25 April 2015 earthquake, inferring high-stress buildup. This might indicate the high probability of occurrence of a large earthquake, particularly in the eastern zone. This work examines the spatio-temporal variation of the *b*-value in the previously mentioned faults in the region after the Gorkha earthquake of 2015.

4. Data and methodology

The catalog in this study is prepared from the two different datasets containing well-located earthquakes. The first one is the bulletin of the permanent National Seismological Centre (NSC) network [3] and the second is a well-resolved aftershock catalog for the 2015 Gorkha earthquake detected by the NAMASTE temporary seismic network that is densely distributed over the rupture area [42]. We got 15,275 earthquake events from the above sources. The magnitude of completeness (M_c) is calculated by the maximum curvature technique [43], and it was estimated to be M_L2.0. The final dataset contains 10,500 earthquakes of magnitude ≥2.0 M_L (Local-scale) from 2015.4.25 to 2016.5.14 within the study area. The *b*-value for the total dataset was found to be 0.61 ± 0.01 (Fig. 2).

To investigate the variation of *b*-values along the aforementioned faults, an area of fixed-width 20 km and variable-length

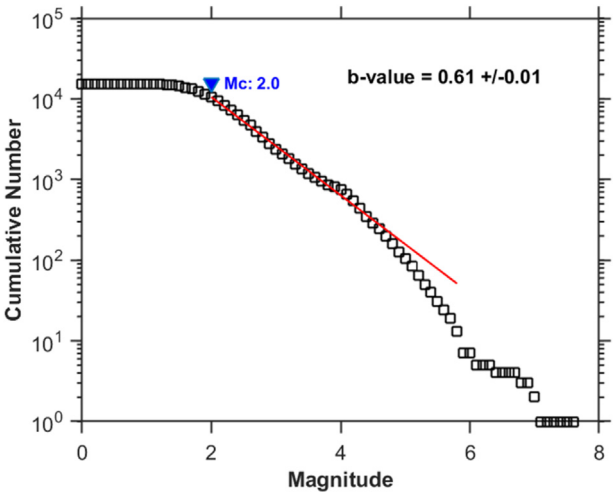

Fig. 2. Magnitude of completeness (M_c) and b-value for the entire dataset.

from south to north is considered and analysis is carried out by the software package ZMAP [44]. We computed the maximum likelihood of b-values using the equation (2) [45,46].

$$b = \frac{1}{\overline{M} - (M_c - \frac{\Delta M}{2})} \log e \tag{2}$$

where $\overline{M}$ is the mean magnitude, M_c is the completeness magnitude and ΔM is the binning width. The confidence limit of this estimation is given by [47].

$$\delta b = 2.30 * b^2 \sqrt{\sum_{i=1}^{n} \frac{(M_i - \overline{M})^2}{n_s(n_s - 1)}} \tag{3}$$

where n_s is the total number of events in the sample window, and δb is actual standard deviation of b-value. For the time series analysis of b-value, the window size of 200 was taken with the minimum number of events 50 and a window overlap of 4%, while for the b-value cross-section study, a minimum number of nearest events was taken 50 and the minimum number of events > M_c per node was taken 50. Similarly, for b-value variation with depth number of events in each window is taken at 150 with an overlap factor of 5.

4.1. b-value variation along the Judi fault

The cross-section along the Judi fault (84.30°E, 27.72°N and 85.10°E, 28.50°N) bounded by the length 117.0 km and width of 20 km is considered for the study.

From the log-linear frequency-magnitude plot of the Gutenberg–Richter distributions, the b-value is estimated as 0.45 ± 0.02 for this area (Fig. 3a). The b-value is the slope of the red line obtained from the linear regression of the observed events with $M_c \geq 2.0$. It is the significantly low value of b comparing to the remaining four areas selected for the study. The temporal variation of the b-values is depicted by the Fig. 3b, where the b-values are represented by a solid line, and the standard deviation is represented as dashed lines. The b-value was noticed 0.76 on 12 August 2015 and 0.67 on 18 August 2015. It shows a sharp rise, fall within a

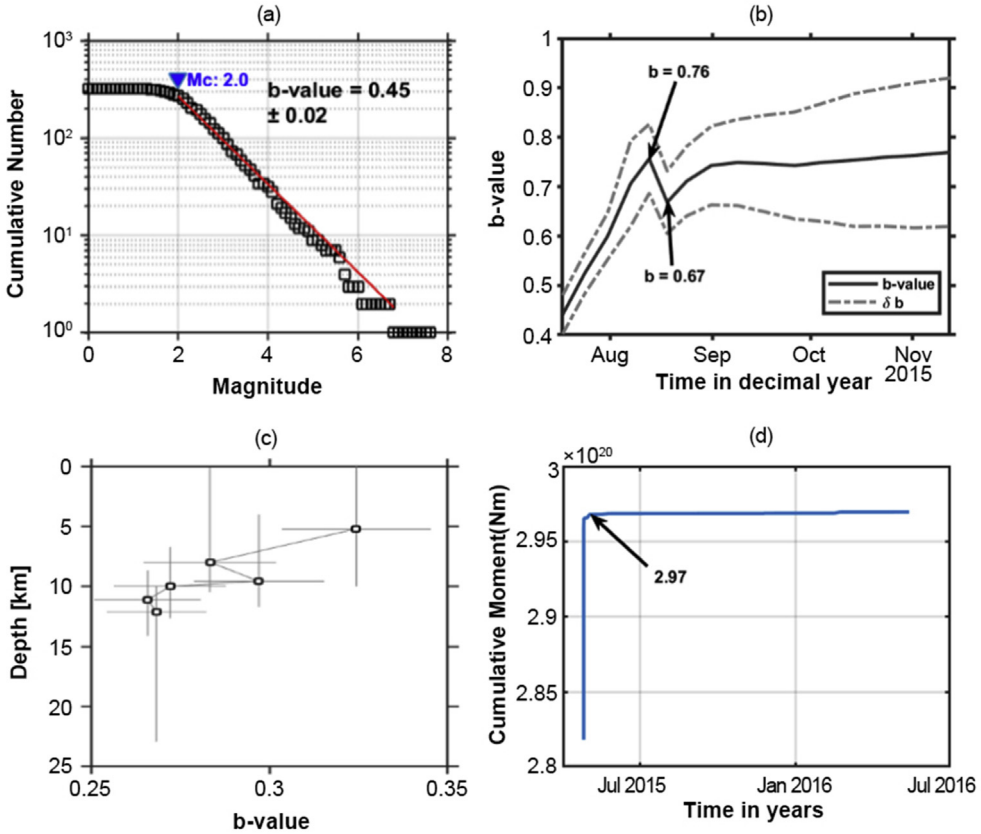

Fig. 3. Graphs representing b-value variation for the area along Judi fault. (a), (b), (c) and (d) depict frequency magnitude distribution (FMD), b-value variation with time, b-value variation with depth, and temporal variation of cumulative seismic moment release for the area.

week, and settles within the range 0.75–0.8 after September 2015. The depth variation of *b*-value shows the lowest value below the depth of 10 km, which could be the indication that the stress was most concentrated near this depth (Fig. 3c). The recurrent existence of earthquakes is at depth <12 km and within this depth the *b*-value changes from ~0.27 to 0.33. The cumulative moment release curve (Fig. 3d) shows the large amount of strained energy gets released from this area. It rises sharply from 2.82×10^{20} Nm on 25 April 2015 to 2.97×10^{20} Nm on 2 May 2015 indicating the quick release of the energy.

4.2. *b*-value variation along the Thaple fault

The area along the Thaple fault (84.64°E, 27.58°N and 87.15°E, 29.55°N) bounded by the length 328.6 km and width of 20 km is considered for the study.

A log-linear frequency-magnitude plot for the Gutenberg–Richter distributions gives the *b*-value of 0.48 ± 0.02 (Fig. 4a). It is estimated as the slope of the red line obtained from the linear regression of the observed events for ($M_c \geq 2.0$). The *b*-value estimated is again significantly low. In the temporal variation of the *b*-values plot (Fig. 4b), the *b*-values are represented by a solid line, and the standard deviation is represented as dashed lines. The *b*-value shows roughly cyclic variation with a maximum value of 0.97 on 1 September 2015. The *b*-value was smallest (around 0.23) at a depth of 10 km, indicating that the stress was accumulated around this depth. It was around 0.39 at a depth of around 13 km (Fig. 4c). The cumulative moment curve (Fig. 4d) for this area shows a significant rise to 1.37×10^{18} Nm on 1 May 2015, and after that, it shows a gradual increase.

4.3. *b*-value variation along the Kathmandu fault

The area selected along the Kathmandu fault (85.14°E, 27.14°N and 86.0°E, 28.05°N) is bounded by a length of 130.9 km and a width of 20 km.

A log-linear frequency-magnitude plot for the Gutenberg–Richter distributions is depicted in Fig. 5a. The slope of the red line obtained for the linear regression of the events ($M_c \geq 2.0$) gives the *b*-value as 0.64 ± 0.01. The estimated *b*-value is low compared to the average value of 1.0. The temporal variation of the *b*-values is revealed by the plot (Fig. 5b), where the *b*-values are represented by a solid line, and the standard deviation is represented as dashed lines. The *b*-value shows roughly cyclic variation with decreasing trend and the lowest value was observed as 0.55 on 29 January 2015 and the highest *b*-value 1.10 on 7 June 2015. The *b*-value was smallest (<0.2) at a depth of 10 km, so the concentration of the stress is near this depth for this region. It was around 0.38 at a depth of 15 km (Fig. 5c). The cumulative moment release curve (Fig. 5d) for this area shows a significant rise from 0.398×10^{18} Nm to 4.07×10^{18} Nm within the period of 25 April 2015 to 12 May 2015, and thereafter it shows a very small increment.

4.4. *b*-value variation along the Motihari-GauriShanker fault

To study the *b*-value variation for the area along the Motihari-GauriShanker fault (84.82°E, 26.67°N and 86.83°E, 28.58°N), we considered the area bounded by the length 289.3 km and width of 20 km.

For the area considered, the *b*-value (0.69 ± 0.02) is estimated as the slope of the red line in the Gutenberg-Richter frequency

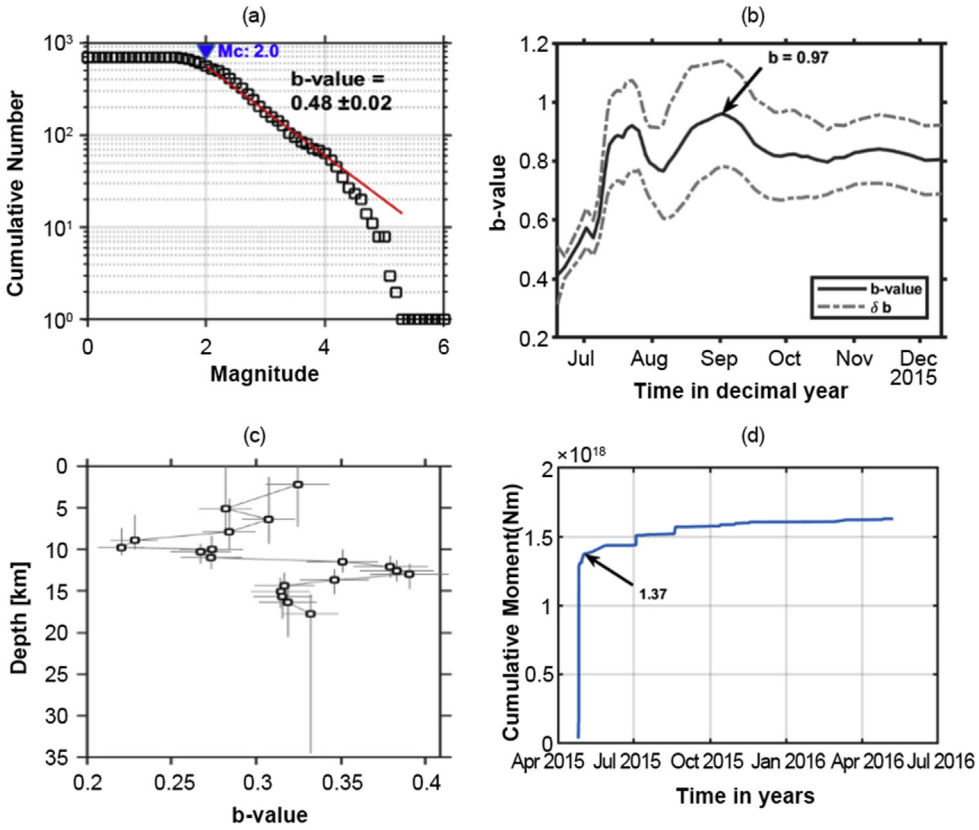

Fig. 4. Graphs representing *b*-value variation for the area along the Thaple fault. (a), (b), (c) and (d) depict frequency magnitude distribution (FMD), *b*-value variation with time, *b*-value variation with depth, and temporal variation of cumulative seismic moment release for the area.

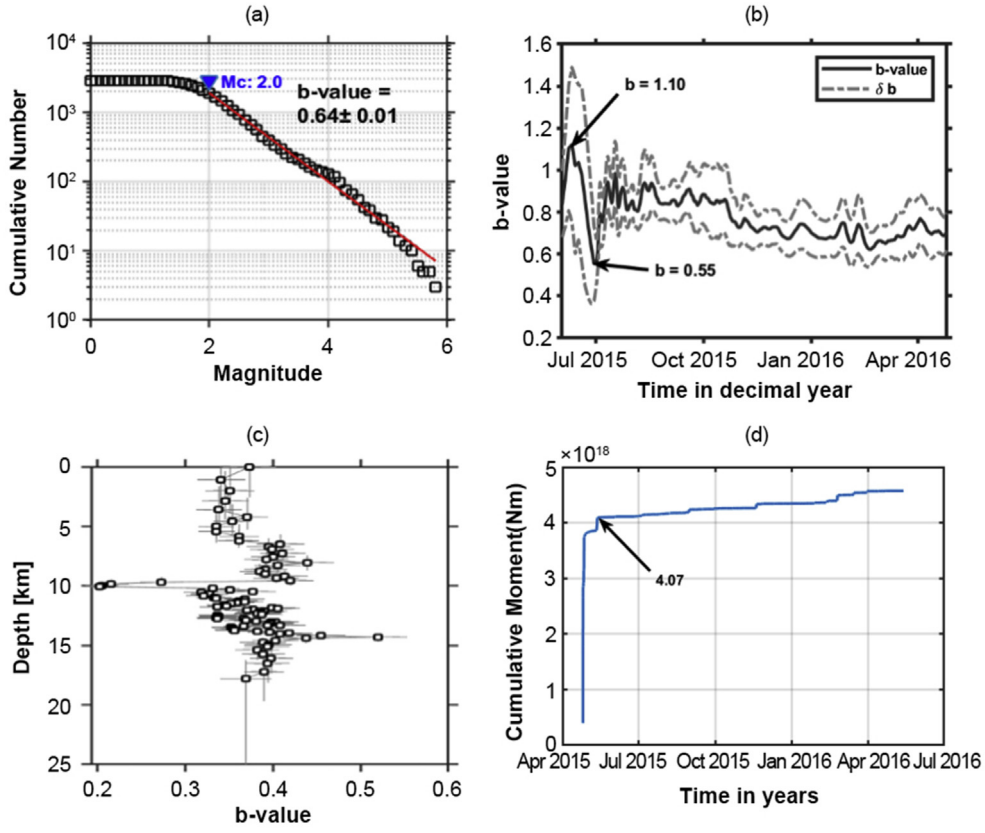

Fig. 5. Graphs representing *b*-value variation for the area along the Kathmandu fault. (a), (b), (c) and (d) depict the frequency magnitude distribution (FMD), *b*-value variation with time, *b*-value variation with depth, and temporal variation of cumulative seismic moment release.

magnitude distribution. It is estimated from the linear regression of the observed events with $M_c \geq 2.0$ (Fig. 6a). In the temporal variation of the *b*-values plot (Fig. 6b), the *b*-values are represented by a solid line, and the standard deviation is represented as dashed lines. The sharp fluctuation in *b*-value from 0.42 to 1.22 was noticed from 22 June 2015 to 22 July 2015. After July 2015, a gradual decrease in *b*-value was noticed. The *b*-value is smallest (around 0.2) at a depth of 10 km, and its variation is from 0.3 to 0.55 between 10 km and 17 km. The results indicate a concentration of the stress within this depth (Fig. 6c). The cumulative moment curve (Fig. 6d) shows a sharp rise of energy up to 2.63×10^{19} Nm within a single day (25 April 2015–26 April 2015). Thus, there is a release of a massive amount of energy in a noticeably short time interval. This may be the cause behind the occurrences of many aftershocks in a noticeably short time.

4.5. *b*-value variation along the Motihari-Everest fault

For this fault, the area covered by the length of 341.0 km and width of 20 km bounded by the geographical points 84.92°E, 26.55°N and 87.69°E, 28.41°N is considered for the study.

From the log-linear frequency-magnitude plot of the Gutenberg–Richter distributions, the *b*-value (0.55 ± 0.04) is estimated (Fig. 7a). The *b*-value is the slope of the red line obtained for the linear regression line of the observed events with $M_c \geq 2.0$. For this area, the *b*-value obtained is very low compared to the global average value of 1.0. Fig. 7b shows the temporal variation of the *b*-values where a solid line represents the *b*-values, and the standard deviation is represented as dashed lines. The *b*-value shows rapid fluctuations from 0.74 to 0.67 within one week (7 September 2015 to 14 September 2015), thereafter it settles around 0.7. The *b*-value was the smallest (around 0.303) at a depth of ~7 km (Fig. 7c). The cumulative moment release curve (Fig. 7d) shows that the release of strain energy is not sharp but in a stepwise process. The energy released was 2.51×10^{16} Nm on 12 May 2015. It was 2.94×10^{16} Nm on 23 May 2015, 3.57×10^{16} Nm on 16 September 2015, and 3.93×10^{16} Nm on 3 December 2015. This stepwise energy release process indicates that seismogenic sources are mechanically locked, and earthquakes occurrence is random to time due to frictional and mechanical reasons.

5. Focal mechanism of Gorkha earthquake and its major aftershocks

The CMT solution for the mainshock (M_L7.6) of 25 April 2015 given by Global-CMT [48,49] shows a predominantly thrust fault on a shallow N–E dipping plane (Fig. 8). The propagation of rupture is eastward and is consistent with Main Frontal Thrust [50,51]. The aftershock (M_L6.7) on the same day shows a similar mechanism to the mainshock with a small oblique component on it. Another aftershock of M_L5.7 had a normal fault mechanism with the east-west orientation of nodal planes, which could be interpreted as an extension after the mainshock. The M_L6.0 event showed a normal fault mechanism with a strong oblique component on the same day. The two aftershocks (M_L6.9 and M_L5.8) of 26 April originated on the eastern edge of the main rupture, also showed a predominant fault mechanism initiated by severe compressive stresses. The fault planes for those earthquakes are low angled, which results in a significant horizontal movement. The M_L6.9 event had a close match with the dip of the mainshock. On 12 May

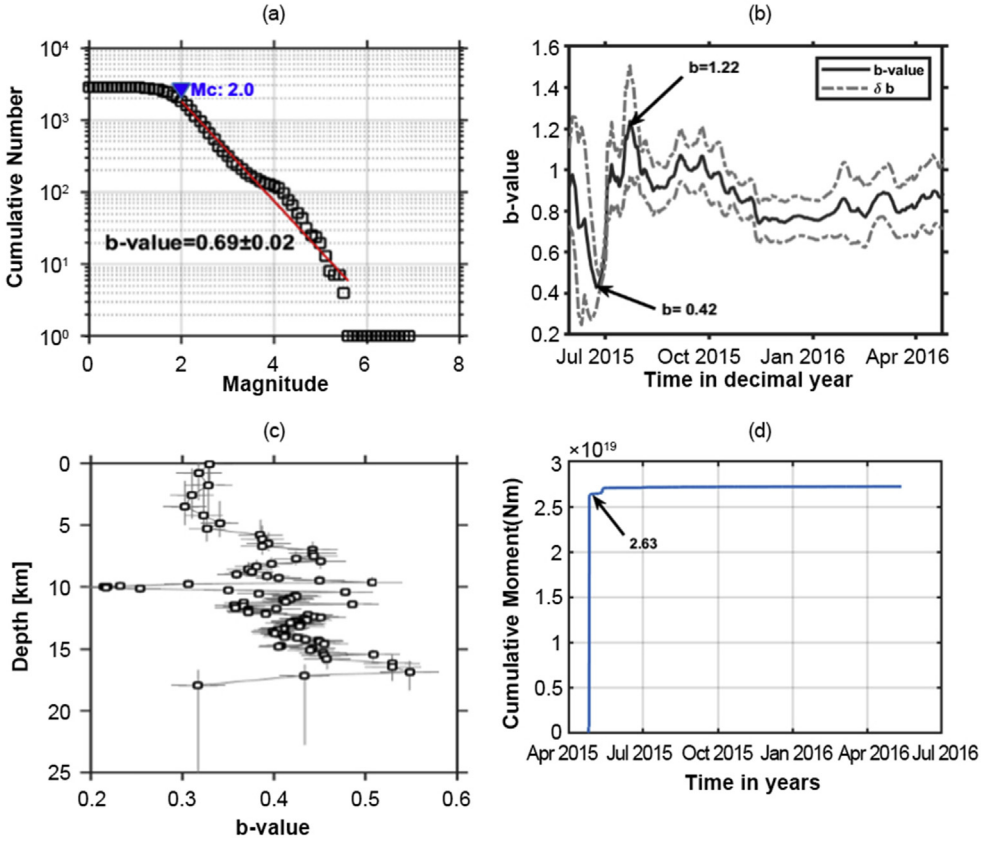

Fig. 6. Graphs representing *b*-value variation for the area along the Motihari-GauriShanker fault. (a), (b), (c) and (d) depict frequency magnitude distribution (FMD), *b*-value variation with time, *b*-value variation with depth, and temporal variation of cumulative seismic moment release.

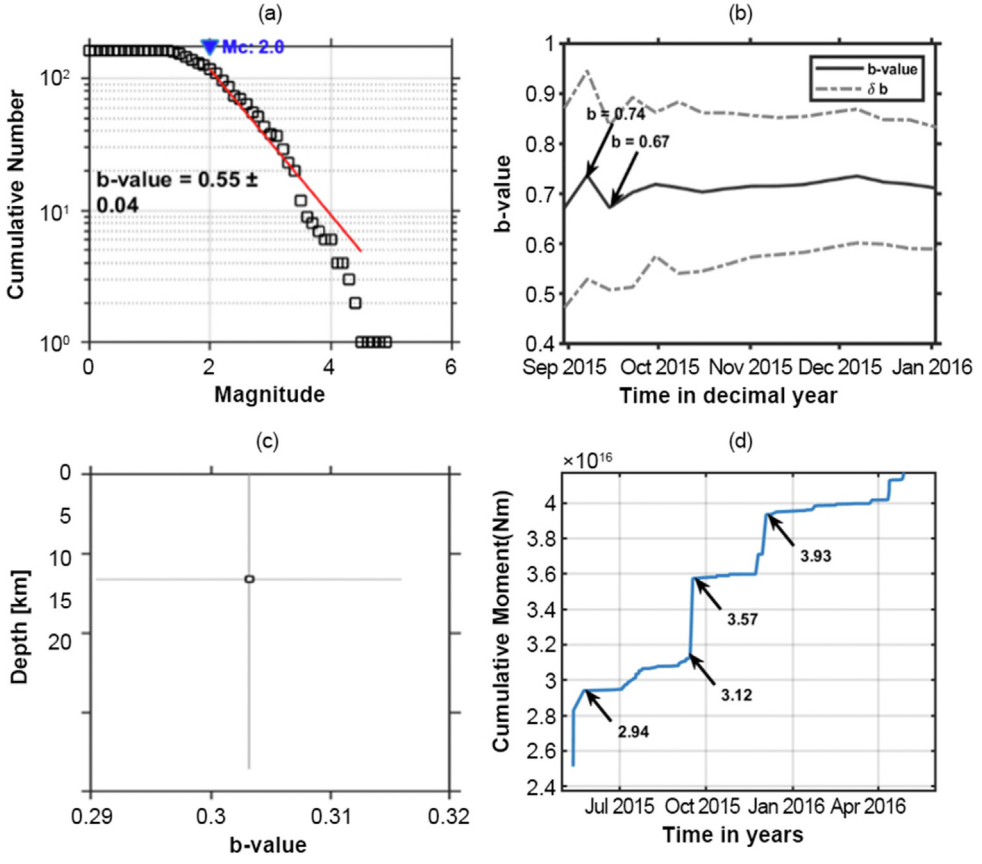

Fig. 7. Graphs representing *b*-value variation for the area along the Motihari-Everest fault. (a), (b), (c) and (d) depict frequency magnitude distribution (FMD), *b*-value variation with time, *b*-value variation with depth, and temporal variation of cumulative seismic moment release.

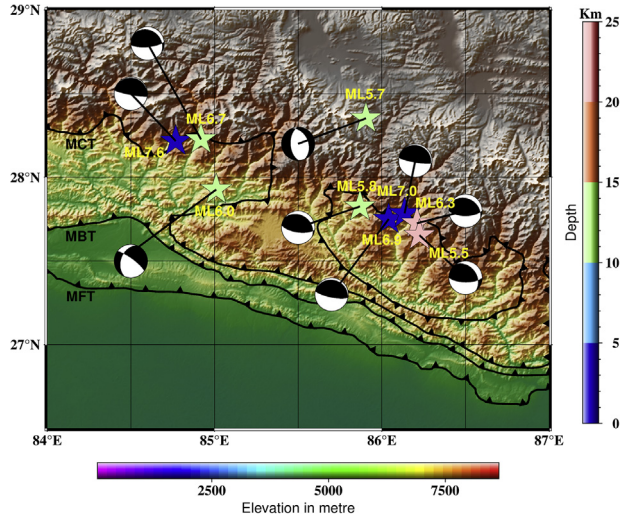

Fig. 8. Focal mechanism of mainshock and major aftershocks where color of the stars indicate the depth of the earthquakes.

2015, M_L7.0 event originated on the eastern end of the mainshock, having the characteristic of the shallow northeast dipping thrust fault. The M_L6.3 aftershock of the same day and M_L5.5 aftershock of 16 May show similar thrust mechanisms with small oblique components.

6. Discussion

The *b*-values reported for the faults (0.45–0.69) from the frequency magnitude plot are remarkably low compared to the global average value of 1.0 as accepted for the aftershock sequences. These low *b*-values are also associated with the thrust faulting [52] and may correspond with a strong and homogeneous stress field or asperities [34,37]. The low *b*-values for the Judi fault (0.45 ± 0.02) and Motihari-Everest fault (0.55 ± 0.4) suggest that the stress level in this area is relatively high that may have a high potentiality of causing a possible moderate or larger event [53]. The strain energy released in the area along the Judi fault is 10^{20} Nm, which is the largest value, while the energy released along the Motihari-Everest fault is 10^{16} Nm, which is the lowest value. The quick-release of strain energy for the Judi fault, Thaple fault, Katmandu fault, and Motihari-GauriShanker fault show how events occur in those areas. The results of this work can be compared with the preceding works. The study carried out by researchers [54] reported the *b*-value (0.75 ± 0.03) for the aftershock sequences of the 25 April earthquakes. In the other study [55] *b*-value was estimated as 0.93 for the aftershock sequences of the Gorkha earthquake. In the study [56], the *b*-value (0.78 ± 0.08) was computed for aftershock sequences after the Kodari earthquake (major aftershock). The estimated *b*-values in this work are low compared with earlier works for the region. This may be because of the abundant number of small magnitude earthquakes in the dataset.

7. Conclusion

In this paper, the spatial and temporal distribution of *b*-value for areas along the aforementioned five faults was studied to understand how the *b*-value distribution occurs after a major earthquake. From frequency magnitude distribution, variation of the *b*-value along the selected areas was reported from 0.45 to 0.69, which is accepted for the aftershock sequences. These low *b*-values regions have a low degree of heterogeneity of the materials, and they experience high stress and are associated with large faults. The results may reflect that the underlying crust bears the fracture of the firmly locked segment and the accumulated stress in the region is released through many small earthquakes. These significantly low *b*-values are also related to thrust faulting in the region as supported by the focal mechanism of the mainshock and the aftershocks. The Gorkha earthquake occurred on a low-angle fault plane and the thrust fault movements with more or less similar geodynamics may be the cause of its origin. The results from the temporal variation of the cumulative moment showed that the higher strain energy was released quickly in the area along the Judi fault and lower strain energy was released in a stepwise pattern in the area along the Motihari-Everest fault. The temporal variation of the *b*-value shows a specific rise in the *b*-value after the Gorkha earthquake. This study, which was based on the progression of the *b*-value and focal mechanism, might be helpful in understanding the rupture extent and stress changes after the Gorkha earthquake in the central Himalayan region.

Conflicts of interest

The authors declare that there is no conflicts of interest.

Acknowledgments

One of the authors RKT would like to acknowledge Tribhuvan University, Nepal for providing sabbatical leave and University Grants Commission (UGC), Nepal for providing financial support in the form of fellowship. We would also like to acknowledge three anonymous reviewers for their suggestions for the improvement of the quality of the manuscript.

References

[1] R. Bilham, Himalayan earthquakes: a review of historical seismicity and early 21st century slip potential, Geol. Soc. Spec. Publ. 483 (2019) 423–482, https://doi.org/10.1144/SP483.16.
[2] M.R. Pandey, R.P. Tandukar, J.P. Avouac, J. Lavé, J.P. Massot, Interseismic strain accumulation on the Himalayan crustal ramp (Nepal), Geophys. Res. Lett. 22 (1995) 751–754, https://doi.org/10.1029/94GL02971.
[3] L.B. Adhikari, U.P. Gautam, B.P. Koirala, M. Bhattarai, T. Kandel, R.M. Gupta, C. Timsina, N. Maharjan, K. Maharjan, T. Dahal, R. Hoste-Colomer, Y. Cano, M. Dandine, A. Guilhem, S. Merrer, P. Roudil, L. Bollinger, The aftershock sequence of the 2015 april 25 Gorkha-Nepal earthquake, Geophys. J. Int. 203 (2015) 2119–2124, https://doi.org/10.1093/gji/ggv412.
[4] L. Bollinger, P. Tapponnier, S.N. Sapkota, Y. Klinger, Slip deficit in central Nepal: omen for a repeat of the 1344 AD earthquake? The 2015 gorkha, Nepal, earthquake and Himalayan studies 4, Seismology, Earth, Planets Sp. 68 (2016) 1–12, https://doi.org/10.1186/s40623-016-0389-1.
[5] D. Hazarika, M. Wadhawan, A. Paul, N. Kumar, K. Borah, Geometry of the main Himalayan thrust and Moho beneath Satluj valley, northwest Himalaya: constraints from receiver function analysis, J. Geophys. Res. Solid Earth Res. 122 (2017) 2929–2945, https://doi.org/10.1002/2016JB013783.
[6] J.P. Avouac, L. Meng, S. Wei, T. Wang, J.P. Ampuero, Lower edge of locked main Himalayan thrust unzipped by the 2015 gorkha earthquake, Nat. Geosci. 8 (2015) 708–711, https://doi.org/10.1038/ngeo2518.
[7] J.R. Elliott, R. Jolivet, P.J. Gonzalez, J.P. Avouac, J. Hollingsworth, M.P. Searle, V.L. Stevens, Himalayan megathrust geometry and relation to topography revealed by the Gorkha earthquake, Nat. Geosci. 9 (2016) 174–180, https://doi.org/10.1038/ngeo2623.
[8] K. Wang, Y. Fialko, Slip model of the 2015 Mw 7.8 Gorkha (Nepal) earthquake from inversions of ALOS-2 and GPS data, Geophys. Res. Lett. 42 (2015) 7452–7458, https://doi.org/10.1002/2015GL065201.
[9] D. Gautam, Hugo Rodrigues, K. Kumar Bhetwal, P. Neupane, Y. Sanada, Common structural and construction deficiencies of Nepalese buildings, Innov. Infrastruct. Solut. 1 (2016), https://doi.org/10.1007/s41062-016-0001-3.

[10] E.O. Lindsey, R. Natsuaki, X. Xu, M. Shimada, M. Hashimoto, D. Melgar, D.T. Sandwell, Line-of-sight displacement from ALOS-2 interferometry: Mw 7.8 gorkha earthquake and Mw 7.3 aftershock, Geophys. Res. Lett. 42 (2015) 6655–6661, https://doi.org/10.1002/2015GL065385.
[11] C. Baillard, H. Lyon-Caen, L. Bollinger, A. Rietbrock, J. Letort, L.B. Adhikari, Automatic analysis of the Gorkha earthquake aftershock sequence: evidences of structurally segmented seismicity, Geophys. J. Int. 209 (2017) 1111–1125, https://doi.org/10.1093/gji/ggx081.
[12] M.M. Mendoza, A. Ghosh, M.S. Karplus, S.L. Klemperer, S.N. Sapkota, L.B. Adhikari, A. Velasco, Duplex in the main Himalayan thrust illuminated by aftershocks of the 2015 M w 7.8 gorkha earthquake, Nat. Geosci. 12 (2019) 1018–1022, https://doi.org/10.1038/s41561-019-0474-8.
[13] L. Bai, S.L. Klemperer, J. Mori, M.S. Karplus, L. Ding, H. Liu, G. Li, B. Song, S. Dhakal, Lateral variation of the Main Himalayan Thrust controls the rupture length of the 2015 Gorkha earthquake in Nepal, Sci. Adv. 5 (2019) 1–8, https://doi.org/10.1126/sciadv.aav0723.
[14] W. An, X. Hu, E. Garzanti, J.G. Wang, Q. Liu, New precise dating of the India-Asia collision in the Tibetan Himalaya at 61 Ma, Geophys. Res. Lett. 48 (2021) 1–10, https://doi.org/10.1029/2020GL090641.
[15] R. Bilham, D. Mencin, R. Bendick, R. Bürgmann, Implications for elastic energy storage in the Himalaya from the Gorkha 2015 earthquake and other incomplete ruptures of the Main Himalayan Thrust, Quat. Int. 462 (2017) 3–21, https://doi.org/10.1016/j.quaint.2016.09.055.
[16] F. Herman, P. Copeland, J.P. Avouac, L. Bollinger, G. Maheo, P. Le Fort, S. Rai, D. Foster, A. Pecher, K. Stuwe, P. Henry, Exhumation, crustal deformation, and thermal structure of the Nepal Himalaya derived from the inversion of thermochronological and thermobarometric data and modeling of the topography, J. Geophys. Res. Solid Earth 115 (2010) 1–38, https://doi.org/10.1029/2008JB006126.
[17] B.R. Arora, B.K. Bansal, S.K. Prajapati, A.K. Sutar, S. Nayak, Seismotectonics and seismogenesis of Mw7.8 Gorkha earthquake and its aftershocks, J. Asian Earth Sci. 133 (2017) 2–11, https://doi.org/10.1016/j.jseaes.2016.07.018.
[18] H. Yue, M. Simons, Z. Duputel, J. Jiang, E. Fielding, C. Liang, S. Owen, A. Moore, B. Riel, J.P. Ampuero, S.V. Samsonov, Depth varying rupture properties during the 2015 Mw 7.8 Gorkha (Nepal) earthquake, Tectonophysics 714–715 (2017) 44–54, https://doi.org/10.1016/j.tecto.2016.07.005.
[19] K.M. Sreejith, P.S. Sunil, R. Agrawal, A.P. Saji, A.S. Rajawat, D.S. Ramesh, Audit of stored strain energy and extent of future earthquake rupture in central Himalaya, Sci. Rep. 8 (2018), https://doi.org/10.1038/s41598-018-35025-y.
[20] J.L. Mugnier, F. Jouanne, R. Bhattarai, J. Cortes-Aranda, A. Gajurel, P. Leturmy, X. Robert, B. Upreti, R. Vassallo, Segmentation of the Himalayan megathrust around the gorkha earthquake (25 april 2015) in Nepal, J. Asian Earth Sci. 141 (2017) 236–252, https://doi.org/10.1016/j.jseaes.2017.01.015.
[21] R. Prakash, R.K. Singh, H.N. Srivastava, Nepal earthquake 25 April 2015: source parameters, precursory pattern and hazard assessment, Geomatics, Nat. Hazards Risk 7 (2016) 1769–1784, https://doi.org/10.1080/19475705.2016.1155504.
[22] S. Dasgupta, M. Mukhopadhyay, D.R. Nandy, Active transverse features in the central portion of the Himalaya, Tectonophysics 136 (1987) 255–264, https://doi.org/10.1016/0040-1951(87)90028-X.
[23] D. Shanker, H. Paudyal, H.N. Singh, Discourse on seismotectonics of Nepal Himalaya and vicinity:appraisal to earthquake hazard, J. Geo-Sciences. 1 (2012) 1–15, https://doi.org/10.5923/j.geo.20110101.01.
[24] W.D. Smith, The *b*-value as an earthquake precursor, Nature 289 (1981) 136–139, https://doi.org/10.1038/289136a0.
[25] P. Nuannin, O. Kulhánek, L. Persson, Variations of b-values preceding large earthquakes in the Andaman-Sumatra subduction zone, J. Asian Earth Sci. 61 (2012) 237–242, https://doi.org/10.1016/j.jseaes.2012.10.013.
[26] H. Hussain, Z. Shuangxi, M. Usman, M. Abid, Spatial variation of b-values and their relationship with the fault blocks in the western part of the Tibetan plateau and its surrounding areas, Entropy 22 (2020), https://doi.org/10.3390/e22091016.
[27] B. Gutenberg, C.F. Richter, Frequency of earthquakes in California, Bull. Seismol. Soc. Am. 34 (1944) 185–188.
[28] Z.H. El-Isa, D.W. Eaton, Spatiotemporal variations in the *b*-value of earthquake magnitude-frequency distributions: classification and causes, Tectonophysics 615–616 (2014) 1–11, https://doi.org/10.1016/j.tecto.2013.12.001.
[29] E. Görgün, Analysis of the *b*-values before and after the 23 October 2011 Mw 7.2 Van–Erciş, Turkey earthquake, Tectonophysics 603 (2013) 213–221, https://doi.org/10.1016/J.TECTO.2013.05.030.
[30] D. Kalafat, E. Görgün, Source characteristics and *b*-values of the Tuz Gölü fault zone in central Anatolia, Turkey, J. Asian Earth Sci. 179 (2019) 337–349, https://doi.org/10.1016/J.JSEAES.2019.05.005.
[31] E. Görgün, A. Zang, M. Bohnhoff, C. Milkereit, G. Dresen, Analysis of Izmit aftershocks 25 days before the November 12th 1999 Düzce earthquake, Turkey, Tectonophysics 474 (2009) 507–515, https://doi.org/10.1016/j.tecto.2009.04.027.
[32] K. Mogi, Earthquakes and fractures, Tectonophysics 5 (1967) 35–55, https://doi.org/10.1016/0040-1951(67)90043-1.
[33] L. Gulia, S. Wiemer, The influence of tectonic regimes on the earthquake size distribution: a case study for Italy, Geophys. Res. Lett. 37 (2010) 1–6, https://doi.org/10.1029/2010GL043066.
[34] D. Schorlemmer, S. Wiemer, M. Wyss, Variations in earthquake-size distribution across different stress regimes, Nature 437 (2005) 539–542, https://doi.org/10.1038/nature04094.
[35] C.H. Scholz, The frequency-magnitude relation of microfracturing in rock and its relation to earthquakes, Bull. Seismol. Soc. Am. 58 (1968) 399–415, https://doi.org/10.1785/bssa0580010399.
[36] C.H. Scholz, On the stress dependence of the earthquake b value, Geophys. Res. Lett. 42 (2015) 1399–1402, https://doi.org/10.1002/2014GL062863.
[37] M. Wyss, C.G. Sammis, R.M. Nadeau, S. Wiemer, Fractal dimension and *b*-value on creeping and locked patches of the San Andreas fault near Parkfield, California, Bull. Seismol. Soc. Am. 94 (2004) 410–421, https://doi.org/10.1785/0120030054.
[38] P. Senatorski, Gutenberg–Richter's b value and earthquake asperity models, Pure Appl. Geophys. 177 (2020) 1891–1905, https://doi.org/10.1007/s00024-019-02385-z.
[39] M. Spada, T. Tormann, S. Wiemer, B. Enescu, Generic dependence of the frequency-size distribution of earthquakes on depth and its relation to the strength profile of the crust, Geophys. Res. Lett. 40 (2013) 709–714, https://doi.org/10.1029/2012GL054198.
[40] Y. Ogata, H. Tsuruoka, Statistical monitoring of aftershock sequences: a case study of the 2015 Mw7.8 gorkha, Nepal, earthquake the 2015 gorkha, Nepal, earthquake and Himalayan studies: first results 4. Seismology, Earth Planets Space 68 (2016), https://doi.org/10.1186/s40623-016-0410-8.
[41] P. Ramesh, T.R. Martha, K.V. Kumar, Regional variation of stress level in the Himalayas after the 25 April 2015 Gorkha earthquake (Nepal) estimated using *b*-values, J. Geophys. Eng. 15 (2018) 921–927, https://doi.org/10.1088/1742-2140/aaa26c.
[42] M. Yamada, T. Kandel, K. Tamaribuchi, A. Ghosh, 3D fault structure inferred from a refined aftershock catalog for the 2015 gorkha earthquake in Nepal, Bull. Seismol. Soc. Am. 110 (2020) 26–37, https://doi.org/10.1785/0120190075.
[43] S. Wiemer, M. Wyss, Minimum magnitude of completeness in earthquake catalogs: examples from Alaska, the Western United States, and Japan, Bull. Seismol. Soc. Am. 90 (2000) 859–869, https://doi.org/10.1785/0119990114.
[44] S. Wiemer, A software package to analyze seismicity: ZMAP, Seismol Res. Lett. 72 (2001) 373–382, https://doi.org/10.1785/gssrl.72.3.373.
[45] T. Utsu, Instructions for use aftershocks and earthquake statistics (I), J. Fac. Sci. Hokkaido Univ. 3 (1969) 129–195.
[46] K. Aki, Maximum likelihood estimate of b in the formula Log N= a − bM _ and its confidence limits, Bull Earthq. Res. Inst. Tokyo Univ. 43 (1965) 237–239.
[47] Y. Shi, A.B. Bolt, The standard error of the magnitude-frequency b value, Bull. Seismol. Soc. Am. 72 (1982) 1677–1687.
[48] A.M. Dziewonski, T.A. Chou, J.H. Woodhouse, Determination of earthquake source parameters from waveform data for studies of global and regional seismicity, J. Geophys. Res. 86 (1981) 2825–2852, https://doi.org/10.1029/JB086IB04P02825.
[49] G. Ekström, M. Nettles, A.M. Dziewoński, The global CMT project 2004-2010: centroid-moment tensors for 13,017 earthquakes, Phys. Earth Planet. In. 200–201 (2012) 1–9, https://doi.org/10.1016/J.PEPI.2012.04.002.
[50] Y. Yagi, R. Okuwaki, Integrated seismic source model of the 2015 Gorkha, Nepal, earthquake, Geophys. Res. Lett. 42 (2015) 6229–6235, https://doi.org/10.1002/2015GL064995.
[51] L. Zhang, J. Li, W. Liao, Q. Wang, Source rupture process of the 2015 Gorkha, Nepal Mw7.9 earthquake and its tectonic implications, Geod. Geodyn. 7 (2016) 124–131, https://doi.org/10.1016/J.GEOG.2016.03.001.
[52] M. Kawamura, K.H. Chen, Influences on the location of repeating earthquakes determined from a and b value imaging, Geophys. Res. Lett. 44 (2017) 6675–6682, https://doi.org/10.1002/2017GL073335.
[53] T. Tormann, S. Wiemer, S. Metzger, A. Michael, J.L. Hardebeck, Size distribution of parkfield's microearthquakes reflects changes in surface creep rate, Geophys. J. Int. 193 (2013) 1474–1478, https://doi.org/10.1093/gji/ggt093.
[54] P. Chingtham, B. Sharma, S. Chopra, P. SinghaRoy, Statistical analysis of aftershock sequences related with two major Nepal earthquakes: april 25, 2015, MW 7.8, and May 12, 2015, MW 7.2, Ann. Geophys. 59 (2016), https://doi.org/10.4401/ag-7025.
[55] D.R. Thapa, X. Tao, F. Fan, Z. Tao, Aftershock analysis of the 2015 Gorkha-Dolakha (Central Nepal) earthquake doublet, Heliyon 4 (2018) 678, https://doi.org/10.1016/J.HELIYON.2018.E00678.
[56] R.K. Tiwari, H. Paudyal, Variability of b-value before and after the Gorkha earthquake in the central Himalaya and vicinity, 18, 2021, pp. 32–42, https://doi.org/10.3126/bibechana.v18i2.31207.

Mr. Ram Krishna Tiwari received the M.Sc. degree in Physics from Tribhuvan University in 2004. Currently, he is pursuing the Ph.D. degree in Geophysics at Central Department of physics, Tribhuvan University, Nepal. His research interests include fractal approach to the study of the seismicity of Himalayan region and the seismic hazard.

Harihar Paudyal received the M.Sc. degree in Physics from Tribhuvan University in 1994 and the Ph.D. degree in Geophysics (Seismicity and Seismotectonics of Nepal and adjoining regions) from Banaras Hindu University, India in 2008. He is a faculty of Physics in Tribhuvan University from 1994 and is a professor of Physics from 2013. His research interests include seismotectonics, seismic hazard and seismicity of Himalayan region.

Prof. Daya Shanker received M.Sc. Tech. in Geophysics from Banarus Hindu University, Varanasi, India in 1986 and Ph.D. degree in Geophysics (Seismology) from Banaras Hindu University, India in 1991. He joined faculty of Engineering Seismology, Department of Earthquake Engineering, Indian Institute of Technology Roorkee, Roorkee from 1999 as assistant Professor of Engineering Seismology and is an associate professor from 2018. His research interests include seismicity and seismtectonics of the Northeast India, seismic hazard and seismicity of Himalayan region.

Earthquake Science 35 (2022) 193–204

Contents lists available at ScienceDirect

Earthquake Science

Journal homepage: https://www.keaipublishing.com/en/journals/earthquake-science/

Article

Gorkha earthquake (M_W7.8) and aftershock sequence: A fractal approach

Ram Krishna Tiwari[1,2,✉] and Harihar Paudyal[2]

[1] *Central Department of Physics*, *Tribhuvan University*, *Kirtipur*, *Kathmandu* 44618, *Nepal*
[2] *Birendra Multiple Campus*, *Tribhuvan University*, *Bharatpur*, *Chitwan* 44200, *Nepal*

Key points:

- The aftershock sequence of the 2015 Gorkha earthquake was analyzed to estimate the seismicity parameter *b*-value, *D*-value, and *p*-value.
- The very low *b*-value (0.57 ± 0.04), the highest *D*-value (1.65 ± 0.02), and rate of aftershock decay (p = 0.86 ± 0.04) were observed for the Gorkha earthquake sequence.
- The level of stress and seismicity patterns of the region between 26.5°N–29°N latitude and 84°E–87°E longitude in the central Himalayan region are explained.

A B S T R A C T

On April 25, 2015, Nepal was struck by the M_W7.8 Gorkha earthquake followed by an intense aftershock sequence. It was one of the most destructive earthquakes in the Himalayan arc, causing more than 8900 fatalities. In this study, we analyzed the dataset (429 events, magnitude of completeness (M_c) ≥ 4.2 local magnitude) of the first 45 days after the Gorkha earthquake to estimate the seismicity parameters *b*-value, *D*-value, and *p*-value. We used the maximum likelihood method to estimate the *b*-value and Omori-Utsu parameters, whereas the correlation integral method was applied to estimate the fractal dimension (*D*-value). The analysis was carried out using running and sliding window techniques. The lowest *b*-value (0.57 ± 0.04) and the highest *D*-value (1.65 ± 0.02) were computed at the time of the Gorkha earthquake, after which the *b*-value significantly increased to a maximum of 1.57. It again dropped to 0.93 at the time of the major aftershock on May 12, 2015. The *D*-value showed an initial quick drop and then decreased in a wavy pattern until the end of the study period, indicating the clustering and scattering of earthquakes in a fault region. The *b*-value contour map identified the eastern part of the study area as a high stress region (b = ~0.8), implying that the stress shifted to that region. The *D*-value contour map reveals that the seismogenic structure shifted from linear to planar in the region. The rate of aftershock decay (p = 0.86 ± 0.04) for a short period reflects that the level of stress decreased rapidly. This study helps to understand the level of stress and seismicity pattern of a region, which could be useful for aftershock studies.

✉ **Corresponding author.** Tiwari RK, email: ram.tiwari@bimc.tu.edu.np

Article history:
Received 15 December 2021
Received in revised form 27 April 2022
Accepted 29 April 2022
Available online 31 May 2022

https://doi.org/10.1016/j.eqs.2022.06.001

Keywords: Omori-Utsu law; correlation integral; fractal dimension; *b*-value; central Himalaya.

Citation: Tiwari RK and Paudyal H (2022). Gorkha earthquake (M_W7.8) and aftershock sequence: A fractal approach. Earthq Sci **35**(3): 193–204, doi: 10.1016/j.eqs.2022.06.001

1. Introduction

Earthquakes are a manifestation of complex non-linear threshold dynamics in the brittle part of Earth's crust. Multiple feedback cycles, such as crustal deformation, crustal shortening, and post-seismic creep, occurring over millions of years beneath the Himalaya have evolved into a non-linear dynamic system that may cause earthquakes (Shcherbakov et al., 2005, 2015; Dal Zilio et al., 2021). Therefore, the Himalayan orogeny, delineated by major continental thrusts, is a natural laboratory for the study of earthquake systematics. Despite their complexities, earthquakes can be considered as a point process in space and time that occurs within seismically dynamic fault sectors (Ogata, 1999; Ogata and Tsuruoka, 2016). Moreover, these sectors are complex systems with heterogeneously distributed stress and strength (Huang J and Turcotte, 1988). The continuous process of slow energy accumulation and fast energy redistribution inside the crust drives it towards the self-organized critical point, i.e., the mainshock (Mandal and Rastogi, 2005; Teotia and Kumar, 2011; Pastén et al., 2015; Aggarwal et al., 2017).

The spatiotemporal distribution of earthquake epicenters is fractal (Turcotte, 1989; Dimri, 2005; Nampally et al., 2018). Fractal scaling relation is used to characterize the mathematical expression of the natural pattern of an earthquake; therefore, it can be used to study the seismicity of a region. Numerous studies have been conducted in the factors that trigger earthquakes. This study focuses on three of the most used techniques, i.e., determining the *b*-value of the Gutenberg-Richter relation, fractal dimension or *D*-value, and *p*-value of the Omori-Utsu relation (Bachmann et al., 2012; Jena et al., 2021), to study earthquake distribution in the Himalayan region. These scaling exponents obey fractal statistics, and their behavior can be considered as the end-product of a self-organized critical state of the Earth's crust at the time of the mainshock. This study estimates the stress level, frequency, and patterns of earthquakes of the region between 26.5°N–29°N latitude and 84°E–87°E longitude in the central Himalaya.

1.1. *b*-value estimation

The *b*-value in the Gutenberg-Richter frequency-magnitude relation (Gutenberg and Richter, 1944; Huang J and Turcotte, 1988; Dimri, 2005) is the power law indicating a self-similar fractal property of earthquakes. This relation can be expressed as

$$\log N = a - bm, \tag{1}$$

where N is an integer describing the number of earthquakes per unit time, with magnitudes greater than or equal to m for a given time and space. The constant "a" denotes the seismicity and the constant "b" denotes the level of stress in the region. The *b*-value is the ratio of the number of weak and strong events, and is estimated to be 0.8–1.2 (Enescu and Ito, 2002; Enescu et al., 2011). An increased *b*-value denotes a rise in the number of weak events compared to strong events, and vice versa (Caneva and Smirnov, 2004). Several studies have shown orderly variations in *b*-values throughout major earthquake sequences, with changes in the ambient stress level and fractal dimension of the stress-strength distribution (Jiang HK and Diao SZ, 1995; Yeken, 2016; Nava et al., 2017; Hussain et al., 2020). It was observed that major earthquakes generally happen in areas with small *b*-values (El-Isa and Eaton, 2014; Wang R et al., 2021), which varies with time showing a decreasing trend before major earthquakes (Smith, 1981; Rehman et al., 2015; Chiba, 2019; Jena et al., 2021).

1.2. Fractal dimension

It is believed that a straight line, plane, and volume have dimensions of 1, 2, and 3, respectively. However, if we consider a rough surface covering a part of a plane, its dimensions would lie between 1 and 2, and a rougher surface corresponds to dimensions close to two. Fractals are rough objects with no specific scale, and cannot be described using traditional measurement procedures, i.e., length or area. The concept of fractal dimension was proposed during a problem encountered while measuring the length of a coastline (Mandelbrot, 1967; Mandelbrot and Wheeler, 1983). Fractal methods describe the properties of an object by estimating its fractal dimension (Chen YG and Wang JJ, 2013). A smaller value of the fractal dimension represents smooth coastlines, while a larger value represents rugged coastlines (Smalley et al., 1987). In fractal distribution, the number of objects N with a characteristic size greater than r can be expressed as

$$N(r) = C\frac{1}{r^D}, \tag{2}$$

where D is the fractal dimension and C is a proportionality constant. Fractal statistics are associated with several natural processes (Mandelbrot, 1967; Mandelbrot and

Wheeler, 1983; Goltz, 1997; Malischewsky, 2014). For earthquake distribution, the D-value characterizes the degree of homogeneity of spatial events, and its decrease suggests the grouping of earthquake events (Caneva and Smirnov, 2004). Several authors have observed a decrease in the value of the fractal dimension before a large earthquake (Wyss et al., 2004; Fayou et al., 2010; Ghosal et al., 2012; Hamdache et al., 2019; Yin LR et al., 2019). Fractal dimensions increase with an increase in the differential stress and decrease with the evolution of the fracture process (Lei XL and Kusunose, 1999; Chingtham et al., 2016; Firoozfar and Ansari, 2019; Lei XL, 2019). The spatial correlation dimension, a lower level of fractal dimension, is a measure of scaling in the spatial distribution of events, and is calculated by defining the correlation integral function $c(r)$ for the epicenter distribution (Roy and Padhi, 2007; Roy and Mondal, 2009; Mondal et al., 2019) as follows:

$$c(r) = \frac{2}{N(N-1)} \sum_{\substack{i,j=1 \\ i \neq j}}^{N} H\left(r - \left|X_i - X_j\right|\right), \quad (3)$$

where N is the total number of earthquakes in the given window, $X_i - X_j$ is the angular distance between two events calculated by the spherical triangle method (Hirata, 1989), $H(\cdot)$ is the Heaviside step function, and r is the scaling radius. After calculating $c(r)$, the spatial correlation dimension can be defined from the power-law relation (Kagan, 1981, 2007; Kagan and Houston, 2005):

$$c(r) \sim r^D, \quad (4)$$

The slope of the linear part of the $\log r - \log c(r)$ plot provides the correlation fractal dimension (D), as explained in the data and methodology section.

1.3. Omori-Utsu law

Aftershocks are manifestations of relaxation phenomena observed in various physical systems, such as solar flares, acoustic emissions, and seismicity. In seismicity, aftershocks indicate that the total strain energy was not released by the mainshock of the earthquake. Occurrence of aftershocks in a brief period and in small areas provide information about the Earth's crust and helps understand the mechanism of earthquakes. Omori Law (Omori, 1894; Žalohar, 2018) states that the frequency of aftershocks decays with time in a hyperbola that involves the statistics of both mainshocks and aftershocks, indicating that they are created by the same mechanism. After being replaced by a power-law function (Utsu, 1969; Utsu et al., 1995; Guglielmi, 2016, 2017), it can be written as

$$n(t) = \frac{K}{(t+c)^p}, \quad (5)$$

where K, c, and p are constants that represent the number of observed earthquakes, rate of decay, and delay of the decay, respectively; t is the time since the mainshock and $n(t)$ is the aftershock frequency measured over a certain interval of time. This equation can be temporally integrated to estimate the expected number of aftershocks.

This decay law reflects the temporal self-similarity of earthquake source processes. p varies according to the heterogeneity, stress, and temperature of the crust (Mogi, 1967; Trivedi, 2015; Guglielmi, 2016). It widely differs among different locations and cases, indicating the rapid rate of decay of aftershocks, and has a value close to 1.0. For example, p-values denoting seismicity are usually in the range of 0.8 to 1.2 (Utsu et al., 1995), and a p-value of 0.5–1.5 was observed for the earthquake study in California (Reasenberg and Jones, 1989; Guglielmi, 2016). Generally, a reliable p-value is required to understand the mechanism of stress relaxation and the friction law in seismic zones (Hainzl et al., 1999; Helmstetter and Shaw, 2006). The parameter K represents productivity, while the constant c is necessary to avoid singularity in the number of aftershocks. However, the value of c and its significance remain debatable. It has been suggested that the value of c is essentially zero, and all reported positive values are owing to incomplete sequencing in the early stage of an aftershock (Utsu, 1971; Utsu et al., 1995).

The Himalaya is divided into four litho-tectonic units, from north to south: the Tethyan Himalaya, Higher Himalaya, Lesser Himalaya, and Sub-Himalaya (Figure 1). These units are separated by the South Tibet Detachment (STD), Main Central Thrust (MCT), Main Boundary Thrust (MBT), and Main Frontal Thrust (MFT), respectively (Bai L et al., 2016). The MCT is the oldest thrust in the Himalayan region, and was activated at ~22 Ma followed by reactivation ~15 Ma and 6 Ma (Yin A et al., 2010). The MFT and MBT also run along the strike of the Himalaya, and the MFT is the youngest of the three.

The slip along a major basal thrust, the Main Himalayan Thrust (MHT), which surfaces along the front of the Himalayan foothills, contributes majorly to the convergence rate between the Indian and Tibetan plates across the Himalaya (~17–21 mm/a) (Ader et al., 2012; Mugnier et al., 2013). The MFT, MBT, and MCT are believed to be attached to the MHT at the deeper level (Bilham, 2015, 2019; Elliott et al., 2016; Dal Zilio et al., 2021; Michel et al., 2021). MHT is one of the largest (~2,400 km long), and fastest slipping active continental megathrusts that separates the underthrusting Indian Plate from the overriding Himalayan orogeny. Most earthquakes have occurred in the frictionally sealed part of the MHT in the roots of Nepal Himalaya (Pandey et al., 1995; Mugnier et al., 2013; Bilham, 2019; Ghosh, 2020).

Located in a seismically active region, Nepal has hosted several large earthquakes in the past. The first documented earthquake occurred on June 7, 1255, and had a magnitude of 7.8. The next recorded major earthquake occurred in 1260, and had a magnitude of 7.1 in the Mt. Everest region (Chaulagain et al., 2018). The 1408 earthquake of magnitude 8.2 is another mega event that killed around 2500 people. The devastating earthquake of 1767 (M7.9) took 4000 lives. The M_S8.0 Kathmandu-Bihar earthquake of August 26, 1833 struck Nepal and the northern part of India and was equally devastating, taking 6500 lives (Martin et al., 2015; Bilham, 2019). On January 15, 1934, the greatest earthquake (M_W8.0) of modern times, known as the Nepal-Bihar earthquake, occurred in the eastern mountains of Nepal. The Udayapur earthquake (M_W6.9) in 1988, 240 km southeast of the Gorkha event, led to ~1500 fatalities (Chen H et al., 2017).

On April 25, 2015, a major earthquake (M_W7.8) occurred in the Himalayan region of central Nepal (Adhikari et al., 2015; Baillard et al., 2017). The event was followed by thousands of aftershocks, with some of them even having magnitude $M_W > 6$, and it triggered the M_W7.3 event (Kodari earthquake) to the east 17 days after the mainshock. Aftershocks were generated at the boundary of these ruptures, predominantly in the droopy part of the MHT (Letort et al., 2016; Miyake et al., 2017; Yamada et al., 2020). The Gorkha and Kodari events are the latest major earthquakes in the Himalaya, and the best-recorded events in the region (Figure 1). The amount of energy dissipated by these events to nearby faults is sufficient to activate earthquakes in adjacent areas (Avouac et al., 2015; Bilham et al., 2017). This study attempts to understand the behavior of the aftershocks to examine the future seismicity pattern.

2. Data and methodology

In this work, earthquake data for the first 45 days after the Gorkha earthquake (2015-4-25–2015-06-07) was analyzed. Earthquake data were collected from the local network of the National Seismic Center, Nepal (Adhikari

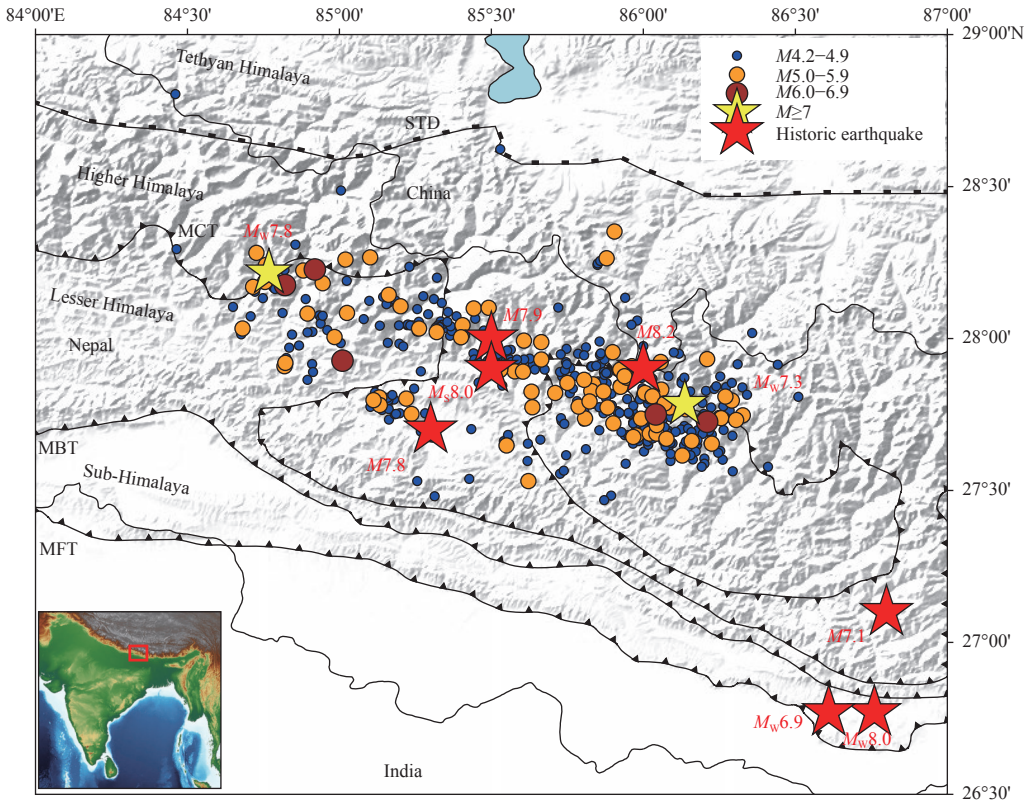

Figure 1. Epicenter location of the 429 earthquake events. Yellow stars stand for the M_W7.8 Gorkha earthquake and its largest aftershock, the Kodari earthquake (M_W7.3). MCT: Main Central Thrust, MBT: Main Boundary Thrust, and MFT: Main Frontal Thrust. Red stars represent historical earthquakes in the region. M7.8: 1255 Kathmandu earthquake, M7.1: 1260 Everest earthquake, M8.2: 1408 Nepal-Tibet earthquake, M7.9: 1767 northern-Bagmati region earthquake, M_S8.0: 1833 Kathmandu-Bihar earthquake, M_W8.0: 1934 Nepal-Bihar earthquake, and M_W6.9: 1988 Udayapur earthquake (Goda et al., 2015; Chaulagain et al., 2018). The red box in the inset map marks the study region.

et al., 2015). The total number of recorded earthquakes in the catalog was 554. Completeness of the data was estimated to be 4.2 using the maximum curvature technique in the software ZMAP (Wiemer, 2001). Therefore, the final dataset comprised 429 earthquakes with magnitude of completeness 4.2 (Figure 2). For the accuracy and precision of the estimated *b*-value and *D*-value, a time window of 100 events was considered, having an interval of 20 events (Table 1).

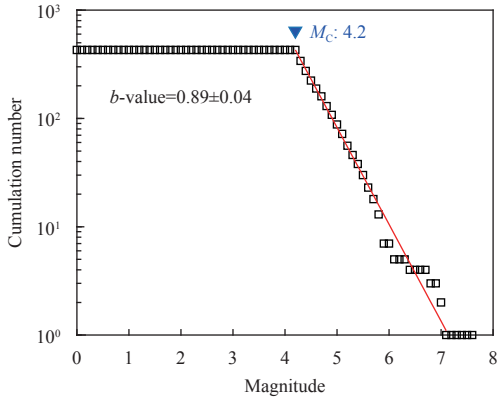

Figure 2. Frequency magnitude (*b*-value) and magnitude of completeness (M_c) of the earthquake's distribution.

The temporal distribution of magnitude and 3D distributions of the earthquakes are depicted in Figure 3.

The *b*-value of the frequency magnitude distribution was calculated using the maximum likelihood estimation method (Aki, 1965; Bender, 1983)

$$b = \frac{\log_{10} e}{M_a - \frac{\Delta M}{2}}, \tag{6}$$

where M_a is the average of all magnitudes, ΔM is the binning width of the catalogue, and the standard error in the *b*-value calculation is computed using the technique by Shi YL and Bolt (1982).

$$(\delta b)_s = 2.3 \times b^2 \sqrt{\frac{\sum_i^N (M_i - M_a)^2}{n_s(n_s - 1)}}, \tag{7}$$

where n_s is the number of earthquakes in the given sample.

The fractal dimension was calculated using the correlation integral method (Grassberger and Procaccia, 1983). The correlation dimension *D*, in terms of the correlation sum $c(r)$ is defined as

$$D = \lim_{r \to 0} \frac{\log c(r)}{\log r}. \tag{8}$$

To demonstrate the fractal nature of the aftershock

Table 1. Data for the time window, number of earthquakes, frequency size distribution (*b*-value), correlation fractal dimension (*D*), and coefficient of determination (R^2).

Window	Event range	Period	Number of events	*b*-value	*D*	R^2
W1	0–100	2015-4-25–2015-4-25	100	0.57±0.04	1.65±0.02	0.992
W2	20–120	2015-4-25–2015-4-25	100	0.76±0.06	1.57±0.01	0.997
W3	40–140	2015-4-25–2015-4-26	100	0.86±0.08	1.54±0.02	0.995
W4	60–160	2015-4-25–2015-4-26	100	0.96±0.10	1.47±0.02	0.996
W5	80–180	2015/4-25–2015-4-26	100	1.03±0.12	1.46±0.02	0.992
W6	100–200	2015-4-25–2015-4-27	100	1.12±0.14	1.51±0.02	0.996
W7	120–220	2015-4-25–2015-4-28	100	1.15±0.14	1.59±0.03	0.991
W8	140–240	2015-4-26–2015-4-30	100	1.20±0.01	1.57±0.02	0.993
W9	160–260	2015-4-26–2015-5-02	100	1.42±0.15	1.43±0.01	0.998
W10	180–280	2015-4-26–2015-5-08	100	1.52±0.14	1.38±0.01	0.999
W11	200–300	2015-4-27–2015-5-12	100	1.11±0.13	1.44±0.01	0.999
W12	220–320	2015-4-28–2015-5-12	100	0.91±0.09	1.43±0.03	0.986
W13	240–340	2015-4-30–2015-5-12	100	0.86±0.08	1.44±0.03	0.980
W14	260–360	2015-5-02–2015-5-13	100	0.78±0.06	1.50±0.05	0.963
W15	280–380	2015-5-08–2015-5-16	100	0.77±0.07	1.47±0.06	0.950
W16	300–400	2015-5-12–2015-5-24	100	0.97±0.08	1.35±0.06	0.942
W17	320–420	2015-5-12–2015-5-29	100	1.15±0.10	1.36±0.05	0.951
W18	340–429	2015-5-12–2015-6-07	89	1.23±0.13	1.34±0.05	0.959
Total data	0– 429	2015-4-25–2015-6-07	429	0.89±0.04	1.56±0.02	0.992

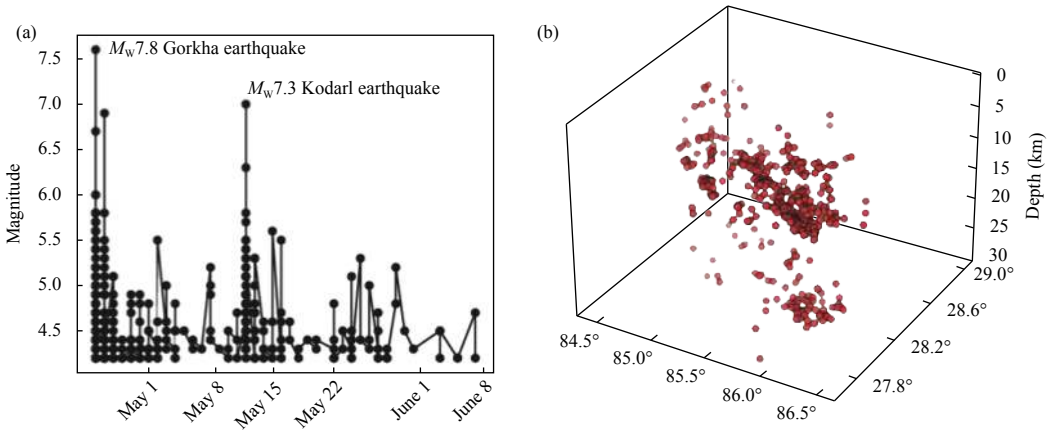

Figure 3. Graphs showing temporal distribution of earthquakes magnitude for the study period (a) geographical distribution of earthquakes along with their depth (b).

sequence, we depicted the log$r$ – log$c$ (r) plot for window 1 containing the Gorkha earthquake (2015-4-25–2015-4-25) and window 11 containing the Kodari earthquake (2015-4-27–2015-5-12) (Table 1 and Figure 4). Although, Nerenberg and Essex (1990) provided a formula for selecting the scaling region between depopulation and saturation, we used a conservative approach to identify the D-value for the range of $r \in [1, 38.90]$ km.

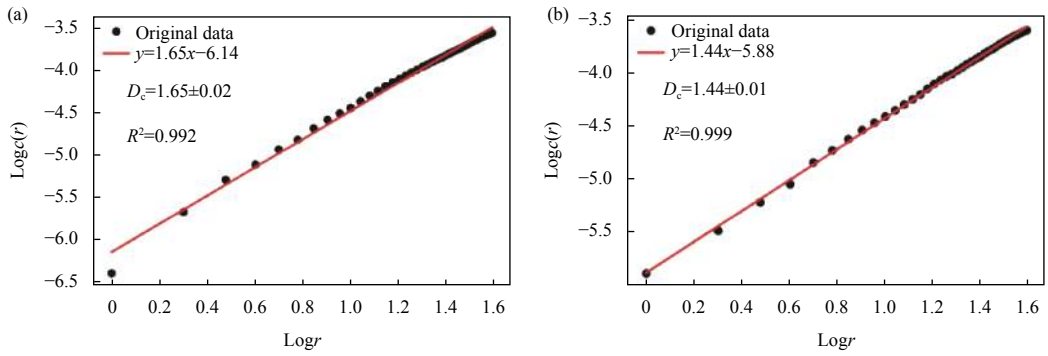

Figure 4. An example of D-value estimation from the correlation integral for the time windows including (a) the mainshock (2015-4-25–2015-4-25) and (b) the major aftershock (2015-4-27–2015-5-12).

The parameters of the Omori-Utsu law (p, c, and K values) were estimated using the maximum likelihood method (Omori, 1894; Utsu et al., 1995).

3. Results and discussion

A significant variation was observed in the b-values from analysis of the aftershock sequence, which increased rapidly after the main shock from 0.57 ± 0.04 to 1.52 ± 0.14 within 14 days, and then decreased to 0.77 ± 0.07 till the occurrence of the largest aftershock (Kodari earthquake); subsequently, it increased again to 1.23 ± 0.13 after the Kodari event (Table 1). The drop in the b-value before both earthquakes are consistent with the results of Chingtham et al. (2016), and indicates that the critically stressed fault could be the source of these earthquakes. The increase in b-value after the main event implies that most of the energy was released through the aftershocks, especially toward the east of the main event and might have also activated the nearby faults.

Decrease in the b-value before a large earthquake reflects the fluctuations in the order parameter upon approaching the critical point, i.e., occurrence of the mainshock (Zhuang JC et al., 2021), and are normally linked to asperities (Oncel and Wilson, 2002; Kawamura and Chen KH, 2017). Low b-value during the Gorkha earthquake indicates that the event could have been initiated by breaking of the asperity of the region. This study also showed that b-values are highly sensitive to variations in temporal stress. At the beginning of the event, the b-value was ~0.9, and increased rapidly to 1.55 around May 1, 2015 (Figure 5). By May 13, 2015, the b-value decreased rapidly to 0.93. b-values <1 indicate areas of crustal homogeneity and high stress, and vice versa

(Bridges and Gao SS, 2006). Therefore, the increasing *b*-value after the Gorkha and Kodari earthquakes indicates that although some stress is released in both events, the material heterogeneity increased in the region and could contribute to moderate to large earthquakes in the future.

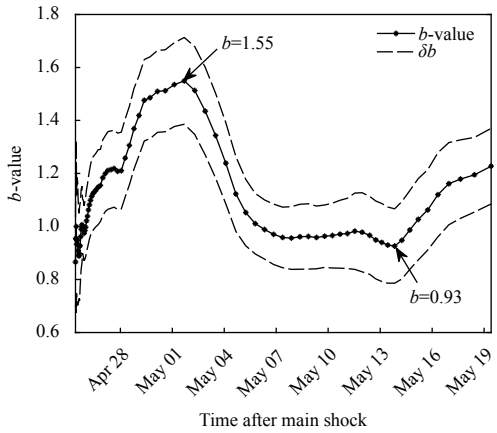

Figure 5. Temporal variation of the *b*-value for sample window of 100 events with a 4% window overlap. The *b*-value is maximum after the Gorkha earthquake and decreases by the time of the Kodari earthquake. It rises again after the Kodari earthquake.

Fractal dimension generally fluctuates following a large earthquake (Tang YS et al., 2020). The *D*-value range from 1.65±0.02 to 1.34±0.05 (Table 1) observed during period between the Gorkha and Kodari earthquakes may indicate such fluctuations. Decrease in the fractal dimension from 1.65 ± 0.02 to 1.46 ± 0.02 just after the Gorkha event indicates clustering of epicenters during a large event (Bayrak and Bayrak, 2012). The limiting value of the dimension can be interpreted as *D* close to 0, signifying that the earthquakes are concentrated in a limited area or are sparsely distributed. *D* close to 1 suggests a linear configuration of the epicenters, and *D* close to 2 indicates that the earthquakes are densely distributed over the entire area (Rodríguez Pascua et al., 2003; Borgohain et al., 2018; Mondal et al., 2019; Hussain et al., 2020; Tosi, 1998). Moreover, it is believed that *D* is regulated by pre-existing geological, mechanical, structural, and stress field heterogeneity (Öncel et al., 1996). Therefore, the range of fractal dimension (1.34–1.65) estimated in this study indicates a shift from linear to more planar structure of the seismogenic source, with densely distributed events. The spatial correlation dimensions exhibited one slope, indicating a single source. The *D*-value estimated in this study can be related to the previous work of Nampally et al. (2018), in which a fractal correlation dimension of 1.66 was estimated for 820 aftershocks of the Gorkha earthquake between April 25 and November 12, 2015.

Faulting is generally scale invariant, and the fractal dimension (*D*) of the source can be related to the *b*-value of the earthquake distribution (Huang J and Turcotte, 1988). The temporal variation of *b*-value represents differential stress conditions, and the fractal dimension acts as an indicator of material heterogeneity and strength (Srivastava et al., 2015). A sudden decrease in the *D*-value followed by an increase (Figure 6) immediately after the mainshock can be easily correlated with the clustering and scattering of earthquakes in a fault zone, and reflect the stress accumulation and strain release patterns in the region (Roy and Nath, 2007). Increased *b*-value (from <0.6 to >1.5) after the Gorkha earthquake may be associated with a decrease in the fractal dimension (from 1.65 to <1.40) of the associated heterogeneities and supports the theory that most of the large earthquakes are marked by relatively a high *D*-value and low *b*-value. The Gorkha event might have witnessed the introduction of small-scale heterogeneities (compared to the size of the fault zone) by stress accumulation after a major shock and led to the associated aftershock sequence. This result supports the findings of Bayrak and Öztürk (2004), where a comparatively low *b*-value and high *D*-value were correlated to a small degree of heterogeneity of the cracked surface, substantial stress, and large faults, with broadly distributed significantly stressed asperities.

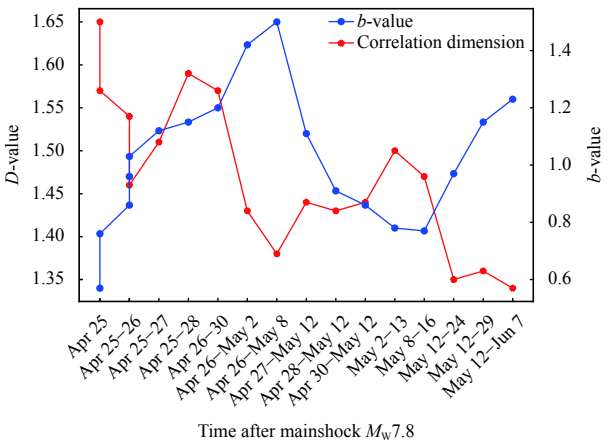

Figure 6. Temporal variation of the *D*-value and *b*-value. Time after the main shock is presented along the x axis.

Previous studies have shown both positive and negative correlation between the *b*-values and the fractal dimension of earthquakes (Ogata, 1999; Dimri, 2005; Teotia and Kumar, 2011). We estimated this correlation to be negative, with the regression function $D = -0.18b + 1.66$ and a coefficient of determination (R^2) = 0.243 (Figure 7). This indicates that the accumulated stress discharged along

the fault zone with a larger surface area, and the medium has not yet achieved a steady state of stress distribution. The negative correlation may have developed in response to an increase in stress (lower *b*) and a decline in epicenter clustering, i.e., an increased *D*-value (Oncel and Wilson, 2002). Similar type of correlation was also observed for the region in a previous study (Ghosh, 2020). Furthermore, a weak correlation was observed between the *D*-value and *b*-values for the earthquake epicenter distribution in western Taiwan region as well (Wang JH and Lee, 1996)

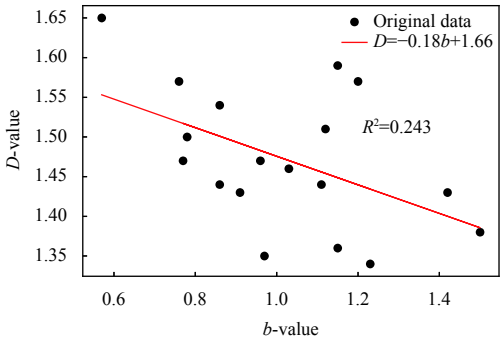

Figure 7. Relationship between fractal dimension (*D*) and *b*-value.

The *b*-value contour map (Figure 8a) depicts the spatial variation of earthquake frequency in the region. A comparatively low *b*-value contour (~0.7–0.9) was observed for the region of 84.5° E–85° E and 28° N–29° N (along the MCT) and the region of 86° E–87° E, 27° N–28.75° N. Comparatively high *b*-value contours (~1.2–1.3) were observed towards the southwest of the study area. The average *b*-value in the study area was 1.04. Areas with low *b*-value are said to be under high stress, i.e., slip movement is yet to occur, and vice versa (Enescu and Ito, 2002). Mapping of the *b*-value identified the high stress region towards the west of the Gorkha earthquake and east of the Kodari earthquake, which can be considered as the future seismogenic sources. The fractal dimension (*D*) value contours reveal spatial variation in the fractal features of the earthquake source. The study area was dominated by *D*-value contours of ~1.4–1.8 (Figure 8b). Low *D*-value contours (~1.4) were observed for the eastern section of the north-dipping active faults (MCT, MBT, and MFT) within the study area. The average *D*-value of the region was observed to be 1.6, indicating that the earthquakes were widely distributed along the fault plane; therefore, the heterogeneity developed in the fault plane may be responsible for triggering the events. Some areas with *D*-value >1.5 reflect a tendency of planar epicenter distribution and low clustering. The relatively high *D*-values and low *b*-values along the west of the Gorkha earthquake and east of the Kodari earthquake indicate a more heterogeneous structure. Such values may be the dominant in these regions and may arise from clusters because the uniform distribution of events decreases with their increased clustering.

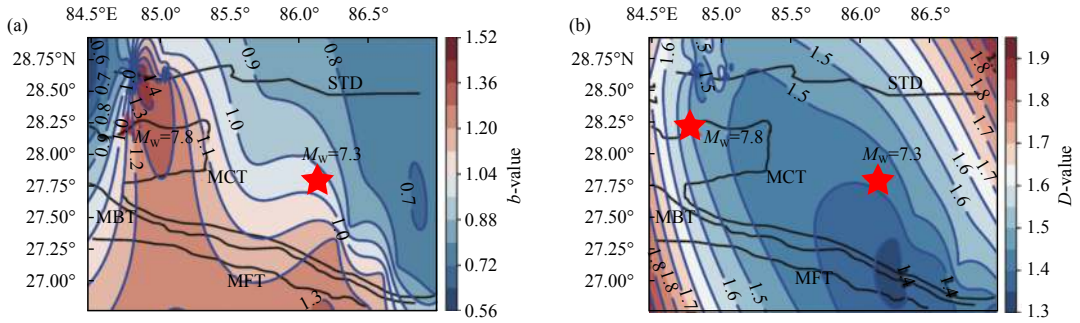

Figure 8. (a) *b*-value contour map for the study region with major faults STD, MCT, MBT, and MFT, (b) *D*-value contour map for the study region. Low *b*-value contour (~0.7–0.9) are observed for the Gorkha (84.5° E–85° E, 28° N–29° N) and Kodari (86° E–87° E, 27° N–28.75° N) earthquake regions.

Figure 9 depicts the rate of occurrence of aftershocks within 45 days of the Gorkha earthquake, which was observed to rise rapidly within the first 10 days and was followed by a steady increase. The modified Omori parameters (p = 0.86 ± 0.04, c = 0.005 1 ± 0.019, and K= 57.9 ± 3.7) were estimated for the aftershock sequence. The exponent p (0.86 ± 0.04) was low compared to the universal value of 1.0, suggesting that the temporal disintegration patterns of aftershock sequences can be efficiently modeled by the Omori-Utsu law. The lower *p*-value also signified that the study area did not experience significant rupture during the earthquake. The parameters of Omori's law mainly vary with the faulting style. Low *p*-values and larger K values denote thrust faulting events (Tahir and Grasso, 2015). The *p*-value estimated by this study (0.86) was slightly greater than the values 0.80 ± 0.4 estimated for the 2015 main cluster (Adhikari et al., 2015), 0.82 ± 0.02 for thrust faulting events (Tahir and Grasso,

2015), and 0.79 ± 0.24 for the 298 aftershocks with $m_b \geq$ 4.0 (Thapa et al., 2018). The small *c*-value (0.051 ± 0.019) observed in this study could be the result of a heterogeneous Coulomb stress adjustment (Dieterich, 1994; Helmstetter and Shaw, 2006). Understanding the decay rate of early aftershocks is significant in aftershock risk assessments (Mignan and Woessner, 2012). Therefore, characterization of aftershock parameters (this study) provides useful information for aftershock estimation.

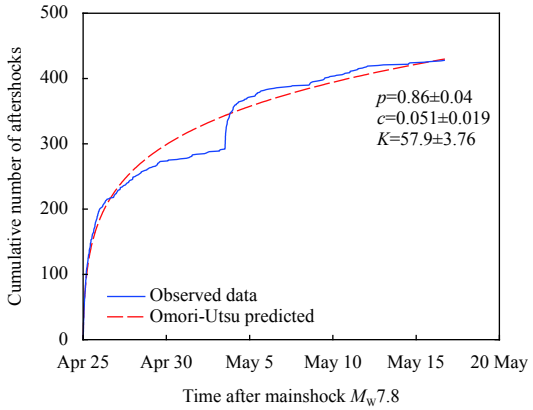

Figure 9. Omori-Utsu parameters and their standard deviations for the 429 aftershocks of the Gorkha earthquake sequence.

4. Conclusions

To determine the seismicity distribution and probability of the occurrence of future earthquakes in central Himalaya, this study analyzed the aftershock sequence of the 2015 Gorkha earthquake covering a period from 2015-4-25 to 2015-06-07. The *b*-value and Omori-Utsu parameters (*p*, *c*, and *K*) were estimated using the maximum likelihood method, while the fractal dimension was estimated using the correlation integral method. Very low *b*-value was observed during the Gorkha earthquake, after which it increased. The *b*-value again decreased at the time of the Kodari earthquake. This reduced *b*-value before the earthquakes reflects the situation when the stress of the subsurface rock mass reaches a critical value, transforming the stable locked segment into a comprehensive fault failure. Continuous aftershock activity was observed in response to the high-stress level of the underlying crust.

The *D*-value rapidly decreased initially, after which an undulating decrease was observed during the study period. This variation can be correlated with the clustering and scattering of earthquakes along a fault. This study suggests that the *D*-value and *b*-values can gradually increase and decrease, respectively, before a large earthquake. The *b*-value contour map identified the eastern part of the study region as a high stress region (*b* = ~0.8), implying that the stress shifted to that region. The *D*-value contour map reveals that the seismogenic structure (fault) acquires shifts from a linear to a planar structure in this region. The *D*-value correlated negatively with the *b*-value, indicating that the medium has not yet achieved a steady state of stress distribution. The decay rate of aftershocks (*p* = 0.86 ± 0.04) for a brief period reflects that the stress-release process is fast, and can be used to evaluate the degree of destruction of the aftershocks. The results of this study are useful for explaining the level of stress patterns in earthquake activity and provide information on aftershock decay.

Acknowledgements

This investigation was funded by the University Grant Commission (UGC) Nepal as a PhD fellowship and supported by Tribhuvan University, Nepal that allowed a sabbatical leave to the author Tiwari RK. The authors would like to thank the two anonymous reviewers and the associate editor for their suggestions on improving the quality of the manuscript.

References

Ader T, Avouac JP, Liu-Zeng J, Lyon-Caen H, Bollinger L, Galetzka J, Genrich J, Thomas M, Chanard K, Sapkota SN, Rajaure S, Shrestha P, Ding L and Flouzat M (2012). Convergence rate across the Nepal Himalaya and interseismic coupling on the Main Himalayan Thrust: Implications for seismic hazard. J Geophys Res: Solid Earth **117**(B4): B04403.

Adhikari LB, Gautam UP, Koirala BP, Bhattarai M, Kandel T, Gupta RM, Timsina C, Maharjan N, Maharjan K, Dahal T, Hoste-Colomer R, Cano Y, Dandine M, Guilhem A, Merrer S, Roudil P and Bollinger L (2015). The aftershock sequence of the 2015 April 25 Gorkha-Nepal earthquake. Geophys J Int **203**(3): 2 119–2 124.

Aggarwal SK, Pastén D and Khan PK (2017). Multifractal analysis of 2001 M_W7.7 Bhuj earthquake sequence in Gujarat, Western India. Phys A:Stat Mech Appl **488**: 177–186.

Aki K (1965). Maximum likelihood estimate of *b* in the formula Log*N* = *a*–*bM* and its confidence limits. Bull Earthq Res Inst Tokyo Univ **43**: 237–239.

Avouac JP, Meng LS, Wei SJ, Wang T and Ampuero JP (2015). Lower edge of locked Main Himalayan Thrust unzipped by the 2015 Gorkha earthquake. Nat Geosci **8**(9): 708–711.

Bachmann CE, Wiemer S, Goertz-Allmann BP and Woessner J (2012). Influence of pore-pressure on the event-size distribution of induced earthquakes. Geophys Res Lett **39**(9): L09 302.

Bai L, Liu HB, Ritsema J, Mori J, Zhang TZ, Ishikawa Y and Li

GH (2016). Faulting structure above the Main Himalayan Thrust as shown by relocated aftershocks of the 2015 M_W7.8 Gorkha, Nepal, earthquake. Geophys Res Lett **43**(2): 637–642.

Baillard C, Lyon-Caen H, Bollinger L, Rietbrock A, Letort J and Adhikari LB (2017). Automatic analysis of the Gorkha earthquake aftershock sequence: Evidences of structurally segmented seismicity. Geophys J Int **209**(2): 1 111–1 125.

Bayrak Y and Öztürk S (2004). Spatial and temporal variations of the aftershock sequences of the 1999 İzmit and Düzce earthquakes. Earth Planets Space **56**(10): 933–944.

Bayrak Y and Bayrak E (2012). Regional variations and correlations of Gutenberg-Richter parameters and fractal dimension for the different seismogenic zones in Western Anatolia. J Asian Earth Sci **58**: 98–107.

Bender B (1983). Maximum likelihood estimation of *b* values for magnitude grouped data. Bull Seismol Soc Am **73**(3): 831–851.

Bilham R (2015). Raising Kathmandu. Nat Geosci **8**(8): 582–584.

Bilham R, Mencin D, Bendick R and Bürgmann R (2017). Implications for elastic energy storage in the Himalaya from the Gorkha 2015 earthquake and other incomplete ruptures of the Main Himalayan Thrust. Quat Int **462**: 3–21.

Bilham R (2019). Himalayan earthquakes: A review of historical seismicity and early 21st century slip potential. Geol Soc Spec Publ **483**(1): 423–482.

Borgohain JM, Borah K, Biswas R and Bora DK (2018). Seismic *b*-value anomalies prior to the 3rd January 2016, M_W = 6.7 Manipur earthquake of northeast India. J Asian Earth Sci **154**: 42–48.

Bridges DL and Gao SS (2006). Spatial variation of seismic *b*-values beneath makushin Volcano, Unalaska Island, Alaska. Earth Planet Sci Lett **245**(1-2): 408–415.

Caneva A and Smirnov V (2004). Using the fractal dimension of earthquake distributions and the slope of the recurrence curve to forecast earthquakes in Colombia. Earth Sci Res J **8**(1): 3–9.

Chaulagain H, Gautam D, and Rodrigues H (2018). Revisiting major historical earthquakes in Nepal: Overview of 1833, 1934, 1980, 1988, 2011, and 2015 seismic events. In: Gautam D, and Rodrigues H eds. Impacts and Insights of the Gorkha Earthquake. Elsevier, Amsterdam, pp 1–17.

Chen H, Xie QC, Li ZQ, Xue W and Liu K (2017). Seismic damage to structures in the 2015 Nepal earthquake sequences. J Earthq Eng **21**(4): 551–578.

Chen YG and Wang JJ (2013). Multifractal characterization of urban form and growth: The case of Beijing. Environ Plan B:Plan Des **40**(5): 884–904.

Chiba K (2019). Spatial and temporal distributions of *b*-values related to long-term slow-slip and low-frequency earthquakes in the Bungo Channel and Hyuga-nada regions, Japan. Tectonophysics **757**: 1–9.

Chingtham P, Sharma B, Chopra S and SinghaRoy P (2016). Statistical analysis of aftershock sequences related with two major Nepal earthquakes: April 25, 2015, M_W7.8, and May 12, 2015, M_W7.2. Ann Geophys **59**(5): S0 540.

Dal Zilio L, Hetényi G, Hubbard J and Bollinger L (2021). Building the Himalaya from tectonic to earthquake scales. Nat Rev Earth Environ **2**(4): 251–268.

Dieterich J (1994). A constitutive law for rate of earthquake production and its application to earthquake clustering. J Geophys Res **99**(B2): 2 601–2 618.

Dimri VP (2005). Fractals in geophysics and seismology: An introduction. In: Dimri VP ed. Fractal Behaviour of the Earth System. Springer, Berlin, Heidelberg, pp 1–22, doi: 10.1007/3-540-26536-8_1.

El-Isa ZH, and Eaton DW (2014). Spatiotemporal variations in the *b*-value of earthquake magnitude-frequency distributions: Classification and causes. Tectonophysics **615–616**: 1–11, doi: 10.1016/j.tecto.2013.12.001.

Elliott JR, Jolivet R, González PJ, Avouac JP, Hollingsworth J, Searle MP and Stevens V (2016). Himalayan megathrust geometry and relation to topography revealed by the Gorkha earthquake. Nat Geosci **9**(2): 174–180.

Enescu B and Ito K (2002). Spatial analysis of the frequency-magnitude distribution and decay rate of aftershock activity of the 2000 Western Tottori Earthquake. Earth Planets Space **54**(8): 847–859.

Enescu B, Enescu D and Ito K (2011). Values of *b* and *p*: Their variations and relation to physical processes for earthquakes in Japan and Romania. Rom J Phys **56**(3-4): 590–608.

Fayou A, Kong JM, Tian SJ, Cui Y, and Wu WP (2010). A study on aftershock spatio-temporal fractal and *b*-value variation rule of Wenchuan earthquake. In: 2010 Seventh International Conference on Fuzzy Systems and Knowledge Discovery. IEEE, Yantai, China, pp 2721–2725, doi: 10.1109/FSKD.2010.5569510.

Firoozfar A and Ansari B (2019). *b*-value and fractal dimension variations in Iran. Earthq Sci **32**(2): 57–63.

Ghosal A, Ghosh U and Kayal JR (2012). A detailed *b*-value and fractal dimension study of the March 1999 Chamoli earthquake (M_S6.6) aftershock sequence in western Himalaya. Geomat Nat Hazards Risk **3**(3): 271–278.

Ghosh U (2020). Seismic characteristics and seismic hazard assessment: Source region of the 2015 Nepal earthquake M_W7.8 in Central Himalaya. Pure Appl Geophys **177**(1): 181–194.

Goda K, Kiyota T, Pokhrel RM, Chiaro G, Katagiri T, Sharma K and Wilkinson S (2015). The 2015 Gorkha Nepal earthquake: Insights from earthquake damage survey. Front Built Environ **1**: 8.

Goltz C (1997). Fractal and Chaotic Properties of Earthquakes. Springer, Berlin, Heidelberg.

Grassberger P and Procaccia I (1983). Measuring the strangeness of strange attractors. Phys D: Nonlinear Phenom **9**(1-2): 189–208.

Guglielmi AV (2016). Interpretation of the Omori law. Izv Phys Solid Earth **52**(5): 785–786.

Guglielmi AV (2017). Omori's law: A note on the history of geophysics. Physics-Uspekhi **60**(3): 319–324.

Gutenberg B and Richter CF (1944). Frequency of earthquakes in California. Bull Seismol Soc Am **34**(4): 185–188.

Hainzl S, Zöller G and Kurths J (1999). Similar power laws for foreshock and aftershock sequences in a spring-block model for earthquakes. J Geophys Res: Solid Earth **104**(B4): 7 243–7 253.

Hamdache M, Henares J, Peláez JA and Damerdji Y (2019). Fractal analysis of earthquake sequences in the Ibero-Maghrebian Region. Pure Appl Geophys **176**(4): 1 397–1 416.

Helmstetter A and Shaw BE (2006). Relation between stress heterogeneity and aftershock rate in the rate-and-state model. J Geophys Res: Solid Earth **111**(B7): B07 304.

Hirata T (1989). A correlation between the *b* value and the fractal dimension of earthquakes. J Geophys Res **94**(B6): 7 507–7 514.

Huang J and Turcotte DL (1988). Fractal distributions of stress and strength and variations of *b*-value. Earth Planet Sci Lett **91**(1-2): 223–230.

Hussain H, Zhang SX, Usman M and Abid M (2020). Spatial variation of *b*-values and their relationship with the fault blocks in the western part of the tibetan plateau and its surrounding areas. Entropy **22**(9): 1 016.

Jena R, Ghansar TAA, Pradhan B and Rai AK (2021). Estimation of fractal dimension and *b*-value of earthquakes in the Himalayan region. Arab J Geosci **14**(10): 867.

Jiang HK and Diao SZ (1995). A model of seismicity with fractal structures and a preliminary discussion on the relation between *D* and *b* value. Acta Seismol Sin **8**(4): 647–652.

Kagan YY (1981). Spatial distribution of earthquakes: The four-point moment function. Geophys J Int **67**(3): 719–733.

Kagan YY and Houston H (2005). Relation between mainshock rupture process and Omori's law for aftershock moment release rate. Geophys J Int **163**(3): 1 039–1 048.

Kagan YY (2007). Earthquake spatial distribution: The correlation dimension. Geophys J Int **168**(3): 1 175–1 194.

Kawamura M and Chen KH (2017). Influences on the location of repeating earthquakes determined from *a* and *b* value imaging. Geophys Res Lett **44**(13): 6 675–6 682.

Lei XL and Kusunose K (1999). Fractal structure and characteristic scale in the distributions of earthquake epicentres, active faults and rivers in Japan. Geophys J Int **139**(3): 754–762.

Lei XL (2019). Evolution of *b*-value and fractal dimension of acoustic emission events during shear rupture of an immature fault in granite. Appl Sci **9**(12): 2 498.

Letort J, Bollinger L, Lyon-Caen H, Guilhem A, Cano Y, Baillard C and Adhikari LB (2016). Teleseismic depth estimation of the 2015 Gorkha-Nepal aftershocks. Geophys J Int **207**(3): 1 584–1 595.

Malischewsky PG (2014). A very special fractal: Gingko of Jena. Geofis Int **53**(1): 95–100.

Mandal P and Rastogi BK (2005). Self-organized fractal seismicity and *b* value of aftershocks of the 2001 Bhuj earthquake in Kutch (India). Pure Appl Geophys **162**(1): 53–72.

Mandelbrot B (1967). How long is the coast of Britain? Statistical self-similarity and fractional dimension. Science **156**(3775): 636–638.

Mandelbrot BB and Wheeler JA (1983). The fractal geometry of nature. Am J Phys **51**(3): 286–287.

Martin SS, Hough SE and Hung C (2015). Ground motions from the 2015 M_W7.8 Gorkha, Nepal, Earthquake constrained by a detailed assessment of macroseismic data. Seismol Res Lett **86**(6): 1 524–1 532.

Michel S, Jolivet R, Rollins C, Jara J and Dal Zilio L (2021). Seismogenic potential of the Main Himalayan thrust constrained by coupling segmentation and earthquake scaling. Geophys Res Lett **48**(13): e2 021GL093 106.

Mignan A and Woessner J (2012). Estimating the magnitude of completeness for earthquake catalogs. Community Online Resource for Statistical Seismicity Analysis, doi:10.5078/corssa-00180805.

Miyake H, Sapkota SN, Upreti BN, Bollinger L, Kobayashi T and Takenaka H (2017). Special issue "The 2015 Gorkha, Nepal, earthquake and Himalayan studies: First results". Earth Planets Space **69**(1): 12.

Mogi K (1967). Earthquakes and fractures. Tectonophysics **5**(1): 35–55.

Mondal SK, Roy PNS, Catherine JK and Pandey AK (2019). Significance of fractal correlation dimension and seismic *b*-value variation due to 15th July 2009, New Zealand earthquake of M_W7.8. Ann Geophys **62**(5): SE568.

Mugnier JL, Gajurel A, Huyghe P, Jayangondaperumal R, Jouanne F and Upreti B (2013). Structural interpretation of the great earthquakes of the last millennium in the central Himalaya. Earth-Sci Rev **127**: 30–47.

Nampally S, Padhy S and Dimri VP (2018). Characterizing spatial heterogeneity based on the *b*-value and fractal analyses of the 2015 Nepal earthquake sequence. Tectonophysics **722**: 154–162.

Nava FA, Márquez-Ramírez VH, Zúñiga FR, Ávila-Barrientos L and Quinteros CB (2017). Gutenberg-Richter *b*-value maximum likelihood estimation and sample size. J Seismol **21**(1): 127–135.

Nerenberg MAH and Essex C (1990). Correlation dimension and systematic geometric effects. Phys Rev A **42**(12): 7 065–7 074.

Ogata Y (1999). Seismicity analysis through point-process modeling: A review. Pure Appl Geophys **155**(2-4): 471–507.

Ogata Y and Tsuruoka H (2016). Statistical monitoring of aftershock sequences: A case study of the 2015 M_W7.8 Gorkha, Nepal, earthquake. Earth Planets Space **68**(1): 44.

Omori F (1894). On the aftershocks of earthquakes. J Coll Sci Imp Univ Tokyo **7**: 111–120.

Öncel AO, Main I, Alptekin Ö and Cowie P (1996). Spatial variations of the fractal properties of seismicity in the Anatolian fault zones. Tectonophysics **257**(2-4): 189–202.

Oncel AO and Wilson TH (2002). Space-time correlations of seismotectonic parameters: Examples from Japan and from Turkey preceding the İzmit earthquake. Bull Seismol Soc Am **92**(1): 339–349.

Pandey MR, Tandukar RP, Avouac JP, Lavé J and Massot JP (1995). Interseismic strain accumulation on the Himalayan crustal ramp (Nepal). Geophys Res Lett **22**(7): 751–754.

Pastén D, Estay R, Comte D and Vallejos J (2015). Multifractal analysis in mining microseismicity and its application to

seismic hazard in mine. Int J Rock Mech Min Sci **78**: 74–78.
Reasenberg PA and Jones LM (1989). Earthquake hazard after a mainshock in California. Science **243**(4895): 1 173–1 176.
Rehman K, Ali A, Ahmed S, Ali W, Ali A and Khan MY (2015). Spatio-temporal variations of *b*-value in and around north Pakistan. J Earth Syst Sci **124**(7): 1 445–1 456.
Rodríguez Pascua MA, De Vicente G, Calvo JP and Pérez-López R (2003). Similarities between recent seismic activity and paleoseismites during the late miocene in the external Betic Chain (Spain): Relationship by "*b*" value and the fractal dimension. J Struct Geol **25**(5): 749–763.
Roy PNS and Nath SK (2007). Precursory correlation dimensions for three great earthquakes. Curr Sci **93**(11): 1 522–1 529.
Roy PNS and Padhi A (2007). Multifractal analysis of earthquakes in the Southeastern Iran-Bam Region. Pure Appl Geophys **164**(11): 2 271–2 290.
Roy PNS and Mondal SK (2009). Fractal nature of earthquake occurrence in northwest Himalayan region. J Ind Geophys Union **13**(2): 63–68.
Shcherbakov R, Yakovlev G, Turcotte DL and Rundle JB (2005). Model for the distribution of aftershock interoccurrence times. Phys Rev Lett **95**(21): 218501.
Shcherbakov R, Turcotte DL, and Rundle JB (2015). Complexity and earthquakes. In: Schubert G and Kanamori H eds. Treatise on Geophysics. 2nd ed. Elsevier, Oxford, pp 627–653.
Shi YL and Bolt BA (1982). The standard error of the magnitude-frequency *b* value. Bull Seismol Soc Am **72**(5): 1 677–1 687.
Smalley RFJr, Chatelain JL, Turcotte DL and Prévot R (1987). A fractal approach to the clustering of earthquakes: Applications to the seismicity of the New Hebrides. Bull Seismol Soc Am **77**(4): 1 368–1 381.
Smith WD (1981). The *b*-value as an earthquake precursor. Nature **289**(5794): 136–139.
Srivastava K, Rani S and Srinagesh D (2015). A review of *b*-value imaging and fractal dimension studies in the Andaman Sumatra subduction. Nat Hazards **77**(1): 97–107.
Tahir M and Grasso JR (2015). Faulting style controls for the space–time aftershock patterns. Bull Seismol Soc Am **105**(5): 2 480–2 497.
Tang YS, Liu S, Li XL, Fan YL, Deng YR, Liu Y and Yin LR (2020). Earthquakes spatio-temporal distribution and fractal analysis in the Eurasian seismic belt. Rend Fis Acc Lincei **31**(1): 203–209.
Teotia SS and Kumar D (2011). Role of multifractal analysis in understanding the preparation zone for large size earthquake in the North-Western Himalaya region. Nonlin Process Geophys **18**(1): 111–118.
Thapa DR, Tao XX, Fan F and Tao ZR (2018). Aftershock analysis of the 2015 Gorkha-Dolakha (Central Nepal) earthquake doublet. Heliyon **4**(7): e00 678.
Tosi P (1998). Seismogenic structure behaviour revealed by spatial clustering of seismicity in the Umbria-Marche Region (Central Italy). Ann Geofis **41**(2): 215–224.
Trivedi PC (2015). Application of Omori's Decay Law to the 2001 Bhuj aftershock sequence for Kachchh region of western India. Open J Earthq Res **4**(3): 94–101.
Turcotte DL (1989). Fractals in geology and geophysics. Pure Appl Geophys **131**(1): 171–196.
Utsu T (1969). Aftershocks and earthquake statistics (I): Some parameters which characterize an aftershock sequence and their interrelations. J Fac Sci Hokkaido Univ, Japan, Ser. VII **3**(3): 129–195.
Utsu T (1971). Aftershocks and earthquake statistics (III): Analyses of the distribution of earthquakes in magnitude, time, and space with special considertion to clustering characteristics of earthquake occurrence (1). J Fac Sci Hokkaido Univ, Ser VII **3**(5): 379–441.
Utsu T, Ogata Y, Ritsuko S and Matsu'ura (1995). The centenary of the omori formula for a decay law of aftershock activity. J Phys Earth **43**(1): 1–33.
Wang JH and Lee CW (1996). Multifractal measures of earthquakes in west Taiwan. Pure Appl Geophys **146**(1): 131–145.
Wang R, Chang Y, Miao M, Zeng ZY, Chen HY, Shi HX, Li DN, Liu LF, Su YJ and Han P (2021). Assessing earthquake forecast performance based on *b* value in Yunnan province, China. Entropy **23**(6): 730.
Wiemer S (2001). A software package to analyze seismicity: ZMAP. Seismol Res Lett **72**(3): 373–382.
Wyss M, Sammis CG, Nadeau RM and Wiemer S (2004). Fractal dimension and *b*-value on creeping and locked patches of the San Andreas fault near Parkfield, California. Bull Seismol Soc Am **94**(2): 410–421.
Yamada M, Kandel T, Tamaribuchi K and Ghosh A (2020). 3D fault structure inferred from a refined aftershock catalog for the 2015 Gorkha earthquake in Nepal. Bull Seismol Soc Am **110**(1): 26–37.
Yeken T (2016). Spatial analysis of *b*-value variability in Armutlu Peninsula (NW Turkey). Open Geosci **8**(1): 548–555.
Yin A, Dubey CS, Webb AAG, Kelty TK, Grove M, Gehrels GE and Burgess WP (2010). Geologic correlation of the Himalayan orogen and Indian craton: Part 1. Structural geology, U-Pb zircon geochronology, and tectonic evolution of the Shillong Plateau and its neighboring regions in NE India. GSA Bull **122**(3-4): 336–359.
Yin LR, Li XL, Zheng WF, Yin ZT, Song LH, Ge LJ and Zeng QC (2019). Fractal dimension analysis for seismicity spatial and temporal distribution in the circum-Pacific seismic belt. J Earth Syst Sci **128**: 22.
Žalohar J (2018). Omori's Law. In: Developments in Structural Geology and Tectonics. Elsevier, Amsterdam, pp 123–134.
Zhuang JC, Matsu'ura M and Han P (2021). Critical zone of the branching crack model for earthquakes: Inherent randomness, earthquake predictability, and precursor modelling. Eur Phys J Spec Top **230**(1): 409–424.

sciendo

Geologos 28, 2 (2022): 115–128
DOI: 10.2478/logos-2022-0009

GEOLOGOS

Frequency magnitude distribution and spatial correlation dimension of earthquakes in north-east Himalaya and adjacent regions

Ram Krishna Tiwari[1,2]*, Harihar Paudyal[2]

[1] Central Department of Physics, Tribhuvan University, Kirtipur, Kathmandu, Nepal
[2] Birendra Multiple Campus, Tribhuvan University, Bharatpur, Chitwan, Nepal
* corresponding author, e-mail: ram.tiwari@bimc.tu.edu.np

Abstract

The north-east sector of the Himalaya is one of the most active tectonic belts, with complex geological and tectonic features. The b-value and spatial correlation dimension (D_c) of earthquake distribution in the north-east Himalaya and its adjacent regions (20–32°N and 88–98°E) are estimated in the present study. Based on seismicity and faulting pattern, the region is divided into five active regions, namely the (i) South-Tibet, (ii) Eastern-Syntaxis, (iii) Himalayan-Frontal Arc, (iv) Arakan-Yoma belt and (v) Shillong-Plateau. A homogeneous catalogue of 1,416 earthquakes (mb ≥ 4.5) has been prepared from a revised catalogue of the ISC (International Seismological Centre). The b-value has been appraised by the maximum likelihood estimation method, while D_c values have been calculated by the correlation integral method; b-values of 1.08 ± 0.09, 1.13 ± 0.05, 0.92 ± 0.05, 1.00 ± 0.03 and 0.98 ± 0.08 have been computed for the South-Tibet, Eastern-Syntaxis, Himalayan-Frontal Arc, Arakan-Yoma belt and Shillong-Plateau region, respectively. The D_c values computed for the respective regions are 1.36 ± 0.02, 1.74 ± 0.04, 1.57 ± 0.01, 1.8 ± 0.01, and 1.83 ± 0.02. These values are > 1.5, except for the South-Tibet (1.36 ± 0.02). The b-values around the global average value (1.0) reflect the stress level and seismic activity of the regions, while high D_c values refer to the heterogeneity of the seismogenic sources.

Key words: North-east India, b-value, maximum likelihood estimation, correlation dimension

1. Introduction

With regard to time, space and size, earthquake occurrences own a power-law relation. The b-value (Gutenberg & Richter, 1944) and fractal dimension – D_c (Grassberger & Procaccia, 1983) are two scale-invariant exponents in earthquake data analysis that obey a power law relation. The spatio-temporal variations of these parameters have importance in our understanding of stress environments and features of seismogenic structures. The b-value is associated to variations in both local and regional stresses (Mogi, 1967; Scholz, 1968; Wiemer & Wyss, 1997; Khan & Chakraborty, 2007; Bora & Baruah, 2012; El-Isa & Eaton, 2014; Mousavi, 2017a, b; Bora et al., 2018), types of faults (Ishibe et al., 2015) and creeping segment of the fault and asperity existing in the fault (Zhao & Wu, 2008), while the fractal dimension can be used to explain the complexity present in a ruptured surface (Kagan & Knopoff, 1978; Mandelbrot & Wheeler, 1983; Turcotte, 1989). The D_c in different zones may vary and the variation can be related to geo-structural heterogeneity (Aviles et al., 1987). The relation between the b-value and D_c has been studied widely during the last three decades (Hirata, 1989a; Öncel et al., 1996; Legrand, 2002; Wyss et al., 2004; Ghosal et al., 2012; Pailoplee & Choowong, 2014; Wu et al., 2017; Mondal et al., 2019; Chen & Zhu, 2020).

The Himalaya was created due to continuous convergence and under-thrusting of the Indian continental plate below the Eurasian plate. Its northern boundary is the Tibetan plateau; the southern boundary is the Indo-Gangetic plane. Here, we select the north-east Himalayan region, which is bounded by 20–32°N and 88–98°E, in order to study the fractal nature of earthquake distribution. This region includes Sikkim, Bhutan, north-east Himalaya, and its adjoining Tibet region, Arakan-Yoma belt and adjoining parts of Bangladesh and Myanmar (Fig. 1). It is characterised by a complex geological and tectonic setting with several thrusts, faults, folds and lineaments (Berthet et al., 2014; Dasgupta et al., 2021).

Having an intricate geotectonic setup, the seismicity of the region is remarkably high in which earthquakes with wide-range magnitude have been a common phenomenon since historical times (Angelier & Baruah, 2009; Bhattacharya et al., 2010; Zhang et al., 2012). The great Shillong earthquake of June 12, 1897 (Mw 8.0) was in the northern parts of the Shillong Plateau, while on August 15, 1950, the great Assam earthquake (Mw 8.6) occurred in the Mishmi tectonic block (Kayal, 2010; Liu et al., 2015). These great earthquakes have made the region seismically very active (Bilham et al., 2017). The Kopili Fault zone, which separates the Shillong Plateau and the Mikir Massif (Fig. 1; Kayal et al., 2006, 2012) had earlier produced two strong earthquakes, i.e., in 1869 (Mw 7.7) Cachar earthquake (Nandy, 2005) and in 1943 (Mw 7.1) earthquake (Nandy & Dasgupta, 1991) and has the potential to experience strong earthquake in the future (Bora et al., 2013). The segment of the crust between the rupture zone of the Shillong and Assam earthquakes has been identified as a potential host of a future great earthquake (Khattri & Tyagi, 1983; Angelier & Baruah, 2009). In addition, the area bounded by the Dhubri-Chungthang fault (DCF) zone and the Main Himalayan Thrust (MHT) may potentially host M7 to M8 earthquakes (Fig. 1; Diehl et al., 2017).

Most earthquakes in the Himalaya are shallow and intermediate in focus and the major cause of these earthquakes is a shallow dipping-downward motion of the Indian plate under the Eurasian landmass (Molnar & Tapponnier, 1975; Kayal et al., 1993). Furthermore, the subducting Indo-Bur-

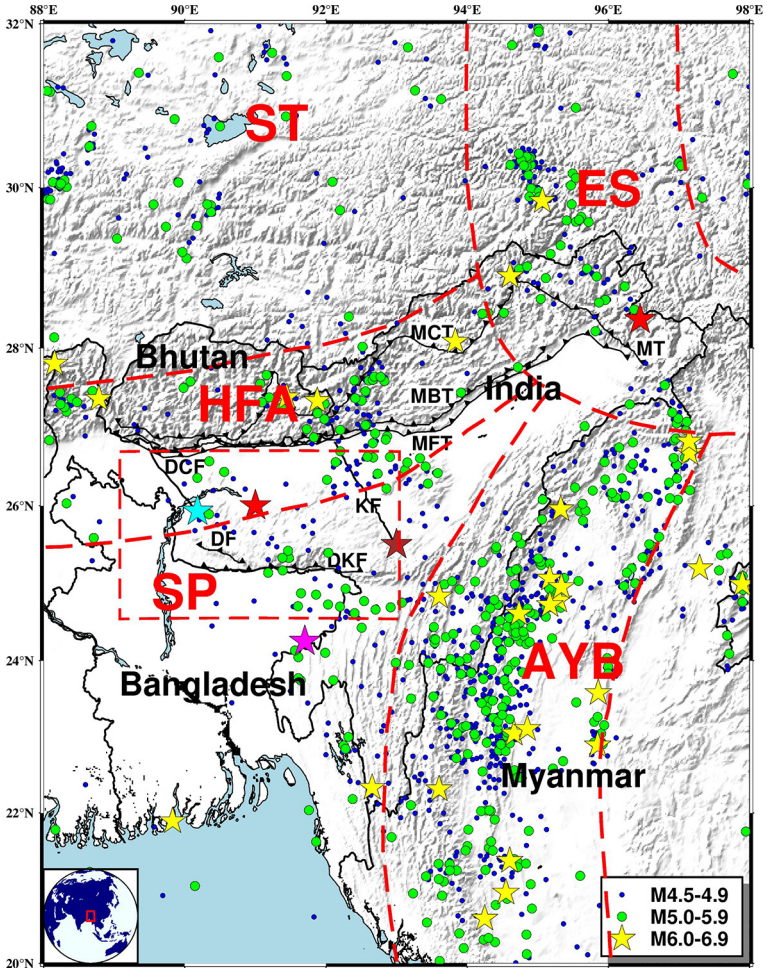

Fig. 1. Epicentral distribution of earthquakes (Mc ≥ 4.5) in the study region. The yellow stars in different blocks stand for earthquakes (magnitude ≥ 6.0mb). Regions are as follows: ST - South Tibet; ES – Eastern-Syntaxis; HFA – Himalayan-Frontal Arc; AYB – Arakan-Yoma belt; SP – Shillong-Plateau (Panthi et al., 2013). The red star in region ES stands for the 1950 Assam earthquake, while that inside the rectangular box signifies the 1897 Shillong earthquake. The cyan star is for the 1930 Dhubri earthquake, a brown star for the 1869 Cacher earthquake and a magenta star for the 1918 Srimangal earthquake. Abbreviations: MCT – Main Central Thrust; MBT – Main Boundary Thrust; MFT – Main Frontal Thrust; KF – Kopili Fault; MT – Mishimi Thrust; DCF – Dhubri–Chungthang Fault; DF – Dapsi Fault; DKF – Dauki Fault. The red box in the inset map at the bottom left-hand corner of the map depicts the study area in a global scenario.

ma Range (IBR) in the east is also responsible for a prominent level of seismic activity in the region (Verma et al., 1976; Thingbaijam et al., 2008; Bora et al., 2022a, b). From our study of the literature, the north-east Himalaya and its nearby regions are demarcated as a potential zone for strong seismic activity in the future. Therefore, the present study attempts to enhance our understanding of regional features of seismicity, stress level and crustal heterogeneity.

2. Seismicity of the region and division of seismic zones

A total of 22 large earthquakes with M ≥ 7, including the Shillong earthquake of Mw 8.0 (1897) and Assam earthquake of Mw 8.6 (1950), have occurred in the north-east region between 1897 and 1962 (Kayal et al., 1993; Islam et al., 2011; Tandon & Gupta, 2020). Other notable events are the 1869 Cachar earthquake (Mw 7.7), the 1918 Srimangal earthquake (Mw 7.5) and the 1930 Dhubri (Mw 7.1) (see Raghu Kanth & Dash, 2010). The high seismicity of this region can also be understood from the fact that it has experienced 29 events (magnitude ≥ 6.0mb) for the period 1964–2020. Thus, it can be inferred that a considerable amount of strain energy is stored along this part of the Himalaya and the regions divided are tectonically active.

The division of the study area into five regions (Fig. 1) is based on the seismic activity and nature of faulting (Panthi et al., 2013). These regions are the South-Tibet (ST), Eastern-Syntaxis (ES), Himalayan-Frontal Arc (HFA), Arakan-Yoma belt (AYB) and Shillong-Plateau (SP). The normal faulting pattern is predominant in South-Tibet. Eastern-Syntaxis is made up with both thrust fault and transverse faults. The Himalayan-Frontal Arc shows thrust faulting with predominant major faults such as the MCT (Main Central Thrust) and MBT (Main Boundary Thrust; Fig. 1). The Arakan-Yoma region has more complex tectonics compared to others, in which a near-equal percentage of normal and thrust faulting is established (Bora, 2016). The Shillong-Plateau shows a tectonically important pop-up structure induced by plate convergence (Islam et al., 2011). These five regions enclose only 1,347 earthquakes with the Arakan-Yoma belt having a large number of earthquakes (727) and the Shillong Plateau having fewer (83) (Table 1).

3. Compilation of a seismicity database and methodology

A comprehensive and reliable seismicity database covering a wide range of magnitudes is needed to draw meaningful inferences from seismicity studies. For the preparation of a homogeneous catalogue, we have used the revised earthquake catalogue of the International Seismological Centre, ISC (Bondár & Storchak, 2011; Storchak et al., 2017, 2020). We have retrieved 5,013 earthquakes having body wave magnitude (mb) for the region 20–32°N and 88–98°E between January 22, 1964 and May 25, 2020. The declustering of the catalogue has been performed by the linked-window method (Reasenberg, 1985) in order to remove dependent events such as foreshocks and aftershocks. We have then retained 4,845 earthquakes whose completeness (Mc) has been checked for a time window of 20 years from the maximum curvature technique in ZMAP package (Wiemer, 2001). For the time window from 1964 to 1984, Mc has been found to be 4.8. The Mc is 4.0 for the time window from 1984 to 2004 and 3.8 for 2004 to 2020. Although the average value of Mc for these three time windows is 4.2, the best fitted line is obtained for a completeness magnitude Mc ≥ 4.5 mb with a b-value of 1.01 ± 0.02. Thus, the final analysis is best on earthquake data with completeness magnitude 4.5 mb (Fig. 2). The completeness magnitude of the prepared catalogue is in agreement with the completeness magnitude of the preceding work (Sarkar et al., 2020). The maximum curvature technique has been used for estimation of Mc and b-value, because it gives a stable result even for fewer events. Thus, it has an advantage over other techniques such as the b-value stability technique (Cao & Gao, 2002) and the entire

Table 1. Information on the number of earthquakes, duration, focal depth and magnitude range in the five regions studied. For location of the regions see Figure 1.

Region	Number of earthquakes	Time period	Depth (km)	Magnitude (mb)
South-Tibet (ST)	124	1964/06/10–2020/01/29	2.30–101.90	4.5–6.5
Eastern-Syntaxis (ES)	247	1965/06/15–2020/02/01	3.60–51.00	4.5–6.1
Himalayan-Frontal Arc (HFA)	166	1964/02/18–2020/04/15	6.50–65.80	4.5–6.1
Arakan-Yoma belt (AYB)	727	1964/01/22–2020/05/25	6.10–84.70	4.5–6.9
Shillong-Plateau (SP)	83	1966/02/24–2020/04/05	1.70–50.20	4.5–5.9

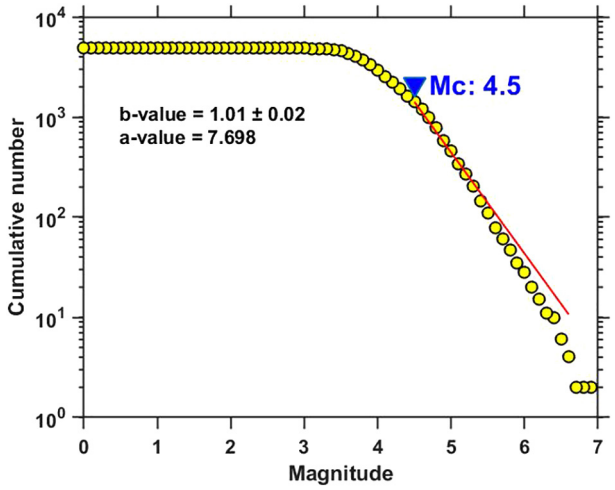

Fig. 2. b-value (1.01 ± 0.02) and magnitude of completeness (Mc ≥ 4.5 mb) of dataset. The slope of the fitted red line gives the b-value.

magnitude range technique (Woessner, 2005). The database then contains 1,416 earthquakes covering the entire study region.

The power law relating magnitude of the earthquakes and their frequency of occurrence (Gutenberg & Richter, 1944; Nava et al., 2017) is:

$$\log N_e(M_e) = a - b(M_e - M_c);\ M_e \geq M_c \qquad (1)$$

In equation (1), N_e is the numeral of earthquakes with magnitude M_e with $M_e \geq M_c$. The constant 'a' is the intercept on the y axis which depends on the region and timeframe of the study and describes the seismic assembly (El-Isa & Eaton, 2014). The other constant b is the slope of the linearly fitted line, also known as b-value, which gives the relative number of small to large earthquakes (Nava et al., 2017). A high value of b means that the fraction of smaller events is large and a low value of b means that the fraction of larger events is greater. It has an inverse relation with the stress level of the region (Ghosal et al., 2012; Scholz, 2015), and many studies have found a drop in the b-value prior to large earthquakes, tailed by an increase in the b-value after the main shock (Wiemer & Wyss, 1997, 2000; Pudi et al., 2020).

The b-value in the present study is estimated by the maximum likelihood method (Aki, 1965):

$$b = \frac{\log_{10} e}{\overline{M} - (M_e - \frac{\Delta M_e}{2})} \qquad (2)$$

In equation (2), $\overline{M}$ is the average value of the magnitudes, M_e is minimum magnitude of the sample and ΔM_e is the binning thickness of the data considered. The standard error (Δb) on the value of b is estimated by (Shi & Bolt, 1982):

$$\Delta b = 2.30 \times b^2 \sqrt{\sum_{i=1}^{n_e} \frac{(M_i - M)^2}{n_e(n_e - 1)}} \qquad (3)$$

In equation (3), n_e is the total number of earthquakes in a sample window. For all five regions considered the standard errors, $\Delta b \leq 0.09$, confirm fewer uncertainties in the evaluation of the b-value (Table 2).

The correlation dimension is obtained from the correlation integral method (Grassberger & Procaccia, 1983) in which the correlation function is defined as:

$$C(r) = \frac{2}{N_c(N_c - 1)} \sum_i^{N_c} \sum_{i \neq j}^{N_c} H(r - r_{ij}). \qquad (4)$$

In equation (4), N_c is the total number of earthquakes in the window considered, $H(r - r_{ij})$ is the Heaviside step function, r is the scaling radius, and r_{ij} is the distance between the two epicentres determined by the spherical triangle method (Hirata, 1989a, 1989b) by the formula:

$$r_{ij} = \cos^{-1}(\cos\theta_i \cos\theta_j + \sin\theta_i \sin\theta_j \cos(\emptyset_i - \emptyset_j)) \qquad (5)$$

Where θ_i and θ_j are the latitudes, while $\emptyset_i$ and $\emptyset_j$ are the longitudes of the epicentres of the earthquake. The arc distance between the two epicentres $(\theta_i, \emptyset_i)$ and $(\theta_j, \emptyset_j)$ is then obtained by multiplying r_{ij} with the radius of the earth. The correlation integral is related to the correlation dimension by the power law in the scaling region as:

Table 2. Magnitude of completeness (Mc), a-value, frequency magnitude distribution b-value, correlation dimension (D_c) and coefficient of determination (R^2) of the regions studied. For location of the regions see Figure 1.

Region	Mc	a-value	b-value	D_c	R^2 for D_c
South-Tibet (ST)	4.5	6.150	1.08 ± 0.09	1.36 ± 0.02	0.997
Eastern-Syntaxis (ES)	4.5	7.482	1.13 ± 0.05	1.74 ± 0.04	0.997
Himalayan-Frontal Arc (HFA)	4.5	6.363	0.92 ± 0.05	1.57 ± 0.01	0.999
Arakan-Yoma belt (AYB)	4.5	7.374	1.00 ± 0.03	1.80 ± 0.01	0.988
Shillong-Plateau (SP)	4.5	6.333	0.98 ± 0.08	1.83 ± 0.02	0.996

$$C(r) = r^D \tag{6}$$

The scaling region of is selected between the saturation and depopulation limits (Nerenberg & Essex, 1990). The slope of fitted straight line in the linear part of the plot between logC(r) and log(r) estimates the correlation dimension as

$$D_c = \lim_{r \to 0} \frac{\log C(r)}{\log(r)} \tag{7}$$

The uncertainty in calculation of correlation dimension (root mean square error) is estimated by the formula:

$$RMSE = \sqrt{\frac{(P_i - O_i)^2}{n}} \tag{8}$$

where is Pi the ith predicted value and O_i is the ith observed value and n is the number of observations. The uncertainty in $D_c \leq 0.04$ indicates fewer uncertainties in the estimation of fractal dimension (Table 2).

The seismic moment curve shows two jumps in the years 1988 and 2016, releasing 0.79 x 10^{20} Nm and 1.83 x 10^{20} Nm energy, respectively, from the study region (Fig. 3). The range of the seismic moment (0.54–0.79) x 10^{20} Nm may be attributed to a seismic energy release after the Indo-Burma earthquake on August 6, 1988 (Mw 7.2) (Devi et al., 2021), while the range (1.57–1.83) x 10^{20} Nm may be attributed to the seismic energy release after the Manipur earthquake on January 3, 2016 (Mw 6.7) (Fig. 3; Borgohain et al., 2018). These values are comparable with the seismic moment estimated from the spectral analysis of P-waves of 162 local earthquakes in the Shillong-Mikir Hills plateau and its adjoining region in north-east India (Bora et al., 2013; Bora, 2016).

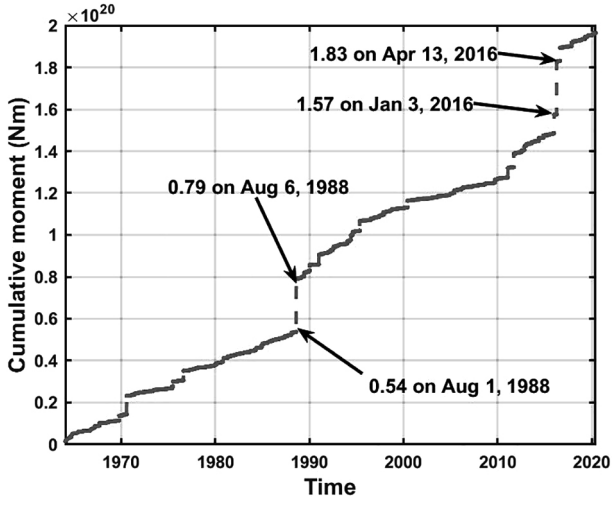

Fig. 3. Seismic moment release curve showing quick jumps in 1988 and 2016.

4. Results and discussion

4.1. b-value and earthquake occurrences

The frequency of earthquake occurrences in the five regions are explained on the basis of seismic a-values and b-values. The b-value ranges from 0.92 to 1.13 for these regions. The lowest b-value 0.92 ± 0.05 has been computed for the Himalayan-Frontal Arc region, while the highest value 1.13 ± 0.05 is seen for the Eastern-Syntaxis region. The b-value is 1.08 ± 0.09 for the South-Tibet, 1.00 ± 0.03 for the Arakan-Yoma belt and 0.98 ± 0.08 for the Shillong-Plateau (Fig. 4; Table 2).

The b-values obtained for these regions are close to the global mean value of 1.0. This indicates that the regions selected are seismically active. The observed a-values and b-values for the South-Tibet (6.15 and 1.08 ± 0.09), Eastern-Syntaxis (7.48 and 1.13 ± 0.05) and Arakan-Yoma belt (7.37 and 1.00 ± 0.03) reflect the high seismic activity due to the increment of heterogeneity in the crust (Khan et al., 2011; Akol & Bekler, 2013). The crustal heterogeneity may be linked to deformation on the crust caused by folding, faulting and cracking of the rock. The relatively low b-values 0.92 ± 0.05 and 0.98 ± 0.08 observed for the Himalayan-Frontal Arc and the Shillong Plateau (Fig. 4; Table 2) may indicate the accumulation of stress caused by the tectonic interaction between these landmasses (Panthi et al., 2013; Bora, 2016).

The temporal variation of the b-value has been determined for the five selected regions. For the South-Tibet region, a small increment in the b-value is noted from 1.15 to 1.22 during the study period (Fig. 5a). The gradual decrease in the b-value from 2.52 to 1.30 is seen for the Eastern-Syntaxis region (Fig. 5b), while the Himalayan-Frontal Arc (Fig. 5c) demonstrates a rise in the b-value from 1.36 to 1.61 and then a falls down to 1.37. An oscillating nature of variation in the b-value is noted for the Arakan-Yoma belt (Fig. 5d), between ~1.5 to ~1.1 for the study period. Finally, for the Shillong-Plateau, the b-value rises from 1.11 to 1.20 and then falls to 1.10 (Fig. 5e). The lowering trend of the b-value for the Eastern-Syntaxis may be the cause of the earthquakes of similar magnitude in the region and suggests an accumulation of stress in the region. The oscillating variation for the Arakan-Yoma belt indi-

cates continuous accumulation and release of stress in the region through small to moderate earthquakes. A similar type of variation in the b-value was also recorded for north-east India during 1975 to 2015 by Kumar & Sharma (2019).

From the b-value contour map of the region (Fig. 6), it is inferred that the seismic b-values obtained are evenly distributed over the entire region and dominated by b-values of ≤ 1.0. Relatively low b-value contours (0.8–0.9) have been obtained along the Dhubri-Chungthang Fault (DCF) zone in the Himalayan-Frontal Arc region (HFA), the Dapsi Fault (DF) zone, the Dauki Fault (DKF) zone and the Kopili Fault (KF) zone in the Shillong Plateau region (SP). Furthermore, b-value contours (0.9) have been obtained along the Mishimi Thrust (MT) zone in the Eastern-Syntaxis region (ES). Relatively high b-value contours (1.1–1.2) have been found for

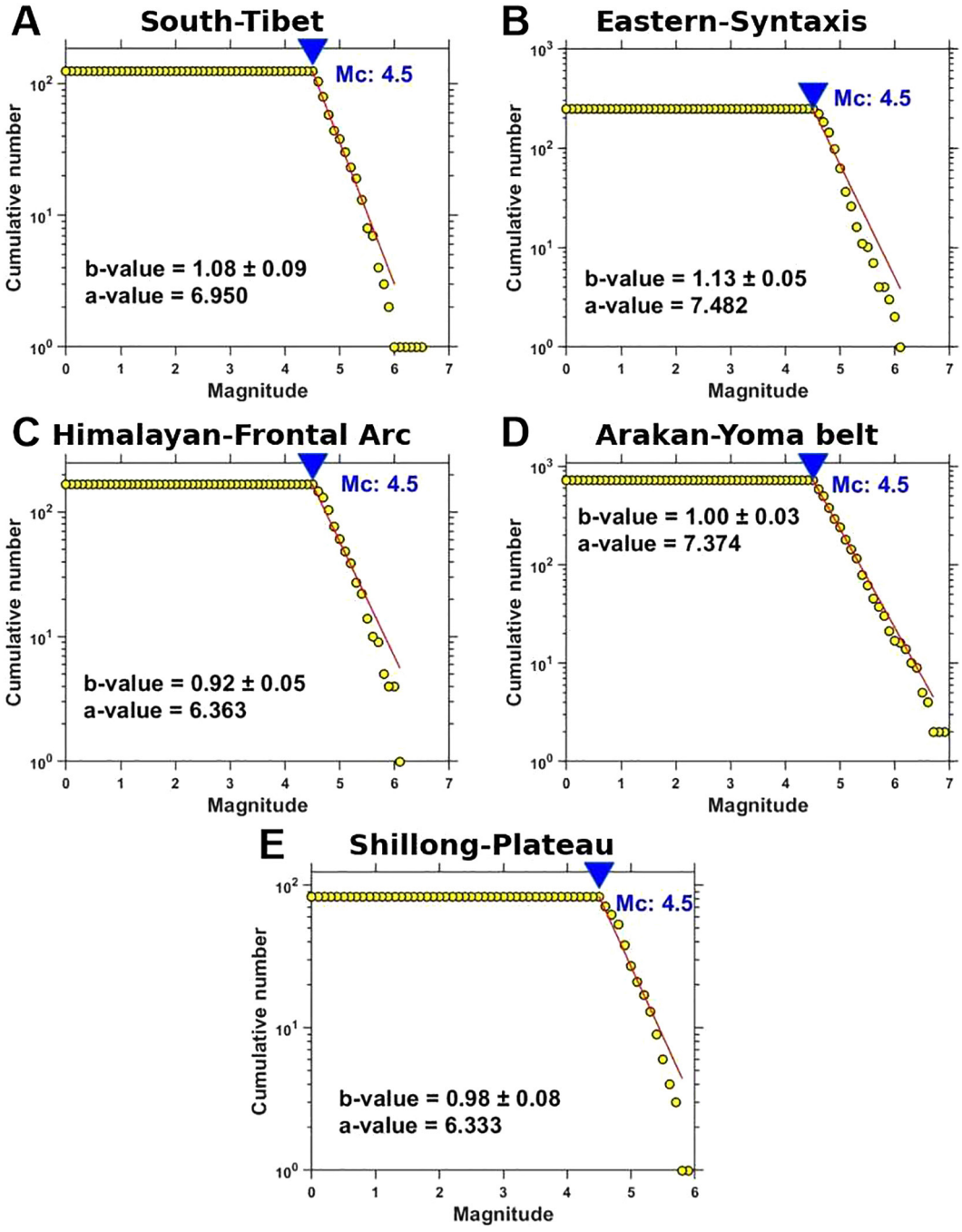

Fig. 4. Magnitude-frequency plots computed from the maximum likelihood solution for selected regions. For location of the regions see Figure 1.

the latitude 22–24°N and longitude 92.5–95°E in the Arakan-Yoma belt region (AYB; Fig. 6). The higher b-values may be due to reciprocated interaction between the Shillong Plateau, Mikir Hills, Kopili Fault zone and the IBR (Khan et al., 2011).

In earlier papers, b-values were observed to be in the range 0.6 to 1.0 and in particular, higher b-value contours were mapped for the Shillong Plateau (Bhattacharya & Kayal, 2003), b-values from 0.6 to 1.0 were also computed for the same region (Bhattacharya et al., 2010). Thus, the b-values estimated in the present work are in agreement with previous publications. Some researchers have also found b-value variations from 0.75 to 1.54 for the Indo-Burma range – IBR (Bora et al., 2018).

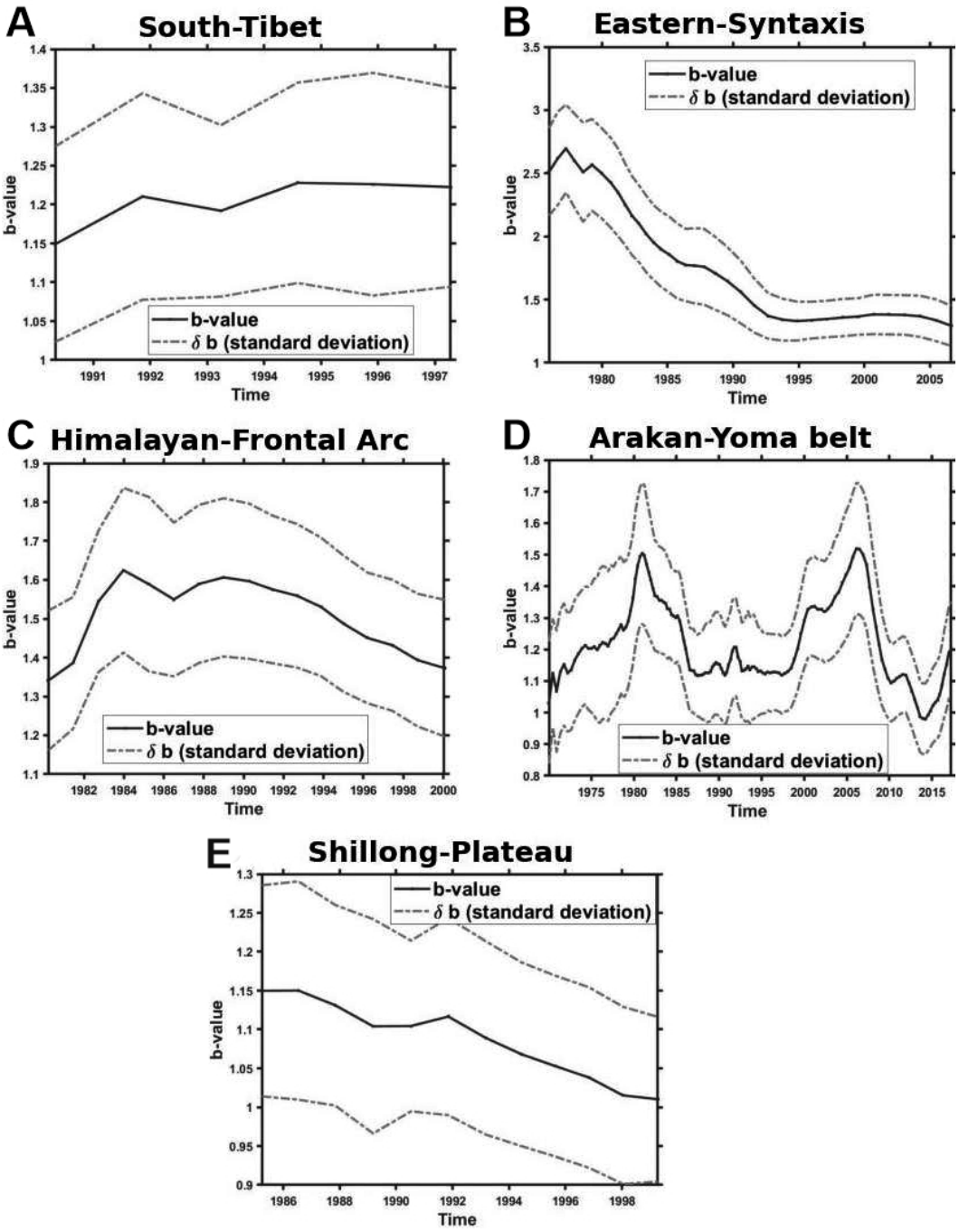

Fig. 5. b-value variation with time for selected regions. The temporal variation of the b-value is studied for a window size of 100 events with an overlap of 4%, except for the Shillong-Plateau region where a window size of only 60 events is taken because of paucity of data. For location of the regions see Figure 1.

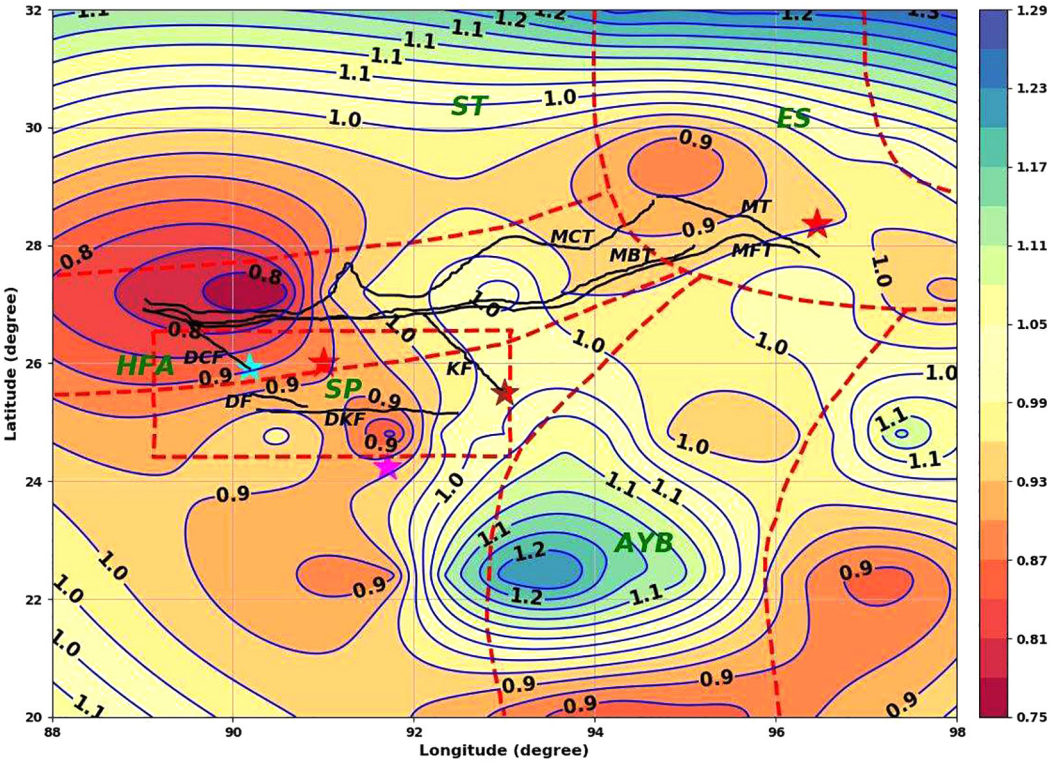

Fig. 6. The contour map of b-values in the study area. The b-values are plotted for the mean value of longitude and latitude of 2° × 2° square grids with window shifting of 0.5° along the direction of longitude. For detailed explanations and location of the regions see Figure 1.

4.2. Fractal correlation dimension of spatial distribution of epicentres

The correlation dimension (D_c) for different regions can be found in Table 2 and D_c value graphs in Figure 7. The correlation dimension obtained for the South-Tibet region is 1.36 ± 0.02. It is 1.74 ± 0.04 for the Eastern-Syntaxis, 1.57 ± 0.01 for the Himalayan Frontal Arc, 1.80 ± 0.01 for the Arakan-Yoma belt and 1.83 ± 0.02 for the Shillong-Plateau. The high D_c value along the Shillong-Plateau (1.83) is followed by the value 1.80 for the Arakan-Yoma belt, while the lowest value (1.36) is noted for the South-Tibet (Fig. 7; Table 2). The D_c value of seismically dynamic sources ranges between 0 and 2 (Tosi, 1998) and a value close to 2 is a sign of the distribution of events over a two-dimensional fault plane (Yadav et al., 2011; Ghosal et al., 2012). Also, the degree of clustering of earthquakes is inversely proportional to the fractal dimension, that is, a high value is associated with a low clustering and vice versa (Hirata, 1989a; Roy & Padhi, 2007; Roy et al., 2015). Therefore, the region under study, with a fractal dimension 1.36–1.83, shows near-plane characteristics of seismogenic structures, where earthquakes are densely distributed. In particular, the Shillong-Plateau (D_c = 1.83 ± 0.02) and the Arakan-Yoma belt with (D_c = 1.80 ± 0.01) indicate a near-planar nature of seismogenic structures and the D_c value < 1.5 for South-Tibet indicates an active linear fault system in the region (Yadav et al., 2011). Although, the D_c value obtained in the present study are higher than results of earlier workers (0.8 to 1.2) for eastern Himalaya and southern Tibet (Singh et al., 2009) these results agree with the D_c value range (0.37 to 1.81) obtained by Sarkar et al. (2020).

The contour map (Fig. 8) shows both low D_c contours (~1.1) and high D_c contours (~1.9). Comparatively low D_c (1.1–1.5) contours are noted in the South-Tibet region (ST; see Fig. 1) while an intermediate values of D_c contour (1.2–1.6) are seen in the Eastern-Syntaxis region (ES). In addition, D_c contours of a high range from 1.5 to 1.6 are also noted along the Mishimi Thrust (MT) zone in the Eastern-Syntaxis region. High D_c contours (1.8–1.9) are demonstrated in the Himalayan-Frontal Arc region (HFA), and Shillong Plateau region (SP), accommodating underlined faults DCF, DF KF, and DKF (Fig. 8; Table 2). Moreover, high D_c contours (1.6–1.8) are also seen for the Arakan-Yoma belt (AYB). These results indicate the gathering of epicentres around a two-dimensional space. This ultimately reduces the stress-bearing capacity of the rocks, making the

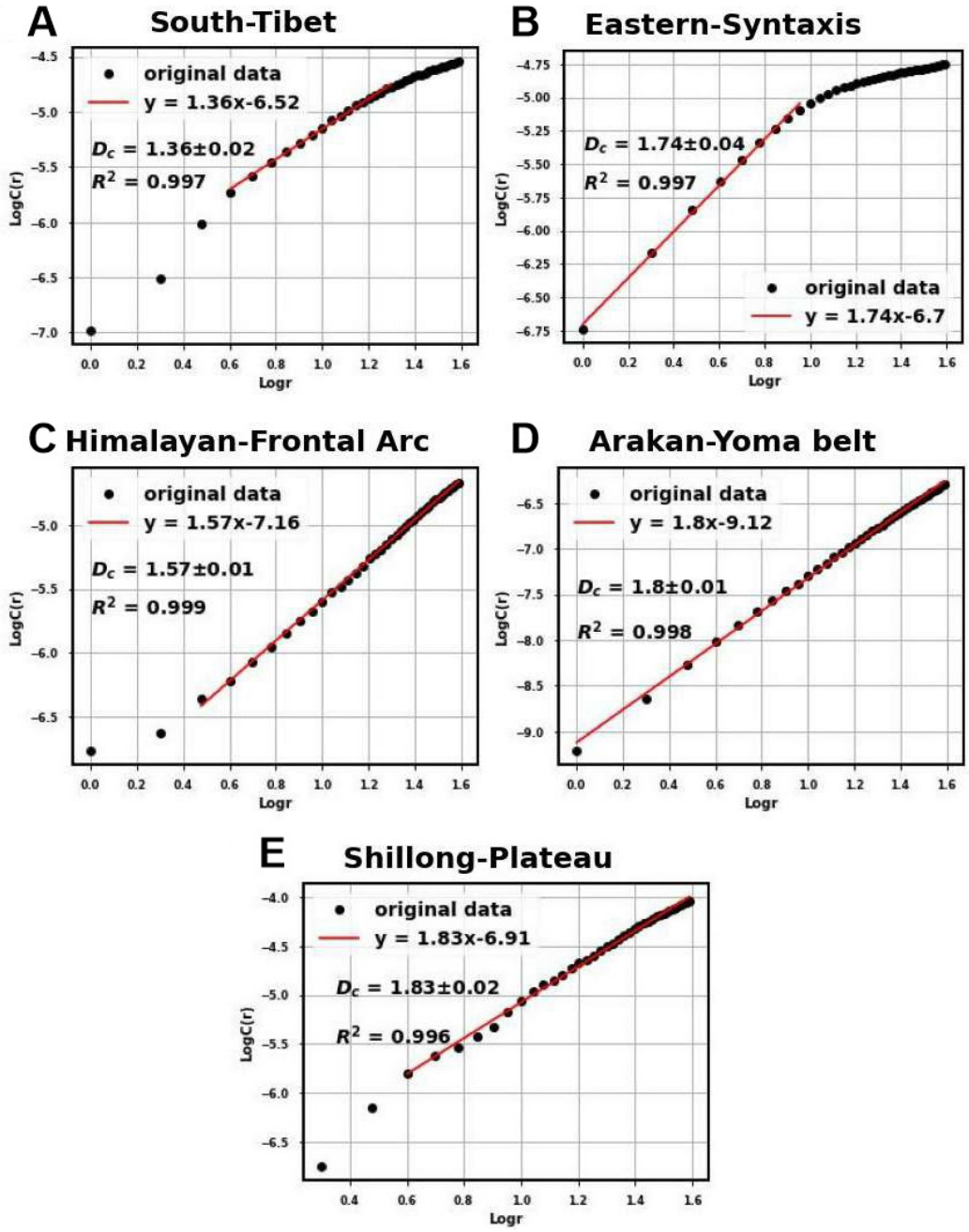

Fig. 7. The plot of LogC(r) *vs* Logr for five selected regions under study. The C in LogC along y-axis is the correlation integral function, while r in Logr along x-axis is the scaling radius. The slope of the linear part of the plot estimates the fractal dimension D_c. For location of the regions see Figure 1.

crustal surface heterogeneous. A heterogeneous crustal structure is responsible for a heterogeneous stress field that makes the region favourable for the growth of a tremor.

The interrelationship between D_c and b-value has been calculated for different regions of the world. A positive co-relationship between them was proposed for intermediate events with $D_c = 2b$ (Aki, 1965), which is supported by studies carried out in the south-eastern Iran-Bam region (Roy & Padhi, 2007) and in İzmit, Turkey (Oncel & Wilson, 2002, 2007). The negative co-relationship reported by Hirata (1989b) between two scaling exponents has also been supported by a study carried out in the north Anatolian fault zone (Öncel et al., 1995, 1996). As far as the present study is concerned, no correlation has been found between D_c and b-value as depicted by the correlation function $D_c = -0.08b + 1.6$ and $R^2 = 0.002$ (Fig. 9).

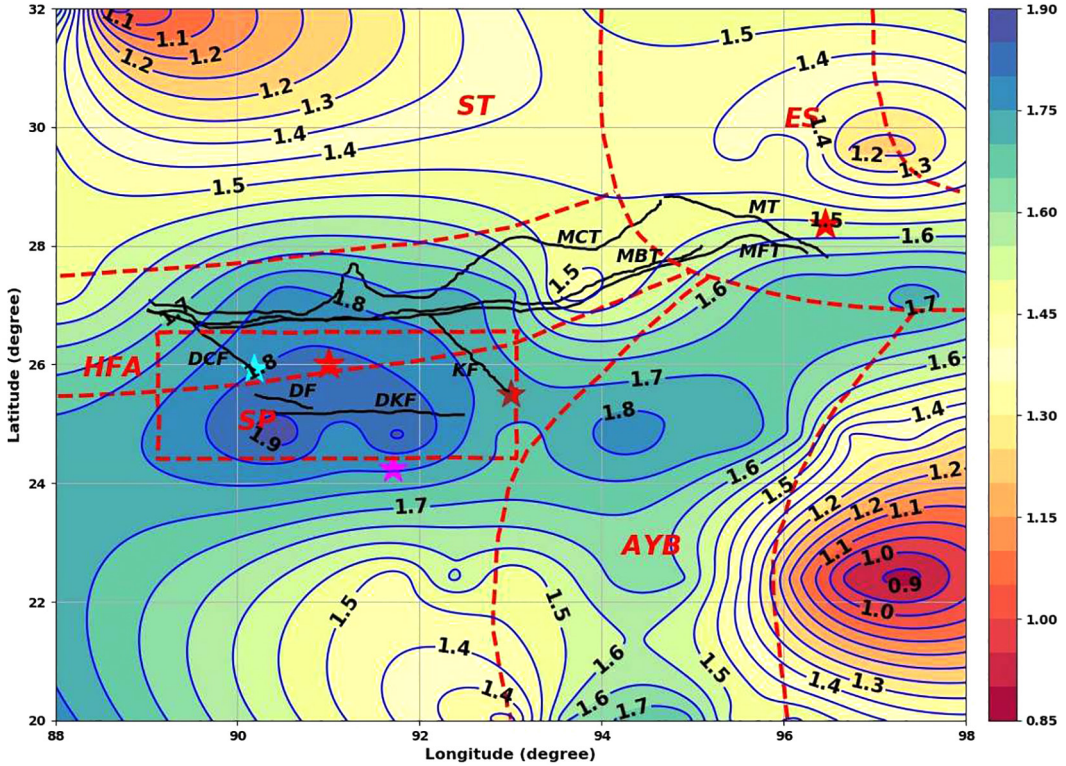

Fig. 8. Spatial fractal dimension (D_c) contour map of the study area. D_c values are plotted for the mean value of longitude and latitude of 2° x 2° square grid with window shifting of 0.5° along the direction of longitude. For detailed explanations and location of the regions see Figure 1.

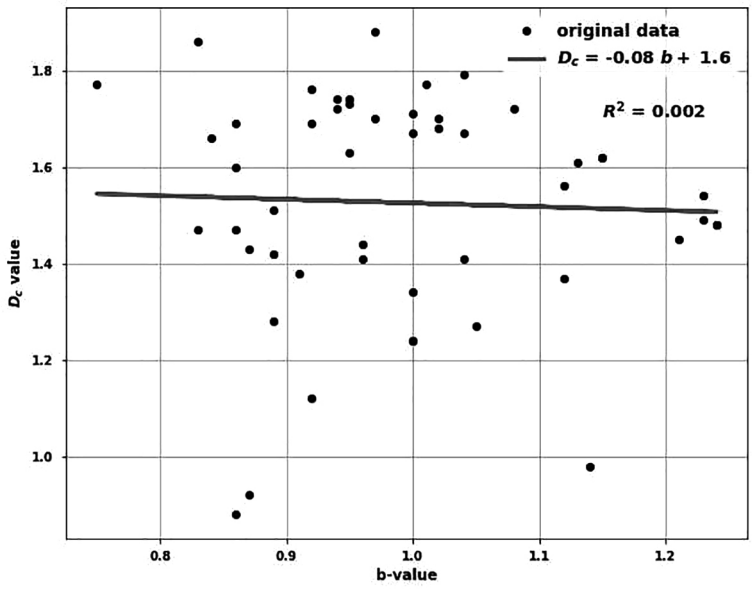

Fig. 9. Correlation between b-value and D_c for the entire study area. The straight line represents the fitted regression line. The b-values and D_c are obtained for 2° × 2° square grid of selected regions. For location of the regions see Figure 1.

5. Conclusions

To assess the level of stress and understand the seismic characteristics of the region between 20–32˚N and 88–98°E, the b-value and fractal correlation dimension (D_c) of seismic event epicentres were estimated. These parameters were obtained for five different regions by analysing the homogeneous database of 1,347 events (mb ≥ 4.5) from January 1964 to May 2020. High D_c (> 1.5), except for the South-Tibet region, and b-values around 1.0 reported for regions considered in the present study suggest a high-stress concentrated locked region that signifies the arbitrary occurrence of mostly strong

earthquakes. The subduction thrust on the Indian plate due to external forces generated by the overriding Burmese plate may be the cause of the greater stress concentration in the region. Therefore, from the present study, we may conclude that:

The regions selected were identified as seismically active with b-values close to 1.0. Relatively low b-value contours (0.8–0.9) are obtained along the Dhubri-Chungthang Fault (DCF) zone, the Dapsi Fault (DF) zone, the Dauki Fault (DKF) zone and the Kopili Fault (KF) zone. These b-values are attributed to the continuous release of strain energy in the region that was accumulated because of northward drifting of the Indian plate towards the Eurasian landmass.

High D_c indicates that the clustering of earthquakes is over a two-dimensional plane and D_c = 1.36 obtained for South-Tibet shows the existence of the active linear fault in the region. Higher D_c contours near the Shillong Plateau are due to the heterogeneous fracture structures along the Dauki, Dapsi and Kopili faults. Likewise, the higher D_c obtained for the Arakan-Yoma belt represents a greater stress concentration because of the interaction between the subducting Indian plate and the superseding Burmese plate. By indexing the b-value and correlation fractal dimension, the present study improves our understanding of the regional features of seismicity, stress level and crustal heterogeneity.

Software resources

The plots were made using Python, Generic Mapping Tools (Wessel et al., 2013) and ZMAP (Wiemer, 2001).

Acknowledgements

The first author wishes to recognise the Tribhuvan University (Nepal) for providing study leave and the University Grants Commission-UGC (Nepal) for providing financial support in the form of a fellowship. Furthermore, both authors are grateful to two anonymous reviewers for their valuable comments.

References

Aki, K., 1965. Maximum likelihood estimate of b in the formula Log N = a - bM and its confidence limits. *Bulletin of Earthquake Research Institute Tokyo University* 43, 237–239.

Akol, B. & Bekler, T., 2013. Assessment of the statistical earthquake hazard parameters for NW Turkey. *Natural Hazards* 68, 837–853.

Angelier, J. & Baruah, S., 2009. Seismotectonics in Northeast India: A stress analysis of focal mechanism solutions of earthquakes and its kinematic implications. *Geophysical Journal International* 178, 303–326.

Aviles, C.A., Scholz, C.H. & Boatwright, J., 1987. Fractal analysis applied to characteristic segments of the San Andreas fault (USA). *Journal of Geophysical Research* 92, 331–344.

Berthet, T., Ritz, J.F., Ferry, M., Pelgay, P., Cattin, R., Drukpa, D., Braucher, R. & Hetényi, G., 2014. Active tectonics of the eastern Himalaya: New constraints from the first tectonic geomorphology study in southern Bhutan. *Geology* 42, 427–430.

Bhattacharya, P.M. & Kayal, J.R., 2003. Mapping the b-value and its correlation with the fractal dimension in the northeast region of India. *Journal of the Geological Society of India* 62, 680–695.

Bhattacharya, P.M., Kayal, J.R., Baruah, S. & Arefiev, S.S., 2010. Earthquake Source Zones in Northeast India: Seismic Tomography, Fractal Dimension and b Value Mapping. *Pure and Applied Geophysics* 167, 999–1012.

Bilham, R., Mencin, D., Bendick, R. & Bürgmann, R., 2017. Implications for elastic energy storage in the Himalaya from the Gorkha 2015 earthquake and other incomplete ruptures of the Main Himalayan Thrust. *Quaternary International* 462, 3–21.

Bondár, I. & Storchak, D., 2011. Improved location procedures at the International Seismological Centre. *Geophysical Journal International* 186, 1220–1244.

Bora, D.K., 2016. Scaling relations of moment magnitude, local magnitude, and duration magnitude for earthquakes originated in northeast India. *Earthquake Science* 29, 153–164.

Bora, D.K. & Baruah, S., 2012. Mapping the crustal thickness in Shillong-Mikir Hills Plateau and its adjoining region of northeastern India using Moho reflected waves. *Journal of Asian Earth Sciences* 48, 83–92.

Bora, D.K., Baruah, S., Biswas, R. & Gogoi, N.K., 2013. Estimation of sourceparameters of local earthquakes originated in Shillong-Mikir plateau and its adjoining region of Northeastern India. *Bulletin of Seismological Society of America* 103, 437–446.

Bora, D.K., Borah, K., Mahanta, R. & Borgohain, J.M., 2018. Seismic b-values and its correlation with seismic moment and Bouguer gravity anomaly over Indo-Burma ranges of northeast India: Tectonic implications. *Tectonophysics* 728–729, 130–141.

Bora, D.K., Mukherjee, P., Singh, A.P., Borah, K. & Biswas, R., 2022a. Source parameters and scaling relations for small to moderate earthquakes in the Indo-Burma Ranges, North-east India, and its seismotectonic implications. *Geological Journal* 57, 863–876.

Bora, D.K., Singh, A.P., Borah, K., Anand, A., Biswas, R. & Mishra, O.P., 2022b. Crustal Structure Beneath the Indo-Burma Ranges from the Teleseismic Receiver Function and Its Implications for Dehydration of the Subducting Indian Slab. *Pure and Applied Geophysics* 179, 197–216.

Borgohain, J.M., Borah, K., Biswas, R. & Bora, D.K., 2018. Seismic b-value anomalies prior to the 3rd January 2016, Mw = 6.7 Manipur earthquake of northeast India. *Journal of Asian Earth Sciences* 154, 42–48.

Cao, A. & Gao, S.S., 2002. Temporal variation of seismic b-values beneath northeastern Japan island arc. *Geophysical Research Letters* 29, 481–483.

Chen, J. & Zhu, S., 2020. Spatial and temporal b-value precursors preceding the 2008 Wenchuan, China, earthquake (Mw = 7.9): implications for earthquake prediction. *Geomatics, Natural Hazards and Risk* 11, 1196–1211.

Dasgupta, S., Mukhopadhyay, B., Mukhopadhyay, M. & Pande, P., 2021. Geo- and seismo- tectonics of Eastern Himalaya: Exploring earthquake source zones from foredeep to Tibetan hinterland. *Physics and Chemistry of the Earth* 123, 103013.

Devi, S., Arora, S., Kumar, P. & Yadov, M., 2021. Strong-Motion Simulation of the 1988 Indo-Burma and Scenario Earthquakes in NE India by Integrating Site Effects in a Semi-Empirical Technique. *Pure and Applied Geophysics* 178, 2839–2854.

Diehl, T., Singer, J., Hetényi, G., Grujic, D., Clinton, J., Giardini, D. & Kissling, E., 2017. Seismotectonics of Bhutan: Evidence for segmentation of the Eastern Himalayas and link to foreland deformation. *Earth and Planetary Science Letters* 471, 54–64.

El-Isa, Z.H. & Eaton, D.W., 2014. Spatiotemporal variations in the b-value of earthquake magnitude-frequency distributions: Classification and causes. *Tectonophysics* 615–616, 1–11.

Ghosal, A., Ghosh, U. & Kayal, J.R., 2012. A detailed b-value and fractal dimension study of the March 1999 Chamoli earthquake (Ms 6.6) aftershock sequence in western Himalaya. *Geomatics, Natural Hazards and Risk* 3, 271–278.

Grassberger, P. & Procaccia, I., 1983. Characterization of strange attractors. *Physical Review Letters* 50, 346–349.

Gutenberg, B. & Richter, C.F., 1944. Frequency of earthquakes in California. *Bulletin of the Seismological Society of America* 34, 185–188.

Hirata, T., 1989a. A correlation between the b value and the fractal dimension of earthquakes. *Journal of Geophysical Research* 94, 7507–7514.

Hirata, T., 1989b. Fractal Dimension of Fault Systemss in Japan: Fractal Structure in Rock Fracture Geometry at Various Scales. *Pure and Applied Geophysics* 131, 157–170.

Ishibe, T., Satake, K., Sakai, S., Shimazaki, K., Tsuruoka, H., Yokota, Y., Nakagawa, S. & Hirata, N., 2015. Correlation between Coulomb stress imparted by the 2011 Tohoku-Oki earthquake and seismicity rate change in Kanto, Japan. *Geophysical Journal International* 201, 112–134.

Islam, M.S., Shinjo, R. & Kayal, J.R., 2011. Pop-up tectonics of the Shillong Plateau in northeastern India: Insight from numerical simulations. *Gondwana Research* 20, 395–404.

Kagan, Y. & Knopoff, L., 1978. Statistical study of the occurrence of shallow earthquakes. *Geophysical Journal of the Royal Astronomical Society* 55, 67–86.

Kayal, J.R., 2010. Himalayan tectonic model and the great earthquakes: An appraisal. *Geomatics, Natural Hazards and Risk* 1, 51–67.

Kayal, J.R., Arefiev, S.S., Baruah, S., Hazarika, D., Gogoi, N., Gautam, J.L., Baruah, S., Dorbath, C. & Tatevossian, R., 2012. Large and great earthquakes in the Shillong plateau-Assam valley area of Northeast India Region: Pop-up and transverse tectonics. *Tectonophysics* 532–535, 186–192.

Kayal, J.R., Arefiev, S.S., Baruah, S., Hazarika, D., Gogoi, N., Kumar, A., Chowdhury, S.N. & Kalita, S., 2006. Shillong plateau earthquakes in northeast India region: Complex tectonic model. *Current Science* 91, 109–114.

Kayal, J.R., Reena, D. & Chakraborty, P.P., 1993. Microearthquakes at the main boundary thrust in Eastern Himalaya and the present-day tectonic model. *Tectonophysics* 218, 375–381.

Khan, P.K. & Chakraborty, P.P., 2007. The seismic b-value and its correlation with Bouguer gravity anomaly over the Shillong Plateau area: Tectonic implications. *Journal of Asian Earth Sciences* 29, 136–147.

Khan, P.K., Ghosh, M., Chakraborty, P.P. & Mukherjee, D., 2011. Seismic b-Value and the assessment of ambient stress in Northeast India. *Pure and Applied Geophysics* 168, 1693–1706.

Khattri, K.M. & Tyagi, A.K., 1983. Seismicity patterns in the Himalayan plate boundary and identification of the areas of high seismic potential. *Tectonophysics* 96, 281–297.

Kumar, S. & Sharma, N., 2019. The seismicity of central and north-east Himalayan region. *Contributions to Geophysics and Geodesy* 49, 265–281.

Legrand, D., 2002. Fractal dimensions of small, intermediate, and large earthquakes. *Bulletin of the Seismological Society of America* 92, 3318–3320.

Liu, J., Ji, C., Zhang, J., Zhang, P., Zeng, L., Li, Z. & Wang, W., 2015. Tectonic setting and general features of coseismic rupture of the 25 April, 2015 Mw 7.8 Gorkha, Nepal earthquake. *Kexue Tongbao/Chinese Science Bulletin* 60, 2640–2658.

Mandelbrot, B.B. & Wheeler, J.A., 1983. The Fractal Geometry of Nature. *American Journal of Physics* 51, 286–287.

Mogi, K., 1967. Earthquakes and fractures. *Tectonophysics* 5, 35–55.

Molnar, P. & Tapponnier, P., 1975. Cenozoic tectonics of Asia: Effects of a continental collision. *Science* 189, 419–426.

Mondal, S.K., Roy, P.N.S., Catherine, J.K. & Pandey, A.K., 2019. Significance of fractal correlation dimension and seismic b-value variation due to 15th July 2009, New Zealand earthquake of mw 7.8. *Annals of Geophysics* 62, 1–17.

Mousavi, S.M., 2017a. Mapping seismic moment and b-value within the continental-collision orogenic-belt region of the Iranian Plateau. *Journal of Geodynamics* 103, 26–41.

Mousavi, S.M., 2017b. Spatial variation in the frequency-magnitude distribution of earthquakes under the tectonic framework in the Middle East. *Journal of Asian Earth Sciences* 147, 193–209.

Nandy, D.R., 2005. Geodynamics and Seismicity of Northeast India and its Adjoining areas. *Special Publication Geological Survey of India* 85, 49–59.

Nandy, D.R. & Dasgupta, S., 1991. Seismotectonic Domains of Northeastern India and Adjacent areas. *Physics and Chemistry of the Earth* 18, 371–384.

Nava, F.A., Márquez-Ramírez, V.H., Zúñiga, F.R. & Lomnitz, C., 2017. Gutenberg–Richter b-value determination and large-magnitudes sampling. *Natural Hazards* 87, 1–11.

Nerenberg, M.A.H. & Essex, C., 1990. Correlation dimension and systematic geometric effects. *Physical Review A* 42, 7065–7074.

Oncel, A.O. & Wilson, T., 2002. Space-time correlations of seismotectonic parameters: Examples from Japan and from Turkey preceding the İzmit earthquake. *Bulletin of the Seismological Society of America* 92, 339–349.

Oncel, A.O. & Wilson, T., 2007. Anomalous seismicity preceding the 1999 Izmit event, NW Turkey. *Geophysical Journal International* 169, 259–270.

Öncel, A.O., Alptekin, Ö. & Main, I., 1995. Temporal variations of the fractal properties of seismicity in the western part of the north anatolian fault zone: Possible artifacts due to improvements in station coverage. *Nonlinear Processes in Geophysics* 2, 147–157.

Öncel, A.O., Main, I., Alptekin, Ö. & Cowie, P., 1996. Spatial variations of the fractal properties of seismicity in the Anatolian fault zones. *Tectonophysics* 257, 189–202.

Pailoplee, S. & Choowong, M., 2014. Earthquake frequency-magnitude distribution and fractal dimension in mainland Southeast Asia. *Earth, Planets and Space* 66, 1–10.

Panthi, A., Singh, H.N. & Shanker, D., 2013. Revisiting State of Stress and Geodynamic Processes in Northeast India Himalaya and Its Adjoining Region. *Geosciences* 3, 143–152.

Pudi, R., Martha, T.R., Kumar, K.V., Ramesh, P., Martha, T.R. & Kumar, K.V., 2020. Regional variation of stress level in the Himalayas after the 25 April 2015 Gorkha earthquake (Nepal) estimated using b-values. *Journal of Geophysics and Engineering* 15, 921–927.

Raghu Kanth, S.T.G. & Dash, S.K., 2010. Deterministic seismic scenarios for North East India. *Journal of Seismology* 14, 143–167.

Reasenberg, P., 1985. Second-order moment of central California seismicity, 1969-1982. *Journal of Geophysical Research: Solid Earth* 90, 5479–5495.

Roy, P.N.S. & Padhi, A., 2007. Multifractal analysis of earthquakes in the Southeastern Iran-Bam Region. *Pure and Applied Geophysics* 164, 2271–2290.

Roy, P.N.S., Chowdhury, S., Sarkar, P. & Mondal, S.K., 2015. Fractal study of seismicity in order to characterize the various tectonic blocks of North-east Himalaya, India. *Natural Hazards* 77, S5–S18.

Sarkar, P., Roy, P.N.S. & Pal, S.K., 2020. Rejuvenation of 'pop-up' tectonics for Shillong Plateau in NE Himalayan region. *Journal of Earth System Science* 129, 123.

Scholz, C.H., 1968. The frequency-magnitude relation of microfracturing in rock and its relation to earthquakes. *Bulletin of the Seismological Society of America* 58, 399–415.

Scholz, C.H., 2015. On the stress dependence of the earthquake b value. *Geophysical Research Letters* 42, 1399–1402.

Shi, Y. & Bolt, A.B., 1982. The standard error of the magnitude-frequency b value. *Bulletin of the Seismological Society of America* 72, 1677–1687.

Singh, C., Singh, A. & Chadha, R.K., 2009. Fractal and b-value mapping in eastern Himalaya and southern Tibet. *Bulletin of the Seismological Society of America* 99, 3529–3533.

Storchak, D.A., Harris, J., Brown, L., Lieser, K., Shumba, B. & Di Giacomo, D., 2020. Rebuild of the Bulletin of the International Seismological Centre (ISC) – part 2: 1980–2010. *Geoscience Letters* 7, 1980–2010.

Storchak, D.A., Harris, J., Brown, L., Lieser, K., Shumba, B., Verney, R., Di Giacomo, D. & Korger, E.I.M., 2017. Rebuild of the Bulletin of the International Seismological Centre (ISC). *Geoscience Letters* 4, 1964–1979.

Tandon, S.K. & Gupta, N., 2020. Introduction to geodynamics of the indian plate: Evolutionary perspectives. In: N. Gupta & S. Tandon (Eds): *Geodynamics of the Indian Plate. Springer Geology*. Springer, Cham. https://doi.org/10.1007/978-3-030-15989-4_1

Thingbaijam, K.K.S., Nath, S.K., Yadav, A., Raj, A., Walling, M.Y. & Mohanty, W.K., 2008. Recent seismicity in Northeast India and its adjoining region. *Journal of Seismology* 12, 107–123.

Tosi, P., 1998. Seismogenic structure behaviour revealed by spatial clustering of seismicity in the Umbria-Marche Region (Central Italy). *Annals of Geophysics* 41, 215–224.

Turcotte, D.L., 1989. Fractals in geology and Geophysics. *Pure and Applied Geophysics* 131, 171–196.

Verma, R.K., Mukhopadhyay, M. & Ahluwalia, M.S., 1976. Earthquake mechanisms and tectonic features of Northern Burma. *Tectonophysics* 32, 387–399.

Wessel, P., Smith, W.H.F., Scharroo, R., Luis, J. & Wobbe, F., 2013. Generic mapping tools: Improved version released. *Eos* 94, 409–410.

Wiemer, S., 2001. A software package to analyze seismicity: ZMAP. *Seismological Research Letters* 72, 373–382.

Wiemer, S. & Wyss, M., 1997. Mapping the frequency-magnitude distribution in asperities: An improved technique to calculate recurrence times? *Journal of Geophysical Research: Solid Earth* 102, 15115–15128.

Wiemer, S. & Wyss, M., 2000. Minimum magnitude of completeness in earthquake catalogs: Examples from Alaska, the Western United States, and Japan. *Bulletin of the Seismological Society of America* 90, 859–869.

Woessner, J., 2005. Assessing the Quality of Earthquake Catalogues: Estimating the Magnitude of Completeness and Its Uncertainty. *Bulletin of the Seismological Society of America* 95, 684–698.

Wu, H.Y., Liu, H.F., Xu, W.J. & Wang, X., 2017. Fractal dimension and b value of the aftershock sequence of the 2008 Ms 8.0 wenchuan earthquake. *Natural Hazards* 88, 315–325.

Wyss, M., Sammis, C.G., Nadeau, R.M. & Wiemer, S., 2004. Fractal dimension and b-value on creeping and locked patches of the San Andreas fault near Park-

field, California. *Bulletin of the Seismological Society of America* 94, 410–421.

Yadav, R.B.S., Tripathi, J.N., Shanker, D., Rastogi, B.K., Das, M.C. & Kumar, V., 2011. Probabilities for the occurrences of medium to large earthquakes in northeast India and adjoining region. *Natural Hazards* 56, 145–167.

Zhang, J., Santosh, M., Wang, X., Guo, L., Yang, X. & Zhang, B., 2012. Tectonics of the northern Himalaya since the India-Asia collision. *Gondwana Research* 21, 939–960.

Zhao, Y.Z. & Wu, Z.L., 2008. Mapping the -values along the Longmenshan fault zone before and after the 12 May 2008, Wenchuan, China, MS 8.0 earthquake. *Natural Hazards and Earth System Sciences* 8, 1375–1385.

Manuscript submitted: 23 March 2022
Revision accepted: 19 July 2022

Indian Geotech J
https://doi.org/10.1007/s40098-022-00704-1

ORIGINAL PAPER

Fractal Characteristics of the Seismic Swarm Succeeding the 2015 Gorkha Earthquake, Nepal

Ram Krishna Tiwari[1,2] · **Harihar Paudyal**[2]

Received: 24 August 2022 / Accepted: 21 December 2022

Abstract This study discusses the regional distribution of the b-value, box counting fractal dimension (D_0) and correlation fractal dimension (D_2) of the 2017–2019 seismic swarm. The location of swarm was about 30 km north of the epicenter of 2015 Gorkha earthquakes in high topography of the Manaslu-Himalchuli range. The b-values are estimated from the maximum likelihood approach, while fractal dimensions are estimated from the generalized fractal dimension approach. The b-value estimated was 1.82 ± 0.02 for the swarm sequence, while its maximum value was 2.97 ± 0.14 and minimum value was 1.81 ± 0.07 for different temporal windows. D_0 values range from 0.55 ± 0.02 to 1.68 ± 0.08 for different temporal windows and correlation fractal dimension ranges from 0.27 ± 0.07 to 0.78 ± 0.02 for the same windows. Positive correlation between fractal dimensions D_0 and D_2 and a negative correlation between fractal dimensions and b-value were observed from the study. The seismic moment released during the 2017–2019 swarm was around 2.0×10^{17} Nm. The large b-value (1.82) obtained for the whole sequence signifies the typical characteristic of swarm earthquakes. The variation in b and fractal dimensions can be related to the highly heterogeneous environment caused by the thermal cracking of the weak zone. Furthermore, reduced value of effective stress might have caused the failure of isolated and small asperities and consequently the earthquakes occurred in clusters. The occurrence of swarms may be associated with the formation of new fractures in the region.

Keywords Swarm activity · Temporal variation · b-value · Fractal dimension · Positive and negative correlation

Introduction

Earthquake sequences not having clear triggering mainshock are referred to as earthquake swarms and better stated in volcanic and hydrothermal areas [1, 2]. Another category of swarms associated with active tectonic regions and coinciding with aseismic slip is tectonic earthquake swarms which sometimes occur preceding the more damaging earthquakes [3, 4]. Swarm earthquakes are seen along the active faults that undergo slip at a very slow rate in contrast to the tectonic earthquakes that occur on active faults having faster slip rate [5, 6]. Swarms can occur beyond the aftershocks zone, in and around the rupture zone as a stress adjustment mechanism after the regional and local events and due to the passage of the seismic waves from large distant earthquakes [3, 7]. Such swarms may help to diagnose the stress conditions of the seismogenic crust and fluid diffusion in the crust [8].

Nepal lies at the center of 2500 km seismically active Himalayan zone where convergence rate of India-Eurasia plate is about 20 mm per year [9, 10]. The seismicity of the Himalaya is mainly focused along a north dipping detachment separating the downgoing Indian plate from the overriding Himalayan wedge surface known as the Main Himalayan Thrust (MHT). According to the theory of plate tectonics, the Indian plate underthrusts the Eurasian plate along MHT [11]. Recently on April 25, 2015, the block

✉ Ram Krishna Tiwari
ram.tiwari@bimc.tu.edu.np

[1] Central Department of Physics, Tribhuvan University, Kirtipur, Kathmandu, Nepal

[2] Birendra Multiple Campus, Tribhuvan University, Bharatpur, Chitwan, Nepal

Published online: 14 January 2023

below the MHT slipped to the north beneath Tibet and the upper block moves to the south that triggered massive earthquake in the Gorkha District of Nepal, known as Gorkha earthquake [12–17]. Succeeding the Gorkha earthquake in the summer of 2017, an intense swarm was recorded outside the aftershock zone of the Gorkha earthquake under the very high topography of the Manaslu-Himalchuli range [18]. The swarm was confined within a northward dipping steep area about 30 km north of the epicenter of Gorkha earthquake (Fig. 1). The area covered by the swarms is situated at the northeastern edge of a large MHT segment with the distribution of thermal springs and fumaroles and has not ruptured since the fourteenth century [19], so the occurrence of the swarm is a major worry.

The study of earthquake swarm has given considerable attention in various parts of the world as found in the literature. The study form Japan shows the association of swarms with the aseismic slip before the 2011 Mw 9.0 Tohoku and 2014 Mw 8.2 Iquique earthquakes [20–22]. From the three-dimensional mapping of fractal correlation dimensions and b-values of Palghar (Maharashtra) and Pulichintala (Andhra Pradesh), India swarm sequences, the Pulichintala region is identified as less earthquake hazard region compared to the Palghar region [23]. From the study of seismicity pattern of swarm occurred in South Gujarat, India, the swarm activity was identified as the consequence of hydro seismicity [24]. Similarly, from the study of the earthquake swarm that occurred in 2000 in Vogtland (northeast Bohemia, Central Europe), an increase in pore pressure was identified as the main cause of the swarm [3]. From the study, it was inferred that the patterns of anomalous seismicity (earthquake swarms) may be considered as an important parameter for the forecasting of long range earthquake hazards in the Nepal Himalaya [25].

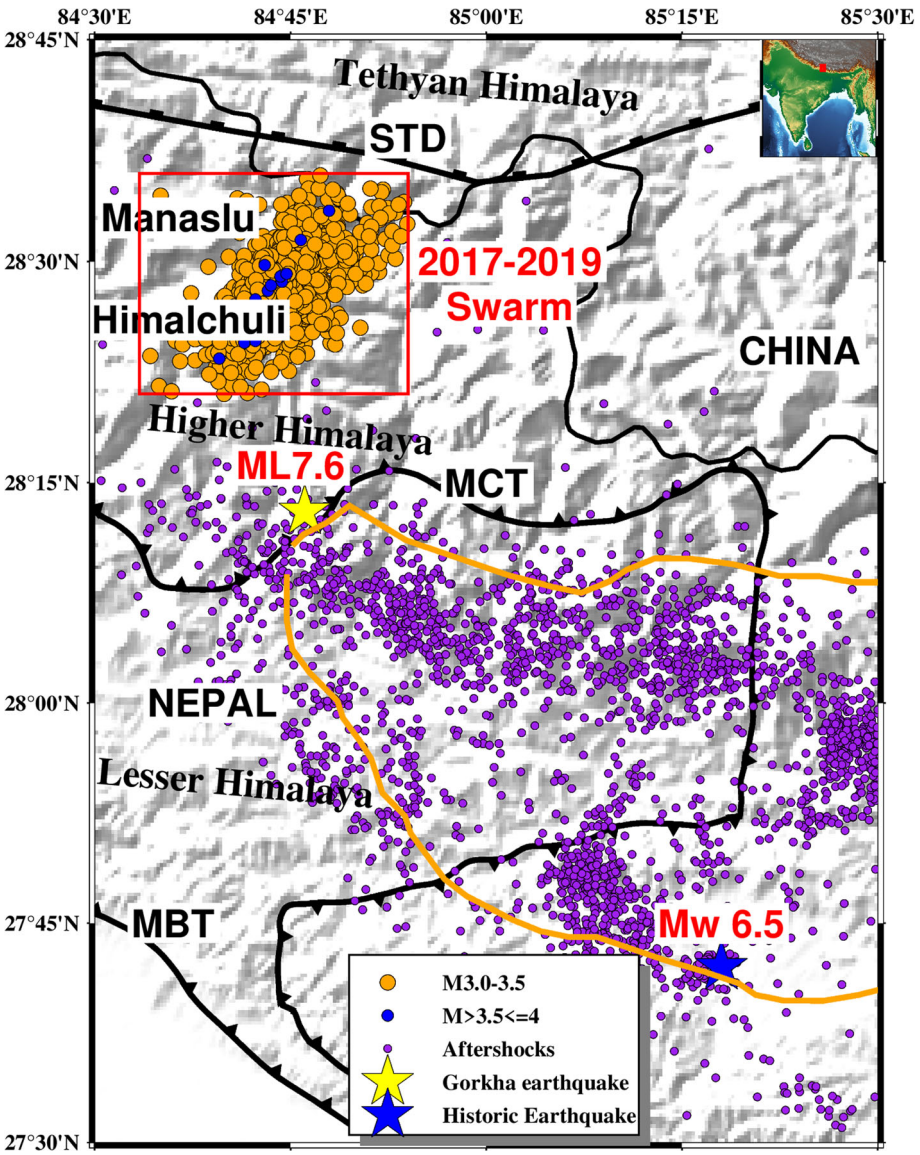

Fig. 1 Location map showing epicenters of earthquakes used in this study (2906 events depicted by orange and blue circles) and epicenters of aftershocks of Gorkha earthquakes (Purple circles) [33, 34]. Yellow star stands for ML 7.6 mainshock of Gorkha earthquake 2015, and blue star is for magnitude 6.5 Mw historical earthquake of 1808 [35]. Orange contour represents the rupture area of mainshock of Gorkha earthquake [13]. The red box at upper left corner shows 2017–2019 swarms, and the red box in the inset map (upper right) shows the study area

In a study, swarm at the foot of the Himalchuli summit initiated in August 2017 reveals tangled localized interaction between orogenic collapse and stress adjustments [18]. Under the hypothesis that the prime causes of most of the earthquakes swarm are the stress changes in the shallow and brittle crustal due to magmatic intrusions, tectonic faulting, or hydrothermal cooling [26, 27], the present paper explains the fractal nature of the swarm activities occurring between 2017 and 2019 near MCT which probably help to demarcate the zone for future earthquakes.

Tectonic Structure of the Study Area

The Himalaya, lying at the northern margin of the Indian continent, is a wedge-shaped structure formed by folding and thrusting mechanism on the under-thrusting Indian plate and overlying Himalayan mass. The formation process started between 40 and 50 million years ago and still continuing [28, 29]. It consists of three thrust-bounded litho-tectonic units and the overlying Tethys Himalaya from south to north. The Main Frontal Thrust (MFT) is the boundary between the sub-Himalaya and Indo Gangetic plain, the sub-Himalaya and the lesser Himalaya are separated by the Main Boundary Thrust (MBT), the lesser Himalaya and the higher Himalaya are separated by the Main Central Thrust (MCT), and the higher Himalaya and Tethys Himalaya are separated by the South Tibet Detachment (STD) [30]. The MFT, MBT, and MCT are the splays off an underlying sub-horizontal decollement the Main Himalaya Thrust (MHT) [13, 16]. Among these thrusts, MCT zone has played a significant role in Himalayan tectonics. It is one of the key high strain zones in Himalaya having an intense shearing capacity and neotectonic movements. It accommodates at least 90 km of shortening which exhumed and buried hanging wall and footwall rocks due to geometric and kinematic association between the MCT and the structurally overlying STD [31, 32].

Data and Methodology

More than 31,000 aftershocks of the Gorkha earthquake were identified out of 43,000 earthquakes recorded by National Seismic Centre (NSC) network (www.seismonepal.gov.np) and local networks in Nepal between April 2015 and April 2020 [18]. From the same networks, an intense seismic swarm (6756 seismic events) was recorded within 30 km north from the Gorkha mainshock epicenter mainly in 2017 and with lower intensity in 2018 [17, 36, 37] (Fig. 2). The relations between magnitude of the earthquakes and their depth of occurrence are

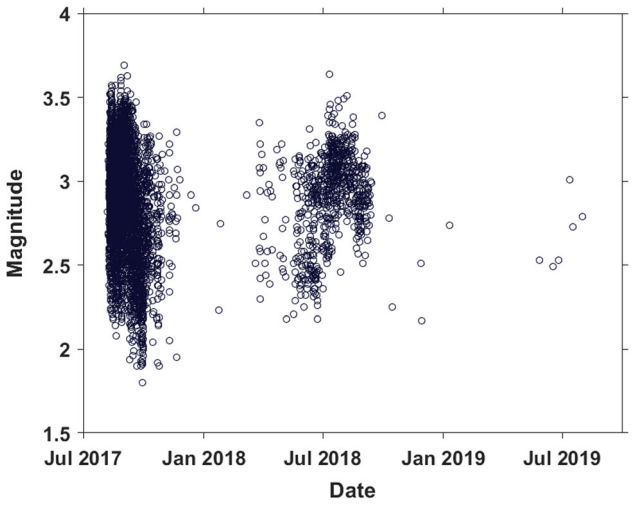

Fig. 2 Temporal variations of the magnitude of the earthquake swarms showing two clustered first in August 2017 and second between April and July 2018. The swarms contain events with minimum magnitude 1.8 to maximum magnitude 3.69 in local scale

depicted in Fig. 3. We determined the magnitude of completeness (MC) by the maximum curvature technique in the ZMAP software [38], and accordingly, the further analysis was limited to the catalog of 2906 events with magnitude ML $>$ = 3.0 (Fig. 4). In this study, we adopt the fixed number of events (200) method and the window is shifted throughout the dataset for the reliable estimation of b-value, D_0 and D_2 [39].

The magnitude versus depth plot (Fig. 3) shows that there is no effect of the change in the depth of hypocenter on the magnitude of the swarms.

The fractal dimensions and b-values have fundamental importance in understanding the characteristic of the source zone and the seismogenic active fault [40–43]. Fractal dimension of earthquakes quantity the clustering of events and material heterogeneity [44, 45]. The b-values

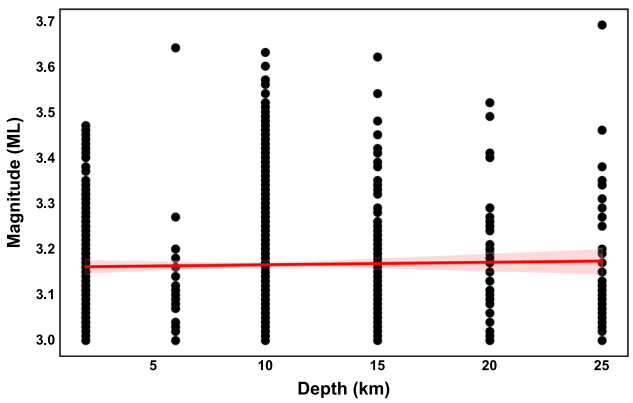

Fig. 3 The linear regression plot between magnitude and depth shows that the magnitude of the earthquakes is independent of the focal depth. The red line is the regression line and shaded area is the confidence interval of regression estimates

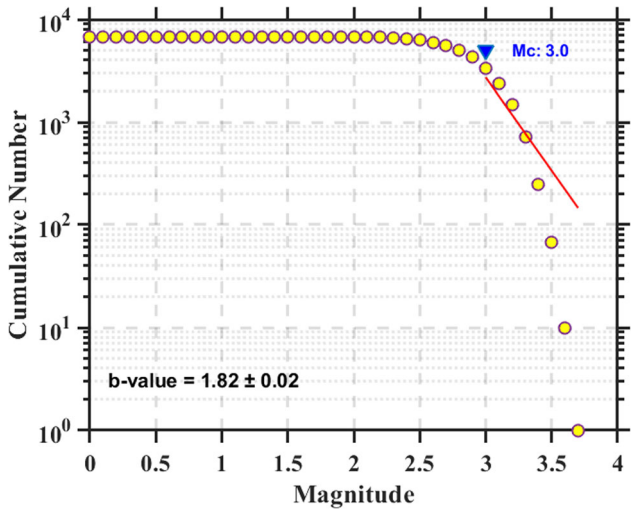

Fig. 4 b-value and magnitude of completeness (Mc) of the earthquake data set

correlate with material properties, degree of stress concentration, stress level changes, and pore-fluid pressure, etc. [46]. Here, we have estimated fractal dimension (D_0 and D_2) as the cases of the generalized fractal dimension D_q[47] and the b-values from maximum likelihood methods [48–50]

Gutenberg-Richter (G-R) Law

A empirical G-R law [51] connecting the frequency of occurrence of the earthquakes with associated magnitudes is the function of the total number of earthquakes (N) with magnitude $\geq$ m, intercept (a) and the slope of the straight line (b) in the semi log plot and written as

$$\log_{10} N = a - bm$$

The y intercept of above equation (a-value) depends on the area and temporal window of consideration and describes the productivity, while the slope (b-value) describes the relative size distribution of earthquakes. The b-value is high in the area having high geothermal activities [52], area with the increased value of pore pressure [53], high thermal stresses [54, 55], and an increased value of shallow crustal heterogeneities [56]. Although the average value of b is found close to unity for seismically active areas [57–59], the b-value variation in wide range from 0.3 to 2.5 has also been reported in the literature [60–63]. For natural seismicity, the b-values estimated are less than 2 [55, 64], whereas for the induced type of seismicity, its value up to 3 is estimated [65, 66]. In the region having b-value equal to 1, the frequency of earthquakes with magnitude 2 is 10 times the frequency of the earthquakes with magnitude 3. If b-value is less than 1, then high-magnitude earthquakes occur in the region, and if b-value is greater than 1, then small magnitude earthquakes occur [67]. This makes the b-value the key parameter for the estimation of the seismic hazard. The cause of the variability of b-value may be stress state, crustal heterogeneity, pore pressure, tectonic setting, geothermal gradient, etc. The studies suggest that swarms and high b-values are associated with heterogeneous materials and structures [68, 69]. The creeping sections of faults have high b-values, while asperities present in the faults show a low b-value [70–73]. The b-value increases for isolated asperities and decreases for interconnected asperities [55, 63].

The b-value is estimated by the formula

$$b = \frac{1}{M_{mean} - M_{min}} \log e$$

where M_{mean} denotes the mean magnitude and $M_{min} = Mc - \frac{\Delta m}{2}$ is the correction on magnitude of completeness [74]. The certainty limit of this approximation is given by the relation [75].

$$\sigma(b) = 2.3 \times b^2 \sqrt{\frac{\sum_{i=1}^{n} (M_i - M_{mean})^2}{n(n-1)}}$$

where n is the number of events considered.

Fractal Dimension

The generalized correlation integral $C_q(r)$ discovers the section of couples of earthquakes (i, j) which are partitioned by the distance less than r [47] and defined as

$$C_q(r) = \left[\frac{1}{N_p} \sum_{i=1}^{N_p} \left[\frac{1}{N_p - 1} \sum_{j=1, i \neq j}^{N_p} H\left(r - \left|x_i - x_j\right|\right) \right]^{q-1} \right]^{\frac{1}{q-1}}$$

In the above equation, $H\left(r - \left|x_i - x_j\right|\right) = \begin{cases} 1, if \left|x_i - x_j\right| \leq r \\ 0, if \left|x_i - x_j\right| > r \end{cases}$ is the Heaviside step or unit step function, r is the scaling radius, $\left|x_i - x_j\right|$ is the distance between two points x_i and x_j, and N_p is the total number of earthquakes within the sample taken. The generalized dimension (D_q) can be obtained as the gradient of the linear portion of the plot between $\log r$ and $\log\left(C_q(r)\right)$ for $r \to 0$ for every value of q

$$D_q = \lim_{r \to 0} \frac{1}{q-1} \frac{\log C_q(r)}{\log r}$$

For q = 0, the formula above gives a box counting dimension and is equivalent to a capacity dimension mathematically. D_0 value quantifies the geometrical pattern

Table 1 Characteristics of the data showing event window, region covered by the events, time duration, magnitude of completeness (Mc = 3.1), b-value, a-value, box counting fractal dimension (D_0), correlation fractal dimension (D_2) and respective coefficient of determination (R^2)

SN	Event window	Region	Time duration	b-value	a-value	D_0	R^2	D_2	R^2
1	0–200	84.664–84.864 28.351–28.593	2017.08.08–2017.08.13	2.20 ± 0.11	8.937	1.14 ± 0.03	0.97	0.66 ± 0.01	0.98
2	20–220	84.81–84.663 28.351–28.593	2017.08.10–2017.08.13	2.16 ± 0.10	8.812	1.14 ± 0.03	0.97	0.65 ± 0.01	0.98
3	40–240	84.663–84.81 28.379–28.593	2017.08.10–2017.08.13	2.04 ± 0.10	8.441	1.00 ± 0.03	0.97	0.59 ± 0.01	0.97
4	60–260	84.41–84.663 28.379–28.593	2017.08.11–2017.08.13	1.97 ± 0.09	8.223	0.95 ± 0.03	0.95	0.51 ± 0.02	0.96
5	80–280	84.663–84.81 28.379–28.593	2017.08.11–2017.08.13	1.91 ± 0.08	8.058	0.93 ± 0.03	0.95	0.50 ± 0.02	0.96
6	100–300	84.81–84.663 28.379–28.582	2017.08.12–2017.08.13	1.89 ± 0.08	8.011	0.81 ± 0.03	0.95	0.50 ± 0.02	0.96
7	120–320	84.663–84.81 28.404–28.582	2017.08.12–2017.08.13	1.93 ± 0.08	8.134	0.78 ± 0.03	0.94	0.47 ± 0.02	0.95
8	140–340	84.663–84.81 28.404–28.582	2017.08.12–2017.08.13	1.88 ± 0.08	7.992	0.77 ± 0.03	0.95	0.49 ± 0.02	0.96
9	160–360	84.663–84.81 28.404–28.582	2017.08.12–2017.08.14	1.82 ± 0.07	7.799	0.78 ± 0.03	0.94	0.49 ± 0.02	0.95
10	180–380	84.66–84.835 28.404–28.582	2017.08.12–2017.08.14	1.84 ± 0.07	7.872	0.77 ± 0.03	0.94	0.48 ± 0.02	0.95
11	200–400	84.66–84.835 28.399–28.582	2017.08.13–2017.08.14	1.79 ± 0.07	7.712	0.76 ± 0.03	0.93	0.45 ± 0.02	0.94
12	220–420	84.66–84.835 28.399–28.546	2017.08.13–2017.08.14	1.81 ± 0.07	7.759	0.59 ± 0.03	0.91	0.41 ± 0.02	0.93
13	240–440	84.66–84.835 28.399–28.546	2017.08.13–2017.08.14	1.85 ± 0.07	7.898	0.57 ± 0.03	0.91	0.41 ± 0.02	0.93
14	260–460	84.66–84.835 28.399–28.546	2017.08.13–2017.08.14	1.89 ± 0.07	8.024	0.58 ± 0.02	0.93	0.44 ± 0.02	0.94
15	280–480	84.66–84.835 28.376–28.554	2017.08.13–2017.08.15	1.99 ± 0.07	8.329	0.88 ± 0.04	0.90	0.45 ± 0.02	0.94
16	300–500	84.655–84.835 28.376–28.554	2017.08.13–2017.08.15	2.00 ± 0.08	8.341	0.93 ± 0.04	0.91	0.48 ± 0.02	0.95
17	320–520	84.655–84.835 28.355–28.554	2017.08.13–2017.08.15	2.01 ± 0.08	8.400	0.87 ± 0.03	0.92	0.49 ± 0.02	0.95
18	340–540	84.655–84.835 28.355–28.554	2017.08.13–2017.08.15	2.04 ± 0.08	8.489	0.88 ± 0.04	0.92	0.50 ± 0.02	0.95
19	360–560	84.835–84.655 28.355–28.554	2017.08.14–2017.08.15	2.18 ± 0.09	8.897	0.89 ± 0.04	0.92	0.49 ± 0.02	0.95
20	380–580	84.655–84.819 28.355–28.554	2017.08.14–2017.08.16	2.27 ± 0.10	9.179	0.86 ± 0.04	0.92	0.48 ± 0.02	0.95
21	400–600	84.655–84.819 28.355–28.554	2017.08.14–2017.08.16	2.37 ± 0.10	9.518	0.84 ± 0.04	0.92	0.48 ± 0.02	0.95
22	420–620	84.655–84.868 28.355–28.581	2017.08.14–2017.08.17	2.41 ± 0.10	9.605	1.24 ± 0.04	0.92	0.49 ± 0.02	0.96
23	440–640	84.655–84.868 28.355–28.581	2017.08.14–2017.08.17	2.51 ± 0.10	9.916	1.24 ± 0.04	0.96	0.54 ± 0.01	0.97
24	460–660	84.655–84.868 28.355–28.581	2017.08.14–2017.08.17	2.56 ± 0.10	10.062	1.23 ± 0.04	0.96	0.52 ± 0.02	0.97

Table 1 continued

SN	Event window	Region	Time duration	b-value	a-value	D_0	R^2	D_2	R^2
25	480–680	84.655–84.868 28.355–28.581	2017.08.15–2017.08.17	2.53 ± 0.10	9.960	0.76 ± 0.02	0.98	0.52 ± 0.02	0.96
26	500–700	84.668–84.868 28.355–28.581	2017.08.15–2017.08.17	2.57 ± 0.10	10.091	0.73 ± 0.02	0.98	0.50 ± 0.02	0.95
27	520–720	84.668–84.868 28.377–28.581	2017.08.15–2017.08.17	2.59 ± 0.11	10.133	0.73 ± 0.02	0.98	0.49 ± 0.02	0.95
28	540–740	84.668–84.868 28.377–28.581	2017.08.15–2017.08.18	2.56 ± 0.10	10.033	0.96 ± 0.02	0.99	0.50 ± 0.02	0.95
29	560–760	84.571–84.868 28.377–28.581	2017.08.15–2017.08.18	2.55 ± 0.10	9.990	0.99 ± 0.02	0.99	0.51 ± 0.02	0.95
30	580–780	84.571–84.868 28.377–28.581	2017.08.16–2017.08.18	2.53 ± 0.10	9.933	1.22 ± 0.03	0.97	0.54 ± 0.02	0.96
31	600–800	84.571–84.868 28.377–28.581	2017.08.16–2017.08.18	2.44 ± 0.10	9.656	1.18 ± 0.03	0.97	0.51 ± 0.02	0.96
32	620–820	84.571–84.863 28.378–28.553	2017.08.17–2017.08.19	2.34 ± 0.09	9.353	1.28 ± 0.07	0.89	0.50 ± 0.02	0.96
33	640–840	84.571–84.863 28.378–28.553	2017.08.17–2017.08.19	2.30 ± 0.09	9.225	1.28 ± 0.08	0.86	0.43 ± 0.02	0.94
34	660–860	84.571–84.863 28.378–28.553	2017.08.17–2017.08.19	2.28 ± 0.09	9.174	1.30 ± 0.08	0.86	0.40 ± 0.01	0.94
35	680–880	84.571–84.863 28.378–28.553	2017.08.17–2017.08.19	2.22 ± 0.08	8.980	1.00 ± 0.05	0.90	0.40 ± 0.01	0.94
36	700–900	84.571–84.863 28.378–28.553	2017.08.17–2017.08.20	2.22 ± 0.08	8.961	1.01 ± 0.05	0.90	0.36 ± 0.01	0.95
37	720–920	84.571–84.863 28.378–28.553	2017.08.18–2017.08.20	2.22 ± 0.08	8.958	1.38 ± 0.09	0.85	0.37 ± 0.01	0.95
38	740–940	84.571–84.826 28.378–28.553	2017.08.18–2017.08.20	2.27 ± 0.09	9.105	0.97 ± 0.05	0.91	0.36 ± 0.01	0.94
39	760–960	84.593–84.826 28.389–28.553	2017.08.18–2017.08.20	2.25 ± 0.09	9.037	0.91 ± 0.05	0.90	0.33 ± 0.01	0.94
40	780–980	84.637–84.826 28.389–28.553	2017.08.18–2017.08.21	2.23 ± 0.09	8.982	1.03 ± 0.05	0.89	0.28 ± 0.01	0.92
41	800–1000	84.637–84.826 28.389–28.553	2017.08.18–2017.08.21	2.34 ± 0.09	9.313	1.03 ± 0.05	0.89	0.27 ± 0.01	0.92
42	820–1020	84.637–84.806 28.389–28.57	2017.08.19–2017.08.21	2.37 ± 0.10	9.390	1.11 ± 0.05	0.91	0.32 ± 0.01	0.93
43	840–1040	84.637–84.806 28.389–28.57	2017.08.19–2017.08.21	2.39 ± 0.10	9.451	0.86 ± 0.07	0.94	0.37 ± 0.01	0.95
44	860–1060	84.645–84.806 28.389–28.57	2017.08.19–2017.08.22	2.41 ± 0.10	9.508	0.88 ± 0.03	0.94	0.37 ± 0.01	0.94
45	880–1080	84.645–84.855 28.402–28.57	2017.08.19–2017.08.22	2.47 ± 0.10	9.704	0.89 ± 0.04	0.92	0.43 ± 0.02	0.94
46	900–1100	84.645–84.855 28.394–28.57	2017.08.20–2017.08.22	2.45 ± 0.10	9.657	0.84 ± 0.04	0.92	0.47 ± 0.02	0.94
47	920–1120	84.645–84.855 28.394–28.57	2017.08.20–2017.08.22	2.44 ± 0.10	9.636	0.81 ± 0.03	0.93	0.47 ± 0.02	0.94
48	940–1140	84.645–84.855 28.394–28.57	2017.08.20–2017.08.23	2.40 ± 0.10	9.523	0.73 ± 0.03	0.91	0.41 ± 0.02	0.93

Table 1 continued

SN	Event window	Region	Time duration	b-value	a-value	D_0	R^2	D_2	R^2
49	960–1160	84.645–84.855 28.394–28.57	2017.08.20–2017.08.23	2.44 ± 0.10	9.646	0.73 ± 0.03	0.91	0.43 ± 0.02	0.93
50	980–1180	84.645–84.855 28.394–28.57	2017.08.21–2017.08.24	2.48 ± 0.11	9.748	0.75 ± 0.03	0.92	0.47 ± 0.02	0.93
51	1000–1200	84.645–84.855 28.394–28.57	2017.08.21–2017.08.24	2.40 ± 0.10	9.511	0.77 ± 0.03	0.92	0.49 ± 0.02	0.93
52	1020–1220	84.628–84.855 28.388–28.544	2017.08.21–2017.08.24	2.43 ± 0.10	9.606	0.87 ± 0.05	0.88	0.46 ± 0.02	0.93
53	1040–1240	84.628–84.855 28.388–28.54	2017.08.21–2017.08.25	2.51 ± 0.10	9.858	0.83 ± 0.05	0.86	0.41 ± 0.02	0.91
54	1060–1260	84.628–84.855 28.388–28.54	2017.08.22–2017.08.25	2.49 ± 0.11	9.795	0.83 ± 0.05	0.87	0.42 ± 0.02	0.92
55	1080–1280	84.628–84.825 28.386–28.54	2017.08.22–2017.08.25	2.43 ± 0.10	9.590	0.93 ± 0.06	0.86	0.40 ± 0.02	0.92
56	1100–1300	84.628–84.811 28.386–28.54	2017.08.22–2017.08.25	2.41 ± 0.10	9.537	0.82 ± 0.05	0.88	0.41 ± 0.02	0.93
57	1120–1320	84.628–84.811 28.386–28.533	2017.08.22–2017.08.26	2.31 ± 0.10	9.240	0.82 ± 0.04	0.89	0.45 ± 0.02	0.93
58	1140–1340	84.628–84.854 28.386–28.528	2017.08.23–2017.08.26	2.28 ± 0.10	9.177	0.83 ± 0.04	0.89	0.46 ± 0.02	0.93
59	1160–1360	84.628–84.854 28.386–28.528	2017.08.23–2017.08.26	2.26 ± 0.10	9.090	0.77 ± 0.04	0.90	0.46 ± 0.02	0.93
60	1180–1380	84.628–84.854 28.386–28.577	2017.08.24–2017.08.27	2.25 ± 0.09	9.063	0.76 ± 0.03	0.92	0.49 ± 0.02	0.94
61	1200–1400	84.628–84.854 28.386–28.577	2017.08.24–2017.08.27	2.16 ± 0.09	8.789	0.76 ± 0.03	0.94	0.54 ± 0.02	0.95
62	1220–1420	84.639–84.854 28.386–28.577	2017.08.24–2017.08.27	2.04 ± 0.09	8.427	0.71 ± 0.03	0.95	0.55 ± 0.02	0.95
63	1240–1440	84.582–84.854 28.359–28.577	2017.08.25–2017.08.27	1.97 ± 0.09	8.216	0.73 ± 0.01	0.98	0.60 ± 0.02	0.96
64	1260–1460	84.582–84.854 28.35–28.577	2017.08.25–2017.08.27	1.95 ± 0.09	8.180	1.27 ± 0.05	0.94	0.64 ± 0.02	0.97
65	1280–1480	84.582–84.854 28.35–28.577	2017.08.25–2017.08.28	1.99 ± 0.09	8.294	1.23 ± 0.05	0.93	0.62 ± 0.02	0.96
66	1300–1500	84.582–84.854 28.35–28.577	2017.08.26–2017.08.28	2.01 ± 0.09	8.352	1.22 ± 0.05	0.93	0.60 ± 0.02	0.96
67	1320–1520	84.582–84.854 28.35–28.577	2017.08.26–2017.08.29	2.05 ± 0.09	8.472	1.55 ± 0.06	0.93	0.61 ± 0.02	0.96
68	1340–1540	84.582–84.866 28.35–28.578	2017.08.26–2017.08.29	2.07 ± 0.09	8.564	1.33 ± 0.04	0.96	0.63 ± 0.02	0.96
69	1360–1560	84.582–84.866 28.35–28.578	2017.08.26–2017.08.29	2.07 ± 0.09	8.559	1.33 ± 0.04	0.96	0.65 ± 0.02	0.96
70	1380–1580	84.582–84.866 28.35–28.578	2017.08.27–2017.08.29	2.00 ± 0.09	8.339	1.61 ± 0.06	0.94	0.65 ± 0.02	0.97
71	1400–1600	84.582–84.866 28.35–28.578	2017.08.27–2017.08.29	2.06 ± 0.09	8.533	1.65 ± 0.06	0.93	0.65 ± 0.02	0.97
72	1420–1620	84.582–84.866 28.35–28.578	2017.08.27–2017.08.30	2.22 ± 0.10	9.000	1.61 ± 0.06	0.94	0.66 ± 0.02	0.97

Table 1 continued

SN	Event window	Region	Time duration	b-value	a-value	D_0	R^2	D_2	R^2
73	1440–1640	84.623–84.866 28.35–28.578	2017.08.27–2017.08.30	2.34 ± 0.11	9.358	1.40 ± 0.05	0.94	0.62 ± 0.02	0.97
74	1460–1660	84.623–84.866 28.376–28.578	2017.08.27–2017.08.31	2.36 ± 0.10	9.417	1.09 ± 0.05	0.95	0.57 ± 0.02	096
75	1480–1680	84.623–84.866 28.376–28.578	2017.08.28–2017.08.31	2.23 ± 0.10	9.038	1.02 ± 0.03	0.96	0.56 ± 0.02	0.96
76	1500–1700	84.623–84.866 28.376–28.578	2017.08.28–2017.08.31	2.17 ± 0.09	8.847	1.06 ± 0.03	0.96	0.55 ± 0.02	0.96
77	1520–1720	84.664–84.866 28.376–28.578	2017.08.29–2017.08.31	2.18 ± 0.09	8.880	0.92 ± 0.03	0.95	0.51 ± 0.02	0.94
78	1540–1740	84.664–84.811 28.376–28.555	2017.08.29–2017.08.31	2.16 ± 0.09	8.815	0.87 ± 0.03	0.95	0.53 ± 0.02	0.95
79	1560–1760	84.664–84.811 28.376–28.555	2017.08.29–2017.09.01	2.14 ± 0.09	8.742	0.94 ± 0.03	0.95	0.54 ± 0.02	0.94
80	1580–1780	84.664–84.853 28.376–28.561	2017.08.29–2017.09.01	2.20 ± 0.09	8.931	0.99 ± 0.03	0.96	0.56 ± 0.02	0.95
81	1600–1800	84.657–84.853 28.376–28.571	2017.08.29–2017.09.01	2.18 ± 0.09	8.886	1.06 ± 0.03	0.96	0.59 ± 0.02	0.96
82	1620–1820	84.657–84.853 28.376–28.571	2017.08.30–2017.09.01	2.16 ± 0.09	8.835	1.02 ± 0.04	0.95	0.55 ± 0.02	0.96
83	1640–1840	84.657–84.853 28.376–28.571	2017.08.31–2017.09.01	2.09 ± 0.08	8.618	1.03 ± 0.04	0.94	0.50 ± 0.02	0.96
84	1660–1860	84.657–84.853 28.376–28.571	2017.08.29–2017.09.01	2.18 ± 0.09	8.886	1.06 ± 0.04	0.94	0.48 ± 0.02	0.96
85	1680–1880	84.657–84.853 28.376–28.571	2017.08.31–2017.09.02	2.05 ± 0.08	8.490	1.08 ± 0.04	0.93	0.48 ± 0.02	0.95
86	1700–1900	84.657–84.853 28.376–28.571	2017.08.31–2017.09.02	2.03 ± 0.08	8.448	1.13 ± 0.05	0.94	0.46 ± 0.02	0.94
87	1720–1920	84.657–84.853 28.376–28.571	2017.08.31–2017.09.02	2.01 ± 0.08	8.393	1.13 ± 0.05	0.92	0.44 ± 0.02	0.94
88	1740–1940	84.657–84.853 28.376–28.571	2017.08.31–2017.09.02	1.99 ± 0.08	8.352	1.16 ± 0.05	0.91	0.44 ± 0.02	0.94
89	1760–1960	84.657–84.853 28.382–28.571	2017.09.01–2017.09.03	1.91 ± 0.07	8.100	1.89 ± 0.05	0.92	0.47 ± 0.02	0.94
90	1780–1980	84.657–84.853 28.382–28.571	2017.09.01–2017.09.03	1.86 ± 0.07	7.947	1.10 ± 0.05	0.92	0.50 ± 0.02	0.95
91	1800–2000	84.659–84.884 28.382–28.569	2017.09.01–2017.09.03	1.89 ± 0.07	8.039	0.90 ± 0.03	0.96	0.45 ± 0.02	0.94
92	1820–2020	84.659–84.884 28.382–28.582	2017.09.01–2017.09.03	1.87 ± 0.07	7.997	1.41 ± 0.06	0.92	0.45 ± 0.02	0.95
93	1840–2040	84.659–84.884 28.382–28.582	2017.09.01–2017.09.04	1.87 ± 0.07	7.990	1.39 ± 0.06	0.92	0.50 ± 0.02	0.96
94	1860–2060	84.66–84.884 28.382–28.582	2017.09.02–2017.09.04	1.93 ± 0.07	8.159	1.40 ± 0.06	0.92	0.52 ± 0.02	0.96
95	1880–2080	84.66–84.884 28.382–28.582	2017.09.02–2017.09.04	1.99 ± 0.07	8.340	1.42 ± 0.07	0.91	0.52 ± 0.02	0.95
96	1900–2100	84.66–84.884 28.382–28.582	2017.09.02–2017.09.04	2.06 ± 0.08	8.541	1.42 ± 0.07	0.91	0.56 ± 0.02	0.95

Table 1 continued

SN	Event window	Region	Time duration	b-value	a-value	D_0	R^2	D_2	R^2
97	1920–2120	84.66–84.884 28.382–28.582	2017.09.02–2017.09.05	2.13 ± 0.08	8.747	1.45 ± 0.06	0.92	0.60 ± 0.02	0.96
98	1940–2140	84.66–84.884 28.382–28.582	2017.09.02–2017.09.05	2.18 ± 0.08	8.897	1.45 ± 0.06	0.92	0.57 ± 0.02	0.96
99	1960–2160	84.664–84.892 28.401–28.582	2017.09.03–2017.09.06	2.34 ± 0.09	9.375	1.40 ± 0.07	0.91	0.53 ± 0.02	0.95
100	1980–2180	84.653–84.892 28.393–28.582	2017.09.03–2017.09.06	2.42 ± 0.10	9.603	1.39 ± 0.06	0.92	0.55 ± 0.02	0.96
101	2000–2200	84.653–84.892 28.393–28.597	2017.09.03–2017.09.06	2.38 ± 0.11	9.477	1.13 ± 0.03	0.97	0.59 ± 0.02	0.97
102	2020–2220	84.653–84.892 28.393–28.597	2017.09.03–2017.09.07	2.40 ± 0.11	9.552	1.02 ± 0.04	0.98	0.66 ± 0.02	0.97
103	2040–2240	84.612–84.892 28.393–28.597	2017.09.04–2017.09.07	2.35 ± 0.11	9.393	1.10 ± 0.03	0.97	0.66 ± 0.02	0.97
104	2060–2260	84.612–84.895 28.393–28.597	2017.09.04–2017.09.07	2.39 ± 0.11	9.531	1.38 ± 0.05	0.95	0.69 ± 0.02	0.97
105	2080–2280	84.612–84.895 28.393–28.597	2017.09.04–2017.09.08	2.31 ± 0.11	9.273	1.45 ± 0.05	0.94	0.75 ± 0.02	0.95
106	2100–2300	84.612–84.895 28.393–28.597	2017.09.04–2017.09.08	2.22 ± 0.10	9.002	1.43 ± 0.05	0.94	0.74 ± 0.02	0.98
107	2120–2320	84.612–84.895 28.392–28.597	2017.09.05–2017.09.09	2.18 ± 0.10	8.863	1.45 ± 0.05	0.94	0.73 ± 0.02	0.98
108	2140–2340	84.612–84.895 28.392–28.597	2017.09.06–2017.09.10	2.15 ± 0.10	8.770	1.44 ± 0.05	0.95	0.76 ± 0.02	0.97
109	2160–2360	84.612–84.895 28.364–28.597	2017.09.06–2017.09.11	2.10 ± 0.10	8.619	1.56 ± 0.06	0.94	0.78 ± 0.02	0.97
110	2180–2380	84.612–84.895 28.364–28.597	2017.09.06–2017.09.12	2.13 ± 0.10	8.707	1.62 ± 0.06	0.94	0.76 ± 0.02	097
111	2200–2400	84.612–84.895 28.364–28.567	2017.09.06–2017.09.14	2.11 ± 0.09	8.644	1.64 ± 0.07	0.92	0.75 ± 0.02	0.97
112	2220–2420	84.612–84.895 28.36–28.567	2017.09.07–2017.09.16	2.09 ± 0.09	8.557	1.67 ± 0.08	0.91	0.72 ± 0.02	0.97
113	2240–2440	84.669–84.895 28.36–28.575	2017.09.07–2017.09.17	2.17 ± 0.10	8.826	1.68 ± 0.08	0.91	0.67 ± 0.02	0.97
114	2260–2460	84.669–84.884 28.36–28.581	2017.09.07–2017.09.18	2.15 ± 0.09	8.760	1.52 ± 0.06	0.93	0.67 ± 0.02	0.97
115	2280–2480	84.665–84.884 28.36–28.581	2017.09.08–2017.09.22	2.21 ± 0.10	8.936	1.34 ± 0.04	0.96	0.61 ± 0.02	0.96
116	2300–2500	84.659–84.899 28.36–28.581	2017.09.08–2017.09.27	2.39 ± 0.11	9.271	1.31 ± 0.03	0.97	0.64 ± 0.02	0.97
117	2320–2520	84.658–84.899 28.36–28.581	2017.09.09–2017.10.05	2.36 ± 0.11	9.359	1.37 ± 0.03	0.98	0.67 ± 0.02	0.97
118	2340–2540	84.658–84.899 28.36–28.581	2017.09.10–2017.10.08	2.40 ± 0.11	9.503	1.40 ± 0.03	0.98	0.61 ± 0.01	0.98
119	2360–2560	84.646–84.899 28.36–28.581	2017.09.11–2017.10.27	2.49 ± 0.11	9.773	1.33 ± 0.02	0.99	0.65 ± 0.01	0.98
120	2380–2580	84.628–84.899 28.36–28.581	2017.09.12–2018.04.30	2.25 ± 0.11	9.963	1.32 ± 0.01	0.99	0.63 ± 0.01	0.98

Table 1 continued

SN	Event window	Region	Time duration	b-value	a-value	D_0	R^2	D_2	R^2
121	2400–2600	84.584–84.899 28.36–28.581	2017.09.14–2018.06.10	2.72 ± 0.12	10.465	1.19 ± 0.02	0.99	0.61 ± 0.01	0.98
122	2420–2620	84.584–84.899 28.364–28.581	2017.09.16–2018.06.25	2.88 ± 0.13	10.937	1.15 ± 0.02	0.98	0.61 ± 0.01	0.98
123	2440–2640	84.584–84.899 28.364–28.581	2017.09.17–2018.07.7	2.97 ± 0.14	11.221	1.14 ± 0.02	0.99	0.61 ± 0.01	0.98
124	2460–2660	84.584–84.899 28.364–28.574	2017.09.18–2018.07.11	2.84 ± 0.15	10.835	1.25 ± 0.04	0.99	0.57 ± 0.01	0.97
125	2480–2680	84.584–84.899 28.364–28.574	2017.09.22–2018.07.13	2.82 ± 0.15	10.767	1.23 ± 0.02	0.99	0.54 ± 0.01	0.97
126	2500–2700	84.584–84.899 28.364–28.574	2017.10.01–2018.07.15	2.76 ± 0.14	10.577	1.25 ± 0.02	0.99	0.48 ± 0.01	0.97
127	2520–2720	84.584–84.888 28.372–28.574	2017.10.05–2018.07.18	2.74 ± 0.13	10.539	1.18 ± 0.02	0.99	0.41 ± 0.01	0.95
128	2540–2740	84.584–84.888 28.372–28.574	2017.10.09–2018.07.21	2.72 ± 0.13	10.477	1.02 ± 0.07	0.81	0.45 ± 0.02	0.95
129	2560–2760	84.584–84.888 28.358–28.574	2017.10.29–2018.07.24	2.74 ± 0.14	10.523	0.82 ± 0.17	0.58	0.36 ± 0.02	0.92
130	2580–2780	84.584–84.853 28.358–28.574	2018.05.01–2018.07.27	2.72 ± 0.14	10.460	0.77 ± 0.15	0.63	0.33 ± 0.02	0.90
131	2600–2800	84.609–84.853 28.358–28.539	2018.06.10–2018.07.31	2.66 ± 0.13	10.279	0.55 ± 0.02	0.92	0.41 ± 0.02	0.93
132	2620–2820	84.609–84.85 28.358–28.528	2018.06.26–2018.08.03	2.58 ± 0.12	10.057	0.60 ± 0.02	0.93	0.44 ± 0.02	0.94
133	2640–2840	84.598–84.826 28.353–28.568	2018.07.07–2018.08.08	2.50 ± 0.12	9.815	0.58 ± 0.01	0.98	0.44 ± 0.02	0.94
134	2660–2860	84.598–84.826 28.353–28.568	2018.07.11–2018.08.04	2.60 ± 0.12	10.114	0.60 ± 0.01	0.98	0.43 ± 0.02	0.95
135	2680–2880	84.598–84.826 28.353–28.568	2018.07.14–2018.08.09	2.60 ± 0.12	10.150	0.61 ± 0.01	0.98	0.42 ± 0.02	0.95
136	2700–2906	84.598–84.891 28.353–28.568	2018.07.15–2019.07.12	2.70 ± 0.13	10.440	1.12 ± 0.03	0.97	0.47 ± 0.02	0.96

of a fractal in a space and characterizes the occupancy of fracture system or the roughness of fracturing [76]. The box counting fractal dimension values gives the dimension of the active fractal fault system [77–80]. For q = 2 it is termed as correlation dimension. D_2 quantifies the degree of fractal clustering of points in a space, where the lower fractal dimensions reflect tighter clusters [81].

Results and Discussion

Frequency magnitude distributions b-values and fractal dimensions (D_0 and D_2) are estimated for earthquakes swarm following the 2015 Gorkha earthquake and presented in Table 1.

The b-value calculated for the entire dataset was found to be 1.82 ± 0.02, while it was maximum 2.97 ± 0.14 and minimum 1.81 ± 0.07 for different temporal windows. These values are totally different from the average b-value around 1.0 determined for the earthquake distributions in active faults [33, 82]. As recent studies of the seismicity accompanying injections indicate that the fluid triggering of seismicity is manifested by increased b-value [86, 87], we can conclude that the earthquake swarms may have triggered by high-pressured migrating fluids and the large b-value 2.97 reflects the distinctive behavior of swarm earthquakes attributed to the smaller fault lengths or movement of fluids [64, 83–85]. The results further suggest that the earthquake swarms may have been produced by a concentrated source of stress. The localized sources of high

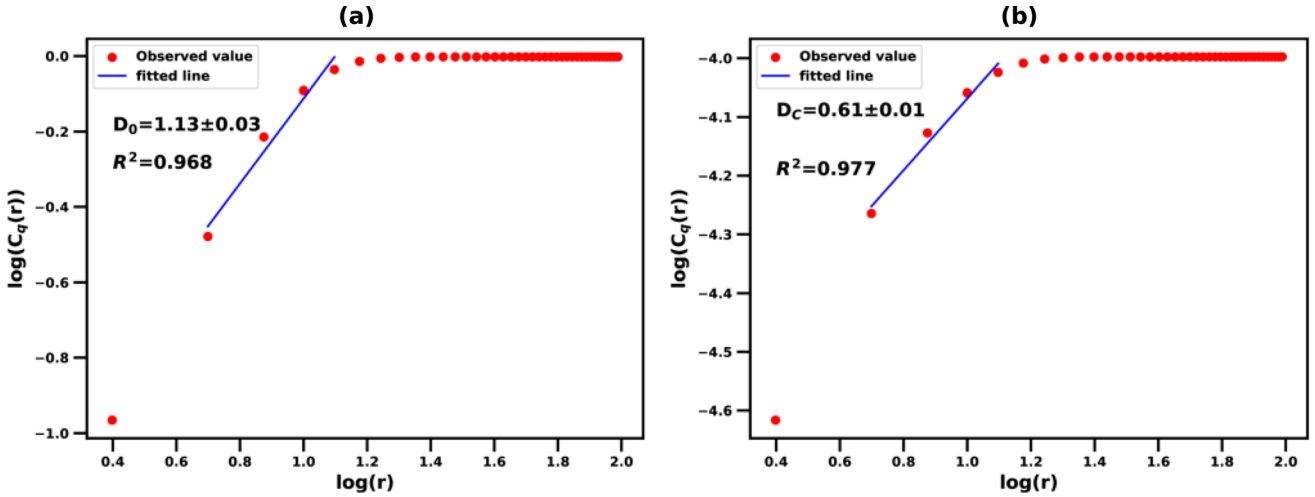

Fig. 5 Log–log regression plot for the estimation of the fractal dimension for the temporal window 1 of period 2017.08.08–2017.08.13 within the range 84.664°– 84.864° east and 28.351° –28.593° north **a** box counting dimension **b** correlation dimension. The regression line is fitted for the range of scaling distance r = 4.99 km to r = 15 km

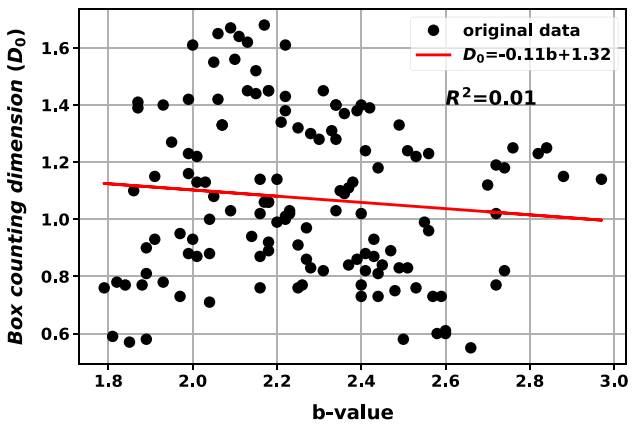

Fig. 6 Relationship between box counting fractal dimension (D_0) and b-values for 136 temporal windows. The straight line is the linear regression and R^2 is the coefficient of determination

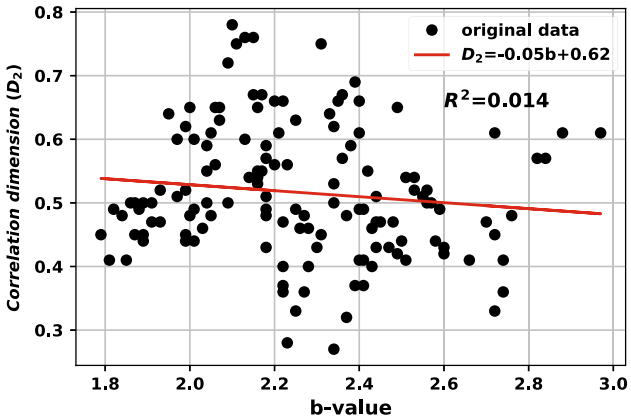

Fig. 7 Relationship between correlation dimension (D_2) and b-values for 136 temporal windows. The straight line is the linear regression, and R^2 is the coefficient of determination

fluid pressures may have lowered the effective strength which essentially act as concentrated sources of stress [68, 88]. The larger b-value also suggests the presence of a high number of smaller shocks in the swarm sequence.

Box counting fractal dimension value (D_0) ranges from 0.55 ± 0.02 to 1.68 ± 0.08, while correlation fractal dimension value (D_2) ranges from 0.27 ± 0.07 to 0.78 ± 0.02 for different temporal windows. As an example, box counting dimension value (D_0) plot and correlation dimension value (D_2) plot for the temporal window 1 of period 2017.08.08–2017.08.13 within the range 84.664°–84.864° east and 28.351° –28.593° north are depicted in Fig. 5. These low fractal dimension values for temporal distribution are significant for the intra-plate seismicity. These values reflect the strong degree of temporal clustering explaining the episodic character of

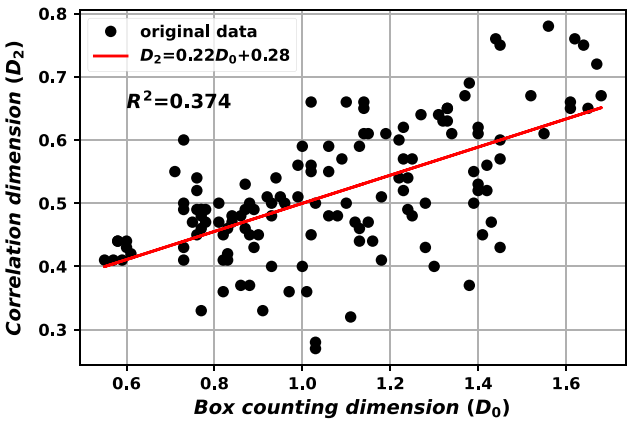

Fig. 8 The relationship between the correlation fractal dimension (D_2) and the box counting fractal dimensions (D_0) of the epicentral distributions of swarms

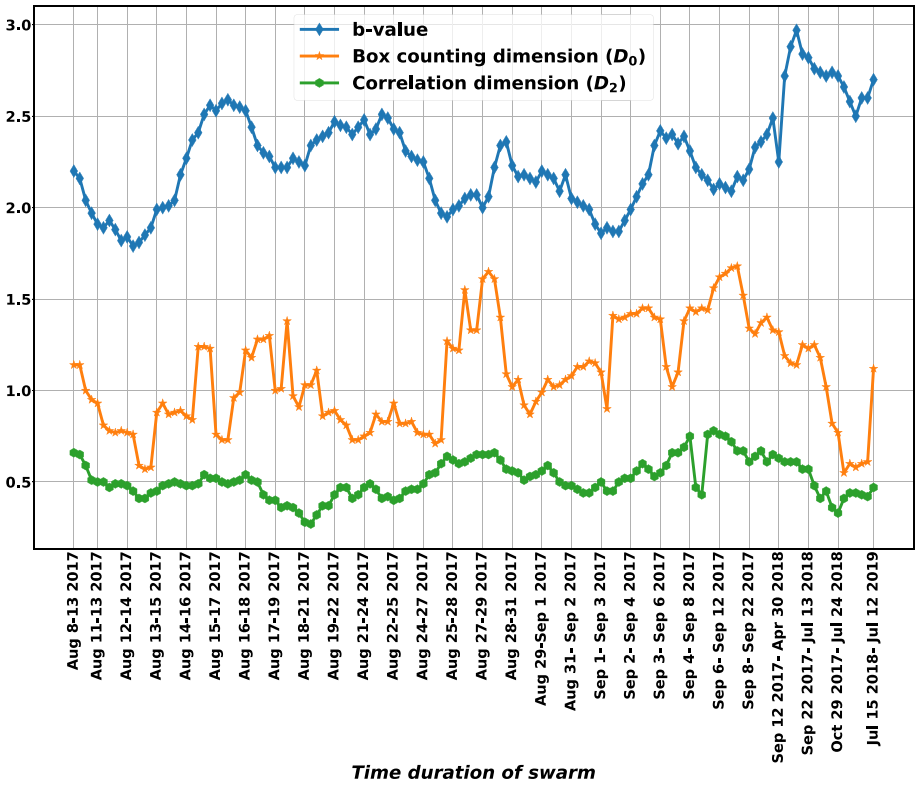

Fig. 9 Temporal changes in the fractal dimensions (Box counting dimension and correlation dimension) and the b-value for 136 temporal windows

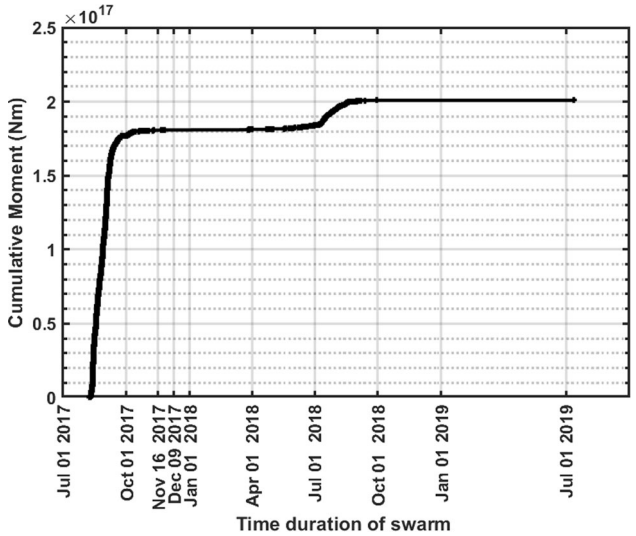

Fig. 10 Cumulative seismic moment release during the swarm

swarms which in turn supports the idea of impulse like triggering of earthquake avalanches. In addition, the seismogenic zone is characterized by low D_2 values together with some small patches of high D_2 values. This probably reflects small zones of high material heterogeneities or asperities within the area of swarms. From these results, we can infer that the study area is relatively more prone for the occurrences of moderate future earthquakes.

The box counting fractal dimension (D_0) and b-values are negatively correlated defined by the equation $D_0 = -0.11b + 1.32$ (Fig. 6) with coefficient of determination (R^2) = 0.01. The negative correlation between b and D_0 values is concordance with the past studies [41, 89]. The poor correlations among these parameters indicate that the parameters are independent of each other.

The fractal correlation dimension (D_2) and b-values are negatively correlated defined by the equation $D_2 = -0.05b + 0.62$ with coefficient of determination (R^2) = 0.014 (Fig. 7). The negative correlation may have develop in response to the decrease in stress concentration (higher b) and an increase in epicenter clustering (decreased D_2). From the negative correlation between D_2 and b-values, the study region can be inferred to have small and isolated asperities and by the failure of those asperities' earthquake swarm may have occurred in clusters.

D_2 estimated for epicenter distribution is less than 1, and D_0 estimated is less than 2 (Table 1). A positive correlation (solid red line) is obtained with $D_2 = 0.22D_0 + 0.28$ with coefficient of determination (R^2) = 0.374 (Fig. 8). The fractal dimension of faults is related to the spatial distribution of earthquakes and strain release modes [90, 91]. The poor correlation between D_2 and D_0 suggests that their variation may not strongly influence one another. There is no strong relationship between distribution of aftershocks

and occupancy of fracture system and the roughness of fracturing. The spatial distribution of aftershocks tend to become more random and unpredictable with increasing the fractal dimensions of active fault systems in aftershock regions [76]. Similar relations (a positive correlation) between fractal dimensions and earthquake density was also noticed for the 1999 Chi–Chi aftershock [92] and the 2001 Bhuj aftershock data [93].

The variation in the b-value, D_0 value and D_2 value with time (Fig. 9) shows oscillating behavior. This pattern of variation could be related with stress build-up process and release process of strain energy through the clusters of the events. Similar patterns were also observed for fractal dimensions in acoustic emission, micro-seismicity studies in the laboratory, and rock burst seismicity in mines [68, 94]. During the period of swarm, the majority of the b-values are greater than 2.5 and at the end of swarm, few of them are even close to 3. These relatively high b-values might suggest low confining stress, the presence of fluids or the presence of highly fractured rocks in the fault areas. The most of D_0 values estimated are less than 1.5 and few of them are greater than 1.5, while all the estimated D_2 values are less than 1. These results are consistent with low-magnitude clustered activity. The greater D_0 shows more irregular shape of the fault structure and a small D_2 value indicates a tight earthquake distribution within the faults.

There is a quick release of seismic moment at the beginning of the swarm, and by the end of September 2017 cumulative seismic moment is about 1.8×10^{17} Nm. It is about 2.0×10^{17} Nm by the end of the swarm seismic (Fig. 10). The release of huge energy is attributed to the high seismic activity indicated by the high a-value of the frequency magnitude distribution (Table 1). According to the previous work [18], the total seismic moment released was 1.11×10^{17} Nm, which is in the same order but half of the moment released calculated in this study.

Conclusion

The b-value, D_0 of active faults and D_2 of spatial distributions of aftershocks are computed for earthquake swarms initiated in August 2017 at the front of the High Himalayas, about 30 km north-west of the epicenter of the 2015 Gorkha earthquake. The maximum b-value was 2.97 ± 0.14 and minimum value was 1.81 ± 0.07 for different temporal windows. The a-value range from 7.712 to 11.221 and b-value range from 1.81 to 2.97 reflect the fact that swarms can occur as the post-seismic relaxation process after the large earthquake. Box counting fractal dimension value (D_0) ranges from 0.55 ± 0.02 to 1.68 ± 0.08, while correlation fractal dimension value (D_2) ranges from 0.27 ± 0.07 to 0.78 ± 0.02. Low dimension values (D_2) of spatial distribution of earthquakes reflect a predominantly linear configuration of epicenters. The b-value estimated is found to be negatively correlated with both D_0 and D_2 as defined by the equations $D_0 = -0.11b + 1.32$ and $D_2 = -0.05b + 0.62$, respectively. D_0 and D_2 are positively correlated with each other defined by the equation $D_2 = 0.22D_0 + 0.28$. The variation in b and D can be explained by the existence of the hydrothermal zone of weakness that was active prior to August 2017. The seismic moment released during the 2017–2019 swarm is around 2.0×10^{17} Nm. The occurrence of swarms may be associated with the development of new ruptures in the region. Many small faults and small-scale structures could have provided an extremely heterogeneous background. In addition, reduced effective stresses could be the leading factor for the occurrences of the swarm sequences. The associated smaller earthquakes also suggest the fact that the region can accumulate low levels of tectonic stress, thereby releasing stored strain energy in the form of smaller events. This study provides valuable insights into the seismo genesis and the future earthquake potential in the region.

Acknowledgements One of the authors (RKT) would like to express acknowledgements to Tribhuvan University of Nepal for providing the sabbatical leave and to the University Grants Commission, Nepal, for providing the financial support under the PhD grant S&T -14-075/76. The authors would also like to thank the reviewers for their suggestions and comments to improve the quality of this manuscript.

Funding There is an agreement between author and publisher that the method of publishing is traditional and author do not have to pay any APC (Article publishing charge).

Declarations

Conflict of interests The authors declare that they have no competing interests that could have appeared to influence the work.

References

1. Amezawa Y, Maeda T, Kosuga M (2021) Migration diffusivity as a controlling factor in the duration of earthquake swarms. Earth, Planets Sp 73:148
2. Kundu B, Legrand D, Gahalaut K et al (2012) The 2005 volcano-tectonic earthquake swarm in the Andaman Sea: triggered by the 2004 great Sumatra-Andaman earthquake. Tectonics 31:1–11. https://doi.org/10.1029/2012TC003138
3. Hainzl S (2004) Seismicity patterns of earthquake swarms due to fluid intrusion and stress triggering. Geophys J Int 159:1090–1096. https://doi.org/10.1111/j.1365-246X.2004.02463.x
4. Passarelli L, Rivalta E, Jónsson S et al (2018) Scaling and spatial complementarity of tectonic earthquake swarms. Earth Planet Sci Lett 482:62–70. https://doi.org/10.1016/j.epsl.2017.10.052
5. Godano M, Larroque C, Bertrand E et al (2013) The October-November 2010 earthquake swarm near Sampeyre (Piedmont region, Italy): a complex multicluster sequence. Tectonophysics 608:97–111. https://doi.org/10.1016/j.tecto.2013.10.010

6. Hauksson E, Stock J, Bilham R et al (2013) Report on the august 2012 brawley earthquake swarm in Imperial Valley, Southern California. Seismol Res Lett 84:177–189. https://doi.org/10.1785/0220120169
7. Brodsky EE, Mori JJ, Anderson L et al (2020) The state of stress on the fault before, during, and after a major earthquake. Annu Rev Earth Planet Sci 48:49–74. https://doi.org/10.1146/annurev-earth-053018-060507
8. Hoste-Colomer R, Bollinger L, Lyon-Caen H et al (2017) Lateral structure variations and transient swarm revealed by seismicity along the Main Himalayan Thrust north of Kathmandu. Tectonophysics 714–715:107–116. https://doi.org/10.1016/j.tecto.2016.10.004
9. Bilham R (2004) Earthquakes in India and the Himalaya: tectonics, geodesy and history. Ann Geophys 47:839–858
10. Mullick M, Mukhopadhyay D (2017) Quantitative analysis of the Nepal earthquake on 25 April, 2015 in the perspective of future earthquake hazard. Geod Geodyn 8:77–83. https://doi.org/10.1016/j.geog.2017.02.003
11. Seeber L, Armbruster JG (1981) Great detachment earthquakes along the Himalayan arc and long- term forecasting. Earthq Predict an Int Rev. https://doi.org/10.1029/me004p0259
12. Avouac JP, Meng L, Wei S et al (2015) Lower edge of locked Main Himalayan Thrust unzipped by the 2015 Gorkha earthquake. Nat Geosci 8:708–711. https://doi.org/10.1038/ngeo2518
13. Elliott JR, Jolivet R, Gonzalez PJ et al (2016) Himalayan megathrust geometry and relation to topography revealed by the Gorkha earthquake. Nat Geosci 9:174–180. https://doi.org/10.1038/ngeo2623
14. Grandin R, Vallée M, Satriano C et al (2015) Rupture process of the Mw = 7.9 2015 Gorkha earthquake (Nepal): insights into Himalayan megathrust segmentation. Geophys Res Lett 42:8373–8382. https://doi.org/10.1002/2015GL066044
15. Gualandi A, Avouac JP, Galetzka J et al (2017) Pre- and post-seismic deformation related to the 2015, Mw7.8 Gorkha earthquake. Nepal Tectonophysics 714–715:90–106. https://doi.org/10.1016/j.tecto.2016.06.014
16. Wang K, Fialko Y (2015) Slip model of the 2015 Mw 7.8 Gorkha (Nepal) earthquake from inversions of ALOS-2 and GPS data. Geophys Res Lett 42:7452–7458. https://doi.org/10.1002/2015GL065201
17. Zhang J, Zhao B, Wang D et al (2021) Dynamic modeling of postseismic deformation following the 2015 Mw 7.8 Gorkha earthquake, Nepal. J Asian Earth Sci. https://doi.org/10.1016/j.jseaes.2021.104781
18. Adhikari LB, Bollinger L, Vergne J et al (2021) Orogenic Collapse and Stress Adjustments Revealed by an Intense Seismic Swarm Following the 2015 Gorkha Earthquake in Nepal. Front Earth Sci 9:1–13. https://doi.org/10.3389/feart.2021.659937
19. Bollinger L, Tapponnier P, Sapkota SN, Klinger Y (2016) Slip deficit in central Nepal: Omen for a repeat of the 1344 AD earthquake? the 2015 Gorkha, Nepal, Earthquake and Himalayan Studies 4 Seismology. Earth Planets Sp. https://doi.org/10.1186/s40623-016-0389-1
20. Ito Y, Hino R, Kido M et al (2013) Episodic slow slip events in the Japan subduction zone before the 2011 Tohoku-Oki earthquake. Tectonophysics 600:14–26. https://doi.org/10.1016/j.tecto.2012.08.022
21. Kato A, Nakagawa S (2014) Multiple slow-slip events during a foreshock sequence of the 2014 Iquique, Chile Mw 8.1 earthquake. Geophys Res Lett 41:5420–5427. https://doi.org/10.1002/2014GL061138
22. Ruiz S, Metois M, Fuenzalida A et al (2014) Intense foreshocks and a slow slip event preceded the 2014 Iquique Mw8.1 earthquake. Science 80:1165–1169. https://doi.org/10.1126/science.1256074
23. Mandal P, Srinagesh D, Suresh G et al (2021) Characterization of earthquake hazard at the Palghar and Pulichintala swarm activity regions (India) through three-dimensional modelling of b-value and fractal (correlation) dimensions. Nat Hazards 108:1183–1196. https://doi.org/10.1007/s11069-021-04726-5
24. Sateesh A, Mahesh P, Singh AP et al (2019) Are earthquake swarms in South Gujarat, northwestern Deccan Volcanic Province of India monsoon induced? Environ Earth Sci 78:1–13. https://doi.org/10.1007/s12665-019-8382-1
25. Paudyal H, Singh HN, Shanker D, Singh VP (2008) Stress pattern in two seismogenic sources in Nepal-Himalaya and its vicinity. Acta Geophys 56:313–323. https://doi.org/10.2478/s11600-008-00013-2
26. Ruch J, Keir D, Passarelli L et al (2021) Revealing 60 years of Earthquake swarms in the Southern Red Sea, Afar and the Gulf of Aden. Front Earth Sci 9:9. https://doi.org/10.3389/feart.2021.664673
27. Sykes LR (1970) Earthquake swarms and sea- floor spreading. J Geophys Res 75:6578–6611. https://doi.org/10.1029/jb075i032p06598
28. An W, Hu X, Garzanti E et al (2021) New precise dating of the India-Asia collision in the Tibetan Himalaya at 61 Ma. Geophys Res Lett 48:1–10. https://doi.org/10.1029/2020GL090641
29. Decelles PG, Kapp P, Gehrels GE, Ding L (2014) Paleocene-Eocene foreland basin evolution in the Himalaya of southern Tibet and Nepal: implications for the age of initial India-Asia collision. Tectonics 33:824–849. https://doi.org/10.1002/2014TC003522
30. Bai L, Liu H, Ritsema J et al (2016) Faulting structure above the Main Himalayan Thrust as shown by relocated aftershocks of the 2015 Mw7.8 Gorkha, Nepal, earthquake. Geophys Res Lett 43:637–642. https://doi.org/10.1002/2015GL066473
31. Gansser A (1964) The Geology of the Himalaya. Wiley Interscience, New York
32. Martin AJ (2017) A review of definitions of the Himalayan Main Central Thrust. Int J Earth Sci 106:2131–2145. https://doi.org/10.1007/s00531-016-1419-8
33. Adhikari LB, Gautam UP, Koirala BP et al (2015) The aftershock sequence of the 2015 april 25 Gorkha-Nepal earthquake. Geophys J Int 203:2119–2124. https://doi.org/10.1093/gji/ggv412
34. Yamada M, Kandel T, Tamaribuchi K, Ghosh A (2020) 3D fault structure inferred from a refined aftershock catalog for the 2015 gorkha earthquake in Nepal. Bull Seismol Soc Am 110:26–37. https://doi.org/10.1785/0120190075
35. Bilham R (2015) Raising Kathmandu Nat Geosci 8:582–584. https://doi.org/10.1038/ngeo2498
36. Jouanne F, Gajurel A, Mugnier JL et al (2019) Postseismic deformation following the April 25, 2015 Gorkha earthquake (Nepal): afterslip versus viscous relaxation. J Asian Earth Sci 176:105–119. https://doi.org/10.1016/j.jseaes.2019.02.009
37. Liu G, Yang SM, Shi HB et al (2017) A unified source model of the 2015 Gorkha earthquake. Acta Geophys Sin 60:2663–2679. https://doi.org/10.6038/cjg20170714
38. Wiemer, (2001) A software package to analyze seismicity: ZMAP. Seismol Res Lett 72:373–382. https://doi.org/10.1785/gssrl.72.3.373
39. De RV, Dimitriu P, Papadimitriou E, Tosi P (1993) Recurrent patterns in the spatial behaviour of italian seismicity revealed by the fractal approach. Geophys Res Lett 20:1911–1914
40. Aki K (1967) Scaling law of seismic spectrum. J Geophys Res 72:1217–1231. https://doi.org/10.1029/jz072i004p01217
41. Hirata T (1989) A correlation between the b value and the fractal dimension of earthquakes. J Geophys Res 94:7507–7514. https://doi.org/10.1029/JB094iB06p07507
42. Main IG (1992) Damage mechanics with long-range interactions: correlation between the seismic b-value and the fractal two-point

correlation dimension. Geophys J Int 111:531–541. https://doi.org/10.1111/j.1365-246X.1992.tb02110.x
43. Mandelbrot B (1967) How long is the coast of Britain? Statistical self-similarity and fractional dimension. Science 156:636–638. https://doi.org/10.1126/science.156.3775.636
44. Aviles CA, Scholz CH, Boatwright J (1987) Fractal analysis applied to characteristic segments of the San Andreas fault (USA). J Geophys Res 92:331–344. https://doi.org/10.1029/JB092iB01p00331
45. Öncel AO, Main I, Alptekin Ö, Cowie P (1996) Spatial variations of the fractal properties of seismicity in the Anatolian fault zones. Tectonophysics 257:189–202. https://doi.org/10.1016/0040-1951(95)00132-8
46. Utsu T (1969) Aftershocks and earthquake statistics(1): some parameters which characterize an aftershock sequence and their interrelations. J Fac Sci Hokkaido Univ 3:129–195
47. Grassberger P, Procaccia I (1983) Measuring the strangeness of strange attractors. Phys D Nonlinear Phenom 9:189–208. https://doi.org/10.1016/0167-2789(83)90298-1
48. Aki K (1965) Maximum likelihood estimate of b in the formula Log N = a - bM and its confidence limits. Bull Earthq Res Inst Tokyo Univ 43:237–239
49. Bender B (1983) Maximum likelihood estimation of b values for magnitude grouped data. Bull Seismol Soc Am 73:831–851. https://doi.org/10.1785/bssa0730030831
50. Utsu T (1969) Instructions for use aftershocks and earthquake statistics (I). J Fac Sci Hokkaido Univ 3:129–195
51. Gutenberg B, Richter CF (1944) Frequency of earthquakes in California. Bull Seismol Soc Am 34:185–188
52. Wiemer S, Katsumata K (1999) Spatial variability of seismicity parameters in aftershock zones. J Geophys Res Solid Earth 104:13135–13151. https://doi.org/10.1029/1999jb900032
53. Murru M, Console R, Falcone G et al (2007) Spatial mapping of the b value at Mount Etna, Italy, using earthquake data recorded from 1999 to 2005. J Geophys Res Solid Earth. https://doi.org/10.1029/2006JB004791
54. Marzocchi W, Sandri L (2003) A review and new insights on the estimation of the b-value and its uncertainty. Ann Geophys 46:1271–1282. https://doi.org/10.4401/ag-3472
55. Wiemer S, Wyss M (1997) Mapping the frequency-magnitude distribution in asperities: an improved technique to calculate recurrence times? J Geophys Res Solid Earth 102:15115–15128. https://doi.org/10.1029/97jb00726
56. Enescu B, Enescu D, Ito K (2011) Values of b and p: their variations and relation to physical processes for earthquakes in Japan and Romania. Rom Reports Phys 56:590–608
57. Cheng QM, Sun HY (2018) Variation of singularity of earthquake-size distribution with respect to tectonic regime. Geosci Front 9:453–458. https://doi.org/10.1016/j.gsf.2017.04.006
58. Sreejith KM, Sunil PS, Agrawal R et al (2018) Audit of stored strain energy and extent of future earthquake rupture in central Himalaya. Sci Rep 8:1–9. https://doi.org/10.1038/s41598-018-35025-y
59. Wang F, Zai Y (2021) Fractal and multifractal characteristics of shale nanopores. Results Phys. https://doi.org/10.1016/j.rinp.2021.104277
60. Legrand D, Villagómez D, Yepes H, Calahorrano A (2004) Multifractal dimension and b value analysis of the 1998–1999 Quito swarm related to Guagua Pichincha volcano activity, Ecuador. J Geophys Res Solid Earth 109:1–9. https://doi.org/10.1029/2003jb002572
61. Rodríguez-Pérez Q, Monterrubio-Velasco M, Zúñiga FR et al (2021) Spatial and temporal b-value characterization at Popocatépetl volcano, Central Mexico. J Volcanol Geotherm Res. https://doi.org/10.1016/j.jvolgeores.2021.107320
62. Rydelek PA, Sacks IS (2003) Comment on "Minimum Magnitude of Completeness in Earthquake Catalogs: Examples from Alaska, the Western United States, and Japan", by Stefan Wiemer and Max Wyss. Bull Seismol Soc Am 93:1862–1867. https://doi.org/10.1785/0120020035
63. Senatorski P (2020) Gutenberg–Richter's b value and earthquake asperity models. Pure Appl Geophys 177:1891–1905. https://doi.org/10.1007/s00024-019-02385-z
64. Spada M, Tormann T, Wiemer S, Enescu B (2013) Generic dependence of the frequency-size distribution of earthquakes on depth and its relation to the strength profile of the crust. Geophys Res Lett 40:709–714. https://doi.org/10.1029/2012GL054198
65. Bachmann CE, Wiemer S, Goertz-Allmann BP, Woessner J (2012) Influence of pore-pressure on the event-size distribution of induced earthquakes. Geophys Res Lett 39:1–7. https://doi.org/10.1029/2012GL051480
66. López-Comino JA, Cesca S, Heimann S et al (2017) Characterization of Hydraulic Fractures Growth During the Äspö Hard Rock Laboratory Experiment (Sweden). Rock Mech Rock Eng 50:2985–3001. https://doi.org/10.1007/s00603-017-1285-0
67. Fiedler B, Hainzl S, Zöller G, Holschneider M (2018) Detection of gutenberg-richter b-value changes in earthquake time series. Bull Seismol Soc Am 108:2778–2787. https://doi.org/10.1785/0120180091
68. Mogi K (1963) Some discussions on aftershocks, foreshocks and earthquake swarms—the fracture of a semi- infinite body caused by an inner stress origin and its relation to the earthquake phenomena (third paper). Bull Earthq Res Inst 41:615–658
69. Mogi K (1967) Earthquakes and fractures. Tectonophysics 5:35–55. https://doi.org/10.1016/0040-1951(67)90043-1
70. Amelung F, King G (1997) Earthquake scaling laws for creeping and non-creeping faults. Geophys Res Lett 24:507–510. https://doi.org/10.1029/97GL00287
71. Chen KH, Bürgmann R (2017) Creeping faults: good news, bad news? Rev Geophys 55:282–286. https://doi.org/10.1002/2017RG000565
72. Harris RA (2017) Large earthquakes and creeping faults. Rev Geophys 55:169–198
73. Wyss M (2001) Locked and creeping patches along the Hayward fault, California. Geophys Res Lett 28:3537–3540. https://doi.org/10.1029/2001GL013499
74. Schorlemmer D, Wiemer S, Wyss M (2004) Earthquake statistics at Parkfield: 1. Stationarity of b values. J Geophys Res Solid Earth 109:1–17. https://doi.org/10.1029/2004JB003234
75. Shi Y, Bolt AB (1982) The standard error of the magnitude-frequency b value. Bull Seismol Soc Am 72:1677–1687
76. Nanjo K, Nagahama H (2004) Fractal properties of spatial distributions of aftershocks and active faults. Chaos, Solitons Fractals 19:387–397. https://doi.org/10.1016/S0960-0779(03)00051-1
77. Mandal P, Mabawonku AO, Dimri VP (2005) Self-organized fractal seismicity of reservoir triggered earthquakes in the Koyna-Warna seismic zone, Western India. Pure Appl Geophys 162:73–90. https://doi.org/10.1007/s00024-004-2580-8
78. Setyawan B, Sapiie B (2019) Correlation between the fractal of aftershock spatial distribution and active fault on Sumatra. Nat Hazards Earth Syst Sci. https://doi.org/10.5194/nhess-2019-215
79. Tiwari RK, Paudyal H (2021) Box counting fractal dimension and frequency size distribution of earthquakes in the central Himalaya region. J Inst Sci Technol 26:127–136. https://doi.org/10.3126/jist.v26i2.41664
80. Xu J (2011) Fractal analysis to study the structural distribution of Wenchuan earthquake in China. Adv Mater Res 243–249:4097–4100. https://doi.org/10.4028/www.scientific.net/AMR.243-249.4097

81. Hirata T, Satoh T, Ito K (1987) Fractal structure of spatial distribution of microfracturing in rock. Geophys J R Astron Soc 90:369–374. https://doi.org/10.1111/j.1365-246X.1987.tb00732.x
82. Pandey MR, Tandukar RP, Avouac JP et al (1995) Interseismic strain accumulation on the Himalayan crustal ramp (Nepal). Geophys Res Lett 22:751–754. https://doi.org/10.1029/94GL02971
83. Gulia L, Wiemer S (2010) The influence of tectonic regimes on the earthquake size distribution: a case study for Italy. Geophys Res Lett 37:1–6. https://doi.org/10.1029/2010GL043066
84. Mori J, Abercrombie RE (1997) Depth dependence of earthquake frequency-magnitude distributions in California: Implications for rupture initiation. J Geophys Res Solid Earth 102:15081–15090. https://doi.org/10.1029/97jb01356
85. Nuannin P, Kulhánek O, Persson L (2012) Spatial and temporal characteristics of aftershocks of the December 26, 2004 and March 28, 2005 earthquakes off NW Sumatra. J Asian Earth Sci 46:150–160. https://doi.org/10.1016/j.jseaes.2011.12.004
86. Farrell J, Husen S, Smith RB (2009) Earthquake swarm and b-value characterization of the Yellowstone volcano-tectonic system. J Volcanol Geotherm Res 188:260–276. https://doi.org/10.1016/j.jvolgeores.2009.08.008
87. Abu El-Nader IF, Shater A, Hussein HM (2016) Mapping b -values beneath Abu Dabbab from June to August 2004 earthquake swarm. NRIAG J Astron Geophys 5:403–412. https://doi.org/10.1016/j.nrjag.2016.07.002
88. Scholz CH (2002) The Mechanics of Earthquakes and Faulting. Cambridge University Press
89. Öncel AO, Main I, Alptekin Ö, Cowie P (1996) Temporal variations in the fractal properties of seismicity in the north anatolian fault zone between 31°E and 41°E. Pure Appl Geophys 147:147–159. https://doi.org/10.1007/bf00876441
90. Okubo PG, Aki K (1987) Fractal geometry in the San Andreas fault system (USA). J Geophys Res 92:345–355. https://doi.org/10.1029/JB092iB01p00345
91. Ram A, Roy PNS (2005) Fractal dimensions of blocks using a box-counting technique for the 2001 Bhuj earthquake, Gujarat, India. Pure Appl Geophys 162:531–548. https://doi.org/10.1007/s00024-004-2620-4
92. Chen CC, Wang WC, Chang YF et al (2006) A correlation between the b-value and the fractal dimension from the aftershock sequence of the 1999 Chi-Chi, Taiwan, earthquake. Geophys J Int 167:1215–1219. https://doi.org/10.1111/j.1365-246X.2006.03230.x
93. Mandal P, Rodkin MV (2011) Seismic imaging of the 2001 Bhuj Mw7.7 earthquake source zone: B-value, fractal dimension and seismic velocity tomography studies. Tectonophysics 512:1–11. https://doi.org/10.1016/j.tecto.2011.09.004
94. Goebel THW, Sammis CG, Becker TW et al (2015) A comparison of seismicity characteristics and fault structure between stick-slip experiments and nature. Pure Appl Geophys 172:2247–2264. https://doi.org/10.1007/s00024-013-0713-7

APPLIED GEOPHYSICS, Vol.19, No.3 (September 2022), P. 458–469, 8 Figures.
DOI:10.1007/s11770-022-0956-0

Spatio-temporal distribution of earthquake occurrence in Eastern Himalaya and vicinity (26°N – 31°N and 87°E – 98°E) based on b-value and fractal dimension

Ram Krishna Tiwari[1,2]*, Harihar Paudyal[2], and Daya Shanker[3]

Abstract: This study investigates the spatial and temporal variation of fractal dimension and b-value for the eastern part of the Himalaya and adjoining area (26°N – 31°N and 87°E – 98°E). The analysis is carried out on the earthquake dataset of 1373 events (Mc = 4.0) by sliding window technique for the period 1964 to 2020. The region is divided into three sub regions A (87°E – 92°E), B (92°E – 94°E) and C (94°E – 98°E). The b-value computed for the region A comprising eastern Nepal is smaller compared to other two regions which infers the possible high stress and asperities in the region. High spatial fractal dimension ($D_c > 1.5$) and low temporal fractal dimension ($D_t < 0.31$) are computed for the regions. High spatial fractal dimension may indicate that fractures generating earthquakes are approaching a 2D structure and low temporal fractal dimension implies high clustering of earthquake's epicenters. The b value shows a weak negative correlation with Dc for regions A and C while a weak positive correlation is observed for the region B. Based on b-value and fractal dimension, this study explains the frequency of earthquakes and heterogeneity of the seismogenic structure in this part of the Himalaya.
Keywords: Eastern Himalaya, fault, b-value, fractal dimension, earthquake clustering

Introduction

The Himalaya is one of the largest orogenic and seismically active belt, where the Indian continental crust is forced down beneath the Eurasian continental crust (Coudurier-Curveur et al., 2020; Dasgupta et al., 1987; Molnar and Pandey, 1989; Tapponnier et al., 1982). The several thrusts, lineaments, folded belts present in the Himalayas are found to be responsible for frequent earthquake occurrences in the region (Angelier and Baruah, 2009; Shanker et al., 2010; Verma, 1991). At the eastern part, the Himalaya structure deviates from its continuous gentle curvature and takes a sharp turn of about 90° (near 28°N latitude and 96°E longitude) along the Assam syntaxis. The most devastating earthquakes i.e. 1897 Mw 8.0 earthquake over the Shillong Plateau and 1950 Mw 8.6 earthquake in the Assam syntaxial region have occurred in this segment of the Himalaya. The main shock of the August 15, 1950 earthquake was located beyond the conventional limit of the eastern Himalaya, in the Assam syntaxial region, nearly 100 km

Manuscript received by the Editor December 12, 2021; revised manuscript received September 23, 2022.
1. Central Department of Physics, Tribhuvan University, Kirtipur, Kathmandu, Nepal.
2. Birendra Multiple Campus, Tribhuvan University, Bharatpur, Chitwan, Nepal.
3. Department of Earthquake Engineering, Indian Institute of Technology Roorkee, Roorkee, Uttarakhand, India.
*Corresponding author: Ram Krishna (Email: ram.tiwari@bimc.tu.edu.np).

east of the Mishmi thrust. Other notable earthquakes of the region are Cachar earthquake of 7.4 Mw (1869), Srimangal earthquake of 7.5 Mw (1918), Dhubri earthquake of 7.1 Mw (1930), and Manipur earthquake of 7.3 Mw (1988). The seismicity in eastern Himalaya is concentrated near Sikkim in the west, near longitude 92°– 94° E in the central part, and in the eastern part near the Mishmi Thrust (MT) (Baruah et al., 2013; Mugnier et al., 2013; Raghu Kanth and Dash, 2010). Recently, an earthquake of magnitude 6.9 Mw occurred on 18th of September, 2011 in Sikkim - Nepal Border region and the devastating earthquake of 7.8 Mw happened at the Gorkha district of Nepal followed by large number of aftershocks. The eastward propagation of the rupture of the mainshock of 2015 Gorkha, Nepal earthquake led to enhanced stresses on the eastern segment of the Main Himalayan Thrust (MHT) (Bilham, 2019; Bilham et al., 2017). The findings of Baillard et al. (2017) showed termination of seismic activity is characterized by subsequent jump-offs towards east, reaching almost 25 km after the May 12 Mw 7.3 main aftershock.

A research group have identified block of Eastern Himalaya near Main Central Thrust, Main Boundary Thrust, north of Kopili lineament and block of Shillong plateau near Dauki fault area as the most potential zone to have a strong event (Roy et al., 2015). The group of investigators estimated the spatial variation of seismic b-value in the Indo-Myanmar subduction zone of northeast India for the period 1996 – 2015, varying from 0.75 to 1.54 (Borgohain et al., 2018). For the period of 1973 – 2015, the b-values and fractal dimensions of entire Himalayan range was estimated (Jena et al., 2021). Their results showed an increase in b-value and clustering of epicenter from northwest to northeast Himalaya. Thus, the possibility of the occurrence of earthquakes in this part of the Himalayas cannot be overlooked. This study, therefore, focuses on this segment of the Himalayas (~1225 km) including the eastern part of Nepal, Bhutan, and northeast part of India (Figure 1). For this we have analyses the homogeneous earthquake data set of 1373 events (Mc = 4.0) to relate fractal correlation dimension (D_c) and frequency-magnitude relation characteristics of the seismogenic structures.

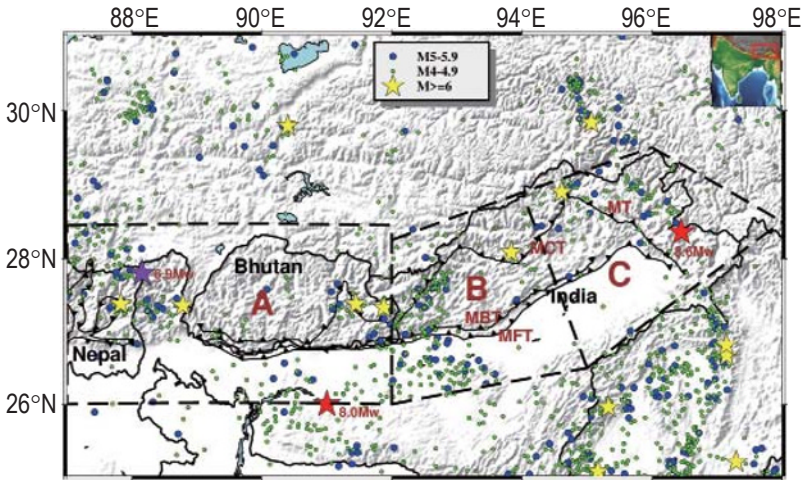

Figure 1. The distribution of 1373 earthquakes in the study region from 1964 to 2020. The areas of the present interest are outlined by black boxes into A, B, C. Red star at the boundary of region A is the Shillong earthquake of 1897 (8.0 Mw) and the red star in region C is the Assam earthquake of 1950 (8.6 Mw).The purple star is for 18 September 2011 (6.9 Mw) Sikkim earthquake. MCT stands for Main Central Thrust, MBT stands for Main Boundary Thrust, MFT stands for the Main Frontal Thrust and MT stands for the Mishimi Thrust.

The spatial and temporal variations of earthquake precursor (b-value and correlation fractal dimension) have been the focus of many studies (Bayrak and Bayrak, 2012; Bhattacharya et al., 2010; Mondal and Roy, 2016; Sarkar et al., 2020). The spatio-temporal variations in b-values are utilized to study structural heterogeneity and earthquakes forecast. The b-value varies mostly from 0.5 to 1.5 in a tectonically active region like Himalaya (Bhattacharya and Kayal, 2003; Kayal et al., 2012; Smith, 1981). Similarly, the space-time distributions of fractal dimension of earthquake quantify the randomness and clustering of seismic events with in each region. The fractal properties are considered as a consequence of a self-organized critical state of the earth's crust that is intimately linked to the stress in the crust (Schorlemmer et al., 2005; Shcherbakov et al., 2015; Smalley et al., 1987). Jiang and Diao (1995) derived the quantitative relationship between fractal dimension of seismic activities in spatial distribution and b-value. The b-value has a positive correlation with the fractal dimension of the distribution and is inversely

related to the ambient stress level (Huang and Turcotte, 1988). Roy et al. (2011) found that the smaller b-value zones are corroborated with lower fractal correlation dimension (0.5 – 0.9) and they have a positive correlation for the Andaman-Sumatra subduction zone. A negative correlation between the b-value and the fractal dimension of the spatial distribution of earthquakes was observed in the Tohoku region of the Japan (Hirata, 1989).

Data and method

In this work, we have analyzed the earthquake data from period 1964 to 2020 prepared from the available catalogs of the International Seismological Centre (ISC) (https://www.isc.ac.uk) and the United States Geological Survey (USGS) (https://earthquake.usgs.gov). For the preparation of the database, we retrieved the earthquake data from the above sources and obtained 2941 earthquakes. For the homogeneity of the data, we use the global magnitude conversion relation (Das et al., 2011). According to the relation, the Mw scale is converted into mb as

$$mb=M_w\,(0.65\pm0.003)+(1.65\pm0.02) \text{ with } R^2=0.54. \quad (1)$$

After de-clustering the catalog and removing all foreshocks and aftershocks by window method (Gardner and Knopoff, 1974), we retained only 2187 events. Magnitude of completeness is then calculated by maximum curvature technique (Wiemer and Wyss, 2000) and it was found to be 4.0 (Figure 2). Now, we left with 1373 events having magnitude ≥4.0 mb. Moreover, the segment of eastern Himalaya ~1225 km (26°N – 31°N and 87°E – 98°E) is subdivided into three regions stretching from the eastern Nepal (aftershocks dominant region of 2015 Gorkha event) to the eastern syntaxis of the Himalaya. The whole idea is to cover the bent structure of the eastern Himalaya excluding the Arakan-Yoma fold belt. The subdivided regions encloses only 499 events for the period of 1964.02.01 to 2020.12.10. The details of the subdivisions are presented as:

Region A - 87°E – 92°E (eastern Nepal, Sikkim and Bhutan comprising 214 events)

Region B - Near longitude 92°E – 94°E (Central part of eastern Himalaya where it takes sharp turn comprising 197 events)

Region C- 94°E–98°E (Near the Mishmi Thrust region in the Assam syntaxis comprising 88 events)

Different models have been developed to describe the statistical properties of earthquake distributions in time, space, and magnitude domains. Some models explain the occurrence of earthquake events as quasi-periodic while the other says earthquake events are randomly distributed and follow the Poisson distribution (Werner and Sornette, 2008). Recent results (Matcharashvili et al., 2018) indicate that the sequences of earthquake in the Caucasus mountains are low-dimensional and nonlinear. A similar result was noticed for the temporal distribution of Japanese earthquakes (Goltz, 1997). Sobolev (2011) reported the existence of deterministic chaos in (smoothed) seismic time series. From these literature, it can be concluded that the real seismic processes show intermediate behavior between random and deterministic process which can be explained by fractal geometry. By computing b-value and correlation dimension from sliding window technique (Chen et al., 2006; Prokoph, 1999; Öncel et al., 1995), the present investigation attempts to explain the fractal properties of earthquakes in Eastern Himalaya. A window containing a fixed number of events rather than a fixed period was chosen to ensure the existence of enough points for the reliable value of b and fractal dimension.

Frequency magnitude distribution

The b-value is an important parameter that describes the characteristics of an ensemble of earthquakes. Geometrically, it is the negative slope of the log-cumulative-frequency versus magnitude plot (Figure 2). The calculation of b-value has been successfully used by

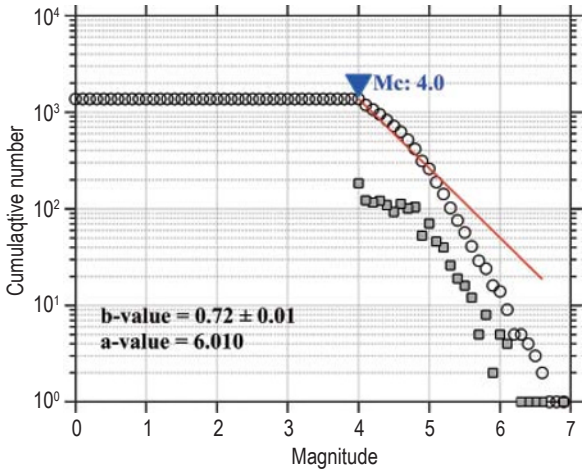

Figure 2. Magnitude of completeness (Mc = 4.0) and b-value (0.72 ± 0.01) of the frequency magnitude distribution of de-clustered catalog. The gray filled squares indicate the number of earthquakes in individual magnitude level.

several authors since the 1940s for different regions of the world. For example, the seismic b value in northeast India is found to vary from 0.6 to 1.0 (Bhattacharya et al., 2010), the b-values (0.5–0.9) obtained for the earthquakes ($2.5 \leq M \leq 5.0$) in the northeast region of the India (Bhattacharya and Kayal, 2003), relatively high b-values (b = 1.5) is obtained for Shinmoe-dake, Kirishima volcano, Japan (Chiba and Shimizu, 2018), and the higher b-value was found for events accompanied frictional sliding and deformation of a ductile rock (Scholz, 1968). Guttenberg and Richter (1944) relation has been suggested as a generalized fractal dimension of earthquake magnitude. The relation is expressed as:

$$\log_{10} N = a - bM_c. \quad (2)$$

In the relation above, constant 'a' indicates the seismicity level with 10a, the total number of earthquakes, and another constant b also known as b-value indicates the relative earthquake size distribution. A high b-value region has a low level of stress accumulation and a low b-value region has a prominent level of stress accumulation. In other words, a low b-value indicates an active region subjected to higher applied shear stress after the mainshock and overwhelmed by large events whereas regions with higher b-values have experienced slip (Wyss, 1973). The letter N in the above relation is the number of earthquakes in the group having magnitudes larger than equal to completeness magnitude Mc. The magnitude of completeness is a statistical way to determine the quality of an earthquake catalog which gauges how detailed our monitoring is in the region of study. The b-value is calculated by the maximum likelihood method (Aki, 1965) from the software ZMAP (Wiemer and Wyss, 2000). A maximum likelihood estimation of b-value is given by:

$$b = \log_{10} e \left(\frac{1}{\bar{M} - M_{min}} \right), \quad (3)$$

where $\bar{M}$ is the average magnitude and M_{min} is the minimum magnitude of the data set. An estimate of the standard deviation (δb) of the b-value is given as suggested by (Shi and Bolt, 1982)

$$\delta b = 2.3 b^2 \sqrt{\frac{\sum_i^N (M_i - \bar{M})^2}{n(n-1)}}, \quad (4)$$

where n is the sample size (total number of events in the given window).

The spatial variations in the b-value have been reported for diverse stress regimes worldwide. The studies indicate that normal and thrust faulting regimes have higher and lower b-values, respectively, while strike-slip faulting regimes have intermediate b-values. The b-value variations in different tectonic domains may also be related to structural heterogeneity and stress distribution (Mogi, 1967; Scholz, 1968). For areas with greater geological complexity, a high b-value was reported, indicating the existence of the multiple fracture. In contrast, a low b-value was reported for the areas having no uniformities of a cracked medium and a low degree of variation in rock properties like large stress, high deformation rate, and large faults (Bridges and Gao, 2006; Wiemer and Wyss, 2000).

Fractal dimension

The spatial and temporal distribution patterns of fault and earthquake seismicity were demonstrated to be fractal (Goltz, 1997; Huang and Turcotte, 1988). The fractal dimension of seismicity is a measure of the degree of both the heterogeneity of the process and the clustering of the seismic activity (Öncel et al., 1995). It can be quantified by the correlation dimension based on the correlation integral technique (Grassberger and Procaccia, 1983).

Spatial fractal correlation dimension

The spatial correlation dimension, a lower bound of the fractal dimension is a measure of the scaling in the spatial distribution of events. Being straightforward and quick, it has an advantage over other dimensions like the Hausdorff dimension, the box-counting dimension, etc. It is less noisy even when only a small number of points is available, and is often in agreement with other calculations of dimension. The correlation integral method (Mondal et al., 2019; P. Roy and Mondal, 2009; Roy and Padhi, 2007) is used for the given set of earthquakes in which correlation integral function C(r) is defined as,

$$C(r) = \frac{2}{N(N-1)} \sum_{\substack{i,j=1 \\ i \neq j}}^{N} H(r - |X_i - X_j|), \quad (5)$$

where N is the number of total earthquakes in the given window, X_i–X_j is the angular distance between two events calculated by the spherical triangle method (Hirata, 1989) and H (.) is the Heaviside step function. After calculating the correlation integral, the spatial correlation dimension can be defined from the power-law relation (Kagan, 2007)

$$C(r) \sim r^{D}. \quad (6)$$

The graph is then plotted for *logr–log C*(*r*) and D is obtained as the slope of the linear segment of the graph.

Temporal fractal correlation dimension

A seismic process can be characterized by its fluctuating behavior, with temporal phases of low activity interspersed between highly active phases where the density of the events is relatively large. The time between two successive seismic events follows power-law distribution. To investigate the temporal fluctuations of seismic sequences, the temporal correlation dimension is calculated (Telesca et al., 2001, 2012; Mondal and Roy, 2016). The correlation function $C(\tau)$ is defined as

$$C(\tau) = \frac{2}{N(N-1)} \sum_{\substack{i,j=1 \\ i \neq j}}^{N} H(\tau - |t_i - t_j|), \quad (7)$$

where N is the total number of earthquakes in the given window, τ is scaling time, t_i - t_j is the inter occurrence time and H (.) is the Heaviside step function. Now the temporal correlation dimension can be defined from the power-law relation

$$C(\tau) \sim \tau^{D}. \quad (8)$$

The graph is plotted for $log\tau$–$log\ C(\tau)$ then D is obtained as the slope of the linear segment of the graph. The temporal correlation fractal dimension provides the information of clustering nature of earthquake distribution in the time domain which is the most important marker of the changes of the physical state of the earthquake (Enescu et al., 2005; Hirata and Imoto, 1991).

Results and discussion

In the present study, b-value of Gutenberg-Richter relation and correlation fractal dimension are computed by sliding window technique for the three sub regions and the results are presented in table 1, table 2 and table 3. After performing the several test for varying number of events for different windows, 100 event window is decided as optimal size for detection of sudden temporal change of estimated parameter.

Table 1: Time window, b-value, temporal correlation dimension (D_t), and spatial correlation dimension (D_c) with their coefficient of determination (R^2) for 7 windows (6 windows of 100 events and 7th window of 94 events) of region A.

Window	Time	b-value	D_t	R^2	D_c	R^2
1	1964-02-01- 2000-03-17	0.56 ± 0.03	0.24 ± 0.009	0.986	1.88 ± 0.04	0.990
2	1975-04-24-2004-08-09	0.67 ± 0.05	0.26 ± 0.009	0.992	1.75 ± 0.02	0.995
3	1986-01-07-2007-08-11	0.76 ± 0.06	0.24 ± 0.003	0.998	1.88 ± 0.05	0.978
4	1994-03-24- 2012-09-18	0.81 ± 0.07	0.26 ± 0.005	0.997	1.79 ± 0.03	0.991
5	1997-09-13-2015-09-11	0.80 ± 0.07	0.25 ± 0.007	0.992	1.68 ± 0.03	0.988
6	2005-05-14-2018-07-19	0.85 ± 0.08	0.25 ± 0.006	0.993	1.56 ± 0.02	0.995
7	2004-09-27-2020-12-10	0.83 ± 0.08	0.25 ± 0.006	0.994	1.63 ± 0.03	0.988
Entire region A	1964-02-01-2020-12-10	0.68 ± 0.04	0.24 ± 0.006	0.994	1.80 ± 0.02	0.995

The temporal occurrence of the events (Figure 3a) and the magnitude density distribution (Figure 3b) gives the knowledge of the earthquake dataset we are going to analyze for region A. The frequency magnitude distribution b-value for 7 fixed events windows varied from 0.56 to 0.85. The increment in the b-value was noticed in the recent years (Table 1). The lowest b-values 0.56 ± 0.03 was observed for window 1 (1964.02.01 to 2000.03.17). The frequency magnitude distribution b-value for the entire region A was found to be 0.68 ± 0.04 (Figure 3c). A b-value less than average value of 1 reported for all windows and for entire region A indicate the high-stress level in the region. The temporal variation of b-value (Figure 3d) shows the lowest value 0.85 on 30 November 2007 i.e. before the 2011 Sikkim earthquake (6.9 Mw), a notable earthquake of the region in the recent past. From 2011 onwards it was reported to rise and seems to settle around the global mean value of 1. The b-values reported are accepted for the seismically active continental collision zone indicating the release of strain energy through the small to moderate earthquakes. These results are comparable with the work of other groups of researchers for the same region. According to Singh et al. (2009), the b value varies from 0.61 to 1.36 and it was reported from 0.6 to 1.0 by Bhattacharya and Kayal (2003).

The value of spatial correlation dimension (Dc) ranges from 1.56 to 1.88. For window 1 of period 1964.02.01 to 2000.03.17 and window 3 of period 1986.01.17 to 2007.08.11, it has the highest values. It assigns the lowest value (1.56 ± 0.02) for window 6 of period 2005.05.14 to 2018.07.19 (Table 1) and 1.80 ± 0.02 for the entire region A (Figure 4a). The spatial correlation dimension gives an estimate of the fractal characteristics of the fault system. According to Tosi (1998), the D_c values close to 2 imply the earthquake sources are distributed in 2-dimensional space, and the Dc values close to 1 means the events are distributed in line sources. D_c values computed for the region A are > 1.5 indicating the near planar nature of the seismogenic sources. High D_c and low b values obtained for this region suggest the formation of heterogeneity across the underlying faults that could generate a medium to strong earthquake in the region. Our work is comparable with the work of Sarkar et al. (2020), according to them, the Dc value varies in northeast India from 0.37 to 1.82. The temporal correlation dimension ranges from 0.24 to 0.25 for 7 windows (Table 1) and it is 0.24 ± 0.006 with R^2 = 0.994 for the entire study period (Figure 4b). The range of temporal variation of correlation is small with a low value. These results suggest the strong and homogeneous level of the clustering of events in the region. Moreover, the seismicity is distributed more uniformly which may lead to activation of nearby faults for probable future large events. The b-value and Dc value variation with different window shows that there is not any clear trend of variation between them (Figure 4c). The b-Dc relationship is proposed as an effective indicator of seismic hazards (Bayrak and Bayrak, 2012). It was revealed as D_c = -0.81b+2.35 with R^2 = 0.477 (Figure 4d) for the region A. Two parameters are negatively correlated though it is a weak correlation.

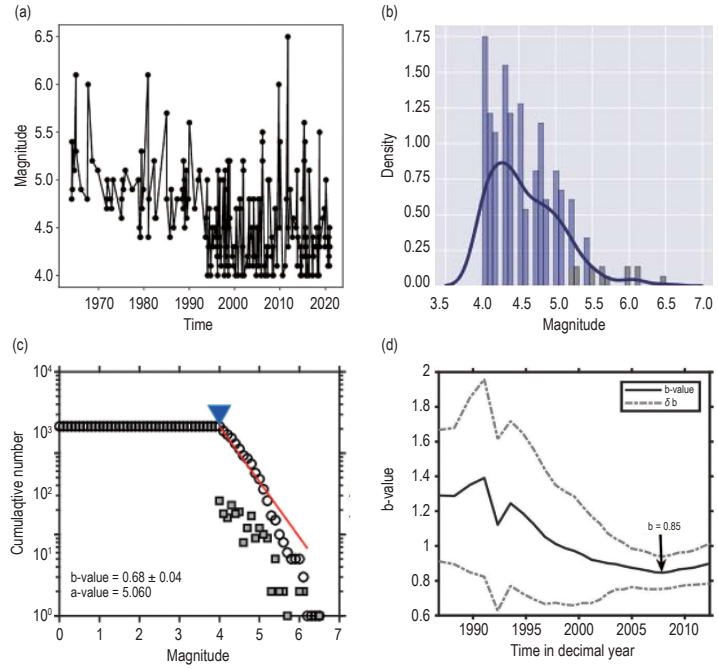

Figure 3. Seismic character parameter for for region A. (a) Temporal evolution of magnitude of the earthquake for the study period. (b) Distribution of magnitude in terms of probability density plot (blue curve) and histogram depicting unimodel and left skewed distribution of magnitude. (c) Frequency magnitude distribution b-value. magnitude. (c)–(d) b-value variation with time where dashed lines represent the standard deviation. The temporal variation b-value is obtained for sample window size of 100 events with overlap of 4%.

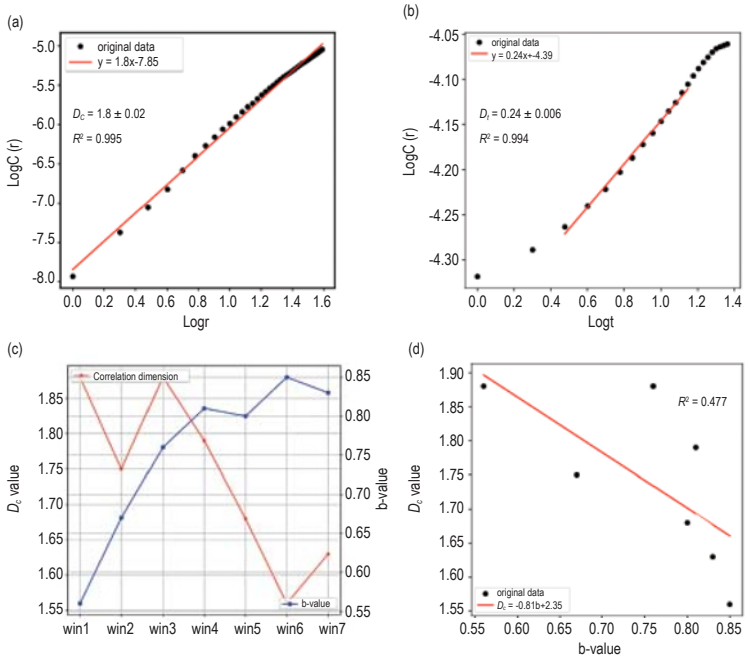

Figure 4. Graphs showing (a) spatial fractal correlation dimension, (b) temporal fractal correlation dimension, (c) Variation of b-value and D_c value for different windows, and (d) Empirical relationships between the b and Dc value for the region A.

The temporal distribution (Figure 5a) and the density functions (Figure 5b) of earthquake magnitude are for the knowledge of dataset we are going to analyze for region B. We computed the frequency magnitude distribution b-value for 6 windows and noticed to range from 0.56 to 1.01. The b-value 1.01 ± 0.08 was reported for window 5 (1995.09.29 to 2015.11.25) while the lowest value 0.56 ± 0.03 was reported for window 1 (1964.09.01 to 1997.06.02). The b values close to 1 were reported for time windows after 1991 (Table 2). These value are acceptable for the seismically active continental collision zone of the Himalaya. The b-value for entire region B (Figure 5c) is smaller than the global average value of 1. The time variation of the b-value shows the cyclic decreasing trend for the study period (Figure 5d). These findings reflect the high probability of occurrence of small events than large events.

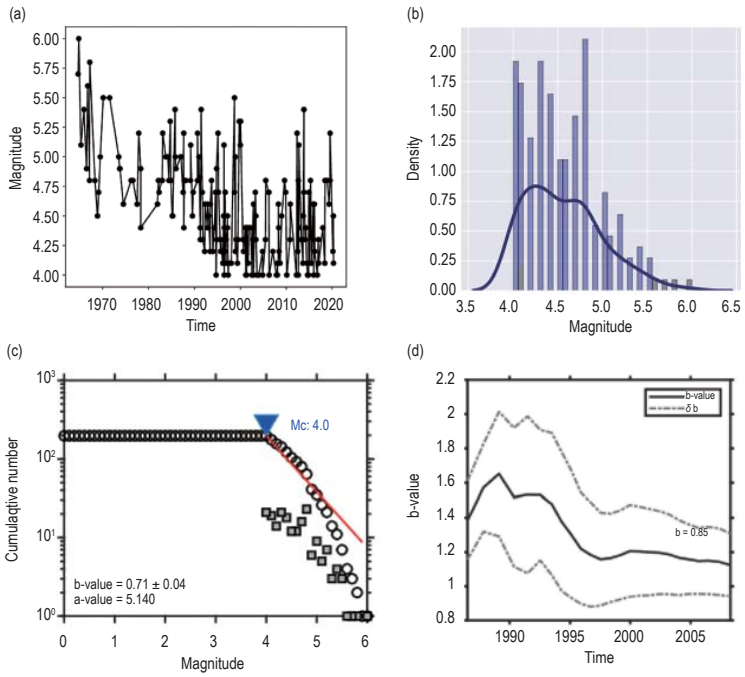

Figure 5. Seismic character parameter for region B. (a) Temporal evolution of magnitude of the earthquake for the study period, (b) Distribution of magnitude in terms of probability density plot (blue curve) and histogram depicting bimodel distribution of magnitude (c) Frequency magnitude distribution b-value, and (d) b-value variation with time where dashed lines represent the standard deviation. The temporal variation b-value is obtained for sample window size of 100 events with overlap of 4%.

The spatial correlation dimension ranges from 1.55 ± 0.01 to 1.73 ± 0.01 for 6 different windows. The highest D_c (1.73 ± 0.01) was reported for window 1 of period 1964.09.01 to 1997.06.02 and the lowest D_c (1.55 ± 0.01) for window 2 of period 1986.12.31 to 2006.06.20 (Table 2). The D_c value of 1.72 ± 0.01 was noticed for the entire region of the study with R^2 = 1.0 (Figure 6a). The high values of D_c and global average value of b are supposed to represent the occurrence of a small to moderate earthquake in the region. The temporal correlation dimension ranged from 0.25 ± 0.004 to 0.31 ± 0.008 for 6 different windows (Table 2) and it is 0.28 ± 0.005 with R^2 = 0.997 for the entire study period (Figure 6b). This low value of temporal dimension may be the indicator of intense temporal clustering of events that could trigger large events in the future. The D_c and b-value plot for different windows (Figure 6c) does not show any trend in their variation. The correlation between D_c value and b-value is negative and not significant as given by the equation D_c = -0.07b+1.71 with R^2 = 0.044 (Figure 6d).

The temporal distribution (Figure 7a) and the density functions of magnitude of the earthquake

Table 2: Time window, b-value, temporal correlation dimension (D_t), and spatial correlation dimension (D_c) with their coefficient of determination (R^2) for 6 windows (5 windows of 100 events and 6th window of 97 events) of region B.

Window	Time	b-value	D_t	R^2	D_c	R^2
1	1964-09-01- 1997-06-02	0.56 ± 0.03	0.27 ± 0.002	0.998	1.73 ± 0.01	0.998
2	1986-12-31-2001-06-20	0.74 ± 0.05	0.25 ± 0.004	0.998	1.55 ± 0.01	0.997
3	1986-12-31-2006-04-11	0.81 ± 0.06	0.29 ± 0.006	0.995	1.64 ± 0.01	0.999
4	1991-11-11- 2012-08-09	0.98 ± 0.08	0.31 ± 0.008	0.993	1.65 ± 0.03	0.991
5	1995-09-29-2015-11-25	1.01 ± 0.08	0.29 ± 0.008	0.992	1.62 ± 0.02	0.994
6	1997-08-06-2020-04-17	0.98 ± 0.08	0.25 ± 0.006	0.993	1.69 ± 0.02	0.993
Entire region B	1964-09-01-2020-04-17	0.71 ± 0.04	0.28 ± 0.005	0.997	1.72 ± 0.01	0.998

(Figure 7b) reflect the nature of the earthquake occurred in the region C for the study period. The frequency magnitude distribution

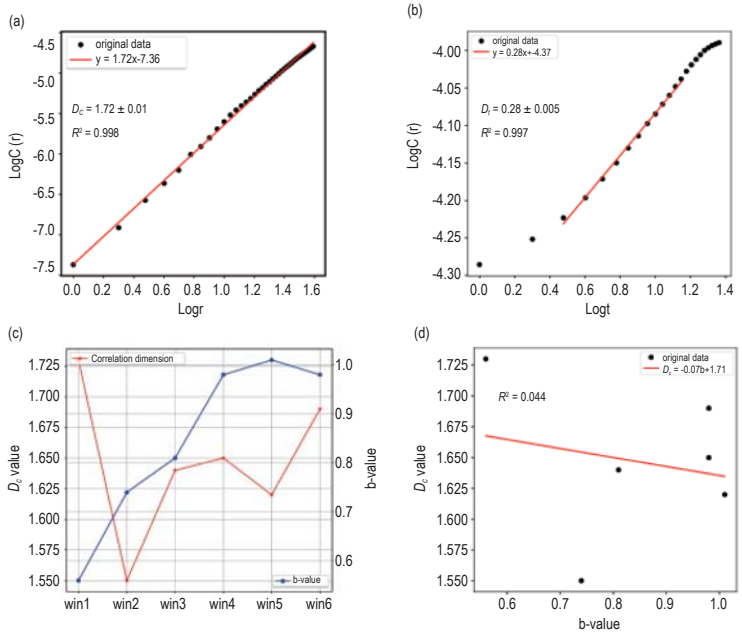

Figure 6. Graphs showing (a) spatial fractal correlation dimension, (b) temporal fractal correlation dimension, (c) Variation of b-value and D_c value for different windows, and (d) Empirical relationships between the b and D_c value for the region B.

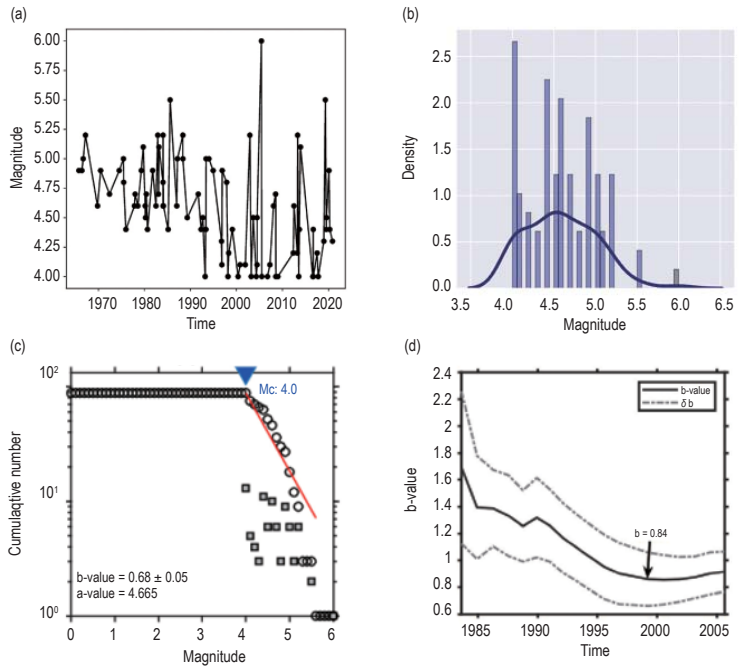

Figure 7. Seismic character parameter for region C. (a) Temporal evolution of magnitude of the earthquake for the study period, (b)) Distribution of magnitude in terms of probability density plot (blue curve) and histogram depicting unimodel and no skewed distribution of magnitude, (c) Frequency magnitude distribution b-value, and (d) b-value variation with time where dashed lines represent the standard deviation. The temporal variation b-value for region is obtained for sample window size of 50 events with overlap of 4% of the events due to paucity of data.

b-value ranges from 0.55 ± 0.03 to 0.89 ± 0.12. It is the lowest 0.55 ± 0.03 for window 1 for the period of 1965.10.06 to 1998.02.21 and the highest 0.89 ± 0.12 for window 3 for the period of 1993.04.12 to 2020.11.08 (Table 3). The b-value was computed 0.68 ± 0.05 for the entire region C (Figure 7c). The b-values in recent time is close to global average value of 1 and reasonable for the seismically active region. The temporal variation of b-value shows initial decreasing trend and the lowest value is observed as 0.84 on 8 April 1999 and thereafter it is gradually increasing towards the stable value (Figure 7d). These findings suggest that accumulated stress is releasing through the small to moderate earthquake in the region. The earlier work in the region by Kumar and Sharma (2019) conclude that stress is accumulating in the upper part of Assam and eastern parts of Arunachal Pradesh near Mishmi hills and the region may experience moderate to large magnitude earthquakes in the future.

High Dc 1.73 ± 0.04 is observed for window 2 from 1981.10.14 to 2012.05.04 and low Dc 1.52 ± 0.03 is observed for window 3 from 1993.04.12 to 2020.11.08. Dc for the entire region is 1.67 ± 0.04 with R2 = 0.992 (Figure 8a). High Dc values obtained for the region show the formation of heterogeneity across the underlying faults. The temporal correlation dimension ranges from 0.25 to 0.26 for 3 windows (Table 3) and it is 0.26 ± 0.009 with R^2 = 0.998 for the entire study period (Figure 8b). The lowest value of the temporal fractal dimension observed in this region may be the indication of the strong clustering of the events. The increasing or decreasing trend of the D_c and b-value does not show any particular trend (Figure 8c). Statistically, there is a negative

correlation between Dc and b value defined by the equation Dc = - 0.2b + 1.75 with R^2 = 0.096 (Figure 8d). The positive correlation between these precursor parameters agrees with the previous work that investigated at the earthquake source zone in northeast India (Bhattacharya et al., 2010).

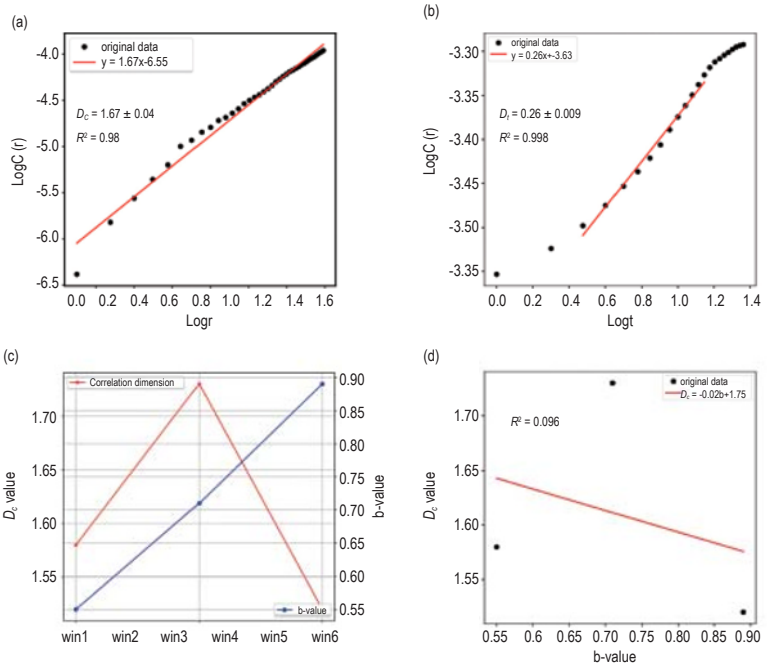

Figure 8. Graphs showing (a) spatial fractal correlation dimension, (b) temporal fractal correlation dimension, (c) Variation of b-value and D_c value for different windows, and (d) Empirical relationships between the b and D_c value for the region C.

Conclusions

In this study, the evolution of the seismicity is characterized by the b-value of frequency magnitude distribution and the fractal dimension at the selected regions A, B, and C of the Himalaya. The measurements are carried out by sliding window technique with a window advanced of 20 events. We have employed the maximum likelihood method for the evaluation of the b-value and the correlation integral method to calculate the fractal dimension. The b-value for region A is 0.68 ± 0.04. It is 0.71 ± 0.04 for region B and 0.68 ± 0.05 for region C. The observed b-values are less than the average value of 1. The b-value is similar for the sub regions that signifies the same seismicity behavior in the regions. The b value is related to the stability of the crust and when it is perturbed from its equilibrium value of 1 it tends to regain its average values by oscillating back and forth. These oscillations are manifested as earthquakes. Thus, the possibility of a future large event cannot be underrated for this part of the Himalayas. The spatial correlation dimension is 1.73 ± 0.02 for region A. It is 1.70 ± 0.02 for region B and 1.61 ± 0.02 for region C. In terms of temporal fractal dimension region, A owned the value 0.27 ± 0.004, region B owned 0.27 ± 0.004, and region C owned the value 0.25 ± 0.006. The spatial correlation dimension (D_c) >1.5 indicates near the planar structure of the fault in the region. The high value of D_c and low b-value indicates the chances of arbitrary occurrence of large events in the region. The highest D_c value, low b-value, and the low value of temporal fractal dimension (D_t) indicate the clustering of small events which could transfer the stress in the nearby fault triggering large future events in the region.

Table 3: Time window, b-value, temporal correlation dimension (Dt), and spatial correlation dimension (Dc) with their coefficient of determination (R2) for 3 windows (2 windows of 50 events and 3rd window of 49 events) of region C.

Window	Time	b-value	D_t	R^2	D_c	R^2
1	1965-10-06-1998-02-21	0.55 ± 0.03	0.26 ± 0.008	0.990	1.58 ± 0.02	0.992
2	1981-10-14-2012-05-04	0.71 ± 0.08	0.25 ± 0.007	0.992	1.73 ± 0.04	0.984
3	1993-04-12-2020-11-08	0.89 ± 0.12	0.25 ± 0.011	0.980	1.52 ± 0.03	0.982
Entire region C	1965-10-06-2020-11-08	0.68 ± 0.05	0.26 ± 0.009	0.998	1.67 ± 0.04	0.992

Acknowledgments

One of the authors (RKT) would like to acknowledge Tribhuvan University, Nepal for providing sabbatical leave and University Grants Commission (UGC), Nepal for providing financial support in the form of fellowship. We would also like to acknowledge two anonymous reviewers for their suggestions for the improvement of

the manuscript.

References

Aki, K., 1965, Maximum likelihood estimate of b in the formula Log N = a - bM and its confidence limits: Bulletin of Earthquake Research Institute Tokyo University, **43**, 237–239.

Angelier, J., and Baruah, S., 2009, Seismotectonics in Northeast India: A stress analysis of focal mechanism solutions of earthquakes and its kinematic implications: Geophysical Journal International, **178**(1), 303–326. https://doi.org/10.1111/j.1365-246X.2009.04107.x

Baillard, C., Lyon-Caen, H., Bollinger, L., Rietbrock, A., Letort, J., and Adhikari, L. B., 2017, Automatic analysis of the Gorkha earthquake aftershock sequence: Evidences of structurally segmented seismicity: Geophysical Journal International, **209**(2), 1111–1125. https://doi.org/10.1093/gji/ggx081

Baruah, S., Baruah, S., and Kayal, J. R., 2013, State of tectonic stress in Northeast India and adjoining south Asia region: An appraisal: Bulletin of the Seismological Society of America, **103**(2 A), 894–910. https://doi.org/10.1785/0120110354

Bayrak, Y., and Bayrak, E., 2012, Regional variations and correlations of Gutenberg-Richter parameters and fractal dimension for the different seismogenic zones in Western Anatolia: Journal of Asian Earth Sciences, **58**, 98–107. https://doi.org/10.1016/j.jseaes.2012.06.018

Bhattacharya, and Kayal, J. R., 2003, Mapping the b-value and its correlation with the fractal dimension in the northeast region of India: Journal of the Geological Society of India, **62**(6), 680–695.

Bhattacharya, P. M., Kayal, J. R., Baruah, S., and Arefiev, S. S., 2010, Earthquake Source Zones in Northeast India: Seismic Tomography, Fractal Dimension and b Value Mapping: Pure and Applied Geophysics, **167**(8–9), 999–1012. https://doi.org/10.1007/s00024-010-0084-2

Bilham, R., 2019, Himalayan earthquakes: A review of historical seismicity and early 21st century slip potential: Geological Society Special Publication, **483**(1), 423–482. https://doi.org/10.1144/SP483.16

Bilham, R., Mencin, D., Bendick, R., and Bürgmann, R., 2017, Implications for elastic energy storage in the Himalaya from the Gorkha 2015 earthquake and other incomplete ruptures of the Main Himalayan Thrust: Quaternary International, **462**, 3–21. https://doi.org/10.1016/j.quaint.2016.09.055

Borgohain, J. M., Borah, K., Biswas, R., and Bora, D. K., 2018, Seismic b-value anomalies prior to the 3rd January 2016, Mw = 6.7 Manipur earthquake of northeast India: Journal of Asian Earth Sciences, **154**, 42–48. https://doi.org/10.1016/j.jseaes.2017.12.013

Bridges, D. L., and Gao, S. S., 2006, Spatial variation of seismic b-values beneath makushin Volcano,Unalaska Island,Alaska: Earth and Planetary Science Letters, **245**, 408–415. https://doi.org/10.1016/j.epsl.2006.03.010

Chen, C. C., Wang, W. C., Chang, Y. F., Wu, Y. M., and Lee, Y. H., 2006, A correlation between the b-value and the fractal dimension from the aftershock sequence of the 1999 Chi-Chi, Taiwan, earthquake: Geophysical Journal International, **167**(3), 1215–1219. https://doi.org/10.1111/j.1365-246X.2006.03230.x

Chiba, K., and Shimizu, H., 2018, Spatial and temporal distributions of b-value in and around Shinmoe-dake, Kirishima volcano, Japan: Earth, Planets and Space, **70**(1). https://doi.org/10.1186/s40623-018-0892-7

Coudurier-Curveur, A., Tapponnier, P., Okal, E., Van der Woerd, J., Kali, E., Choudhury, S., Baruah, S., Etchebes, M., and Karakaş., 2020, A composite rupture model for the great 1950 Assam earthquake across the cusp of the East Himalayan Syntaxis: Earth and Planetary Science Letters, **531**, 1–13. https://doi.org/10.1016/j.epsl.2019.115928

Das, R., Wason, H. R., and Sharma, M. L., 2011, Global regression relations for conversion of surface wave and body wave magnitudes to moment magnitude: Natural Hazards, **59**(2), 801–810. https://doi.org/10.1007/s11069-011-9796-6

Dasgupta, S., Mukhopadhyay, M., and Nandy, D. R., 1987, Active transverse features in the central portion of the Himalaya: Tectonophysics, **136**(3–4), 255–264. https://doi.org/10.1016/0040-1951(87)90028-X

Enescu, B., Ito, K., Radulian, M., Popescu, E., and Bazacliu, O., 2005, Multifractal and chaotic analysis of Vrancea (Romania) intermediate-depth earthquakes: Investigation of the temporal distribution of events: Pure and Applied Geophysics, **162**(2), 249–271. https://doi.org/10.1007/s00024-004-2599-x

Gardner, J. K., and Knopoff, L., 1974, Is The Sequence of Earthquakes in Southern California, With Aftershocks Removed, Poissonian?: Bulletin of the Seismological Society of America, **64**(5), 1363–1367. https://doi.org/10.1.1.467.2509

Goltz, C., 1997, Earthquakes and Fractals. In Fractal and Chaotic Properties of Earthquakes (p. 182): Springer, Berlin, Heidelberg. https://doi.org/10.1007/BFb0028315

Grassberger, P., and Procaccia, I., 1983, Characterization of strange attractors: Physical Review Letters, **50**(5), 346–349. https://doi.org/10.1103/PhysRevLett.50.346

Gutenberg, B., and Richter, C. F., 1944, Frequency of earthquakes in California: Bulletin of the

Seismological Society of America, **34**, 185–188.

Hirata, T., 1989, A correlation between the b value and the fractal dimension of earthquakes: Journal of Geophysical Research, **94**(B6), 7507–7514. https://doi.org/10.1029/JB094iB06p07507

Hirata, T., and Imoto, M., 1991, Multifractal analysis of spatial distribution of microearthquakes in the Kanto region. Geophysical Journal International: **107**(1), 155–162. https://doi.org/10.1111/j.1365-246X.1991.tb01163.x

Huang, J., and Turcotte, D. L., 1988, Fractal distributions of stress and strength and variations of b-value: Earth and Planetary Science Letters, **91**(1–2), 223–230. https://doi.org/10.1016/0012-821X(88)90164-1

Jena, R., Ghansar, T. A. A., Pradhan, B., and Rai, A. K., 2021, Estimation of fractal dimension and b-value of earthquakes in the Himalayan region: Arabian Journal of Geosciences, **14**(10). https://doi.org/10.1007/s12517-021-07271-4

Jiang, H. K., and Diao, S. Z., 1995, A model of seismicity with fractal structures and a preliminary discussion on the relation between D and b value: Acta Seismologica Sinica, **8**(4), 647–652. https://doi.org/10.1007/BF02650533

Kagan, Y. Y., 2007, Earthquake spatial distribution: The correlation dimension: Geophysical Journal International, **168**(3), 1175–1194. https://doi.org/10.1111/j.1365-246X.2006.03251.x

Kayal, J. R., Arefiev, S. S., Baruah, S., Hazarika, D., Gogoi, N., Gautam, J. L., Baruah, S., Dorbath, C., and Tatevossian, R., 2012, Large and great earthquakes in the Shillong plateau-Assam valley area of Northeast India Region: Pop-up and transverse tectonics: Tectonophysics, 532–535, 186–192. https://doi.org/10.1016/j.tecto.2012.02.007

Kumar, S., and Sharma, N., 2019, The seismicity of central and north-east Himalayan region: Contributions to Geophysics and Geodesy, **49**(3), 265–281. https://doi.org/10.2478/congeo-2019-0014

Matcharashvili, T., Chelidze, T., Javakhishvili, Z., Zhukova, N., Jorjiashvili, N., Shengelia, I., Mepharidze, E., and Sborshchikovi, A., 2018, Analysis of the Complexity of Seismic Data Sets: Case Study for Caucasus: In Complexity of Seismic Time Series (pp. 3-24). Elsevier.

Mogi, K., 1967, Earthquakes and fractures: Tectonophysics, **5**(1), 35–55. https://doi.org/10.1016/0040-1951(67)90043-1

Molnar, P., and Pandey, M. R., 1989, Rupture zones of great earthquakes in the Himalayan region: Proceedings of the Indian Academy of Sciences - Earth and Planetary Sciences, **98**(1), 61–70. https://doi.org/10.1007/BF02880376

Mondal, S. K., and Roy, P. N. S., 2016, Temporal multifractal pattern of seismicity in northwest Himalayan region: Journal of the Geological Society of India, **88**(5), 569–575. https://doi.org/10.1007/s12594-016-0522-6

Mondal, S. K., Roy, P. N. S., Catherine, J. K., and Pandey, A. K., 2019, Significance of fractal correlation dimension and seismic b-value variation due to 15th July 2009, New Zealand earthquake of mw 7.8: Annals of Geophysics, **62**, 1–17. https://doi.org/10.4401/ag-8020

Mugnier, J. L., Gajurel, A., Huyghe, P., Jayangondaperumal, R., Jouanne, F., and Upreti, B., 2013, Structural interpretation of the great earthquakes of the last millennium in the central Himalaya: Earth-Science Reviews, **127**, 30–47. https://doi.org/10.1016/j.earscirev.2013.09.003

Öncel, A. O., Alptekin, Ö., and Main, I., 1995, Temporal variations of the fractal properties of seismicity in the western part of the north anatolian fault zone: Possible artifacts due to improvements in station coverage: Nonlinear Processes in Geophysics, **2**(3–4), 147–157. https://doi.org/10.5194/npg-2-147-1995

Prokoph, A., 1999, Fractal, multifractal and sliding window correlation dimension analysis of sedimentary time series: Computers and Geosciences, **25**(9), 1009–1021. https://doi.org/10.1016/S0098-3004(99)00063-1

Raghu Kanth, S. T. G., and Dash, S. K., 2010, Deterministic seismic scenarios for North East India: Journal of Seismology, **14**(2), 143–167. https://doi.org/10.1007/s10950-009-9158-y

Roy, P., and Mondal, S., 2009, Fractal nature of earthquake occurrence in northwest Himalayan region: Journal of Indian Geophysical Union, **13**(2), 63–68.

Roy, P. N. S., Chowdhury, S., Sarkar, P., and Mondal, S. K., 2015, Fractal study of seismicity in order to characterize the various tectonic blocks of North-east Himalaya, India: Natural Hazards, **77**, S5–S18. https://doi.org/10.1007/s11069-014-1188-2

Roy, P. N. S., and Padhi, A., 2007, Multifractal analysis of earthquakes in the Southeastern Iran-Bam Region: Pure and Applied Geophysics, **164**(11), 2271–2290. https://doi.org/10.1007/s00024-007-0272-x

Roy, S., Ghosh, U., Hazra, S., and Kayal, J. R., 2011, Fractal dimension and b-value mapping in the Andaman-Sumatra subduction zone: Natural Hazards, **57**(1), 27–37. https://doi.org/10.1007/s11069-010-9667-6

Sarkar, P., Roy, P. N. S., and Pal, S. K., 2020, Rejuvenation of 'pop-up' tectonics for Shillong Plateau in NE Himalayan region: Journal of Earth System Science, **129**(1). https://doi.org/10.1007/s12040-020-01389-x

Scholz, C. H.,1968, The frequency-magnitude relation of microfracturing in rock and its relation to earthquakes: Bulletin of the Seismological Society of America, **58**(1), 399–415. https://doi.org/10.1785/

bssa0580010399
Schorlemmer, D., Wiemer, S., and Wyss, M. (2005). Variations in earthquake-size distribution across different stress regimes: Nature, **437**(7058), 539–542. https://doi.org/10.1038/nature04094
Shanker, D., Singh, H. N., Paudyal, H., Kumar, A., Panthi, A., and Singh, V. P. (2010). Searching for an earthquake Precursor-A case study of precursory swarm as a real seismic pattern before major shocks: Pure and Applied Geophysics, **167**(6), 655–666. https://doi.org/10.1007/s00024-010-0067-3
Shcherbakov, R., Turcotte, D. L., and Rundle, J. B., 2015, Complexity and Earthquakes. In Treatise on Geophysics: Second Edition (Vol. 4, Issue April). Elsevier B.V. https://doi.org/10.1016/B978-0-444-53802-4.00094-4
Shi, Y., and Bolt, A. B.,1982, The standard error of the magnitude-frequency b value: Bulletin of the Seismological Society of Americaletin, **72**(5), 1677–1687.
Singh, C., Singh, A., and Chadha, R. K., 2009, Fractal and b-value mapping in eastern Himalaya and southern Tibet: Bulletin of the Seismological Society of America, **99**(6), 3529–3533. https://doi.org/10.1785/0120090041
Smalley, R. F., Chatelain, J.-L., Turcotte, D. L., and Pevot, R., 1987, A Fractal Approach To The Clustering Of Earthquakes: Applications To The Seismicity Of The New Herbides: Bulletin of the Seismological Society of America, **77**(4), 1368–1381.
Smith, W. D., 1981, The b-value as an earthquake precursor: Nature, 289(5794), 136–139. https://doi.org/10.1038/289136a0
Sobolev, G. A., 2011, Seismicity dynamics and earthquake predictability: Natural Hazards and Earth System Science, **1**1(2), 445–458. https://doi.org/10.5194/nhess-11-445-2011
Tapponnier, P., Peltzer, G., Le Dain, A. Y., Armijo, R., and Cobbold, P.,1982, Propagating extrusion tectonics in Asia: new insights from simple experiments with plasticine: Geology, **10**(12), 611–616. https://doi.org/10.1130/0091-7613(1982)10<611:PETIAN>2.0.CO;2
Tosi, P.,1998, Seismogenic structure behaviour revealed by spatial clustering of seismicity in the Umbria-Marche Region (Central Italy): Annals of Geophysics, **41**(2), 215–224. https://doi.org/10.4401/ag-4331
Verma, R. K., 1991, Seismicity of the Himalaya and the northeast India, and nature of continent-continent collision: Physics and Chemistry of the Earth, **18**(1), 345–370. https://doi.org/10.1016/0079-1946(91)90009-5
Werner, M. J., and Sornette, D., 2008, Magnitude uncertainties impact seismic rate estimates, forecasts, and predictability experiments: Journal of Geophysical Research: Solid Earth, **113**(8). https://doi.org/10.1029/2007JB005427
Wiemer, S., and Wyss, M., 2000, Minimum magnitude of completeness in earthquake catalogs: Examples from Alaska, the Western United States, and Japan: Bulletin of the Seismological Society of America, **90**(4), 859–869. https://doi.org/10.1785/0119990114
Wyss, M., 1973, Towards a Physical Understanding of the Earthquake Frequency Distribution: Geophysical Journal of the Royal Astronomical Society, **31**(4), 341–359. https://doi.org/10.1111/j.1365-246X.1973.tb06506.x

Mr. Ram Krishna Tiwari received the M.Sc. degree in Physics from Tribhuvan University in 2004. From 2006 to 2011, he had served as a part time teaching assistant at Birendra Multiple Campus (Tribhuvan University), Bharatpur, Chitwan 44200, Nepal. From 2011 to 2017, he had served as a full time teaching assistant at the same campus. Since 2017, he took permanent position as an assistant professor of physics. He has supervised half dozen of under graduate thesis (B. Sc. student project) and co supervised three M. Sc. thesis. Currently, he is pursuing the Ph.D. degree in Geophysics at Central Department of physics, Tribhuvan University, Kirtipur, Kathmandu 44618, Nepal. His research interest includes fractal approach to the study of the seismicity of Himalayan region and the seismic hazard. He has four national and three international publications in the field related to the fractal study of the central Himalayan seismicity so far.

Prof. Harihar Paudyal, received the M.Sc. degree in Physics from Tribhuvan University in 1994 and the Ph.D. degree in Geophysics (Seismicity and Seismotectonics of Nepal and adjoining regions) from Banaras Hindu University, India in 2008. He joined faculty of Physics in Tribhuvan University in 1994 as Assistant Lecturer and is a professor of Physics from 2013. His research interests include seismotectonics, seismic hazard and seismicity of Himalayan region. He has about 40 research publications in international and national journals. Till date, he has supervised 18 MSc thesis and supervising one PhD work.
(E-mail: hariharpaudyal@gmail.com)

PLOS ONE

RESEARCH ARTICLE

Spatial mapping of b-value and fractal dimension prior to November 8, 2022 Doti Earthquake, Nepal

Ram Krishna Tiwari[1,2]*, **Harihar Paudyal**[2]

1 Central Department of Physics, Tribhuvan University, Kirtipur, Kathmandu, Nepal, **2** Birendra Multiple Campus, Tribhuvan University, Bharatpur, Chitwan, Nepal

* ram.tiwari@bimc.tu.edu.np

OPEN ACCESS

Citation: Tiwari RK, Paudyal H (2023) Spatial mapping of b-value and fractal dimension prior to November 8, 2022 Doti Earthquake, Nepal. PLoS ONE 18(8): e0289673. https://doi.org/10.1371/journal.pone.0289673

Editor: Yang Li, Florida Atlantic University, UNITED STATES

Received: January 1, 2023

Accepted: July 24, 2023

Published: August 9, 2023

Peer Review History: PLOS recognizes the benefits of transparency in the peer review process; therefore, we enable the publication of all of the content of peer review and author responses alongside final, published articles. The editorial history of this article is available here: https://doi.org/10.1371/journal.pone.0289673

Data Availability Statement: All data are freely available from International Seismological Centre (ISC) catalog (Bondár, I., & Storchak, D. (2011). Improved location procedures at the International Seismological Centre. Geophysical Journal

Abstract

An earthquake of magnitude 5.6 mb (6.6 ML) hit western Nepal (Doti region) in the wee hours of wednesday morning local time (2:12 AM, 2022.11.08) killing at least six people. Gutenberg-Richter b-value of earthquake distribution and correlation fractal dimension (D_2) are estimated for 493 earthquakes with magnitude of completeness 3.6 prior to this earthquake. We consider earthquakes in western Nepal Himalaya and adjoining region (80.0–83.5˚E and 27.3–30.5˚N) for the period of 1964 to 2022 for the analysis. The b-value 0.68 ±0.03 implies a high stress zone and the spatial correlation dimension 1.81±0.02 implies a highly heterogeneous region where the epicenters are spatially distributed. Low b-values and high D_2 values identify the study region as a high hazard zone. Focal mechanism styles and low b-values correlate with thrust nature of earthquakes and show that the earthquake's occurrence is associated with the dynamics of the faults responsible for generating the past earthquakes.

Introduction

The magnitude distribution of earthquakes, the spatial distribution of epicenter/hypocenter, frequency of aftershocks etc., satisfy the power law distribution [1, 2]. Hence, earthquakes can be described by the scaling parameter obeying power law, known as the fractal dimension [3–5]. The b-value of frequency-magnitude is a power law involving magnitude while the two-point spatial correlation dimension of earthquake's epicenter distribution displays a power law that quantifies the proportion of randomness and clusterization. The b-value measures the material heterogeneities within a fault zone and decreases with increasing stress in the brittle part of the Earth's crust. It suggests an increasing possibility of occurrence of large magnitude earthquakes (lower b-value) and smaller magnitude earthquakes (higher b-value) [6–8]. For the regions having complex tectonic activity, b-values deviates significantly from 1.0 and in the regions characterized by stable tectonic conditions and low seismicity rates its value approaches to 1.0 over long periods of time, on the order of decades or centuries [9–11]. The b-value linked with the dynamics of individual faults is universal whereas the fractal dimension of the fault network can vary depending on geological heterogeneity [12]. Different tectonic

International, 186(3), 1220–1244. https://doi.org/10.1111/j.1365-246X.2011.05107.x). All figures were created using the free available software Python, and Generic Mapping Tools (GMT) (Wessel et al., 2013).

Funding: authors received no salary or no specific funding for this work.

Competing interests: no competing interest.

processes undergoing inside the earth generally activate the fault systems in asperity zones from where generous size earthquakes nucleate [13, 14].

Nepal rests on the boundary of Eurasian plate and Indian plate with major faults parallel to its length, and is vulnerable to earthquakes [15, 16]. From the northern belt to the southern belt, the South Tibetan Detachment (STD), Main Central Thrust (MCT), Main Boundary Thrust (MBT), and Main Frontal Thrust (MFT) are major faults system in the Himalaya [17, 18]. The MCT, MBT, and MFT sole into a gentle dipping detachment called the Main Himalayan Thrust (MHT) [19]. The present-day convergence between the Indian and Eurasian plates is mostly accommodated along the MHT whose surface trace is MFT. Along with these major faults, some northeast-southwest trending transverse lineaments like Tanakpur lineament, Karnali lineament, and Samea lineament are also responsible for seismic activity of the western Nepal [20]. In the past work related with anomalous seismicity of western Nepal Himalaya, potential zone for the medium size earthquakes was identified within an area bounded by 29.3˚-30.5˚N and 81.2˚-81.9˚E [21]. The recent work identified the existence of asperity capable of hosting the future earthquake with similar character of the 2015 Gorkha earthquake towards west of the epicenter of Gorkha earthquake [22]. The research carried out by separate groups [23–25] highlights the presence of a crucial seismic gap in western Nepal and adjoining region. Thus, the prime objective of this paper is to characterize the stress level and heterogeneity of the seismogenic sources by mapping b-value and fractal dimension in the region.

In record, Nepal has the long history of moderate to large earthquakes since 1255 [26]. The western region of Nepal is seismically most active segment of central Himalaya and had also hosted many earthquakes in the past and few of them are notable [20]. An earthquake of 26 September, 1964 (6.0 mb) occurred in Nepal- India border 4 km from Dharchula, Uttarakhand, India. The 6.0 mb earthquake on 27 June 1966, at the depth of 23.80 km in border of Nepal and India took the lives of 80 people [27]. The 6.1 mb Bajhang earthquakes on July 29, 1980 affected Baitadhi, Bajhang and Darchula region of western Nepal and took 125 lives [28, 29]. Following the history, a magnitude 5.6 mb or 6.6 ML earthquake hit western Nepal in the wee hours of wednesday morning local time (2:12 AM, 2022.11.08) killing at least six people [30]. The epicenter of the shock was 21 km east of Dipayal (Headquarter of Doti District), at a depth of 15.7 km. Cracks have surfaced in most of the houses in the aftermath of the event. As per the National Earthquake Monitoring & Research Center (seismonepal.gov.np), a 5.7 ML earthquake was reported in the area at 9:07 pm prior to the stronger one that was felt later. Many aftershocks had been felt after the two bigger quakes throughout the night. The jolt was felt in and around Bajhang, Kailali, Kanchanpur, Banke, Rukum west and far up to the Indian capital Delhi and lasted for about 10 seconds [31]. The fault plane solutions from the catalog of Global Centroid Moment Tensor (GCMT) [32, 33] depict the Doti earthquake as shallow angle north east dipping thrust fault event. The fault geometry of this earthquake is similar to the 1980, Bajhang earthquake (Fig 1).

Data and methodology

For better understanding of earthquake phenomena, a decent dataset is essential. The dataset used in this study is from the catalog of International Seismological Centre (ISC) [34, 35]. We retrieved 634 earthquakes from the ISC catalog. After declustering and removing dependent events [36], only 609 earthquakes were retained. The completeness magnitude (Mc) is checked by the ZMAP software [37] which gives only 493 events with Mc $\geq$ 3.6 for final analysis (Figs 2 and 3). The final data set contains 442 events having magnitude between 3.6 and 4.9, 48 events having magnitude between 5.0 and 5.9, and three events having magnitude greater than or equal to 6.0. To map the b-value and fractal dimension, the study area was gridded at 1˚×1˚

spacing with an overlapping of 0.2˚. The correlation dimension (D_2) and b-value are estimated only for the grids containing events ≥25 for the reliable values of these parameters. The b-value is calculated by maximum likelihood estimation (MLE) method [38, 39] with standard deviation [40]. The formula used is

$$b = \frac{\log_{10} e}{M_a - \left(M_c - \frac{\Delta M}{2}\right)} \tag{1}$$

where M_a is average magnitude, M_c = 3.6, and ΔM = 0.1. The spatial correlation dimension is calculated from correlation integral function $c(r)$ [41–43] as,

$$c(r) = \frac{2}{N(N-1)} \sum_{\substack{i,j=1 \\ i \neq j}}^{N} H(r - |X_i - X_j|) \tag{2}$$

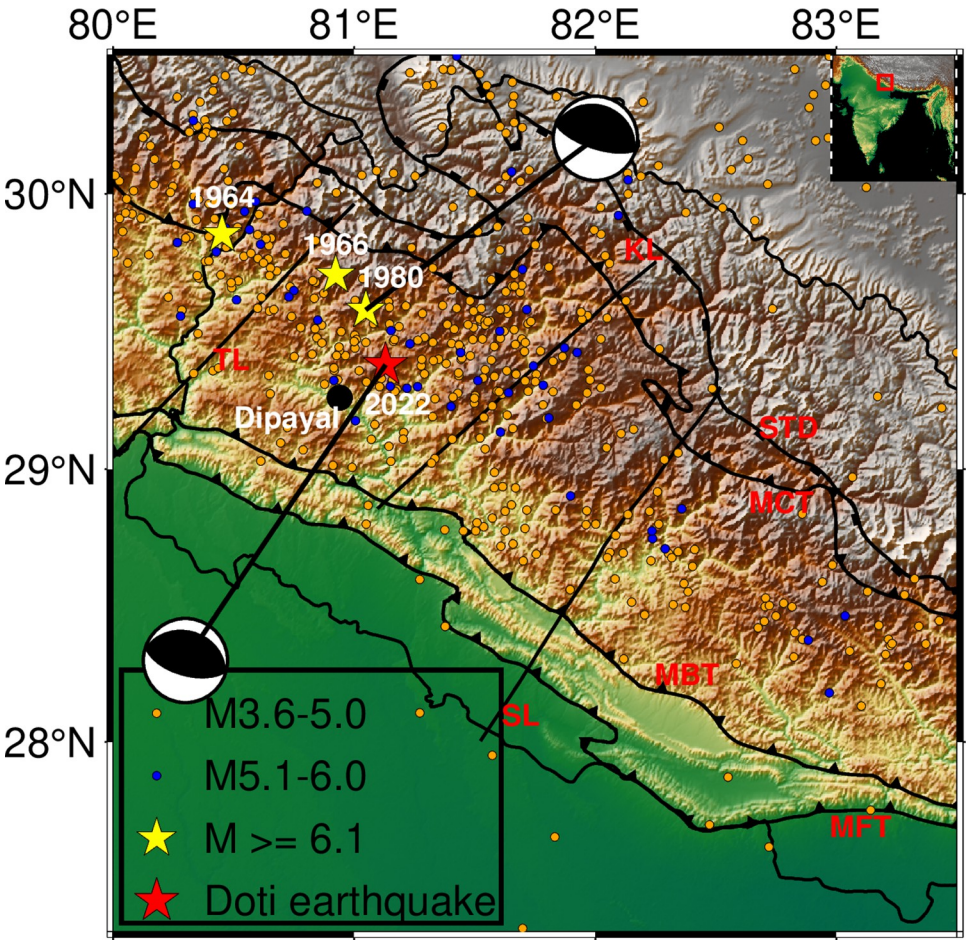

Fig 1. Western Nepal and adjoining regions showing moderate historical earthquakes, viz.1964 earthquake, 1966 earthquake, and 1980 Bajhang earthquake (Yellow stars). Recent Doti earthquake (2022) is represented by red star. Black sphere is indicating the Dipayal (Head quarter of Doti district). Tiny spheres (orange) indicate the earthquakes having magnitude between 3.6 and 5.0 and blue spheres indicate the earthquakes having magnitude between 5.1 and 6.0. Beach balls depict the focal mechanism solutions of July 29, 1980 Bajhang earthquake and 8 November, 2022 Doti earthquake. STD is South Tibetan Detachment, MCT is Main Central Thrust, MBT is the Main Boundary Thrust, and MFT is the Main Frontal Thrust. TL is the Tanakpur lineament, KL is Karnali lineament, and SL is Samea lineament [20].

https://doi.org/10.1371/journal.pone.0289673.g001

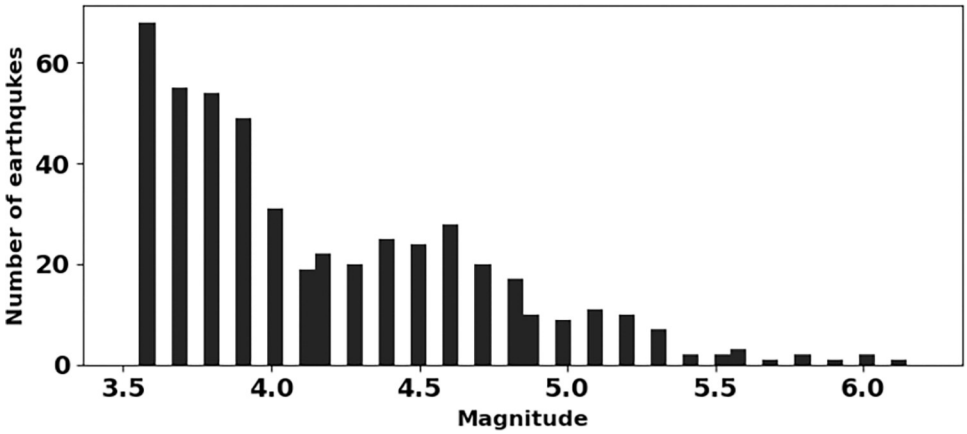

Fig 2. Magnitude histogram of the dataset under study.

https://doi.org/10.1371/journal.pone.0289673.g002

Where r is the scaling radius (r = 5 km to r = 35 km for this study), N ranges between 25 to 171 for different grids (Table 1). The angular distance X_i–X_j is evaluated by the spherical triangle method [44]. The slope of the linear part of plot for *logr*–log *c*(*r*) gives the correlation fractal dimension (D_2) as depicted for the window containing all 493 earthquakes (Fig 4). The estimated values of D_2 and b are presented in the Table 1.

Results

From the earthquake data of ISC catalog, we have estimated the values of power law exponents namely, the b-value and fractal dimension for 39 grids (sub-catalogs) and are presented in

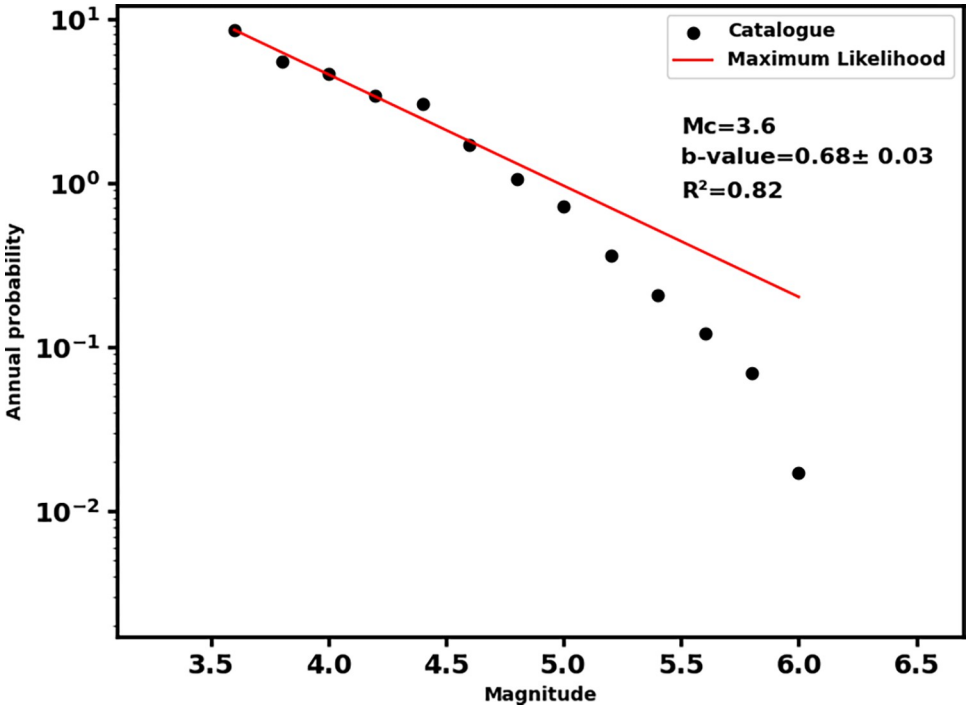

Fig 3. Magnitude of completeness (Mc) of data set and b-value of earthquake distribution with coefficient of determination (R^2).

https://doi.org/10.1371/journal.pone.0289673.g003

Table 1. List of estimated parameters of 39 grids including number of events in grid, b-value, and fractal dimension (D_2) with standard deviation, and respective coefficient determination (R^2). Grids containing events ≥ 25 are only analyzed for reliable values of estimated parameters.

S.N.	Grid	No. of events	b-value	R^2	D_2	R^2
1	80.00–81.00˚E 27.30–28.30˚N	0	–	–	–	–
2	80.20–81.20˚E 27.30–28.30˚N	0	–	–	–	–
3	80.40–81.40˚E 27.30–28.30˚N	1	–	–	–	–
4	80.60–81.60˚E 27.30–28.30˚N	2	–	–	–	–
5	80.80–81.80˚E 27.30–28.30˚N	3	–	–	–	–
6	81.00–82.00˚E 27.30–28.30˚N	4	–	–	–	–
7	81.20–82.20˚E 27.30–28.30˚N	4	–	–	–	–
8	81.40–82.40˚E 27.30–28.30˚N	3	–	–	–	–
9	81.60–82.60˚E 27.30–28.30˚N	5	–	–	–	–
10	81.80–82.80˚E 27.30–28.30˚N	5	–	–	–	–
11	82.00–83.00˚E 27.30–28.30˚N	5	–	–	–	–
12	82.20–83.20˚E 27.30–28.30˚N	8	–	–	–	–
13	82.40–83.50˚E 27.30–28.30˚N	9	–	–	–	–
14	80.00–81.00˚E 28.30–29.30˚N	18	–	–	–	–
15	80.20–81.20˚E 28.30–29.30˚N	17	–	–	–	–
16	80.40–81.40˚E 28.30–29.30˚N	28	0.57 ± 0.02	0.89	1.72 ± 0.03	0.99
17	80.60–81.60˚E 28.30–29.30˚N	47	0.65 ± 0.03	0.86	1.56 ± 0.01	1.00
18	80.80–81.80˚E 28.30–29.30˚N	62	0.61 ± 0.04	0.88	1.54 ± 0.03	0.99
19	81.00–82.00˚E 28.30–29.30˚N	68	0.62 ± 0.04	0.88	1.61 ± 0.04	0.99
20	81.20–82.20˚E 28.30–29.30˚N	72	0.66 ± 0.05	0.85	1.62 ± 0.04	0.99
21	81.40–82.40˚E 28.30–29.30˚N	79	0.65 ± 0.05	0.94	1.58 ± 0.04	0.99
22	81.60–82.60˚E 28.30–29.30˚N	63	0.62 ± 0.05	0.96	1.67 ± 0.03	0.99
23	81.80–82.80˚E 28.30–29.30˚N	50	0.65 ± 0.06	0.95	1.55 ± 0.02	1.00

(*Continued*)

Table 1. (Continued)

S.N.	Grid	No. of events	b-value	R^2	D_2	R^2
24	82.00–83.00˚E	49	0.63 ± 0.05	0.97	1.47 ± 0.02	1.00
	28.30–29.30˚N					
25	82.20–83.20˚E	42	0.61 ± 0.03	0.96	1.38 ± 0.01	1.00
	28.30–29.30˚N					
26	82.40–83.50˚E	34	0.69 ± 0.04	0.92	1.49 ± 0.02	1.00
	28.30–29.30˚N					
27	80.00–81.00˚E	133	0.60 ± 0.11	0.88	1.67 ± 0.02	1.00
	29.30–30.50˚N					
28	80.20–81.20˚E	147	0.59 ± 0.11	0.87	1.60 ± 0.03	0.99
	29.30–30.50˚N					
29	80.40–81.40˚E	140	0.62 ± 0.11	0.84	1.64 ± 0.04	0.99
	29.30–30.50˚N					
30	80.60–81.60˚E	146	0.64 ± 0.12	0.83	1.66 ± 0.03	0.99
	29.30–30.50˚N					
31	80.80–81.80˚E	171	0.66 ± 0.15	0.82	1.67 ± 0.03	0.99
	29.30–30.50˚N					
32	81.00–82.00˚E	159	0.69 ± 0.14	0.81	1.68 ± 0.03	1.00
	29.30–30.50˚N					
33	81.20–82.20˚E	141	0.72 ± 0.15	0.84	1.64 ± 0.03	0.99
	29.30–30.50˚N					
34	81.40–82.40˚E	120	0.70 ± 0.12	0.86	1.55 ± 0.03	0.99
	29.30–30.50˚N					
35	81.60–82.60˚E	83	0.73 ± 0.10	0.81	1.48 ± 0.01	1.00
	29.30–30.50˚N					
36	81.80–82.80˚E	40	0.86 ± 0.06	0.76	1.61 ± 0.02	1.00
	29.30–30.50˚N					
37	82.00–83.00˚E	36	1.07 ± 0.08	0.72	1.72 ± 0.03	1.00
	29.30–30.50˚N					
38	82.20–83.20˚E	25	1.40 ± 0.19	0.72	1.64 ± 0.03	0.99
	29.30–30.50˚N					
39	82.40–83.50˚E	30	1.55 ± 0.25	0.67	1.67 ± 0.01	1.00
	29.30–30.50˚N					

https://doi.org/10.1371/journal.pone.0289673.t001

Table 1. The b-value describes the slope of power law and explain frequency magnitude distribution of earthquakes while fractal dimension describes the complexity of the fault system and seismogenic sources.

The b-value for whole data set is found to be 0.68 ± 0.03 while the b-value map shows the broad variation for different grids i.e., between 0.48 and 1.55 (Table 1 and Fig 3). This type of variation is acceptable for the seismically active Himalayan region [46, 47]. The broad patch of low b-value between 0.48 and 0.64 is noticed for the region occupied by historical earthquakes and the recent Doti earthquake as well (Fig 5). The low b-value areas also coincide with the major thrust system (MCT, MBT, MFT etc.) of the western Nepal.

The fractal dimension value 1.81 ± 0.02 for whole data set (Table 1 and Fig 4) and the variation between 1.36 and 1.92 for different grids indicate that the epicenters are distributed in 2D seismogenic structures. High D_2 contours (1.5 to 1.92) are identified for the area occupied by the past moderate earthquakes and recent Doti earthquake (Fig 6). The areas east of Dipayal are identified as the low D_2 contours (1.36–1.52) area. These areas could be inferred as the

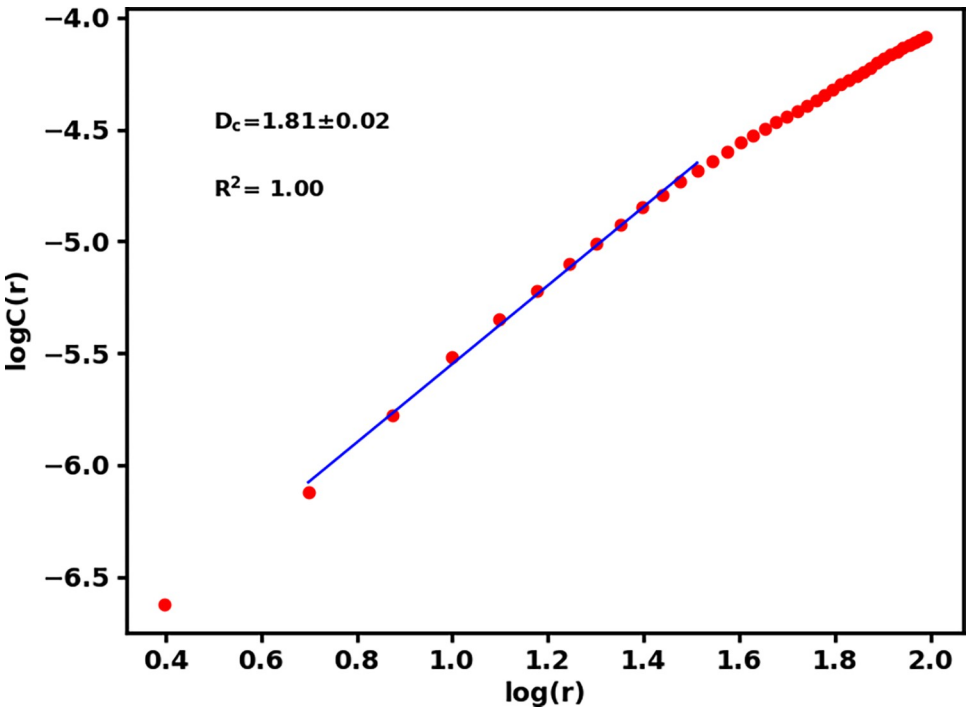

Fig 4. The method of estimation of correlation fractal dimension as the slope of the linear part of the plot between where r = 5 km to r = 35 km is set as the distance between depopulation and saturation [45].

https://doi.org/10.1371/journal.pone.0289673.g004

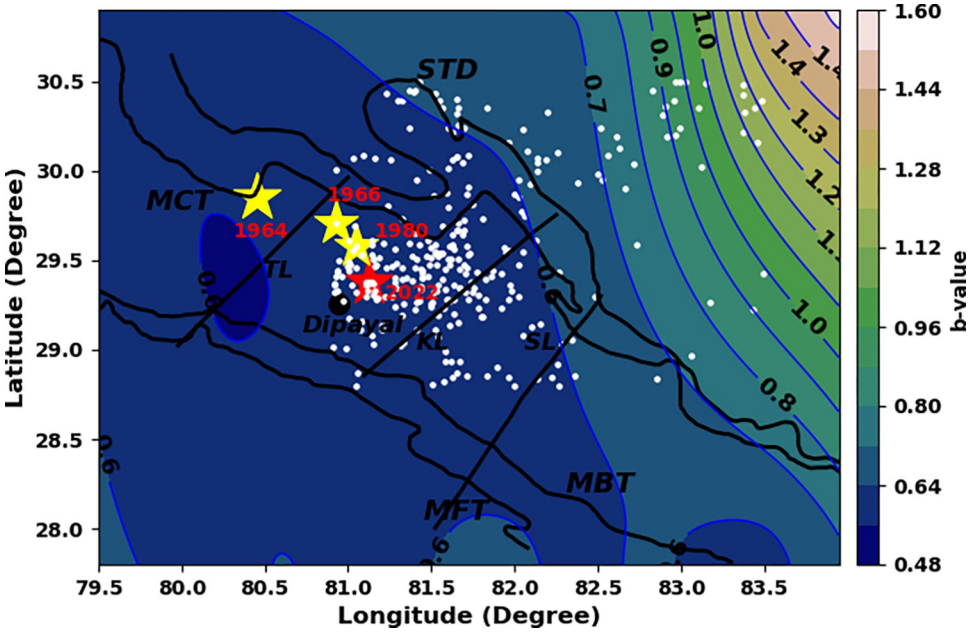

Fig 5. b-value contours of the study region. The b-values are calculated for the grids of size 1˚×1˚ with overlapping of 0.2˚. STD, MCT, MBT, MFT, TL, KL, and SL are as mentioned in the captions of the Fig 1. The seismic activity of the region is depicted by white dots.

https://doi.org/10.1371/journal.pone.0289673.g005

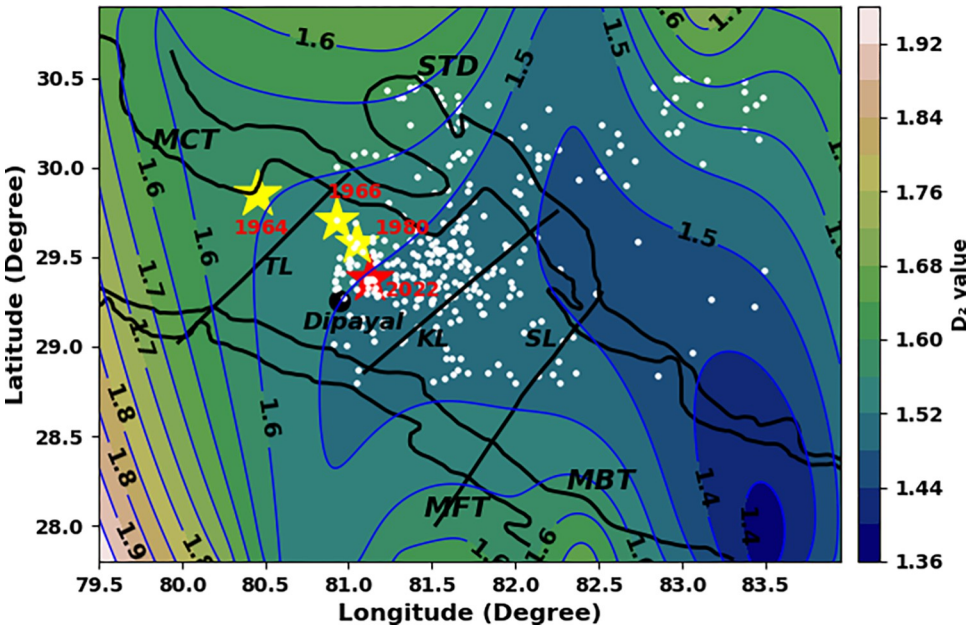

Fig 6. D_2-value contours of the study region. The D_2-values are calculated for the grids of size 1˚×1˚ with overlapping of 0.2˚. STD, MCT, MBT, MFT, TL, KL, and SL are as mentioned in the captions of the Fig 1. The seismic activity of the region is depicted by white dots.

https://doi.org/10.1371/journal.pone.0289673.g006

asperity zones along the fault systems. The remarkably low b-value reflects that the subsurface rock mass is under stress closing to the ultimate strength, and as a result the firmly locked segment within the fault zone transforms into the state of complete failure. Moreover, high fractal dimension reflects an increase in heterogeneity of the seismogenic sources.

Fig 7 illustrates the temporal changes in b-value and D_2-value over a decade-long time window, with a 2-year shift between each window. To ensure reliable estimates of these parameters, only windows with 25 or more earthquakes are considered. The estimated values are presented in the Table 2. The b-value exhibits a slight increase from 1970 to 1998, followed by a sharp rise. In contrast, the D_2-value experiences a gradual decrease during this same time period, with a significant dip between 1988 and 1998. Subsequently, the D_2-value continues to decrease, with another dip observed between 2000 and 2010.

Discussion

The low b-values estimated are the indicator of a more stressed zone or presence of asperity in the region [48, 49]. The observed low b-values can be attributed to the prevalence of dominant reverse faulting mechanisms in the area, specifically the presence of major thrusts MCT, MBT, and MFT. Thus, the area enclosed between Tanakpur Lineament and Samea lineament could be the host region of the future large earthquake. The north east corner of the study region is reflected with high b-value contours (1.00 to 1.50), so can be inferred as less probable region for the future large earthquake. Fractal dimension (D_2) is a measure of resistance of material against the fracture, so the fragile material had a smaller fractal dimension. The fractal dimension would increase with an increase in the energy density available for fracture [50, 51]. D_2 is a measure of spatial clustering and can take a value from 0 to 2. Its value close to 0 signifies that earthquakes are centralized in a small locality and the value close to 2 signifies that the earthquakes are spatially distributed [52, 53]. The higher values of fractal dimensions (between 1.36 and 1.92) obtained from this study suggest the presence of spatially distributed

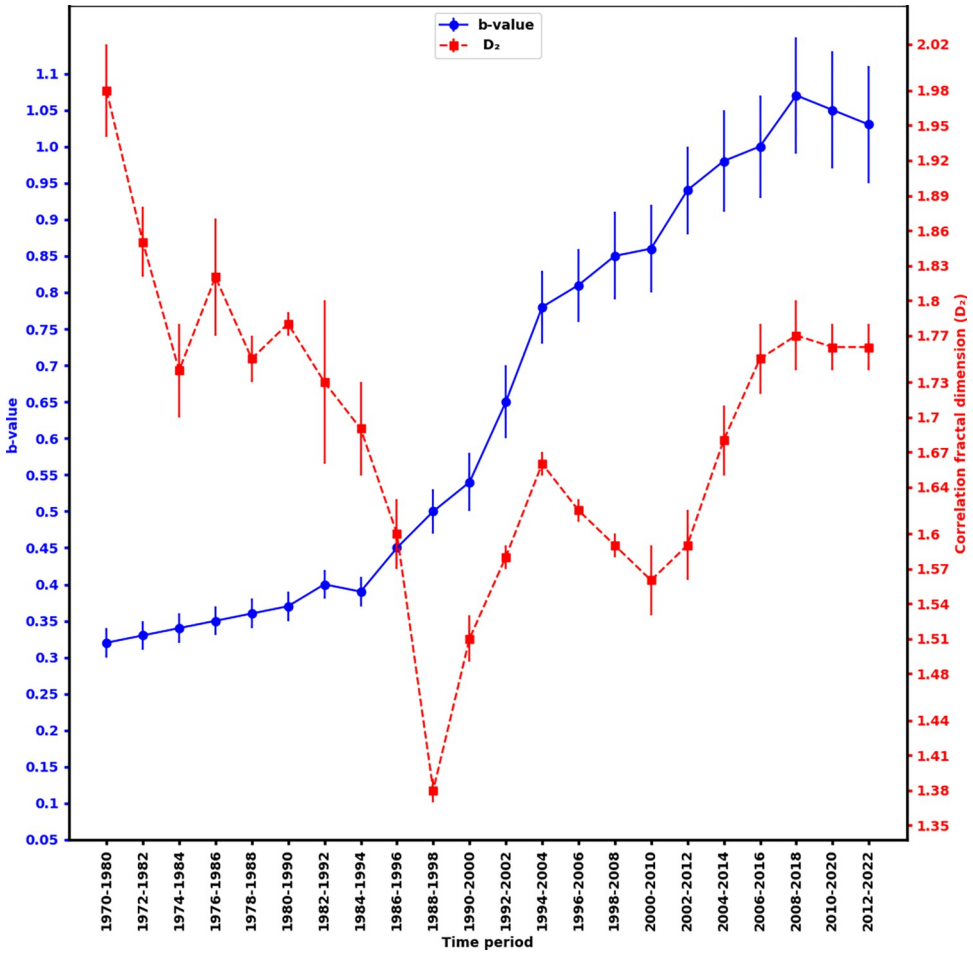

Fig 7. The temporal changes in b-value and D_2-value over the period of 1970 to 2022.

https://doi.org/10.1371/journal.pone.0289673.g007

heterogeneous faults in the region and the region are seismically active. The smaller b-value zones (0.48–0.60) are corroborated with higher D_2 (1.5–1.9), implying negative correlation. The areas with low b-value and high D_2 and are expected to accumulate prominent levels of tectonic stress, which could be the risk factor for generating large earthquakes in the future [54–56]. The area identified as high risk zone in this study is within the zone identified as anomalous seismicity zone in the past work [21]. In addition, A decade wise study of b-values and D_2 revealed that during the initial period (1970–1994), low b-values and a gradual decrease in D_2 were noted, which may be related to the preparation phenomenon for the occurrence of the 1980 Bajhang earthquake. The occurrence of this earthquake would have altered the stress state of the surrounding rocks, potentially leading to the observed changes in earthquake parameters. The low b-values may indicate a gradual change in the stress field over time. A subsequent jump in b-value after the Bajhang earthquake may be due to changes in tectonic stress causing an increase in the number of small earthquakes. This increase in seismicity may have caused a temporary decrease in the fractal correlation dimension as seismic activity became more clustered around the mainshock location. As time passes and aftershocks occur, the fractal correlation dimension may increase again as the seismic activity spreads out and becomes more diffuse, leading to a more complex pattern of earthquake epicenters. Overall, these changes in the b-value and fractal correlation dimension suggest a more complex

Table 2. List of estimated parameters of 25 windows including number of events in window, b-value, and fractal dimension (D_2) with standard deviation, and respective coefficient determination (R^2). Windows containing events ≥ 25 are only analyzed for reliable values of estimated parameters.

S.N.	Window	No. of events	b-value	R^2	D_2	R^2
1	1964–1974	24	-	–	–	–
2	1966–1976	20	–	–	–	–
3	1968–1978	17	–	–	–	–
4	1970–1980	26	0.32 ± 0.02	0.92	1.98 ± 0.04	0.99
5	1972–1982	34	0.33 ± 0.02	0.91	1.85 ± 0.03	1.00
6	1974–1984	44	0.34 ± 0.02	0,91	1.74 ± 0.04	0.99
7	1976–1986	43	0.35 ± 0.02	0.90	1.82 ± 0.05	0.99
8	1978–1988	48	0.36 ± 0.02	0.88	1.75 ± 0.02	1.00
9	1980–1990	50	0.37 ± 0.02	0.87	1.78 ± 0.01	1.00
10	1982–1992	49	0.40 ± 0.02	0.89	1.73 ± 0.07	0.97
11	1984–1994	51	0.39 ± 0.02	0.90	1.69 ± 0.04	0.99
12	1986–1996	55	0.45 ± 0.02	0.92	1.60 ± 0.03	0.99
13	1988–1998	67	0.50 ± 0.03	0.94	1.38 ± 0.01	1.00
14	1990–2000	72	0.54 ± 0.04	0.92	1.51 ± 0.02	1.00
15	1992–2002	90	0.65 ± 0.05	0.90	1.58 ± 0.01	1.00
16	1994–2004	110	0.78 ± 0.05	0.83	1.66 ± 0.01	1.00
17	1996–2006	136	0.81 ± 0.05	0.81	1.62 ± 0.01	1.00
18	1998–2008	147	0.85 ± 0.06	0.81	1.59 ± 0.01	1.00
19	2000–2010	165	0.86 ± 0.06	0.81	1.56 ± 0.03	1.00
20	2002–2012	185	0.94 ± 0.06	0.77	1.59 ± 0.03	1.00
21	2004–2014	177	0.98 ± 0.07	0.75	1.68 ± 0.03	0.99
22	2006–2016	186	1.00 ± 0.07	0.73	1.75 ± 0.03	1.00
23	2008–2018	190	1.07 ± 0.08	0.70	1.77 ± 0.03	1.00
24	2010–2020	186	1.05 ± 0.08	0.71	1.76 ± 0.02	1.00
25	2012–2022	169	1.03 ± 0.08	0.73	1.76 ± 0.02	1.00

https://doi.org/10.1371/journal.pone.0289673.t002

pattern of seismic activity in the region. The recent seismic activity observed in western Nepal can be described as a micro-fracturing process taking place within the Earth's crust prior to a major earthquake.

Conclusion

After the analysis of earthquake dataset for the period of 58 years (1964–2022), the b-value earthquake distribution and the fractal dimension (D_2) of epicenter distribution are mapped for the tectonic structures of western Nepal and adjoining region. The maximum likelihood method is used for the estimation of b-value and correlation integral method is employed for the estimation of fractal dimension. The results identify the region under study as a high hazard zone with low b-values and high D_2 values. A high D_2 value obtained for the region indicates strong heterogeneity at this part of the Himalaya, may be due to varied stress level in the crust. A study conducted over multiple decades on the b-value and D_2 reveal the precursor signal before the Bajhang earthquake. The fault geometry of 2022 Doti earthquake and 1980 Bajhang earthquake revealed by focal mechanism solutions show the similar characteristics, so the occurrence of the earthquake could be related to the previous earthquakes. The thrust nature of focal mechanism associated with earthquakes in a region is typically the result of tectonic plate compression, which leads to a low b-value and a clustered pattern of seismicity near the fault line. This can result in a lower fractal dimension during the main shock. The mapped

region can be inferred to be most hazardous, which correlate well with seismic gap mentioned in the past literature. Finally, this study sheds new light in the understanding the characteristics of the seismogenic sources in western Nepal Himalaya.

Data and software resources

All data are freely available from International Seismological Centre (ISC) catalog [34, 35]. All figures were created using the free available software Python, and Generic Mapping Tools (GMT) [57].

Acknowledgments

One of the authors (RKT) would like to acknowledge both University Grant Commission (UGC), Nepal and the Tribhuvan University, Nepal for providing PhD fellowship and sabbatical leave, respectively.

Author Contributions

Conceptualization: Harihar Paudyal.

Data curation: Ram Krishna Tiwari, Harihar Paudyal.

Formal analysis: Harihar Paudyal.

Investigation: Ram Krishna Tiwari.

Methodology: Ram Krishna Tiwari.

References

1. Pilgrim I, Taylor RP. Fractal Analysis of Time-Series Data Sets: Methods and Challenges. Fractal Analysis. IntechOpen; 2019. https://doi.org/10.5772/intechopen.81958
2. Roy A, Perfect E, Dunne WM, McKay LD. Fractal characterization of fracture networks: An improved box-counting technique. J Geophys Res Solid Earth. 2007; 112: 1–9. https://doi.org/10.1029/2006JB004582
3. Huang J, Turcotte DL. Fractal distributions of stress and strength and variations of b-value. Earth Planet Sci Lett. 1988; 91: 223–230. https://doi.org/10.1016/0012-821X(88)90164-1
4. Mandlebrot BB. Multifractal Measures, Especially for the Geophysicist. Pure Appl Geophys. 1989;131.
5. Shcherbakov R, Yakovlev G, Turcotte DL, Rundle JB. Model for the distribution of aftershock interoccurrence times. Phys Rev Lett. 2005;95. https://doi.org/10.1103/PhysRevLett.95.218501 PMID: 16384191
6. Gulia L, Wiemer S. The influence of tectonic regimes on the earthquake size distribution: A case study for Italy. Geophys Res Lett. 2010; 37: 1–6. https://doi.org/10.1029/2010GL043066
7. Ogata Y, Tsuruoka H. Statistical monitoring of aftershock sequences: A case study of the 2015 Mw7.8 Gorkha, Nepal, earthquake the 2015 Gorkha, Nepal, Earthquake and Himalayan Studies: First Results 4. Seismology. Earth, Planets Sp. 2016; 68: 44. https://doi.org/10.1186/s40623-016-0410-8
8. Wyss M, Sammis CG, Nadeau RM, Wiemer S. Fractal dimension and b-value on creeping and locked patches of the San Andreas fault near Parkfield, California. Bull Seismol Soc Am. 2004; 94: 410–421. https://doi.org/10.1785/0120030054
9. Arroyo-Solórzano M, Linkimer L. Spatial variability of the b-value and seismic potential in Costa Rica. Tectonophysics. 2021;814. https://doi.org/10.1016/j.tecto.2021.228951
10. El-Isa ZH. Frequency-Magnitude Distribution of Earthquakes. Earthquakes—Forecast, Prognosis and Earthquake Resistant Construction. 2018. https://doi.org/10.5772/intechopen.77294
11. Ketthong T, Pailoplee S. Frequency-magnitude Distribution and Fractal Dimension of the Seismicity along the Sumatra-Andaman Subduction Zone: A Temporal Comparison Bulletin of Earth Sciences of Thailand. Bull Earth Sci Thail. 2012; 8: 12–23.
12. Lomnitz-Adler J. Interplay of fault dynamics and fractal dimension in determining Gutenberg & Richter's b-value. Geophys J Int. 1992; 108: 941–944. https://doi.org/10.1111/j.1365-246X.1992.tb03482.x

13. Legrand D. Fractal dimensions of small, intermediate, and large earthquakes. Bull Seismol Soc Am. 2002; 92: 3318–3320. https://doi.org/10.1785/0120020025

14. Roy S, Ghosh U, Hazra S, Kayal JR. Fractal dimension and b-value mapping in the Andaman-Sumatra subduction zone. Nat Hazards. 2011; 57: 27–37. https://doi.org/10.1007/s11069-010-9667-6

15. Bai L, Liu H, Ritsema J, Mori J, Zhang T, Ishikawa Y, et al. Faulting structure above the Main Himalayan Thrust as shown by relocated aftershocks of the 2015 Mw7.8 Gorkha, Nepal, earthquake. Geophys Res Lett. 2016; 43: 637–642. https://doi.org/10.1002/2015GL066473

16. Pei S, Liu H, Bai L, Liu Y, Sun Q. High-resolution seismic tomography of the 2015 Mw7.8 Gorkha earthquake, Nepal: Evidence for the crustal tearing of the Himalayan rift. Geophys Res Lett. 2016; 43: 9045–9052. https://doi.org/10.1002/2016GL069808

17. Grandin R, Vallée M, Satriano C, Lacassin R, Klinger Y, Simoes M, et al. Rupture process of the Mw = 7.9 2015 Gorkha earthquake (Nepal): Insights into Himalayan megathrust segmentation. Geophys Res Lett. 2015; 42: 8373–8382. https://doi.org/10.1002/2015GL066044

18. Upreti BN. An overview of the stratigraphy and tectonics of the Nepal Himalaya. J Asian Earth Sci. 1999; 17: 577–606. https://doi.org/10.1016/S1367-9120(99)00047-4

19. Sathiakumar S, Barbot S. The stop-start control of seismicity by fault bends along the Main Himalayan Thrust. Commun Earth Environ. 2021;2. https://doi.org/10.1038/s43247-021-00153-3

20. Paudyal H, Shanker D, Singh H, Panthi A, Kumar A, Singh V. Current understanding of the seismotectonics of Western Nepal Himalaya and vicinity. Acta Geod Geophys Hungarica. 2010; 45: 195–209. https://doi.org/10.1556/AGeod.45.2010.2.5

21. Paudyal H, Singh HN. Anomalous Seismicity Prceeding Moderate Size Earthquake in Nepal Himalaya and its Adjoining region. Varanasi, India: Department of Geophysics, Banaras Hindu University,Varanasi, India; 2008. pp. 86–129.

22. Sreejith KM, Sunil PS, Agrawal R, Saji AP, Rajawat AS, Ramesh DS. Audit of stored strain energy and extent of future earthquake rupture in central Himalaya. Sci Rep. 2018; 8: 1–9. https://doi.org/10.1038/s41598-018-35025-y PMID: 30420673

23. Bilham R. Himalayan earthquakes: A review of historical seismicity and early 21st century slip potential. Geol Soc Spec Publ. 2019; 483: 423–482. https://doi.org/10.1144/SP483.16

24. Mencin D, Bendick R, Upreti BN, Adhikari DP, Gajurel AP, Bhattarai RR, et al. Himalayan strain reservoir inferred from limited afterslip following the Gorkha earthquake. Nat Geosci. 2016; 9: 533–537. https://doi.org/10.1038/ngeo2734

25. Molnar P, Pandey MR. Rupture zones of great earthquakes in the Himalayan region. Proc Indian Acad Sci—Earth Planet Sci. 1989; 98: 61–70. https://doi.org/10.1007/BF02880376

26. Joshi VM, Kaushik HB. Historic earthquake-resilient structures in nepal and other himalayan regions and their seismic restoration. Earthq Spectra. 2017; 33: S299–S319. https://doi.org/10.1193/121616EQS240M

27. Agrawal P. N. Structural Response Results During the June 27, 1966 Earthquakes in Nepal-India Border Region. Bull Seismol Soc Am. 1969; 59: 771–775. https://doi.org/10.1086/622062

28. Chaulagain H, Gautam D, Rodrigues H. Revisiting major historical earthquakes in Nepal: Overview of 1833, 1934, 1980, 1988, 2011, and 2015 seismic events. Impacts and Insights of the Gorkha Earthquake. Elsevier Inc.; 2018. https://doi.org/10.1016/B978-0-12-812808-4.00001–8

29. Khanal KN. Source parameters estimation of the 1980 Bajhang Earthquake, far western Nepal. J Nepal Geol Soc. 1997; 15: 45–51. https://doi.org/10.3126/jngs.v15i0.32123

30. Pokharel S, Wang P. Western Nepal hit by magnitude 5.6 earthquake killing at least six people, officials say. Cable News Network. 9 Nov 2022. Available: https://www.cnn.com/2022/11/08/asia/delhi-nepal-earthquake-today-nepal-earthquake-today/index.html

31. Joshi P. Earthquake kills six, injures five others in Doti. myRepublica. 9 Nov 2022. Available: https://myrepublica.nagariknetwork.com

32. Dziewonski AM, Chou T-A, Woodhouse JH. Determination of earthquake source parameters from waveform data for studies of global and regional seismicity. J Geophys Res. 1981; 86: 2825–2852. https://doi.org/10.1029/JB086iB04p02825

33. Ekström G, Nettles M, Dziewoński AM. The global CMT project 2004–2010: Centroid-moment tensors for 13,017 earthquakes. Phys Earth Planet Inter. 2012;200–201: 1–9. https://doi.org/10.1016/j.pepi.2012.04.002

34. Bondár I, Storchak D. Improved location procedures at the International Seismological Centre. Geophys J Int. 2011; 186: 1220–1244. https://doi.org/10.1111/j.1365-246X.2011.05107.x

35. Storchak DA, Harris J, Brown L, Lieser K, Shumba B, Di Giacomo D. Rebuild of the Bulletin of the International Seismological Centre (ISC)—part 2: 1980–2010. Geoscience Letters. 2020. pp. 1980–2010. https://doi.org/10.1186/s40562-020-00164-6

36. Reasenberg P. Second-order moment of central California seismicity, 1969–1982. J Geophys Res Solid Earth. 1985; 90: 5479–5495. https://doi.org/10.1029/jb090ib07p05479

37. Wiemer. A software package to analyze seismicity: ZMAP. Seismol Res Lett. 2001; 72: 373–382. https://doi.org/10.1785/gssrl.72.3.373

38. Aki K. Maximum likelihood estimate of b in the formula Log N = a—bM and its confidence limits. Bull Earthq Res Inst Tokyo Univ. 1965; 43: 237–239.

39. Bender B. Maximum likelihood estimation of b values for magnitude grouped data. Bull Seismol Soc Am. 1983; 73: 831–851. Available: http://www.bssaonline.org/cgi/content/abstract/73/3/831

40. Shi Y, Bolt BA. The standard error of the magnitude-frequency b value. Bull Seismol Soc Am. 1982; 72: 1677–1687. https://doi.org/10.1785/bssa0720051677

41. Mondal SK, Roy PNS, Catherine JK, Pandey AK. Significance of fractal correlation dimension and seismic b-value variation due to 15th July 2009, New Zealand earthquake of mw 7.8. Ann Geophys. 2019; 62: 1–17. https://doi.org/10.4401/ag-8020

42. Roy P, Mondal S. Fractal nature of earthquake occurrence in northwest Himalayan region. J Indian Geophys Union. 2009; 13: 63–68.

43. Roy PNS, Padhi A. Multifractal analysis of earthquakes in the Southeastern Iran-Bam Region. Pure Appl Geophys. 2007; 164: 2271–2290. https://doi.org/10.1007/s00024-007-0272-x

44. Hirata T. Fractal Dimension of Fault Systemss in Japan: Fractal Structure in Rock Fracture Geometry at Various Scales. Pure Appl Geophys. 1989;131.

45. Nerenberg MAH, Essex C. Correlation dimension and systematic geometric effects. Phys Rev A. 1990; 42: 7065–7074. https://doi.org/10.1103/physreva.42.7065 PMID: 9904020

46. Gui Z, Bai Y, Wang Z, Li T. Seismic b-value anomalies in the Sumatran region: Seismotectonic implications. J Asian Earth Sci. 2019; 173: 29–41. https://doi.org/10.1016/j.jseaes.2019.01.015

47. Zhu S. Estimation of seismic hazard around the Ordos Block of China based on spatial and temporal variations of b-values. Geomatics, Nat Hazards Risk. 2021; 12: 2048–2069. https://doi.org/10.1080/19475705.2021.1949394

48. Kumar N, Yadav DK, Mondal SK, Roy PNS. Stress drop and its relation to tectonic and structural elements for the meizoseismal region of great 1905 Kangra earthquake of the NW Himalaya. Nat Hazards. 2013; 69: 2021–2038. https://doi.org/10.1007/s11069-013-0793-9

49. Nakaya S. Spatiotemporal variation in b value within the subducting slab prior to the 2003 Tokachi-oki earthquake (M 8.0), Japan. J Geophys Res Solid Earth. 2006; 111: 3311. https://doi.org/10.1029/2005JB003658

50. Bardeji SZ. Fractal Distribution of Earthquake Epicenter and Faulting in the Sepidar Anticline, Sw Zagros. 2018; 9: 20–21.

51. Turcotte L. Fractal and fragmentation. New York. 1986; 91: 1921–1926.

52. Kagan YY. Earthquake spatial distribution: The correlation dimension. Geophys J Int. 2007; 168: 1175–1194. https://doi.org/10.1111/j.1365-246X.2006.03251.x

53. Mandal P, Rodkin M V. Seismic imaging of the 2001 Bhuj Mw7.7 earthquake source zone: B-value, fractal dimension and seismic velocity tomography studies. Tectonophysics. 2011; 512: 1–11. https://doi.org/10.1016/j.tecto.2011.09.004

54. Mandal P, Srinagesh D, Suresh G, Naresh B, Singh DK, Swathi K, et al. Three-dimensional b-value and Fractal Dimension Mapping of the Uttarakhand Himalayan Region. J Geol Soc India. 2022; 98: 1365–1379.

55. Sarkar P, Roy PNS, Pal SK. Rejuvenation of 'pop-up' tectonics for Shillong Plateau in NE Himalayan region. J Earth Syst Sci. 2020;129. https://doi.org/10.1007/s12040-020-01389-x

56. Tiwari R, Paudyal H. Statistics of the earthquakes in the central Himalaya and its vicinity in last 56 years, with an emphasis in the 25 April 2015 Gorkha, Nepal earthquake. Contrib to Geophys Geod. 2021; 51: 321–343. https://doi.org/10.31577/congeo.2021.51.4.2

57. Wessel P, Smith WHF, Scharroo R, Luis J, Wobbe F. Generic mapping tools: Improved version released. Eos (Washington DC). 2013; 94: 409–410. https://doi.org/10.1002/2013EO450001

Volume 9, December 2020 ISSN 2542-2545

The HIMALAYAN PHYSICS

A peer-reviewed Journal of Physics

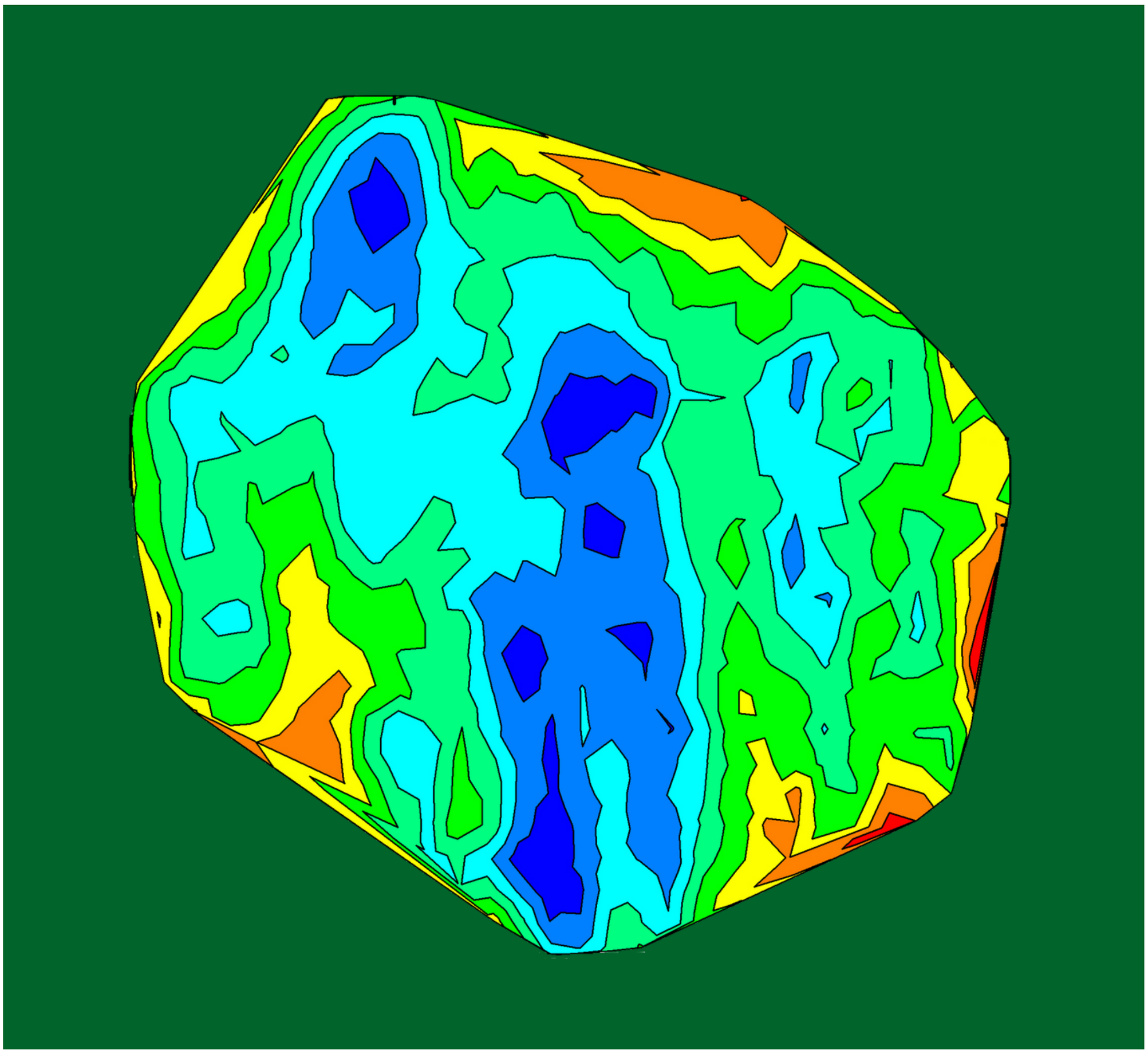

Department of Physics, Prithvi Narayan Campus, Pokhara
Nepal Physical Society, Western Chapter, Pokhara

Publisher

Department of Physics, Prithvinarayan Campus, Pokhara
Nepal Physical Society, Western Chapter, Pokhara

The Himalayan Physics

Volume 9, December 2020

ISSN 2542-2545

The Himalayan Physics (HimPhys) is an open access peer-reviewed journal that publishes quality articles which make innovative contributions in all areas of Physics. HimPhys is published annually by Nepal Physical Society (Western Regional Chapter), and Department of Physics, Prithvi Narayan Campus, Pokhara. The goal of this journal is to bring together researchers and practitioners from academia in Nepal and abroad to focus on advanced techniques and explore new avenues in all areas of physical sciences and establishing new collaborations with physics community in Nepal.

Cover: Contour map of dust mass. © Mijas Tiwari. Printed from article in the current issue, with permission.

Volume 9, December 2020 ISSN 2542-2545

The HIMALAYAN PHYSICS

A peer-reviewed Journal of Physics

Publisher
Department of Physics, Prithvi Narayan Campus, Pokhara
Nepal Physical Society, Western Chapter, Pokhara

Nepal Physical Society

Western Regional Chapter

Pokhara, Nepal

Himalayan Physics Vol-9 (2020)

TABLE OF CONTENTS

****

Him. Phys. **9** 103-109, (2020)

Himalayan Physics

Geodynamics of Gorkha earthquake (Mw 7.9) and its aftershocks

Research Article

Ram Krishna Tiwari[1,2*], H. Paudyal[2]

1 Tribhuvan University, Kirtipur, Kathmandu

2 Birendra Multiple Campus, Tribhuvan University, Bharatpur, Chitwan

Abstract: A devastating earthquake (Mw 7.9) occurred in Gorkha region on 25 April 2015 caused loss of 8964 human lives and huge property in Central Nepal and adjoining region. Sequence of aftershocks, including four having magnitude greater than 6 occurred within 18 days, confined in a distance of about 150 km from Gorkha to Dolakha. Main shock and its aftershocks series confined in a depth range of 12 to 21 km. In this study, using 11 CMT solutions of earthquakes with magnitude 5 and above, occurred between 2014.12.18 and 2016.11.27 within 84° to 87°E and 27° to 29°N, we analyze faulting pattern of the Gorkha earthquake and associated large aftershocks to reveal recent geodynamics pattern in the central Himalayan region.

Nodal planes of mainshock and four large aftershocks have east west orientation and shallow dip (6° to 23°) towards north, exhibit strong thrust mechanism. Smaller aftershocks scattered within 150 km long rupture zone along NW to SE direction show similar mechanism with large thrust component. Collective dips of nodal plane of ten events indicate northward under thrusting of the Indian plate at shallow angle, though the nodal plane of individual event differ slightly in their orientation. The cross-sectional study of focal mechanism shows the clustering of the seismic events at different depth with diverse faulting pattern. It is inferred that recent seismic activity in central Nepal region is dominated by thrust faulting and the mechanism which were responsible for the formation of Himalaya are still continuing.

Keywords: Seismotectonics • Central Himalaya • Nepal • Clustering

1. Introduction

On 25th April 2015 an intense ground shaking struck Central Nepal that caused tremendous damage and loss. The earthquake occurred as a result of the northward under thrusting of India beneath Eurasia. The main shock, approximately 80 km to the northwest of Kathmandu, occurred in Gorkha at 11:56 (NST) with a magnitude of Mw 7.9 at latitude 27.9°N and 85.3°E which triggered numerous aftershocks [1]. The biggest of the aftershocks was of the magnitude Mw 7.2 approximately 90 km southeast from the Mainshock [1]. Multiple studies were carried out by the researchers on the Gorkha Earthquake and its aftershocks sequence to retrieve the rupture process and its tectonic implications [2–4]. A multi-disciplinary effort to understand the earthquake in the context of tectonic evolution of the Himalaya and associated seismic hazards was carried out and the findings suggest

* *Corresponding Author: ram.tiwari@bimc.tu.edu.np*

that segments of the MHT, up-dip of the 2015 Gorkha rupture, likely have high hazard for future damaging earthquakes in this densely populated and vulnerable region [4]. In this study we analyze the faulting pattern of this devastating event and its major aftershocks using CMT moment tensor solutions.

Geo-tectonics of the region

Central Nepal represents a part of Himalayan geo-tectonic belt. The region is classically divided into four tectonic units from south to north;

1. Sub-Himalaya
2. Lesser Himalaya
3. Higher Himalaya
4. Tethyan Himalaya

Main Frontal Thrust (MFT), Main Boundary Thrust (MBT), Main Central Thrust (MCT) and South Tibet Detachment (STD) separate the four tectonic units (Fig. 1). MFT is the active thrust fault which exposed along the southern edge of the Sub-Himalayan foothills. Both the MFT and MBT sole into the Main Himalaya Thrust (MHT), the detachment along which the Indian plate subducts beneath the Himalaya [5, 6]. MHT dips gently to the north beneath the Lesser Himalaya and further it steepens downward onto a ramp that dives beneath the Higher Himalaya before flattening again northward under the Tethys Himalaya of southern Tibet [7]. It accommodates approximately a half of tectonic convergence between Indian plate and Eurasian plates. Apart from these major thrusts, large number of active faults are identified in the region responsible for frequent generation of earthquake [8] .

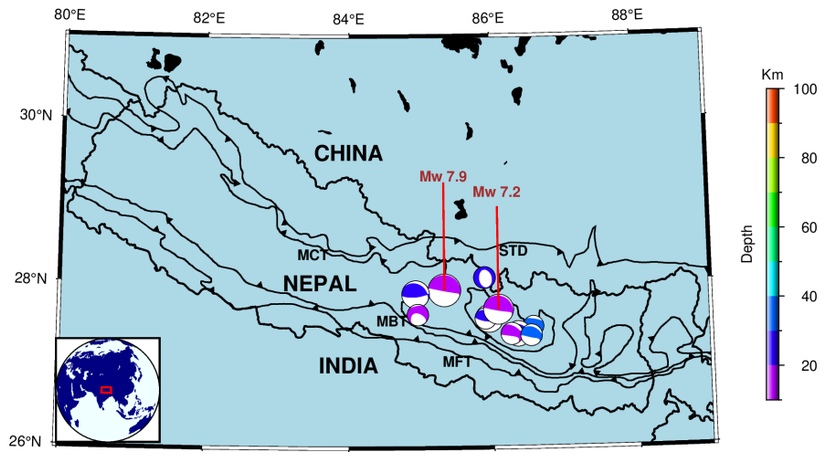

Figure 1. Focal mechanism beachballs solutions of earthquake events (magnitude 5 and above) in the region (26°N-31°N and 80°E-89°E). The red box in the inset map indicates the Nepal in the gobal scenario. The color of the beachball depends on the depth of the event depicted by color bar.

The term focal mechanism is used to refer to the parameters that characterizes an earthquake rupture. It presents the characteristics of the two orthogonal possible ruptures planes on the basis of strike, dip and rake of the slip vector over the plane. Focal mechanism by Centroid Moment Tensor (CMT) method were constrained by first motion solutions and waveform modelling. The method is based on the linear relationship that exists between the six independent elements of a zeroth order moment tensor representation of an earthquake and the ground motion that the earthquake generates [9]. A moment tensor is a complete description of equivalent forces of a general seismic point source [10] in an elastic medium [11]. The term centroid refers to the center of the earthquake moment distribution in time and space defined by four parameters like centroid latitude, longitude, depth and centroid time. Thus, ten parameters altogether provide the point source CMT representation of an earthquake [1].

Focal mechanism analysis able to describe the source mechanism for the fault planes geometrically and mathematically when the earthquakes occurred. In order to understand the various aspects of earthquake like stress perturbation, aftershocks pattern and faulting geometry etc., an immediate determination of focal mechanism is exceedingly important [12–14]. Focal mechanism data also help in assignment of the tectonic regime by providing information on the relative magnitudes of the principal stresses. In the prediction of ground shaking for early warning purpose, the timely derived focal mechanism can provide significant information such as fault orientation and slipping mode. The faults parameters like strike, dip and slip angles are useful to find out whether the earthquakes have similar source mechanism characteristics or not. The objective of this work is to explain focal mechanism of Gorkha earthquakes of magnitude 5 and above to analyze faulting pattern which could reveal recent geodynamics pattern in the region.

2. Data and Methodology

The moment tensor solutions are available for this region in the Harvard CMT Catalogue [3, 4] [Table 1 and Table 2]. We compile the data for the period 2014-1-1 to 2016-12-30 for latitude range 27°N to 29°N and longitude range 84°E to 87°E. The original method of constructing beach ball diagrams was the result of analysis of waveforms (the P-wave first motion) generated by an earthquake and recorded by at least 10 seismographs distributed geographically around the epicenter. Here we use the Generic Mapping Tool (GMT) package to construct the map and visualization of beach balls on the map [15]. More precisely, the syntax 'psmeca' is used for representation of the focal mechanism on map of Nepal (Fig. 1) and the syntax 'pscoupe' to plot cross section of focal mechanism (Fig. 2).

Table 1. : Fault-plane solution parameters of eleven earthquakes from Central Nepal Himalaya and its adjoining regions.

S.N	Date	Centroid Time (GMT)	Lat.	Lon.	Depth (km)	Mw	Ms	Strike (°)	Dip (°)	Slip (°)
1	2014-12-18	15:32:15.4	27.46	86.56	30.3	5.0	5.0	248	26	44
								117	72	110
2	2015-04-25	6:11:58.6	27.91	85.33	12.0	7.9	7.8	287	6	96
								101	84	89
3	2015-04-25	6:45:53.3	27.86	84.93	21.0	6.7	6.6	308	23	131
								85	73	74
4	2015-04-25	17:42:53.3	28.06	85.89	20.8	5.3	5.1	339	40	-105
								178	52	-78
5	2015-04-25	23:16:18.1	27.61	84.96	15.0	5.1	5.1	201	40	-20
								306	77	-129
6	2015-04-26	7:9:20.1	27.56	85.95	20.6	6.7	6.7	289	14	98
								101	76	88
7	2015-04-26	16:26:9.6	27.56	85.95	19.8	5.2	5.0	305	26	115
								98	66	78
8	2015-05-12	7:5:27.5	27.67	86.08	12.0	7.2	7.3	307	11	117
								99	81	85
9	2015-05-12	7:36:59.6	27.37	86.35	20.1	6.1	6.3	299	28	116
								90	65	77
10	2015-05-16	11:34:12.6	27.37	86.26	12.0	5.3	5.5	324	34	138
								91	68	63
11	2016-01-12	23:35:26.0	27.35	86.53	35.4	5.2	5.4	305	24	113
								100	67	80

Table 2. : CMT Harvard Centroid Moment Tensor data (psmeca compatible) where mrr, mtt, mpp, mrt, mrp and mtp are six components of moment Tensor (r for up, t for south and p for east) and Iexp is exponent used to convert the scalar moment to units of dyne-cm

S.N	Lon.	Lat.	Depth (km)	mrr	mtt	mpp	mrt	mrp	mtp	Iexp (dyne-cm)
1	86.56	27.46	30	1.20	-3.08	1.88	2.48	-0.64	1.07	23
2	85.33	27.91	12	1.76	-1.82	0.06	8.04	-1.51	0.48	27
3	84.93	27.86	21	0.68	-0.74	0.06	0.96	0.19	0.25	26
4	85.89	28.06	21	-1.04	0.16	0.87	0.16	0.26	-0.17	24
5	84.96	27.61	15	-2.08	-2.46	4.54	5.53	-0.90	-1.20	23
6	85.95	27.56	21	0.60	-0.67	0.07	1.20	-0.23	0.20	26
7	85.90	27.56	20	5.38	-5.14	-0.24	5.14	-0.18	2.23	23
8	86.08	27.67	12	2.70	-2.62	-0.08	8.25	-1.28	1.22	26
9	86.35	27.37	20	1.37	-1.54	0.17	1.24	0.14	0.43	25
10	86.26	27.37	12	0.75	-0.95	0.20	0.83	0.04	0.63	24
11	86.53	27.35	35	0.56	-0.61	0.05	0.62	-0.08	0.29	24

3. Results and Discussion

The mainshock (7.9Mw) shows N17°E dipping with strike direction N73°W while the aftershocks (Mw 6.6) occurred in the same day shows N38°E dipping with strike direction N52°W. The aftershock (Mw 6.7) on the day after the mainshock shows the dipping with direction N19°E and N71°W and the major aftershocks on 12 May 2015 has again shows dipping with dip direction N37°E and striking with direction N53°W. This indicates that the strike direction is confined on NW and the propagation of the rupture is mainly concentrated along NE direction. The angle of dip of mainshock was 6° and its largest aftershock was 11°. Nodal planes of mainshock and three large aftershocks have east west orientation and shallow dip (6° to 23°) towards north, exhibit strong thrust mechanism. The dips of nodal plane of other larger aftershocks (Mw 5.1 to 6.7) lying between 14° to 40° indicate dipping process at shallow angle in the region, steeper than the detachment MHT which is demarcated as a low-angle northeast dipping at depth of 12-21 km [9].

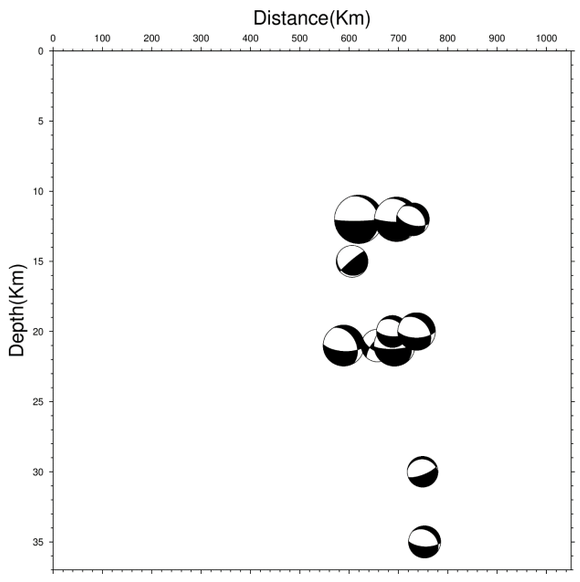

Figure 2. Focal mechanism cross-section of 11 events having magnitude 5 and above (26°N-31°N and 80°E-89°E) with depth.

The cross-section map (Fig. 3) associated with mainshock and aftershocks shows the depth range from 10 km to 35 km. The mainshock (Mw7.9) and major aftershock (Mw7.2) both occurred at depth of 12 km. The focal mechanism cross section map (Fig. 2) shows two remarkable clustering. There is one cluster around depth 12 km and another cluster around 20 km to 21 km. The seismic event gap was noticed between these two clusters. The group of researchers [16] noticed the thrusting on a sub horizontal fault dipping about 10° northwards and the 15 km hypo central depth. They made the conclusion that this earthquake ruptured the MHT, the main fault along which northern India underthrusts the Himalaya at a rate of approximately 2 cmyr^{-1}. Zhang et al. [2] reported the focal mechanism of this earthquake is a thrust fault type and is consistent with the Main Frontal Thrust.

Thus, focal mechanism of Gorkha earthquake explained in this study is agreement with the earlier works.

4. Conclusion

The focal mechanism of the 2015 Nepal earthquake was the thrust fault type, which is consistent with the Main Frontal Thrust. The rupture propagated from the hypocenter toward southeast and did not cause surface rupture. Clustering patterns of events is observed following NW-SE trend of the major thrust. Most of the aftershocks are occurred to the SE of main shock than that in NW of it and within 10 to 35 km depth range. The strong thrust mechanism was exhibited by the events as noticed from orientation of nodal planes of mainshock and four large aftershocks. They have east west orientation and shallow dip (6° to 23°) towards north. The strain resulting from on-going collision between India and Eurasian plates could have cause large slip on the locked segment of the detachment (MHT) to generate the Mw7.9 devastating Gorkha earthquake. Focal mechanism cross sections highlight a region of the MHT that has not ruptured in this event, but is locked, and therefore still has the potential to fail seismically.

5. Acknowledgements

One of the authors RKT would like to acknowledge Tribhuvan University, Nepal for providing sabbatical leave and University Grants Commission (UGC), Nepal for providing financial support in the form of fellowship.

References

[1] Ekstrom G, Nettles M, Dziewo'nski A. The global CMT project 2004–2010 Centroid-moment tensors for 13,017 earthquakes. Physics of the Earth and Planetary Interiors. 2012;200:1–9.

[2] Zhang L, Li J, Liao W, Wang Q. Source rupture process of the 2015 Gorkha, Nepal Mw7. 9 earthquake and its tectonic implications. Geodesy and geodynamics. 2016;7(2):124–131.

[3] Fan W, Shearer PM. Detailed rupture imaging of the 25 April 2015 Nepal earthquake using teleseismic P waves. Geophysical Research Letters. 2015;42(14):5744–5752.

[4] Arora B, Bansal B, Prajapati SK, Sutar AK, Nayak S. Seismotectonics and seismogenesis of Mw7. 8 Gorkha earthquake and its aftershocks. Journal of Asian Earth Sciences. 2017;133:2–11.

[5] Paudyal H, Shanker D, Singh H, Panthi A, Kumar A, Singh V. Current understanding of the seismotectonics of Western Nepal Himalaya and vicinity. Acta Geodaetica et Geophysica Hungarica. 2010;45(2):195–209.

[6] Thapa DR, Tao X, Fan F, Tao Z. Aftershock analysis of the 2015 Gorkha-Dolakha (Central Nepal) earthquake doublet. Heliyon. 2018;4(7):e00678.

[7] Elliott J, Jolivet R, González PJ, Avouac JP, Hollingsworth J, Searle M, et al. Himalayan megathrust

geometry and relation to topography revealed by the Gorkha earthquake. Nature Geoscience. 2016;9(2):174–180.

[8] Dasgupta S, Mukhopadhyay M, Nandy D. Active transverse features in the central portion of the Himalaya. Tectonophysics. 1987;136(3-4):255–264.

[9] Gilbert F. Excitation of the normal modes of the Earth by earthquake sources. Geophysical Journal International. 1971;22(2):223–226.

[10] Jost Mu, Herrmann R. A students guide to and review of moment tensors. Seismological Research Letters. 1989;60(2):37–57.

[11] Shearer P, Hauksson E, Lin G. Southern California hypocenter relocation with waveform cross-correlation, Part 2: Results using source-specific station terms and cluster analysis. Bulletin of the Seismological Society of America. 2005;95(3):904–915.

[12] Michael AJ. Use of focal mechanisms to determine stress: a control study. Journal of Geophysical Research: Solid Earth. 1987;92(B1):357–368.

[13] King GC, Stein RS, Lin J. Static stress changes and the triggering of earthquakes. Bulletin of the Seismological Society of America. 1994;84(3):935–953.

[14] Moore G, Bangs N, Taira A, Kuramoto S, Pangborn E, Tobin H. Three-dimensional splay fault geometry and implications for tsunami generation. Science. 2007;318(5853):1128–1131.

[15] Wessel P, Luis J, Uieda L, Scharroo R, Wobbe F, Smith W, et al. The generic mapping tools version 6. Geochemistry, Geophysics, Geosystems. 2019;20(11):5556–5564.

[16] Avouac JP, Meng L, Wei S, Wang T, Ampuero JP. Lower edge of locked Main Himalayan Thrust unzipped by the 2015 Gorkha earthquake. Nature Geoscience. 2015;8(9):708–711.

BIBECHANA
ISSN 2091-0762 (Print), 2382-5340 (Online)
Journal homepage: http://nepjol.info/index.php/BIBECHANA
Publisher: Department of Physics, Mahendra Morang A.M. Campus, TU, Biratnagar, Nepal

Variability of b-value before and after the Gorkha earthquake in the central Himalaya and vicinity

Ram Krishna Tiwari[1, 2,*], Harihar Paudyal[2]
[1]Central Department of Physics, Tribhuvan University, Kirtipur, Kathmandu, Nepal
[2]Birendra Multiple Campus, Tribhuvan University, Bharatpur, Chitwan, Nepal
* Email: tiwari.ram77@gmail.com

Article Information:
Received: September 9, 2020
Accepted: February 11, 2021

Keywords:
G-R (Gutenberg Richter) law
b-value
Stress heterogeneity
Gorkha
Central Himalaya

ABSTRACT

This study computes the b-value of Gutenberg-Richter relation associated with the 25 April 2015 Gorkha earthquake and its aftershock sequences. For this the homogeneous catalogue of 769 earthquakes that occurred in the Himalayan compressed belt and its vicinity was analyzed by three different approaches. The minimum b-values 0.60±0.07 and 0.63±0.06 were observed for windows containing Gorkha earthquake. For time window before Gorkha earthquake, the b-value was noted as 0.89±0.12. It was noted 0.81±0.04 for time window between Gorkha earthquake and Dolakha earthquake and 0.78±0.08 for time window after Dolakha earthquake. The results revealed the fact that b-value starts to decrease for strong earthquake. About 17% jumps of the b value were observed within 17 days between Gorkha earthquake and its largest aftershock, the Dolakha earthquake. The b-value 1.16±0.09 was obtained for the depth range of 0-10 km, 0.89±0.4 for the depth range 10-20 km and 0.65±0.08 for the depth range of 20-30 km. The results strongly support the global trends of decreasing b-value with depth in the continental crust and subduction zones. The low b-value patch observed in the west of Gorkha from contour map depicts the region as the potential zone of future strong seismic activity.

DOI: https://doi.org/10.3126/bibechana.v18i2.31207

1. Introduction

The entire Himalayan terrain and its surroundings is a highly active seismic zone on the earth. Nepal lying at the center of the 2500 km long Himalayan range, has encountered 19 devastating earthquakes since the twelfth century. A catastrophic earthquake (7.8 Mw) on 25 of April 2015 has left the entire nation stunned with the casualty of about 8900 people. The effect was felt in some adjoining parts

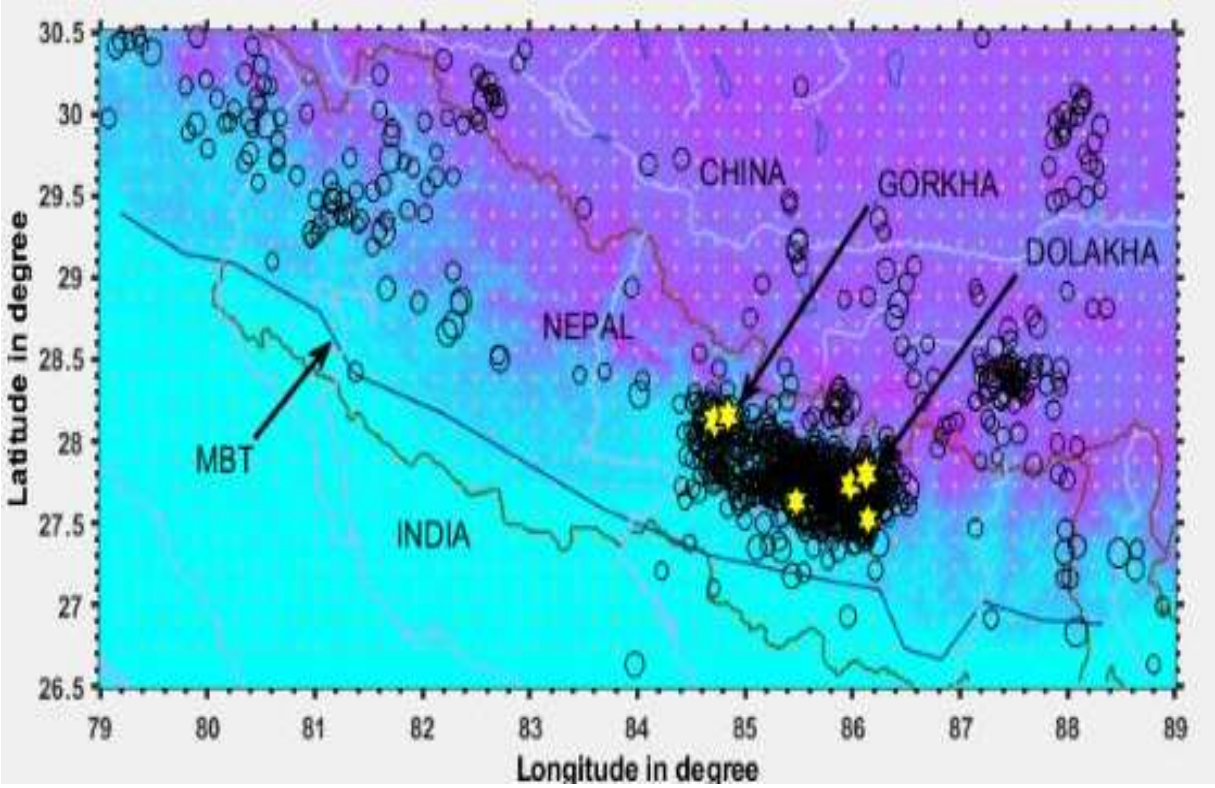

Fig. 1: Map of Central Himalaya and adjoining region showing location of earthquake epicenter from 1 Jan. 2013 to 31 Dec. 2016. Events with magnitude 6 and above are depicted by yellow stars.

of India, Bangladesh and the Tibet [1]. The event was followed by hundreds of aftershocks throughout Nepal, with one shock reaching a magnitude of 6.6 mb on 26 April and the major aftershock of 6.7 mb (7.3 Mw) on 12 May 2015. The Gorkha earthquake ruptured ~ 150 × 60 km patch of the Main Himalayan Thrust (MHT), the decollement defining the plate boundary at depth and locations of aftershocks are at or below the mainshock rupture plane [2]. The seismicity distribution and the cumulative number of events are depicted in Fig. 1 and Fig. 2.

The fundamental seismic parameter used to describe the ensemble of earthquakes is b value of the Gutenberg-Richter distribution which is power law size distribution described in terms of magnitude [3]. The distribution is

$$\log N(M) = a - bM$$

where N(M) is the number of earthquakes in the group having magnitudes ≥M. A constant parameter a is the logarithm of the total number of earthquakes with magnitudes greater than or equal to completeness magnitude that depends on the seismicity rate and the length of the observation time. The b value can be obtained from the slope of frequency magnitude distribution of the earthquakes. The spatial and temporal variation of b value is regarded as key clues for the future large earthquake precursors [4].

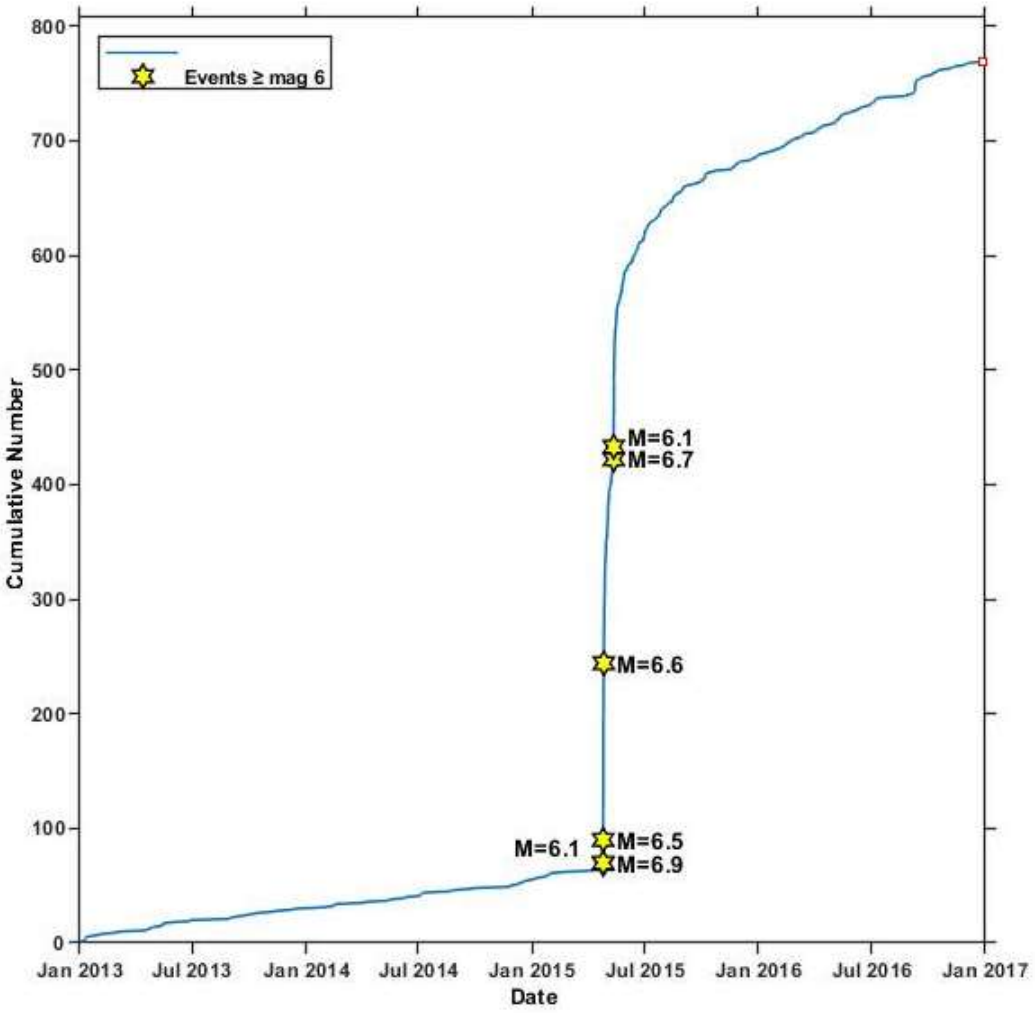

Fig. 2: Time series analysis of 769 earthquake occurred in Central Himalayan compression zone showing events (>6 mb) for the study period.

A high b value means a predominance of small earthquakes while a low b value means that the large earthquake dominates over smaller earthquakes. The b value is also associated with geotectonic features of an area so it has important value in seismology. A decreased in stress results in high b values whereas the increase in applied stress decreases b value [5-7] thus it decreases laterally with depth possibly because of increased stress [8], [9]. Large heterogeneity present in material corresponds to higher b value [10]. Aftershocks have large b values while foreshocks on the other hand show low b-value [11], [12]. Numerous workers have disclosed that foreshocks before strong earthquakes often have low b-value. The variation of b values before the mainshock usually experience three stages, an increase in the first, followed by a drop and another increase prior to the major event. [13-15]. A decrease in b value is interpreted because of stress increase prior to a seismic event [12], [16]. So, it is especially important to understand the b value of the frequency magnitude distribution. The objective of the study is to examine temporal and spatial variation of b value to understand the stress condition before and after the earthquake.

2. Data and method

A homogeneous earthquake catalogue is a prerequisite for the study of seismic activity of any region. We get 881 earthquake data (≥ 3.2 mb), for the period 1 Jan. 2013 to 31 Dec. 2017) from the catalogue of International Seismological Centre (ISC) for the region 26.5 °N-30.5 °N and 79 °E-89 °E. Out of these earthquakes, 112 are found to occur in adjoining Tibetan normal faulting environment. Since this study is limited to Himalayan compressive zone, these 112 earthquakes are removed from the catalogue for further study. Thus, the subset of catalogue including 769 events is prepared by considering the earthquake data within central Himalaya and its closed surrounding for the period of 2013-01-01 to 2016-12-31. Gardner and Knopoff [17] algorithm was used for declusterising the catalogue. The catalogue is analyzed by three different approaches. First one is by dividing the catalogue into fixed event window; the second approach is by dividing catalogue into three different time window and, the third approach is by dividing the catalogue into subsets of depth ranges. The event time windows were prepared by taking 100 events with overlapping of 60 events. The magnitude of completeness (M_c) is computed by the maximum curvature [18] approach using ZMAP-7.1 software [19]. The b-value is calculated by maximum likelihood estimation (MLE) method which is not affected by large magnitude earthquake. The formula [20] for b-value estimation is

$$b = \frac{\log_{10} e}{M_a - \left(M - \frac{\Delta M}{2}\right)}$$

where M_a is average of all magnitudes, M is minimum magnitude in the catalogue and ΔM is binning width of the catalogue. The b-value of all the 769 events is computed as 0.77±0.09 as depicted in Fig. 3.

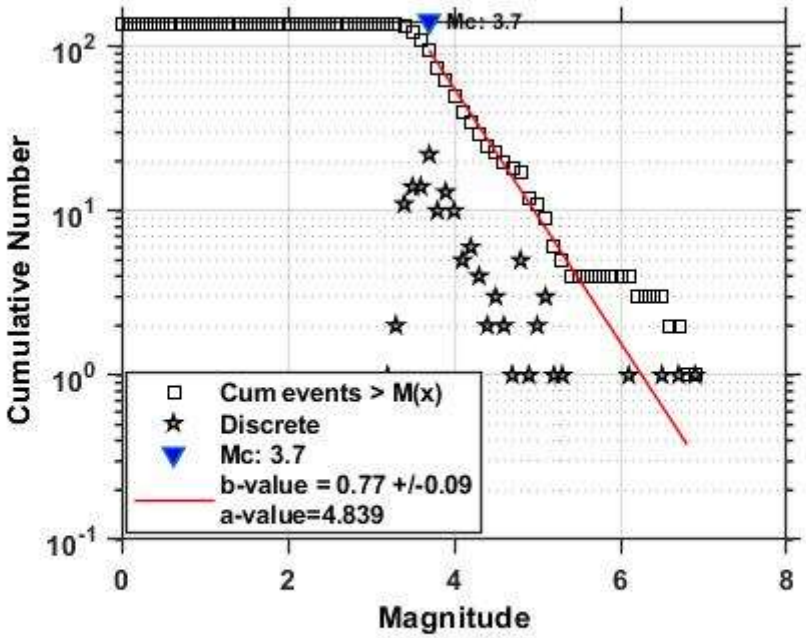

Fig. 3: Frequency magnitude distribution of GR (Gutenberg Richter) relationship for the earthquake sequences for the period Jan. 2013 to Jan. 2017 where cum events in legend is for cumulative number of events and discrete is for discrete events.

Frequency magnitude distribution of GR relationship for the earthquake sequences before the Gorkha earthquake of Mw 7.8 (from 1 Jan. 2013 to 25 April 2015), between Gorkha earthquake and Dolakha earthquake (from 25 April to 12 May 2015) and after Dolakha earthquake (from 12 May 2015 to 31 Dec. 2017) are shown in Figs. 4, 5 and 6 respectively. The b-value is observed to increase ~ 17% within 17 days between the Gorkha earthquake and the Dolakha earthquake (Fig. 7).

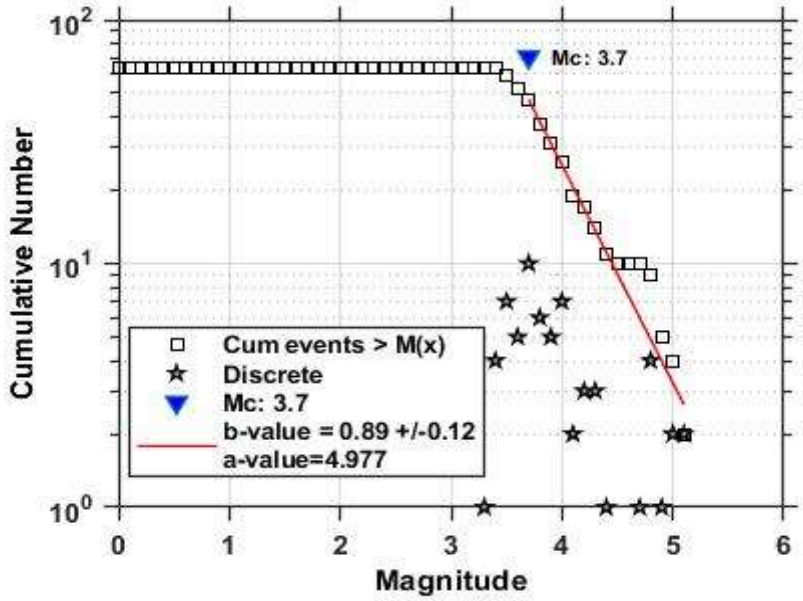

Fig. 4: Frequency magnitude distribution of GR relationship for the earthquake sequences (from 1 Jan. 2013 to 25 April 2015) before the Gorkha earthquake of Mw 7.8 where cum events in legend is for cumulative number of events and discrete is for discrete events.

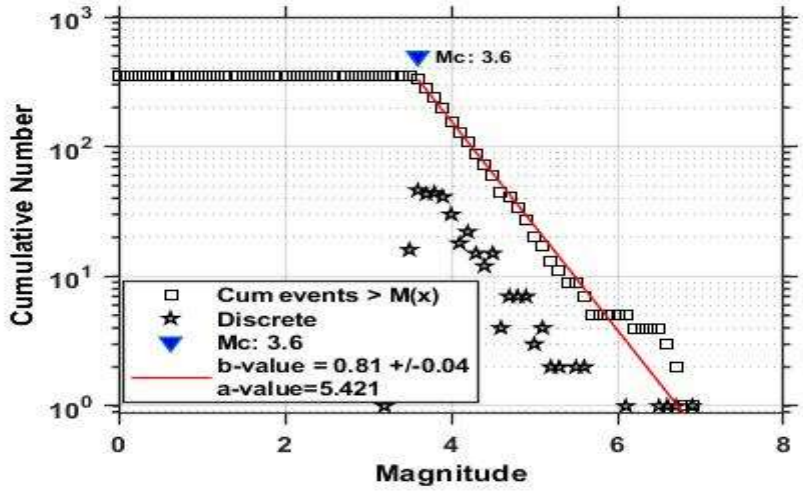

Fig. 5: Frequency magnitude distribution of GR relationship for the earthquake sequences (from 25 April to 12 May 2015) between Gorkha earthquake and Dolakha earthquake where cum events in legend is for cumulative number of events and discrete is for discrete events.

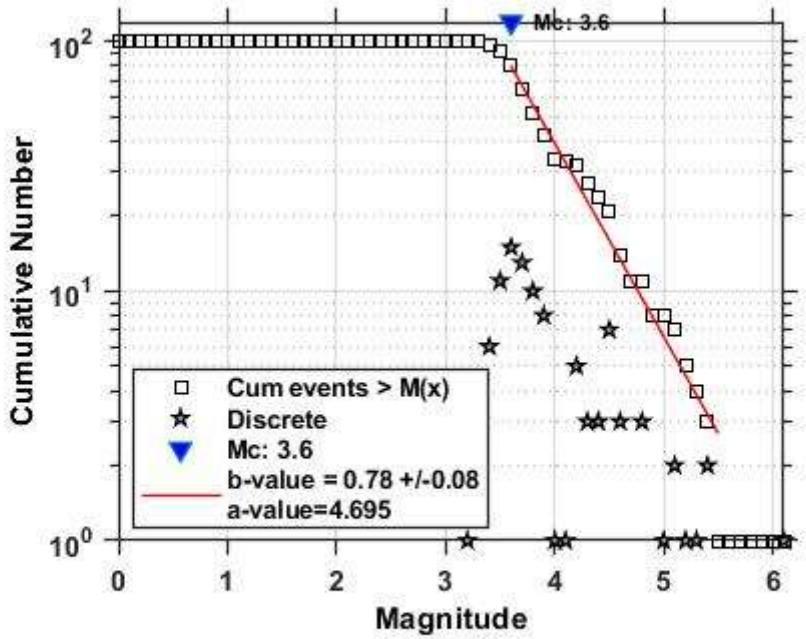

Fig. 6: Frequency magnitude distribution of GR relationship for the earthquake sequences (from 12 May 2015 to 31 Dec. 2017) after Dolakha earthquake where cum events in legend is for cumulative number of events and discrete is for discrete events.

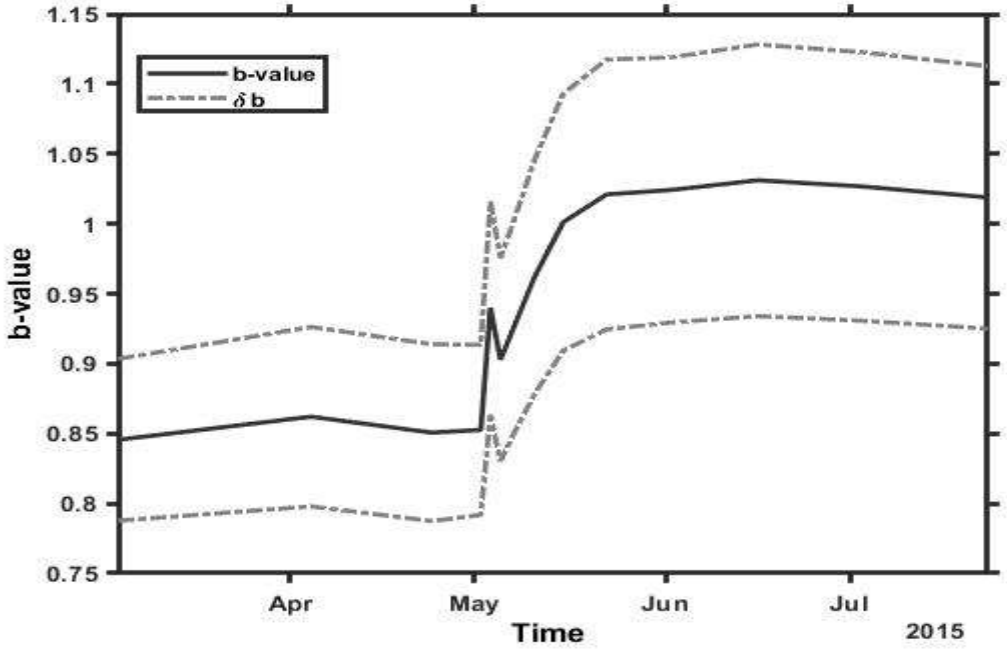

Fig. 7: Time series analysis of b-value over the study period showing sudden jumps of b-value after the 25 of April 2015 Gorkha earthquake.

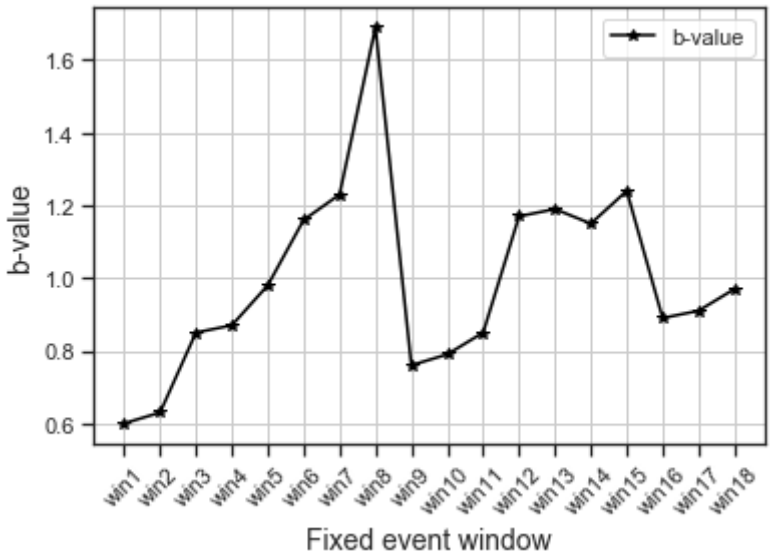

Fig. 8: Variation of b-value with time window. For time window 1 (2013/01/01 - 2015/04/25) b-value is lowest indicating the accumulation of stress and for time window 8 (2015/04/26 - 2015/05/03) b-value rises to 1.69 indicating release of stress after the large earthquake.

3. Results and Discussion

Seismic b-value for fixed 100 events window with overlapping of 60 events is given in Table 1. The lowest b-value was observed as 0.60±0.07 and 0.63±0.06 for first and second windows, prior to and during the Gorkha earthquake (6.9 mb). It was 0.79±0.08 for the period 2015/05/01-2015/05/12 during which 6.7 mb Dolakha earthquake occurred in the region. After the Gorkha earthquake, the b-value was increased to 0.85±0.08 and further up to 1.69±0.23. The b-value was found increased even after the Dolakha earthquake up to 1.19±0.14 (Table 1). Thus, the results agree with hypotheses that b-value decreases before a strong event and increases after the event (Fig. 8). The increase in b-value indicates the releasing of the accumulated strain in the region. The frequency magnitude distribution (FMD) plots for the earthquake sequences are depicted in the Figs. 3, 4, 5 and 6. The b-value is 0.77±0.09 for the entire study period. It was 0.89±0.12 before the earthquake (2013/01/01-2015/04/23).It was computed 0.81±0.04 between the Gorkha earthquake and Dolakha earthquake (2015/4/25-2015/5/12) and 0.78±0.08 after the earthquake (2015/05/12-2016/12/31). The most dominant range of earthquake magnitude in this period is indicated by a-value variation of 4.977 to 5.421 (Table 2). The low b-value for aftershock sequences may correspond to the generation of enormous size asperities in the hypocentral area of the MHT [21] by the mainshock. These observed b-values indicate that it is increasing after the Dolakha earthquake showing the gradual release of stress in the region. The b-value variation with the depth range is given in Table 3. By dividing the full depth range (0 km-100 km) into two groups (0-40 km and 30 –100 km), the b-value estimation shows variation from 0.83± 0.03 to 1.29±0.16 respectively, indicating high strain accumulation in the crust. It is also the indication of more heterogeneous stress distribution in the depth range 0-40 km compared to the depth below 30 km. For the depth ranges of 10 km, the smallest b- value is 0.65±0.08 for the depth range 20 km to 30 km and the highest b-value is 1.42±0.17 for the depth range 30 km to 40 km. The lowest b-value for the depth range 20-30 km may be because of increased applied stress at greater depth [8], [9]. The higher b-value (1.16 ±0.09) for the 0-10

km range suggests higher heterogeneity. It may also indicate the low strength of rock's that are present in the crust [22]. The depth versus b-value analysis for the region shows a continuous decrease from 0 km to 30 km (Table 3). The b-value observed lower than the global b value of 1.0 from 10 km to 30 km reveal a highly differential stressed regime [9]. These observations also indicate the reverse relationship between b-value and differential stress in the crust. The Gorkha earthquake exposed an asymmetric fault rupture scattering eastward from the epicenter [23]. The observed low b-value patch in the region (Fig. 9) in conjunction with asymmetric fault rupture indicates the possibility of future earthquakes in the west of epicenter of the Gorkha earthquake.

Table 1: Seismic b-value for fixed 100 events window with overlapping of 60 events.

Window	No. of events	Time period	Depth range (km)	Magnitude range	M_c	b-value
1	100	2013/01/01 - 2015/04/25	2.70 - 99.0	3.3 - 6.9	4.0	0.60±0.07
2	100	2014/07/03 - 2015/04/25	3.50 - 99.0	3.3 - 6.9	4.0	0.63±0.06
3	100	2015/04/25 - 2015/04/25	3.50 - 28.7	3.4 - 6.5	4.0	0.85±0.08
4	100	2015/04/25 - 2015/04/25	3.50 - 28.7	3.2 - 5.2	3.7	0.87±0.08
5	100	2015/04/25 - 2015/04/26	7.90 - 28.7	3.2 - 6.6	3.7	0.98±0.12
6	100	2015/04/25 - 2015/04/27	4.50 - 22.8	3.2 - 6.6	3.9	1.16±0.21
7	100	2015/04/26 - 2015/04/29	4.50 - 22.8	3.4 - 6.6	3.8	1.23±0.19
8	100	2015/04/26 - 2015/05/03	7.60 - 35.0	3.4 - 4.8	3.8	1.69±0.23
9	100	2015/04/28 - 2015/05/11	4.50 - 19.60	3.4 - 5.2	3.8	0.76±0.22
10	100	2015/05/01 - 2015/05/12	2.20 - 35.0	3.5 - 6.7	3.6	0.79±0.08
11	100	2015/05/07- 2015/05/12	2.20 - 20.30	3.4 - 6.7	3.9	0.85±0.11
12	100	2015/05/12 - 2015/05/15	0.70 - 35.0	3.4 - 5.2	3.9	1.17±0.14
13	100	2015/05/12 - 2015/05/27	0.70 - 35.0	3.4 - 5.6	3.9	1.19±0.14
14	100	2015/05/13 - 2015/07/01	4.50 - 35.0	3.4 - 5.6	3.9	1.15±0.15
15	100	2015/05/21 - 2015/09/02	4.50 - 35.0	3.4- 5.1	3.9	1.24±0.14
16	100	2015/06/15 - 2016/02/23	5.70 - 100.0	3.2 - 5.3	3.6	0.89±0.08
17	100	2015/07/30 - 2016/08/27	5.70 - 100.0	3.2 - 5.3	3.7	0.91±0.09
18	89	2015/11/29 - 2015/12/31	0.70 - 68.0	3.2 - 5.4	3.6	0.97±0.12

Table 2: Seismic b-value and a value comparison for different period

SN	No of events	Time duration	M_c	b-value	a-value
1	769	2013-01-02 - 2016-12-28	3.7	0.77±0.09	4.839
2	68	2013/01/02 - 2015/04/23 (Before Mainshock)	3.7	0.89±0.12	4.977
3	354	2015/4/25-2015/5/12 (Between mainshock and largest aftershock)	3.6	0.81±0.04	5.421
4	430	2015/05/12 - 2016/12/31 (After Dolakha earthquake)	3.6	0.78±0.08	4.695

Table 3: Seismic b-value at different depths

Depth	Mean Longitude	Mean Latitude	No. of events	M_c	b-value
0-10	84.95	28.00	345	3.8	1.16±0.09
10-20	85.21	27.95	713	3.7	0.89±0.04
20-30	83.42	28.78	55	3.6	0.65±0.08
30-40	84.33	28.55	123	3.5	1.42±0.17
0-40	85.07	28.02	957	3.6	0.83±0.03
30-100	84.65	28.49	143	3.5	1.29±0.16

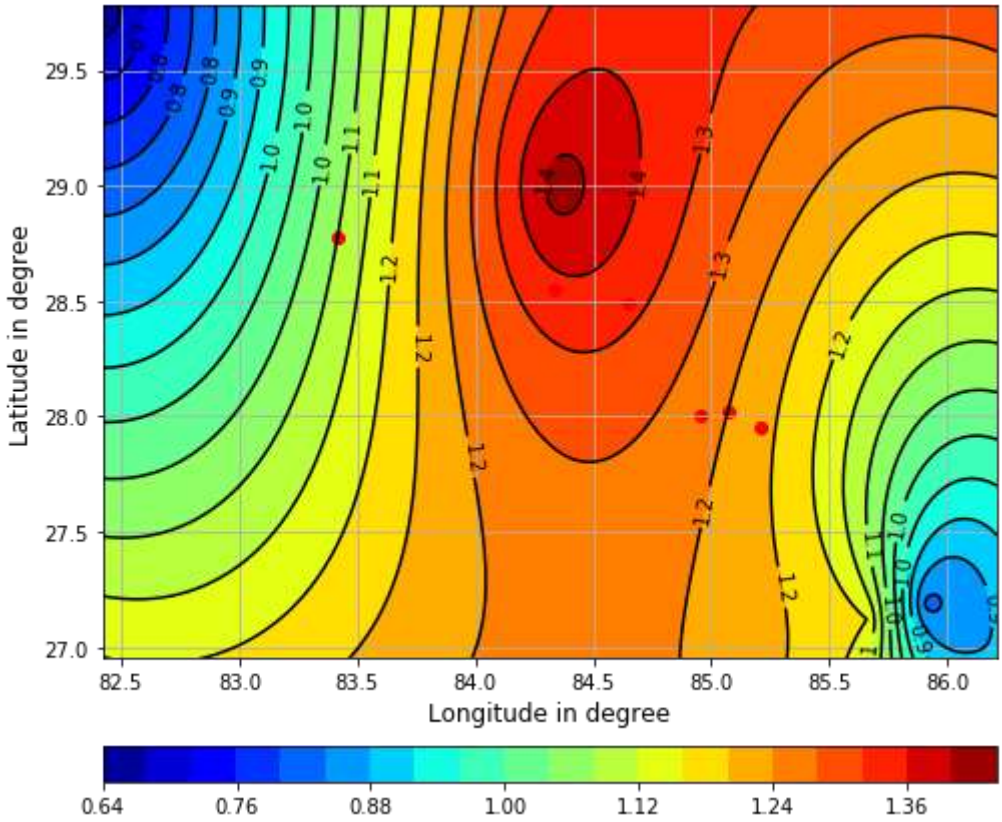

Fig. 9: Contour map for b-value variation with depth. Solid dots are b-value plotted for mean longitude and latitude (Table 3)

4. Conclusion

The statistical parameter b-value of GR relation has been investigated. The b-value for the overall study period was found to be 0.77±0.09. Before the Gorkha earthquake, it was computed as 0.89±0.12. The b-value for the period between the Gorkha earthquake and the Dolakha earthquake was noted as 0.81±0.04. It was found decreasing even after the Dolakha earthquake as 0.78±0.08. The distinct drop of b-value before two strong events is the exhibition of rupture nucleation points of stressed region of Himalaya. The analysis of b-value based on fixed event window shows gradual increase after the Gorkha earthquake and reaches the maximum value of 1.69±0.23 and again drops to the low value of 0.76±0.22. Thus, there is a sudden variation of b-value within a noticeably brief period of 17 days.

The b-value for depth range indicates the presence of heterogeneous crust with differential stress in the region. This observation of variation of b-value with depth agrees with other studies in various parts of the worlds. The contour map (Fig. 9) shows low b-value patch west of Gorkha region which could be the region of future seismic activity. This study presents the stress level in the region before and after the Gorkha earthquake in term of earthquake precursor parameter b-value of earthquake frequency magnitude distribution.

Acknowledgements

One of the authors RKT would like to acknowledge Tribhuvan University, Nepal for providing sabbatical leave and University Grants Commission (UGC), Nepal for providing financial support in the form of fellowship.

References

[1] S. Subedi, and M. B. Poudyal Chhetri, impacts of the 2015 Gorkha Earthquake: Lessons Learnt from Nepal, Earthquakes - Impact, Community Vulnerability and Resilience Intech Open (2019). http://dx.doi.org/10.5772/intechopen.85322

[2] D. E. McNamara et al., Source modeling of the 2015 Mw 7.8 Nepal (Gorkha) earthquake sequence: Implications for geodynamics and earthquake hazards, Tectonophys. 21-30 (2017) 714–715. https://doi.org/10.1016/j.tecto.2016.08.004.

[3] B. Gutenberg and C. F. Richter, Magnitude and energy of earthquakes, Ann. Geophys. 9(1) (1956) 1-15. https://dx.doi.org/10.4401/ag-5590.

[4] W. Smith, The *b*-value as an earthquake precursor, Nature 289 (1981) 136–139. https://doi.org/10.1038/289136a0.

[5] C. H. Scholz, The frequency-magnitude relation of micro fracturing in rock and its relation to earthquakes, Bull. Seis. Soc. Am. 58 (1968) 399–415

[6] C. H. Scholz, On the Stress Dependence of the Earthquake b value, Geophys. Res. Lett. 42 (2015) 1399–1402. https://doi.org/10.1002/2014GL062863.

[7] M. Wyss, The Thickness of Deep Seismic Zones, *Nature* 242 (1973) 255–256. https://doi.org/10.1038/242255a0.

[8] J. Mori and R. E. Abercrombie, Depth dependence of earthquake frequency-magnitude distributions in California: Implications for rupture initiation, J. Geophys. Res. 102(B7) (1997) 15081–15090. https://doi.org/10.1029/97JB01356.

[9]. Wiemer and M. Wyss, Mapping the frequency-magnitude distribution in asperities: An improved technique to calculate recurrence times? J. Geophys. Res. 102 (B7) (1997) 15115–15128. https://doi.org/10.1029/97JB00726.

[10] K. Mogi, Magnitude-Frequency Relationship for Elastic Shocks Accompanying Fractures of Various Materials and Some Related Problems in Earthquakes, Bull. Earthq. Res. Inst. University of Tokyo, 40 (1962) 831-853.

[11] S. Suyehiro et al., Foreshocks and aftershocks accompanying a perceptible earthquake, Meteorol. Geophys. 15 (1964) 71–88.

[12] K. Z. Nanjo and A. Yoshida, Anomalous decrease in relatively large shocks and increase in the *p* and *b* values preceding the April 16, 2016, *M* 7.3 earthquake in Kumamoto, Japan. Earth Planets Space 6913(2017). https://doi.org/10.1186/s40623-017-0598-2.

[13] J. Chen and Z. Shoubiao, Spatial and temporal b-value precursors preceding the 2008 Wenchuan, China, earthquake (Mw = 7.9): implications for earthquake prediction, Geomatics, Nat. Haz. Risk 11(1) (2020) 1196-1211. https://doi.org/10.1080/19475705.2020.1784297

[14] S. Nakaya, Spatiotemporal variation in b value within the subducting slab prior to the 2003 Tokachi-oki earthquake (M 8.0), Japan, J. Geophys. Res. 111 (2006) B03311. https://doi.org/10.1029/2005JB003658

[15] P. Nuannin et al., Spatial, and temporal b value anomalies preceding the devastating off coast of NW Sumatra earthquake of December 26, 2004 Geophys. Res. Lett. 32 (2005) L11307. https://doi.org/10.1029/2005GL022679

[16] C. H. Scholz, The frequency–magnitude relation of micro fracturing in rocks and its relation to earthquakes, Bull. Seis. Soc. Am. 58 (1968) 399–415.

[17] J. K. Gardner and L. Knopoff, Is the sequence of earthquakes in Southern California, with aftershocks removed, Poissonian?, Bull. Seis. Soc. Am. 64(5) (1974) 1363–1367.

[18] S. Wiemer and M. Wyss, Minimum magnitude of completeness in earthquake catalogs: Examples from Alaska, the western US and Japan, Bull. Seism. Soc. Am. 90 (2000) 859-869.

[19] S. Wiemer, A software package to analyze seismicity: ZMAP, Seism. Res. Lett. 72 (3) (2001) 373-382. https://doi.org/10.1785/gssrl.72.3.373.

[20] K. Aki, Maximum likelihood estimate of b in the formula logN = a-bM and its confidence limits, Bull. Seism. Soc. Am. 43 (1965) 237–239.

[21] J. Galetzka et al., Slip pulse and resonance of Kathmandu basin during the 2015 Mw 7.8 Gorkha earthquake, Nepal imaged with geodesy, Science (2015)1091-1095. https://doi.org/10.1126/science.aac6383.

[22] H. R. Wason et al., Analysis of aftershocks of the Chamoli earthquake of March 29, 1999, using broadband seismic data, J. Himal. Geol. 23 (2002) 7–18.

[23] J. P. Avouac et al., Lower edge of locked Main Himalayan Thrust unzipped by the 2015 Gorkha earthquake, Nat. Geosci. 8 (2015)708–711. https://doi.org/10.1038/ngeo2518.

Journal of Institute of Science and Technology, 26(2), 127-136 (2021)
ISSN: 2467-9062 (print), e-ISSN: 2467-9240
https://doi.org/10.3126/jist.v26i2.41664

Research Article

BOX COUNTING FRACTAL DIMENSION AND FREQUENCY SIZE DISTRIBUTION OF EARTHQUAKES IN THE CENTRAL HIMALAYA REGION

Ram Krishna Tiwari[1,2,*] and Harihar Paudyal[2]
[1]Central Department of Physics, Tribhuvan University, Kirtipur, Kathmandu
[2]Birendra Multiple Campus, Tribhuvan University, Bharatpur, Chitwan
**Corresponding author: E-mail: ram.tiwari@bimc.tu.edu.np*
(Received:** July 30, 2021; **Revised:** December 25, 2021; **Accepted:** December 28, 2021**)

ABSTRACT

To establish the relations between b-value and fractal dimension (D_0) for the earthquake distribution, we study the regional variations of those parameters in the central Himalaya region. The earthquake catalog of 989 events (Mc = 4.0) from 1994.01.31 to 2020.10.28 was analyzed in the study. The study region is divided into two sub-regions (I) Region A: 27.3°N -30.3°N and 80°E -84.8°E (western Nepal and vicinity) and (II) Region B: 26.4°N -28.6°N and 84.8°E -88.4°E (eastern Nepal and vicinity). The b-value observed is within the range between 0.92 to 1.02 for region A and 0.64 to 0.74 for region B showing the homogeneous nature of the variation. The seismic a-value for those regions ranges respectively between 5.385 to 6.007 and 4.565 to 5.218. The low b-values and low seismicity noted for region B may be related with less heterogeneity and high strength in the crust. The high seismicity with average b-values obtained for region A may be related with high heterogeneity and low strength in the crust. The fractal dimension ≥1.74 for region A and ≥ 1.82 for region B indicate that the earthquakes were distributed over two-dimensional embedding space. The observed correlation between D_0 and b is negative for western Nepal and positive for eastern Nepal while the correlation between D_0 and a/b value is just opposite for the respective regions. The findings identify both regions as high-stress regions. The results coming from the study agree with the results of the preceding works and reveal information about the local disparity of stress and change in tectonic complexity in the central Himalaya region.

Keywords: b-value, complexity, fractal dimension, central Himalaya, stress

INTRODUCTION

On 25 April of 2015, the central Nepal was struck by Mw 7.8 (6.9 mb) earthquake. The event took place on the Main Himalayan Thrust (MHT) (Adhikari *et al.*, 2015; Yue *et al.*, 2017) and was resulted from unfastening of the lower edge of the sealed portion of the MHT, along which the Himalayan hunk is thrust over India (Avouac *et al.*, 2015). The MHT is the dynamic structure along the Himalayan arc and reaches the surface at Main Frontal Thrust (MFT) as observed by the Japanese Agency (Hubbard *et al.*, 2015). Within the 17 days (on 12 May 2015), the nation was again struck by another earthquake of Mw 7.3 (6.7 mb) (Lindsey *et al.*, 2015). These two large events with their aftershocks have partly released the strain accumulated between seismic events along the MHT (Hayes *et al.*, 2015; Sreejith *et al.*, 2018). The mainshock and prompt running aftershock sequence caused strong ground shaking not only in Nepal but also in some parts of neighboring nations India and China, causing more than 8900 deaths (Lindsey *et al.*, 2015). Ground shaking in Kathmandu basin was strong enough to collapse many historical structures that had persisted the preceding earthquakes(Galetzka *et al.*, 2015).

From the study of literatures, the spreading of the rupture in the past Himalayan earthquakes were understood to be organized by asperities and supplementary structural complexities (Bilham, 2019; Mugnier *et al.*, 2017). Since the Gorkha earthquake of 2015 happened between the rupture areas of the 1505 Ms 8.2 Lo-Mustang earthquake in western Nepal (Ghazoui *et al.*, 2019) and Nepal-Bihar earthquake (Mw 8.2) of 1934, it was expected to have the magnitude greater than 8 (Letort *et al.*, 2016). Sreejith *et al.* (2018) disclose the existence high strain and stress region (asperity), one towards the west and the other towards the east of the 2015 Gorkha epicenter. Although, the asperity found in the eastern side had broken partially in the Gorkha earthquake, the asperity in the western side is still unbroken and preparing to host the future large earthquake. Furthermore, it is known that the elastic potential energy releasing process in the Himalaya is either by the large rupture reaching the surfaces or by incomplete rupture (Scholz & Campos, 2012). The case of partial rupture for Gorkha earthquake indicates the event did not release all the stored strain in the region and the region is overdue for major earthquake (Avouac *et al.*, 2015; Ghazoui *et al.*, 2019). This investigation applies the theory of nonlinear dynamics (Helmstetter *et al.*, 2005; Yin *et al.*, 2019) to identify the stress regions in terms of b-values and box counting fractal dimension of epicenter distribution. Based on the previous studies on the aftermath of the Gorkha earthquake, the study region is divided into two sub-regions (Fig. 1).

(I) Region A: 27.3°N - 30.3°N and 80°E - 84.8°E (western Nepal and vicinity) consisting of 348 earthquakes.
(II) Region B: 26.4°N - 28.6°N and 84.8°E - 88.4°E (eastern Nepal and vicinity) consisting of 274 earthquakes.

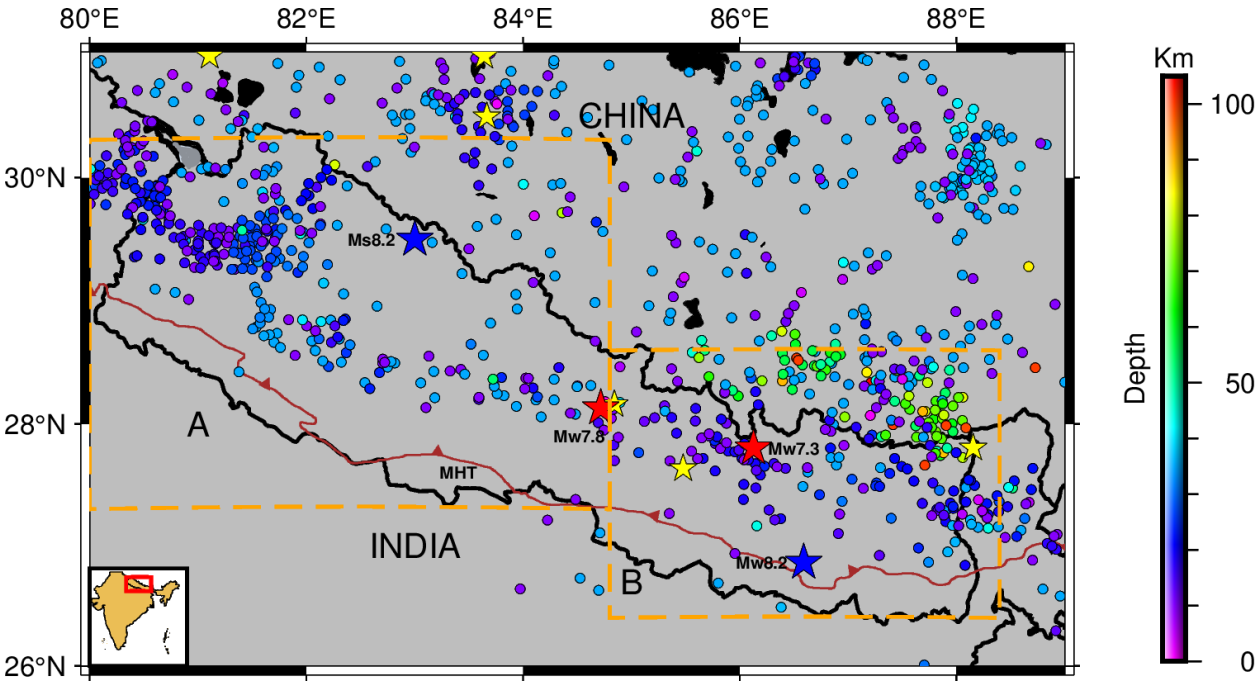

Figure 1. Epicentral locations of the 1189 earthquakes events out of which 1181 events with magnitude ≤ 5.9 mb are represented by solid circle. The color of the circle indicates the depth of the earthquake events. Yellow stars stand for the 6 earthquake events ≥ 6 mb after 1994 and two red stars stand for Mw 7.8 Gorkha earthquake and Mw 7.3 Dolakha earthquake. Blue star in the region A stands for 1505 Lo-Mustang earthquake (Ms 8.2) and blue star in the region B stands for 1934 Nepal-Bihar earthquake (Mw 8.2). Regions of interest are demarcated by orange box into regions A and B. Inset map at bottom left corner of the map shows study region bounded by red box.

Data

The earthquake events were collected from International Seismological Centre (ISC) catalog and United States Geological Survey (USGS) catalog. While selecting the events priority was given to ISC catalog and events were scrutinized on the basis of locations (latitude and longitude) and date with time of occurrence The Mw scale of USGS catalog were converted into mb scale from the relation given by Das *et al.* (2011). We found 2457 events for the period 1964-02-01 to 2020-11-23 with in the latitude 26°N to 31°N and longitude 80°E to 89°E. After declustering the catalog (Gardner & Knopoff, 1974) from the software ZMAP (Wiemer, 2001) , we only retained 1185 events. The software ZMAP is the widely accepted tool for the statistical analysis of the seismicity pattern so equally applicable for the study in the Himalayan region. The cumulative curve (Fig. 2) shows straight line with constant slope after January 1994 giving the completeness (Mc=4.0) of catalog, so the catalog starts from 1994 with 989 events. For the analysis of the epicenters, we have selected rectangular areas of dimension 3°×3° in the region A (sub-regions A1 to A10) and 3°×2.2° in the region B (sub-regions B1to B4) as mentioned in the Table 1 and Table 2. The variation between b and D_0 over time was evaluated using sliding windows of aforementioned areas with window advance of 0.2 degree along the direction of longitude in order to cover region of the study. The time number histograms (Fig. 3) display the high seismic activity in region A compared to region B whereas the increase of seismic activity around the year 2015 is observed for both regions.

METHODOLOGY

Earthquake frequency size distribution b-value

The cumulative frequency size dispersal of earthquakes is given by the relation.

$$Log\ N_c = a - bM$$

where N_c is the number of earthquakes with magnitude greater or equal to M, a is the constant signifying the level of the productivity and b is the constant known as b-value that signifies magnitude distribution (Gutenberg & Richter, 1944). The frequency-magnitude analysis of the data is done by the maximum curvature technique and the b-value is estimated by maximum likelihood approach (Aki, 1965).

$$\mathrm{b} = \frac{\log_{10} e}{M_{av.} - (M - \Delta M/2)}$$

where $M_{av.}$ is the average value of the magnitudes, M is the lower limit of the magnitude in the catalog and ΔM is the binning width of the catalog. The uncertainty occurred in the estimation of the b-value is given by the relation below (Shi & Bolt, 1982).

$$\delta \mathrm{b} = 2.3 * \mathrm{b}^2 \sqrt{\frac{\sum_i^N (M_i - M_{av.})^2}{n_c(n_c - 1)}}$$

where n_c is the number of earthquakes in the given sample. The magnitude of completeness (Mc) was determined as 4.0 (for 989 events) using the iterative method (Wiemer & Wyss, 2000). The b-value is normally inferred as the sign of the heterogeneity present in the material of the medium and found to fluctuate from 1.0 to 1.6 for the global seismicity (Mogi, 1967; Sobiesiak *et al.*, 2007). Also, it is interpreted as the indicator of applied tangential stresses (Scholz, 1968; Schorlemmer *et al.*, 2005; Singh *et al.*, 2009). For the earthquakes in the California, the b-values found to vary from 0.45 to 1.5 (Gutenberg & Richter, 1944). The b-value of 0.80 ± 0.05 is computed for aftershocks sequences of Gorkha earthquake between 2015 May 25 and June 8 (Adhikari *et al.*, 2015). For the 820 aftershocks (2.7 < M < 7.3) of the Gorkha earthquake, the b-value of 1.11 ± 0.08 was computed during the period April 25 – November 12, 2015 (Nampally *et al.*, 2018). The b-values for the longitude range 80°E to 89°E and latitude range 26°N to 31°N found to vary from 0.5 to 1.6 for the period 1964-2015 (Ghosh, 2020). Furthermore, the b-value contour map depicts the low b-value patch in the western part of the Gorkha region as the possible zone of future robust seismic activity (Tiwari & Paudyal, 2021).

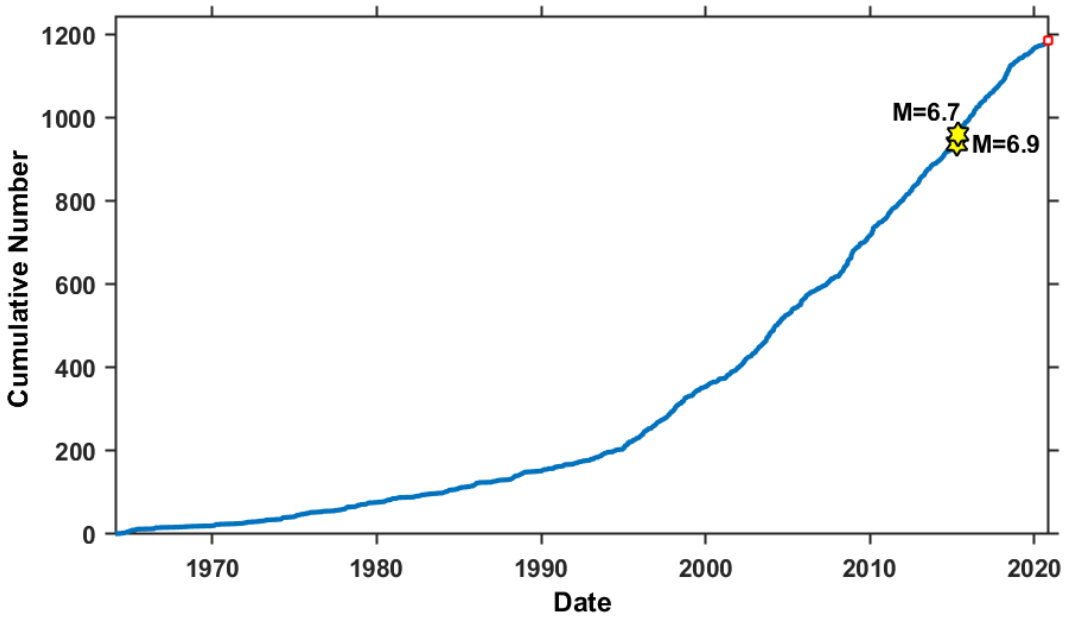

Figure 2. Cumulative number of events with time showing 6.9 mb Gorkha earthquake and 6.7 mb major aftershock

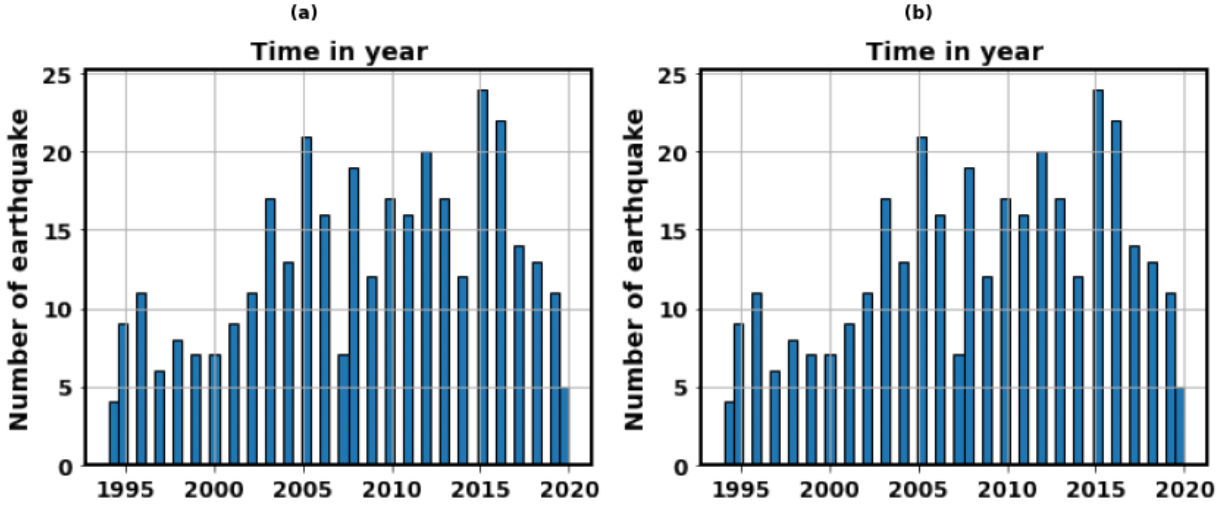

Figure 3. Time histograms of the earthquakes for (a) region A and (b) region B

Fractal distribution

A distribution with fracture or uneven basic structure reiterate in different scales is a fractal. The index providing a statistical value to compare how a pattern alters with the measuring scale is the fractal dimension (Lopes & Betrouni, 2009). Earthquakes are known as self-organized dynamical

system progressing spatially and temporarily towards a critical stationary stage, so the fractal theories are beneficial in learning seismic activities (Rodríguez Pascua *et al.*, 2003). The spectrum of the fractal dimension can be obtained from the generalized fractal dimension D_q and it is calculated from the relation (Grassberger & Procaccia, 1983).

$$C_q\,(N_c,r) = [\frac{1}{N_c}\sum_{i=1}^{N_c}[\frac{1}{N_c-1}\sum_{j=1,i\neq j}^{N}\theta\big(r - \|X_i - X_j\|\big)]^{q-1}]^{\frac{1}{q-1}}$$

In above equation, $\theta\big(r - \|X_i - X_j\|\big) = \begin{cases} 1, if\ \|X_i - X_j\| < r \\ 0, if\ \|X_i - X_j\| \geq r \end{cases}$ is the Heaviside step function, r is the scaling radius, N_c is the total number of pair of data points within the sample volume, X_i and X_j are the location of the epicenter in latitude and longitude of the i^{th} event and the j^{th} event while $C_q\,(N_c,r)$ is the q^{th} integral.

The generalized dimension D_q, in terms of generalized correlation sum can be written as,

$$D_q = \lim_{r\to 0}\frac{1}{q-1}\frac{\log C_q(N_c,r)}{\log r}$$

For the monofractal having homogeneous epicentral distribution, D_q has the constant values for all q values (Zamani & Agh-Atabai, 2011).

Moreover, $\lim_{N_c\to\infty} C_q(N_c,r) = C_q(r)$

Finally, the generalized dimension$\big(D_q\big)$, in terms of the generalized correlation sum

$$D_q = \lim_{r\to 0}\frac{1}{q-1}\frac{\log C_q(r)}{\log r}$$

For q = 0, the above formula gives capacity dimension. It gives information dimension for q=1, and correlation dimension for q=2 (Roy & Padhi, 2007). Therefore, for q = 0, the formula reduces to

$$D_0 = -\lim_{r\to 0}\frac{\log C_q(r)}{\log r}$$

The above formula is similar to the box counting technique (Aggarwal *et al.*, 2017; Mandal & Rodkin, 2011; Radziminovich *et al.*, 2019) as

$$D_0 = -\lim_{r\to 0}\frac{\log N_c(r)}{\log r}$$

where N_c(r) is the number of boxes of side r occupied by point sources. With the advantage of simple mathematical formulation and empirical estimation, box-counting dimension becomes the widely used dimension (Falconer, 1997). The box counting technique estimates the capacity dimension by measuring the space-filling characters of a fracture set with the change in grid of the scale (Gospodinov *et al.*, 2010; Mandal & Rodkin, 2011). In the box-counting method, the epicenter distribution is covered by squares or cubes of decreasing size (r). If the epicenter distribution points have fractal character the slope of the $\log C_q(r) - \log r$ curve, in particular range of r, provides capacity dimension.

RESULTS AND DISCUSSION

The b-value of the region A ranges from 0.91 ± 0.08 to1.02 ± 0.10 (Table 1; Fig. 4a) while b-value of Region B ranges from 0.64 ± 0.04 to 0.78 ± 0.06 (Table 2; Fig. 5a). The relatively high b-value and high seismicity observed in the region A may indicate that the area is linked with high material heterogeneity and low strength in the crust as explained in the literatures Mogi (1967) and Scholz (1968). Many small earthquakes can be expected in regions. The low b-values and relatively low seismicity in the region B may be linked with low degree of heterogeneity and strong rheological strength in the crust that approves the preceding works (Bayrak *et al.*, 2013; Khan *et al.*, 2011; Khattri & Tyagi, 1983; Wyss, 1973). The creeping process occurring in the faults is generally related with higher b-value, and asperities present in the faults are often related to lower b-value (Kawamura & Chen, 2017; Oncel & Wilson, 2002). Thus, the earthquakes in the region A may be due to the creeping process and the dominating number of aftershock in the region B are related to the asperities found in the region.

The fractal dimension of the region A ranges from 1.79 ± 0.01 to 1.89 ± 0.03 (Table 1; Fig. 4b). Similarly, for the region B it ranges from 1.82 ± 0.02 to 1.86 ± 0.02 (Table 2; Fig. 5b). These non-integers values of the dimension between 1 and 2 indicates that the earthquakes are spread on the boundary between a line and a plane (Rodríguez Pascua *et al.*, 2003). Tosi (1998) explained that possible values of fractal dimensions do not depend on the dimension of the embedding space and the value ranges between 0 and 2. The limiting value of dimension can be interpreted as D_0 close to 0 has all events bunched into single point, D_0 near to 1 means the source region has linear nature and D_0 near to 2 shows that the epicenters are casually or evenly spread over a two-dimensional (2D) implanting space (Roy & Ram, 2006; Tosi, 1998). Thus, the higher D_0 (1.79 -1.89) obtained for the regions may be the indication of scattered epicenter distributions. The lowest b-values and the highest D_0 computed for region B indicate the vulnerability of the region for occurrence of the large earthquakes (Naimi-Ghassabian *et al.*, 2018). The works similar to the present investigation have been carried out by the previous researchers. The fractal correlation dimension of 1.66 is noted for 820 aftershocks between April 25 – November 12, 2015 for Gorkha earthquake (Nampally et al., 2018). The fractal dimension of 1.69 ± 0.05 is obtained for the epicenter distribution of 2001 Bhuj earthquake (Mw 7.7) in Gujarat, India (Aggarwal et al., 2017).

Table 1. Subdivided regions of A with period, location, earthquakes numbers, frequency magnitude distribution coefficients a-value and b-value, ratio of a and b, fractal dimension (D_0) and coefficient of determination (R^2)

Region/period	Latitude/Longitude	No. of events	a-value	b-value	a/b	D_0	R^2
A1 (1994-01-31—2020-10-28)	27.3°N-30.3°N 80.0°E-83.0°E	277	5.817	0.92 ± 0.06	6.32	1.88 ± 0.03	0.993
A2 (1994-01-31—2020-10-28)	27.3°N-30.3°N 80.2°E-83.2°E	267	5.809	0.93 ± 0.06	6.24	1.87 ± 0.03	0.993
A3 (1994-01-31—2020-10-28)	27.3°N-30.3°N 80.4°E-83.4°E	250	5.763	0.92 ± 0.06	6.26	1.89 ± 0.03	0.994
A4 (1994-01-31—2020-10-28)	27.3°N-30.3°N 80.6°E-83.6°E	241	5.780	0.93 ± 0.07	6.21	1.88 ± 0.02	0.995
A5 (1994-01-31—2020-10-28)	27.3°N-30.3°N 80.8°E-83.8°E	228	5.894	0.97 ± 0.07	6.07	1.88 ± 0.02	0.994
A6 (1994-01-31—2020-03-15)	27.3°N-30.3°N 81.0°E-84.0°E	224	5.897	0.97 ± 0.07	6.08	1.86 ± 0.02	0.994
A7 (1994-01-31—2020-03-15)	27.3°N-30.3°N 81.2°E -84.2°E	210	5.995	1.00 ± 0.01	6.00	1.82 ± 0.03	0.993
A8 (1994-01-31—2020-03-15)	27.3°N-30.3°N 81.4°E -84.4°E	200	5.868	0.97 ± 0.01	6.04	1.79 ± 0.02	0.994
A9 (1994-01-31—2020-03-15)	27.3°N-30.3°N 81.6°E -84.6°E	168	5.979	1.02 ± 0.10	5.87	1.79 ± 0.01	0.999
A10 (1994-05-10—2020-03-15)	27.3°N-30.3°N 81.8°E -84.8°E	139	5.385	0.91 ± 0.08	5.92	1.74 ± 0.01	0.998
Entire A (1994-01-31—2020-10-28)	27.3°N-30.3°N 80.0°E -84.8°E	348	6.007	0.95 ± 0.06	6.32	1.87 ± 0.02	0.995

Table 2. Subdivided regions of B with period, location, earthquakes numbers, frequency magnitude distribution coefficients a-value and b-value, ratio of a and b, fractal dimension (D_0) and coefficient of determination (R^2)

Region/Period	Latitude/Longitude	No. of events	a-value	b-value	a/b	D_0	R^2
B1 (1994-06-25—2020-11-23)	26.4°N -28.6°N 84.8°E -87.8°E	202	4.565	0.64 ± 0.04	7.13	1.82 ± 0.02	0.997
B2 (1994-05-25—2020-11-23)	26.4°N -28.6°N 85.0°E -88.0°E	234	5.218	0.78 ± 0.06	6.69	1.82 ± 0.02	0.995
B3 (1994-05-25—2020-11-23)	26.4°N -28.6°N 85.2°E -88.2°E	250	5.211	0.78 ± 0.06	6.68	1.84 ± 0.02	0.996
B4 (1994-05-25—2020-11-23)	26.4°N -28.6°N 85.4°E -88.4°E	257	5.205	0.77 ± 0.05	6.76	1.85 ± 0.02	0.996
Entire B (1994-05-25—2020-11-23)	26.4°N -28.6°N 84.8°E -88.4°E	274	5.137	0.74 ± 0.05	6.94	1.86 ± 0.02	0.996

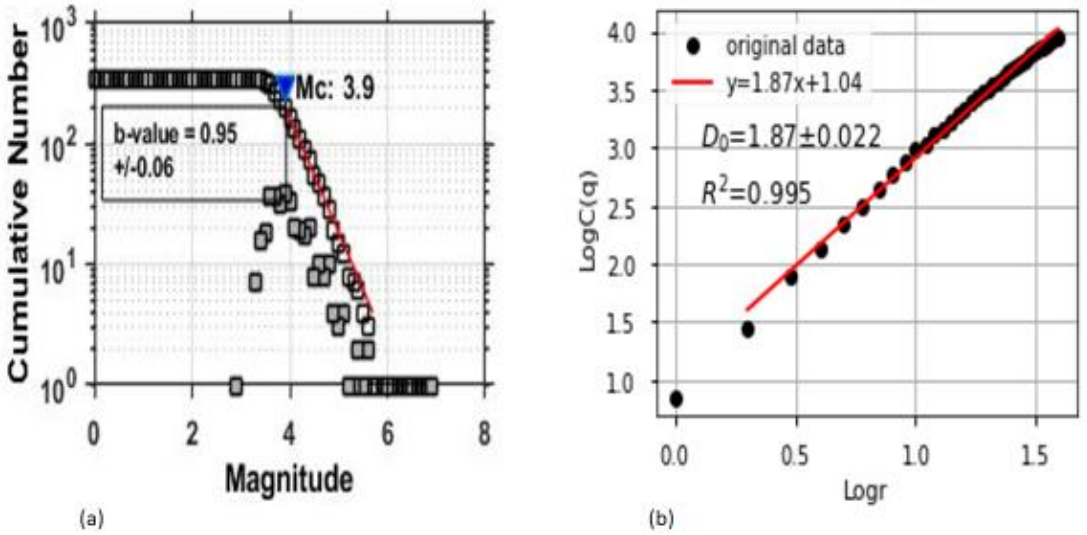

Figure 4. Graphs showing (a) Frequency magnitude distribution b-value and (b) D_0 for the entire region A.

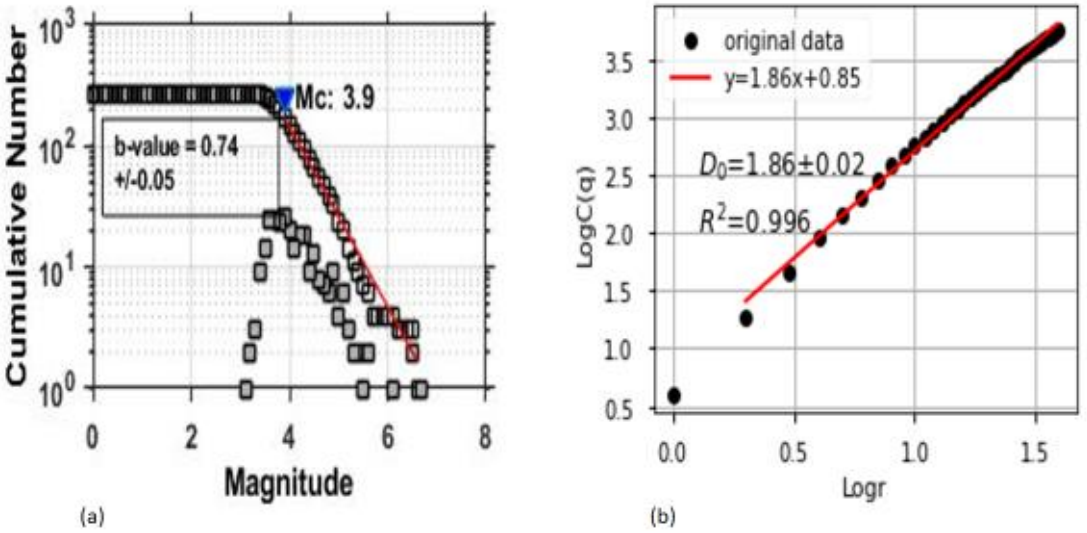

Figure 5. Graphs showing (a) Frequency magnitude distribution b-value and (b) D_0 for the entire region B

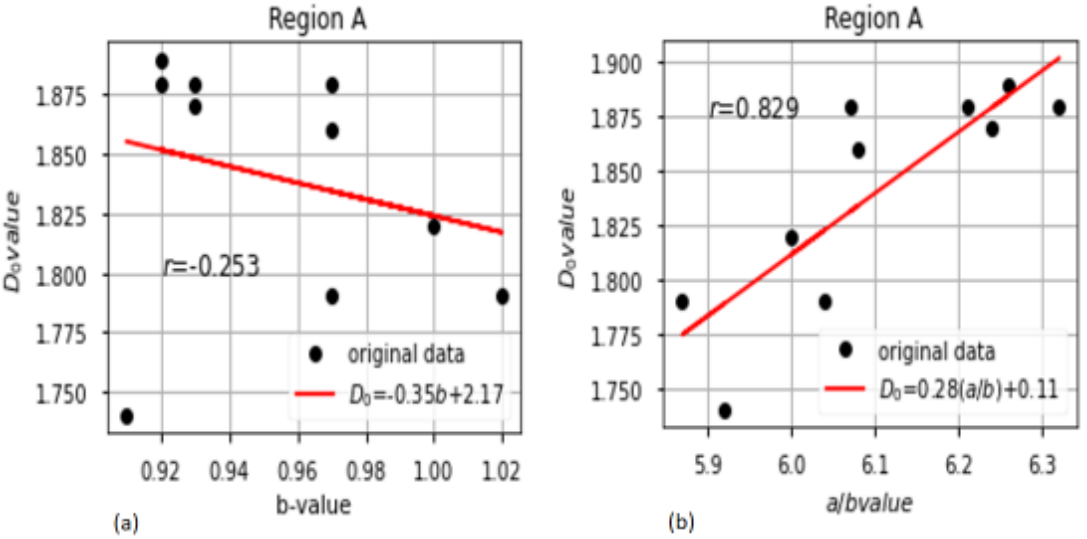

Figure 6. Correlation between variations in D_0 and (a) b-value and (b) the ratio a/b for region A

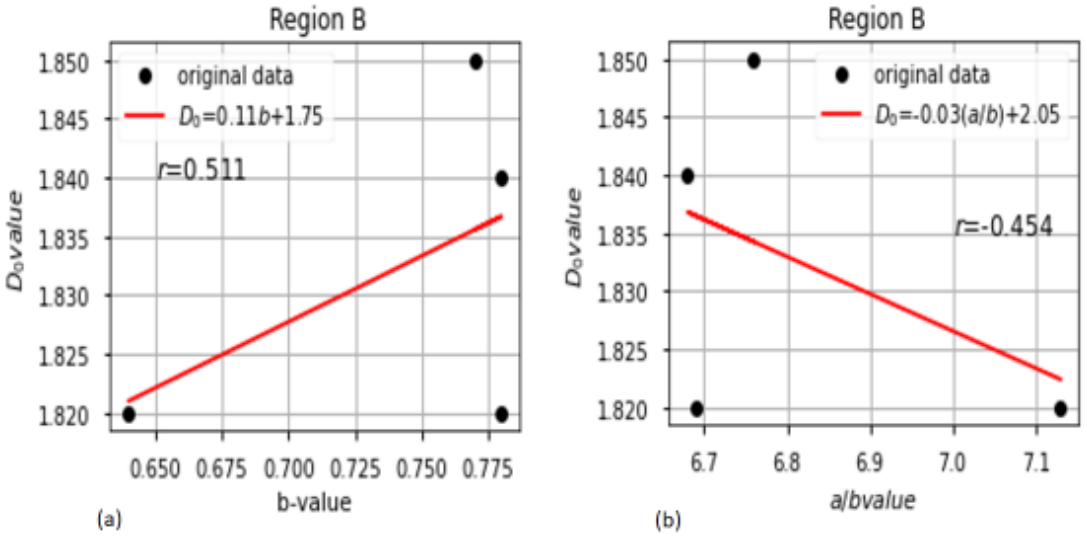

Figure 7. Correlation between variations in D_0 and (a) b-value and (b) the ratio a/b for region B

The D_0 – b and D_0 – (a/b) relations could possibly replicate regional seismicity and earthquake threat and believed to be applicable in earthquake hazard related studies (Bayrak & Bayrak, 2012; Pailoplee & Choowong, 2014). The negative correlations between b-value and D_0 (r = - 0.253) is obtained for the region A (Fig. 6a) while the positive correlation (r = 0.511) is observed in the region B (Fig. 6b). The positive correlations between a/b and D_0 (r = 0.829) is observed for the region A (Fig. 6b) and negative correlation (r = - 0.454) is observed for the region B (Fig. 7b). The D_0 – (a/b) correlation was explained to be quite dependable and effective comparing to the D_0 – b correlation for indicating seismic hazards(Bayrak & Bayrak, 2012), but in this work, it is justified only for the region A showing the significant of the distribution of D_0 – a/b with r = 0.829. The negative correlations mean the drop in one parameter for rise in another and the positive correlations means parallel increase or decrease in corresponding parameters. The drop in D_0 and rise in b-value or parallel rise or fall in D_0 and a/b for the region A indicate the presence of dense and complex network of faults having likelihood of occurring earthquake with larger magnitude (Oncel & Wilson, 2007). The positive correlation between D_0 and b or negative correlation between D_0 and a/b in region B can be interpreted as reduced probability of larger magnitude earthquake because the stress in the region is reducing through lower magnitude events. The preceding study had also noticed negative correlation between b-value and fractal dimension for this region from the earthquake data of seismological catalogs of the USGS and ISC (Ghosh, 2020).

For the region A, there is a decrease in D_0 and increase in b-value as the sliding windows move from west to east while for the region B both parameters increase as the window moves from west to east (Fig. 8). Thus, the spatial variation of D_0 and b-value is in the negative correlation for the region A and in the positive correlation for the region B. The negative spatial correlation may be responsible to the rise in stress concentration (lower b) and a decline in the clustering of the epicenter (increased D_0).

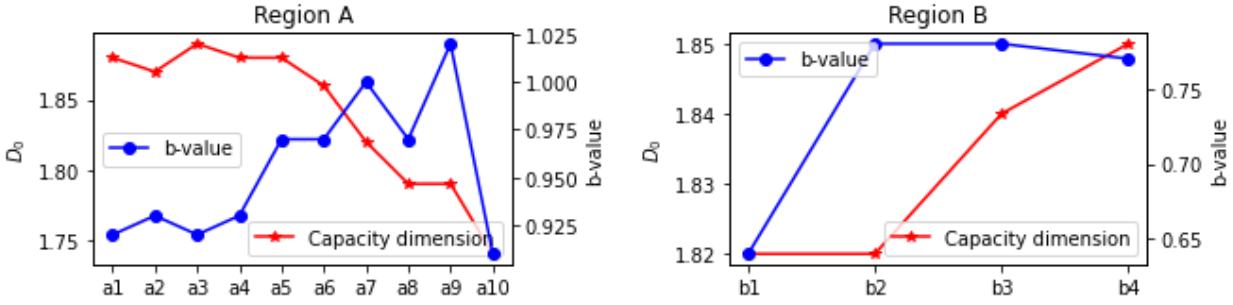

Figure 8. Regional variation of b-value and D_0 depending on the windows selected

CONCLUSIONS

The analysis is carried out on earthquake catalog (Mc = 4.0) of 989 events from January 1994 to November 2020. The spatial variation of fractal dimension (D_0) with b-value shows negative correlation for western Nepal and vicinity while correlation is positive for eastern Nepal and vicinity. The correlation of D_0 with a/b ratio is just opposite. From these results, it can be inferred that regions considered are under high stress and posing risk for generating large earthquake in the future. The western Nepal is safe against the seismic hazards as the b-value of the region is getting average b-value of 1.0 through the small earthquakes event. The observed low b values for eastern Nepal imply that it is highly stressed and could be a source region for future strong events. The high fractal dimension value ≥1.74 obtained for both regions indicate the earthquake events are distributed in two-dimensional embedding space (source zones). This study indicates the regional variation of stress level and difference in tectonic complexity.

ACKNOWLEDGEMENTS

The first author (Ram Krishna Tiwari) would like to acknowledge Tribhuvan University, Nepal, and University Grants Commission (UGC), Nepal for the sabbatical leave and financial support, respectively.

AUTHOR CONTRIBUTIONS

HP conceived and designed the research. RKT handled the software, analyzed and interpreted the data. Both authors wrote and revised the manuscript.

CONFLICT OF INTEREST

The authors declare no conflict of interest.

DATA AVAILABILITY STATEMENT

The data that support the findings of this study are available from the corresponding author, upon reasonable request.

REFERENCES

Adhikari, L.B., Gautam, U.P., Koirala, B.P., Bhattarai, M., Kandel, T., Gupta, R.M., Timsina, C., Maharjan, N., Maharjan, K., Dahal, T., Hoste-Colomer, R., Cano, Y., Dandine, M., Guilhem, A., Merrer, S., Roudil, P., & Bollinger, L. (2015). The aftershock sequence of the 2015 April 25 Gorkha-Nepal earthquake. *Geophysical Journal International*, *203*(3), 2119–2124. https://doi.org/10.1093/gji/ggv412.

Aggarwal, S.K., Pastén, D., & Khan, P.K. (2017). Multifractal analysis of 2001 Mw7.7 Bhuj earthquake sequence in Gujarat, Western India. *Physica A: Statistical Mechanics and its Applications*, *488*, 177–186. https://doi.org/10.1016/j.physa.2017.06.022.

Aki, K. (1965). Maximum likelihood estimate of *b* in the formula Log *N*= *a* – *bM* and its confidence limits. *Bulletin of the Earthquake Research Institute, 43*, 237–239.

Avouac, J.P., Meng, L., Wei, S., Wang, T., & Ampuero, J.P. (2015). Lower edge of locked Main Himalayan Thrust unzipped by the 2015 Gorkha earthquake. *Nature Geoscience*, 8(9), 708–711. https://doi.org/10.1038/ngeo2518.

Bayrak, Y., & Bayrak, E. (2012). Regional variations and correlations of Gutenberg-Richter parameters and fractal dimension for the different seismogenic zones in Western Anatolia. Journal of Asian Earth Sciences, 58, 98–107. https://doi.org/10.1016/j.jseaes.2012.06.018.

Bayrak, Y., Yadav, R.B.S., Kalafat, D., Tsapanos, T.M., Çinar, H., Singh, A.P., Bayrak, E., Yilmaz, Ş., Öcal, F., & Koravos, G. (2013). Seismogenesis and earthquake triggering during the Van (Turkey) 2011 seismic sequence. *Tectonophysics, 601*, 163–176. https://doi.org/10.1016/j.tecto.2013.05.008.

Bilham, R. (2019). Himalayan earthquakes: A review of historical seismicity and early 21st century slip potential. *Geological Society Special Publication, 483*(1), 423–482. https://doi.org/10.1144/SP483.16.

Das, R., Wason, H.R., & Sharma, M.L. (2011). Global regression relations for conversion of surface wave and body wave magnitudes to moment magnitude. *Natural Hazards, 59*(2), 801–810. https://doi.org/10.1007/s11069-011-9796-6.

Falconer, K. (1997). Fractal Geometry. Biometrics, 53(3), 1183. https://doi.org/10.2307/2533585

Galetzka, J., Melgar, D., Genrich, J.F., Geng, J., Owen, S., Lindsey, E.O., Xu, X., Bock, Y., Avouac, J.-P., Adhikari, L.B., Upreti, B.N., Pratt-Sitaula, B., Bhattarai, T.N., Sitaula, B.P., Moore, A., Hudnut, K.W., Szeliga, W., Normandeau, J., Fend, M., Flouzalt, M. Bollinger, L., Shrestha, P., Koirala, B., Gautam, U., Bhattarai, M., Gupta, R., Kandel, T., Timsina, C., Sapkota, S.N., Rajaure, S., & Maharjan, N. (2015). Slip pulse and resonance of Kathmandu basin during the 2015 Mw 7.8 Gorkha earthquake, Nepal imaged with space geodesy. Science, 349(6252), 1091–1095. https://doi.org/10.1126/science.aac6383.

Gardner, J.K., & Knopoff, L. (1974). Is The Sequence of Earthquakes in Southern California, With Aftershocks Removed, Poissonian? *Bulletin of the Seismological Society of America, 64*(5), 1363–1367.

Ghazoui, Z., Bertrand, S., Vanneste, K., Yokoyama, Y., Nomade, J., Gajurel, A.P., & van der Beek, P.A. (2019). Potentially large post-1505 AD earthquakes in western Nepal revealed by a lake sediment record. *Nature Communications, 10*(1), 1–9. https://doi.org/10.1038/s41467-019-10093-4.

Ghosh, U. (2020). Seismic Characteristics and Seismic Hazard Assessment: Source Region of the 2015 Nepal Earthquake Mw 7.8 in Central Himalaya. *Pure and Applied Geophysics, 177*(1), 181–194. https://doi.org/10.1007/s00024-019-02318-w.

Gospodinov, D., Marekova, E., & Marinov, A. (2010). Verifying the dependence of fractal coefficients on different spatial distributions. *AIP Conference Proceedings, 1203*, 731–736. https://doi.org/10.1063/1.3322545.

Grassberger, P., & Procaccia, I. (1983). Characterization of

strange attractors. *Physical Review Letters, 50*(5), 346–349. https://doi.org/10.1103/PhysRevLett.50.346.

Gutenberg, B., & Richter, C.F. (1944). Frequency of earthquakes in California. *Bulletin of the Seismological Society of America*, 34, 185–188.

Hayes, G.P., Briggs, R.W., Barnhart, W.D., Yeck, W.L., McNamara, D.E., Wald, D.J., Nealy, J.L., Benz, H.M., Gold, R.D., Jaiswal, K.S., Marano, K., Earle, P.S., Hearne, M.G., Smoczyk, G.M., Wald, L.A., & Samsonov, S.V. (2015). Rapid characterization of the 2015 Mw 7.8 Gorkha, Nepal, earthquake sequence and its seismotectonic context. *Seismological Research Letters, 86*(6), 1557–1567. https://doi.org/10.1785/0220150145.

Helmstetter, A., Kagan, Y.Y., & Jackson, D.D. (2005). Importance of small earthquakes for stress transfers and earthquake triggering. *Journal of Geophysical Research: Solid Earth, 110*(5), 1–13. https://doi.org/10.1029/2004JB003286.

Hubbard, J., Almeida, R., Foster, A., Sapkota, S.N., Bürgi, P., Tapponnier, P., Wang, K., & Fialko, Y. (2015). Source characteristics of the 2015 Mw 7.8 Gorkha earthquake and its MW 7.2 aftershock from space geodesy. *Geology, 44*, 639–642. https://doi.org/10.1002/2015GL065201.

Kawamura, M., & Chen, K.H. (2017). Influences on the location of repeating earthquakes determined from a and b value imaging. *Geophysical Research Letters, 44*(13), 6675–6682. https://doi.org/10.1002/2017GL073335.

Khan, P.K., Ghosh, M., Chakraborty, P.P., & Mukherjee, D. (2011). Seismic b-value and the assessment of ambient stress in Northeast India. *Pure and Applied Geophysics, 168*(10), 1693–1706. https://doi.org/10.1007/s00024-010-0194-x.

Khattri, K.M., & Tyagi, A.K. (1983). Seismicity patterns in the Himalayan plate boundary and identification of the areas of high seismic potential. *Tectonophysics, 96*(3–4), 281–297. https://doi.org/10.1016/0040-1951(83)90222-6.

Letort, J., Bollinger, L., Lyon-Caen, H., Guilhem, A., Cano, Y., Baillard, C., & Adhikari, L.B. (2016). Teleseismic depth estimation of the 2015 Gorkha-Nepal aftershocks. *Geophysical Journal International, 207*(3), 1584–1595. https://doi.org/10.1093/gji/ggw364.

Lindsey, E.O., Natsuaki, R., Xu, X., Shimada, M., Hashimoto, M., Melgar, D., & Sandwell, D.T. (2015). Line-of-sight displacement from ALOS-2 interferometry: Mw 7.8 Gorkha Earthquake and Mw 7.3 aftershock. *Geophysical Research Letters, 42*(16), 6655–6661. https://doi.org/10.1002/2015GL065385.

Lopes, R., & Betrouni, N. (2009). Fractal and multifractal analysis: A review. *Medical Image Analysis, 13*(4), 634–649. https://doi.org/10.1016/j.media.2009.05.003.

Mandal, P., & Rodkin, M.V. (2011). Seismic imaging of the 2001 Bhuj Mw 7.7 earthquake source zone: B-value, fractal dimension and seismic velocity tomography studies. *Tectonophysics, 512*(1–4), 1–11. https://doi.org/10.1016/j.tecto.2011.09.004.

Mogi, K. (1967). Earthquakes and fractures. *Tectonophysics, 5*(1), 35–55. https://doi.org/10.1016/0040-1951(67)90043-1.

Mugnier, J.L., Jouanne, F., Bhattarai, R., Cortes-Aranda, J., Gajurel, A., Leturmy, P., Robert, X., Upreti, B., & Vassallo, R. (2017). Segmentation of the Himalayan megathrust around the Gorkha earthquake (25 April 2015) in Nepal. *Journal of Asian Earth Sciences, 141*, 236–252. https://doi.org/10.1016/j.jseaes.2017.01.015.

Naimi-Ghassabian, N., Khatib, M.M., Nazari, H., & Heyhat, M.R. (2018). Regional variations and earthquake frequency–magnitude distribution and fractal dimension in the North of Central-East Iran Blocks (NCEIB). *Arabian Journal of Geosciences, 11*(11), 243–264. https://doi.org/10.1007/s12517-018-3506-6.

Nampally, S., Padhy, S., & Dimri, V.P. (2018). Characterizing spatial heterogeneity based on the b-value and fractal analyses of the 2015 Nepal earthquake sequence. *Tectonophysics, 722*, 154–162. https://doi.org/10.1016/j.tecto.2017.11.004.

Oncel, A.O., & Wilson, T. (2007). Anomalous seismicity preceding the 1999 Izmit event, NW Turkey. *Geophysical Journal International, 169*(1), 259–270. https://doi.org/10.1111/j.1365-246X.2006.03298.x.

Oncel, A.O., & Wilson, T.H. (2002). Space-time correlations of seismotectonic parameters: Examples from Japan and from Turkey preceding the İzmit earthquake. *Bulletin of the Seismological Society of America, 92*(1), 339–349. https://doi.org/10.1785/0120000844.

Pailoplee, S., & Choowong, M. (2014). Earthquake frequency-magnitude distribution and fractal dimension in mainland Southeast Asia. *Earth, Planets and Space, 66*(1), 1–10. https://doi.org/10.1186/1880-5981-66-8.

Radziminovich, N.A., Miroshnichenko, A.I., & Zuev, F.L. (2019). Magnitude of completeness, b-value, and spatial correlation dimension of earthquakes in the South Baikal Basin, Baikal Rift System. *Tectonophysics, 759*, 44–57. https://doi.org/10.1016/j.tecto.2019.04.002.

Rodríguez Pascua, M.A., De Vicente, G., Calvo, J.P., & Perez-Lopez, R. (2003). Similarities between recent seismic activity and paleoseismites during the late miocene in the external Betic Chain (Spain): Relationship by "b" value and the fractal dimension. *Journal of Structural Geology, 25*(5), 749–763. https://doi.org/10.1016/S0191-8141(02)00078-0.

Roy, P.N.S., & Padhi, A. (2007). Multifractal analysis of earthquakes in the Southeastern Iran-Bam Region. *Pure and Applied Geophysics, 164*(11), 2271–2290. https://doi.org/10.1007/s00024-007-0272-x

Roy, P.N.S., & Ram, A. (2006). A correlation integral approach to the study of 26 January 2001 Bhuj earthquake, Gujarat, India. *Journal of Geodynamics, 41*(4), 385–399. https://doi.org/10.1016/j.jog.2005.10.003.

Scholz, C.H. (1968). The frequency-magnitude relation of microfracturing in rock and its relation to earthquakes. Bulletin of the Seismological Society of America, 58(1),

399–415. https://doi.org/10.1785/bssa0580010399

Scholz, C.H., & Campos, J. (2012). The seismic coupling of subduction zones revisited. *Journal of Geophysical Research: Solid Earth, 117*(5), 1–22. https://doi.org/10.1029/2011JB009003.

Schorlemmer, D., Wiemer, S., & Wyss, M. (2005). Variations in earthquake-size distribution across different stress regimes. *Nature, 437*(7058), 539–542. https://doi.org/10.1038/nature04094.

Shi, Y., & Bolt, A.B. (1982). The standard error of the magnitude-frequency b value. *Bulletin of the Seismological Society of America*, 72(5), 1677–1687.

Singh, C., Singh, A., & Chadha, R.K. (2009). Fractal and b-value mapping in eastern Himalaya and southern Tibet. *Bulletin of the Seismological Society of America, 99*(6), 3529–3533. https://doi.org/10.1785/0120090041.

Sobiesiak, M., Meyer, U., Schmidt, S., Götze, H.J., & Krawczyk, C.M. (2007). Asperity generating upper crustal sources revealed by b value and isostatic residual anomaly grids in the area of Antofagasta, Chile. *Journal of Geophysical Research: Solid Earth, 112*(12). https://doi.org/10.1029/2006JB004796.

Sreejith, K.M., Sunil, P.S., Agrawal, R., Saji, A.P., Rajawat, A.S., & Ramesh, D.S. (2018). Audit of stored strain energy and extent of future earthquake rupture in central Himalaya. *Scientific Reports, 8*(1), 1–9. https://doi.org/10.1038/s41598-018-35025-y.

Tiwari, R.K., & Paudyal, H. (2021). Variability of b-value before and after the Gorkha earthquake in the central Himalaya and vicinity. *Bibechana, 18*(2), 32–42. https://doi.org/10.3126/bibechana.v18i2.31207.

Tosi, P. (1998). Seismogenic structure behaviour revealed by spatial clustering of seismicity in the Umbria-Marche Region (Central Italy). *Annali Di Geofisica, 41*(2), 215–224. https://doi.org/10.4401/ag-4331.

Wiemer, S. (2001). A software package to analyze seismicity: ZMAP. *Seismological Research Letters, 72*(3), 373–382. https://doi.org/10.1785/gssrl.72.3.373.

Wiemer, S., & Wyss, M. (2000). Minimum magnitude of completeness in earthquake catalogs: Examples from Alaska, the Western United States, and Japan. *Bulletin of the Seismological Society of America, 90*(4), 859–869. https://doi.org/10.1785/0119990114.

Wyss, M. (1973). Towards a Physical Understanding of the Earthquake Frequency Distribution. *Geophysical Journal of the Royal Astronomical Society, 31*(4), 341–359. https://doi.org/10.1111/j.1365-246X.1973.tb06506.x.

Yin, L., Li, X., Zheng, W., Yin, Z., Song, L., Ge, L., & Zeng, Q. (2019). Fractal dimension analysis for seismicity spatial and temporal distribution in the circum-Pacific seismic belt. *Journal of Earth System Science, 128*(1), 1–7. https://doi.org/10.1007/s12040-018-1040-2.

Yue, H., Simons, M., Duputel, Z., Jiang, J., Fielding, E., Liang, C., Owen, S., Moore, A., Riel, B., Ampuero, J.P., & Samsonov, S.V. (2017). Depth varying rupture properties during the 2015 Mw 7.8 Gorkha (Nepal) earthquake. *Tectonophysics, 714–715*, 44–54. https://doi.org/10.1016/j.tecto.2016.07.005.

Zamani, A., & Agh-Atabai, M. (2011). Multifractal analysis of the spatial distribution of earthquake epicenters in the Zagros and Alborz-Kopeh Dagh regions of Iran. *Iranian Journal of Science and Technology, Transaction A: Science, 35*(1), 39–51. https://doi.org/10.22099/ijsts.2011.2127.

Seismic phases of 25 April 2015 (Mw 7.8) Earthquake and 12 May 2015 (Mw 7.3) Earthquake Predicted by AK135 Model - A comparison

R. K. Tiwari and H. Paudyal

Journal of Nepal Physical Society

Volume 7, Issue 2, June 2021

ISSN: 2392-473X (Print), 2738-9537 (Online)

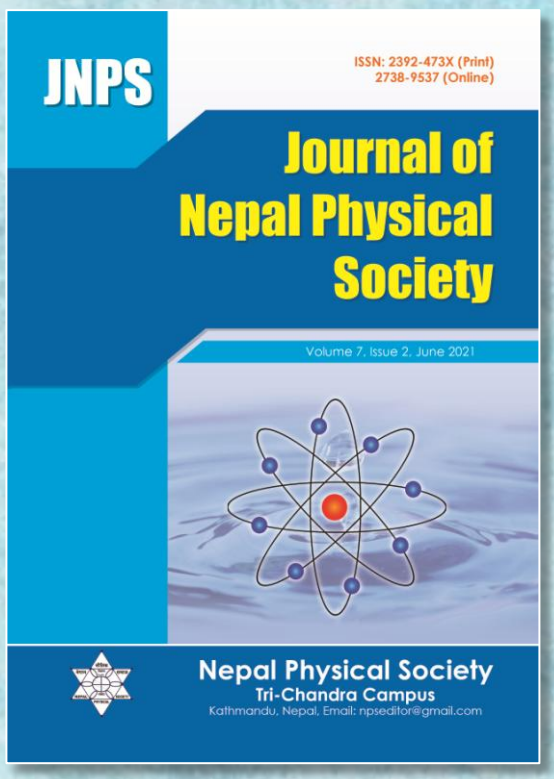

JNPS, **7** (2), 58-64 (2021)

DOI: https://doi.org/10.3126/jnphyssoc.v7i2.38623

Published by:

Nepal Physical Society

P.O. Box: 2934

Tri-Chandra Campus

Kathmandu, Nepal

Email: nps.editor@gmail.com

JNPS 7 (2): 58-64 (2021)
ISSN: 2392-473X (Print), 2738-9537 (Online)
Research Article *© Nepal Physical Society*
DOI: https://doi.org/10.3126/jnphyssoc.v7i2.38623

Seismic phases of 25 April 2015 (Mw 7.8) Earthquake and 12 May 2015 (Mw 7.3) Earthquake Predicted by AK135 Model - A comparison

R. K. Tiwari[1, 2, *] and H. Paudyal[2]
[1]Central Department of Physics, Tribhuvan University, Kirtipur, Kathmandu
[2]Birendra Multiple Campus, Tribhuvan University, Bharatpur, Chitwan
***** Corresponding Email: ram.tiwari@bimc.tu.edu.np

Received: *09 April, 2021;* ***Revised:*** *10 May, 2021;* ***Accepted:*** *22 June, 2021*

ABSTRACT

A strong Mw 7.8 (depth = 8.2 km) earthquake initiated ~80 km northwest of the Kathmandu on 25 April of 2015 was followed by the Mw 7.3 (depth = 15 km) earthquake on 12 May. The seismic phases of these earthquakes were predicted at Kakani, Kathmandu seismic station (27.80°N and 85.28°E) using software model AK135. The model predicts 21 arrivals for Gorkha earthquake with first p phase arriving at incident angle 82.65° in 11.516 seconds and final phase SKIKSSKIKS in 3270.791 seconds with incident angle 0.02°. Similarly, for the Dolakha earthquake 27 arrivals are predicted with the first arrival p phase at incident angle 74.35° in 14.504 seconds and final arrival SKIKSSKIKS phase at incident angle 0.03° in 3268.823 seconds. The 5 depth phases and 8 core phases predicted are similar for both the earthquakes while 8 and 12 mantle phases are predicted for Gorkha earthquake and Dolakha earthquake respectively. In addition, two crustal phases (Pn, Sn) were predicted only for Dolakha earthquake. The additional phases are critically refracted seismic phases indicating the existence of the Moho discontinuity between the crust and upper mantle. Their existence for Dolakha earthquake could be the indication of different geological provinces of the source region of the earthquakes, differing in age, crustal thickness, temperature, and tectonic stress. The ratio of P wave ad S wave velocity is found to be 1.67 for the regions. These seismic phases reflect their sensitivity to different layers of the earth and carry information about the geometrical and physical properties of discontinuities inside the earth.

Keywords: Crustal phase, Mantle phase, Core phase, Depth phase, AK135.

1. INTRODUCTION

On 25 April 2015 11:56 am local time (06:11:26 UTC), Gorkha region, the central Himalayan region was hit by a devastating earthquake of moment-magnitude M_w 7.8 (28.23° N, 84.73° E) and just after 18 days, another large earthquake of M_w 7.3 occurred at Dolakha (27.80° N, 86.06° E), about 140 km away from the epicenter of the mainshock [1]. These two-earthquake doublet effectively unfastened a ~160 km along- strike length at the lower edge of the locked portion of the Main Himalayan Thrust (MHT) beneath central Nepal [2]. The seismic activity of the region is dominated by three major fault systems, namely the Main Central Thrust (MCT), Main Boundary Thrust (MBT) and Main Frontal Thrust (MFT) (Figure 1). The MHT is the root detachment of these major faults. Both the MFT and MBT sole into the MHT. The MHT accommodates crustal shortening of India and Eurasia as a result of the ongoing collision between the Indian and Eurasian plates [3]. The Gorkha earthquake is the largest earthquake occurring on the MHT since the great 1934 Bihar-Nepal earthquake Mw 8.1 [4].

Seismic waves from earthquake hypocenter travel through different layers of Earth. They have non-stationary amplitude and the energy associated with the signal is high at the beginning and decay at the end. This results different types of seismic waves at different time-instants and phenomenon of

distribution [5]. The body waves (the P and S waves) from source are reflected or refracted and also get converted into other phases as they encounter boundary between two layers [6]. These waves can be recorded by seismographs and are useful for velocity and geological structure study of earth's interior [7].

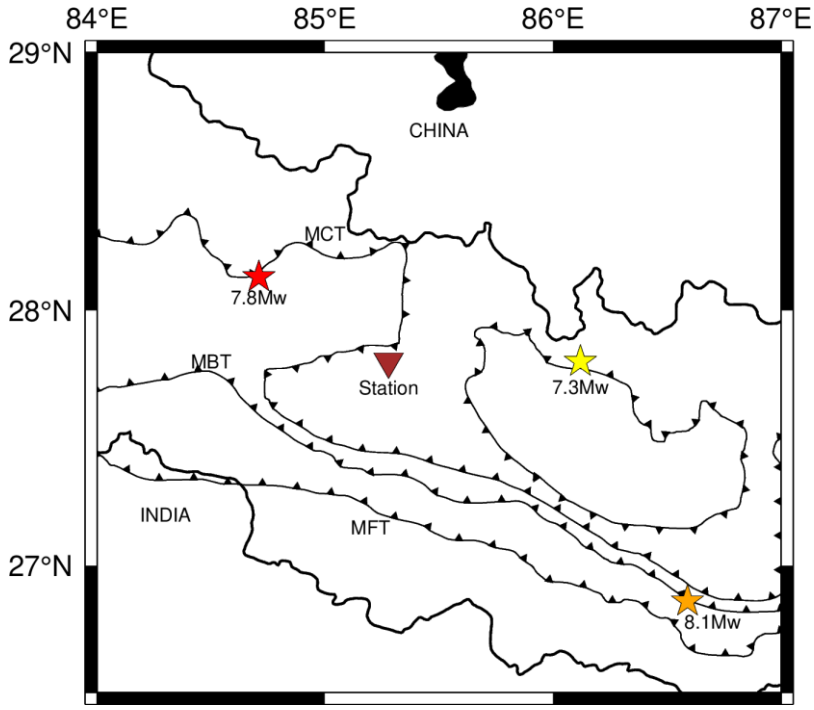

Fig. 1: The tectonic background and locations of two large 2015 Nepal earthquakes, i.e., the Mw 7.8 Gorkha earthquake (left-hand red star) and Mw 7.3 Dolakha earthquake (right-hand yellow star), with 1934 Bihar-Nepal earthquake Mw 8.1 by orange star on bottom right corner. Brown delta shows Kakani, Kathmandu seismic station.

The seismic phases generated by an earthquake at a shallow depth (d < 10 km) and recorded by a station within a few km of the epicenter, are generally identified as direct P and S arrivals. With growing distance more and more secondary seismic body-wave phases are appeared following the direct P-wave and S-wave arrivals in seismic records [8]. Knowing the distance from the epicenter and the arrival times of the different waves, information on the structure of the Earth's interior and composition of Earth's layers can be inferred. The proper identification and complementary use of secondary phases significantly improves the precision and accuracy of seismic event locations, their source depth in particular. The time frequency characteristics of seismic wave signal can be used to study ground motion during earthquake. Based on wavelet transform, the ground motion in Kathmandu valley is estimated [5] and the high amplitude signals are found associated with the horizontal motion with the release of high energy. Similarly, from the multifractal study of seismic signal of Gorkha earthquake, smoother seismic signal was noticed with growing distances and the time duration of main event was noticed to be very short [9]. A group of researchers [10] studied the finite rupture processes and the associated 3D ground motion of the Gorkha earthquake and Dolakha earthquake and concluded that the different rupture features between these events could be related to difference in fault zone structure. Our study aims at adding information about the path traces by seismic wave for their journey from earthquake focus to seismic station. For this, we examine the propagation of seismic wave phases of aforementioned two events predicted by simulation model AK135 [11].

2. METHODOLOGY

There are two default models available for the simulation of travel times. The first one, the International Association of Seismology and Physics of the Earth's Interior (IASP91), developed by Kennett and Engdahl [11] and the second one is a modern global Earth model AK135 developed by Kennett et al. [12]. The AK135 represents an update of the IASP91 model and attempts to match the behavior of a wider range of seismic phases. The model AK135 is the global 1-D earth velocity model that assumes a homogeneous 35 km thick two-layer crust with the intermediate crustal discontinuity at 20 km depth. The AK135 model was developed with a continental style for the uppermost crust and upper mantle so, it is suitable for the study of continental earthquakes in the Himalayan region [13].

3. RESULTS AND DISCUSSION

The different arrivals phases with their characteristics, predicted by the model, for Gorkha earthquake and Dolakha earthquake are presented in Table 1 and Table 2.

Table 1: Twenty-one seismic phases with arrival time and incident angle for Gorkha earthquake

S.N.	Phase name	Arrival Time (S)	Incident Angle (°)	S.N.	Phase name	Arrival Time (S)	Incident Angle (°)
1	p	11.516	82.65	12	PKiKP	993.373	0.04
2	P	12.660	62.81	13	pPKiKP	996.201	0.04
3	P	12.664	64.13	14	sPKiKP	997.157	0.04
4	sP	13.337	89.72	15	SKIKP	1204.466	0.04
5	s	19.304	82.65	16	PKIKKIKP	2123.928	0.04
6	S	21.227	63.62	17	SKIKKIKP	2122.971	0.04
7	S	21.228	64.13	18	PKIKKIKS	2123.928	0.02
8	PcP	510.277	0.17	19	SKIKKIKS	2335.020	0.02
9	ScP	721.375	0.22	20	PKIKPPKIKP	2423.552	0.05
10	PcS	722.331	0.13	21	SKIKSSKIKS	3270.791	0.02
11	ScS	933.433	0.18				

Table 2: Twenty-seven seismic phases with arrival time and incident angle for Dolakha earthquake

S.N.	Phase name	Arrival Time (S)	Incident Angle (°)	S.N.	Phase name	Arrival Time (S)	Incident Angle (°)
1	p	14.504	74.35	15	ScP	719.422	0.27
2	P	14.666	62.81	16	PcS	721.171	0.17
3	P	14.900	72.84	17	ScS	931.485	0.24
4	P	15.970	45.84	18	PKiKP	992.203	0.05
5	Pn	15.970	45.84	19	pPKiKP	997.375	0.05
6	P	16.048	50.39	20	sPKiKP	999.124	0.05
7	sP	17.766	89.68	21	SKiKP	1202.503	0.05
8	s	24.313	63.62	22	PKIKKIKP	1910.704	0.05
9	S	24.644	72.84	23	SKIKKIKP	2121.004	0.05
10	S	24.976	75.06	24	PKIKKIKS	2122.753	0.03
11	S	27.009	50.18	25	SKIKKIKS	2323.053	0.03
12	Sn	27.009	50.18	26	PKIKPPKIKP	2422.377	0.07
13	S	27.012	50.75	27	SKIKSSKIKS	3268.823	0.03
14	PcP	509.115	0.21				

Seismic phases for the Gorkha earthquake (depth 8.2 km) with their properties are listed in Table 1 and depicted in the Figure 2 and Figure 3. The model predicts 21 seismic phases for Gorkha earthquake including 8 mantle phases, 5 depth phases and 8 core phases.

- The seismic ray path p (Lower case letter) indicates pressure (P) wave travelling directly from an earthquake focus to the station (Figure 2).
- P (Upper case letter) indicate a P wave travelling down from the focus, reflected from the upper crust (depth~20 km), which then travelled to station as P wave.
- Second upper-case letter P indicate a P wave travelling down from the focus, travelled along the upper crust and reflected from the upper crust (depth~20 km), which then travelled to station as P wave.
- The lower-case letter p is the relatively short upgoing leg of P phases.
- The seismic phase sP in the sequence sP, s, S, S (Figure 3) is an S wave that started out upward from the source as s, reflected off the earth's surface and converted to a P wave which then travelled to the station as a P wave.
- The seismic wave s (Lower case letter) indicates shear wave (S) wave travelling directly towards the station.

- Seismic phase S (upper case) travels downwards from an earthquake focus, reflected from the upper crust (~20 km), which then travelled to station as S wave.
- Second upper-case letter S in the sequence indicates seismic phase that travels downwards from an earthquake focus, travelled along the upper crust (~20 km), which then reflected to station as S wave.

For Gorkha earthquake, the P wave velocity (V_P) is calculated as 5.75 kms^{-1} and S wave velocity (V_S) is calculated as 3.43 kms^{-1}. Therefore, the ratio of these crustal P wave velocity to the S wave velocity $\left({}^{V_P}/_{V_S}\right)$ is 1.67.

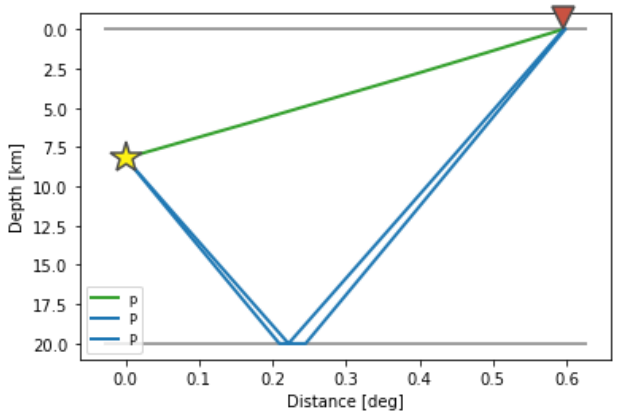

Fig. 2: Seismic ray path of phases p, P, P of Gorkha earthquake where yellow star is for the earthquake focus and brown delta is for seismic station.

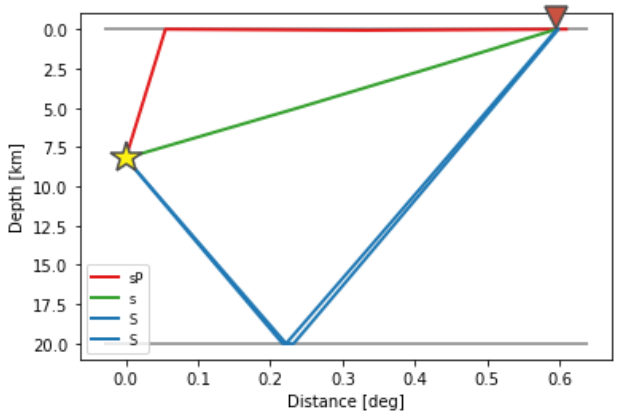

Fig. 3: Seismic ray path of phases sP, s, S, S of Gorkha earthquake where yellow star is for the earthquake focus and brown delta is for seismic station.

Seismic phases for the Dolakha earthquake (depth 15 km) with their properties are listed in Table 2 and depicted in the Figure 4 and Figure 5. The model predicts 27 seismic phases for Dolakha earthquake including 2 crustal phases, 12 mantle phases, 5 depth phases and 8 core phases.

- The lower-case letter p in sequence p, P, P, P, Pn, P indicates longitudinal or pressure (P) wave travelling directly towards the station from an earthquake focus
- The first upper-case letter P (Figure 4) indicate a P wave travelling down from the focus, reflected from the upper crust (depth~20 km), which then travelled to station as P wave.
- The second upper case letter P indicate a P wave travelling down from the focus, travelled along the upper crust, reflected from the upper crust (depth~20km), which then travelled to station as P wave.
- The third upper case letters P in the sequence indicates P wave travelling downwards from the focus, refracted from depth ~20 km and then reflected form the crust mantle boundary (Moho) at ~35 km depth which then travelled towards the station.
- The Pn is compressional or shear wave travelling along (just beneath) the Moho discontinuity called head wave. The Pn phase is a mantle lid guided wave and it is the first phase to arrive when the distance between a station and an earthquake exceeds about 150 km in continental regions with a Moho depth of about 35 km [14]. The head wave Pn is followed by the larger and sharper impulse of short period direct P [15, 16] (Figure 4).
- In the sequence sP, s, S, S, S, Sn, S (Figure 5) the seismic phase sP is an S wave that started out upward from the source (s), reflected off the earth's surface and also converted to a P wave which then travelled to the station as a P wave (P).
- The lower-case letter s indicates shear wave (S) travelling directly from an earthquake focus towards the station.
- The first upper-case letter S in the sequence indicate shear wave travelling down from the focus, reflected from the upper crust (~20 km), which then travelled to station as S wave.
- The second letter S indicate shear wave travelling down form the focus, travel along the upper crust (depth ~20 km) which then travelled to station as S wave.
- The third upper case letter S in the sequence indicates shear wave travelling down from the focus, refracted from the upper crust (~20 km),

and reflected from Moho (~35 km) which then travelled to station as S wave.

- The seismic phase Sn indicates seismic wave bottoming from the focus which then reflected from the Earth's uppermost mantle towards station [17]. The head wave (Sn) is followed by the larger and sharper impulse of short period direct S [16].

For Dolakha earthquake, the P wave velocity (V_P) is calculated as 5.70 kms^{-1} and S wave velocity (V_S) is calculated as 3.40 kms^{-1}. Therefore, the ratio of these crustal P wave velocity to the S wave velocity $\left({V_P}/{V_S}\right)$ is 1.67. The previous studies in the Himalayan region [18] estimated the ratio $\left({V_P}/{V_S}\right)$ to be 1.73. The P wave velocity 5.7 kms^{-1} and S wave velocity 3.6 kms^{-1} ($\leq$ 23 km) were noted for the crust below Nepal [19] giving velocity ratio 1.60. So, the velocity calculated by the model considered in this study is in agreement with previous findings.

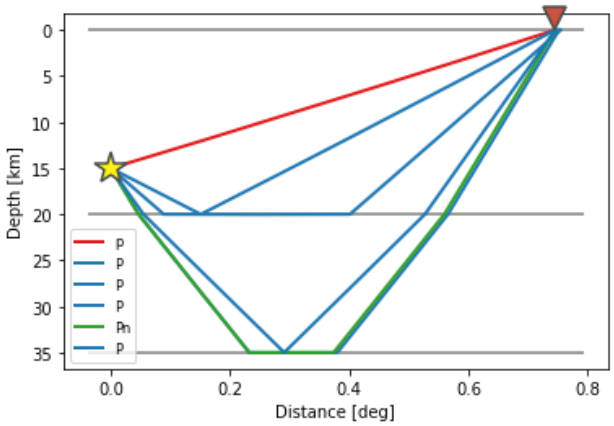

Fig. 4: Seismic ray path of phases p, P, Pn of Dolakha earthquake where yellow star is for the earthquake focus and brown delta is for seismic station.

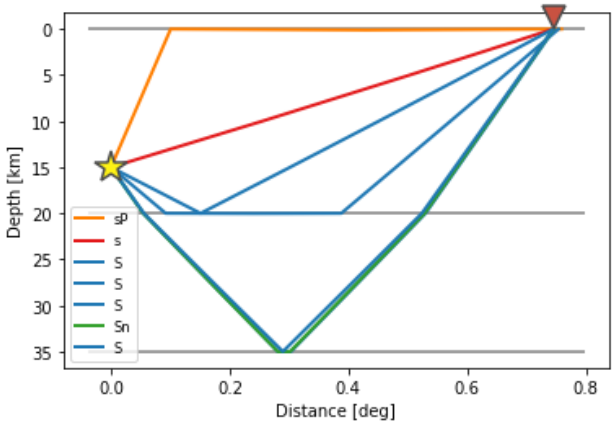

Fig. 5: Seismic ray path of phases sP, s, S, Sn of Dolakha earthquake where yellow star is for the earthquake focus and brown delta is for seismic station.

In addition, in the seismic phases PcP, ScP, PcS and ScS (observed for both earthquakes) symbols c indicates upward reflections from the outer side of the core mantle boundary (CMB) so the phase PcP indicates P reflection from the CMB, ScP indicates S to P converted reflection from CMB, PcS indicates P to S converted reflection from the CMB, while ScS is for S reflection from the CMB. Thus, the phases P, S, PcP, ScP, PcS and ScS are mantle seismic phases. In the phases like PKiKP, PKIKP etc. the symbol K is longitudinal wave which has traveled through the Earth's outer core, I is longitudinal wave which has traveled through the Earth's inner core and i indicates upward reflection from inner core boundary (ICB) so the phase PKiKP is the wave reflected at ICB while the phase PKIKP is a pure refracted longitudinal wave from outermost part of the inner core. It has travelled the first part of its path as P through crust and mantle, the second through the outer core, the third through the inner core, and the fourth and fifth parts back again through outer core and mantle/crust. These two are core phases along with six others (Table 1 and Table 2). The phases p, s, sP, pPKiKP and sPKiKP are depth phases. The phases Pn and Sn are P wave and S wave bottoming in the uppermost mantle and are crustal phases [20]. Seismic wave phases Pn and Sn are essential in exploring regional crustal and mantle lid structure and rheology [21].

The seismic phases listed for Gorkha earthquake (epicenter distance ~66.18 km from the station) and for Dolakha earthquake (epicenter distance ~82.73 km from the station) in this work are found to travel through crust and uppermost mantle. According to Bormann et al. [22] seismic waves arriving at stations at local distances of up to about 150 km from the seismic source have traveled exclusively through the crust or the sub-crustal uppermost mantle. Thus, the seismic wave predicted by the Ak135 model in this work is in agreement with the observed seismic phases.

4. CONCLUSION

Various direct, reflected and converted seismic phases have been predicted for Gorkha earthquake and Dolakha earthquake at Kakani, Kathmandu, Nepal seismic station using TauPy Model (AK135). The ray-geometry as illustrated in Figure (2, 3, 4, 5) show the existence of three primary travel paths between the source and the station: (i) direct arrival p, s (both lower case) which travels in a straight line connecting the source and receiver, (ii)

reflected arrivals and (iii) head waves. Additional rays involving multiple reflections are also predicted by the model. The crustal phases (Pn and Sn) predicted only for Dolakha earthquake indicates geological provinces that differ in age, crustal thickness (pressure), heat flow (temperature), and tectonic regime (stress) [23]. Their existence could also be the indication of difference in fault zone structure of these two earthquakes [10]. The ratio of P wave velocity to the S wave velocity is found to be 1.67 for the regions. Seismic waves predicted at Kakani station from the two earthquake sources have found travelled dominatingly through the crust or the sub-crustal uppermost mantle. Identification of these phases on seismogram is importance for a better event location, and improved source depth in particular [24, 25].

Software resources

The plots were made using Obspy-A Python Tool Box for Seismology [26] and Generic Mapping Tools (GMT) [27]

ACKNOWLEDGEMENTS

One of the authors RKT would like to acknowledge Tribhuvan University for providing sabbatical leave and University Grants Commission (UGC), Nepal for providing financial support in the form of fellowship.

REFERENCES

[1] Thapa, D. R.; Tao, X.; Fan, F. and Tao, Z. Aftershock analysis of the 2015 Gorkha-Dolakha (Central Nepal) earthquake doublet, Heliyon, **4**:e0068 **(**2018).

[2] Mendoza, M. M.; Ghosh, A.; Karplus, M. S.; Klemperer, S. L.; Sapkota, S. N.; Adhikari, L. B. and Velasco, A. Duplex in the Main Himalayan Thrust illuminated by aftershocks of the 2015 M_w 7.8 Gorkha earthquake, *Nature Geoscience*, **12**:1018–1022 **(**2019).

[3] Hubbard, J.; Almeida R.; Foster, A.; Sapkota, S. N.; Bürgi, P. and Tapponnier P. Structural segmentation controlled the 2015 M_w 7.8 Gorkha earthquake rupture in Nepal, *Geology*, **44**: 639–642 **(**2016).

[4] Sapkota, S. N.; Bollinger, L. and Perrier, F. Fatality rates of the Mw ~8.2, 1934, Bihar–Nepal earthquake and comparison with the April 2015 Gorkha earthquake, Earth, *Planets and Space*, **68**:40 (2016).

[5] Adhikari, B.; Dahal, S.; Karki, M.; Mishra, R. K.; Dahal, R. K.; Sasmal, S. and Klausner, V. Application of wavelet for seismic wave analysis in Kathmandu Valley after the 2015 Gorkha earthquake, Nepal, Geoenvironmental Disaster, **7,** (2020).

[6] Letort, J.; Bollinger L.; Lyon-Caen, H.; Guilhem, A.; Cano, Y.; Baillard, C. and Adhikari, L.B. Teleseismic depth estimation of the 2015 Gorkha−Nepal aftershocks, *Geophysical Journal International*, **207**:1584-1595 (2016).

[7] Romanowicz, B. Using seismic waves to image Earth's internal structure, *Nature*, **451**:266–268 (2008).

[8] Sato, H. and Fehler, M. C. Seismic wave propagation and scattering in the heterogeneous Earth, *Springer-Verlag, New York* (1998).

[9] Tiwari, B. R.; Xu, J.; Adhikari, B. and Chapagain, N. P. Multifractal analysis for seismic wave in Kathmandu valley after Gorkha Earthquake-2015, Nepal, *Journal of Nepal Physical Society*, **6**:113-120 (2020).

[10] Wei, S.; Chen, M.; Wang, X.; Graves, R.; Lindsey, E.; Wang, T. and Helmberger, D. The 2015 Gorkha (Nepal) earthquake sequence: I. Source modeling and deterministic 3D ground shaking. *Tectono Physics*, **722**, 447–461(2018).

[11] Kennett, B. L. N. and Engdahl, E. R. Travel times for global earthquake location and phase identification, *Geophysical Journal International*, **122**:429–465 (1991).

[12] Kennet, B. L. N.; Engdahl, E. R. and Buland, R. Constraints on seismic velocities in the Earth from travel times, *Geophysical Journal International*, **122**:108-124 (1995).

[13] Engdahl, E. R.; van der Hilst, R. and Buland, R. Global teleseismic earthquake relocation with improved travel times and procedures for depth determination, *Bulletin of Seismological Society of America*, **88**:722-743 (1998).

[14] Khaled Al-D.; Sandvol E.; Al-Lazki A. and Barazangi M. Regional seismic wave propagation (Lg and Sn) and Pn attenuation in the Arabian Plate and surrounding regions, *Geophysical Journal International*, **157**:775–795 (2004).

[15] Chaklader, A. The Mohorovicic discontinuity, *Nature*, **207**:1082-1083 (1965).

[16] Kulhanek, O. Anatomy of Seismograms, Elsevier, Amsterdam, New York, **178** (1990).

[17] Cook, K. L.; Algermissen, S.T. and Costain, J. L. The status of Ps converted waves in crustal studies. *Journal of Geophysical Research*, **67**:4769-4778 (1962).

[18] Monsalve, G.; Sheehan A.; Schulte-Pelkum, V.; Rajaure, S.; Pandey, M. R. and Wu, F. Seismicity and one dimensional velocity structure of the Himalayan collision zone: Earthquakes in the crust and upper mantle, *Journal of Geophysical Research*, **111**:B10301 (2006).

[19] McNamara, D.E.; Yeck, W.L.; Barnhart, W.D.; Schulte-Pelkum, V.; Bergman, E.; Adhikari, L.B.; Dixit, A.; Hough, S.E.; Benz, H.M. and Earle, P.S. Source modeling of the 2015 Mw 7.8 Nepal (Gorkha) earthquake sequence: Implications for geodynamics and earthquake hazards, *Tectonophysics*, **714–715**: 21-30 (2016).

[20] Storchak, D. A.; Schweitzer J. and Bormann P. The IASPEI Standard Seismic Phase List, *Seismological Research Letters*, **74**: 761-772 (2003).

[21] Chiu, K., and Snyder, D. B. Regional seismic wave propagation (Lg & Sn phases) in the Amerasia Basin and High Arctic, *Polar Science*, **9**:130-145 (2015).

[22] Bormann, P.; Engdahl, B. and Kind, R. Seismic wave propagation and earth models, in New Manual of Seismological Observatory Practice (NMSOP), 1–70, ed. Bormann, P., Potsdam: Deutsches GeoForschungs Zentrum GFZ (2009).

[23] Fuchs, K.; Tittgemeyer, M.; Ryberg, T.; Wenzel, F. and Mooney, W. Global significance of a sub-Moho boundary layer (SMBL) deduced from high-resolution seismic observations, *International Geology Review*, **44**: 671-685 (2002).

[24] Scrase, F. J. The Reflected Waves from Deep Focus Earthquakes, Proceedings of the Royal Society A: Mathematical, *Physical and Engineering Sciences*, **132**:213–235 (1931).

[25] Stechschulte, V. C. The Japanese earthquake of March 29, 1928. Bulletin of Seismological. *Society of America*, **22**:81-137 (1932).

[26] Beyreuther, M.; Barsch, R.; Krischer, L.; Megies, T.; Behr, Y. and Wassermann, J. ObsPy: A Python Toolbox for Seismology, *Seismological Research Letters*, **81**:530-53 (2010).

[27] Wessel, P.; Smith, W. H. F.; Scharroo, R.; Luis, J. and Wobbe, F. Generic Mapping Tools: Improved Version Released, EOS Trans. AGU, **94**; 409–410 (2013).

BMC JOURNAL OF SCIENTIFIC RESEARCH
A Multidisciplinary Peer Reviewed Research Journal
ISSN: 2594-3421 (Print), 2773-8191 (Online)

Fractal Structure of Seismic Signals of 2015 Gorkha-Kodari Earthquakes: A Box Counting Method

Ram Krishna Tiwari [1, 2] Harihar Paudyal [2]

[1] Central Department of Physics, Tribhuvan University, Kirtipur, Kathmandu, Nepal
[2] Department of Physics, Birendra Multiple Campus, Tribhuvan University, Bharatpur, Chitwan, Nepal
*Corresponding Author: ram.tiwari@bimc.tu.edu.np

Received: Aug. 12, 2022, Accepted: Nov. 30, 2022

Abstract

Fractal dimension analysis is a computational image processing technique that allows assessing the degree of complexity in patterns. In seismology, fractal dimensions can be used to describe fractured surfaces quantitatively. The larger the fractal dimension the more rugged is the surface, the more irregular is the line, and the more complex is the pore space. For the present investigation the seismic wave signal of 40 earthquakes including one foreshock, main shock and 38 aftershocks (mb ≥ 5.0) of 2015 Gorkha-Kodari earthquakes from 2015/4/21 to 2016/11/27 were considered. The seismograms were retrieved from the archived waveform data of Incorporated Research Institutions of Seismology (IRIS). The fractal dimension (D) was evaluated by the Python program for box counting. It is found that the fractal dimensions of the seismic wave signal during the active seismic period do not show sudden variation and they are almost identical. The maximum value was noticed to be 1.99±0.006 and the minimum value to be 1.95±0.007. The estimated fractal dimension is greater or equal to 1.95 with an average value of 1.98 which signify the presence of high grade of fractality in seismic wave time series. This suggests that the fractal characteristics of the seismic wave signal of 2015 central Himalayan earthquakes occurrence behavior is nonlinear and coplanar.

Keywords Fractal dimension, Nonlinearity, Central Himalaya, Seismic wave signal

1. Introduction

The Himalayan arc between the Indian plate and the Eurasian plate had hosted many devastating earthquakes in the past. Recently on 25th of April 2015, the region was visited by another devastating earthquake known as Gorkha earthquake (Elliott et al., 2016; Gualandi et al., 2017; He et al., 2018). The main shock of magnitude 7.8 Mw (6.9 mb) hit nearly 80 km N-NE of Kathmandu in central Nepal and the event was followed by thousands of moderate to strong aftershocks (Yamada et al., 2020). A strong aftershock magnitude 6.5 mb occurred on the same day just after the 34 minutes of the main shock. Moreover, on April 26, another strong aftershock of magnitude 6.6 mb struck the region, and the strongest aftershock Mw 7.3 (6.7 mb) of the Gorkha seismic sequence was recorded on May 12, in the Kodari region, north-east of Kathmandu (Adhikari et al., 2015; Baillard et al., 2017). The three-dimensional visualization of earthquakes is depicted in figure1 showing the clustered seismicity around longitude 85°E to 87°E.

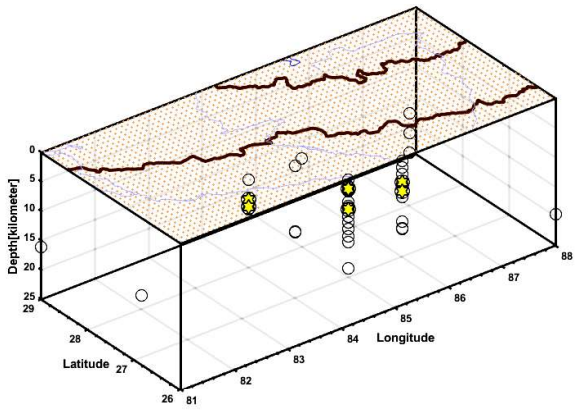

Fig. 1: Three-dimensional visualization of events where circles represent the earthquakes between magnitude 5.0 mb and less than 5.8 mb while yellow hexagrams stand for the earthquake with magnitude ≥ 5.8 mb

Euclidean geometry or plane geometry is capable enough to describe regular structures. In Euclidean geometry, objects are solid and continuous, and they do not have holes or gaps. The dimensions of such objects are integers. It can be normally described by size of length, area, and volume. More importantly, the Euclidean dimension or embedding dimension is always an integer. It is 0 for point, 1 for line, 2 for surface, and 3 for volume and so on. Both a smooth line and a very wiggly line have same dimension 1 according to Euclidean geometry. In real sense, wiggly line could indeed fill up more space than a smooth line and it is the fractal object. It has complex geometry and shows the different length, area, and volume with changes with the scales. Their understandings require a meaning of dimension beyond the idea of conventional approach of dimension we learnt so far. Fractals are rough or discontinuous so they have fractional or fractal dimensions. The idea of fractal dimension had been introduced by Mandelbrot (Mandelbrot, 1967) and it can be applied to determine the self-similarity of the objects (Eke et al., 2002; Kurths et al., 2008). It has been used to identify the patterns in surface electromyography (EMG) signal (Hu et al., 2005). The fractal geometry has ability to express the irregular or fragmented shape of natural features and other complex objects whenever Euclidean geometry fails to analyze (Mandelbrot, 2003,1989; Márquez-Rámirez et al., 2012).
The measurement of the fractal dimension of complex objects was popularized in many scientific fields, especially to time series in physics, engineering, and neurophysiology (Lopes & Betrouni, 2009; Telesca et al., 2015). Seismic wave signals are fractal time series data, and the fractal dimensionality associated with them contains information about the geometrical structure of the source (Maragos & Sun, 1993). In the past studies, the time interval between successive earthquakes of seismically active areas of central Italy was studied by using the Multifractal Detrended Fluctuation Analysis (MF-DFA) (Telesca et al., 2005). In the recent study of the earthquake distribution in the central Himalayan region, high box counting fractal dimension values (≥1.74) were

obtained indicating the near planar structure of the source zones (Tiwari & Paudyal, 2021). This paper is aimed at recognizing dissimilar patterns of seismic wave signals of 2015 Gorkha earthquake sequences according to box counting fractal dimension.

2. Data and methodology

We have retrieved the earthquake data from the catalogue of Internal Seismological Centre (ISC) considered 40 earthquakes (≥5mb) including one foreshock, mainshock and aftershocks from April 2015 to November 2016 (2015/4/21–2016/11/27). The seismic wave signals for corresponding events were retrieved from Incorporated Research Institutions in Seismology (IRIS) for a period of two minutes i.e., one minute before and one minute after the event time mentioned in Table1. We have used network AV, station RSO and channel EHZ for retrieving the signal from ObsPy (A Python Toolbox for Seismology) (Beyreuther et al., 2010). The instrument response of each seismic signal is removed before calculating the fractal dimension. In box counting method, the seismic signal is covered with a grid and numbers of boxes of the grid covering part of the signal are counted. By repeating the procedure with a finer grid having smaller boxes, the fractal dimension of the signal is estimated. The signals retrieved were depicted in figure 2.

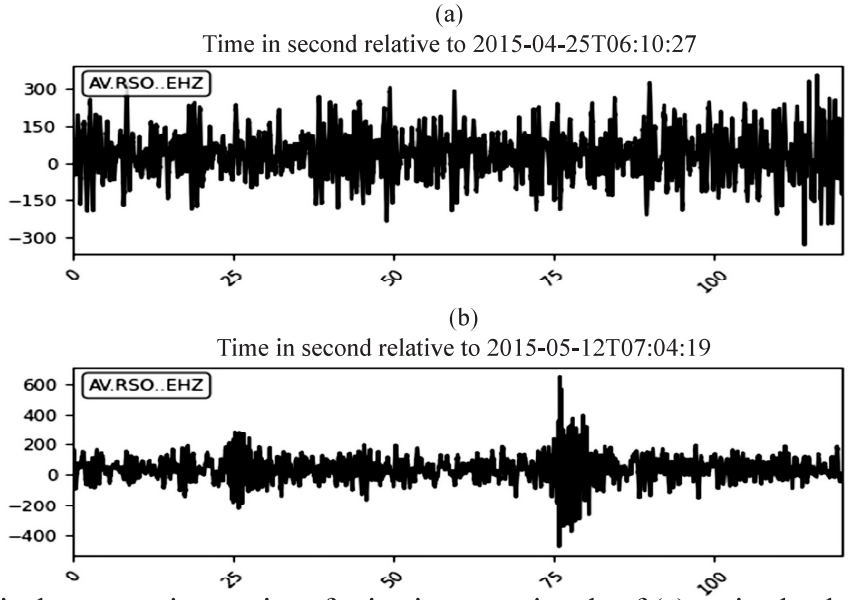

Fig. 2: Displacement time series of seismic wave signals of (a) main shock (7.8Mw) and (b) major aftershock (7.3 Mw)

2.1 Fractal dimension calculation

For the straight line divided into N equal parts to cover the line, each part has a size

$$r(N) = \frac{1}{N} \qquad (1)$$

But to cover the rectangle there is a need for N^2 equal parts and size of single part

$$r(N) = \frac{1}{N^{\frac{1}{2}}} \quad (2)$$

For the parallelepiped

$$r(N) = \frac{1}{N^{\frac{1}{3}}} \quad (3)$$

Generalizing the results, we get

$$r(N) = \frac{1}{N^{\frac{1}{D}}} = N^{-\frac{1}{D}} \quad (4)$$

Where D is the dimension of the objects having non integer or fractional values.

2.2 Box counting dimensions

The generalization of box counting dimension is named after the German mathematician, Felix Hausdorff (Górski, 2001). The method is useful for both describing natural objects and for evaluating trajectories of dynamic systems as well. In box counting algorithm (Grassberger, 1983), a planar set S is enclosed with square boxes of size r and the number of square boxes required to cover S is counted (Gonzato, 1998). For the limiting value of r (r→0), the total area covered with square boxes will converge to the measure of S. It can be expressed mathematically by the relation

$$D = -\lim_{r\to 0} \frac{\log\left(n_r(S)\right)}{\log\left(\frac{1}{r}\right)}$$

The fractal dimension (*D*) is estimated from the slope of straight line obtained from a plot of $\log n_r(S)$ versus log r (Figure 3).

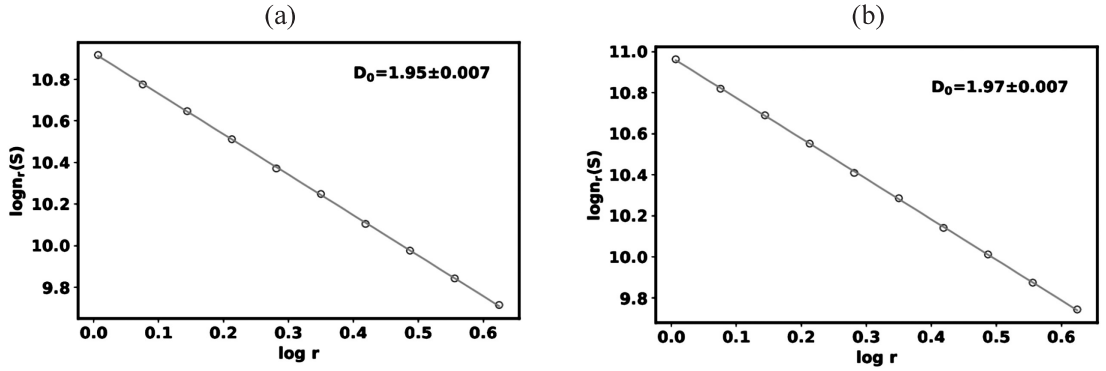

Fig. 3: The estimation of fractal dimension of (a) main shock (7.8Mw) and (b) major aftershock (7.3 Mw)

3. Results and discussion

The fractal dimensions of seismic signal corresponding to each earthquake are computed and presented in table 1. As an example of the dimension calculation procedure, the log-log plots for main shock (Gorkha earthquake) and major after shock (Kodari earthquake) are depicted in figure 3. The fractal dimension of main shock (6.9 mb) signal and 6.5 mb aftershock signal on the same day were found to be 1.95±0.007 and 1.98 ± 0.007, respectively. The fractal dimension is 1.98 ± 0.006 for 6.6 mb aftershock

signal that recorded day after the main event. The fractal dimension (1.97 ± 0.007) for 6.7 mb major aftershock signal on 2015/5/12 is similar to the fractal dimension of 6.1 mb aftershock signal on the same day. We noticed the small variation of fractal dimension from 1.95 ± 0.007 to 1.99 ± 0.006 for all considered seismic wave time series. The estimated fractal dimension is greater or equal to 1.95 with an average value of 1.98. This result assures the presence of a high degree of fractality in the signals. The preceding study also noticed the increase in multifractality of the seismic wave signals of 2015 Gorkha earthquake and its aftershock (Tiwari et al., 2020). A sudden drop of fractal dimension for electromagnetic emission prior to significant earthquake (Lu et al., 2005; Potirakis et al., 2012) and in laboratory experiments (Kapiris et al., 2005) are noticed, however we did not notice such type of variation in the seismic wave time series of Gorkha-Kodari earthquakes.

Table 1: Earthquake events with date of occurrence, time of occurrence, latitude, longitude, depth, magnitude and box counting fractal dimension

SN	Date	time	latitude	longitude	Depth (km)	Magnitude (mb)	Fractal dimension (D)
1	4/21/2015	14:02:17	28.8557	82.359	22.7	5.0	1.98±0.007
2	4/25/2015	06:11:27	28.1302	84.7168	13.4	6.9	1.95±0.007
3	4/25/2015	06:15:23	27.6342	85.4762	10.0	6.1	1.98±0.007
4	4/25/2015	06:18:00	27.7097	85.9014	10.0	5.3	1.96±0.006
5	4/25/2015	06:18:13	27.6955	85.9601	19.0	5.6	1.97±0.006
6	4/25/2015	06:20:40	28.202	84.6237	10.0	5.3	1.98±0.006
7	4/25/2015	06:22:03	27.7884	85.1449	12.1	5.1	1.99±0.006
8	4/25/2015	06:22:23	27.8287	85.455	18.0	5.0	1.99±0.006
9	4/25/2015	06:25:56	27.699	85.5783	15.6	5.0	1.99±0.006
10	4/25/2015	06:37:59	27.8009	85.8073	14.7	5.1	1.98±0.007
11	4/25/2015	06:45:21	28.1603	84.8433	14.7	6.5	1.98±0.006
12	4/25/2015	06:56:34	27.8635	85.7138	8.4	5.5	1.99±0.006
13	4/25/2015	06:58:28	27.7032	85.9789	13.3	5.1	1.99±0.006
14	4/25/2015	07:47:02	27.8734	85.5984	10.1	5.0	1.98±0.007
15	4/25/2015	08:55:56	27.5796	85.5542	12.9	5.2	1.98±0.006
16	4/25/2015	09:17:02	28.3483	87.2873	9.3	5.6	1.98±0.006
17	4/25/2015	12:44:06	28.0803	84.6417	15.1	5.1	1.97±0.006
18	4/25/2015	17:42:52	28.2579	85.8625	9.9	5.3	1.97±0.007
19	4/25/2015	23:16:15	27.7744	84.9497	13.7	5.5	1.96±0.007
20	4/26/2015	07:09:09	27.7365	85.9788	13.4	6.6	1.98±0.006
21	4/26/2015	16:26:06	27.7996	85.8233	16.8	5.6	1.97±0.007
22	4/27/2015	12:35:52	26.8348	88.0797	19.6	5.2	1.99±0.006
23	5/12/2015	07:05:19	27.8014	86.126	12.3	6.7	1.97±0.007
24	5/12/2015	07:17:21	27.7251	86.2083	12.6	5.4	1.99±0.006
25	5/12/2015	07:23:33	27.3792	86.2416	19.0	5.0	1.99±0.006
26	5/12/2015	07:34:23	27.6932	86.2267	11.0	5.3	1.97±0.006

27	5/12/2015	07:36:53	27.5248	86.1418	13.8	6.1	1.97±0.007
28	5/12/2015	08:06:08	27.669	86.088	20.3	5.1	1.98±0.007
29	5/12/2015	08:13:54	27.7404	85.8442	9.5	5.1	1.97±0.006
30	5/12/2015	08:21:10	27.6801	86.1084	9.8	5.2	1.96±0.007
31	5/12/2015	21:25:11	27.7651	84.7136	2.5	5.1	1.98±0.006
32	5/16/2015	11:34:11	27.5175	86.1127	20.1	5.6	1.98±0.006
33	8/23/2015	09:02:04	27.7509	86.0641	8.7	5.1	1.97±0.007
34	11/19/2015	04:15:52	27.7947	85.6871	10.4	5.0	1.97±0.006
35	12/18/2015	22:16:56	29.2787	81.6399	16.1	5.3	1.98±0.006
36	2/5/2016	16:20:11	27.8644	85.457	23.4	5.2	1.97±0.007
37	2/21/2016	18:10:00	27.9582	84.717	13.8	5.0	1.97±0.006
38	5/22/2016	01:48:49	28.3812	87.5079	16.0	5.0	1.98±0.007
39	5/22/2016	02:05:55	28.4487	87.428	12.7	5.1	1.98±0.006
40	11/27/2016	23:35:21	27.7097	86.5045	14.8	5.4	1.98±0.007

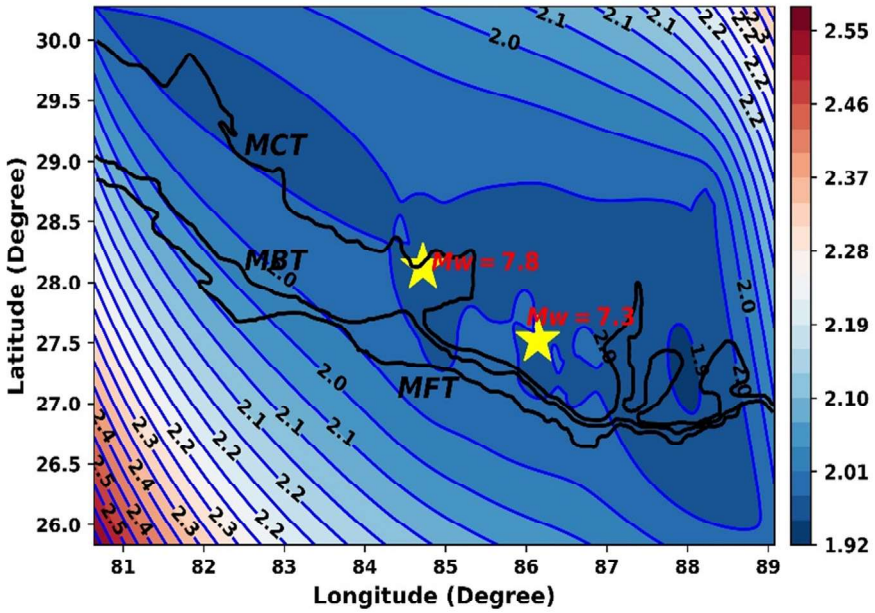

Fig. 4: Contour map of fractal dimension value for the study region where MCT, MBT, and MFT are abbreviations for Main Central Thrust, Main Boundary Thrust, and Main Frontal Thrust, respectively. Two yellow stars stand for the Gorkha earthquake and Kodari earthquake of 2015.

The fractal dimension contour map is depicted in figure 4. The high D value contour lines show that the region is dominated by fractal dimension values between 1.92 to around 2.0. These high values of dimension may be associated with different underlying geometrical structures and different dynamics operating in the region.

4. Conclusion

Fractal objects have non-integer fractional dimension rather than an integer Euclidean dimensionality. All fractal objects exhibit self-similar or self-affine character (exact or statistical); this means that objects look the same at different levels of magnification (Narine & Marangoni, 1999). Fractal geometry has been reported to characterize brittle deformation structures in the crust over several bands of length scales, from regional fault networks through main traces of individual faults to the internal structure of fault zones. Another characteristic of fractal objects is that a specific property should scale in a power-law fashion within a length scale. It has for long been suggested that fractured rock surfaces are fractals. The fractal geometry implies a balance between two competing processes: strain weakening and strain hardening. This balance is critically tuned to produce neither positive nor negative feedback mechanisms during deformation. In such a case, the long-term deformation is accommodated statistically, at all-time intervals, by structures that have no preferred size scale, i.e., structures following a scale free frequency-size distribution. In fact, fault surfaces are fractals can be interpreted as the fractal dimension of the fault system. The application of nonlinear science has been used to find the fractal dimension of the seismic signals recorded at IRIS. Seismic wave signals before and after the Gorkha earthquake have been analyzed in terms of box counting fractal dimension. The results show almost identical value of the fractal dimension for active seismic period. The fractal dimensions of seismic wave signal do not show significant variation during the time of the active seismic period Thus, time series seismic signals are complex and have fractal characteristics that exists self-similarity phenomenon, i.e., pieces of a fractal object are similar to that of the whole implying fractal models of earthquake dynamics.

Acknowledgments

One of the author (RKT) would like to express acknowledgement to Tribhuvan University, Nepal for providing the sabbatical leave and to the University Grants Commission, Nepal for providing the financial support under the PhD grant S&T -14-075/76. The authors would also like to thank the reviewers for their suggestions and comments to improve the quality of this manuscript.

References

Adhikari, L. B., Gautam, U. P., Koirala, B. P., Bhattarai, M., Kandel, T., Gupta, R. M., Timsina, C., Maharjan, N., Maharjan, K., Dahal, T., Hoste-Colomer, R., Cano, Y., Dandine, M., Guilhem, A., Merrer, S., Roudil, P., & Bollinger, L. (2015). The aftershock sequence of the 2015 april 25 Gorkha-Nepal earthquake. *Geophysical Journal International*, *203*(3), 2119–2124. https://doi.org/10.1093/gji/ggv412

Baillard, C., Lyon-Caen, H., Bollinger, L., Rietbrock, A., Letort, J., & Adhikari, L. B. (2017). Automatic analysis of the Gorkha earthquake aftershock sequence: Evidences of structurally segmented seismicity. *Geophysical Journal International*, *209*(2), 1111–1125. https://doi.org/10.1093/gji/ggx081

Beyreuther, M., Barsch, R., Krischer, L., Megies, T., Behr, Y., & Wassermann, J. (2010). ObsPy: A Python Toolbox for Seismology. *Seismological Research Letters*, *81*(3), 530–533. https://doi.org/https://doi.org/10.1785/gssrl.81.3.530

Eke, A., Herman, P., Kocsis, L., & Kozak, L. R. (2002). Fractal characterization of complexity in temporal physiological signals. *Physiological Measurement*, *23*(1). https://doi.org/10.1088/0967-3334/23/1/201

Elliott, J. R., Jolivet, R., Gonzalez, P. J., Avouac, J. P., Hollingsworth, J., Searle, M. P., & Stevens, V. L. (2016). Himalayan megathrust geometry and relation to topography revealed by the Gorkha earthquake. *Nature Geoscience*, *9*(2), 174–180. https://doi.org/10.1038/ngeo2623

Gonzato, G. (1998). A practical implementation of the box counting algorithm. *Computers and Geosciences*, *24*(1), 95–100. https://doi.org/10.1016/S0098-3004(97)00137-4

Górski, A. Z. (2001). Pseudofractals and the box counting algorithm. *Journal of Physics A: Mathematical and General*, *34*(39), 7933–7940. https://doi.org/10.1088/0305-4470/34/39/302

Grassberger, P. (1983). Generalized dimensions of strange attractors. *Physics Letters A*, *97*(6), 227–230. https://doi.org/10.1016/0375-9601(83)90753-3

Gualandi, A., Avouac, J. P., Galetzka, J., Genrich, J. F., Blewitt, G., Adhikari, L. B., Koirala, B. P., Gupta, R., Upreti, B. N., Pratt-Sitaula, B., & Liu-Zeng, J. (2017). Pre- and post-seismic deformation related to the 2015, Mw7.8 Gorkha earthquake, Nepal. *Tectonophysics*, *714–715*, 90–106. https://doi.org/10.1016/j.tecto.2016.06.014

He, P., Lei, J., Yuan, X., Xu, X., Xu, Q., Liu, Z., Mi, Q., & Zhou, L. (2018). Lateral Moho variations and the geometry of the Main Himalayan Thrust beneath the Nepal Himalayan orogen revealed by teleseismic receiver functions. *Geophysical Journal International*, *214*(2), 1004–1017. https://doi.org/10.1093/gji/ggy192

Hu, X., Wang, Z. Z., & Ren, X. M. (2005). Classification of surface EMG signal with fractal dimension. *Journal of Zhejiang University: Science*, *6 B*(8), 844–848. https://doi.org/10.1631/jzus.2005.B0844

Kapiris, P., Nomicos, K., Antonopoulos, G., Polygiannakis, J., Karamanos, K., Kopanas, J., Zissos, A., Peratzakis, A., & Eftaxias, K. (2005). Distinguished seismological and electromagnetic features of the impending global failure: Did the 7/9/1999 M5.9 Athens earthquake come with a warning? *Earth, Planets and Space*, *57*(3), 215–230. https://doi.org/10.1186/BF03351818

Kurths, J., Schwarz, U., Witt, A., Krampe, R. T., & Abel, M. (1996, June). *Measures of complexity in signal analysis*. In AIP Conference Proceedings (Vol. 375, No. 1, PP.(33-54). American Institute of Physics.

Lopes, R., & Betrouni, N. (2009). Fractal and multifractal analysis: A review. *Medical Image Analysis*, *13*(4), 634–649. https://doi.org/10.1016/j.media.2009.05.003

Lu, C., Mai, Y.-W., & Xie, H. (2005). A sudden drop of fractal dimension: a likely precursor of catastrophic failure in disordered media. *Philosophical Magazine Letters*, *85*(1), 33–40. https://doi.org/https://doi.org/10.1080/09500830500153883

Mandelbrot, B. (1967). How long is the coast of Britain? Statistical self-similarity and fractional dimension. *Science*, *156*(3775), 636–638. https://doi.org/10.1126/science.156.3775.636

Mandelbrot, B. B. (2003). Multifractal Power Law Distributions: Negative and Critical Dimensions and Other "Anomalies," Explained by a Simple Example. *Journal of Statistical Physics*, *110*(3–6), 739–774. https://doi.org/10.1023/A:1022159802564

Mandlebrot, B. B. (1989). Multifractal Measures, Especially for the Geophysicist. *Pure and Applied Geophysics*, *131*(1/2).

Maragos, P., & Sun, F. K. (1993). Measuring the Fractal Dimension of Signals: Morphological Covers and Iterative Optimization. *IEEE Transactions on Signal Processing*, *41*(1), 108. https://doi.org/10.1109/TSP.1993.193131

Márquez-Rámirez, V. H., Pichardo, F. A. N., & Reyes-Dávila, G. (2012). Multifractality in Seismicity Spatial Distributions: Significance and Possible Precursory Applications as Found for Two Cases in Different Tectonic Environments. *Pure and Applied Geophysics*, *169*(12), 2091–2105. https://doi.org/10.1007/s00024-012-0473-9

Narine, S. S., & Marangoni, A. G. (1999). Fractal nature of fat crystal networks. *Physical Review E* , *59*(2), 1908–1920. https://doi.org/10.1103/physreve.59.1908

Potirakis, S. M., Minadakis, G., & Eftaxias, K. (2012). Sudden drop of fractal dimension of electromagnetic emissions recorded prior to significant earthquake. *Natural Hazards*, *64*(1), 641–650. https://doi.org/doi:10.1007/s11069-012-0262-x

Telesca, L., Lapenna, V., & MacChiato, M. (2005). Multifractal fluctuations in seismic interspike series. *Physica A: Statistical Mechanics and Its Applications*, *354*(1–4), 629–640. https://doi.org/10.1016/j.physa.2005.02.053

Telesca, L., Lovallo, M., Martì Molist, J., López Moreno, C., & Abella Meléndez, R. (2015). Multifractal investigation of continuous seismic signal recorded at El Hierro volcano (Canary Islands) during the 2011-2012 pre- and eruptive phases. *Tectonophysics*, *642*(1), 71–77. https://doi.org/10.1016/j.tecto.2014.12.019

Tiwari, B. R., Xu, J., Adhikari, B., & Chapagain, N. P. (2020). Multifractal analysis for seismic wave in Kathmandu valley after Gorkha Earthquake-2015, Nepal. *Journal of Nepal Physical Society*, *6*(2), 113–120. https://doi.org/10.3126/jnphyssoc.v6i2.34866

Tiwari, R. K., & Paudyal, H. (2021). Box counting fractal dimension and frequency size distribution of earthquakes in the central Himalaya region. *Journal of Institute of Science and Technology*, *26*(2), 127–136. https://doi.org/https://doi.org/10.3126/jist.v26i2.41664

Yamada, M., Kandel, T., Tamaribuchi, K., & Ghosh, A. (2020). 3D fault structure inferred from a refined aftershock catalog for the 2015 gorkha earthquake in Nepal. *Bulletin of the Seismological Society of America*, *110*(1), 26–37. https://doi.org/10.1785/0120190075

The conference/workshop participation certificates can be accessed afterward.

Certificate of Appreciation

THIS CERTIFICATE IS PRESENTED TO

MR. RAM K. TIWARI

Tribhuvan University, Nepal

FOR YOUR PRESENTATION DURING THE ANPA CONFERENCE 2020

DR. CHET R. BHATT
CHAIR, ANPA CONFERENCE 2020

DR. SHREE K. BHATTARAI
PRESIDENT, ANPA

Geoscience & Technology Division
North East Institute of Science & Technology
(Council of Scientific & Industrial Research)
Jorhat, Assam, India

International Virtual Workshop on Global Seismology & Tectonics

September 14-25, 2020

Certificate of Participation

This e-Certificate is presented to

RAM KRISHNA TIWARI, TRIBHUVAN UNIVERSITY, NEPAL, NEPAL

for participating in the International Virtual Workshop on "Global Seismology & Tectonics" held during September 14 - 25, 2020 via MS Teams, YouTube and Facebook live stream platform organized by the Geoscience & Technology Division, CSIR-NEIST, Jorhat, Assam, India.

The virtual workshop was participated by more than 1000 students, researchers, academicians and scientists from 31 countries including Albania, Algeria, Argentina, Australia, Bangladesh, Canada, Colombia, Comalcalco Tabasco, Democratic Republic of Congo, Dominican Republic, Ecuador, Iceland, Indonesia, Iran, Israel, Japan, Malaysia, México, Myanmar, Nepal, Nigeria, Philippines, Poland, Russia, Singapore, Sri Lanka, Taiwan, Tajikistan, Turkey & US apart from India.

Sixteen keynote lectures were presented by eminent personalities from diverse forums and institutes such as USGS, USA; Chapman University, USA; Dalhousie University, Canada; University of Malta, Malta; International Institute of Earthquake Engineering and Seismology, Iran; Obafemi Awolowo University, Nigeria; Bangladesh University of Engineering and Technology, Bangladesh; Geological Survey of India, Kolkata, India; Kurukshetra University, India; CSIR-4 PI, India; CSIR-NGRI, India & CSIR-NEIST, Jorhat, India.

We wish you good luck for your future endeavors.

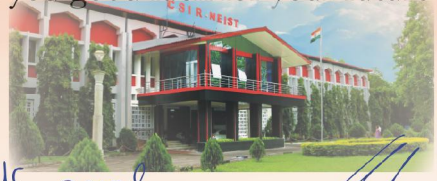

G. Narahari Sastry	J. R. Kayal	Andrew Michael	Santanu Baruah
Director	Sessions' Chairperson	USGS, USA	Convener
CSIR-NEIST, Jorhat	IVWGST-2020	Advisor, IVWGST-2020	IVWGST-2020

GSTD/IVWGST-20/0745/1025

The Abdus Salam
International Centre
for Theoretical Physics

This is to certify that

Ram Krishna TIWARI

participated in and completed online

Citizen Science with Application to Nuclear, Seismic and Air Quality Monitoring: INTRODUCTION

08 - 12 Mar 2021

Directors:
Francois Guy Foulon (IAEA, Austria)
Davide Storti (UNESCO Headquarters, France)
Marco Zennaro (ICTP, Italy)

Atish Dabholkar, Director

The Abdus Salam
International Centre
for Theoretical Physics

This is to certify that

Ram Krishna TIWARI

participated in and completed online

Citizen Science with Application to Nuclear, Seismic and Air Quality Monitoring: APPLICATIONS in Seismic Monitoring

15 - 19 Mar 2021

Directors:
Francois Guy Foulon (IAEA, Austria)
Davide Storti (UNESCO Headquarters, France)
Marco Zennaro (ICTP, Italy)

Atish Dabholkar, Director

Certificate of Appreciation

THIS CERTIFICATE IS PRESENTED TO

MR. RAM KRISHNA TIWARI

Central Department of Physics

Tribhuvan University, Nepal

FOR YOUR PRESENTATION DURING THE ANPA CONFERENCE 2021

Nmalakar

DR. NABIN MALAKAR
CHAIR, ANPA CONFERENCE 2021

DR. JAGAN DEVKOTA
PRESIDENT, ANPA

Joint Scientific Assembly
IAGA-IASPEI 2021
21-27 August 2021 | VIRTUAL CONFERENCE
INDIAN INSTITUTE OF TECHNOLOGY ROORKEE

On the spatio-temporal variation in b-value After 25 April 2015 Gorkha, Nepal earthquake

Ram Krishna Tiwari*[1,2], Harihar Paudyal[2] and Daya Shanker[3]

[1]Central Department of Physics, Tribhuvan University, Kirtipur, Kathmandu, Nepal
[2]Birendra Multiple Campus, Bharatpur, Chitwan, Nepal
[3]Department of Earthquake Engineering Indian Institute of Technology Roorkee, Roorkee, Uttarakhand, India
*Email: ram.tiwari@bimc.tu.edu.np

INTERNATIONAL VIRTUAL WORKSHOP ON GLOBAL SEISMOLOGY & TECTONICS

IVWGST 2021

20-30 September, 2021

ORGANIZED BY

Geoscience & Technology Division

North East Institute of Science & Technology
(Council of Scientific & Industrial Research)
Jorhat, Assam, India

Certificate of Participation

This e-Certificate is presented to

Mr. Ram Krishna Tiwari

Tribhuvan University, Nepal

for attending the International Virtual Workshop on Global Seismology and Tectonics (IVWGST2021), during 20th to 30th September 2021, organized by CSIR North East Institute of Science and Technology, Jorhat under the aegis of Diamond jubilee year of the institute.

We wish them good luck for their future endeavors.

Santanu Baruah	Andrew J. Michael	Dapeng Zhao	G. Narahari Sastry
Convener, IVWGST	USGS International Advisor, IVWGST	Tohoku University Session Advisor, IVWGST	Director, CSIR NEIST Patron, IVWGST

IVWGST-2021-0875

Participants from 42 Nations

WORKSHOP ON

SCIENTIFIC RESEARCH WRITING

15 - 19 Sept. 2021

Certificate of Participation

Ram Krishna Tiwari

Participated in the Training Program.

Organized by:

Research Management Cell

Birendra Multiple Campus, Bharatpur

Supported by:

University Grants Commission, Nepal

Prof. Dr. Sita Ram Bdr. Thapa
Co-ordinator
Research Management Cell
Bharatpur, Chitwan

Prof. Daya Ram Paudyal
Campus Chief
Birendra Multiple Campus
Bharatpur, Chitwan

TRAINING PROGRAME ON

CAPACITY DEVELOPMENT IN LINUX OPERATING SYSTEM

19 - 25 Sept. 2021

Certificate of Participation

Ram Krishna Tiwari

Participated in the Training Program.

Organized by:

Research Management Cell

Birendra Multiple Campus, Bharatpur

Supported by:

University Grants Commission, Nepal

Prof. Dr. Sita Ram Bdr. Thapa
Co-ordinator
Research Management Cell
Bharatpur, Chitwan

Prof. Daya Ram Paudyal
Campus Chief
Birendra Multiple Campus
Bharatpur, Chitwan

CONIAPS-27/26-28/RAES/2021/P0014

27TH INTERNATIONAL CONFERENCE
OF
INTERNATIONAL ACADEMY OF PHYSICAL SCIENCES
(CONIAPS XXVII)
On
"RECENT ADVANCES IN EARTH SCIENCES"
OCTOBER 26-28, 2021
Organized by
INSTITUTE OF EARTH AND ENVIRONMENTAL SCIENCES
DR. RAMMANOHAR LOHIA AVADH UNIVERSITY, AYODHYA

E-CERTIFICATE

Issued on October 28, 2021 to Prof./Dr./Mr./Mrs. ***Dr. Ram Krishna Tiwari*** from *Tribhuvan university of Nepal* for his/her active Participation in the conference and presentation of the paper entitled *"Study of 25 April 2015 Gorkha Earthquake (Mw 7.8) and aftershock Sequence: A Fractal Approach".*

Prof. Jaswant Singh
Convener
CONIAPS XXVII

Prof. Ravi Shankar Singh
Vice- Chancellor
Dr. RML Avadh University

Prof. P.N. Pandey
General Secretary
IAPS

Nepal Physical Society

Ghantaghar, Kathmandu, Nepal

Presenting this certificate to **Ram Krishna Tiwari** from Central Department of Physics, Tribhuvan University, Kirtipur, Kathmandu Nepal

for attending the

International Conference on Frontiers of Physics -2022

(ICFP-2022)

held on January ual platform.

Prof. Dr. Narayan P. Chapagain
Conference Chair, ICFP-2022
President, Nepal Physical Society

February 1, 2022

CERTIFICATE

This is to certify that

Ram Krishna Tiwari

has presented **Oral** presentation for the paper entitled "**The p and b values succeeding the 25 April and 12 May, 2015 Central Himalayan earthquakes.**" in the **58th Annual Convention of IGU "Recent Advances in Earth Sciences with Special Emphasis - Natural Hazards"** jointly organised by Indian Geophysical Union and North-Eastern Hill University, Shillong between **2nd and 4th February 2022.**

Prof. Shailesh Nayak
President, IGU
Director, NIAS, Bengaluru

Prof. Devesh Walia
LOC-58th AC IGU-NEHU
Head, Geology Department NEHU

Nepal Academy of Science and Technology (NAST)

CERTIFICATE OF PARTICIPATION

Awarded to

RAM KRISHNA TIWARI

for Presentation in Oral / ~~Poster~~ / ~~Participation~~ in the

9th National Conference on Science and Technology

June 26-28,2022 (Asar 12-14, 2079)

Khumaltar, Lalitpur, Nepal

Ms. Luna Vajra Chief, Promotion Division	Prof. Dr. Mahesh K. Adhikari Secretary	Dr. Sunil Babu Shrestha Vice Chancellor

CERTIFICATE

OF COMPLETION

This Certifies that

Ram Krishna Tiwari

Has successfully completed the short course training program requirement for

THE GENERIC MAPPING TOOL (GMT) FOR GEODESY
JULY 5-7, 2022

DR. PAUL WESSEL, PH.D.
UNIVERSITY OF HAWAII, MANOA

DR. DONNA J. CHARLEVOIX, PH.D.
UNAVCO

GAGE
National Science Foundation's Geodetic Facility for the Advancement of Geoscience

Operated by UNAVCO

INTERNATIONAL VIRTUAL WORKSHOP ON GLOBAL SEISMOLOGY & TECTONICS (IVWGST) 2022

20-30 September 2022

ORGANIZED BY

GEOSCIENCE & TECHNOLOGY DIVISION

NORTH EAST INSTITUTE OF SCIENCE & TECHNOLOGY

(COUNCIL OF SCIENTIFIC & INDUSTRIAL RESEARCH)

JORHAT, ASSAM, INDIA

CERTIFICATE FOR PARTICIPATION

THIS E-CERTIFICATE IS PRESENTED TO

Mr. Ram Krishna Tiwari

Tribhuvan University, Nepal

for attending the 3rd International Virtual Workshop on Global Seismology and Tectonics (IVWGST 2022), from 20th to 30th September 2022, organized by Geoscience and Technology Division, CSIR- North East Institute of Science & Technology, Jorhat, Assam, India.

We wish them good luck for their future endeavors.

Santanu Baruah	Andrew J. Michael	Dapeng Zhao	G. Narahari Sastry
Convenor (CSIR-NEIST)	**International Advisor (USGS)**	**International Advisor (Tohoku University, Japan)**	**Chief Patron (Director, CSIR-NEIST)**

CERTIFICATE NO.: IVWGST-2022/484

"GeoSynergy"

A collaboration of

SEG Student Chapters of IIT Kharagpur, Dibrugarh University and Delhi University

CERTIFICATE OF COMPLETION

Presented to

RAM KRISHNA TIWARI

for successfully completing the "**2-day Hands-on Workshop on OpendTect Software**" through online platform on 25th and 26th March, 2023.

Pavel Karmanov
Workshop Instructor
Senior Research Fellow
Dept of Geology and Geophysics
IIT Kharagpur

Akash Nair
President
SEG IIT Kharagpur SC

Moinak Sinha
President
SEG Delhi University SC

Md Sohail Khan
President
SEG Dibrugarh University SC